



THE UNIVERSITY OF  
**SYDNEY**

## **COPYRIGHT AND USE OF THIS THESIS**

This thesis must be used in accordance with the provisions of the Copyright Act 1968.

Reproduction of material protected by copyright may be an infringement of copyright and copyright owners may be entitled to take legal action against persons who infringe their copyright.

Section 51 (2) of the Copyright Act permits an authorized officer of a university library or archives to provide a copy (by communication or otherwise) of an unpublished thesis kept in the library or archives, to a person who satisfies the authorized officer that he or she requires the reproduction for the purposes of research or study.

The Copyright Act grants the creator of a work a number of moral rights, specifically the right of attribution, the right against false attribution and the right of integrity.

You may infringe the author's moral rights if you:

- fail to acknowledge the author of this thesis if you quote sections from the work
- attribute this thesis to another author
- subject this thesis to derogatory treatment which may prejudice the author's reputation

For further information contact the University's Director of Copyright Services

**[sydney.edu.au/copyright](http://sydney.edu.au/copyright)**

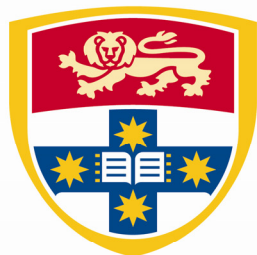
# **SYSTEM RELIABILITY-BASED DESIGN OF 2D STEEL FRAMES BY ADVANCED ANALYSIS**

BY

Shabnam Shayan

B.Sc. (Civil Engineering), M.E. (Hons) (Structural Engineering)

A thesis submitted in fulfilment of the requirements for the degree of  
Doctor of Philosophy  
School of Civil Engineering  
The University of Sydney



THE UNIVERSITY OF  
**SYDNEY**

Sydney, Australia  
August 2013



## **Certificate of originality**

I hereby declare that this thesis is my own work and that, to the best of my knowledge and belief, it contains no material previously published or written by another person, nor material which to a substantial extent has been accepted for the award of any other degree or diploma at The University of Sydney or any other educational institution, except where due acknowledgment is made in the thesis.

I also declare that the thesis has been written by me. Any help that I have received in my research work and the presentation of the thesis itself has been acknowledged. In addition, I clarify that all information sources and literature used are indicated in the thesis.

## **Abstract**

The design of steel frames by geometric and material nonlinear analysis also referred to as “inelastic” or “advanced” analysis, is permitted by most specifications such as AISC360-10 and AS4100. In these specifications, the strength of a structural frame can be determined by system analysis in lieu of checking member resistances to the specific provisions of the Specification, provided a comparable or higher level of structural reliability. In designing by advanced analysis, the system resistance factor ( $\phi_s$ ) is applied to the frame strength determined by analysis. Provided that the design strength exceeds the required strength, the design is deemed adequate, requiring no further check of individual member resistance. The system-based design of steel structures by advanced analysis leads to a more efficient structural design process and achieves a more uniform level of structural reliability. The main impediment to adopting the procedure in practical applications is the apparent difficulty in assigning an appropriate resistance factor to the structural system.

This thesis illustrates the novel framework of the system design-by-analysis approach and how to determine suitable system resistance factors accounting for inherent uncertainties in the ultimate strength of a frame. All key parameters influencing the frame strength are modelled as random and Monte-Carlo type simulations are conducted. New approaches for modelling initial geometric imperfections and residual stresses are introduced. The simulation results for a series of 2D low-to-mid-rise steel frames, which represent typical steel building inventory as well as frames from the literature, are presented obtained according to the proposed methodology. Braced and moment resisting (sway) frames including regular and irregular configurations are analysed under various load combinations and the system resistance factors are derived for different reliability levels. Member cross-sections are selected to provide different system failure modes such as through beam or column yielding, column buckling and elastic sway buckling. Recommendations are made about the appropriate target reliabilities to apply in designing steel frames at system level by advanced analysis and corresponding system resistance factors are derived.

## Dedication

This thesis is lovingly dedicated to my parents, Saeed and Pari Shayan, who taught me to dream big, stay strong and never give up on my goals. There are no words that can truly express the level of gratitude and appreciation I have for you. I am forever grateful for your support, encouragement and unconditional love.

I would not be where I am today without you.

## **Acknowledgments**

Completing my PhD degree was probably one of the most challenging activities of the first 30 years of my life. The best moments of my doctoral journey have been shared with many people I want to thank.

First and foremost, I would like to express my sincere gratitude to my supervisors Dr. Hao Zhang and Prof. Kim Rasmussen for their excellence guidance, caring and patience in all stages of this research. I simply could not wish for better supervisors. Without their support this work would not have been started or completed.

I am especially grateful to Prof. Bruce R. Ellingwood, for his insightful comments, discussion, ideas, and feedback on this study. I would also like to acknowledge Mrs. Kate Kernaghan for providing editorial corrections for this thesis. I would like to thank postgraduate students in Room 360 (Blue room) for their friendship and all good moments that we had together. Special thanks go to my former colleague Dr. Yao (Eric) Zhenyu for all that I have learned from him when I was new to the office.

There are people in everyone's lives who make the tough times easier and more enjoyable. Special thanks are dedicated to my best friends Ms Taraneh Shenassa, Ms Shiva Shahrampour and Ms Naghmeh Saeidi who have supported me in any stage of my life for more than 20 years. Your friendship is one of the most valuable things in my life. Also I would like to thank my friend Bella Gomrokchi for cheering me up and pushing me forward whenever I thought things were not going my way, for being my friend and for the crazy and exciting fun we always have. I would like to thank Dr. Emmanuel Blanchard, who supported, advised and encouraged me through the toughest time of this journey. Thanks Emmanuel for everything. You have really changed my life.

Last, but not least I would like to thank my lovely sister, Shadi Shayan, who is my best friend in life, for always believing on me, supporting me and loving me.

Finally, I would like to express my appreciation to all people, who are not explicitly mentioned here, but have happened to cross my life during these years and to some extent have taught me a special lesson during this period. They have defiantly contributed to this journey by making these years more pleasurable and memorable.

# TABLE OF CONTENTS

<b>ABSTRACT</b> .....	<i>ii</i>
<b>ACKNOWLEDGMENTS</b> .....	<i>iv</i>
<b>LIST OF FIGURES</b> .....	<i>x</i>
<b>LIST OF TABLES</b> .....	<i>xvii</i>
<b>ABBREVIATIONS</b> .....	<i>xxv</i>
<b>PRINCIPAL NOTATIONS</b> .....	<i>xxvi</i>
<b>CHAPTER 1-INTRODUCTION</b> .....	<b>1</b>
1.1 BACKGROUND.....	1
1.1.1.2 AIMS AND OBJECTIVES.....	3
1.3 INNOVATION AND BENEFITS.....	4
1.4 RESEARCH METHODOLOGY.....	5
1.5 THESIS OUTLINE.....	5
1.6 PUBLICATIONS AND AWARDS.....	7
1.6.1 Journal papers.....	7
1.6.2 Conference papers.....	8
1.6.3 Research reports.....	8
1.6.4 Awards.....	9
<b>CHAPTER 2- LITERATURE REVIEW</b> .....	<b>10</b>
2.1 INTRODUCTION.....	10
2.2 CURRENT STEEL STRUCTURAL DESIGN SPECIFICATIONS.....	11
2.3 STRUCTURAL ANALYSIS OF STEEL FRAMES.....	14
2.3.1 First-order elastic analysis.....	15
2.3.2 Second-order elastic analysis.....	16
2.3.3 First-order elastic-plastic hinge analysis.....	16
2.3.4 Second-order elastic-plastic hinge analysis.....	17
2.3.5 Second-order inelastic analysis (Advanced analysis).....	17
2.4 ADVANCE ANALYSIS METHODS.....	19
2.4.1 Plastic hinge analysis.....	19
2.4.1.1 Refined (modified) plastic hinge method.....	19
2.4.1.2 Quasi-plastic hinge method.....	20
2.4.1.3 Notional load plastic hinge method.....	20
2.4.1.4 Hardening plastic hinge method.....	21
2.4.2 Plastic zone analysis.....	22
2.5 ADVANCED ANALYSIS REQUIREMENTS.....	23
2.5.1 Material nonlinearity.....	23
2.5.2 Geometric nonlinearity.....	25
2.5.3 Initial geometric imperfection.....	29
2.5.3.1 Scaling of the first eigenbuckling mode (EBM).....	30
2.5.3.2 Notional horizontal force (NHF).....	31
2.5.3.3 Further reduction of member stiffness ( $Et'$ ).....	32
2.5.3.4 Explicit modelling of initial geometric imperfections (IGI).....	32



2.5.3.5 Deterministic modelling of initial geometric imperfection.....	33
2.5.3.6 Probabilistic modelling .....	34
2.5.3.6.1 Probabilistic SBRA method.....	35
2.5.3.6.2 Proposed method by Bjorhovde.....	36
2.5.3.6.3 Fuzzy analysis method.....	38
2.5.3.7 Experimental data .....	40
2.5.3.7.1 Initial out-of-straightness.....	40
2.5.3.7.2 Initial out-of-plumb .....	45
2.5.4 Residual stress .....	49
2.5.5 Warping torsion .....	50
2.6 RELIABILITY ANALYSIS .....	55
2.7 SIMULATION METHODS.....	57
2.7.1 First-order Reliability Method.....	58
2.7.2 Monte-Carlo (MC) method.....	60
2.8 SAMPLING TECHNIQUES.....	61
2.9 CODE DEVELOPMENT PROCEDURES .....	65
2.10 STRUCTURAL SAFETY AND TARGET RELIABILITY.....	66
2.11 CONCLUSION .....	67
<b>CHAPTER 3- ADVANCED ANALYSIS MODELS OF STEEL STRUCTURAL</b>	
<b>SYSTEMS.....</b>	<b>69</b>
3.1 INTRODUCTION.....	69
3.2 FINITE ELEMENT MODEL .....	71
3.3 ELEMENTS.....	72
3.4 MATERIAL MODEL.....	73
3.5 RESIDUAL STRESS AND INITIAL GEOMETRIC IMPERFECTION.....	75
3.6 STRENGTH AND SERVICEABILITY LIMIT STATE .....	76
3.7 EFFECT OF STRAIN HARDENING ON THE FRAME ULTIMATE STRENGTH .....	79
3.8 MODEL CALIBRATION.....	80
3.9 MESH SENSITIVITY (CONVERGENCE STUDY) .....	85
3.10 CONCLUSION .....	88
<b>CHAPTER 4- A MODEL FOR WARPING TRANSMISSION THROUGH JOINTS</b>	
<b>OF STEEL FRAMES .....</b>	<b>89</b>
4.2 CONTEXT.....	89
4.2 INTRODUCTION.....	89
4.3 SUBSTRUCTURING AND STATIC CONDENSATION .....	94
4.4 JOINT MODEL.....	96
4.4.1 The basics- 2D model.....	96
4.4.2 3D model .....	102
4.5 IMPLEMENTATION OF THE MODEL.....	104
4.6 VERIFICATION AND ILLUSTRATIVE EXAMPLES.....	107
4.6.1 Planer Frames .....	108
4.6.1.1 L-Shape frame.....	108
4.6.1.2 One-bay, one -storey frame with an overhanging member.....	111
4.6.1.3 One-bay, two-story frame .....	114

4.6.2 Space Frames.....	116
4.6.2.1 One-bay, one storey frame.....	116
4.6.2.2 One-bay, one storey frame.....	118
4.7 OBSERVATIONS AND REMARKS.....	120
4.8 CONCLUSION.....	121
<b>CHAPTER 5- MODELING OF INITIAL GEOMETRIC IMPERFECTIONS OF STEEL STRUCTURAL FRAMES .....</b>	<b>123</b>
5.1 INTRODUCTION.....	123
5.2 STATISTICAL DATA FOR INITIAL GEOMETRIC IMPERFECTION .....	125
5.2.1 Initial out-of-straightness.....	125
5.2.2 Initial out-of-plumb .....	129
5.3 INITIAL GEOMETRIC IMPERFECTION BY LINEAR COMBINATIONS OF EIGENBUCKLING MODES .....	131
5.3.1 Amplitudes of eigenmodes .....	131
5.3.2 Number of eigenmodes .....	138
5.4 VERIFICATION AND ILLUSTRATIVE EXAMPLES.....	144
5.4.1 Unbraced frames.....	144
5.4.2 Braced frames.....	149
5.5 CONCLUSION.....	152
<b>CHAPTER 6- PROBABILISTIC MODELING OF RESIDUAL STRESS IN ADVANCED ANALYSIS OF STEEL FRAMES .....</b>	<b>153</b>
6.1 INTRODUCTION.....	153
6.2 THE PROPOSED APPROACH.....	156
6.3 FRAME ANALYSIS .....	158
6.3.1 Deterministic study.....	160
6.3.2 Probabilistic study .....	165
6.4 RELIABILITY ANALYSIS .....	168
6.5 CONCLUSION.....	171
<b>CHAPTER 7- SYSTEM RELIABILITY-BASED DESIGN OF STEEL FRAMES BY ADVANCED ANALYSIS .....</b>	<b>172</b>
7.1 INTRODUCTION.....	172
7.2 METHODOLOGY.....	176
7.3 STRUCTURAL FRAMING SYSTEM .....	177
7.3.1 Loading.....	179
7.3.2 System failure criterion .....	180
7.4 PROBABILISTIC ANALYSIS .....	183
7.4.1 Uncertainties in steel structures.....	185
7.4.1.1 Variability in yield stress and elastic modulus.....	187
7.4.1.2 Variability in cross-section dimensions .....	187
7.4.1.3 Variability in initial geometric imperfection .....	188
7.4.1.4 Variability in residual stress.....	189
7.5 SENSITIVITY ANALYSIS.....	189
7.6 SYSTEM RELIABILITY AND MODEL UNCERTAINTY.....	193

7.7 SIMULATION RESULTS TO DETERMINE APPROPRIATE SYSTEM RESISTANCE FACTORS	196
7.7.1 Proposed methods to plot $\beta - \varphi_s$ curves	197
7.7.1.1 Cross-Section Scaling Method (CSM)	197
7.7.1.2 Load Scaling Method (LSM)	200
7.7.2 Simulation results for sway frames under gravity loading	201
7.7.2.1 Ziemian's frames	201
7.7.2.2 Proposed sway frames	205
7.7.3 Verification of FORM against Direct Monte-Carlo for frames under gravity	208
7.7.4 Simulation results for frames under gravity plus wind loading	211
7.7.5 Simulation results for braced frames under gravity loading	217
7.8 EFFECT OF MEMBER YIELD STRESS CORRELATION ON THE SYSTEM RESISTANCE FACTOR	222
7.9 EFFECT OF STRAIN HARDENING ON THE SYSTEM RESISTANCE FACTOR	223
7.10 TARGET RELIABILITY AND DESIGN EXAMPLE	226
7.11 CONCLUSIONS	229
<b>CHAPTER 8- CONCLUSION</b>	<b>231</b>
8.1 SUMMARY	231
8.2 REMARKS	232
<b>REFERENCES</b>	<b>239</b>
<b>APPENDIX A- RESIDUAL STRESS SUBROUTINE</b>	<b>251</b>
<b>APPENDIX B- WARPING TORSION</b>	<b>252</b>
7.9 B.1 EXAMPLE OF A PERL SCRIPT FOR CREATING A SHELL FINITE ELEMENT MODEL OF THE CORNER BOX-STIFFENED JOINT SHOWN IN FIGURE 4-4	252
B.2 AN ABAQUS INPUT FILE FOR ANALYSING THE JOINT SHOWN IN FIGURE 4-4 AS A SUBSTRUCTURE	257
B.3 A SAMPLE ABAQUS INDATA FILE FOR ANALYSING PLANAR L-SHAPE FRAME USING THE B-FEA SPRING MODEL WITH A BOX-STIFFENED JOINT	261
<b>APPENDIX C- INITIAL GEOMETRIC IMPERFECTION</b>	<b>264</b>
C.1 FRAME LAYOUTS TO FIND THE AMPLITUDE OF EIGEN BUCKLING MODES	264
7.7.4 C.1.1 Unbraced frames	264
C.1.2 Braced frames	267
C.2 SCALE FACTORS	270
C.2.1 Unbraced frames	270
C.2.2 Braced frames	281
C.3 LOAD-DEFLECTION RESPONSE OF FRAMES FOR VERIFICATION EXAMPLES	292
C.3.1 Unbraced frames	292
C.3.2 Braced frames	296
C.4 ULTIMATE STRENGTH DISTRIBUTION OF FRAMES FOR VERIFICATION EXAMPLES	300
C.4.1 Unbraced frames	300
C.4.2 Braced frames	304
<b>APPENDIX D- SCALE FACTORS FOR RESIDUAL STRESS</b>	<b>308</b>
D.1 NON-AMERICAN SECTIONS	308

D.2 AMERICAN SECTIONS .....	308
<b>APPENDIX E- SYSTEM-BASED DESIGN .....</b>	<b>311</b>
E.1 SYSTEM-BASED DESIGN OF SWAY FRAMES UNDER GRAVITY, CSM .....	311
E.2 SYSTEM-BASED DESIGN OF SWAY FRAMES UNDER GRAVITY PLUS WIND, CSM .....	329
E.3 SYSTEM-BASED DESIGN OF HINGED JOINT BRACED FRAMES UNDER GRAVITY, LSM	359
E.4 SYSTEM-BASED DESIGN OF RIGID JOINT BRACED FRAMES UNDER GRAVITY, LSM....	365
E.5 SELECTED HISTOGRAMS OF ULTIMATE LOAD FACTORS, SWAY FRAMES UNDER GRAVITY LOADS .....	371
E.6 SELECTED HISTOGRAMS OF ULTIMATE LOAD FACTORS, SWAY FRAMES UNDER GRAVITY PLUS WIND LOADS .....	376
E.7 SELECTED HISTOGRAMS OF ULTIMATE LOAD FACTORS, HINGED JOINT BRACED FRAMES UNDER GRAVITY LOADS .....	379
E.8 SELECTED HISTOGRAMS OF ULTIMATE LOAD FACTORS, RIGID JOINT BRACED FRAMES UNDER GRAVITY LOADS .....	381
E.9 SELECTED $\beta - \varphi_s$ PLOTS, SWAY FRAMES UNDER GRAVITY LOADS .....	383
E.10 SELECTED $\beta - \varphi_s$ PLOTS, SWAY FRAMES UNDER GRAVITY PLUS WIND LOADS .....	385
E.11 SELECTED $\beta - \varphi_s$ PLOTS, HINGED JOINT BRACED FRAMES UNDER GRAVITY LOADS .....	387
E.12 SELECTED $\beta - \varphi_s$ PLOTS, RIGID JOINT BRACED FRAMES UNDER GRAVITY LOADS	388
E.13 CODES .....	389
E.14 PRACTICAL APPLICATION AND DESIGN EXAMPLES .....	411

## List of figures

Figure 2-1: Strength and stability check for member based on AISC-ASD .....	11
Figure 2-2: Curves of LRFD interaction equations .....	13
Figure 2-3: Curve of AS4100 interaction equation.....	13
Figure 2-4: Structural analysis methods .....	15
Figure 2-5: Plastic zone method for frame analysis (a) frame discretization (b) section discretization.....	22
Figure 2-6: Concept of Yield Surface.....	24
Figure 2-7: Hardening response of material .....	25
Figure 2-8: Newton-Raphson Method .....	27
Figure 2-9: Modified Newton-Raphson Method .....	27
Figure 2-10: The displacement control method.....	28
Figure 2-11: The arc-length control method.....	29
Figure 2-12: (a) Initial out-of-straightness, (b) Initial out-of-plumb .....	29
Figure 2-13: Initial out-of-straightness distribution, SBRA method.....	35
Figure 2-14: Negatively skewed distribution.....	36
Figure 2-15: Initial out-of-straightness proposed by Bjorhovde (1972).....	38
Figure 2-16: Random field of beam axis curvature .....	38
Figure 2-17: Example of the beam initial out-of-straightness, depending on the correlation length.....	39
Figure 2-18: Initial out-of-straightness of IPE 160 column tested by ECCS reported by Fukumoto and Itoh (1983) .....	41
Figure 2-19: Statistical characteristics of measured imperfection by ECCS reported by Roorda (1974).....	41
Figure 2-20: Initial out-of-straightness of columns tested by ECCS as reported by Strating and Vos (1973).....	42
Figure 2-21: Initial out-of-straightness reported by Itoh (1984).....	43
Figure 2-22: Initial crookedness measured in Kasumigaseki Building (Tomonaga 1971).....	43
Figure 2-23: Initial out-of-plumb of a multistorey building measured by ECCS (a) first floor (b) sixth floor (c) eleventh floor.....	45
Figure 2-24: Column out-of-plumb distribution measured by Beaulieu and Adams (1977) .....	46
Figure 2-25: Absolute values of 725 measured out-of-plumb reported by Lindner and Gietzelt (1984) .....	47
Figure 2-26: Out-of-plumb reported by Lindner and Gietzelt (1984) (a) actual values with sign (b) Absolute values.....	47
Figure 2-27: Effect of residual stresses (Szalai and Papp 2005) (a) on the ultimate strength of a column (b) on the buckling curve.....	50
Figure 2-28: Joints configuration (a) warping free (b) warping fully prevented.....	51
Figure 2-29: Joint configuration considered by Baigent and Hancock (1982).....	52
Figure 2-30: Joints details considered by Renton (1974) .....	53

Figure 2-31: Connection element proposed by Blandford (1990).....	53
Figure 2-32: (a) Angle joint under load (b) joint stiffening arrangements (Vacharajittiphan and Trahair 1975).....	54
Figure 2-33: Structural reliability problem, PDF of load, resistance and safety margin ...	55
Figure 2-34: Safe domain and failure domain in a two-dimensional space.....	56
Figure 2-35: Reliability index defined as the shortest distance in the space of reduced variables .....	57
Figure 2-36: Two-dimensional scatter plots of different point sets.....	62
Figure 2-37: Halton sequence and scrambled Halton sequence .....	63
Figure 2-38: Latin-Hypercube sampling.....	64
Figure 2-39: Evaluating the rate of convergence using both Monte Carlo and LHS .....	64
Figure 3-1: Integration points of (a) two-node, linear beam (B31) and (b) three-node, quadratic beam (B32) elements of ABAQUS.....	72
Figure 3-2: Default ABAQUS section points, (a) beam in a plane (b) beam in space .....	73
Figure 3-3: Comparison of nominal and true stress-strain relationship.....	74
Figure 3-4: Stress-strain relationship .....	75
Figure 3-5: Residual stress pattern, ECCS model.....	76
Figure 3-6: Examples of load-deflection response .....	77
Figure 3-7: Step-by-step procedure to find the structural collapse load.....	78
Figure 3-8: 3-bay irregular frame to investigate the effect of strain hardening.....	79
Figure 3-9: Load-deflection response of 3-bay irregular frame.....	80
Figure 3-10: 3-bay irregular frame, failure modes.....	80
Figure 3-11: (a) Configuration of Vogel’s six-storey frame (b) ABAQUS model.....	81
Figure 3-12: Load-lateral displacement of Vogel’s frame.....	82
Figure 3-13: Vogel’s frame, (a) ABAQUS failure mode (b) Plastic hinge locations by Barsan and Chiorean (1999) .....	82
Figure 3-14: Ziemian’s frame, UP36HA .....	83
Figure 3-15: Comparison of load-displacement response of frame UP36HA by ABAQUS, Ziemian (1992) and NIFA (Chen and Toma (1997)).....	84
Figure 3-16: Ziemian’s frame, ABAQUS failure mode .....	84
Figure 3-17: Mesh convergence study, ABAQUS, Vogel’s frame .....	85
Figure 3-18: Mesh convergence study, ABAQUS, Ziemian’s frame.....	86
Figure 3-19: Mesh sensitivity analysis of Ziemian’s frame.....	87
Figure 3-20: Mesh sensitivity analysis of Vogel’s frame .....	87
Figure 4-1: Warping torsion in a doubly symmetric I section (a) cross-sectional displacement (b) axial stress (c) bimoment .....	91
Figure 4-2: Configurations of joints between channel members (Basaglia et al.(2010)) (a) unstiffened with flange continuity, (b) diagonal stiffened, (c) box stiffened, (d) diagonal/box stiffened joints.....	92
Figure 4-3: Example of mixed dimensional model (combination of 1D and 3D elements) .....	93
Figure 4-4: (a) Longitudinal displacements to generate a single warping degree of freedom, (b) Rigid bar model, (c) Retained degrees of freedom for an angle box joint, (d) Joint deformations due to applied warping.....	97

Figure 4-5: Warping compatibility of adjoining members .....	99
Figure 4-6: Joint spring model, 2D .....	102
Figure 4-7: 3D corner joint .....	102
Figure 4-8: Joint spring model, 3D .....	104
Figure 4-9: ABAQUS substructure (a) box joint (b) box joint with one diagonal stiffener .....	105
Figure 4-10: ABAQUS joint spring model, (a) 3D, (b) 2D .....	106
Figure 4-11: Out-of-plane restraint model in S-FEA .....	107
Figure 4-12: Configuration and dimension of L-shape plane frame .....	108
Figure 4-13: Load-deflection curve of L-shape planner frame (a) first-order elastic analysis, (b) nonlinear inelastic analysis .....	110
Figure 4-14: Joint stress contour for nonlinear analysis of L-shape planner frame .....	111
Figure 4-15: Configuration and dimension of plane portal frame with an overhanging member .....	111
Figure 4-16: Nonlinear load-deflection response of one-bay, one storey frame with overhanging member .....	113
Figure 4-17: Joint stress contour for nonlinear analysis of one-bay, one-storey planner frame with overhanging member .....	114
Figure 4-18: Configuration and dimension of two-storey plane portal frame .....	114
Figure 4-19: Joint stress contour for nonlinear analysis of one-bay, two-storey planner frame, $f_y=320$ MPa .....	115
Figure 4-20: Nonlinear load-deflection response of one-bay, two-storey frame .....	115
Figure 4-21: Joint stress contour for nonlinear analysis of one-bay, two-storey planner frame, $f_y =450$ MPa .....	116
Figure 4-22: Configuration and joint types of the one-bay, one-storey space frame .....	117
Figure 4-23: B-FEA and S-FEA critical buckling modes of the space frame with transverse beam .....	118
Figure 4-24: Configuration and joint types of the one-bay, two-storey space frame .....	119
Figure 4-25: B-FEA and S-FEA critical buckling modes of the one-bay, two-storey space frame .....	120
Figure 5-1: First three buckling modes of simply supported, axially loaded column .....	126
Figure 5-2: Example of random shape of initial out-of-straightness for a simply-supported column .....	129
Figure 5-3: Initial out-of-plumb along the height (a) same direction (b) different direction .....	129
Figure 5-4: Out-of-plumb statistics reported by Lindner and Gietzelt (1984) .....	130
Figure 5-5: (a) Examples of randomly generated shapes of initial imperfection for a simple portal frame (b) Example of buckling mode ( $j$ ) for a simple portal frame .....	133
Figure 5-6: (a) Sway mode, (b) Sway mode, (c) Sway mode, (d) Non-sway mode, (e) Non-sway mode, (f) Non-sway mode .....	134
Figure 5-7: Comparison of randomly generated initial imperfection with imperfection modelled by scaling two and ten modes .....	139
Figure 5-8: Steel frame layouts to determine the appropriate number of eigenmodes .....	140
Figure 5-9: Mean value of bias for 200 simulations .....	141

Figure 5-10: COV of bias for 200 simulations .....	142
Figure 5-11: Mean of absolute error (%) for 200 simulations .....	142
Figure 5-12: Maximum of absolute error (%) for 200 simulations .....	143
Figure 5-13: Steel frame layouts of verification examples, unbraced frames .....	146
Figure 5-14: Absolute error (%) between $\bar{\lambda}$ and $\lambda_n^i$ , unbraced frame .....	147
Figure 5-15: F-UB 2, (a) Column slenderness parameter $\lambda_c = 0.88$ (b) Column slenderness parameter $\lambda_c = 1.37$ .....	148
Figure 5-16: Steel frame layouts of verification examples, braced frames .....	150
Figure 5-17: Absolute error (%) between $\bar{\lambda}$ and $\lambda_n^i$ , un-braced frame .....	151
Figure 6-1: Residual stress patterns (a) Cross-sectional dimensions (b) Measured data (Beedle 1958) (c) Measured data (Chen and Sohal 1995) (d) Galambos and Ketter (1959) (e) ECCS (1976) (f) Bild and Trahair (1989) .....	154
Figure 6-2: Residual stress statistics of reported by Fukumoto and Itoh (1980).....	155
Figure 6-3: Histogram of scale factor for residual stress, ECCS model.....	157
Figure 6-4: Histogram of scale factor for residual stress, Trahair model .....	158
Figure 6-5: Histogram of scale factor for residual stress, Galambos model.....	158
Figure 6-6: Steel frame layouts.....	159
Figure 6-7: Load-deflection curve of Frame 1 with ECCS residual stress model .....	162
Figure 6-8: Load-deflection curve of Frame 2 with ECCS residual stress model .....	162
Figure 6-9: Load-deflection curve of Frame 3 with ECCS residual stress model .....	163
Figure 6-10: Load-deflection curve of Frame 4 with ECCS residual stress model .....	163
Figure 6-11: Column strength for different levels of residual stress, ECCS (1976).....	164
Figure 6-12: Histograms of ultimate frame strength for Frame 1 using ECCS and Galambos models.....	166
Figure 6-13: Histograms of ultimate frame strength for Frame 2 using ECCS and Galambos models.....	166
Figure 6-14: Histograms of ultimate frame strength for Frame 3 using ECCS and Galambos models.....	167
Figure 6-15: Histograms of ultimate frame strength for Frame 4 using ECCS and Galambos models.....	167
Figure 6-16: Histograms of ultimate frame strength using ECCS and Galambos models with both residual stress scale factors and yield stress as random variables, Frame 1 ....	169
Figure 6-17: Histograms of ultimate frame strength using ECCS and Galambos models with both residual stress scale factors and yield stress as random variables, Frame 2 ....	170
Figure 7-1: Layouts for steel framing system.....	178
Figure 7-2: Various failure mechanisms.....	180
Figure 7-3: Schematic moment-curvature relationship of an I-section (Kim and Chen 1996).....	181
Figure 7-4: Simply supported beam used to define yielding criteri.....	181
Figure 7-5: Load-deflection curve of simply supported beam used to define the yielding criteria .....	182
Figure 7-6: Examples of frames failure modes.....	183



Figure 7-7: Example of plotted load-deflection curves using MALTAB script to check the convergence .....	185
Figure 7-8: Cross-section dimensions.....	187
Figure 7-9: Comparison between ultimate load distributions with all random variables and with only yield stress as random, Frame 4.....	191
Figure 7-10: Comparison between ultimate load distributions with all random variables and with only cross-section area as random, Frame 4 .....	192
Figure 7-11: Comparison between ultimate load distributions with all random variables and with only cross-section area as random, Frame 4 .....	192
Figure 7-12: Histogram of ultimate load factor for Frame 5 subjected to gravity with BFY-CPY failure mode for $\phi_s=0.63$ ( $L_n/D_n=1$ ) .....	198
Figure 7-13: $\beta$ vs. $\phi_s$ for Frame 5 using CSM.....	199
Figure 7-14: $\beta$ vs. $\phi_s$ for Frame 5 using LSM.....	201
Figure 7-15: Loads and dimensions of Ziemian's frames .....	202
Figure 7-16: Gravity load distribution .....	203
Figure 7-17: $\beta$ vs. $\phi_s$ curves for Frame 5 under gravity loading using LSM with BPY-CFY failure mode .....	208
Figure 7-18: $\beta$ vs. $\phi_s$ curves for Frame 7 under gravity loading using LSM with CFY failure mode .....	208
Figure 7-19: Estimate of reliability index by direct Monte Carlo simulation, Frame 2 corresponding to live to dead load ratio of 5 and $\phi_s = 0.85$ .....	209
Figure 7-20: $\beta$ vs. $\phi_s$ for Frame 2 (BFY-CPY) subject to gravity loading, using FORM and direct MC simulation.....	210
Figure 7-21: Histogram of ultimate load factor for Frame 5 subjected to gravity plus wind with BFY-CFY for $\phi_s=0.69$ ( $L_n/D_n=2$ , $W_n/(L_n + D_n)=0.1$ ).....	212
Figure 7-22: $\beta$ vs. $\phi_s$ for Frame 5 subject to gravity and wind loading, using FORM and direct MC simulation .....	214
Figure 7-23: $\beta$ vs. $\phi_s$ curves for Frame 3 subject to gravity and wind loading using CSM with BFY-CFY failure mode .....	217
Figure 7-24: $\beta$ vs. $\phi_s$ curves for Frame 8 subject to gravity and wind loading using CSM with BFY-CFY failure mode .....	217
Figure 7-25: $\beta$ vs. $\phi_s$ curves for Frame 3 (braced) with hinged joints with BFY-CFY failure mode .....	218
Figure 7-26: $\beta$ vs. $\phi_s$ curves for Frame 6 (braced) with rigid joints with CFY failure mode .....	218
Figure 7-27: $\beta$ vs. $\phi_s$ curves for Frame 2 under gravity with elastic-perfectly plastic material and 5% of initial slope criteria for choosing ultimate strength.....	225
Figure 7-28: $\beta$ vs. $\phi_s$ curves for Frame 2 under gravity with elastic-perfectly plastic material and maximum criteria for choosing ultimate strength.....	225
Figure 7-29: $\beta$ vs. $\phi_s$ curves for Frame 2 under gravity with material with strain hardening and 5% of initial slope criteria for choosing ultimate strength.....	226
Figure C.1: Unbraced frame layouts to obtain the scale factors of initial geometric imperfection.....	266

Figure C.2: Braced frame layouts to obtain the scale factors of initial geometric imperfection.....	268
Figure C.3: Load-deflection response of F-UB1 .....	292
Figure C.4: Load-deflection response of F-UB2 .....	292
Figure C.5: Load-deflection response of F-UB3 .....	293
Figure C.6: Load-deflection response of F-UB4 .....	293
Figure C.7: Load-deflection response of F-UB5 .....	294
Figure C.8: Load-deflection response of F-UB6 .....	294
Figure C.9: Load-deflection response of F-UB7 .....	295
Figure C.10: Load-deflection response of F-UB8 .....	295
Figure C.11: Load-deflection response of F-B1 .....	296
Figure C.12: Load-deflection response of F-B2 .....	296
Figure C.13: Load-deflection response of F-B3 .....	297
Figure C.14: Load-deflection response of F-B4 .....	297
Figure C.15: Load-deflection response of F-B5 .....	298
Figure C.16: Load-deflection response of F-B6 .....	298
Figure C.17: Load-deflection response of F-B7 .....	299
Figure C.18: Load-deflection response of F-B8 .....	299
Figure C.19: Histogram of ultimate load factor, F-UB1.....	300
Figure C.20: Histogram of ultimate load factor, F-UB2.....	300
Figure C.21: Histogram of ultimate load factor, F-UB3.....	301
Figure C.22: Histogram of ultimate load factor, F-UB4.....	301
Figure C.23: Histogram of ultimate load factor, F-UB5.....	302
Figure C.24: Histogram of ultimate load factor, F-UB6.....	302
Figure C.25: Histogram of ultimate load factor, F-UB7.....	303
Figure C.26: Histogram of ultimate load factor, F-UB8.....	303
Figure C.27: Histogram of ultimate load factor, F-B1.....	304
Figure C.28: Histogram of ultimate load factor, F-B2.....	304
Figure C.29: Histogram of ultimate load factor, F-B3.....	305
Figure C.30: Histogram of ultimate load factor, F-B4.....	305
Figure C.31: Histogram of ultimate load factor, F-B5.....	306
Figure C.32: Histogram of ultimate load factor, F-B6.....	306
Figure C.33: Histogram of ultimate load factor, F-B7.....	307
Figure C.34: Histogram of ultimate load factor, F-B8.....	307
Figure E.1. Histogram of ultimate load factor, Frame 1, BFY-CPY, $\varphi_s=0.64$ .....	371
Figure E.2. Histogram of ultimate load factor, Frame 2, BFY-CPY, $\varphi_s=0.78$ .....	371
Figure E.3. Histogram of ultimate load factor, Frame 2, Instability, $\varphi_s=0.90$ .....	372
Figure E.4. Histogram of ultimate load factor, Frame 3, BPY-CFY, $\varphi_s=0.8$ .....	372
Figure E.5. Histogram of ultimate load factor, Frame 4, CFY, $\varphi_s=0.89$ .....	373
Figure E.6. Histogram of ultimate load factor, Frame 5, BFY-CPY, $\varphi_s=0.74$ .....	373
Figure E.7. Histogram of ultimate load factor, Frame 6, BPY-CFY, $\varphi_s=0.93$ .....	374
Figure E.8. Histogram of ultimate load factor, Frame 7, BPY-CPY, $\varphi_s=0.79$ .....	374
Figure E.9. Histogram of ultimate load factor, Frame 8, BPY-CFY, $\varphi_s=0.88$ .....	375

Figure E.10. Histogram of ultimate load factor, Frame 9, BPY-CPY, $\varphi_s=0.60$ .....	375
Figure E.11. Histogram of ultimate load factor, Frame 1, $W_n/(D_n + L_n)=0.05$ , $\varphi_s=0.90$ .....	376
Figure E.12. Histogram of ultimate load factor, Frame 1, $W_n/(D_n + L_n)=0.25$ , $\varphi_s=0.71$ .....	376
Figure E.13. Histogram of ultimate load factor, Frame 3, $W_n/(D_n + L_n)=0.10$ , $\varphi_s=0.92$ .....	377
Figure E.14. Histogram of ultimate load factor, Frame 5, $W_n/(D_n + L_n)=0.15$ , $\varphi_s=0.81$ .....	377
Figure E.15. Histogram of ultimate load factor, Frame 7, $W_n/(D_n + L_n)=0.25$ , $\varphi_s=1.00$ .....	378
Figure E.16. Histogram of ultimate load factor, Frame 9, $W_n/(D_n + L_n)=0.10$ , $\varphi_s=0.82$ .....	378
Figure E.17. Histogram of ultimate load factor, Frame 2, BFY-CFY, $\varphi_s=0.82$ .....	379
Figure E.18. Histogram of ultimate load factor, Frame 4, CFY, $\varphi_s=0.81$ .....	379
Figure E.19. Histogram of ultimate load factor, Frame 6, CFY-BPY, $\varphi_s=0.87$ .....	380
Figure E.20. Histogram of ultimate load factor, Frame 8, CFY-BFY, $\varphi_s=0.83$ .....	380
Figure E.21. Histogram of ultimate load factor, Frame 3, CFY-BPY, $\varphi_s=0.82$ .....	381
Figure E.22. Histogram of ultimate load factor, Frame 5, CFY-BFY, $\varphi_s=0.88$ .....	381
Figure E.23. Histogram of ultimate load factor, Frame 7, CFY, $\varphi_s=0.82$ .....	382
Figure E.24. Histogram of ultimate load factor, Frame 9, CFY-BFY, $\varphi_s=0.78$ .....	382
Figure E.25. $\beta$ vs. $\varphi_s$ curve, Frame 3, BPY-CFY .....	383
Figure E.26. $\beta$ vs. $\varphi_s$ curve, Frame 6, BFY-CFY .....	383
Figure E.27. $\beta$ vs. $\varphi_s$ curve, Frame 7, CFY .....	384
Figure E.28. $\beta$ vs. $\varphi_s$ curve, Frame 9, BFY-CPY .....	384
Figure E.29. $\beta$ vs. $\varphi_s$ curve, Frame 1, CFY .....	385
Figure E.30. $\beta$ vs. $\varphi_s$ curve, Frame 5, BFY-CFY .....	385
Figure E.31. $\beta$ vs. $\varphi_s$ curve, Frame 7, BFY-CFY.....	386
Figure E.32. $\beta$ vs. $\varphi_s$ curve, Frame 9, BFY-CFY.....	386
Figure E.33. $\beta$ vs. $\varphi_s$ curve, Frame 2, CFY-BPY .....	387
Figure E.34. $\beta$ vs. $\varphi_s$ curve, Frame 4, CFY.....	387
Figure E.35. $\beta$ vs. $\varphi_s$ curve, Frame 7, CPY-BFY-CB.....	388
Figure E.36. $\beta$ vs. $\varphi_s$ curve, Frame 9, CFY-BFY .....	388
Figure E.37: Floor type .....	411
Figure E.38: Example 1, 3-bay, 5-storey frame .....	413
Figure E.39: 3-bay, 5-storey frame, SAP 2000 model .....	414
Figure E.40: 3-bay, 5-storey frame, 2 <sup>nd</sup> order axial force diagram.....	414
Figure E.41: 3-bay, 5-storey frame, in-plane 2 <sup>nd</sup> order bending moment diagram.....	415
Figure E.42: 3-bay, 5-storey frame, 2 <sup>nd</sup> order shear force diagram .....	415
Figure E.43: 3-bay, 5-storey frame, demand to capacity ratios .....	416
Figure E.44: 3-bay, 5-storey frame, ABAQUS failure mode .....	417
Figure E.45: 3-bay, 5-storey frame, load-deflection response .....	418
Figure E.46: Example 2, 2-bay, 2-storey braced frame with rigid joints .....	420

Figure E.47: 2-bay, 2-storey rigid-jointed braced frame, 2th order axial force diagram.	421
Figure E.48: 2-bay, 2-storey rigid-jointed braced frame, in-plane 2th order bending moment diagram .....	421
Figure E.49: 2-bay, 2-storey rigid-jointed braced frame, 2 <sup>nd</sup> order shear force diagram	421
Figure E.50: 2-bay, 2-storey rigid-jointed braced frame, demand to capacity ratio .....	422
Figure E.51: 2-bay, 2-storey rigid-jointed braced frame, load-deflection .....	423
Figure E.52: 2-bay, 2-storey rigid-jointed braced frame, ABAQUS failure mode.....	424
Figure E.53: 2-bay, 2-storey hinged-jointed braced frame, 2th order axial force diagram .....	424
Figure E.54: 2-bay, 2-storey hinged-jointed braced frame, in-plane 2 <sup>nd</sup> order bending diagram .....	425
Figure E.55 2-bay, 2-storey hinged-jointed braced frame, 2 <sup>nd</sup> order shear force diagram .....	425
Figure E.56: 2-bay, 2-storey hinged-jointed braced frame, demand to capacity ratio ....	425
Figure E.57: 2-bay, 2-storey hinged-jointed braced frame, load-deflection response ....	426
Figure E.58: 2-bay, 2-storey hinged-jointed braced frame, ABAQUS failure mode .....	427
Figure E.59: 2-bay, 3-storey sway frame subjected gravity and wind loads .....	428
Figure E.60: 2-bay, 3-storey sway frame, 2 <sup>nd</sup> order axial force diagram .....	428
Figure E.61: 2-bay, 3-storey sway frame, 2 <sup>nd</sup> order bending moment diagram .....	429
Figure E.62: 2-bay, 3-storey sway frame, 2 <sup>nd</sup> order shear force diagram .....	429
Figure E.63: 2-bay, 3-storey sway frame, demand to capacity ratio .....	429
Figure E.64: 2-bay, 3-storey sway frame, load versus top storey lateral deflection .....	432
Figure E.65: 2-bay, 3-storey sway frame, ABAQUS failure mode.....	432
Figure E.66: 4-bay, 2-storey irregular sway frame .....	433
Figure E.67: 4-bay, 2-storey irregular sway frame, 2 <sup>nd</sup> order axial force diagram.....	433
Figure E.68: 4-bay, 2-storey irregular sway frame, 2 <sup>nd</sup> order in-plane bending moment diagram .....	433
Figure E.69: 4-bay, 2-storey irregular sway frame, 2 <sup>nd</sup> order shear force diagram .....	434
Figure E.70: 4-bay, 2-storey irregular sway frame, demand to capacity ratio.....	434
Figure E.71: 4-bay, 2-storey irregular sway frame, load deflection response .....	436
Figure E.72: 4-bay, 2-storey irregular sway frame, ABAQUS failure mode .....	436

## List of Tables

Table 2-1: Summary of suggested Notional Horizontal Force (NHF) by different specifications.....	32
Table 2-2: Summary of suggested imperfection by different specifications .....	34
Table 2-3: Statistical characteristics of measured imperfection by ECCS reported by Roorda (1974).....	42
Table 2-4: Static characteristics of initial out-of-straightness from the literature .....	44
Table 2-5: Static characteristics of initial out-of-plumb from the literature.....	48
Table 2-6: Recommended target reliability index in literature.....	67
Table 4-1: Summary of mechanical characteristic for four specific joint types reported by Basaglia et al. (2010) .....	92
Table 4-2: Spring stiffness, bimoments and critical buckling loads of L-shape frame ...	109
Table 4-3: Spring stiffness of joint 2 and critical buckling loads of portal frame with an overhanging member .....	113
Table 5-1: Measured initial out-of-straightness ( $d$ ) by Sfintesco (1970).....	127
Table 5-2: Scale factors of the first three buckling modes .....	128
Table 5-3: Statistic characteristics of scale factors.....	128
Table 5-4: Scale factors of different buckling modes to model initial geometric imperfection, unbraced frames.....	135
Table 5-5: Scale factors of different buckling modes to model initial geometric imperfection for braced frames.....	135
Table 5-6: Proportion of each mode to model initial geometric imperfection, un-braced frames.....	136
Table 5-7: Proportion of each mode to model initial geometric imperfection, braced frames.....	137
Table 5-10: First ten buckling modes of a 1-bay, 2-story frame (Appendix C.1.1) .....	139
Table 5-11: Material properties, un-braced frames.....	145
Table 5-12: Verification results, unbraced frames.....	148
Table 5-13: Simulation results for F-UB 2 different column slenderness.....	149
Table 5-14: Verification results, braced frames.....	149
Table 6-1: Statistics of scale factors .....	157
Table 6-2: Ultimate load factors ( $\lambda$ ).....	161
Table 6-3: The difference between ultimate load factors (%) by using ECCS and Galambos models.....	161
Table 6-4: Ultimate load factor statistics, using different pattern of residual stress.....	165
Table 6-5: Ultimate load factor statistics and reliability index.....	170
Table 7-1: Statistical characteristics of random variable obtained from the literature ....	186
Table 7-2: Statistical result for cross-section dimensions.....	188
Table 7-3: Correlation matrix for cross-section dimensions.....	188
Table 7-4: Results of sensitivity analysis of Frame 4 corresponding to $\phi_s=0.74$ with BFY-CPY as failure mode .....	191
Table 7-5: System-based design of Frame 5 under gravity loading ( $L_n / D_n = 1$ ) .....	198

Table 7-6: System resistance factors ( $\phi_s$ ) for Frame 5 for different reliability levels, CSM .....	200
Table 7-7: System resistance factors ( $\phi_s$ ) for Frame 5 for different reliability levels, LSM .....	201
Table 7-8: Statistic characteristics for Ziemian's frames (Ziemian 1990) .....	204
Table 7-9: System resistance factors ( $\phi_s$ ) for frames designed by Ziemian (1990) .....	204
Table 7-10: Sway frames under gravity loading design based on AS4100 .....	206
Table 7-11: System resistance factors ( $\phi_s$ ), bias factors and COVs of sway frames under gravity loads.....	207
Table 7-12: Comparison of reliability indices resulting from FORM and direct MC simulation methods for Frame 2 under gravity.....	210
Table 7-13: System-based design of Frame 5 under gravity plus wind loading, BFY-CFY ( $Ln/Dn=2, Wn/(Ln+Dn)=0.1$ ).....	212
Table 7-14: Sway frames under gravity plus wind loading design based on AS4100 ....	213
Table 7-15: Comparison of reliability indices resulting from FORM and direct MC simulation methods for Frame 5 subjected to gravity plus wind.....	215
Table 7-16: System resistance factor ( $\phi_s$ ) for Frame 5 subjected to wind plus gravity for different reliability levels using FORM and MC.....	215
Table 7-17: System resistance factors ( $\phi_s$ ) for sway frames subject to gravity and wind loading.....	216
Table 7-18: System resistance factors ( $\phi_s$ ), Bias factors and COVs of braced frames with hinged connections.....	219
Table 7-19: System resistance factors ( $\phi_s$ ), Bias factors and COVs of braced frames with rigid connections.....	220
Table 7-20: System resistance factors ( $\phi_s$ ), Bias factors and COVs of braced frames with hinged connections and long columns .....	221
Table 7-21: System resistance factors ( $\phi_s$ ), Bias factors and COVs of braced frames with rigid connections and long columns .....	221
Table 7-22: Statistical characteristics of frame strength for different yield stress correlations.....	222
Table 7-23: System resistance factor ( $\phi_s$ ) for different yield stress correlations .....	223
Table 7-24: Comparison of frame ultimate strength statistical data of Frame 2 with and without considering strain hardening.....	224
Table 7-25: Comparison of system resistance factors ( $\phi_s$ ) of Frame 2 with and without considering strain hardening.....	226
Table 7-26: Reliability indices ( $\beta$ ) for frames designed by Elastic-LRFD.....	228
Table 7-27: Comparison of member-based and system-based design of Frame 6 .....	229
Table C.1: Mean scale factors from error minimization between unbraced frames with randomly generated imperfection and first ABAQUS eigenmode .....	270
Table C.2: Mean scale factors from error minimization between unbraced frames with randomly generated imperfection and first two ABAQUS eigenmodes .....	271
Table C.3: Mean scale factors from error minimization between unbraced frames with randomly generated imperfection and first three ABAQUS eigenmodes .....	271

Table C.4: Mean scale factors from error minimization between unbraced frames with randomly generated imperfection and first four ABAQUS eigenmodes .....	272
Table C.5: Mean scale factors from error minimization between unbraced frames with randomly generated imperfection and first five ABAQUS eigenmodes .....	272
Table C.6: Mean scale factors from error minimization between unbraced frames with randomly generated imperfection and first six ABAQUS eigenmodes .....	273
Table C.7: Mean scale factors from error minimization between unbraced frames with randomly generated imperfection and first seven ABAQUS eigenmodes .....	273
Table C.8: Mean scale factors from error minimization between unbraced frames with randomly generated imperfection and first eight ABAQUS eigenmodes .....	274
Table C.9: Mean scale factors from error minimization between unbraced frames with randomly generated imperfection and first nine ABAQUS eigenmodes .....	274
Table C.10: Mean scale factors from error minimization between unbraced frames with randomly generated imperfection and first ten ABAQUS eigenmodes .....	275
Table C.11: Total frame heights or member lengths depending on the eigenmode type	275
Table C.12: Mean non-dimensional scale factors from error minimization between unbraced frames with randomly generated imperfection and first ABAQUS eigenmodes .....	276
Table C.13: Mean non-dimensional scale factors from error minimization between unbraced frames with randomly generated imperfection and first two ABAQUS eigenmodes .....	276
Table C.14: Mean non-dimensional scale factors from error minimization between unbraced frames with randomly generated imperfection and first three ABAQUS eigenmodes .....	277
Table C.15: Mean non-dimensional scale factors from error minimization between unbraced frames with randomly generated imperfection and first four ABAQUS eigenmodes .....	277
Table C.16: Mean non-dimensional scale factors from error minimization between unbraced frames with randomly generated imperfection and first five ABAQUS eigenmodes .....	278
Table C.17: Mean non-dimensional scale factors from error minimization between unbraced frames with randomly generated imperfection and first six ABAQUS eigenmodes .....	278
Table C.18: Mean non-dimensional scale factors from error minimization between unbraced frames with randomly generated imperfection and first seven ABAQUS eigenmodes .....	279
Table C.19: Mean non-dimensional scale factors from error minimization between unbraced frames with randomly generated imperfection and first eight ABAQUS eigenmodes .....	279
Table C.20: Mean non-dimensional scale factors from error minimization between unbraced frames with randomly generated imperfection and first nine ABAQUS eigenmodes .....	280

Table C.21: Mean non-dimensional scale factors from error minimization between unbraced frames with randomly generated imperfection and first ten ABAQUS eigenmodes .....	280
Table C.22: Mean scale factors from error minimization between braced frames with randomly generated imperfection and first ABAQUS eigenmode .....	281
Table C.23: Mean scale factors from error minimization between braced frames with randomly generated imperfection and first two ABAQUS eigenmodes .....	281
Table C.24: Mean scale factors from error minimization between braced frames with randomly generated imperfection and first three ABAQUS eigenmodes .....	282
Table C.25: Mean scale factors from error minimization between braced frames with randomly generated imperfection and first four ABAQUS eigenmodes .....	282
Table C.26: Mean scale factors from error minimization between braced frames with randomly generated imperfection and first five ABAQUS eigenmodes .....	283
Table C.27: Mean scale factors from error minimization between braced frames with randomly generated imperfection and first six ABAQUS eigenmodes .....	283
Table C.28: Mean scale factors from error minimization between braced frames with randomly generated imperfection and first seven ABAQUS eigenmodes .....	284
Table C.29: Mean scale factors from error minimization between braced frames with randomly generated imperfection and first eight ABAQUS eigenmodes .....	284
Table C.30: Mean scale factors from error minimization between braced frames with randomly generated imperfection and first nine ABAQUS eigenmodes.....	285
Table C.31: Mean scale factors from error minimization between braced frames with randomly generated imperfection and first ten ABAQUS eigenmodes .....	285
Table C.32: Total frame heights or member lengths depending on the eigenmode type	286
Table C.33: Mean non-dimensional scale factors from error minimization between braced frames with randomly generated imperfection and first ABAQUS eigenmode .....	286
Table C.34: Mean non-dimensional scale factors from error minimization between braced frames with randomly generated imperfection and first two ABAQUS eigenmodes ....	287
Table C.35: Mean non-dimensional scale factors from error minimization between braced frames with randomly generated imperfection and first three ABAQUS eigenmodes ..	287
Table C.36: Mean non-dimensional scale factors from error minimization between braced frames with randomly generated imperfection and first four ABAQUS eigenmodes ....	288
Table C.37: Mean non-dimensional scale factors from error minimization between braced frames with randomly generated imperfection and first five ABAQUS eigenmodes ....	288
Table C.38: Mean non-dimensional scale factors from error minimization between braced frames with randomly generated imperfection and first six ABAQUS eigenmodes .....	289
Table C.39: Mean non-dimensional scale factors from error minimization between braced frames with randomly generated imperfection and first seven ABAQUS eigenmodes ..	289
Table C.40: Mean non-dimensional scale factors from error minimization between braced frames with randomly generated imperfection and first eight ABAQUS eigenmodes ..	290
Table C.41: Mean non-dimensional scale factors from error minimization between braced frames with randomly generated imperfection and first nine ABAQUS eigenmodes.....	290
Table C.42: Mean non-dimensional scale factors from error minimization between braced frames with randomly generated imperfection and first ten ABAQUS eigenmodes .....	291



Table D.1: Scale factors for residual stress (Non-American sections) .....	308
Table D.2: Scale factors for residual stress (American sections) .....	310
Table E.1: System-based design of Frame 1 (sway) under gravity loading using CSM, BFY-CPY .....	311
Table E.2: System-based design of Frame 2 (sway) under gravity loading using CSM, BFY-CPY .....	312
Table E.3: System-based design of Frame 2 (sway) under gravity loading using CSM, Instability .....	313
Table E.4: System-based design of Frame 2 (sway) under gravity loading using CSM, BPY-CPY .....	313
Table E.5: System-based design of Frame 3 (sway) under gravity loading using CSM, BFY-CPY .....	314
Table E.6: System-based design of Frame 3 (sway) under gravity loading using CSM, BPY-CFY .....	314
Table E.7: System-based design of Frame 3 (sway) under gravity loading using CSM, BPY-CPY .....	315
Table E.8: System-based design of Frame 4 (sway) under gravity loading using CSM, BFY-CPY .....	315
Table E.9: System-based design of Frame 4 (sway) under gravity loading using CSM, CFY .....	316
Table E.10: System-based design of Frame 4 (sway) under gravity loading using CSM, BPY-CFY .....	316
Table E.11: System-based design of Frame 5 (sway) under gravity loading using CSM, BFY-CPY .....	317
Table E.12: System-based design of Frame 5 (sway) under gravity loading using CSM, CFY .....	318
Table E.13: System-based design of Frame 5 (sway) under gravity loading using CSM, BPY-CFY .....	318
Table E.14: System-based design of Frame 6 (sway) under gravity loading using CSM, BFY-CPY .....	319
Table E.15: System-based design of Frame 6 (sway) under gravity loading using CSM, BPY-CFY .....	320
Table E.16: System-based design of Frame 7 (sway) under gravity loading using CSM, BFY-CPY .....	321
Table E.17: System-based design of Frame 7 (sway) under gravity loading using CSM, CFY .....	322
Table E.18: System-based design of Frame 7 (sway) under gravity loading using CSM, BPY-CPY .....	322
Table E.19: System-based design of Frame 8 (sway) under gravity loading using CSM, BFY-CPY .....	323
Table E.20: System-based design of Frame 8 (sway) under gravity loading using CSM, BPY-CFY .....	324
Table E.21: System-based design of Frame 8 (sway) under gravity loading using CSM, BPY-CPY .....	325

Table E.22: System-based design of Frame 9 (sway) under gravity loading using CSM, BFY-CPY .....	326
Table E.23: System-based design of Frame 9 (sway) under gravity loading using CSM, BPY-CPY .....	327
Table E.24: System-based design of Frame 9 (sway) under gravity loading using CSM, BFY-CFY .....	328
Table E.25: System-based design of Frame 1 under gravity and wind loading, $W_n/(D_n + L_n)=0.05$ , CFY .....	329
Table E.26: System-based design of Frame 1 under gravity and wind loading, $W_n/(D_n + L_n)=0.10$ , CFY .....	329
Table E.27: System-based design of Frame 1 under gravity and wind loading, $W_n/(D_n + L_n)=0.15$ , CFY .....	329
Table E.28: System-based design of Frame 1 under gravity and wind loading, $W_n/(D_n + L_n)=0.25$ , CFY .....	330
Table E.29: System-based design of Frame 2 under gravity and wind loading, $W_n/(D_n + L_n)=0.05$ , BFY-CFY .....	330
Table E.30: System-based design of Frame 2 under gravity and wind loading, $W_n/(D_n + L_n)=0.10$ , BFY-CFY .....	331
Table E.31: System-based design of Frame 2 under gravity and wind loading, $W_n/(D_n + L_n)=0.15$ , BFY-CFY .....	332
Table E.32: System-based design of Frame 2 under gravity and wind loading, $W_n/(D_n + L_n)=0.25$ , BFY-CFY .....	333
Table E.33: System-based design of Frame 3 under gravity and wind loading, $W_n/(D_n + L_n)=0.05$ , BFY-CFY .....	333
Table E.34: System-based design of Frame 3 under gravity and wind loading, $W_n/(D_n + L_n)=0.10$ , BFY-CFY .....	334
Table E.35: System-based design of Frame 3 under gravity and wind loading, $W_n/(D_n + L_n)=0.15$ , BFY-CFY .....	335
Table E.36: System-based design of Frame 3 under gravity and wind loading, $W_n/(D_n + L_n)=0.25$ , BFY-CFY .....	336
Table E.37: System-based design of Frame 4 under gravity and wind loading, $W_n/(D_n + L_n)=0.05$ , BFY-CFY .....	337
Table E.38: System-based design of Frame 4 under gravity and wind loading, $W_n/(D_n + L_n)=0.10$ , BFY-CFY .....	338
Table E.39: System-based design of Frame 4 under gravity and wind loading, $W_n/(D_n + L_n)=0.15$ , BFY-CFY .....	339
Table E.40: System-based design of Frame 4 under gravity and wind loading, $W_n/(D_n + L_n)=0.25$ , BFY-CFY .....	340
Table E.41: System-based design of Frame 5 under gravity and wind loading, $W_n/(D_n + L_n)=0.05$ , BFY-CFY .....	341
Table E.42: System-based design of Frame 5 under gravity and wind loading, $W_n/(D_n + L_n)=0.10$ , BFY-CFY .....	342

Table E.43: System-based design of Frame 5 under gravity and wind loading, $W_n/(D_n + L_n)=0.15$ , BFY-CFY .....	343
Table E.44: System-based design of Frame 5 under gravity and wind loading, $W_n/(D_n + L_n)=0.25$ , BFY-CFY .....	344
Table E.45: System-based design of Frame 6 under gravity and wind loading, $W_n/(D_n + L_n)=0.05$ , BFY-CFY .....	344
Table E.46: System-based design of Frame 6 under gravity and wind loading, $W_n/(D_n + L_n)=0.10$ , BFY-CFY .....	345
Table E.47: System-based design of Frame 6 under gravity and wind loading, $W_n/(D_n + L_n)=0.15$ , BFY-CFY .....	345
Table E.48: System-based design of Frame 6 under gravity and wind loading, $W_n/(D_n + L_n)=0.25$ , BFY-CFY .....	346
Table E.49: System-based design of Frame 7 under gravity and wind loading, $W_n/(D_n + L_n)=0.05$ , BFY-CFY .....	347
Table E.50: System-based design of Frame 7 under gravity and wind loading, $W_n/(D_n + L_n)=0.10$ , BFY-CFY .....	348
Table E.51: System-based design of Frame 7 under gravity and wind loading, $W_n/(D_n + L_n)=0.15$ , BFY-CFY .....	349
Table E.52: System-based design of Frame 7 under gravity and wind loading, $W_n/(D_n + L_n)=0.25$ , BFY-CFY .....	350
Table E.53: System-based design of Frame 8 under gravity and wind loading, $W_n/(D_n + L_n)=0.05$ , BFY-CFY .....	351
Table E.54: System-based design of Frame 8 under gravity and wind loading, $W_n/(D_n + L_n)=0.10$ , BFY-CFY .....	352
Table E.55: System-based design of Frame 8 under gravity and wind loading, $W_n/(D_n + L_n)=0.15$ , BFY-CFY .....	353
Table E.56: System-based design of Frame 8 under gravity and wind loading, $W_n/(D_n + L_n)=0.25$ , BFY-CFY .....	354
Table E.57: System-based design of Frame 9 under gravity and wind loading, $W_n/(D_n + L_n)=0.05$ , BFY-CFY .....	355
Table E.58: System-based design of Frame 9 under gravity and wind loading, $W_n/(D_n + L_n)=0.10$ , BFY-CFY .....	356
Table E.59: System-based design of Frame 9 under gravity and wind loading, $W_n/(D_n + L_n)=0.15$ , BFY-CFY .....	357
Table E.60: System-based design of Frame 9 under gravity and wind loading, $W_n/(D_n + L_n)=0.25$ , BFY-CFY .....	358
Table E.61: System-based design of Frame 2 (braced, hinged joint) under gravity loading using LSM .....	359
Table E.62: System-based design of Frame 3 (braced, hinged joint) under gravity loading using LSM .....	359
Table E.63: System-based design of Frame 4 (braced, hinged joint) under gravity loading using LSM .....	360

Table E.64: System-based design of Frame 5 (braced, hinged joint) under gravity loading using LSM .....	361
Table E.65: System-based design of Frame 6 (braced, hinged joint) under gravity loading using LSM .....	362
Table E.66: System-based design of Frame 7 (braced, hinged joint) under gravity loading using LSM .....	363
Table E.67: System-based design of Frame 8 (braced, hinged joint) under gravity loading using LSM .....	364
Table E.68: System-based design of Frame 9 (braced, hinged joint) under gravity loading using LSM .....	364
Table E.69: System-based design of Frame 2 (braced, rigid joint) under gravity loading using LSM .....	365
Table E.70: System-based design of Frame 3 (braced, rigid joint) under gravity loading using LSM .....	365
Table E.71: System-based design of Frame 4 (braced, rigid joint) under gravity loading using LSM .....	366
Table E.72: System-based design of Frame 5 (braced, rigid joint) under gravity loading using LSM .....	367
Table E.73: System-based design of Frame 6 (braced, rigid joint) under gravity loading using LSM .....	368
Table E.74: System-based design of Frame 7 (braced, rigid joint) under gravity loading using LSM .....	369
Table E.75: System-based design of Frame 8 (braced, rigid joint) under gravity loading using LSM .....	369
Table E.76: System-based design of Frame 9 (braced, rigid joint) under gravity loading using LSM .....	370
Table E.77: Summary of all studied frames .....	412
Table E.78: 3-bay, 5-storey frame, first six buckling modes .....	417
Table E.79: Comparison of member-based and system-based design of 3-bay, 5-storey frame .....	419
Table E.80: 2-bay, 2-storey rigid-joint braced frame, first six buckling modes .....	422
Table E.81: Comparison of member-based and system-based design of 2-bay, 2-storey rigid-jointed braced frame .....	423
Table E.82: Comparison of member-based and system-based design of 2-bay, 2-storey hinged-jointed braced frame .....	426
Table E.83: 2-bay, 2-storey hinged-jointed braced frame, first six buckling modes .....	427
Table E.84: 2-bay, 3-storey sway frame, first six buckling modes .....	430
Table E.85: Comparison of member-based and system-based design of 2-bay, 3-storey sway frame .....	431
Table E.86: Comparison of member-based and system-based design of 4-bay, 2-storey irregular sway frame .....	435
Table E.87: 2-bay, 2-storey rigid-joint braced frame, first six buckling modes .....	435

## Abbreviations

ANOVA	Analysis of variance
ASD	Allowable stress design
B-FEA	Beam finite element analysis
BFY	Beam fully yielded
BPY	Beam partially yielded
CB	Column buckling
CFY	Column fully yielded
COV	Coefficient of variation
CPY	Column partially yielded
CSM	Cross-section scaling method
EBM	Scaling of eigenbuckling modes
FEA	Finite element analysis
FORM	First-order reliability method
FOSM	First-order second-moment method
GLP	Good Lattice point set
GMNIA	Geometric and material nonlinear analysis with imperfection
H-W	Hua-Wang point set
IGI	Direct modelling of initial geometric imperfections
LHS	Latin-Hypercube sampling
LRFD	Load and resistance factor design
LSD	Limit state design
LSM	Load scaling method
MC	Monte-Carlo analysis
NDSS	Numerical data-base for steel structures
NHF	Notional horizontal force method
PD	Plastic design
PULD	Partially updated Lagrangian description
QMC	Quasi Monte-Carlo analysis
SBRA	Simulation-based reliability assessment
S-FEA	Shell finite element analysis
TLD	Total Lagrangian description
ULD	Updated Lagrangian description

## Principal notations

$a_i$	Scale factor of $i$ th buckling mode of a simply supported column
$A$	Cross-sectional area; Variation in load
$A_j$	Amplification factor of $j$ th eigenbuckling mode to model initial geometric imperfection
$b_f$	Cross-section flange thickness
$B$	Bimoment; Variation due to the method of applying load
$C$	Variation due to method of analysis
$d$	Initial out-of-straightness
$\bar{D}$	Mean dead load
$D_n$	Nominal dead load
$E$	Young's modulus
$E_0$	Initial Young's modulus
$E_{sh}$	Strain hardening modulus
$E_t$	Tangent modulus
$E'_t$	Reduced member stiffness
$f_{nominal}$	Nominal stress
$f_Q(x)$	Probability density function of $Q$
$f_{true}$	True stress
$f_y$	Yield stress
$F$	Load vector; Variation in fabrication
$F_R(x)$	Cumulative distribution function of $R$
$G$	Limit state function; Shear modulus
$h$	Frame storey height; Cross-section height
$H$	Total frame height
$I$	Second moment of inertia
$I_w$	Warping constant
$J$	Uniform torsion constant
$k$	Effective length factor
$K$	Rotational stiffness
$K_{\varphi'}$	Warping stiffness
$L$	Member length
$\bar{L}$	Mean live load
$L_{apt}$	Arbitrary point-in-time live load

$L_n$	Nominal live load
$m$	Number of eigenbuckling modes
$M$	Variation in strength
$M_{nx}$	Nominal flexural strength about major axis
$M_{ny}$	Nominal flexural strength about minor axis
$M_{ux}$	Required flexural strength about major axis
$M_{uy}$	Required flexural strength about minor axis
$M_z$	Torque at the distance $z$ along the member length
$N$	Number of samples
$N_{Ed}$	Design axial force
$P$	Variation due to the method of analysis
$P_f$	Probability of failure
$P_j$	Normalized scale factor of $j$ th eigenbuckling mode to model initial geometric imperfection
$P_n$	Nominal axial strength
$P_u$	Required axial strength
$Q$	Total load effect
$r$	Radius of gyration
$\bar{R}$	Mean structural resistance
$R$	Structural resistance
$S_i$	First-order sensitivity index
$SF_j$	Scale factor of $j$ th eigenbuckling mode to model initial geometric imperfection
$t_f$	Cross-section flange thickness
$t_w$	Cross-section web thickness
$u$	Longitudinal displacement
$V_Q$	Coefficient of variation of total load
$V_R$	Coefficient of variation of system resistance
$w$	Relative likelihood of load situations; uniformly distributed load
$W_n$	Nominal wind load
$x_i$	Design point
$X_i$	Random variable
$X_{ECCS}$	Scale factor of residual stress using ECCS model
$X_{Galambos}$	Scale factor of residual stress using Galambos model
$X_{Trahair}$	Scale factor of residual stress using Trahair model

$Z_i$	Reduced variable
$\beta$	Reliability index
$\gamma_i$	Load factors
$\varepsilon_{nominal}$	Nominal strain
$\varepsilon_y$	Yield strain
$\varepsilon_{ln}^{pl}$	Logarithmic plastic strain
$\Delta$	Out-of plumb; Sway deflection
$\sigma$	Standard deviation
$\sigma_{exp}$	Residual stress from experimental tests
$\sigma_{model}$	Residual stress of theoretical patterns
$\sigma_R$	Residual stress
$\sigma_{RC}$	Compressive residual stress
$\sigma_{RT}$	tensile residual stress
$\lambda$	Ultimate load factor
$\bar{\lambda}$	Mean value of ultimate load factor
$\lambda_c$	Column slenderness
$\lambda_n$	Nominal ultimate load factor
$\mu$	Statistical mean
$\mu_D$	Mean value of dead load
$\mu_L$	Mean value of live load
$\mu_Q$	Mean value of total load
$\mu_R$	Mean value of system resistance
$\varphi$	Member resistance factor
$\varphi_s$	System resistance factor
$\varphi'$	Warping degree of freedom
$\Phi$	Degree of freedom of warping spring; Standard normal distribution function
$\omega$	Sectorial coordinate





# CHAPTER

# 1 .

## Introduction

---

### **1.1 Background**

The steel structural skeletons offer numerous advantages and are designed according to steel structural specifications on a daily basis by engineers. The current process of steel frame design entails two separate steps: (i) analysis in which the internal forces and moments in the steel frame are obtained and, (ii) the capacity check to a structural standard to verify that all frame components such as beams, columns and connections have adequate strength under applied loads. While the types of analysis have been shifted from hand calculations to linear and more recently second order elastic computational analysis over the last 4 decades, the component-based approach (two-step design) has prevailed for longer than a century.

In the conventional steel design method, a structural system is treated as a set of individual components and the interaction between the structural system and its members is only reflected indirectly through the use of effective length factor ( $k$ ). This component-

based approach cannot accurately capture the influence of the inelastic redistribution of internal forces subsequent to initial yielding. On the other hand, the interaction between members, especially in a large redundant structural system, is too complex to be represented by the simple effective length factor approach (Chen and Kim 1997). Thus, the conventional design approach may not accurately predict the ultimate load-carrying capacity of the structural system. Moreover since the load-deflection response is not traced, the frame failure modes cannot be extrapolated correctly. Furthermore, the effective length factor method is not user friendly and capacity check of each individual frame component is a time consuming process.

Therefore, there are strong economic and safety reasons for developing a practical system-based design method that can account for compatibility between the members and the whole system by use of geometric and material nonlinear (“advanced”) analysis. The change of emphasis from individual member strengths to the overall structural behaviour promotes a more holistic approach and greater innovation in structural design, and is likely to become increasingly used by structural engineers as commercial software packages make geometric and material nonlinear analyses available.

The most important barriers to adopt the system-based design approach in practice can be summarized as:

- a) The advanced analysis requires human capital investment (considerable modelling and design skills are needed). This issue needs to be addressed by software developers.
- b) Current design specifications provide insufficient economic incentive for profession to make transition towards advanced analysis. At the moment advanced analysis is simply used to obtain internal actions and member/section capacity checks are still required.
- c) Current design standards do not specify unambiguous requirements for advanced analysis. The modelling requirements and how to define the nominal model are still unclear.

- d) In addition, steel specifications require the reliability of the structure to be considered when advanced analysis is used, but do not explain how this may be achieved. No information is provided about the appropriate system resistance factors to be assigned to frame systems which can account for potential risk arising from uncertainties.

These issues have been addressed in this study.

## 1.2 Aims and objectives

The overall objective of this research is to lay the foundation of the next generation of steel structural code which will be based on direct design of structural systems by advanced analysis (system-based design). In particular:

- a) Development of an accurate finite element analysis (advanced analysis) model to capture the load-deflection response of steel structural systems, accounting for material nonlinearity (yielding), geometric nonlinearity ( $P - \Delta$  and  $P - \delta$  effects), initial geometric imperfections and residual stresses.
- b) Devising new approaches for statistical modelling of initial geometric imperfection and residual stress in advanced analysis of steel frames.
- c) Identifying the main parameters influencing the system strength and performing a statistical assessment of the system strength which considers structural redundancy, consequences of failure and statistical variations in loading and variables affecting the frame strength.
- d) Providing information about the appropriate target reliability for redundant structural systems subjected to different load combinations by performing reliability assessment of existing structures.
- e) Development of guidelines for the direct design of steel structures by advanced analysis, converting the probabilistic assessment framework to a deterministic

design format with system resistance factors which can be implied to the steel structural codes. This helps to achieve a more consistent reliability of a wide range of steel frames, and shorter, more flexible and more efficient structural design process.

Additionally, a new model for warping transmission through the joints of steel frames when using beam finite element analysis has been developed. This model can be used in future studies of 3D space frames where the effect of warping needs to be taken into account in advanced analysis of steel structures.

### **1.3 Innovation and benefits**

The Australian structural industry is regarded as a preeminent profession in adopting new technologies. Right after the AS4100 was released in 1990, the advantages of second-order elastic analysis were realized by designers and many software developers incorporated such analysis in their finite element packages. Within the last twenty years structural modelling has been significantly improved by computational advances which enable the user to model a structural frame as a system rather than a collection of members. Hence advanced analysis is now available in many finite element software (ANSYS 2000, ABAQUS 2009) and general guidelines are available (Chen and Kim 1997, Chen, Kim and Choi 2001). There is no doubt that engineers will use this type of analysis for the system-based design of steel structures once it is permitted by specifications. The innovation of this project lies in combining state-of-the-art advanced analysis with a probabilistic approach to develop a rational system reliability-based criterion for designing steel frames. This change of emphasis encourages innovation at system level and retains the leadership of the profession nationally and internationally for Australia. Another significance of this research is that it defines a comprehensive reliability-based framework for the use of advanced analysis in design, which can be further used to develop the system-based design codes for other materials and types of structures than those studied in this project.

## **1.4 Research methodology**

To develop a rational system-based design approach, a comprehensive probabilistic study of a diverse range of 2D steel frames was conducted. A Monte-Carlo probability type is used to determine the statistical characteristics of frame strength considering uncertainties in material properties, cross-section dimensions, initial geometric imperfections and residual stresses. While the statistics of most governing random variables can be readily obtained from the literature, modelling initial geometric imperfection and residual stress randomly required new research as detailed in this study. A new perspective has been developed in this study to model initial geometric imperfection as a combination of weighted elastic buckling modes. Residual stress was modelled randomly using the statistics obtained in this study by fitting established residual stress patterns to experimental measurements and performing error minimization. More than 100,000 simulations using advanced analysis with randomly-modelled parameters were run to determine the statistical distributions of ultimate strength for frame structures. Subsequently, First-Order Reliability Method (FORM) analyses were carried out to determine suitable resistance factors for a wide range of frame types under various load combinations. The frames were designed to fail in different modes, such as beam or column yielding, column buckling, sway instability or combination of these modes, to evaluate the dependency of the system resistance factor on the particular failure mode.

## **1.5 Thesis outline**

This thesis is structured as follows:

Chapter 2 presents a review of current literature relevant to system-based design of steel structures. It covers a brief overview of current steel structural design specification followed by a description of all commonly used analysis methods. In addition, it provides information about advanced analysis and all key components influencing the ultimate frame strength such as material and geometric nonlinearity, warping torsion, initial geometric imperfection and residual stress. The important aspects of reliability analysis have also been reviewed and all recommended target reliability indices obtained from the literature have been summarized.

Chapter 3 details accurate two-dimensional advanced analysis models using the commercial finite element (FE) software of ABAQUS (2009). Details about the finite element analysis including material properties, elements, and effect of strain hardening on the frame ultimate strength have been provided in this chapter. A mesh sensitivity analysis is performed to find the optimum number of elements used in FE models. The nonlinear model is calibrated against the load and displacement response of selected frames from the literature. The numerical results indicate an excellent agreement.

Chapter 4 introduces a new model for warping transmission through the joint of steel frames when using beam finite element analysis. Using a condensed stiffness matrix generated by the substructuring technique, warping springs are introduced to represent the condition of partial warping restraint at intersections between members. The general theory of static condensation, which is the basis of substructuring, is briefly explained. The application and performance of the proposed model is demonstrated by a number of planar and space frames. Excellent agreement is achieved comparing the result of beam finite elements using the suggested joint model and accurate shell finite element analysis.

Chapter 5 explains a new approach to model the geometric imperfections of a steel structural system as a combination of scaled frame buckling modes. Statistical data for both initial out-of-straightness and initial out-of-plum are provided. Probabilistic methods were employed to examine the two key questions: (i) the optimal numbers of buckling modes to be incorporated, and (ii) the scaling factors for each buckling mode.

Chapter 6 outlines a new perspective for the probabilistic modeling of residual stress in advanced analysis of steel structures. An extensive survey of literature on a large number of experimental measurements of residual stress in hot-rolled I-sections is presented. An error minimization is then performed to find an appropriate scale factor to apply to common residual stress patterns to obtain the best agreement with available experimental data. Frames with deterministic and random residual stresses are then analysed by advanced geometric and material nonlinear analysis using proposed scale factors to find the influence of different residual stress patterns on the ultimate strength and reliability of steel frames.

Chapter 7 presents the framework of the system design-by-analysis approach and how to determine the appropriate system resistance factors accounting for inherent uncertainties in ultimate strength of a frame. Monte-Carlo simulation results are presented for a wide range of two dimensional frames. Sway as well as braced frames with regular and irregular geometries subjected to gravity and gravity plus wind loading are considered. The appropriate resistance factors and system target reliability are recommended.

Chapter 8 draws conclusions about this research and provides recommendations for future research studies.

## **1.6 Publications and awards**

The following journal papers, conference papers, research reports and awards are based on the research presented in this thesis.

### **1.6.1 Journal papers**

Shayan, S. and Rasmussen, K.J.R. “A model for warping transmission through joints of steel frames”, *Thin-walled Structures* (submitted)

Shayan, S., Rasmussen, K.J.R. and Zhang, H. “On the modeling of initial geometric imperfections of steel structural frames in advanced analysis”, *Journal of Constructional Steel Research* (submitted)

Shayan, S., Rasmussen, K.J.R. and Zhang, H. “On the probabilistic modeling of residual stress in advanced analysis of steel structures”, *Journal of Constructional Steel Research* (submitted)

Shayan, S., Rasmussen, K.J.R., Zhang, H. and Ellingwood, B.R. “System reliability-based design of steel frames by advanced analysis, Part I: Design framework”, *Journal of Structural Engineering, ASCE* (submitted)



Shayan, S., Zhang, H., Rasmussen, K.J.R., and Ellingwood, B.R. “System reliability-based design of steel frames by advanced analysis, Part II: Simulation results and design recommendations”, *Journal of Structural Engineering*, ASCE (submitted)

Shayan, S., Zhang, H., and Rasmussen, K.J.R. “System reliability-based design of steel frames by advanced analysis for Australian code”, *Australian Journal of Structural Engineering* (in preparation)

### **1.6.2 Conference papers**

Shayan, S., Rasmussen, K.J.R. and Zhang, H. (2012), “Transmission of warping through joints of steel frames”, the Seventh International Conference on Advances in Steel Structures (ICASS), Nanjing, China

Shayan, S., Rasmussen, K.J.R. and Zhang, H. (2012), “On the modelling of geometric imperfections of steel structural members and frames”, the Seventh International Conference on Advances in Steel Structures (ICASS), Nanjing, China

Shayan, S., Rasmussen, K.J.R., Zhang, H. and Ellingwood, B.R. (2013), “System reliability of steel frames designed by inelastic analysis”, Annual Stability Conference Structural Stability Research Council (SSRC), St. Louis, Missouri

Shayan, S., Rasmussen, K.J.R. and Zhang, H. (2013), “On the modelling of residual stress in advanced analysis of steel frames”, The Seventh International Structural Engineering and Construction Conference (ISEC-7), Honolulu, Hawaii

### **1.6.3 Research reports**

Shayan, S., Rasmussen, K.J.R. and Zhang, H. (2012), “A new joint model for warping transmission in thin-walled steel frames”, R922, The university of Sydney, Sydney, Australia

Shayan, S., Rasmussen, K.J.R. and Zhang, H. (2012), “On the modelling of initial geometric imperfection and residual stress in advanced analysis of steel frames”, R935, The university of Sydney, Sydney, Australia

#### **1.6.4 Awards**

Annie B Wilson Prize for research in civil engineering, The University of Sydney (2010)

Best presentation award in civil engineering student conference, Sydney (2012)

# CHAPTER

## 2 .

### Literature review

---

#### **2.1 Introduction**

The limit state design of steel structural frames has been a topic of research interest for more than two decades. However, most of the design methods remained component-based in which an interaction equation is used to check the ultimate strength of an individual member through a combination of analytical and empirical means. Shifting the focus of design from component-based design to system-based design criterion needs and provides a sound knowledge of structural behaviour under applied loads. Clearly, this also requires an analysis procedure which can simultaneously consider the key factors influencing the frame ultimate strength. This chapter presents an overview of current literature relevant to different analysis types of steel structures as well as components such as material and geometrical nonlinearity, warping torsion, initial geometric imperfections and residual stresses which mostly influence the load-carrying capacity of a structure. In addition, the chapter explains the system reliability-based design criterion for advanced analysis as an innovative practical tool which is beyond the scope of current specifications for steel structural design. The general recommendations are provided for modelling, analysis and design of steel structures by advanced analysis.

## 2.2 Current steel structural design specifications

Structural design methods may be broadly classified into two main groups: (i) member-based design (ii) system-based design or direct design method. The conventional steel design method is a two-step design procedure which is the basis of most common Specifications, e.g. AS4100 (1998), AISC360-10 (2010) and Eurocode 3 (2003). The process of design needs an analysis (a first-order elastic analysis with amplification factors or direct second-order elastic analysis), which produces internal actions such as moments and axial forces, followed by a design check using semi-empirical interaction equations to verify each member and connection has adequate capacity. The design equations implicitly account for member geometric and material nonlinearity. The design methods used by AISC are the Allowable Stress Design (ASD), the Plastic Design (PD) and the Load and the Resistance Factor Design (LRFD) methods.

In the ASD, the stress is obtained based on the first-order elastic analysis, and the geometric nonlinear effects are implicitly taken into account in the member design equations. Two separate linear interaction equations, one for the strength check and the other for stability check, were adopted by the AISC-ASD (1987) (see Figure 2-1). Mostly, for short members, the strength interaction equation is governing, while for long members, the stability interaction equation controls. This approach of having two separate interaction equations for strength and stability criteria was used successfully for over 50 years.

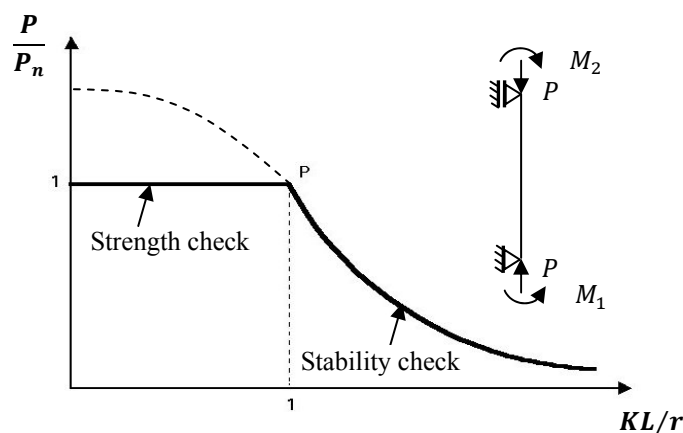


Figure 2-1: Strength and stability check for member based on AISC-ASD

Although this approach is simple to use, it has its own limitations. Firstly, the transition from long to short members (the transition from the stability to the strength equation) is not smooth which makes the design interaction equations either unconservative in the transition region or overly conservative in the rest of the region (Sohal, Duan et al. 1989). Secondly, in this method the maximum second-order moment is determined by applying an elastic moment amplification factor to the first-order moment. It allows the amplification factor to be less than unity, which is physically incorrect for compression members. In plastic design (PD), a first-order plastic-hinge analysis is used in which the geometric and material nonlinearity are not accounted for the analysis and they are approximately taken into account in design equations.

To overcome the limitation of these methods, the LRFD design procedure was introduced and reflected advances in structural design. In all three design methods the members (such as beams and columns) and connections are isolated from the structural system and require separate member capacity checks (member-based design). The LRFD (Load Resistance Factor Design) capacity check has the general format of:

$$\phi R_{ni} \geq \sum \gamma_i Q_{ni} \quad 2-1$$

in which  $R_{ni}$  is the  $i$ th member capacity calculated based on steel design code and  $Q_{ni}$  is the load effect with the span of the corresponding member. The AISC-LRFD Specification (2010) uses the bilinear interaction equations based on the curve fitting to the exact plastic-zone simulations of 82 beam-columns generated by Kanchanalai (1977):

$$\frac{P_u}{\phi_c P_n} + \frac{8}{9} \left( \frac{M_{ux}}{\phi_b M_{nx}} + \frac{M_{uy}}{\phi_b M_{ny}} \right) \leq 1 \quad \text{for} \quad \frac{P_u}{\phi_c P_n} \geq 0.2 \quad 2-2$$

$$\frac{P_u}{2\phi_c P_n} + \frac{M_{ux}}{\phi_b M_{nx}} + \frac{M_{uy}}{\phi_b M_{ny}} \leq 1 \quad \text{for} \quad \frac{P_u}{\phi_c P_n} < 0.2 \quad 2-3$$

where  $P_u$  is the required axial strength,  $P_n$  is nominal axial compressive strength,  $M_{ux}$  and  $M_{uy}$  are required flexural strength,  $M_{nx}$  and  $M_{ny}$  are nominal flexural strength and  $\phi_c$  and  $\phi_b$  are resistance factors for reliability consideration. The interaction curve is presented in Figure 2-2.

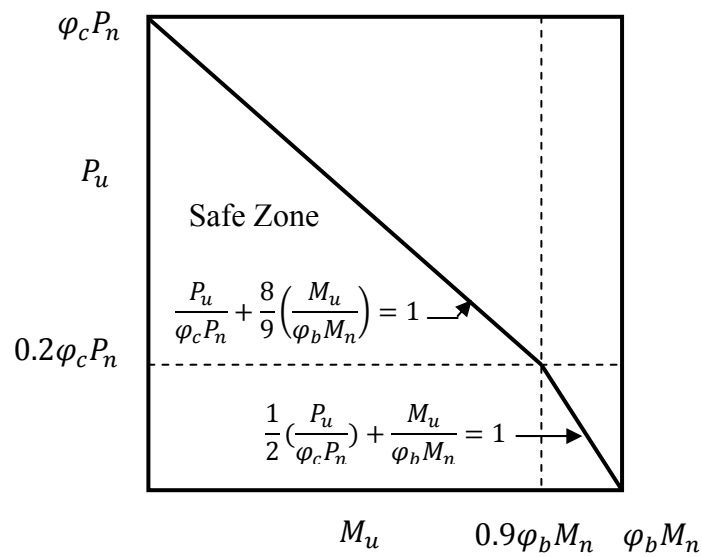


Figure 2-2: Curves of LRFD interaction equations

The Australian steel specification (AS4100 1998) follows the same concept but constitutes a straight line interaction rather than the bilinear relationship. The general interaction equation can be found in Equation 2-4 and the interaction curve is plotted in Figure 2-3.

$$\frac{P}{\phi P_n} + \frac{M_x}{\phi M_{nx}} + \frac{M_y}{\phi M_{ny}} \leq 1 \quad 2-4$$

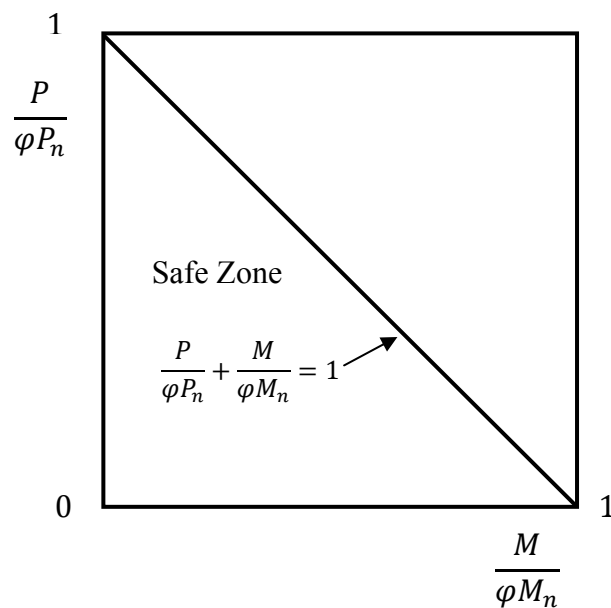


Figure 2-3: Curve of AS4100 interaction equation

The interaction equations can accurately predict the load carrying capacity of a simply-supported beam-column subjected to equal external loads applied at both ends. To account for other loads and boundary conditions, the effective length factor ( $k$ ) is introduced to approximate the influence of a structural system on the strength of individual beam-column members. However, this simple approach cannot accurately predict the complex interactions between members especially in a large structural system. In addition, the inelastic load redistribution subsequent to first yielding is ignored. Consequently, the load-carrying capacity of structural system is overestimated with no or little capability to redistribute loads. In this conventional method, the compatibility between the actual inelastic members as considered in the interaction equations and the elastic structural system as assumed in the elastic frame analysis are not satisfied (Sohal, Duan et al. 1989). Therefore, the load effects obtained from this type of analysis are not accurate. Moreover, as it is mentioned by Kanchanalai (1977) “there is no guarantee that the strength of the member treated as an isolated member can be attained under the geometric configuration imposed by the structural system”. Since this design method is not able to trace the load-deflection response of the structure, the failure modes of the structural system cannot be predicted accurately. To overcome all these limitations, the only rational way is to account for the overall system behaviour and the interaction between system stability and member stability through a direct second-order inelastic frame analysis.

## **2.3 Structural analysis of steel frames**

The most common analysis methods, which can be used to determine the member internal actions, are listed below and shown schematically in Figure 2-4.

- First-order elastic analysis
- Second-order elastic analysis
- First-order elastic-plastic hinge analysis
- Second-order elastic-plastic hinge analysis
- Advanced analysis (Second-order inelastic analysis)

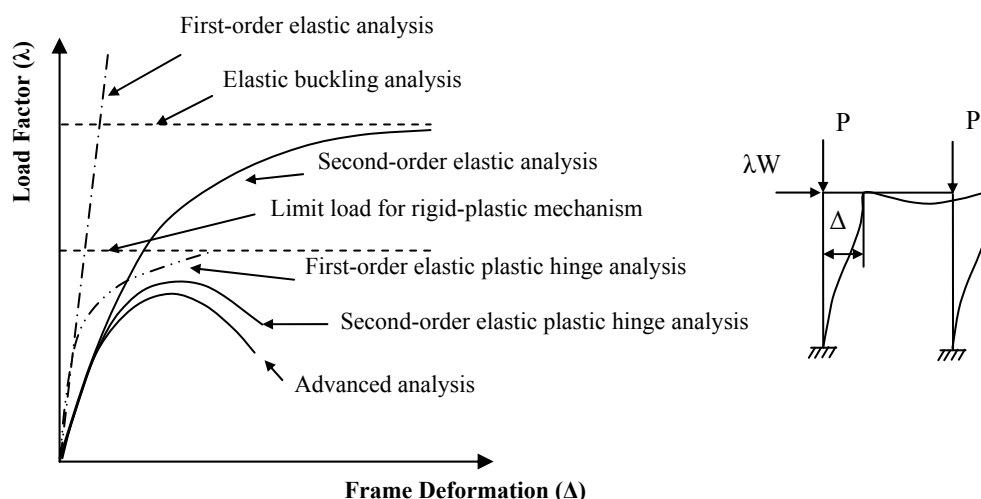


Figure 2-4: Structural analysis methods

Those analysis methods which represent equilibrium on deformed shape are termed as second-order while they are classified as first-order if these effects are not taken into account. Similarly, the analysis is termed as inelastic or elastic depending on whether the effects of the material yielding are modelled or ignored.

### 2.3.1 First-order elastic analysis

First-order elastic analysis is the most basic type of analysis which bases equilibrium calculations on the undeformed shape of the structure and ignores both geometrical nonlinearity ( $P-\Delta$  and  $P-\delta$  effects) and material nonlinearity (yielding). Therefore the second-order effects of the loads acting on the displaced configuration of the structure are ignored. In this analysis a linear relationship between the applied load and the deformations is assumed and the structure follows Hooke's law. The internal force distribution in the frame is assumed to be unaffected by the displacements in the frame and the structure recovers completely to its original state when the load is removed. In this case the deformations are proportional to the applied loads (force-displacement) and therefore the principle of superposition applies which can simplify the analyses for different load combinations.



### **2.3.2 Second-order elastic analysis**

This method is a relatively more complicated approach for analysis of structures taking into account the effect of elastic instability and changes in effective stiffness of the members. The effect of design loads is considered on the structural deformed state and finite displacements of the system are accounted in forming the equations of equilibrium. The principle of superposition does not apply to this type of analysis as the second-order response is nonlinear. As implied by its name, material yielding is not considered in this type of analysis and the members are assumed to remain elastic. The upper limit to a first-order elastic analysis is the elastic buckling limit. The elastic critical load is commonly determined from an eigenvalue analysis of an idealized elastic model of the structure (McGuire et al. 2000).

### **2.3.3 First-order elastic-plastic hinge analysis**

The first-order elastic-plastic redundant hinge method includes yielding by formation of plastic hinges (fully yielded cross-sections), but ignores the second-order stability effects. This means that the material nonlinearity can be captured under incremental loads but the equilibrium equations are formed based on the undeformed shape of the structure. The material is modelled as elastic-perfectly-plastic which means beyond the elastic limit the stress remains constant while the strain increases.

The upper bound for this type of analysis is first-order rigid plastic analysis which ignores the effect of elastic displacements and assumes all rotational deformations are concentrated in discrete regions, called plastic hinges, when the full plastic strength is reached (Beedle 1958; Heyman 1971; Chen and Sohal 1995). The zero length plastic hinges are allowed only at the two ends of each one dimensional beam element (McGuire et al. 2000). Once the cross-section is fully yielded and a plastic hinge is developed, the end sections change abruptly from elastic to fully plastic with no strain hardening and the element exhibits a sudden stiffness reduction (Liew 1992). In first-order rigid plastic analysis, the regions between the plastic hinges remain rigid during the analysis. Therefore, no deformation of the structure is possible until the formation of sufficient plastic hinges to convert the structure into a mechanism. In this method the sequence of

developing the hinges as well as the magnitude of deflections cannot be captured. The analysis can be modified to first-order elastic-plastic, if the members between the “zero-length” plastic hinges are assumed to behave elastically rather than rigid.

The first order elastic-plastic hinge method cannot handle the effect of spread of yielding along the length and through the cross-section in the frame members as well as the second-order geometric effects. Because the segments of member between plastic hinges are modelled as elastic, this method often overestimates the stiffness and always gives an upper-bound prediction of the actual ultimate strength (Li and Lui 1995).

### **2.3.4 Second-order elastic-plastic hinge analysis**

This type of analysis is the most basic type of second-order inelastic analysis in which the analysis traces the development of plastic hinges and also allows for the effects of deformations in formulating equilibrium. The second-order elastic-plastic hinge analysis considers the decrease in stiffness due to both yielding and deformations and usually uses one beam-column element for each frame member. This type of analysis has been classified as an advanced inelastic analysis by Ziemian et al. (1992a; 1992b) if the tangent modulus ( $E_t$ ) is used to capture the distribution of plasticity along the member length and it can accurately approximate frame strength and load-displacement response for reasonably configured structural systems. However, since yielding is only modelled as zero-length plastic hinges and the distributed plasticity as well as associated instability are not considered, this method may over-predict the actual inelastic stiffness and strength of the structure, especially when the instability of a few members is dominant (White et al. 1991a; White and Chen 1993). Although this method is not as accurate as advanced analysis approaches for frames exhibiting significant yielding in beam-column elements, it can be adequate for slender members whose predominant failure mode is elastic instability (Chen 2000). Nevertheless, this method was the basis to develop the more accurate analysis procedures which are termed as the refined plastic hinge methods.

### **2.3.5 Second-order inelastic analysis (Advanced analysis)**

Great attention has been devoted to research on advanced analysis of steel structures over the last two decades (Ziemian 1990; Liew, White et al. 1993a; Chen and Kim 1997;

Surovek, A. E. (Ed.) 2012). This type of analysis which includes significant behavioural effects eliminates the need for checking individual member capacities in the frame. This leads to a substantial simplification of the design process and shifts the focus of design from individual member and connection strength to the overall structural behaviour and strength of the system which is called system-based design. The benefits of using this approach in design are outlined as follows:

- By using advanced analysis, the failure mode of the system becomes apparent and it is possible to consider the consequences of failure in design process. This feature is especially important in the new paradigm of performance-based design.
- System effects are accounted for explicitly which can lead to safer and more efficient designs.
- More consistent system reliability is achieved.
- The one step design procedure is potentially faster and time effective since it completely eliminates the need for separate member or section capacity check based on specifications.
- Advanced analysis overcomes the difficulties due to incompatibility between the elastic global analysis and the limit state member design in the conventional LRFD method (Kim and Chen 1999).
- Advanced analysis is user friendly for computer-based design (Kim and Chen 1999). Most FE commercial software have the ability to run this type of analysis.

As it can be seen in Figure 2-4, among all analysis methods, advanced analysis can accurately predict the behavior and ultimate load carrying capacity of a structural system. In general, the second-order inelastic analysis (“advanced”) falls into two main categories: plastic hinge method (or concentrated plasticity method) and plastic zone method (also known as spread of plasticity method). These methods are explained in Sections 2.4.1 and 2.4.2, respectively. To achieve an accurate result from advanced analysis all key factors influencing the frame ultimate strength including the material

nonlinearity (yielding) and geometric nonlinearity (second-order effects), residual stresses, initial geometric imperfections and warping torsion (connection behaviour) need to be taken into account. All these requirements are discussed in Section 2.5.

## **2.4 Advance analysis methods**

### **2.4.1 Plastic hinge analysis**

The most basic types of plastic hinge method are first-order and second-order elastic-plastic hinge analysis which enable the use of one beam-column element per member (Kim et al. 2004). This provides more computationally efficient approach but at the same time has its own limitations as explained in Section 2.3. Therefore, some considerable refinements have been made to these basic hinge approaches to generalize their application to different types of structural frames. Some of the resulting methods are listed below:

- Refined or modified plastic hinge method
- Quasi-plastic hinge method
- Notional-load plastic hinge method
- Hardening plastic hinge method

#### **2.4.1.1 Refined (modified) plastic hinge method**

The refined plastic hinge method is based on modifications of the elastic-plastic hinge analysis by taking into account the effect of gradual member stiffness degradation and the distributed yielding due to axial force. The distribution of plasticity along the member length caused by residual stresses, large bending and axial forces, is captured by using a tangent modulus ( $E_t$ ) which represents the effective stiffness and a stiffness reduction factor ( $\tau$ ). Significant amount of research has been conducted using this approach for two-dimensional frame analysis (Al-Mashary and Chen 1991; Deierlein, Zhao et al. 1991; King, White et al. 1992; Liew 1992, Ziemian et al. (1992a; 1992b)) and the method was further extended to a 3D formulation (Liew and Tang 1998; Kim and Lee 2002). Later, the effect of local buckling was taken into account by Avery (1998). This method is

proven to be sufficiently accurate in approximating the strength and stability of frame strength, benefiting from the efficiency and simplicity of classical plastic-hinge methods (Liew et al. 1993a).

#### **2.4.1.2 Quasi-plastic hinge method**

An intermediate analysis approach between classic plastic-hinge and plastic-zone methods, which is called quasi-plastic hinge method, was introduced by Attalla et al. (1994). Using this method, the spread of inelasticity in a beam can be captured without discretizing the member along the length and over the cross-section which makes it more computationally efficient. To account for spreading plasticity through members under combined bending and axial force, a 2D element is developed from basic equilibrium, kinematic and constitutive relationships. Gradual plasticisation though the cross-section is captured by fitting nonlinear equations to moment-curvature-axial force behaviour of a unit-length segment of the element. Elastic-plastic flexibility coefficients for the full member are derived by integration along its length. The flexibility coefficients are then employed to form an inelastic element stiffness matrix in which geometric nonlinearity is also taken into account. This method was verified by Attalla et al. (1994) against some benchmark frames in the literature which are sensitive to the effects of distributed plasticity (Kanchanalai 1977; El-Zanaty, Murray et al. 1980; Ziemian 1990) and the error was shown to be less than 5%. However, this method is difficult to extend to 3D since in that case the interaction of axial and biaxial bending forces which cause plastification under longitudinal stress must be taken into account. Moreover, although this method eliminates the need to discretize the members and the cross-sections, it still requires essentially the same run time as the conventional plastic-hinge analysis.

#### **2.4.1.3 Notional load plastic hinge method**

This method permits the use of second-order elastic-plastic hinge analysis for frame design without the risk of overestimating the maximum member strength in the frame (Liew et al. 1994). This can be achieved by the use of equivalent lateral loads which are computed based on gravity loads and account for the influence of residual stresses, gradual yielding and member imperfections by generating larger geometric deformation.

Although this method is simple to use, it is not appropriate for all situations. It was shown by Liew (1992) that this method may over-predict the strength by up to 10% for isolated members subjected to axial force and bending.

#### **2.4.1.4 Hardening plastic hinge method**

The hardening plastic hinge analysis, which is also referred as the modified plastic hinge method, degrades the member stiffness as the cross-section strength is approached at critical locations along the member length (King et al. 1992). This method is based on the assumption that once a plastic hinge is developed, the moment at the plastic hinge remains unchanged as the axial force is increased. A number of benchmark frames were analysed by King et al. (1992) using the modified plastic hinge method and it was found that this method can generally improve the prediction of inelastic load-deflection behaviour and strength for many cases but still has certain limitations. The most important disadvantage is that for an axially loaded member this method still predicts failure at either the elastic critical load or at the member squash load exactly same as conventional elastic-plastic approach. This means that if a column fails inelastically the modified plastic-hinge method does not reduce to the behaviour of the inelastic column for members loaded by axial force alone.

To eliminate this problem, another alternative approach was introduced by King et al. (1992) which is called beam-column strength method. This technique is similar to the modified plastic hinge approach in principle, but this time equations for the entire member are considered rather than equations for the member cross-section strength. In other words, the member stiffness degrades when the overall member strength is reached. However, the beam-column strength method tends to underestimate the column strength in some situations and reduce to the behaviour of a beam member in the limit that the member is subjected only to bending moment.

The modified plastic-hinge method was refined and extended by King and Chen (1994) and called work-hardening plastic hinge approach. In this method, the member stiffness is modified to model the effect of spread of plasticity using the concept of work-hardening in which the average degradation of tangent stiffness of a cross-section is calibrated

against the slope of exact moment-curvature-axial force relationship. Here the terms of “hardening” refers to gradual degradation of tangent stiffness of a cross-section. The load-deflection response of the frames analysed by King and Chen (1994) were found to be identical to the test results. However, this method may underestimate the ultimate bending moment in some columns since the strain hardening of material is neglected.

### 2.4.2 Plastic zone analysis

A plastic-zone analysis is characterized by the spread of plasticity and gradual yielding within members of a framework. Since the main physical attributes affecting the strength and stability of the structural system, such as residual stresses and initial geometric imperfections can be directly incorporated into analysis, this method is generally more accurate than plastic hinge methods. This approach is often considered an “exact” solution and has been used as a benchmark by many researchers to verify the simplified methods such as the modified plastic hinge methods (Vogel 1985; King et al. 1992; Liew 1992; Liew et al. 1993a). Two types of finite elements can be used with this type of analysis: (i) one-dimensional beam elements and 3D shell elements.

In this method frame members are discretized into several finite elements (beam-column elements) and furthermore the cross-section of each member is subdivided into a number of fibers as it is shown in Figure 2-5 (Alvarez and Birnstiel 1969; White 1985; Clarke et al. 1992; Toma and Chen 1992). During the analysis the deflection and stiffness at each point are obtained by numerical integration. Through the incremental load-deflection response at each loading step with updated geometry, the second-order effects can be rigorously captured.

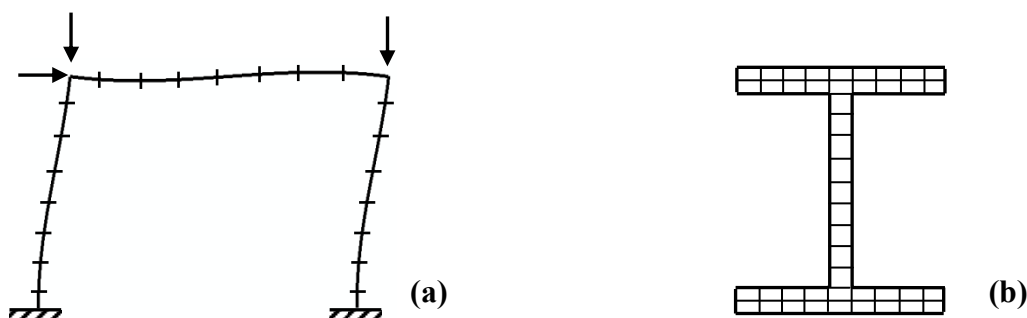


Figure 2-5: Plastic zone method for frame analysis (a) frame discretization (b) section discretization

Due to refined discretization of sections and members, the plastic zone analysis can accurately predict the inelastic behavior of structures and can replace the expensive full-scale testing of steel frames (Toma and Chen 1992). However, in order to obtain an accurate result, a relatively fine discretization is required for frame structures. In the past this type of analysis was computationally intensive for routine design use and limited to special design applications and development of design guidelines (Kim 1996). However, with the developed computer technology, this type of analysis is becoming more practical.

## **2.5 Advanced analysis requirements**

All of these following aspects influencing the behaviour of the steel frame need to be taken into account when using advanced analysis.

- Material nonlinearity (yielding)
- Geometric nonlinearity (second-order effects)
- Initial geometric imperfections
- Residual stress
- Warping torsion

### **2.5.1 Material nonlinearity**

One of the key attributes in modelling limit state behaviour is material nonlinearity. This type of nonlinearity arises when the material exhibits a non-linear stress-strain relationship. For a complete finite element analysis with material nonlinearity, the basic components in the plasticity theory such as a yield criterion, flow rule and hardening rule must be well understood.

The yield criterion describes how the applied stresses are related to the yield strength specified in finite element study. The most popular criterion is the von Mises which can be expressed as:



$$f = \sqrt{\frac{(\sigma_1 - \sigma_2)^2 + (\sigma_2 - \sigma_3)^2 + (\sigma_1 - \sigma_3)^2}{2}} - \sigma_Y = 0 \quad 2-5$$

To plot in two dimensions and for ease of visualization, this problem can be converted to a plane stress case by considering one of the principal stresses equal to zero, and thereby rendering the yield surface of the material (see Figure 2-6).

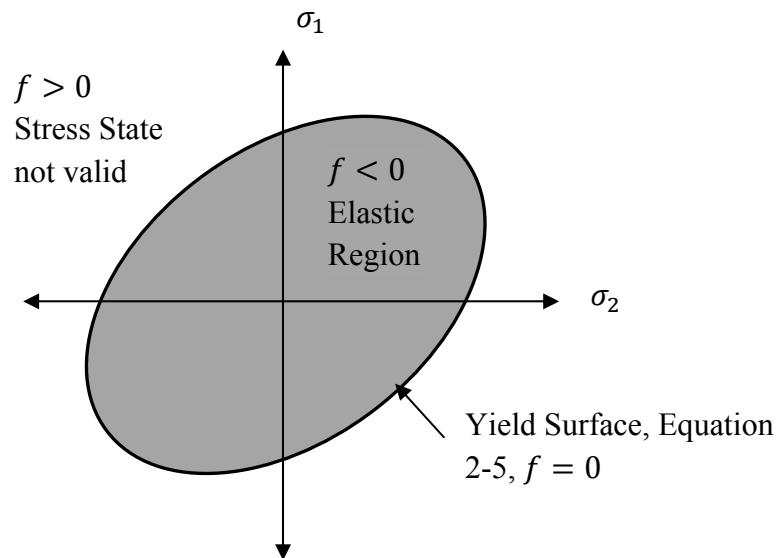


Figure 2-6: Concept of Yield Surface

The yield criterion describes whether plastic deformation occurs or not but it does not provide any information about the behaviour of the material when it becomes plastic. The flow rule concept explains the relationship between stresses and strains for the post-yield behaviour. The final concept which is the hardening rule defines the mechanism for the expansion and translation of the yield surface as the material yields. This means that after the yield point or initial plastic flow, the stress and strain still increase. Moreover, the yield point of the material shows an increase if the material is now unloaded and reloaded (see Figure 2-7).

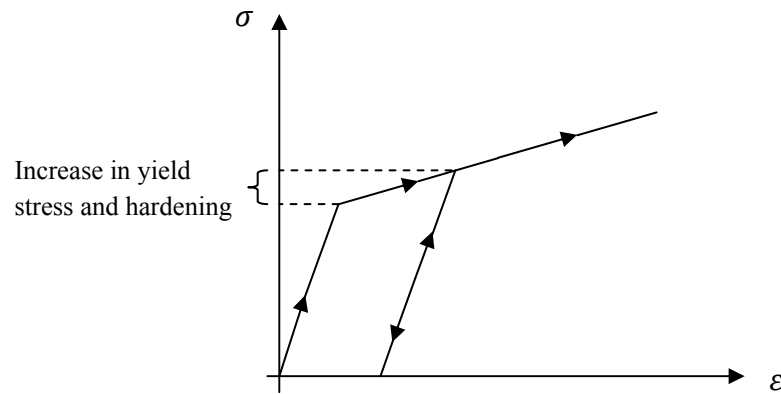


Figure 2-7: Hardening response of material

In the structures made by material with hardening, the members often show larger internal actions e.g. forces and moments. Therefore, the members may show significant hardening before the structure reaches its failure. The material hardening theory is best suited for problems in which the plastic strain is considerably larger than at the onset of yield, such as manufacturing processes (forming, cold working) and large motion dynamic problems.

### 2.5.2 Geometric nonlinearity

If a system contains a level of initial geometric imperfections (member or frame imperfections) and is subjected to lateral loads along with gravity loads, then the deflections start increasing even further developing a second order deflection, as soon as the loads are applied. These second-order effects are termed as P-Delta ( $P - \Delta$  and  $P - \delta$ ) effects. The second-order nonlinear solution for structural analysis is complicated by the fact that the equilibrium equations are formulated with respect to the deformed geometry, which is unknown in advance and keep changing during analysis. Thus, the solution cannot be obtained for each load level in one step and the problem of the geometrically nonlinear behaviour of a structure is usually tackled by tracing the geometrical change by an incremental and iterative algorithm.

One of the most popular theoretical formulations and computational techniques for the geometrically nonlinear finite element analysis is the Lagrangian approach. Three types of Lagrangian approaches can be found in literature which are: Total Lagrangian Description (TLD), Updated Lagrangian Description (ULD) and Partially Updated

Lagrangian Description (PULD). In TLD the deformation of the element is measured with respect to the reference configuration and remains fixed throughout the solution process. This formulation procedure is easy to use but it is only applicable to moderate displacements and strains. Moreover, this method is not able to distinguish the rigid body motion from its local displacement (Wong and Tin-Loi 1990). The second type is the Updated Lagrangian Description (ULD) in which the reference configuration is updated with respect to the current configuration of the element at any time. Thus, in this case the rigid body motion and local deformation can be separated. Although this procedure is more accurate and applicable to large displacements, calculating the local element deformations at any stage of loading requires significant effort. Therefore, this type of displacement description is unnecessary unless an accurate result is needed. This leads to the development of more practical approaches such as PULD. The difference between ULD and PULD is that in the former method the coordinates of each element are updated once and only at the beginning of each load step while in PULD the numerical manipulation is performed by a TLD manner through each load step (Wong and Tin-Loi 1990). Thus, this type of formulation is benefitting from the accuracy inherent in the ULD and from the simplicity of the TLD method.

Considerable information can be found in the literature for the development of numerical solutions for the nonlinear structural problems. One of the earliest and best known methods in this regard is the load controlled Newton-Raphson method (Kao 1974) with an equilibrium check in every load cycle (Figure 2-8). However, when the equilibrium path approaches the limit point, convergence becomes difficult and this method fails. Another drawback of this method is that it completely depends on the initial guess which may be too far from the final result. It should be mentioned that despite this drawback the Newton-Raphson method is still popular in daily design since engineers are not required to design a structure into the post-ultimate regime under typical loads.

The modified Newton-Raphson method (Figure 2-9) shows a dramatic improvement in computation time (performance) by forming the tangent stiffness matrix only one time in the first iteration compared to conventional Newton-Raphson method with reforming the stiffness matrix in every iteration.

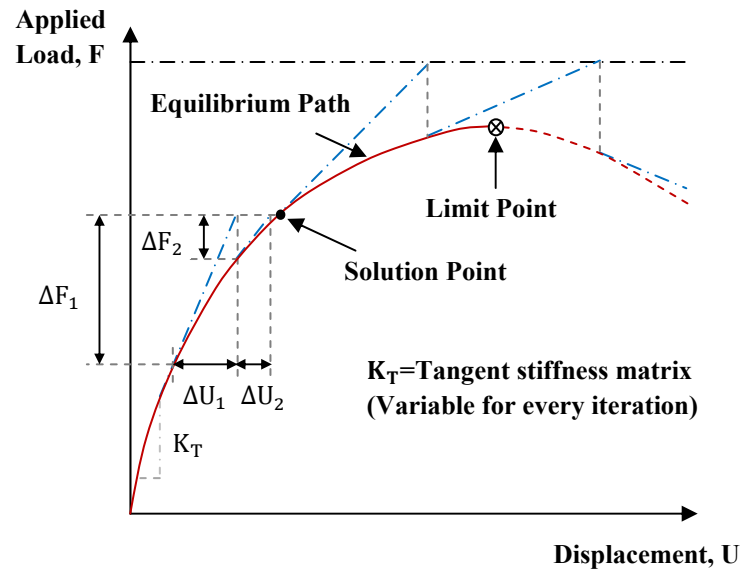


Figure 2-8: Newton-Raphson Method

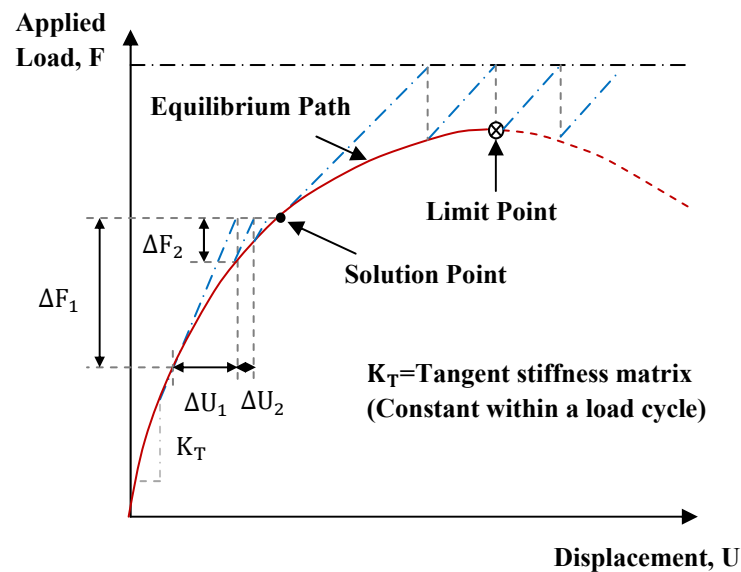


Figure 2-9: Modified Newton-Raphson Method

To overcome the problem of load-control method around load limit points, the displacement control technique was introduced by Argyris (1965), Zienkiewicz (1971) and Sabir and Lock (1972). In this method instead of using load as the control parameter to trace the portion of load-deflection curve around the limit point, displacement increment is used to prevent the applied load being larger than limit load (see Figure

2-10). Using this method, in every incremental step, the equilibrium is satisfied to a pre-defined deflection, which is similar to pre-defined load level in the load-control Newton-Raphson method. A drawback of constant displacement method is that in a structural systems exhibiting snap-through or snap-back behaviour in which the equilibrium path does not increase with the load, this technique leads to error. Moreover, the selection of an appropriate control displacement is not an easy task and has a significant influence on the convergence characteristic of the nonlinear problem.

To obtain a more general technique, the arc-length method was developed by Wempner (1971) and Riks (1979) in which both the load vector and the displacement field are treated as variables and modified at each iteration (Figure 2-11). Therefore, the effects from both load and displacement changes can be captured by the control parameter and subsequently both load limit points (snap-through points) and displacement limit points (snap-back points) can be effectively determined. Although this method can even predict the complex load-deflection behaviour effectively, there are some difficulties in the control of load increment to reach convergence (Sousaa and Pimentab 2010). Therefore, a modification was introduced by Crisfield (1981) to improve the performance analysis of equilibrium path and was adopted by many researchers (Al-Rasby 1991; Fafard and Massicotte 1993; Teng and Luo 1998).

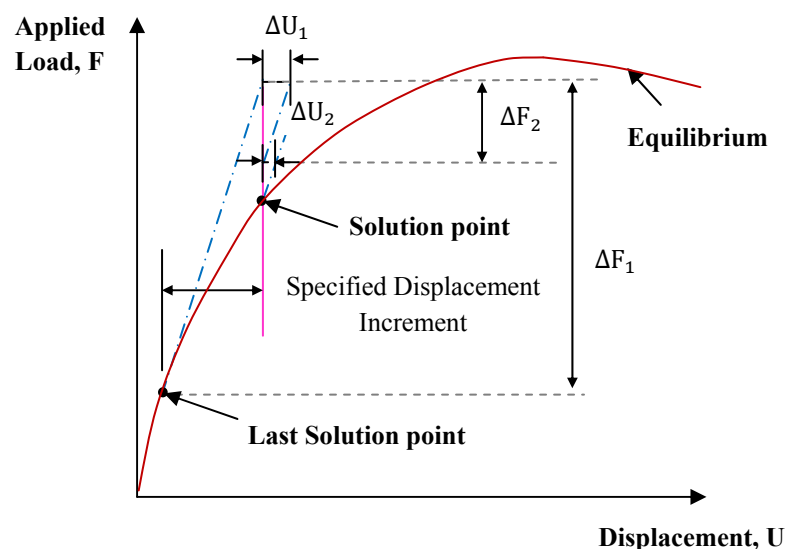


Figure 2-10: The displacement control method

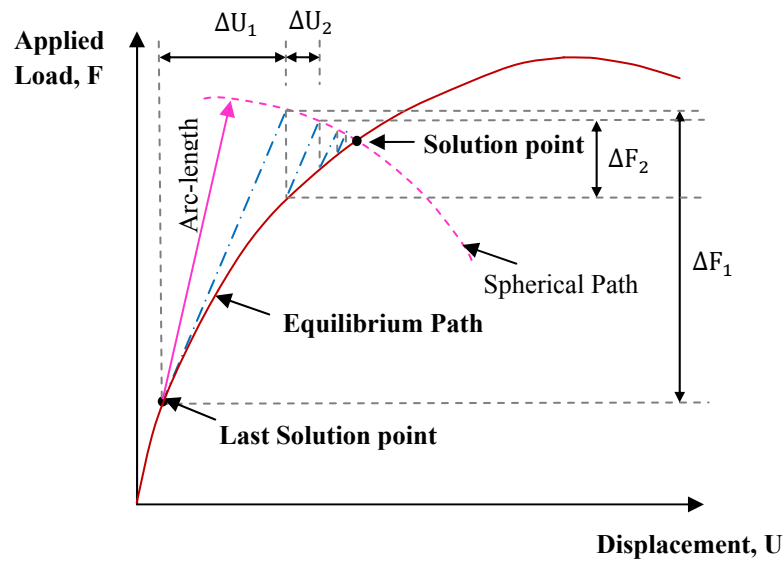


Figure 2-11: The arc-length control method

### 2.5.3 Initial geometric imperfection

In order to determine the load carrying capacity of a practical steel frame, it is important to take into account the effect of initial geometric imperfections which are practically unavoidable. In reality the steel members and the entire structure are not perfectly straight due to manufacturing and erection tolerances. Thus, two types of geometrical imperfections should be taken into account in advanced analysis: the member out-of-straightness (bow imperfection  $\delta$ ) and the frame out-of-plumb (sway imperfection  $\Delta$ ) (see Figure 2-12).

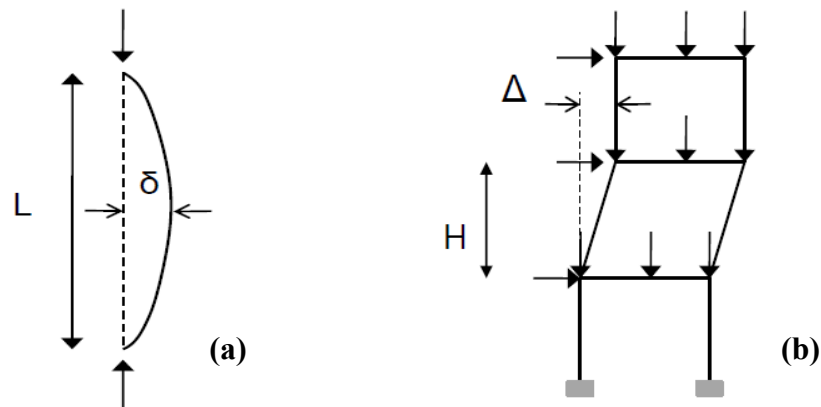


Figure 2-12: (a) Initial out-of-straightness, (b) Initial out-of-plumb

The initial geometric imperfections, which can be the major factors contributing to nonlinear behaviour of structures, may also have a considerable influence on the strength and stability of the whole system. The effect of these imperfections on the strength of a simple elastic two-member frame has been studied by Kounadis and Economou (1984). It was concluded that the influence of imperfection may be detrimental or beneficial depending on the shape and magnitude of the imperfection.

The modelling of imperfection is more complex for a frame compared to a single member because it is not only the magnitude, but the configuration and orientation of the imperfection also have a direct influence on the response of the structure in the ultimate limit state. There are many ways to take geometric imperfection effects into account in the finite element analysis of steel frames. The most well-known approaches to model imperfections are: the scaling of the first eigenbuckling mode (EBM), application of notional horizontal forces (NHF), the direct and explicit modelling of initial geometric imperfections (IGI) (Chan et al. 2005) and a further reduction of member stiffness ( $E_t'$ ) (Chen 2000). In general, both the magnitude and the shape of geometric imperfection can be deterministic or random (Raviprakash et al. 2010).

### **2.5.3.1 Scaling of the first eigenbuckling mode (EBM)**

In the EBM method, a classic elastic buckling analysis of the perfect structure is first performed. The lowest buckling mode is then scaled to represent the imperfect geometry of the frame. This method has been adopted by many researchers to consider the most critical geometric imperfection in their analyses (Hajjar 1997; Kim and Lee 2002; Ofner 2003; Gu and Chan 2005; Mahendran 2007). The concept behind this theory is that the most critical imperfect geometry is similar to the final collapse configuration because it requires the least deformation energy to go from the unload state to the final collapse situation (Alvarenga and Silveira 2009). It is observed that in most cases the first buckling mode can represent the collapse shape however there are also some structures which fail in different shape to the first eigenmode. An alternative approach was proposed by Alvarenga and Silveira (2009) in which a second-order inelastic analysis is run first and the final collapse configuration is determined for specific loading case. Afterwards, the final deformed shape of the structure is used to model the initial geometric

imperfection in the advanced analysis (i.e. the initial imperfect geometry should follow the collapse configuration). However this method may not be reliable for all cases because no effort can be found in (Alvarenga and Silveira 2009) to verify the validity of the proposed model.

### **2.5.3.2 Notional horizontal force (NHF)**

The notional horizontal force method (NHF) was first introduced by Liew et al. (1994) to model geometrical imperfections and has been followed by many researchers (Clarke et al 1992; Kim and Chen 1996; Kim and Chen 1996; Chan et al. 2005). In this method artificial horizontal forces which are a portion of the gravity load ( $P$ ) are added to the top of each story to account for out-of-plumb. Out-of-straightness can also be simulated by applying a lateral distributed force along the member or a concentrated force at the mid-height of the member (Chan et al. 2005).

Recommended values of notional loads are presented in most steel design codes. The value is considered as  $0.002P$  for sway frames and  $0.004P$  for braced frames in AISC (1994) and increases to  $0.005P$  in HKC (2005). Eurocode 3 (2003) suggests  $(\alpha_h \alpha_m / 200) N_{Ed}$  and  $8N_{Ed} / L^2$  for sway and bow imperfection respectively in which  $N_{Ed}$  is the design axial force,  $\alpha_h$  is the reduction factor for height, and  $\alpha_m$  is a reduction factor associated with the number of columns in a row. The notional load in the British standard, BS5950-1 (2003), is equal to 1% of design dead loads or 0.5% of design vertical load (dead plus live) in one floor whichever is greater. The value in the Chinese code (GB50205 2001) is equal to  $(\alpha_i Q_i / 250) \sqrt{0.2 + 1/n_s}$  where  $Q_i$  is the design value of the total gravity load at the  $i$ -th storey top,  $n_s$  is the number of stories in the frame and  $\alpha_i$  is a factor accounting for steel strength effect. The notional load values are summarized in Table 2-1.

The NHF approach is simple and permits the use of straight members in the finite element model. It means that there is no difficulty to deal with representing a member as a sine curve to model out-of-straightness but at the same time it requires tedious input of concentrated or distributed loads for each column. In some cases deciding about the direction of the imperfection which must provide the worst case scenario is difficult or impossible. The requirement in the AISC specification is to apply the notional loads in



the direction that adds to the destabilizing effects. In this case, the behaviour of the structure may be a conservative estimate under the most unfavourable combination of initial imperfection (Zhang et al. 2010).

Table 2-1: Summary of suggested Notional Horizontal Force (NHF) by different specifications

Code	Sway imperfection ( $\Delta$ )	Bow imperfection ( $\delta$ )	Reference
AISC	$0.002P$	$0.004P$	(ANSI/AIS360-05)
Eurocode 3	$(\alpha_h \alpha_m / 200) N_{Ed}$	$8N_{Ed} / L^2$	(Eurocode3 2003)
HKC	$0.005P$		(HKC 2005)
BS 5950-1	1% of design dead loads or 0.5% of design dead plus		(BS5950-1 2003)
GB50205	$(\alpha_i Q_i / 250) \sqrt{0.2 + 1/n_s}$		(GB50205 2001)

### 2.5.3.3 Further reduction of member stiffness ( $E_t'$ )

In 1996, the degradation of member stiffness to model geometric imperfection was introduced by Kim (1996) and called “further reduction of member stiffness”. In this method the modulus  $E$  in the Euler buckling formula is reduced to  $E_t'$  equal to  $0.85E$  to account for unavoidable geometric imperfections. The factor of 0.85 is determined by the calibration with the plastic zone solution and verified with a wide range of frames and columns (Kim and Chen 1996; Kim and Chen 1996). This method has the advantage of eliminating the tedious work of explicit imperfection modelling or notional load application. Another benefit of this method is that it does not need to deal with the direction of geometric imperfections, which is difficult to determine in a large structural frame. This method is applicable for both braced and unbraced members and frames using same factor of 0.85 (Chen 2000). Although this method is simple to use it has not been verified by the probabilistic approach. Details of this model can be found in Chen and Kim (1997).

### 2.5.3.4 Explicit modelling of initial geometric imperfections (IGI)

In the explicit modelling of imperfection (IGI) method, each coordinate of nodal points should be directly and manually set in FE analysis by offsetting the nodes from their original positions. The magnitude and shape of imperfection are implemented into the model in a way to produce largest reduction in strength. Estimating the direction of these

imperfections is difficult and in some cases impossible. Modelling imperfections using the IGI method can be further classified into deterministic and random.

### **2.5.3.5 Deterministic modelling of initial geometric imperfection**

Most of the steel structural design codes present a maximum value of initial imperfection but not the corresponding pattern. When initial geometric imperfections are modelled deterministically, the ideal approach is using the actual shape and data measured from experiment of a type similar to the structure being analysed. The problem is that only few experimental results can be found in the literature to provide both configuration and amplitude of imperfection. When this information is not available two methods are widely used.

The first method is to apply a typical imperfection pattern and magnitude, as obtained from codes and previous studies. The assumed pattern for initial out-of-straightness may be a half-sine wave, which is considered in most research in this field (Chebl and Neale 1984; Kounadis and Economou 1984; Clarke et al. 1992; Kim and Chen 1996; Smith-Pardo and Aristizábal-Ochoa 1999; Kim and Lee 2002; Gu and Chan 2005; Beck and Dória 2008; Buonopane 2008; Xu and Wang 2008; Zhang et al. 2008; Alvarenga and Silveira 2009; Kala 2009). The magnitude of the maximum allowed imperfection is recommended in most specifications. The ECCS (1984; 1991), AS4100 (1998) and CAN/CAS-S16 (1994) specifications recommend an initial out-of-straightness of a column equal to 1/1000 times the column length. The AISC code recommends the same maximum fabrication tolerance of  $L_c/1000$  for out-of-straightness (AISC 1994). The value is  $h/1500$  for columns and  $h/1200$  for beams in GB50205 (2001) and  $L/300$  in Eurocode 3 (2003). The British code suggests the bow imperfection to be 1/1000 of member length or 6mm whichever is greater (BS5950-1 2003).

Each structural specification also recommends maximum amplitude for out-of-plumb and it is assumed that this imperfection follows a linear pattern with all columns leaning in the same direction. AISC (1994) and AS4100 (1998) suggest the out-of-plumb to be equal to  $h/500$  in which  $h$  is the column height. The value is  $(\alpha_h \alpha_m / 200)$  in Eurocode 3 (2003) where  $\alpha_h$  and  $\alpha_m$  are the reduction factor for height and the reduction factor for the

number of columns in a row, respectively. The German stability code DIN18800-2 (1990) defines the magnitude of the initial sway imperfection in a very similar way to Eurocode 3 by value of  $(r_1 r_2/200)$ . The reduction factor  $r_1$  is comparable to  $\alpha_h$ , given by  $\sqrt{5/L}$ , and the reduction factor  $r_2$  is same as  $\alpha_m$  given by  $0.5(1 + \sqrt{1/n})$  where  $n$  is number of columns in a row. BS 5950-1 considers the sway imperfection to be equal to  $h/600$  or 5mm whichever is greater for a column. The corresponding value in GB50205 (2001) is  $h/1000$ . The Canadian Standard S16.1 (CAN/CAS-S16 1994) recommends a constant lean,  $\Delta/L$ , of 0.002 Rad. The ECCS (1991) is more conservative by proposing 0.005 Rad as column slope. The summary of all values is shown in Table 2-2.

Table 2-2: Summary of suggested imperfection by different specifications

Code	Out-of-plumb	Out-of-straightness	Reference
ECCS	$h/200$	$L/1000$	(ECCS 1976)
AS4100	$h/500$	$L/1000$	(AS4100 1998)
CSA	$h/500$	$L/1000$	(CAN/CAS-S16 1994)
AISC	$h/500$	$L_c/1000$	(AISC 1994)
GB50205	$h/1000$	$L/1500$ for columns, $L/1200$ for beams	(GB50205 2001)
Eurocode 3	$\alpha_h \alpha_m/200$	$L/300$	(Eurocode3 2003)
BS 5950-1	$h/600$ or 5mm whichever is greater	$1/1000$ or 6mm whichever is greater	(BS5950-1 2003)
DIN 18800-2	$r_1 r_2/200$	$1/300$ (elastic analysis ,S 235 to S420) $1/250$ (Plastic analysis ,S 235 to S420) $1/350$ elastic analysis ,S 460) $1/300$ (Plastic analysis ,S 460)	(DIN18800-2 1990)

\* Note:  $L$ =member length,  $h$ =story height (column height),  $\alpha_h$ =the reduction factor for height, and  $\alpha_m$ = the reduction factor for number of columns in a row,  $r_1 = \sqrt{5/L}$ ,  $r_2 = 0.5(1 + \sqrt{1/n})$ ,  $n$  is the number of columns in a row

### 2.5.3.6 Probabilistic modelling

Probabilistic modelling treats initial imperfections as a random field (Fraser and Budiansky 1969) (in which both shape and the magnitude can be random). The sway installation tolerances and the out-of-straightness of all members are taken into account randomly. In this method the correct modelling of imperfection requires statistical quantities such as mean and standard deviation. The best way to develop such distribution is to perform numerous experiments. Although a great number of experimental results on column strength can be obtained from literature, few of them report detailed

measurements of initial imperfection along the length of members. The detailed experimental data can be found in Section 2.5.3.7. Alternatively, in the lack of experimental data, some other ways are proposed by researchers to obtain the statistical characteristics of imperfections and are discussed in sections 2.5.3.6.1 to 2.5.3.6.3.

### 2.5.3.6.1 Probabilistic SBRA method

With modern computer technology, the simulation techniques are easy, and powerful structural analysis tools and many reliability assessments such as SBRA (Simulation-Based Reliability Assessment) have been developed. Using the SBRA method, all variables are presented by a nonparametric distribution such as a bounded histogram. The initial geometric imperfections can be implemented in this method (Marek and Křivý ; Omishore and Kala 2009; Marek and Křivý 2010; Omishore 2010). Only the maximum amplitude is considered as random variable and the imperfection follows a sinusoidal shape. In general, the initial bow imperfection  $e_o$  is presented by a normal distribution histogram with a mean value of zero (positive and negative values have same frequency) and the standard deviation is obtained in a way that the random variable  $e_o$  occurs with 95% probability in the interval defined from tolerance limits of the standard e.g.  $(-L/1000, L/1000)$ . The details of this method is presented by Marek and Křivý (2010) (see Figure 2-13). Omishore (2010) and Kala (Kala 2005; Kala 2007) assumed log-normal distribution instead of Gaussian for the out-of-straightness.

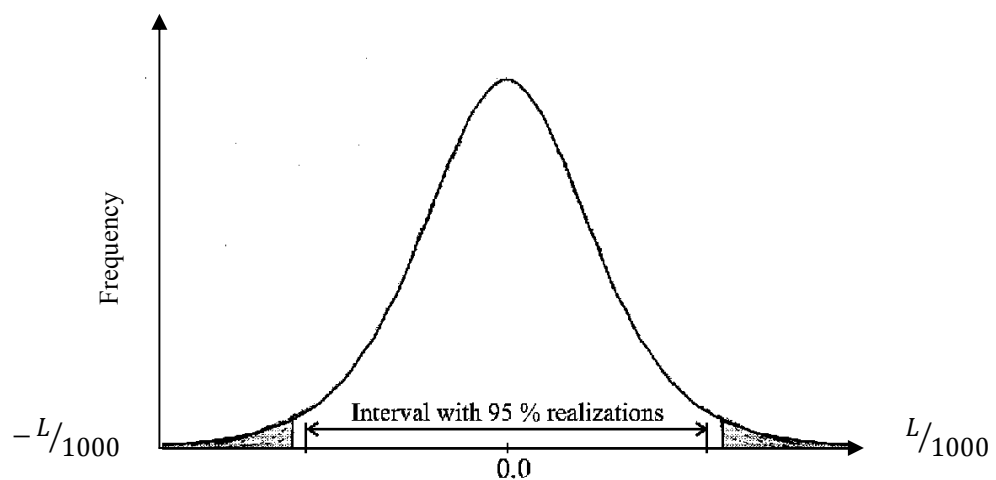


Figure 2-13: Initial out-of-straightness distribution, SBRA method

### 2.5.3.6.2 Proposed method by Bjorhovde

The other method to provide statistical characteristic in the lack of experimental data was proposed by Bjorhovde (1972). A probabilistic method for finding the ultimate strength of a centrally loaded steel column has been developed. Many distributions could be fitted to measured imperfection data obtained from the literature (Tomonaga 1971), e.g. Extreme Type I (Gumbel), Extreme Type III (Weibull) and Rayleigh. Among them the Extreme Type I with negative skewness was chosen by Bjorhovde (1972) to be consistent with the distribution which is assumed for yield stress. The distribution has negative skewness if the tail on the left side of the probability density function is longer than the right side and the bulk of the values lie to the right of the mean (see Figure 2-14).

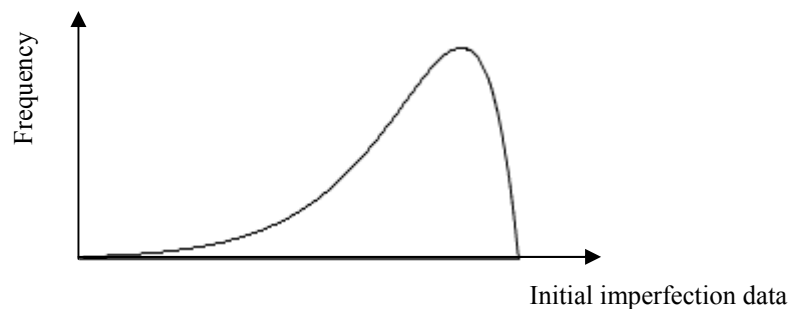


Figure 2-14: Negatively skewed distribution

The distribution function and the probability density function for this type of distribution are considered as:

$$F_{e_L}(e_L) = 1 - \exp(-e^{\mu(e_L - q)}) \quad \text{for} \quad -\infty \leq e_L \leq \infty \quad 2-6$$

$$f_{e_L}(e_L) = \mu \cdot \exp(\mu(e_L - q) - e^{\mu(e_L - q)}) \quad 2-7$$

in which  $e_L$  is initial out-of-straightness. Thus the mean value and standard deviation have the following form:

$$\bar{e}_L = q - \frac{0.577}{\mu} \quad 2-8$$

$$\sigma_{e_L} = \frac{1.282}{\mu} \quad 2-9$$

A transformed out-of-straightness term, which is mentioned to be a more mathematically trustworthy value, is introduced and considered to be equal to  $e_{La} = (e_L - q)\mu$ . Then the maximum allowable out-of-straightness is considered as  $L/1000$  and it is further assumed that the values larger than this occur with a probability of 2.5 percent. This corresponds to a value of  $e_{La}$  of 1.3. Hence

$$e_{L,max} = q + \frac{1.3}{\mu} = \frac{L}{1000} \quad 2-10$$

The smallest possible value is zero in the case of perfectly straight column. It is arbitrarily assumed that this value occurs with a probability of 1 percent and the value of  $e_{La}$  becomes  $-4.6$ . Thus:

$$e_{L,min} = q - \frac{4.6}{\mu} = 0 \quad 2-11$$

By solving the above two equations the values of  $q$  and  $\mu$  are:

$$\mu = \frac{5.9}{(L/1000)} \quad 2-12$$

$$q = 0.78 \left( \frac{L}{1000} \right) = \frac{L}{1280} \quad 2-13$$

It is seen that the most frequently occurring value of out-of-straightness is  $L/1280$ . The mean and standard deviation can then be calculated using the above values of  $q$  and  $\mu$ .

$$\text{Mean: } \bar{e}_L = q - \frac{0.577}{\mu} = 0.78 \left( \frac{L}{1000} \right) - \frac{0.577}{5.9} \cdot \left( \frac{L}{1000} \right) = \frac{L}{1470} \quad 2-14$$

$$\text{Standard deviation: } \sigma_{e_L} = \frac{1.282}{\mu} = \frac{1.282}{5.9} \cdot \frac{L}{1000} = 0.22 \left( \frac{L}{1000} \right) = \frac{L}{4600} \quad 2-15$$

Comparison with actually measured values indicates that the choice made for probability density function as Extreme Type I is reasonable (Tomonaga 1971). Figure 2-15 shows the probability density function for this initial out-of-straightness.

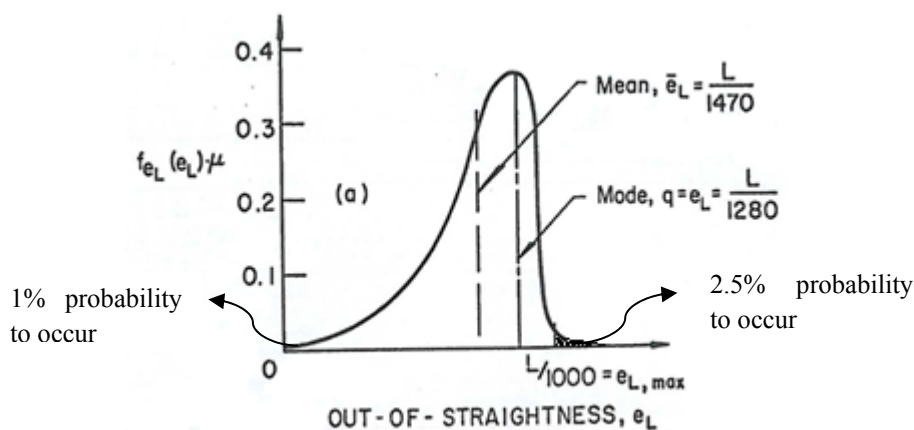


Figure 2-15: Initial out-of-straightness proposed by Bjorhovde (1972)

### 2.5.3.6.3 Fuzzy analysis method

The last method of random modelling of imperfection is the so-called fuzzy analysis and assumes both shape and magnitude as random. This method was introduced by Kala (2003) and extended in his following research (Kala 2005; Kala 2007; Kala 2007; Kala 2007; Kala 2009). The imperfection can be modelled using the following steps:

1. The axis of a member is divided into  $n$  equidistance elements (see Figure 2-16). The displacement  $y_i$  of each  $i$ -th node is a random quantity with normal distribution (Kala 2007).

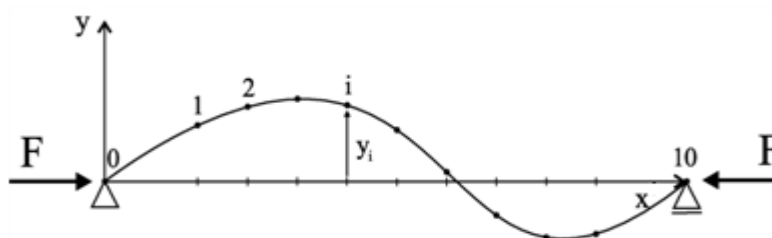


Figure 2-16: Random field of beam axis curvature

2. When the number of nodes is sufficiently large the mean value of  $y$  (nodal displacement in the direction of  $y$  axis) is approximately zero as the positive and negative values have same frequency.

$$\mu_y = \frac{1}{n} \sum_{i=1}^n y_i \approx 0 \quad \text{for} \quad i = 0, 1, \dots, n \quad 2-16$$

3. The standard deviation along the length of the member is approximately given by a sine function as follows (Kala 2007):

$$\sigma_{yi} = \sigma_{ya} \sin(\pi x_i/L) \quad 2-17$$

in which  $\sigma_{ya}$  is constant for all nodes and defined as the standard deviation of the mid span node which is the maximum one. The  $\sigma_{ya}$  can be determined in such a way that 95% of all the realizations of  $\sigma_{ya}$  lie within the tolerance of steel Specifications (see Figure 2-13). Normal or Gauss distributions are considered. The above equation shows that the standard deviation  $\sigma_{yi}$  is zero at both ends and maximum at the centre of the member which is logical.

4. To avoid unreal shapes of imperfection, a pre-selected positive correlation is introduced between deviations of neighbouring nodes. The degree of correlation amongst deviations  $y_i$  is most frequently presented by the Gauss autocorrelation function (Kala 2007), which defines the correlation amongst  $y_j$  and  $y_h$ , two neighbouring nodes by

$$\rho_{jh} = e^{-(\xi_{jh}/L_{cor})^2} \quad 2-18$$

where  $\xi_{jh} = x_h - x_j$  is the distance between nodes  $j$  and  $h$ , and  $L_{cor}$  represent correlation length of the random field. Correlation length is the distance from a point beyond which there is no further correlation associated with that point.

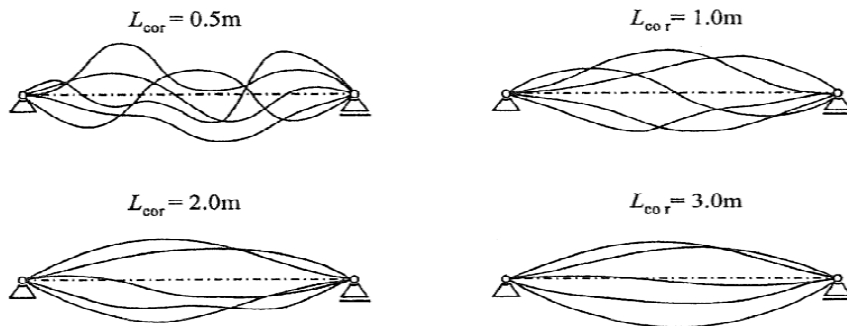


Figure 2-17: Example of the beam initial out-of-straightness, depending on the correlation length



### 2.5.3.7 Experimental data

#### 2.5.3.7.1 Initial out-of-straightness

In 1960s and 1970s numerous experiments were conducted at Lehigh University to develop new column strength curves and published as research reports. The initial geometric imperfection was measured as part of the research study but the detailed reported measurements are still limited. A total of seven experiments have been found in these reports which provide both shape and magnitude of imperfection for American W-sections, at seven levels of the column length about both axes (Tebedge, Marek et al. 1969; Tebedge, Marek et al. 1969). In addition to these data, the initial out-of-straightness of nine IPE 160 columns was undertaken at the University of Politecnico di Milano, Italy (C.E.A.C.M. 1966). Since the American sections indicated larger measured values, combining these data to determine a single histogram for initial out-of-straightness was impossible. Therefore, the experimental measurements of IPE 160 columns which seem to be more similar to Australian sections are used in this study. Nishino and Tall (1970) measured the magnitude and shape of unavoidable initial out-of-straightness for total of 16 columns including welded and rolled box and I-section. Results are provided for welded shape but the report does not have any information about the imperfection of rolled sections. Test measurements of initial geometric imperfection for a single column (10W112) can be obtained in report 290.12 (Ku and Tall 1966).

There are numerous reports and papers that provide only the mid-height imperfection values as measured numbers or as histograms. The result of these measurements for 16 heavy columns is reported by Tebedge et al. (1972). Figure 2-18 shows a histogram of non-dimensionalised initial out-of-straightness  $(f_o/l)_{max}$  for 208 columns with IPE 160 cross-sections tested by ECCS (1984) and reported by Fukumoto and Itoh (1983), in which  $(f_o)_{max}$  is the maximum initial out-of-straightness at mid-height and  $l$  is the length of the columns. The mean and standard deviation are  $\mu = 0.79/1000$  (1/1266) and  $\sigma = 0.326/1000$  (1/3068) respectively.

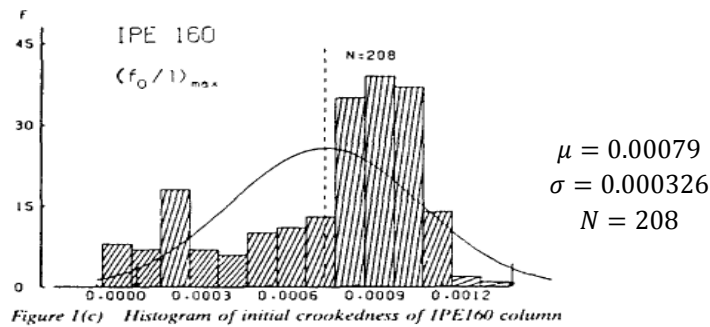


Figure 2-18: Initial out-of-straightness of IPE 160 column tested by ECCS reported by Fukumoto and Itoh (1983)

An extensive survey has been initiated by Fukumoto and Itoh (1983) on column strength tests which covers all imperfection measurements since 1950. All data are sorted in a database known as NDSS (Numerical Data-Base for Steel Structures). The  $(f_0/l)_{max}$  values for 437 of the I-section columns in NDSS have the mean and standard deviation equal to 0.501/1000 (1/1996) and 0.433/1000 (1/2310), respectively.

The statistical evaluation of 160 measurements on ECCS columns are presented by Strating and Vos (1973) and one year later by Roorda (1974). The initial out-of-straightness ( $f_0$ ) was measured for different column lengths. It is assumed that  $f_0$  follows a normal distribution. The relevant statistic characteristics such as mean and standard deviation for each column length are summarized in Table 2-3 and Figure 2-19. These reported values indicate the statistical characteristics of the amplitude of the best-fit sine wave representing the initial deflection.

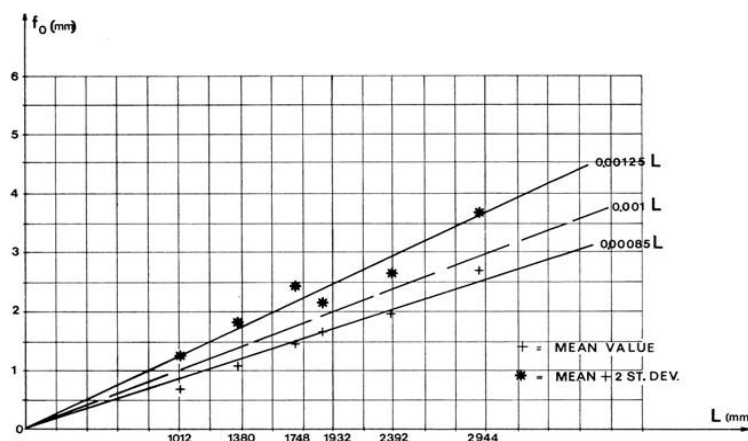


Figure 2-19: Statistical characteristics of measured imperfection by ECCS reported by Roorda (1974)

Table 2-3: Statistical characteristics of measured imperfection by ECCS reported by Roorda (1974)

Length (mm)	Number of samples	Mean, $\bar{f}_o$ (mm)	Standard deviation (mm)
1012	30	0.68 (1/1488)	0.29 (1/3490)
1380	30	1.13 (1/1221)	0.30 (1/4600)
1748	31	1.47 (1/1189)	0.50 (1/3496)
1932	30	1.65 (1/1170)	0.25 (1/7728)
2392	22	1.95 (1/1227)	0.35 (1/6834)
2944	17	2.78 (1/1059)	0.49 (1/6008)

The statistical analysis indicates that the initial deflection in ECCS columns can be fitted by a normal distribution and both mean and standard deviation can be closely approximated as linear function of length ( $l$ ) with values equal to  $0.00085l$  ( $1/1177$ ) $l$  and  $0.0002l$  ( $1/5000$ )  $l$ , respectively. The relevant histogram is shown in Figure 9.

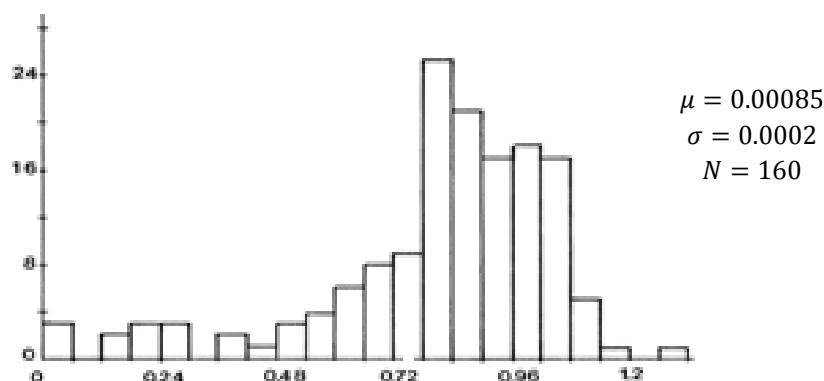


Figure 2-20: Initial out-of-straightness of columns tested by ECCS as reported by Strating and Vos (1973)

The detailed measurements of the initial out-of-straightness about the minor axis and the twist of 75 Japanese I-sections taken at five points along the length is reported by Itoh (1984). Figure 2-21 shows the histogram of non-dimensional initial imperfection at mid-span about the minor axis (Itoh 1984). The mean value of  $f_o/L$  is  $0.00008$  ( $1/12500$ ), which is about only about  $1/10^{\text{th}}$  of the ECCS mean value. The standard deviation is equal to  $0.000053$  ( $1/18868$ ).

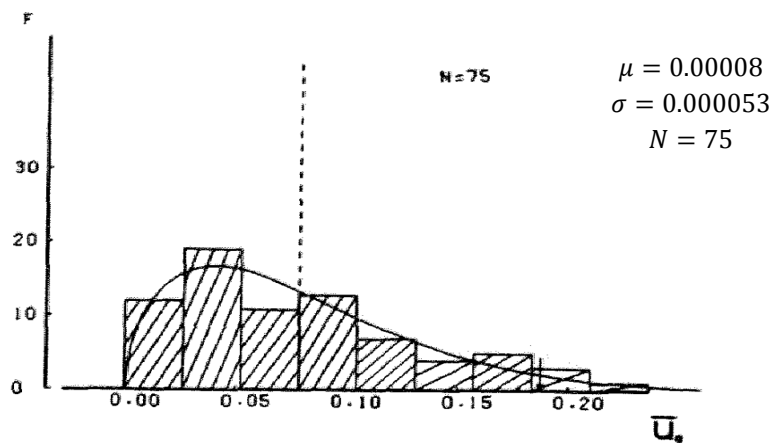


Figure 2-21: Initial out-of-straightness reported by Itoh (1984)

The results of measured out-of-straightness of 350 H-shape member, in the Kasumigaseki Building (Tomonaga 1971), the first high-rise structure in Japan, indicate that the initial imperfection seems to be smaller for Japanese section compared to European (ECCS) and American sections. The mean value of measured data is equal to 0.00025 (1/4000) and the histogram is shown in Figure 2-22.

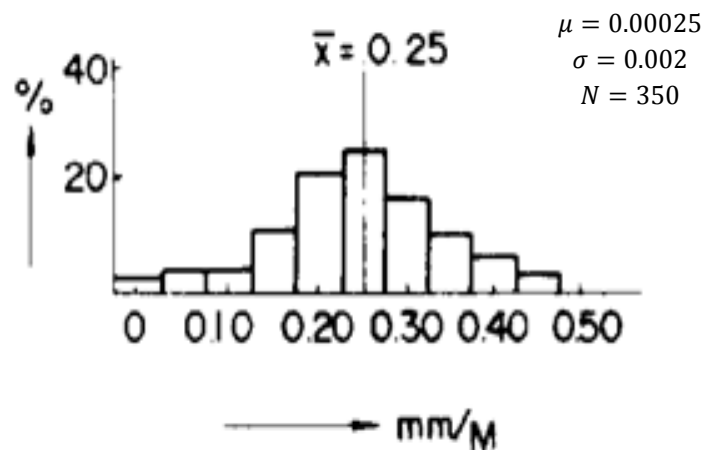
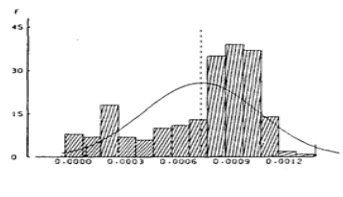
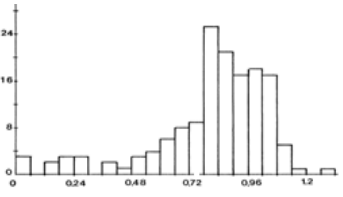
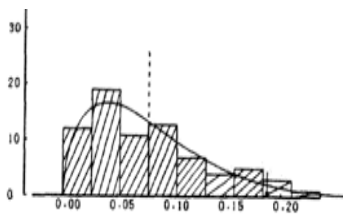
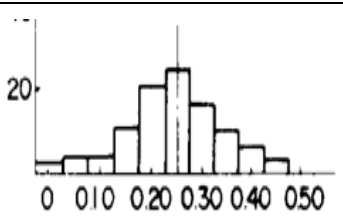


Figure 2-22: Initial crookedness measured in Kasumigaseki Building (Tomonaga 1971)

All statistical data for initial-out-of-straightness at column mid-height found in the literature are summarized in Table 2-4.

Table 2-4: Static characteristics of initial out-of-straightness from the literature

Source	Cross-section	$\mu$	$\sigma$	Number of samples	Reference	Distribution
Lehigh University	W12x161	0.0016* (l/600)	0.0006* (l/1667)	7	(Tebedg et al. 1969; Tebedge et al. 1969)	-
Politecnico di Milano University	IPE 160	0.0002* (l/5000)	0.00016* (l/6250)	9	(C.E.A.C.M. 1966)	-
ECCS	IPE160	0.00079 (l/1266)	0.000326 (l/3068)	208	(Fukumoto and Itoh 1983)	
NDSS	IAP 150 IPE 160 IPE 200 IPN160 DIE 20 DIR 20	0.000501 (l/1996)	0.000433 (l/2310)	437	(Fukumoto and Itoh 1983)	-
ECCS	IPE 160	0.00085 (l/1177)	0.0002 (l/5000)	160	(Strating and Vos 1973)	
Japanese sections (Itoh)	I 200x100x5.5x8	0.00008 (l/12500)	0.000053 (l/18868)	75	(Itoh 1984)	
Kasumigaseki Building	H 478x427x40x60	0.00025 (l/4000)	0.002 (l/500)	350	(Tomonaga 1971)	

\*The mean and standard deviation might be unreliable due to small number of samples

### 2.5.3.7.2 Initial out-of-plumb

In the erection of structural elements, additional geometrical imperfections are superimposed to those existing in members before assembly, called sway imperfection or out-of-plumb. The main cause of such imperfections is fitting the various members together and doing some adjustment on site. It can be assumed that all columns lean in the same direction (Beaulieu and Adams 1977; Buonopane 2008) or each of them has its own direction (Lindner and Gietzelt 1983 ; Lindner 1984 ; Lindner and Gietzelt 1984 ).

If the out-of-plumb is treated as a random variable, statistical data are needed to model the random values of imperfections. Very few detailed measurement studies of sway imperfections can be obtained from the literature. Histograms for the sway imperfection of a multistorey braced steel frame is provided by ECCS (1976). The horizontal displacement in both longitudinal and transverse directions of the building are reported at the first, sixth and eleventh floors (see Figure 2-23).

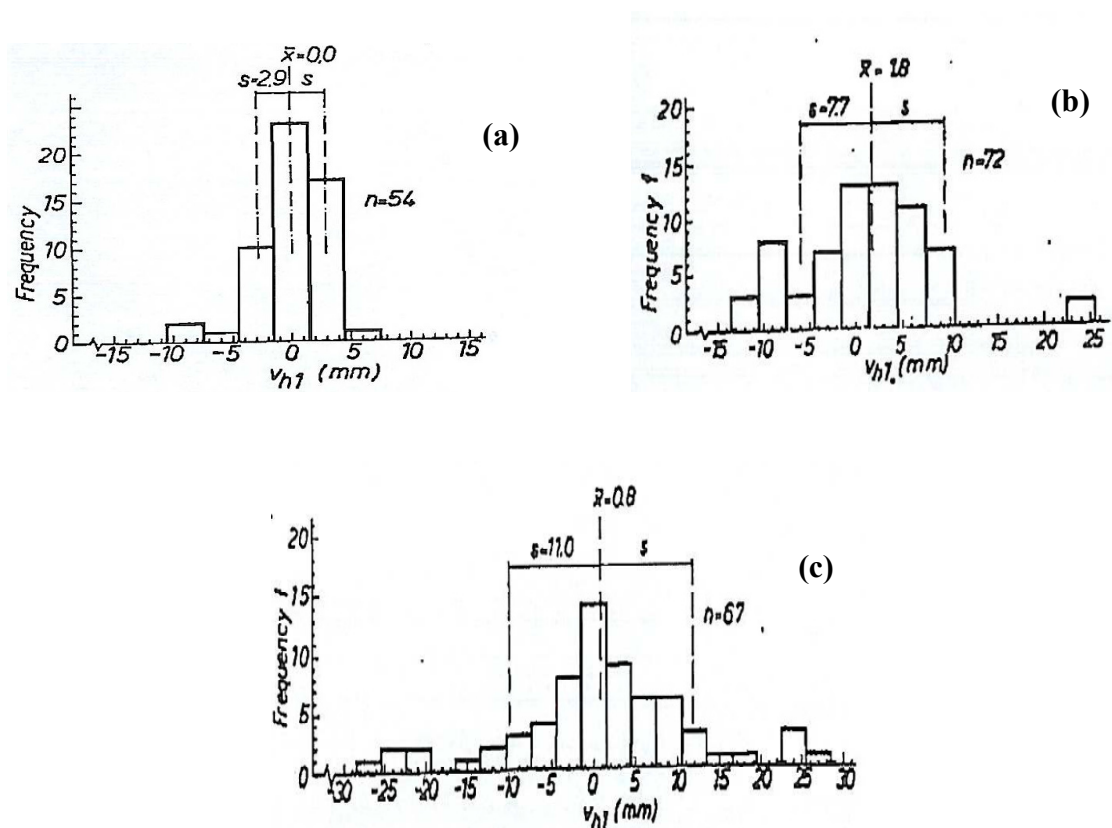


Figure 2-23: Initial out-of-plumb of a multistorey building measured by ECCS (a) first floor (b) sixth floor (c) eleventh floor

Beaulieu and Adams (1977) provides a histogram of the 916 measured out-of-plumb,  $\Delta_o/L$ , which is shown in Figure 2-24. These values are measured in a core-braced building which consists of an exterior steel frame and a central reinforced concrete core. The direction of the inclinations was recorded so that the histogram has both positive and negative values. The distribution shows the non-dimensional mean of  $-0.000044$  for  $\Delta_o/L$  and a standard deviation of  $0.00162$ .

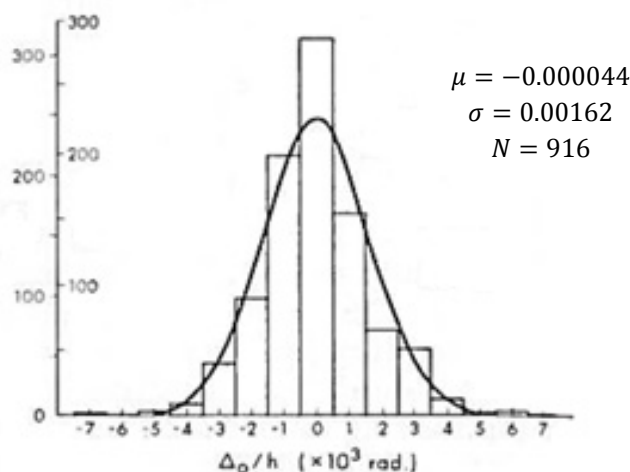


Figure 2-24: Column out-of-plumb distribution measured by Beaulieu and Adams (1977)

Extensive research in this area was carried out by Linder (Lindner and Gietzelt 1983 ; Lindner 1984 ; Lindner and Gietzelt 1984 ), who reported two groups of measurements from different buildings with different column heights. The first group of out-of-plumb measurements (approximately 725) were a second Canadian study by Beaulieu and Adams (1978) on two high rise buildings with a storey height of 3.6m. In the second group, the out-of-plumb of more than 900 German buildings with different heights between 3m and 125m were measured by Lindner and Gietzelt (1983 ). The statistical evaluations lead to a value of  $\phi=1/416$  (based on 725 measurements) and  $\phi=1/481$  (based on 909 measurements). The histograms for the absolute values of misalignment for 725 measurements can be seen in Figure 2-25, in which the mean and standard deviation are  $0.000058$  and  $0.000743$ , respectively.

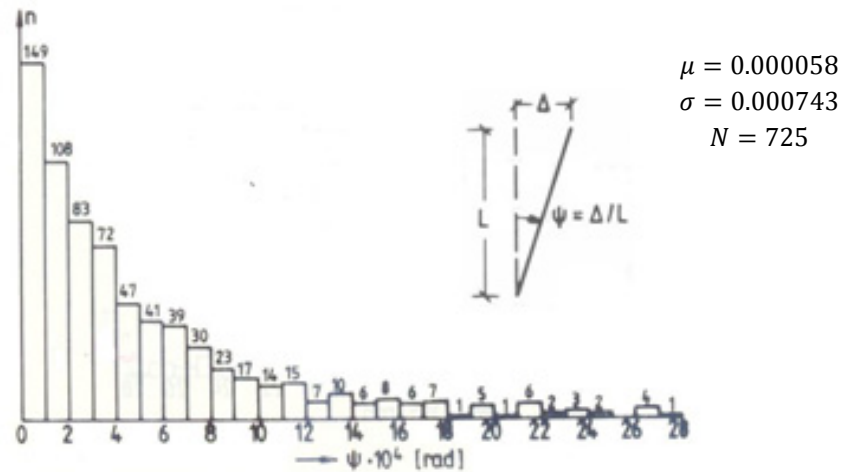


Figure 2-25: Absolute values of 725 measured out-of-plumb reported by Lindner and Gietzelt (1984)

The statistical distributions and the corresponding characteristics for the total number of 1760 measurements which include Canadian (725) and German (more than 900) measurements are presented in Figure 2-26. Both actual and absolute measurements are provided.

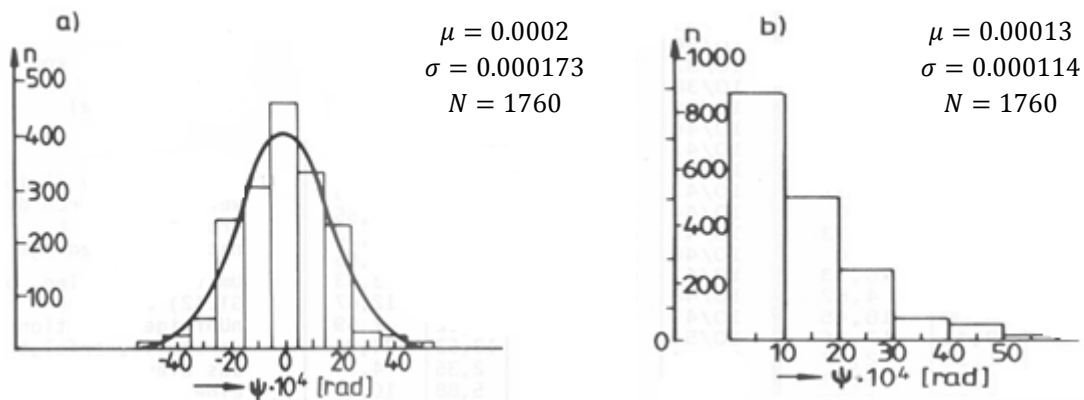
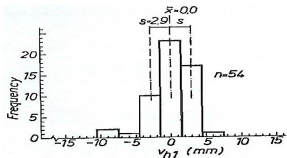
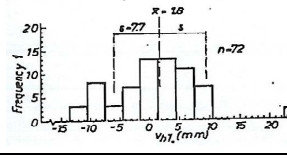
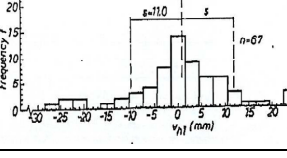
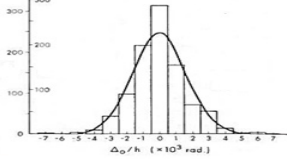
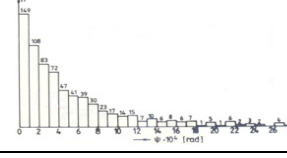
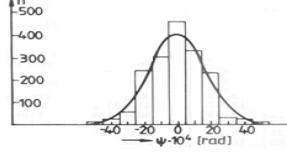
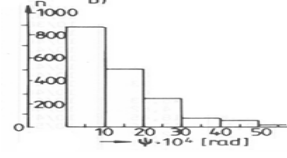


Figure 2-26: Out-of-plumb reported by Lindner and Gietzelt (1984) (a) actual values with sign (b) Absolute values

All the statistical characteristics of measured sway imperfection found in the literature are summarized in Table 2-5.



Table 2-5: Static characteristics of initial out-of-plumb from the literature

Source	$\mu$	$\sigma$	Number of samples	Reference	Distribution
ECCS (first floor measurement)	0*	2.9*	54	(ECCS 1976)	
ECCS (sixth floor measurement)	1.8*	7.7*	72	(ECCS 1976)	
ECCS (eleventh floor measurement)	0.8*	11*	67	(ECCS 1976)	
Measurements by Beaulieu and Adams	-0.000044	0.00162	916	(Beaulieu and Adams 1977)	
Measurements in Canada (absolute values) **	0.000058	0.000743	725	(Lindner and Gietzelt 1983 ; Lindner 1984 ; Lindner and Gietzelt 1984)	
Measurements in Canada & Germany (actual values)	0.00002	0.00173	1760	(Lindner and Gietzelt 1983)	
Measurements in Canada & Germany (absolute values)	0.00013	0.000114	1760	(Lindner and Gietzelt 1983)	

\*There is no information about the non-dimensional out-of-plumbness  $\Delta_0/L$ , for ECCS measurements so the absolute values of mean and standard deviation of  $\Delta_0$  in mm is reported

\*\*No histogram or detail measurements is provided for actual values with sign

### 2.5.4 Residual stress

Hot-rolled steel members usually have significant residual stresses due to uneven cooling of different section parts during the manufacturing process or by fabrication such as cold-bending or welding. These stresses which are internal stresses in an externally unloaded member are in self-equilibrium at any cross-section. For a hot-rolled I-section the portions which are most exposed to air (e.g. the flange tips) cool and shrink first before the other portions such as the flange junctions and the web which have more material inside. As it is mentioned by Szalai and Papp (2005), “the most influential parameter of the distribution and amplitude of residual stresses (considering identical manufacturing processes) is the shape of the profile”. The residual stresses in a straight hot-rolled I-section are usually compression (–) at flange tips and tension at the web to flange junction (+).

When a member is in compression, those portions of the cross-section with compressive stresses yield first and can no longer support additional load. This may lead to a significant decrease of the member ultimate load. Figure 2-27 (a) schematically shows the load-displacement behaviour of a geometrically imperfect beam-column with and without residual stresses. The effect of residual stress is plotted as a function of column slenderness in Figure 2-27 (b). It can be seen that the effect of residual stresses is significant for columns with medium length and tends to be negligible when the column slenderness is small or large. Moreover, it is shown by Buonopane (2008) that residual stress may have a significant impact on the strength of steel frames by increasing lateral deflections and thereby second-order effects. Thus, since these internal longitudinal stresses can cause material nonlinearity and premature yielding, they should be incorporated into finite element analyses of steel structures.

Extensive measurements of residual stresses have been conducted over the last 40 years (Huber and Beedle 1954; Beedle and Tall 1962; Jez-Gala 1962; Lay and Ward 1969; Young 1975) and several residual stress distribution models have been developed based on these experimental data measured in different parts of the world, e.g. Europe, Japan, Australia and America. Generally, the actual residual stress profile is complex and depends on the material properties, section geometry and the manufacturing process.

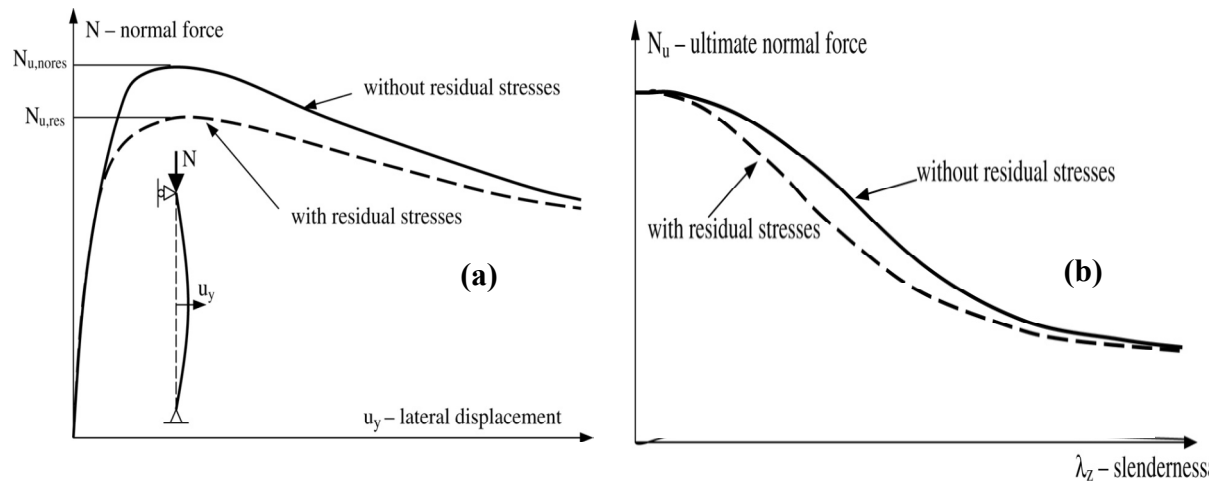


Figure 2-27: Effect of residual stresses (Szalai and Papp 2005) (a) on the ultimate strength of a column (b) on the buckling curve

### 2.5.5 Warping torsion

Thin-walled steel frames with slender open-section members may experience significant torsion and therefore large warping displacement due to applied loads. The warping deformation is generally defined as the longitudinal displacement caused by torsion. For an I-section, the warping displacement consists of longitudinal displacements of the flanges in opposite directions. Past studies of the effects of warping on the behaviour of thin-walled structures may be divided into two distinct categories: The effect of warping and end restraint (i) in an isolated member and (ii) in a joint. The boundary conditions for warping at the ends of an isolated member can be divided into three main groups: completely free, fully restrained or partially restrained. In some cases, a member is connected to a joint such that there is no restraint against warping. Such a condition applies, for example, when an I-section is connected only through its web and the flanges are free to warp (Figure 2-28 (a)). A member can also be rigidly connected to a joint which effectively prevents warping deformations. This situation may occur when the flanges of an I-section are rigidly connected to a stiffened joint (Figure 2-28 (b)). These restraints need to be taken into account in the analysis of thin-walled structures as the magnitude of warping stress can be relatively large and contribute to failure.

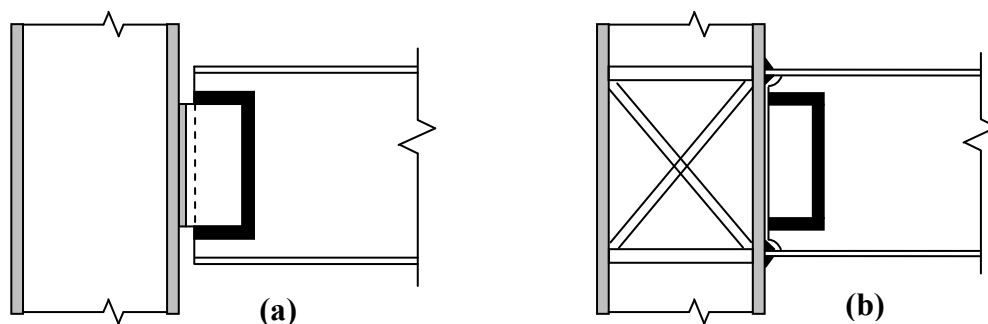


Figure 2-28: Joints configuration (a) warping free (b) warping fully prevented

Most of the early research about warping focused on the response of a single member to warping deformations regardless of the influence of other members connected at the ends. The most important contributions in this context have been made by Timoshenko (1905; Timoshenko and Gere 1961), Wagner (1936) and Vlasov (1939) who studied the warping (or non-uniform) torsion of I-beams and derived a general theory for thin-walled members. In the numerical implementation of the theory, many researchers (Trahair 1966; Krahula 1967; Krajcinovic 1969; Rajasekaran and Murray 1973; Epstein and Murray 1976; Yoo 1980) introduced the first derivative of the twist rotation as the seventh degree of freedom to represent warping deformation. Toward this objective, conventional  $12 \times 12$  stiffness matrices were replaced by the new ones with warping considered as an additional degree of freedom. In these studies, the end warping condition was assumed to be either completely free (Trahair 1966; Kitipornchai and Trahair 1971; Tebedge and Tall 1973) or fully restrained (Dinno and Merchant 1965; Razzaq and Galambos 1979; Chaudhary 1982) at both ends of the member.

The flexural-torsional behaviour of plane frames has been studied by numerous investigators, but in most cases either warping at joints was neglected by assuming six degrees of freedom for beam elements (Orbiso 1982; Liew et al. 2000; Chen et al. 2001; Kim et al. 2001; Jiang et al. 2002) or considered to be fully prevented (Renton 1962; Hartmann and Munse 1966; Trahair 1969; Chu and Rampetsreiter 1972; Vacharajittiphan and Trahair 1975). Baigent and Hancock (1982) investigated the behaviour of a joint in which the webs of two C-profiles were joined by a flat plate. In that case, the members could warp freely and independently (see Figure 2-29) and there was no need to address the problem of transmission of warping through the joint.

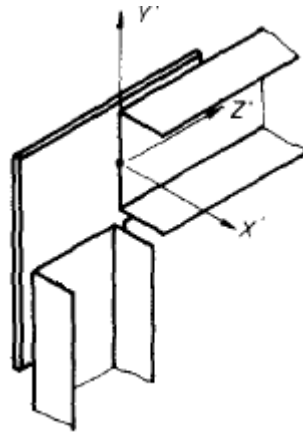


Figure 2-29: Joint configuration considered by Baigent and Hancock (1982)

In subsequent studies, the focus shifted from isolated members to frames by realising that at joints warping displacements in one member may redistribute and produce warping and twisting in other connected members. This implies that when one member warps, the flanges of adjoining members must rotate, causing a distortion of the cross-section. Thus, the resistance of adjoining members to distortion provides a level of restraint on the warping torsion of the loaded member. Several experimental works were conducted to determine the warping restraint at member ends (Dinno and Gill 1964; Ojalvo and Chambers 1977; Beerman 1980). All experiments reported the difficulties of restraining warping and demonstrated that even very stiff end connections do not provide full torsional warping restraint. Consequently, the concepts of continuous warping and partially restrained warping were introduced into research.

Austin et al. (1957) studied the subject of elastic end warping restraint but no information was given to evaluate the degree of warping restraint. Trahair (1968) introduced the ratio between the elastic flange and the fixed-ended flange moments as the degree of warping restraint. Ettouney and Kirby (1981) proposed a warping restraint factor, which is the ratio between the bimoments of the partially and fully restrained cases, similar to the warping “spring” concept introduced by Yang and McGuire (1984). For both studies, static condensation was used to eliminate undesired degrees of freedom. Although the basic idea of the two methods was same, the Yang and McGuire’s procedure seems to be more representative of partial warping restraint between two members as it operates with the warping deformation which is easier to measure than the bimoment. The model featured a hypothetical warping rigidity applied as an internal spring at the joint.

The transmission of warping torsion through the joint was investigated for two special connections by Renton (1974). It was shown that the bimoment of two members at the common node are in equilibrium and equal warping occurs between adjacent elements with the same sign for first joint (a) and opposite sign for second joint (b) (see Figure 2-30).

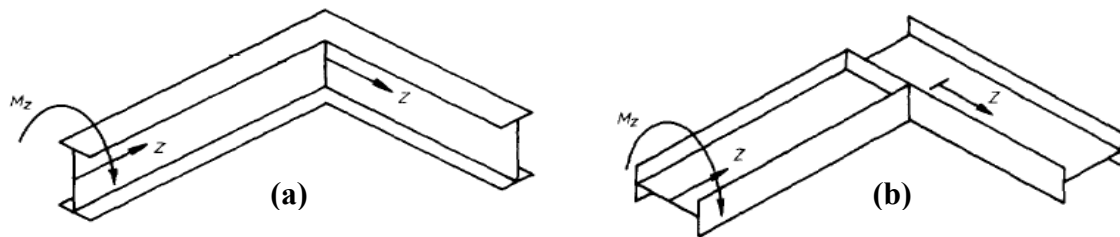


Figure 2-30: Joints details considered by Renton (1974)

Some attempts can be found in the literature to define different warping magnitudes for different members at joints. Bazant and El Nimeiri (1973) considered a unique warping deformation for all elements sharing a node and warping displacement continuity between adjacent elements was imposed on the model. A six DOF, zero-length connection element was presented to model warping deformation discontinuity at the member joints by Blandford (1990) and Chandramouli et al. (1994) (see Figure 2-31). Three moments ( $M_x$ ,  $M_y$  and  $M_z$ ), three rotations ( $\theta_x$ ,  $\theta_y$  and  $\theta_z$ ) and a linear moment-rotation relationship were considered for the joint element. Since multiple nodes were provided for different members in same location, it was possible to have different warping displacements in members connected to the joint.

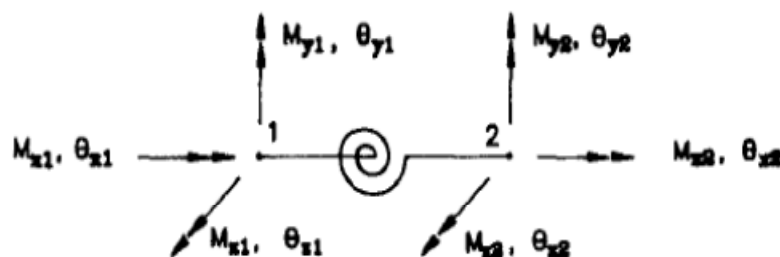


Figure 2-31: Connection element proposed by Blandford (1990)

The warping and distortion at angle joints composed from two steel I-section members of the same cross-section were investigated by Vacharajittiphan and Trahair (1975). Four types of joints were considered in the study (see Figure 2-32) which calculated numerical values of end warping restraint.

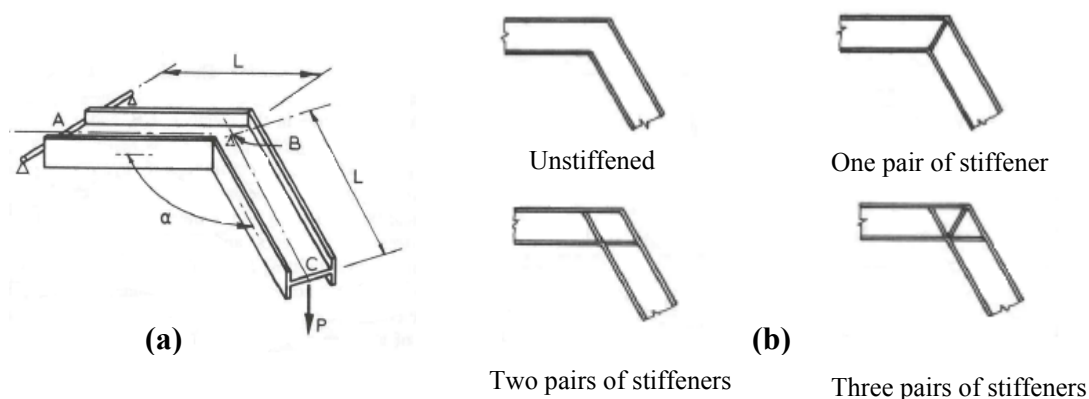


Figure 2-32: (a) Angle joint under load (b) joint stiffening arrangements (Vacharajittiphan and Trahair 1975)

The study concluded that warping and distortion are interdependent and depend on the joint configuration details. Subsequently, these particular types of joints composing two or more channels or I-sections were studied by Sharman (1985), Krenk and Damkilde (1991), Morrell et al. (1996), Masarira (2002), Tong et al. (2005), Camotim et al. (2010) and Basaglia et al. (2009; 2010) to determine the effect of warping transmission through the joints. To investigate the behaviour of these joints, Krenk and Damkilde (1991) considered the continuity conditions for the flanges to express the distortion in terms of warping parameters of the two beams at the joint. They developed a simple method to formulate two elastic-energy components associated with warping and distortion at beam ends. It was concluded that the unstiffened joint has two independent warping parameters while the joints with one and two stiffeners impose equal magnitudes of warping in the connected beams. This result was also proved by Sharman (1985). The joint with three stiffeners provides full warping restraint.

An important contribution to the research on the transfer of warping through joints was presented by Basaglia et al. (2009; 2010) and Camotim et al. (2010) using a numerical model which considered transmission of warping torsion and local displacement

compatibility at frame joints of various configurations. The results of the model were compared with shell element FE analysis using ANSYS and excellent agreement was achieved.

## 2.6 Reliability analysis

Many sources of uncertainty are inherent in structural design. Consequently, structures must be designed to serve its function with low probability of failure. Structural reliability analysis is concerned with treating the uncertainties associated with the design of structures in a rational manner and assess the structural safety. Uncertainties result from the unpredictability of loads and material strength properties, dimensions, natural hazard, insufficient knowledge and human errors during both design and construction phases. The fundamental reliability analysis of technical systems and components is to evaluate the probability of failure ( $P_f$ ) of the structure as defined by:

$$P_f = P(R - Q \leq 0) = P(G(R, Q) \leq 0) = \int F_R(x) f_Q(x) dx \quad 2-19$$

in which  $R$  is the structural resistance and  $Q$  is the total load effects,  $R$  and  $Q$  are modeled as random variables,  $G(R, Q)$  represents the limit state function and  $G(R, Q \leq 0)$  defines the unsafe or failure region,  $F_R(x)$  is the cumulative distribution function of  $R$ , and  $f_Q(x)$  is the probability density function of  $Q$ . Despite the deterministic formwork of common design specifications, both  $R$  and  $Q$  and the quantity  $R - Q$  are random variables with probability density functions (PDF) as shown in Figure 2-33.

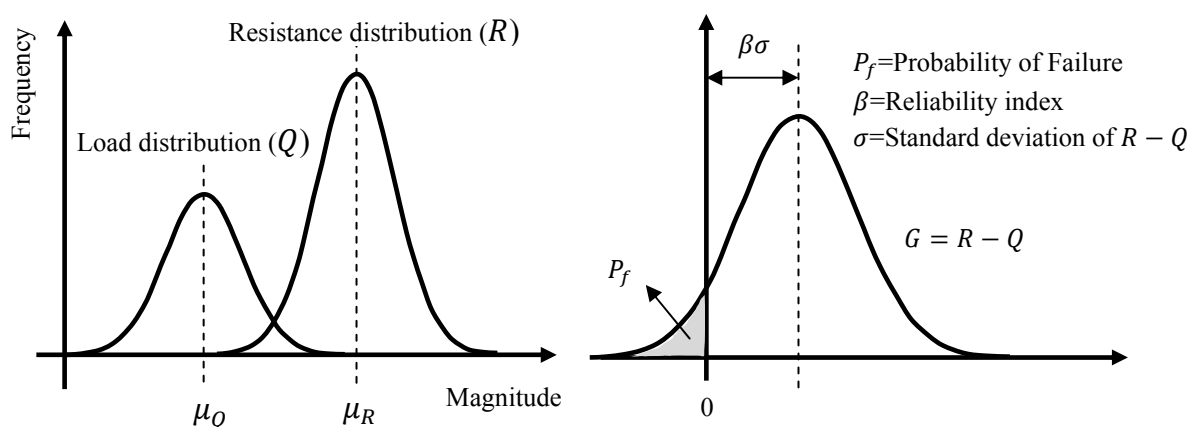


Figure 2-33: Structural reliability problem, PDF of load, resistance and safety margin



If both  $R$  and  $Q$  are independent normal variables and the space of the state variable is a two-dimensional space as shown in Figure 2-34, the “safe domain” is separated from the “failure domain” and the boundary between the two domains is described by the limit state function of  $R - Q = 0$ .

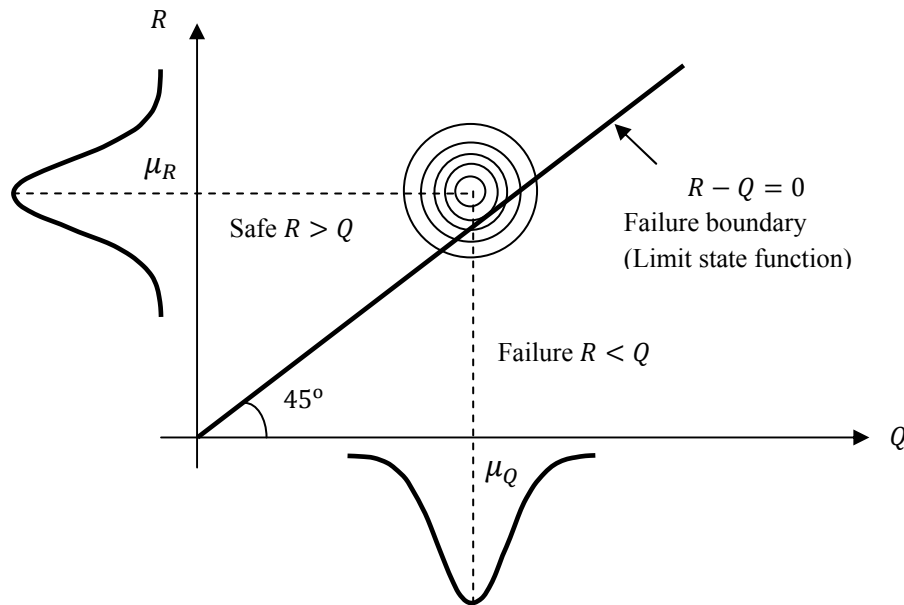


Figure 2-34: Safe domain and failure domain in a two-dimensional space

As an alternative, the concept of a reliability index ( $\beta$ ) was introduced by Hasofer and Lind (1974) as a quantitative measure of structural safety. Generally, the reliability index is evaluated as a function of means and standard deviations of load and resistance. For convenience, the random load and resistance can be converted to their “standard form” as following:

$$R = \mu_R + Z_R \sigma_R \quad 2-20$$

$$Q = \mu_Q + Z_Q \sigma_Q \quad 2-21$$

The variables  $Z_R$  and  $Z_Q$  are called reduced variables. The limit state function can also be expressed in terms of standard the reduced variable  $G(Z_R, Z_Q) = 0$ . In this case, the reliability index is defined as the shortest distance from the origin of reduced variables to the line of  $G(Z_R, Z_Q) = 0$  as presented in Figure 2-35. The probability of failure can then be defined in terms of the reliability index:

$$P_f = \Phi\left(-\frac{\mu_R - \mu_Q}{\sqrt{\sigma_R^2 + \sigma_Q^2}}\right) = \Phi(-\beta) \quad 2-22$$

where  $\Phi()$  is the standard normal distribution function,  $\mu$  and  $\sigma$  represent the mean and standard deviation respectively.

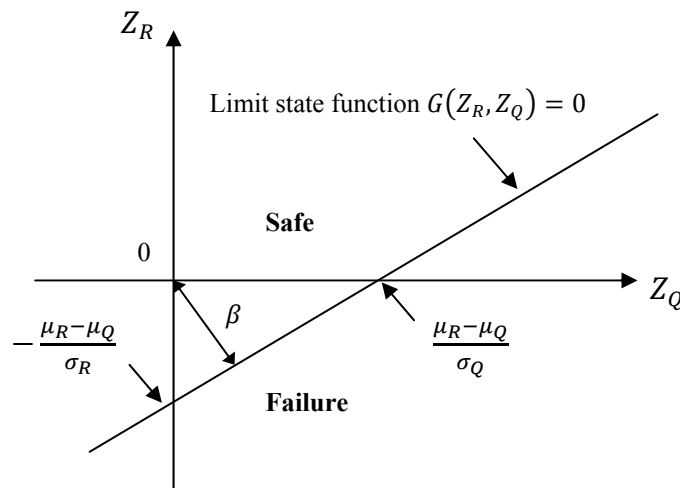


Figure 2-35: Reliability index defined as the shortest distance in the space of reduced variables

## 2.7 Simulation methods

Solving Equation 2-19 in closed-form is impossible and difficulty in computing probability has led to the development of numerous analytical and numerical techniques. These techniques can further be classified into either simulation methods such as direct Monte-Carlo (MC) or approximation methods such as FORM (First Order Reliability Method) or FOSM (First-order Second Order Reliability Method). For small problems with few random variables the approximation methods such as FORM and FOSM are efficient (Frangopol and Moses 1994) but for more complex problem with many random variables MC simulation seems to be more reliable (Papadrakakis and Papadopoulos 1995).

### 2.7.1 First-order Reliability Method

Among all approximation methods, first-order reliability method is considered to be one of the most reliable computational methods. The most basic type of FORM is the first-order second-moment reliability method (FOSM) which is based on the first-order Taylor series approximation of the performance function using mean values of random variables. This method is also referred as Mean Value First-Order Second Moment method (MVFOSM). A Taylor series of the linear performance function is given as

$$g(X_1, X_2, \dots, X_n) = a_0 + \sum_{i=1}^n a_i X_i \quad 2-23$$

where the  $a_i$  terms ( $i=1,2,\dots,n$ ) are constants and the  $X_i$  terms are uncorrelated random variables. By expressing the limit state in terms of the reduced variables ( $Z_i$ ) and finding the shortest distance from the origin in the n-dimensional space of reduced variable as explained in Section 2.6, the reliability index can be determined as:

$$\beta = \frac{a_0 + \sum_{i=1}^n a_i \mu_{X_i}}{\sqrt{\sum_{i=1}^n (a_i \sigma_{X_i})^2}} \quad 2-24$$

This method uses only second moment statistics (mean and standard deviation) of random variables to calculate  $\beta$  while ignoring the information regarding their probability distributions. If the random variables are uncorrelated and defined by normal distributions, this method can exactly predict the reliability index and probability of failure. Otherwise it only provides an approximation of  $\beta$ .

Later, Hasofer and Lind (1974) proposed a modified approach called Hasofer-Lind reliability index by evaluating the limit state function at a point known as the “design point” instead of the mean values. The design point is a point on the failure surface of  $G=0$ . For these methods the detailed information on the distribution type for random variables are not taken into account. The Hasofer-Lind reliability index method can be generally considered as the first-order second-moment mean value method when the limit state function is linear. However, when the limit state function is nonlinear, since the

design point is generally not known a priori, an iteration method is required to determine the reliability index.

The procedures to calculate the reliability index can be improved by considering the probabilistic distributions of all random variables (Rackwitz et al. 1978). The basic idea of this procedure, which is generally called First Order Reliability Method (FORM), is to calculate the “equivalent normal” values of the mean and standard deviation for each non-normal random variable and use them in the iterative analysis. It requires the following steps as set out by Nowak and Collins (2000):

(1) Formulate the limit state function ( $G$ ) and determine the probability distributions with appropriate parameters for all random variables  $X_i$  ( $i = 1, 2, \dots, n$ ) involved.

(2) Acquire an initial design point  $\{x_i^*\}$  by assuming values for  $n - 1$  of the random variables  $X_i$  (usually mean values). The limit state equation  $G = 0$  can then be solved for the remaining random variables. This ensures that the design point is on the failure boundary.

(3) Determine the equivalent normal mean ( $\mu_{x_i}^e$ ) and standard deviation ( $\sigma_{x_i}^e$ ) for each design point ( $x_i^*$ ).

(4) Calculate the reduced variates ( $z_i^*$ ) corresponding to the design point ( $x_i^*$ ) using

$$z_i^* = \frac{x_i^* - \mu_{x_i}^e}{\sigma_{x_i}^e} \quad 2-25$$

(5) Compute the partial derivatives of the limit state function with respect to reduced variates and define a column vector  $\{G\}$  as the vector with elements of partial derivative multiplied by  $-1$ :

$$\{G\} = \begin{Bmatrix} G_1 \\ G_2 \\ \cdot \\ \cdot \\ \cdot \\ G_n \end{Bmatrix} \quad \text{where } G = -\frac{\partial g}{\partial z_i} \Big|_{\text{evaluated at the design point}} \quad 2-26$$

(6) Determine an estimate of  $\beta$  using the following equation:

$$\beta = \frac{\{G\}^T\{z^*\}}{\sqrt{\{G\}^T\{G\}}} \quad \text{where } \{z^*\} = \begin{Bmatrix} z_1^* \\ z_2^* \\ \cdot \\ \cdot \\ \cdot \\ z_n^* \end{Bmatrix} \quad 2-27$$

(7) Find a new design point in reduced variates for  $n - 1$  of the variables from

$$z_i^* = \alpha_i \beta \quad 2-28$$

(8) Calculate a column vector containing the sensitivity factors using

$$\alpha = \frac{\{G\}}{\sqrt{\{G\}^T\{G\}}} \quad 2-29$$

(9) Calculate the values of corresponding design point in original coordinates for the  $n - 1$  using

$$x_i^* = \mu_{x_i}^e + z_i^* \sigma_{x_i}^e \quad 2-30$$

(10) Solve for the value of the remaining random variable by the setting the limit state function  $G = 0$ .

(10) Repeat steps 3 to 10 until  $\beta$  and the design point  $\{x_i^*\}$  converge.

### 2.7.2 Monte-Carlo (MC) method

The Monte Carlo (MC) method is useful for reliability prediction when the system complexity makes the use of approximation methods such as FOSM and FORM unreliable. Monte Carlo simulation technique is a tool to solve the probability integral presented in Equation 2-19 over the failure domain. This method relies on random sampling from random variable distributions to obtain the numerical estimate probability of failure. The most basic version of Monte Carlo technique is called “crude” or “direct”

Monte Carlo simulation in which pseudo-random sampling is used. That method is quite simple and easy to implement as there are only a few requirements that makes the method applicable to very difficult integration problem. The expected error is in order of  $1/N^{-1}$  in which  $N$  is the number of samples and it is fairly independent of the number of random variables. However, if the probability of failure is small the direct MC method demonstrates a poor computational efficiency and needs large number of samples to achieve an estimate of probability of failure with sufficient accuracy. The convergence rate, which means how quickly the error decreases with the number of samples, is proportional to  $1/N^{-1}$ . This means that to halve the error, four times more samples are required. As an alternative to improve the classical Monte Carlo simulation, quasi-random sequences can be used instead of pseudo-random samples which leads to what is known as Quasi-Monte Carlo (QMC) method. These sequences are totally deterministic and used to generate the representative samples from the probability distribution. The quasi-random sequences, also called low-discrepancy sequences, improve the performance of Monte-Carlo simulations, offering shorter computational time and achieving a given accuracy by far fewer samples. The rate of convergence of the Quasi-Monte Carlo method is in order of  $1/N$ .

## 2.8 Sampling techniques

Sampling methods can be classified into the two distinct groups of completely random such as pseudo-random and deterministic point sets such as low-discrepancy sequences. Low-discrepancy point sets utilize more uniformly distributed points in a systematic fashion. Several methods for producing low-discrepancy points have been proposed in which the sample area is filled more efficiently with a lower discrepancy than a pseudo-random number set. Several techniques exist that lead to different solutions for the generation of quasi-random variables. The best known approaches are named Good Lattice Point (GLP) set, Hua-Wang (H-W) point set, Latin-Hypercube set, Halton sequence and Hammersley sequence. The details of these approaches are presented by Dai and Wang (2009). A popular method to compare the uniformity of low-discrepancy sampling methods against pseudo-random methods is to plot their two-dimensional projection (see Figure 2-36).

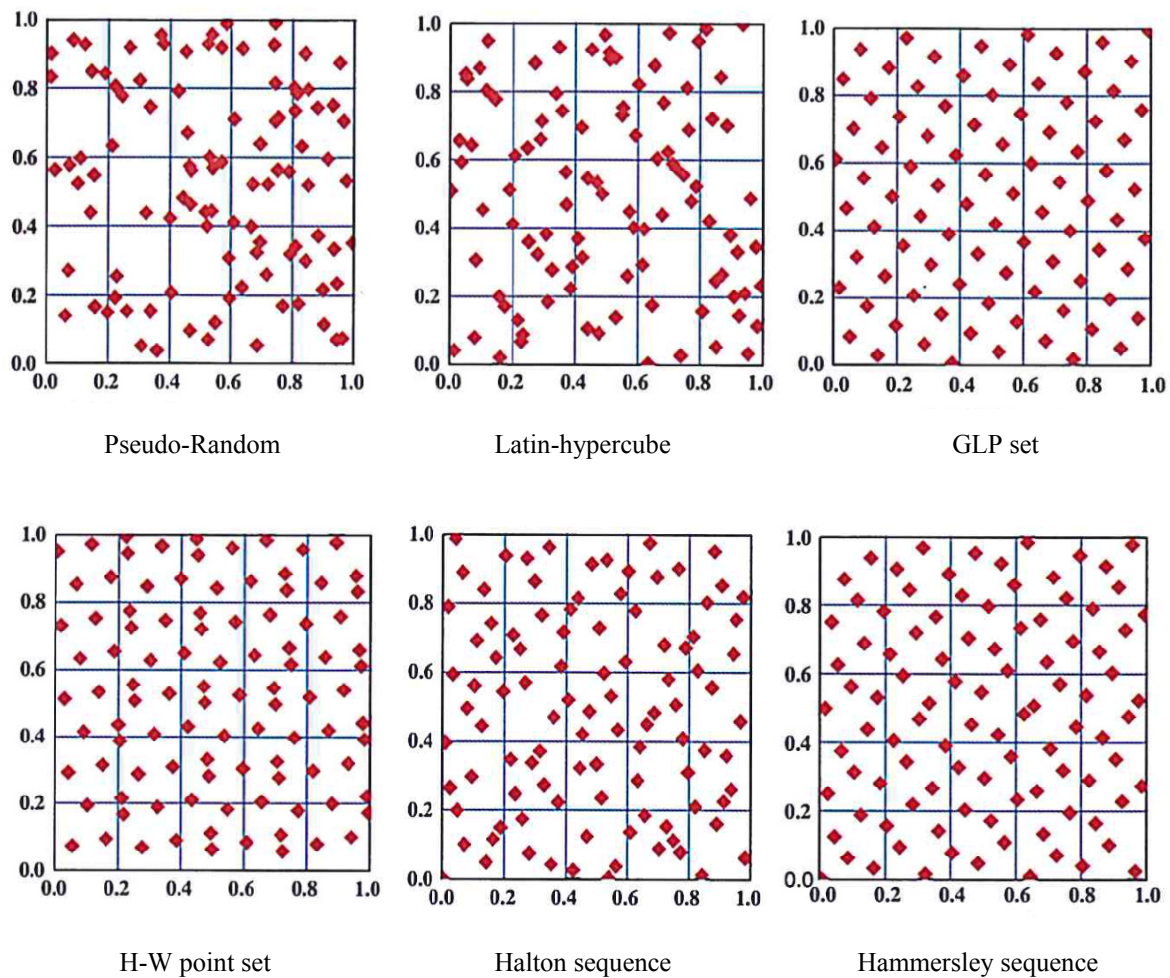


Figure 2-36: Two-dimensional scatter plots of different point sets

As seen in Figure 2-36, the quasi-random techniques result in more uniform distribution of randomly generated variables. This leads to faster rate of convergence and less error in predicting the probability of failure. The major drawback of most of these methods is that the low-discrepancy sequences generally lose their improved accuracy in high dimensional problems due to correlation between two neighbouring components of the points (see Figure 2-37). There are several ways to break or decrease this correlation. The most useful way is scrambling the points (Chai et al. 2005).

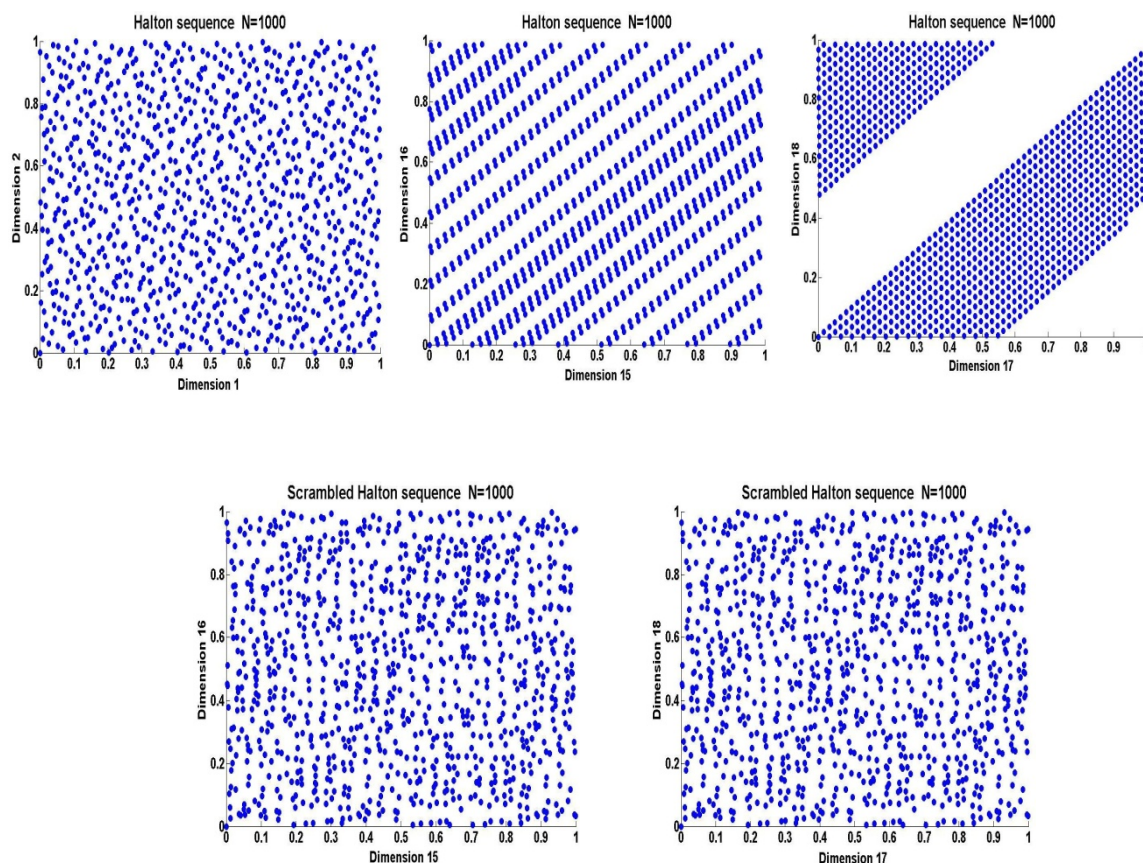


Figure 2-37: Halton sequence and scrambled Halton sequence

One of the low-discrepancy methods which does not suffer from the correlation in high-dimensional problem is Latin-Hypercube sampling. Latin hypercube sampling was first introduced by McKay et al. (1979) and has been further extended for different purposes by several researchers (Iman and Conover 1982; Olsson and Sandberg 2002). In this method the probability distribution is split into  $n$  intervals or “strata” of equal probability, where  $n$  is the number of iterations that are to be performed on the model and a value from each interval is randomly selected as a representative value. The representative value for each random variable are then combined so that each representative value is considered once and only once in the simulation process (Nowak and Collins 2000). In this way, all possible values of the random variables are presented in the simulation. Figure 2-38 illustrates an example of the stratification that is produced for 20 iterations of a normal distribution. It should be noted that this sampling scheme does not require more samples for more variables and this independence is one of the main advantages of the Latin hypercube sampling (LHS) method which might appear in problems with larger number of uncertain parameters.



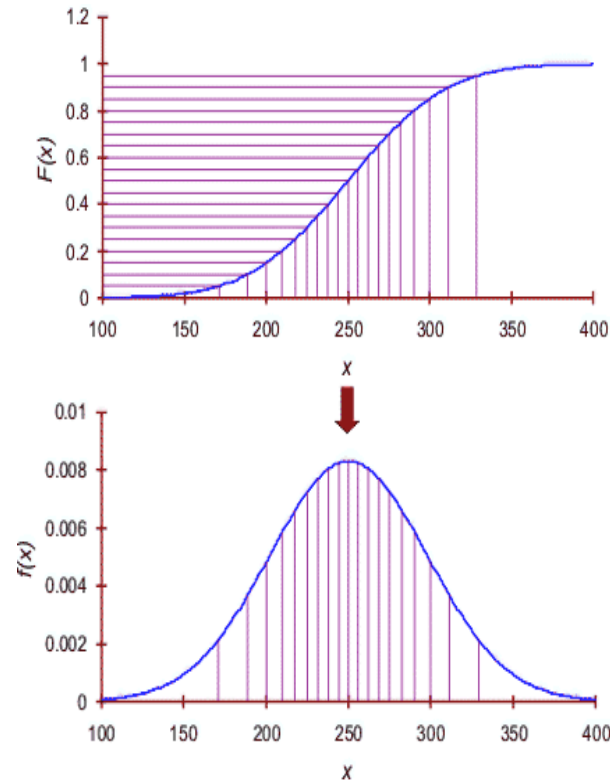


Figure 2-38: Latin-Hypercube sampling

To evaluate the rate of convergence, a simple example is considered where a Normal (1, 0.1) distribution is simulated for 100 iterations with both Monte Carlo sampling and LHS. The mean of generated values versus number of simulation is plotted in Figure 2-39.

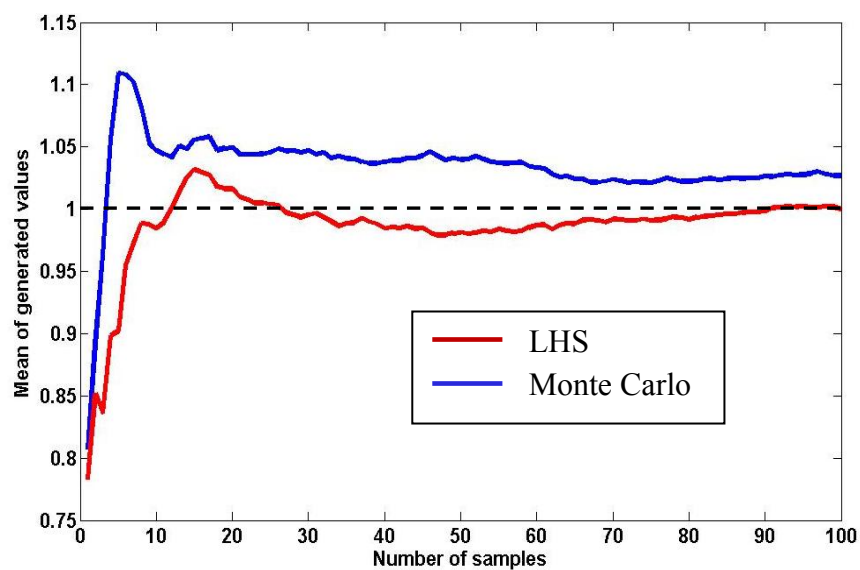


Figure 2-39: Evaluating the rate of convergence using both Monte Carlo and LHS

It is clearly visible that more monotonous convergence behaviour is obtained by using Quasi-Monte Carlo method with Latin-Hypercube sampling technique. Latin hypercube sampling (LHS) is very efficient for estimating mean values and standard deviations in stochastic structural analysis (Olsson and Sandberg 2002) while it is only slightly more efficient than the Direct Monte Carlo for estimating small probabilities (Pebesma and Heuvelink 1999). Therefore, this method is used to determine the statistical characteristic of system strength in this study while the probability of failure is evaluated by simplified FORM.

## **2.9 Code development procedures**

A structural design code is a practical tool, in the sense that if all the requirements are followed by a designer, the resulting structure would be expected to be sufficiently safe and serviceable during the expected life period. However, at the design stage, some matters are not known with any degree of certainty and can only be predicted. The way that a code addresses these uncertainties will affect the expected utility of any structure designed according to it. Current codes have a deterministic format, however the effect of uncertainties is considered through the application of safety factors. Depending on the approach to structural reliability, there are four levels of design codes (Nowak and Collins 2000):

Level 1- Codes use deterministic design formula. The safety margin is introduced through central safety factors (ratio of design resistance to design load) or partial safety factors (load and resistance factors).

Level 2- Codes provides the design acceptance criterion in terms of the “closeness” of the actual reliability index for a design to the target reliability index or other safety-related parameters.

Level 3- Codes require a full reliability analysis to quantify the probability of failure of the structure under various load combinations. The acceptance is defined in terms of the closeness of the actual reliability index to the optimum reliability level.

Level 4- Codes use the total expected cost of the design as the optimization criterion. The acceptable design maximises the utility function, which describes the difference between the benefits and cost associated with a particular design.

The current design codes are basically based on Level 1 code philosophy but to derive the design parameters (load and resistance factors) a Level 2 method was used. The next generation of design codes (system-based design codes), which this study aims to formulate a framework for, will be based on the same deterministic methodology but employ refined probabilistic approaches based on the Level 3 procedure.

## **2.10 Structural safety and target reliability**

Structural failures are always undesirable events. Therefore, as mentioned before structural codes provide a set of technical requirements for safe and acceptable design by implying satisfactory reliability levels into design process. The meaning of “satisfactory safety level” has been addressed for centuries by many researchers. Generally, a structure is designed as safe if it can survive for a number of years without collapse. To achieve a uniform performance for various design situations, the acceptable safety levels must be established. Probabilistic limit state design is based on the notion of a “target” reliability as a quantitative measure of structural safety. Selecting acceptable reliability targets for structural engineering is a difficult task because these values are not readily available and need to be generated or selected by either engineering judgment or assessing the reliability of existing designed frames. In the LRFD specification, the target reliability indices for different steel members range between 2.5 and 3 (Ellingwood and Galambos 1982). Generally, the reliability of redundant structural systems is higher than the reliability of a single member. To calibrate a new design code, the average reliability index from existing structures, which are classified as “safe” designs, is used as target reliability. Target reliability indices ( $\beta$ ) obtained from the literature for different members and systems are summarized in Table 2-6.

Table 2-6: Recommended target reliability index in literature

Structural type	Target Reliability	System/member	Reference(s)
Steel tension member (yield)	3.0	member	(Ellingwood and Galambos 1982)
Steel beam	2.5	member	
Steel column (intermediate slenderness)	3.5	member	
Reinforced concrete beam	3.0	member	
Reinforced concrete tied column	3.5	member	
Masonry unreinforced wall in compression	5.0	member	
Steel beam	2.6	member	(AISC 1987)
Steel column	2.7-3.6	member	
Connection	4.0-6.0	member	
Frame instability under factored gravity loads	4.0	system	(Galambos 1990)
Frame instability under factored gravity loads with cladding	3.0	system	
Rigid frame	2.5	system	
Pile group	3.0-3.5	system	(Zhang al. 2001)
Steel portal frames with tapered members	3.7	system	(Li and Li 2004)
Cantilever retaining walls	3.0-3.2	system	(Sivakumar Babu and Basha 2008)

## 2.11 Conclusion

Substantial research has been devoted to provide guidelines for the modelling, analysis and design of steel structures. This thesis aims to change the paradigm of steel structural design to be based on advanced analysis and provides the basis for next generation of steel structural design codes. Shifting the focus of design from component-based design to system-based design requires a good knowledge of structural behaviour and past studies in this regard. This literature review provides an overview of current guidelines and conventional steel design methods which are based on safety checks of individual members. All factors influencing the ultimate strength of a steel frame including material and geometric nonlinearities, warping torsion and its transmission through the joints, initial geometric imperfection and residual stresses are discussed in this chapter. Among

them, initial geometric imperfection and warping torsion have been reviewed in detail, since new procedures to model these parameters are developed in following chapters. The chapter summarizes the most common reliability analysis and sampling methods. Clearly, one of the most important moves towards the development of the next generation of steel design codes based on system behaviour is to choose an acceptable safety or reliability level which is called “target” reliability. Finally, different values of target reliability obtained from the literature for members and systems are summarized in this chapter.

# CHAPTER

## 3 .

# Advanced analysis models of steel structural systems

---

## 3.1 Introduction

An analysis method can be classified as advanced analysis if all the factors influencing the frame ultimate strength such as material nonlinearity (yielding), geometric nonlinearity (second order effects,  $P - \Delta$  and  $P - \delta$ ), initial geometric imperfections and residual stresses are taken into account. In European terminology this type of analysis is denoted as “GMNIA, Geometric and Material Non-linear with Imperfections Analysis”. A great deal of research has been devoted to advanced analysis of steel structures over the past 20 years (Ziemian 1990; Liew et al. 1993; Chen and Kim 1997). Several guidelines in this regard as well as finite element packages like ABAQUS (2009), ANSYS (2000), NASTRAN (1998), NAF-NIDA (2001) and LUSAS (1998) are well established for advanced analysis of steel structures. Many of these proposed analytical models for advanced analysis are calibrated based on full-scaled tests (Toma and Chen 1992; Toma et al. 1993; Toma and Chen 1994; Kim et al. 2006). The literature shows a wealth of

articles demonstrating that the structural behaviour of systems subject to complex failure modes and/or complex material characteristics can be modelled accurately using advanced finite element software.

Advanced analysis, is also permitted by several design specifications for steel structures. Appendix D of the Australian Steel Structures Standard (AS4100 1998) provides provisions for this type of analysis and states that the members must have compact cross-sections with full lateral restraint to prevent the local buckling and flexural-torsional buckling. The Frame ultimate limit state can be directly obtained by advanced analysis but there is no information provided about the system resistance factors. The Australian provisions for advanced analysis are based on research by Clarke et al. (1992; 1993) aimed at developing “distributed plasticity” analysis models. The “Inelastic Analysis” provisions of Appendix 1 of the AISC360-10 (2010) Specifications allows the geometric and material nonlinear (advanced) analysis to be adapted for accurately determining the internal actions and the frame ultimate strength. The inelastic provision of American standard is based on the large displacement “plastic hinge” type methods proposed by Ziemian et al. (1992), Ziemian and McGuire (2002), Surovek-Maleck and White (2004) and White et al. (2006). The European analysis provisions (Eurocode 3 2005) are based on early research by Horne (1985) and more recent research by Nethercot (2000) and Davies (2002). They implicitly assume 1<sup>st</sup> or 2<sup>nd</sup> order elastic analysis.

Advanced analysis method, if properly implemented in a finite element model, can simplify the design procedure and directly predict the full-range load-deflection response of the frame system. Thus, it is important to have an appropriate finite element model that accounts for all factors influencing the system strength. This chapter presents structural guidelines and modelling requirements for the advanced analysis of a steel structural system. Details about elements selection, material properties, residual stress and structural collapse are summarized in this Chapter. Finally, the finite element model is calibrated against frames from the literature and an excellent agreement is achieved.

## 3.2 Finite element model

In this research, two-dimensional second-order inelastic FE models are developed as a nominal model using one of the most widely used commercial finite element software, ABAQUS (2009). The model details are described in Section 3.3 to 3.7 in order to provide a general guide for advanced analysis of steel frames. There are two types of nonlinear static analysis available in ABAQUS: \*STATIC and \*STATIC, RIKS. The former option traces the load-deflection response of a structure up to the limit state (ascending branch), using the Newton–Raphson solution technique while the later option is able to capture both the ascending and descending parts by applying the arc-length method for solving the equilibrium equations. This method has the ability to change the increment size depending on the nonlinearity of the solution. If the solution is largely linear, the increment size is allowed to increase rapidly while for highly nonlinear analysis the increment size decreases to capture the nonlinearity. The analysis will continue for the specified number of increments defined at the beginning of the analysis. Since we are interested in the post-failure behaviour of the structure, in this study the \*STATIC, RIKS option is used with the minimum and maximum increment sizes of 0.01 and 10, respectively. The non-linear statement of analysis (\*STEP, NLGEOM) is used to take into account the effect of geometric nonlinearity. The plastic-zone formulation is used to model the gradual spread of plasticity across the monitored cross-section and along the elements. As a consequence of the path-dependent nature of plasticity, the current stress and the current level of equivalent plastic strain are stored at each monitoring point and updated incrementally throughout the analysis.

In this research, to model the structural elements of the frame system, nonlinear beam elements are used as described in Section 3.3. A beam in this context is an element in which assumptions are made so that the problem is reduced to one dimension mathematically which is less computational expensive. Recommendations for element selections are subsequently provided. The FE model is then calibrated against the ultimate load and displacement responses of existing frames in the literature in Section 3.8. Finally, a mesh sensitivity analysis is conducted in Section 3.9 to determine the optimum number of elements to use in FE analysis.



### 3.3 Elements

In finite element analysis, the analysis results are very sensitive to the types of elements used. ABAQUS element library contains many different element types for performing various analyses. The ABAQUS three-dimensional Timoshenko beam element types, which allow for transverse shear deformation, are used in this study. The elements are denoted as B31 (two-node beam based on linear interpolation), and B32 (three-node beam based on quadratic interpolation). Both beam elements are modelled in space with six degrees of freedom at each node. The ABAQUS B31 has one integration point along the beam length while the B32 element defines with two integration points as it is shown in Figure 3-1. If warping and flexural torsional buckling are required to be captured in the analysis these elements must be converted to B31OS and B32OS, in which the term “OS” shows the open-section nature of the elements. These elements indicate seven degrees of freedom in which the seventh is warping.

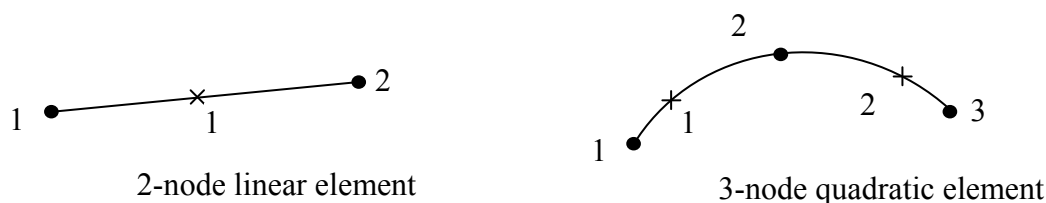


Figure 3-1: Integration points of (a) two-node, linear beam (B31) and (b) three-node, quadratic beam (B32) elements of ABAQUS

In this study all cross-sections are fully compact hot-rolled I-sections and the out-of-plane behaviour is restrained. Thus, local buckling and lateral-torsional buckling are not considered in this study. All members have their webs in the plane of the frame. Since the focus of this study is on two-dimensional frames the 3D beam elements have more degrees of freedom than needed in a plane analysis. However, the distribution of default section points in ABAQUS justifies the need for a full 3D element. As can be seen from Figure 3-2, for two-dimensional elements there are no default section points available on the flanges, nor does ABAQUS allow the user to create any points along the flange. Since the residual stress is modelled by applying an initial axial stress to the section points, as explained in Section 3.5, it is necessary to have section points at the flanges. Thus, 3D

beam elements (B31 and B32) are used and all the out-of plane degrees of freedom are restrained. To achieve this, a boundary condition of “Displacement/Rotation” using \*BOUNDARY command of ABAQUS is created and restricts the displacement component U3 (out-of-plane displacement in global Z direction) and rotation components UR1 and UR2 (rotations about global in-plane X and Y directions).

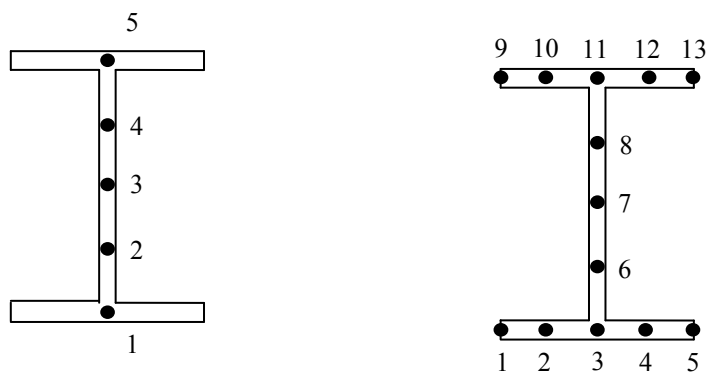


Figure 3-2: Default ABAQUS section points, (a) beam in a plane (b) beam in space

### 3.4 Material model

To model material nonlinearity the classical metal plasticity model in ABAQUS is used in this study. This model uses the von Mises yield surfaces with associated plastic flow to define isotropic yield theory. Perfect plasticity as well as strain hardening are both available in the classical metal plasticity model. To model the stress-strain curve in ABAQUS, the command \*PLASTIC must be used in conjunction with the linear elastic material model (\*ELASTIC) and a multi-linear series of the true stress and true plastic strain values. Quite often material tests supply nominal stress and strain values. The nominal stress (engineering stress) is based on the assumption that the cross-sectional area does not change during deformation, which is a valid approach if the deformations are quite small. However, the change in cross-sectional area is significant if a structure undergoes large deformations and true stress has to be implemented. Thus, the nominal values of stress and strain may be converted to true stress and logarithmic plastic strain as

$$f_{true} = f_{nominal} (1 + \epsilon_{nominal}) \quad 3-1$$

$$\varepsilon_{ln}^{pl} = \ln(1 + \varepsilon_{nominal}) - \frac{f_{true}}{E} \quad 3-2$$

where  $f_{true}$ ,  $f_{nominal}$ ,  $\varepsilon_{ln}^{pl}$ ,  $\varepsilon_{nominal}$  and  $E$  are true stress, nominal stress, logarithmic plastic strain, nominal strain, and Young's modulus, respectively. Figure 3-3 compares the nominal and true stress and strain for a steel material with the Young's modulus of 200 GPa and the yield stress of 320 MPa. As it can be seen from the figure, both nominal and true stresses are almost identical before the strain hardening starts. After this point, the true stress is larger than the nominal stress when the strain increases. This is due to the reduction of the cross sectional area in large deformations. Thus, if strain hardening is taken into account in advanced analysis, it is necessary to implement true stress and strain in order for ABAQUS to interpret the data correctly.

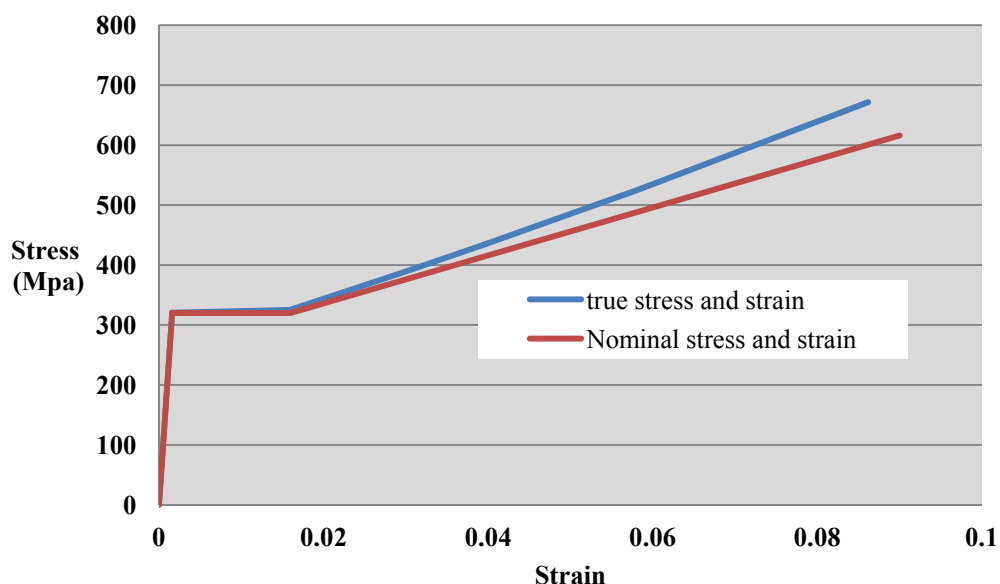


Figure 3-3: Comparison of nominal and true stress-strain relationship

In this study, the nonlinear stress–strain relation of the steel was initially described by a tri-linear curve, consisting of an elastic part and a yield plateau extending to a strain of  $10\varepsilon_y$  followed by a strain-hardening part with a slope of  $E_{sh}=0.02E$ , where  $\varepsilon_y = f_y/E$  is the yield strain,  $E$  is the initial Young's modulus and  $E_{sh}$  is the strain-hardening modulus (Ziemian 1990). The stress-strain curve is presented in Figure 3-4. The influence of strain hardening on the nominal frame ultimate strength is investigated using both deterministic

and probabilistic approaches. The results are presented in Section 3.7 and Section 7.9, respectively. Ultimately, strain hardening was found to have negligible effect on the nominal frame strength and its statistical data and was consequently ignored in this study. Hence, the material is modelled as elastic-perfectly-plastic.

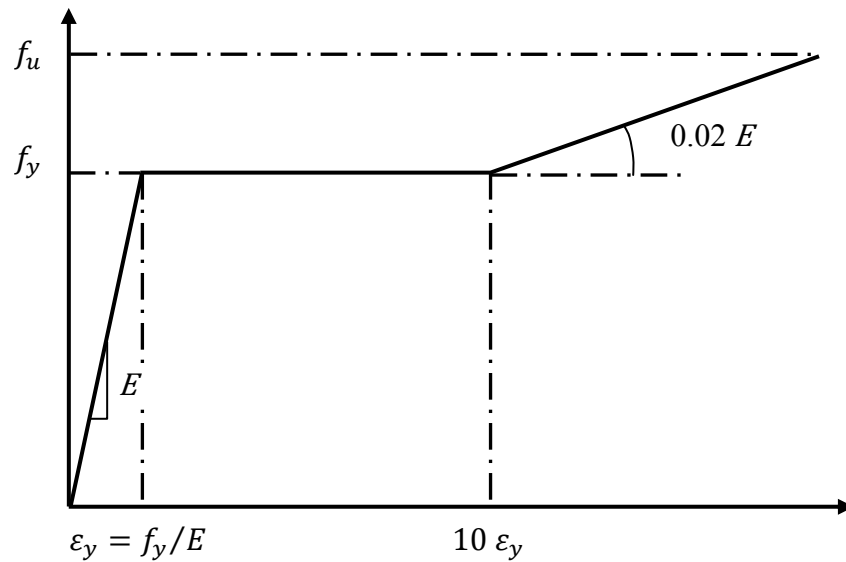


Figure 3-4: Stress-strain relationship

### 3.5 Residual stress and initial geometric imperfection

The uneven rate of cooling after the rolling process creates a set of self-equilibrating initial stresses in the cross section, called residual stress. This is most evident in the case of I-sections in which the flange and web intersections cool much slower than the flange tips or web centre. This induces tensile stress at the flange-to-web junction and compressive stress throughout the rest of the cross-section. In this study, the residual stress distribution proposed by ECCS Technical Committee 8 (1984) is used and presented in Figure 3-5.

A user subroutine (SIGINI) is written in FORTRAN to implement the residual stress into the finite element model in ABAQUS. The SIGINI subroutine enables the user to define the residual stress as the function of the coordinate, element number, or section point number. This subroutine is added to each input file by \*INITIAL CONDITIONS, TYPE=STRESS, USER command and called at the beginning of each analysis. To

implement a more accurate residual stress distribution, the total of 13 default section points of ABAQUS is increased to 25 by creating a section point between each default point. An example of the SIGINI user subroutine and the section points used in this study are presented in Appendix A. More details about the modelling of residual stress can be found in Chapter 6.

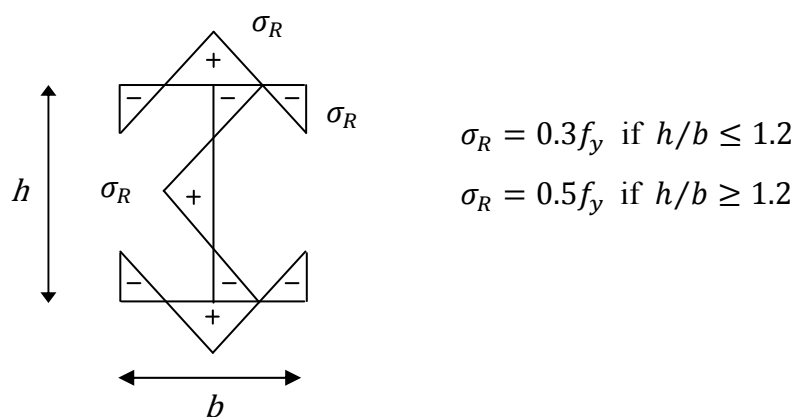


Figure 3-5: Residual stress pattern, ECCS model

Two types of geometric imperfections are considered in this study: the member out-of-straightness (bow imperfection  $\delta$ ) and the frame out-of-plumb (sway imperfection  $\Delta$ ). Initial geometric imperfections are modelled as a linear superposition of the first six elastic buckling modes. First, an elastic buckling analysis is run using the \*BUCKLE option of ABAQUS to obtain the first six eigenmodes. Then the elastic buckling modes are scaled with appropriate factors and implemented into nonlinear inelastic analyses using the \*IMPERFECTION option to model initial geometric imperfections. More detail about this method and appropriate scale factors for each buckling mode can be found in Chapter 5.

### 3.6 Strength and serviceability limit state

The steel structural specifications are based on the limit state design (LSD). Limit states are the conditions beyond that which structure no longer fulfills the specified design criteria. The limit states are classified as strength and serviceability limit states. The strength limit state is associated with the failure of the structure under the most

unfavorable combination of loads while the serviceability limit state is related to the functional performance of the structures and defined as the limit state beyond which service criteria, such as deflection are no longer met (Eurocode 3 2005).

To calculate the ultimate (collapse) strength of the frame, static analyses are conducted until structural collapse which is defined by failure of convergence in finite element analysis. The nominal loads are applied to the frame and proportionally increased to investigate the structural performance against progressive collapse and the load-deflection response is traced. The procedure is referred as a static pushdown analysis if gravity (vertical load) is scaled and pushover analysis if the vertical load is proportionally increased. (Ziemian et al. 1992) defined the frame ultimate load factor as (i) maximum point of load-displacement curve or (ii) the load at which the slope of load-displacement curve becomes less than 5% of its initial value, whichever comes first. Three types of commonly seen load-deflection response in this study are presented in Figure 3-6, in which case (a) mostly happens when strain hardening is taken into account and the failure mode is beam failure while case (b) and (c) are for beam failure without strain hardening and column buckling respectively. The step-by-step procedure to choose the ultimate load from the load-deflection curve is presented in Figure 3-7. The investigation of analysis results of many frames shows that the load factor related to 5% of the initial slope is very close to the maximum point of the load-deflection curve if the strain hardening is not taken into account (see Section 3.7 and Section 7.9 for more details). Accordingly, strain hardening is ignored in this study and the ultimate load factor (collapse) is considered as the maximum point of the load deflection curve.

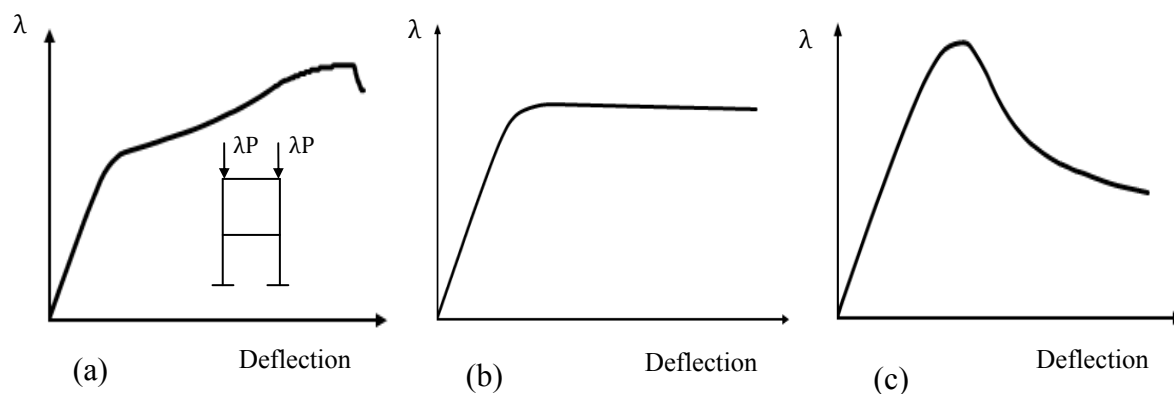


Figure 3-6: Examples of load-deflection response

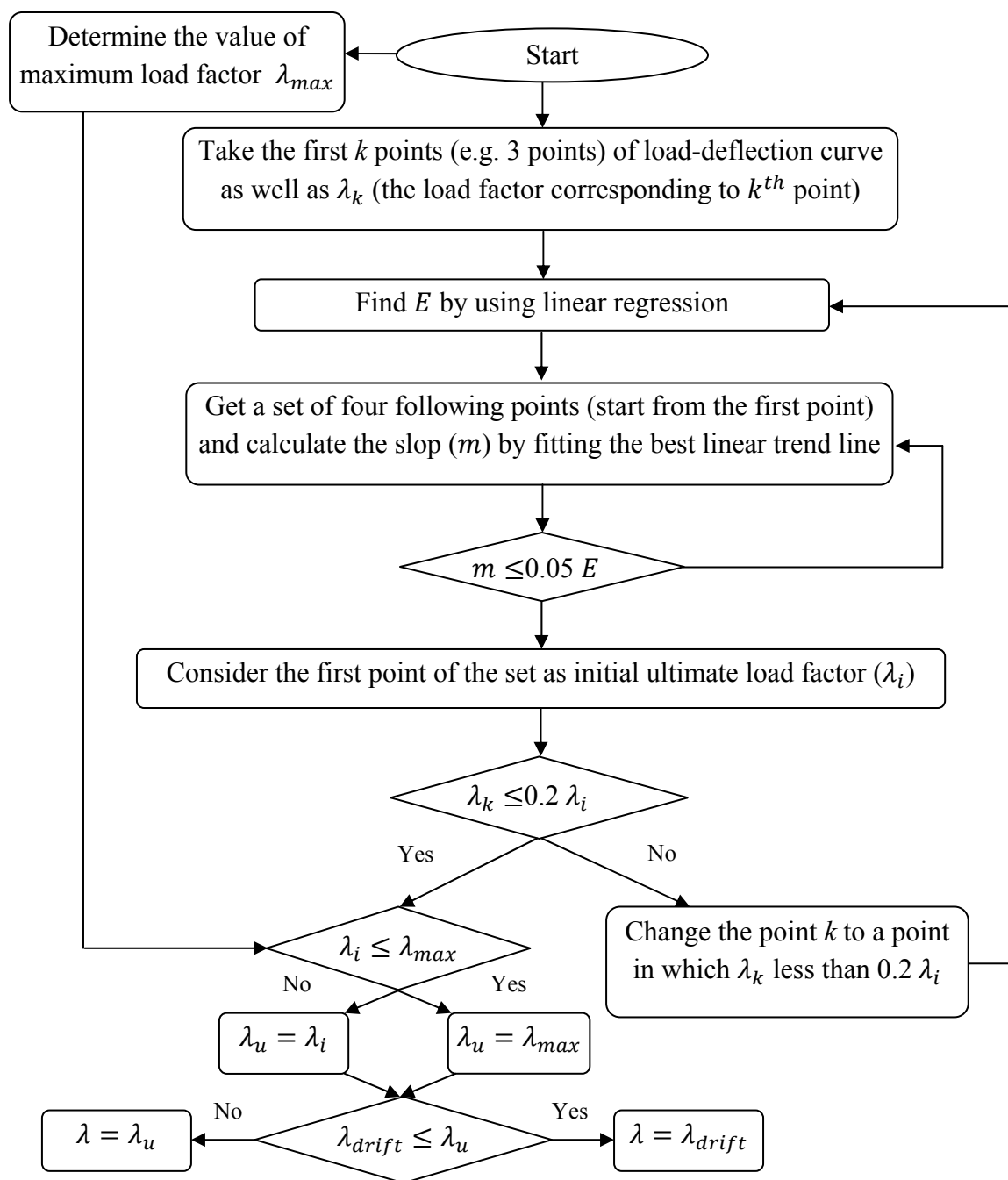


Figure 3-7: Step-by-step procedure to find the structural collapse load

A serviceability storey drift check has been performed in this study which intended to minimize the damage caused by excessive lateral deformation. The storey and the roof drifts are limited to 5% of the storey height and the total structural height, respectively and the corresponding load factor ( $\lambda_{drift}$ ) is obtained. This load factor is then compared with the load factor obtained from the strength limit state check ( $\lambda_u$ ) and the minimum of two is chosen as the structural collapse load.

### 3.7 Effect of strain hardening on the frame ultimate strength

As can be seen from Figure 3-3 and Figure 3-4, strain hardening is only important if those members associated with the frame failure experience large deformations. To see the influence of the strain hardening on the frame ultimate strength, an irregular frame with a 16m span under gravity loading has been studied. The top beam has the capability to undergo large deflection under applied loads. Frame configuration, cross-sections, material properties and loading scheme are presented in Figure 3-8.

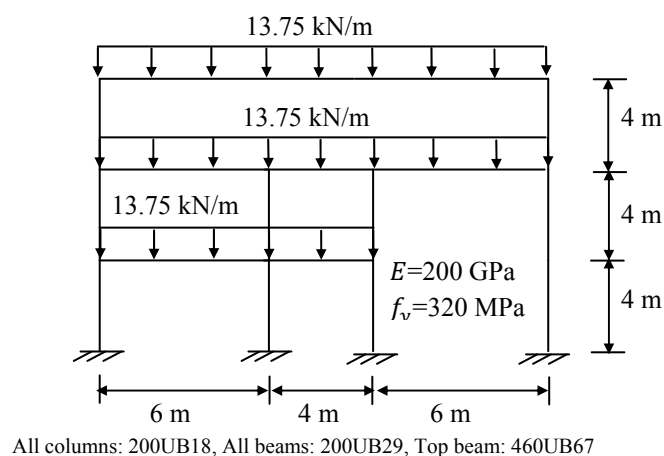


Figure 3-8: 3-bay irregular frame to investigate the effect of strain hardening

The load deflection response of the frame with and without strain hardening is plotted in Figure 3-9. The deformation corresponding to the ultimate points (point (a)) (i.e. ultimate load analysis without strain hardening and 5% initial stiffness with strain hardening) and the end of the analysis (point (b)) as well as the corresponding vertical deflections are presented in Figure 3-10. The ultimate load factor obtained from the analysis including strain hardening using the procedure explained in Figure 3-7 is equal to 1.020 while the load factor for the analysis without hardening is 1.018. As it can be seen from both figures, although the frame including strain hardening can undergo large deflections, the ultimate load factors as well as corresponding deflections for both analyses are quite similar. Thus, since considering strain hardening in the analysis of the frame only influences on the deflection and the load factor remains almost the same, this effect has been ignored in this study. More details about the effect of the strain hardening on the statistics of frame ultimate load can be found in Section 7.9.



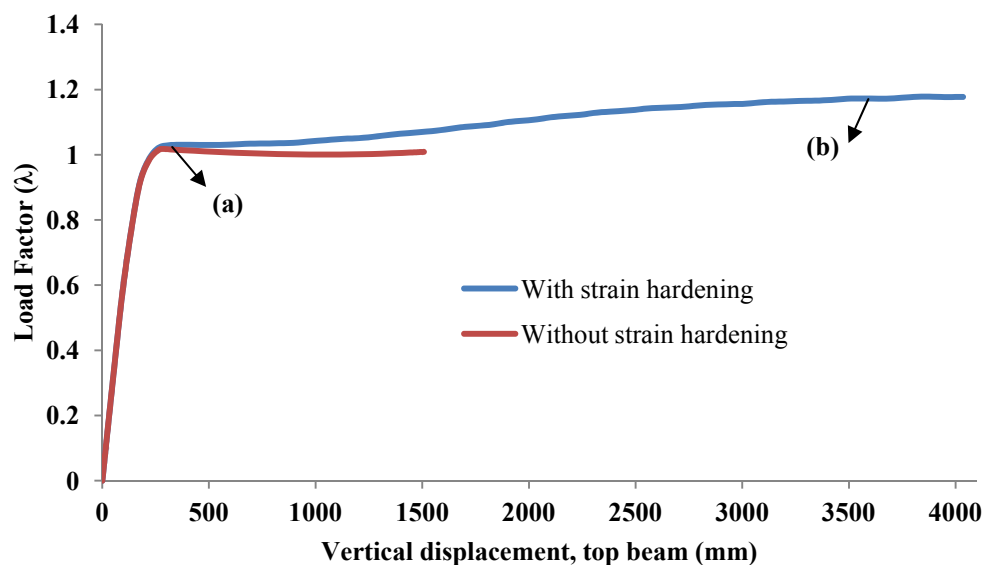


Figure 3-9: Load-deflection response of 3-bay irregular frame

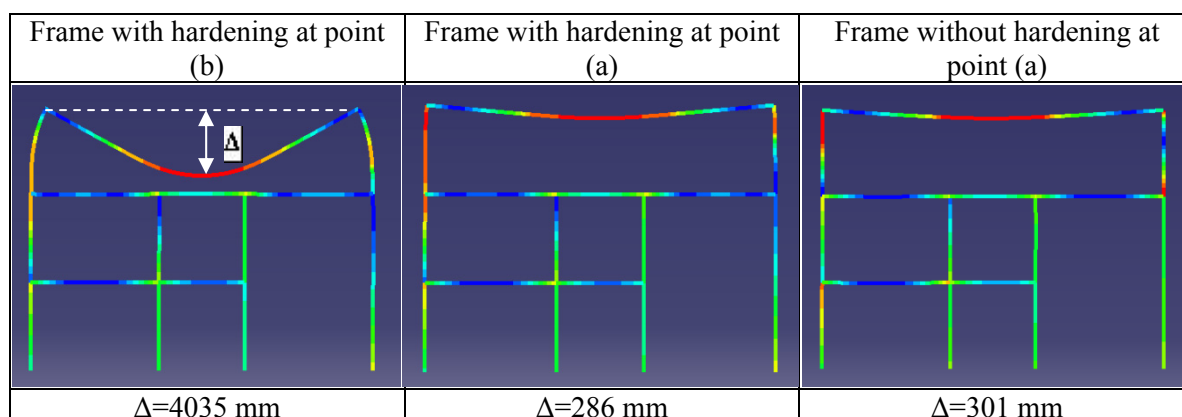


Figure 3-10: 3-bay irregular frame, failure modes

### 3.8 Model calibration

In order to validate the accuracy of the second-order inelastic model presented in this chapter, two planar frames were chosen from the literature as benchmarks. The first frame is the Vogel's six-storey frame which is one of three frames selected by the European Convention for Constructional Steelwork (ECCS) for the calibration of second-order inelastic analysis programs (Vogel 1985). This frame was previously analysed by many researchers (Toma and Chen 1992; Toma et al. 1993; Toma and Chen 1994; Kim et al. 2006). The frame configuration, dimension, cross-sections and loads are presented in Figure 3-11. All cross-sections are compact hot-rolled I-sections and the beam-column

joints are rigid. The frame is subjected to vertical gravity loads and horizontal wind loads, applied to the frame at the same time and scaled simultaneously. The Young's modulus ( $E$ ) and the yield stress ( $f_y$ ) are equal to 200 GPa and 235 MPa, respectively. Initial geometric imperfections and residual stress was modelled as explained in Section 3.5. Strain hardening was ignored and the material was modelled as elastic-perfectly plastic. As it was mentioned in Section 3.3 the frame was modelled using three-dimensional beam element B31 to make sure the residual stress can be applied accurately across the flanges and subsequently the full lateral restraint is applied to make the frame behaviour two-dimensional.

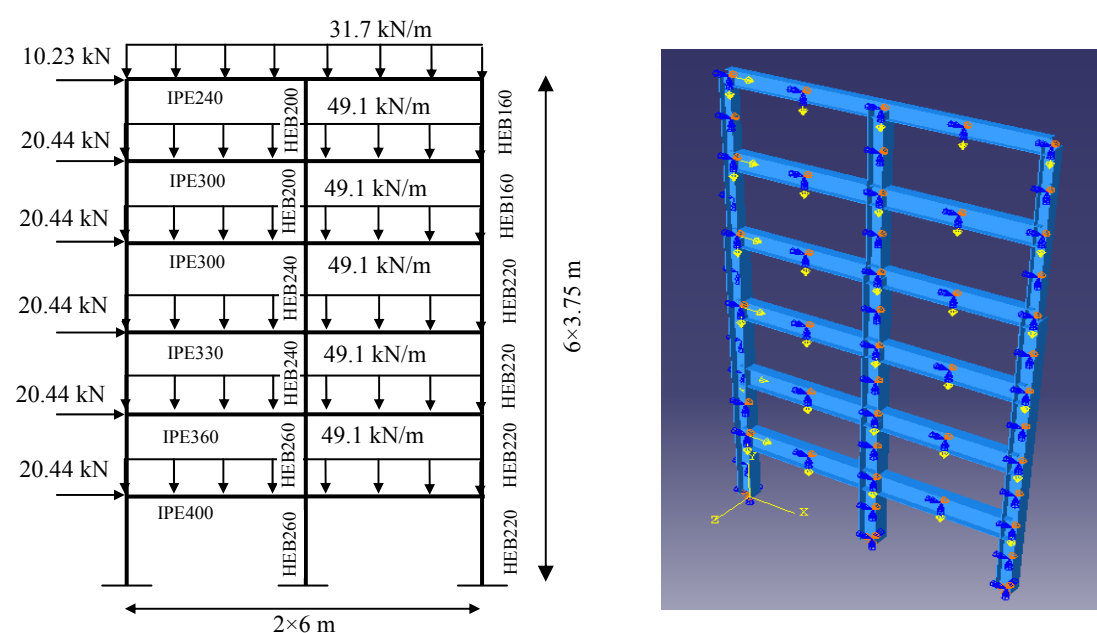


Figure 3-11: (a) Configuration of Vogel's six-storey frame (b) ABAQUS model

The load–deflection curve obtained from the ABAQUS analysis using the advanced analysis model in this study and the result provided by Vogel (1985) have been plotted for comparison in Figure 3-12. An excellent agreement is achieved and both methods result in the same ultimate load factor ( $\lambda$ ) of 1.11. It is worth mentioning that the predicted ultimate load in ABAQUS is sensitive to the mesh size and the presented result is based on the discretization of members into 20 elements. A comprehensive mesh sensitivity study is conducted in Section 3.9. As it can be seen from Figure 3-12, one of the advantages of the nonlinear analysis in ABAQUS (Riks analysis) is that the model is capable of capturing the post-failure behaviour of the structure.

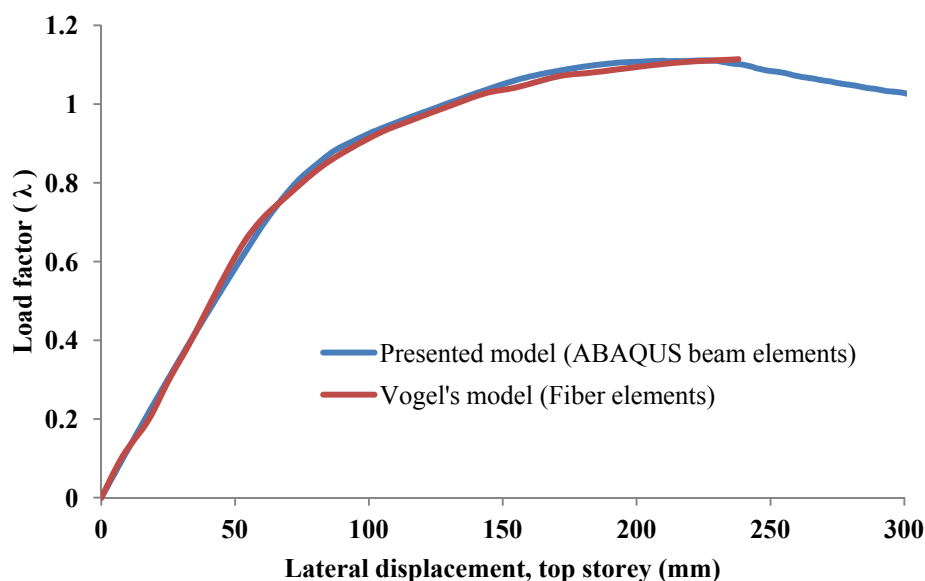


Figure 3-12: Load-lateral displacement of Vogel's frame

The analysis result reveals that the frame fails by sway instability with significant yielding of many beams (especially at upper levels) and columns (particularly in base level) as shown in Figure 3-13 (a). The Vogel frame was previously analysed by Barsan and Chiorean (1999) using a plastic hinge method and the location of plastic hinges are presented in Figure 3-13 (b). Comparison of the results indicates that the spread of plasticity in ABAQUS using the plastic zone method occurred at the exact locations of the plastic hinges presented by Barsan and Chiorean (1999).

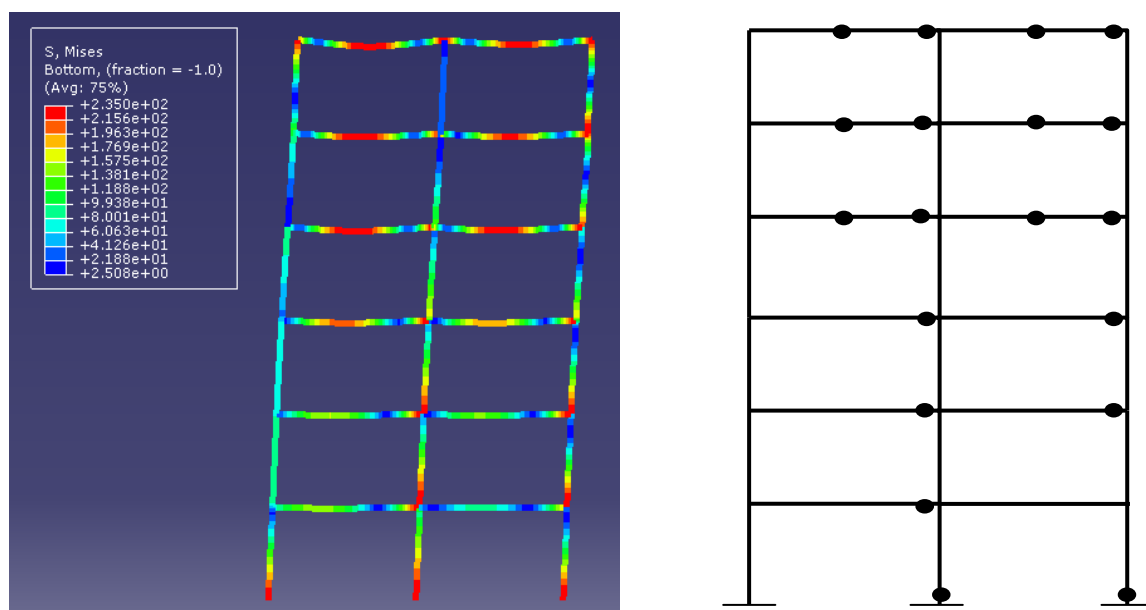


Figure 3-13: Vogel's frame, (a) ABAQUS failure mode (b) Plastic hinge locations by Barsan and Chiorean (1999)

The second calibration frame is one of the sixteen two-bay, two-storey frames proposed by Ziemian (1990), and shown in Figure 3-14. This frame has been studied previously by many researchers (Chen and Toma 1994; Buonopane and Schafer 2006). Both plastic hinge and plastic zone analyses were conducted by Ziemian (1990) in which the frame was assumed to be geometrically perfect. The frame is subjected to gravity loads only. In this study, the material was modelled as elastic-perfectly-plastic. Displacement-based beam-column elements (B31) were used. All members have their webs in the plane of the frame, and out-of-plane behaviour was restrained. Cross-section yielding were captured with a fiber element model (plastic-zone), integrated at 13 integration points in the cross-sections (five points in web, five points in each flange of which two coincide with web points).

The load-lateral displacement response of the frame determined by plastic-zone analysis by Ziemian (1990), plastic-zone analysis by Chen and Toma (1994) referred as NIFA, and ABAQUS model are shown in Figure 3-15. The ultimate load factor ( $\lambda$ ) corresponding to these models are 1.01, 0.985 and 0.976, respectively. Strain hardening, residual stress and initial geometric imperfections were considered in the ABAQUS model although they do not have significant effect. Once again, it should be mentioned that the ABAQUS result is sensitive to the selected element size and the presented load-deflection response here is based on the discretization of beams and columns to 32 and 16 elements, respectively.

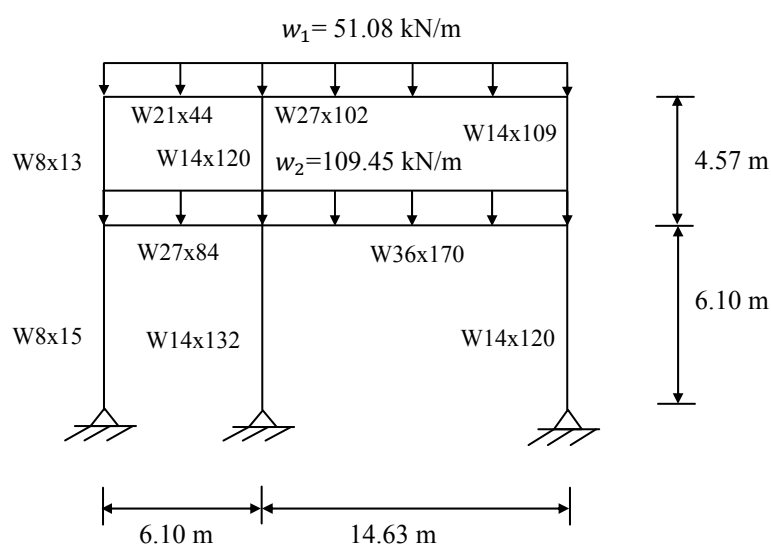


Figure 3-14: Ziemian's frame, UP36HA

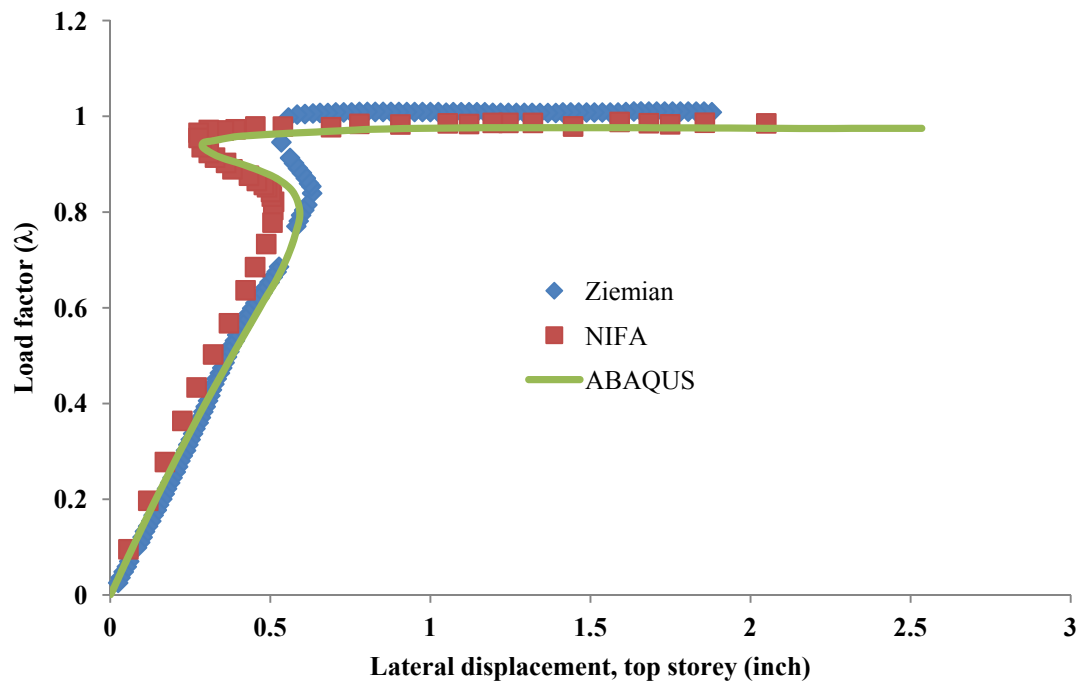


Figure 3-15: Comparison of load-displacement response of frame UP36HA by ABAQUS, Ziemian (1992) and NIFA (Chen and Toma (1997))

Comparison of the results in Figure 3-15 shows that advanced analysis using ABAQUS produces results that are in agreement with other established analysis methods. The frame failure mode is presented in Figure 3-16 and shows the spread of plasticity along the member lengths which matches those presented by Chen and Toma (1994).

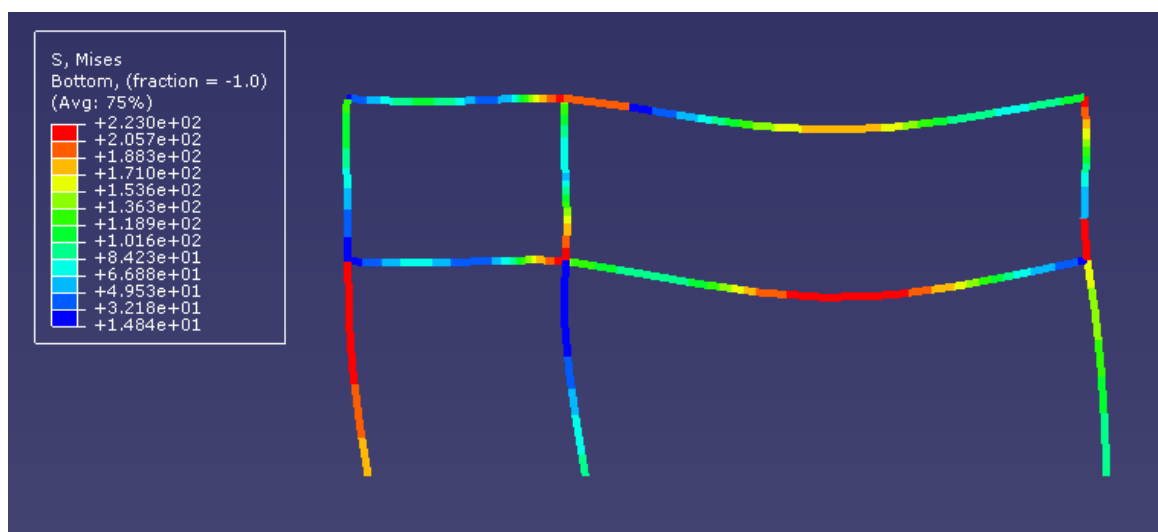


Figure 3-16: Ziemian's frame, ABAQUS failure mode

### 3.9 Mesh sensitivity (Convergence study)

Finite element models are normally sensitive to mesh schemes or number of elements. To gain an appreciation of the sensitivity of the ultimate frame strength to the number of elements and to choose an appropriate mesh size which results in accurate structural responses, a mesh sensitivity analysis is performed in this section for the Vogel and Ziemian frames presented in Section 3.8. Typically, in finite element analysis, a finer mesh results in a more accurate solution. However, increasing mesh density also increases the computational time. The relationship between the ultimate load factors obtained from ABAQUS nonlinear analyses and the number of elements for both Vogel and Ziemian frames are plotted in Figure 3-17 and Figure 3-18, respectively. The results are based on the same number of elements for beams and columns in Vogel frame while the beam mesh size is twice that of the column element size in Ziemian's frame. As it can be seen from the figures, after reaching a specific element size the ultimate load factor remains virtually unchanged for both frames. Thus, to achieve an accurate result in ABAQUS the mesh size should not be coarser than this size.

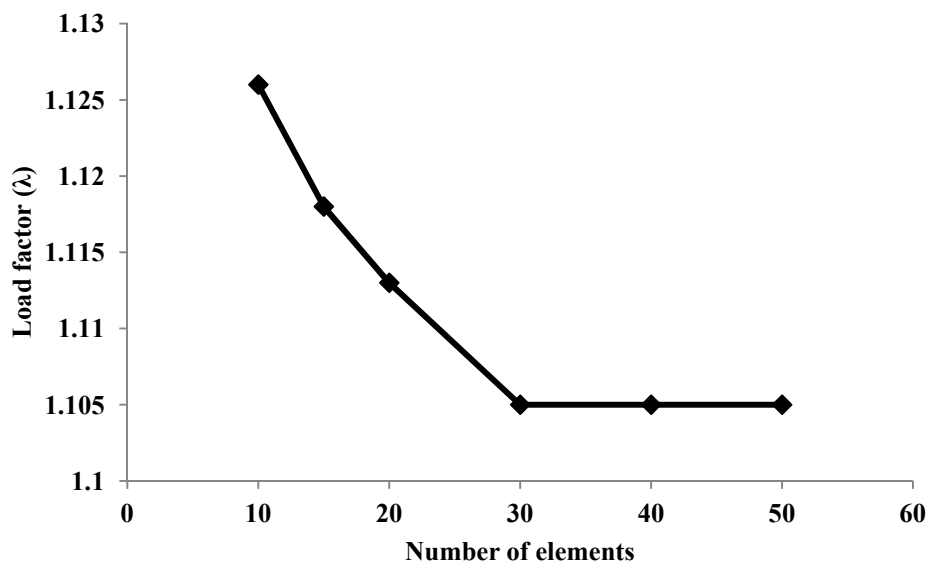


Figure 3-17: Mesh convergence study, ABAQUS, Vogel's frame

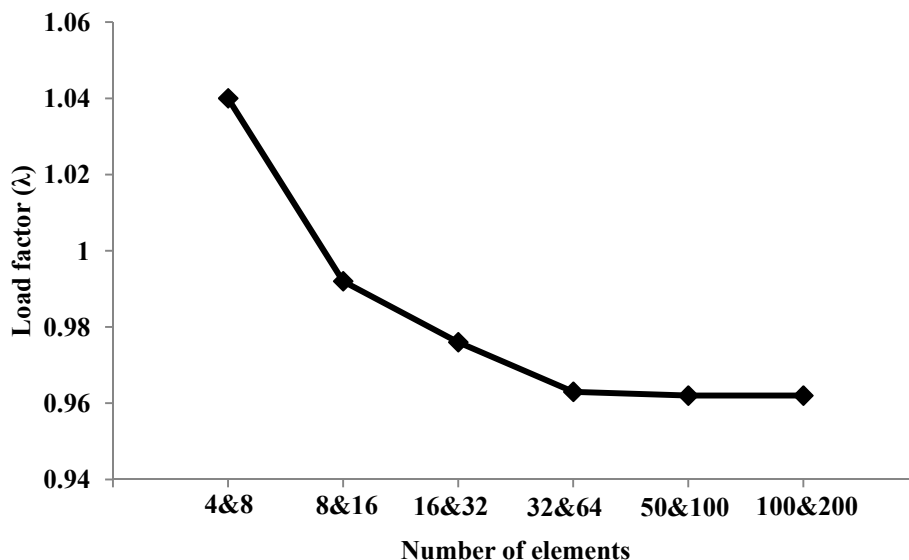


Figure 3-18: Mesh convergence study, ABAQUS, Ziemian's frame

The load-deflection responses of the Ziemian and Vogel frames using different mesh sizes in ABAQUS nonlinear analyses are shown in Figure 3-19 and Figure 3-20, respectively. These results are then compared with the load-deflection curves obtained using Strand 7 (2009). It was observed that while the ultimate load factors obtained from ABAQUS were very sensitive to mesh size, the load-deflection curves using Strand 7 were substantially less sensitive to mesh size. This can be explained by the default number of integration points along the beam length in these software packages. The ABAQUS results presented here are based on the B31 beam element with two integration points along the element length, while the Strand 7 beam element by default has five integration points which proves sufficient to trace the nonlinear behaviour with coarser mesh sizes. It can be seen from Figure 3-19 and Figure 3-20 that if the mesh is fine enough in ABAQUS, the load-deflection curve completely matches the result of Strand 7. It is also clear that if ABAQUS B32 element is used in the analysis the number of elements required to obtain convergence is half that of the B31 element.

It should be mentioned that for these two frames, a short element size is required in ABAQUS because of the concentrated areas of large plastic strain near the joints and beam mid-span. In general, if a frame experience large spread of plasticity and the computational time is an issue, an alternative solution can be using a smaller mesh size of those parts of the frame in which plastic hinges form while coarser mesh sizes can be

used for other frame parts. Since the frame member lengths are different in this study and range from 4 m to 10 m, the global element size of 200 mm is chosen which suggests a consistent mesh size in all frames regardless of member length. This results in typically 20-50 elements per member.

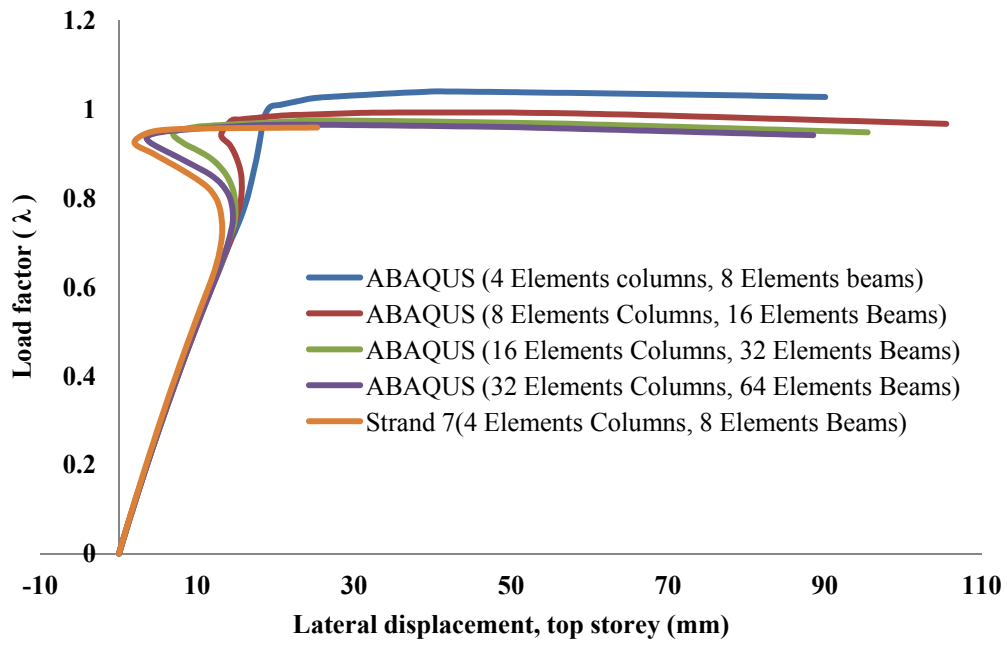


Figure 3-19: Mesh sensitivity analysis of Ziemian's frame

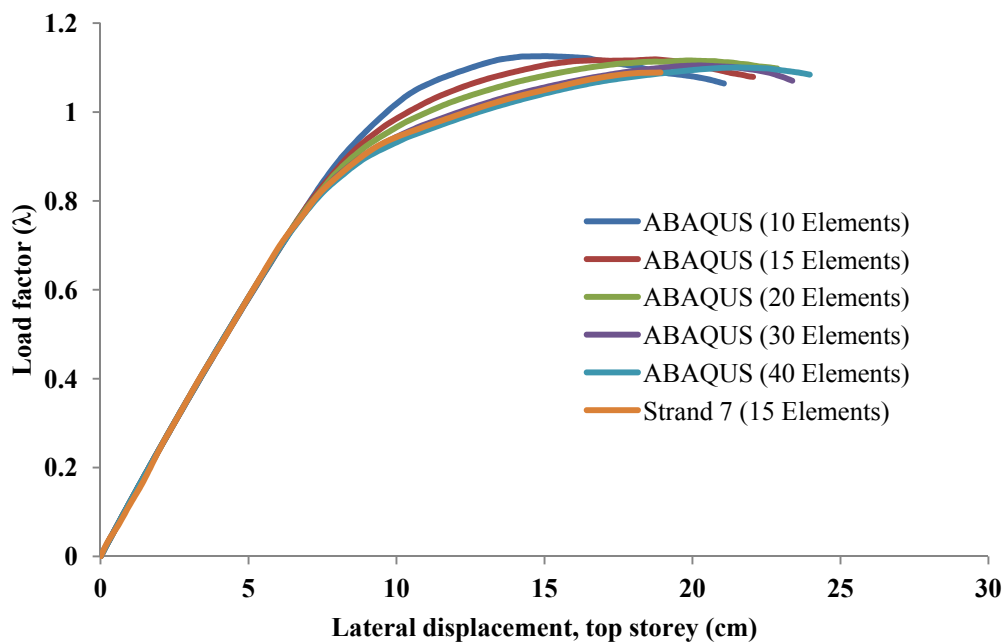


Figure 3-20: Mesh sensitivity analysis of Vogel's frame



### **3.10 Conclusion**

The advanced analysis method, if properly implemented in a finite element model, can simplify the design procedure and directly predict the full-range load-deflection response of frame systems. To capture structural behaviour accurately using advanced analysis, the first step is to have an appropriate finite element model that accounts for all factors influencing the system strength. In this chapter, nonlinear finite element models for two-dimensional steel frames have been developed. Details about element selections, material properties, residual stress and structural collapse are discussed. The finite element model is calibrated against frames from the literature and an excellent agreement is achieved. The effect of strain hardening on the ultimate frame strength is evaluated and appears to be negligible). Mesh sensitivity analysis is conducted. It was concluded that the beam finite element analysis of ABAQUS is very sensitive to the mesh size and after reaching specific element size the ultimate load factor remains unchanged. The global mesh size of 200 mm was chosen.

# CHAPTER

## 4 .

# A model for warping transmission through joints of steel frames

---

## **4.1 Context**

The warping transmission joint model described in this section was developed in the early stages of the research project before it was decided to narrow the scope to 2D frames. Therefore, while the frame analyses described in Chapters 5, 6 and 7 do not feature member torsion or warping, the warping transmission model was fully developed as part of this study and is presented in this chapter.

## **4.2 Introduction**

Steel moment frames are often used in construction and engineering practice. Since steel frames are usually composed of thin-walled open-section members with low torsional stiffness, the members are likely to experience significant torsion and therefore large warping displacements under applied loads. Generally, the applied torque is resisted by

two primary mechanism; St.Venant or uniform torsion ( $GJ\varphi'$ ) and warping or nonuniform torsion ( $EI_w\varphi'''$ ) as shown in Equation 4-1.

$$M_z = GJ\varphi' - EI_w\varphi''' \quad 4-1$$

in which  $M_z$  is the torque at a distance  $z$  along the member length,  $G$  and  $E$  are the shear and Young's modulus of elasticity,  $J$  is the uniform torsion constant and  $I_w$  is the warping section constant. In St.Venant torsion the torque is resisted by shear stresses while in warping torsion the torque is resisted by axial stresses. These contributions vary primarily with the ratio  $L/a$  defined as,

$$\frac{L}{a} = \sqrt{\frac{GJL^2}{EI_w}} \quad 4-2$$

in which  $L$  is the length of the member (Vacharajittiphan and Trahair 1974). In a member with a high  $L/a$ , the uniform torsion (St. Venant theory) is governing and the warping deformations can be ignored. In this case, the member can be modelled assuming only six translational and rotational degrees of freedom in FE formulation. However, when the ratio,  $L/a$ , is small the warping is dominant and needs to be taken into account since it significantly increases the torsional stiffness of the member. In FE formulation each member end nodes is modelled with seven degree of freedom, in which the seventh is warping.

For a doubly symmetric I-section, the warping displacement consists of linear longitudinal displacements in the flanges in opposite directions (see Figure 4-1). The axial stresses can be replaced by two equal moments acting in the planes of the flanges in opposite directions. Statistically, these moments are equivalent to an internal force factor introduced by Vlasov (1961) and called a bimoment. The bimoment for a given torsional load is calculated as the product of flange coupled moments and the section height,

$$B = Mh \quad 4-3$$

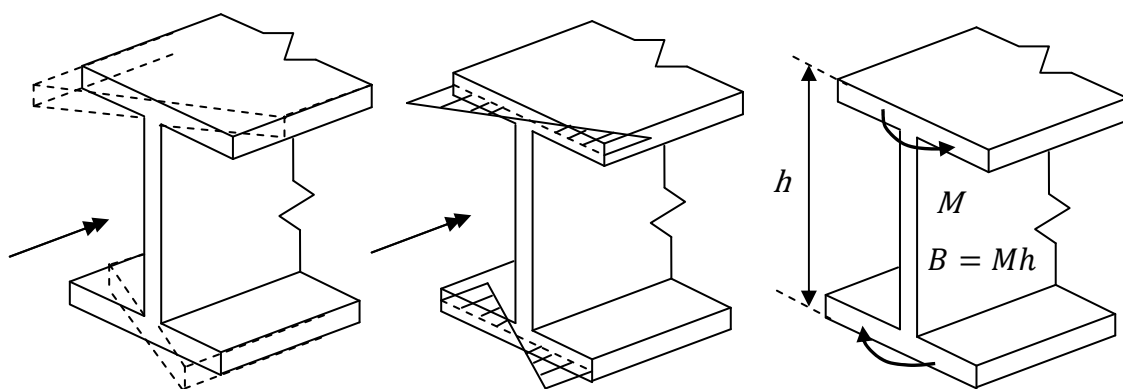


Figure 4-1: Warping torsion in a doubly symmetric I section (a) cross-sectional displacement (b) axial stress (c) bimoment

At joints, warping displacements in one member may redistribute and produce warping and twisting in other attached members. A brief review of the literature on the transmission of warping through joints of thin-walled steel frames shows that all suggested models need substantial numerical or computational effort (Krenk and Damkilde 1991; Masarira 2002; Tong et al. 2005). Warping transmission through the joints can be accurately captured at the expense of substantial computational effort by discretising the entire frame using shell finite elements. However, for one-dimensional beam finite element analyses, the development of a suitable model to incorporate the effects of full or partial warping transmission through joint is a complex task. Due to the complexity of current models, the partial transmission of warping through joints is ignored in most design cases. Even if a designer wanted to consider transmission of warping through joints, available commercial finite element software packages are limited to either completely prevent warping or allow warping to occur freely at joints when using beam finite element analysis (B-FEA).

At this point in time, there appears to be no FE software available that allows the seventh degree of freedom (warping) to be partially transmitted. The only option to model warping accurately is using shell elements (S-FEA), which is not a desired method for complex structures due to its high computational cost. A few models can be found in the literature for the partial transmission of warping at joints when using beam finite elements (Krahula 1967; Basaglia et al. 2010). Basaglia et al. (2010) developed a simple kinematic model to simulate the warping transmission or restraint at the joints of thin-walled frames in the context of beam finite element analysis. The model relies on the facility of most

structural analysis software (e.g. ABAQUS and ANSYS) to impose “linear constraint equations” which establish constraint conditions between the torsion warping degrees of freedom of the member end nodes. The general form of the linear constraint equation which must be imposed in the case of two connected members is:

$$K_1\varphi'_a + K_2\varphi'_b = 0 \quad 4-4$$

where  $a$  and  $b$  refer to the beam and column ends respectively,  $K_i$  are continuity coefficients, which depend on the joint configuration, and  $\varphi'$  is warping degree of freedom. The  $K_i$ -values and mechanical characteristics of the four joint types shown in Figure 4-2 are summarised in Table 4-1.

Table 4-1: Summary of mechanical characteristic for four specific joint types reported by Basaglia et al. (2010)

Joint Type	Warping Transmission	Coefficients
Unstiffened	Complete and direct	$K_1 = 1$ and $K_2 = -1$
Diagonal-stiffened	Complete and direct	$K_1 = 1$ and $K_2 = -1$
Box-stiffened	Complete and inverse	$K_1 = K_2 = 1$
Diagonal/Box stiffened	Null	$\varphi'_a = \varphi'_b = 0$

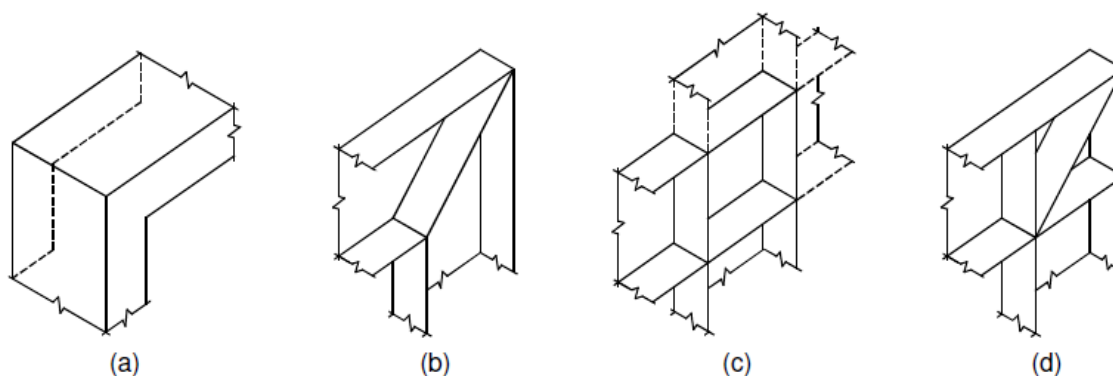


Figure 4-2: Configurations of joints between channel members (Basaglia et al.(2010)) (a) unstiffened with flange continuity, (b) diagonal stiffened, (c) box stiffened, (d) diagonal/box stiffened joints

Despite its simplicity, the model is only applicable to four specific types of joints (see Figure 4-2) and cannot model all possible cases with partially restrained warping. For example, the fully prevented warping assumption implied for diagonal/box stiffened joints may be rather conservative if the stiffeners have relatively small thickness. Also, the method cannot extend to 3D space frames.

A simple theory is developed in this chapter through the use of mixed dimensional analysis which considers the effect of warping continuity through the joint of thin-walled steel frames. The method benefits from the accuracy of 3D shell finite element modelling and from the computational efficiency of using 1D beam elements (see Figure 4-3). Using a condensed stiffness matrix for the joint generated by the substructuring technique, warping springs are introduced to represent the condition of partial warping restraint at intersections between members. In the model, the joint accepts warping deformations from adjoining loaded members and redistributes the deformation to all connected beams and columns. In fact, the suggested joint model acts as a flexible interface between members and provides partial warping restraint by means of springs.

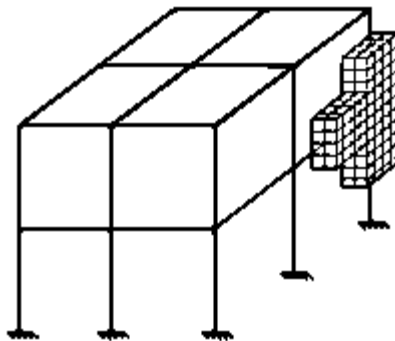


Figure 4-3: Example of mixed dimensional model (combination of 1D and 3D elements)

The suggested model can readily be implemented in conventional types of analysis without the need to modify the stiffness matrix or employ shell finite element analysis, which requires greater computational effort. In addition, the model is general and can be applied to any kind of joint in 2D and 3D thin-walled structural frames. This chapter sets out expressions for the stiffness terms of the joint spring model and how the spring deformations couple with the warping degrees of freedom of adjoining members. Additionally, the general theory of static condensation, which is the basis of

substructuring, is described in this chapter. For validation purposes, the performance of the proposed model is demonstrated through a number of numerical examples. Excellent agreement is achieved between the results of beam finite element analysis using the suggested joint model and accurate shell finite element analysis.

### 4.3 Substructuring and static condensation

Substructuring is a technique commonly used to overcome the difficulty of working with large dimensional problems (Han and Abel 1984). In principle, a structure can be subdivided into smaller parts and each part analysed separately. The basic idea of substructuring analysis is that only certain degrees of freedom are retained while others are eliminated by static condensation. This methodology is available in many finite element software packages and offers many advantages:

- A substantial reduction in analysis time is achieved by modelling only the joints using 3D shell finite elements rather than the entire frame.
- The substructure stiffness matrix needs only to be computed once for each type of joint with similar geometry.
- By writing a script to generate the substructure, the stiffness matrix can be calculated automatically and there is no need to create the joint manually when changing the geometry of the joint.

According to the conventional finite element method, the global stiffness matrix  $\mathbf{K}$  is obtained by assembling the stiffness matrices of all elements. The global stiffness equation can be expressed as:

$$\mathbf{Ku} = \mathbf{F} \quad 4-5$$

where  $\mathbf{K}$  is an  $n \times n$  matrix,  $\mathbf{u}$  and  $\mathbf{F}$  are  $n \times 1$  node-displacement and load vectors respectively and  $n$  is the total number of degrees of freedom. In the substructure analysis, Equation 4-5 is modified to

$$\mathbf{K}^* \mathbf{u}_r = \mathbf{F}^* \quad 4-6$$

where  $\mathbf{K}^*$  and  $\mathbf{F}^*$  are the stiffness matrix and force vector respectively of smaller dimension than  $n$  obtained after static condensation. To obtain Equation 4-6, in first step, the displacement vector ( $\mathbf{u}$ ) is divided into two parts:  $\mathbf{u}_r$  containing degrees of freedom which are to be retained and ( $\mathbf{u}_e$ ) containing degrees of freedom which are to be eliminated, i.e.

$$\mathbf{u} = \begin{bmatrix} \mathbf{u}_r \\ \mathbf{u}_e \end{bmatrix} \quad 4-7$$

In partitioned matrix form, the equation between forces and displacements can be written as

$$\begin{bmatrix} \mathbf{K}_{rr} & \mathbf{K}_{re} \\ \mathbf{K}_{er} & \mathbf{K}_{ee} \end{bmatrix} \begin{bmatrix} \mathbf{u}_r \\ \mathbf{u}_e \end{bmatrix} = \begin{bmatrix} \mathbf{F}_r \\ \mathbf{F}_e \end{bmatrix} \quad 4-8$$

in which  $\mathbf{F}_r$  and  $\mathbf{F}_e$  are force vectors of retained and eliminated DOFs respectively and the  $\mathbf{K}$ -terms are stiffness sub-matrices. Solving the second set of Equation 4-8 with respect to the eliminated DOFs ( $\mathbf{u}_e$ ) provides,

$$\mathbf{u}_e = \mathbf{K}_{ee}^{-1} (\mathbf{F}_e - \mathbf{K}_{er} \mathbf{u}_r) \quad 4-9$$

The condensed equilibrium equation is obtained by substituting Equation 4-9 into the first set of Equation 4-8:

$$(\mathbf{K}_{rr} - \mathbf{K}_{re} \mathbf{K}_{ee}^{-1} \mathbf{K}_{er}) \mathbf{u}_r = (\mathbf{F}_r - \mathbf{K}_{re} \mathbf{K}_{ee}^{-1} \mathbf{F}_e) \quad 4-10$$

which reproduces Equation 4-6 with  $\mathbf{K}^* = \mathbf{K}_{rr} - \mathbf{K}_{re} \mathbf{K}_{ee}^{-1} \mathbf{K}_{er}$  and  $\mathbf{F}^* = \mathbf{F}_r - \mathbf{K}_{re} \mathbf{K}_{ee}^{-1} \mathbf{F}_e$ . After applying static condensation, only the retained degrees of freedom are present in the stiffness equation (Equation 4-10), and each joint can be represented by an equivalent stiffness matrix ( $\mathbf{K}^*$ ).



## 4.4 Joint model

### 4.4.1 The basics- 2D model

A simple 2D angle joint (Figure 4-4 (a)) will be used to explain the model. Subsequently, the model will be set out for the more general case of a 3D joint with multiple adjoining members. The basic idea of the model is to use shell finite elements to discretise the joint, and applying modes of deformation compatible with the warping deformation of adjoining beams to obtain the stiffness of the joint under this mode of deformation. Substructuring is here used to enable a warping deformation to be applied to the joint as a single degree of freedom, which can be linked to the warping degree of freedom of the corresponding adjoining member. A spring model is used to implement the warping stiffness exerted by the joint in the beam-element finite element model.

In the first step, the warping deformation must be mapped onto the 3D joint model by a series of constraint equations which tie the longitudinal displacement of one corner node to the longitudinal displacements of other nodes on the same face so as to represent a warping displacement in the direction of the attached beam (Figure 4-4 (a)). A simple physical interpretation of the model is a set of rigid bar linkages attached to the edge of each component plate which through pivots allow the warping deformation to be represented by a single degree of freedom, shown as  $u_B^1$  in Figure 4-4 (b). The corresponding force required to produce the displacement  $u_B^1$  is denoted by  $F_B^1$ . In this terminology, the subscript “B” refers to “beam” and the superscript “1” refers to the global  $x_1$ -direction. Mathematically, and in the finite element implementation of the model, the warping mode of deformation is implemented using constraint equations, which can be expressed in the general form,

$$a_1 U_i^1 + a_2 U_j^1 = 0 \quad 4-11$$

where  $U_i^1$  and  $U_j^1$  are the longitudinal displacements at adjacent nodes  $i$  and  $j$  in the same plate element (e.g. nodes E and F in Figure 4-4 (a)). For sections composed of three plate elements (e.g. channel and I-sections), three constraint equations are required for each connected face of the joint. For the particular case of a doubly symmetric I-section, the

longitudinal warping displacements of the corner nodes of each component plate element are equal and opposite of each other, i.e.  $U_i^1 = -U_j^1$  and hence  $a_1 = a_2 = 1$ . Thus, the specific constraint equations for the joint shown in Figure 4-4 (a) are  $U_H^1 = -U_G^1$ ,  $U_G^1 = -U_E^1$ , and  $U_E^1 = -U_F^1$ . In general, the constants  $(a_1, a_2)$  are functions of the sectorial coordinate and may be determined as  $(a_1, a_2) = (a_1, -(\omega_i/\omega_j)a_1)$ , where  $\omega_i$  and  $\omega_j$  are the sectorial coordinates of nodes  $i$  and  $j$  respectively.

For each connected face of the joint, one degree of freedom is chosen to represent the warping deformation. For the angle joint, the degrees of freedom are  $u_B^1$  and  $u_C^2$  (Figure 4-4 (c)), both chosen as the longitudinal displacement of a corner node. It follows that the number of degrees of freedom retained in the substructuring process equals the number of adjoining beams and columns. Having chosen the degrees of freedom and corresponding constraint equations, warping deformations can be readily applied to the shell finite element substructure, as exemplified in Figure 4-4 (d).

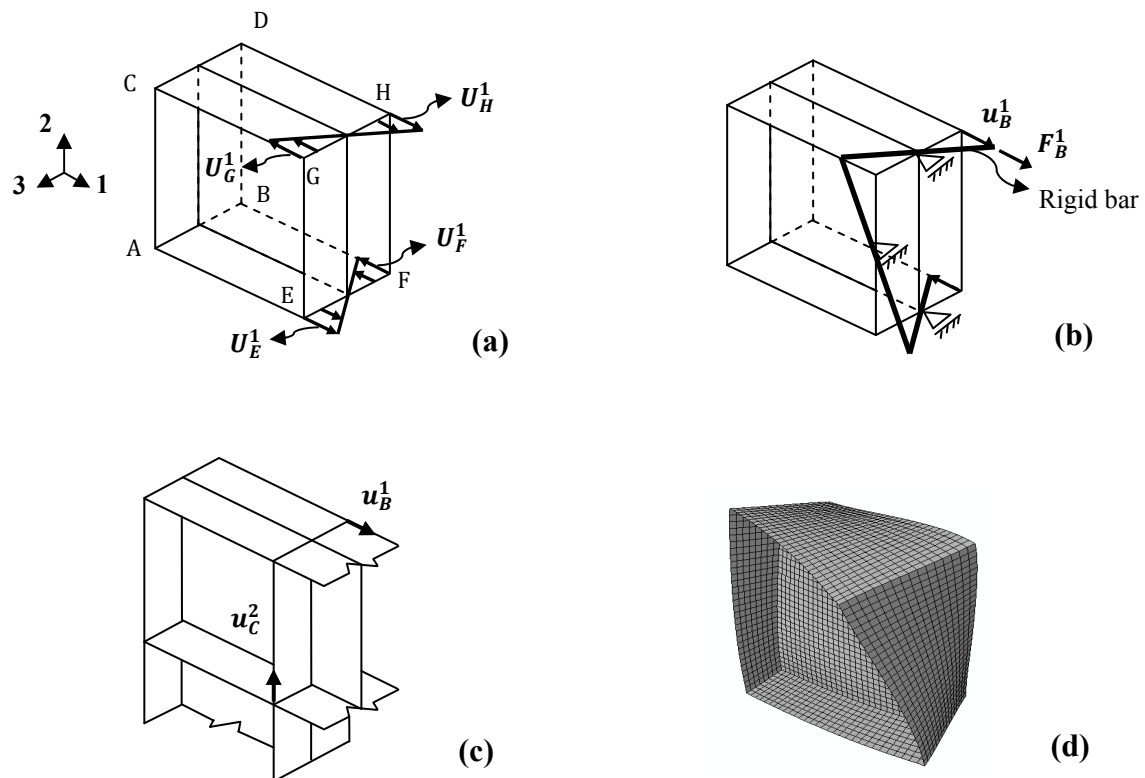


Figure 4-4: (a) Longitudinal displacements to generate a single warping degree of freedom, (b) Rigid bar model, (c) Retained degrees of freedom for an angle box joint, (d) Joint deformations due to applied warping

For the particular angle joint with two degrees of freedom ( $u_B^1, u_C^2$ ), the condensed stiffness matrix has four components: one for the warping displacement ( $u_B^1$ ) of the vertical face connected to the beam ( $K_{BB}$ ), one for the warping displacement ( $u_C^2$ ) of the horizontal face attached to the column ( $K_{CC}$ ) and two off-diagonal components ( $K_{BC}$  and  $K_{CB}$ ) representing interaction between the warping deformations, e.g.  $K_{BC}$  is the force ( $F_B^1$ ) generated in the direction of  $u_B^1$  as a result of a unit warping displacement in the direction of  $u_C^2$ . The stiffness matrix for the substructure after condensation takes the form:

$$\mathbf{K}_u = \begin{bmatrix} K_{BB} & K_{BC} \\ K_{CB} & K_{CC} \end{bmatrix} \text{ where } K_{BC} = K_{CB} \quad 4-12$$

Since the retained degrees of freedom are longitudinal displacements, their multiplication by the stiffness matrix produces forces,

$$\mathbf{F} = \mathbf{K}_u \mathbf{u} \text{ where } \mathbf{F} = \begin{bmatrix} F_B^1 \\ F_C^2 \end{bmatrix} \text{ and } \mathbf{u} = \begin{bmatrix} u_B^1 \\ u_C^2 \end{bmatrix} \quad 4-13$$

The warping deformations of the joint must be compatible with the warping deformations of the adjoining beams. As shown in Figure 4-5, the warping degrees of freedom of the end nodes of the beam and column are denoted by  $\phi'_B$  and  $\phi'_C$  respectively. The corresponding warping displacements at the points where the displacements  $u_B^1$  and  $u_C^2$  are defined are  $\phi'_B \omega_B$  and  $\phi'_C \omega_C$ , respectively, where  $\omega_B$  and  $\omega_C$  are the normalised sectorial coordinates of the same points. Thus,

$$\mathbf{u} = \boldsymbol{\omega} \boldsymbol{\phi}' \text{ where } \boldsymbol{\omega} = \begin{bmatrix} \omega_B & 0 \\ 0 & \omega_C \end{bmatrix} \text{ and } \boldsymbol{\phi}' = \begin{bmatrix} \phi'_B \\ \phi'_C \end{bmatrix} \quad 4-14$$

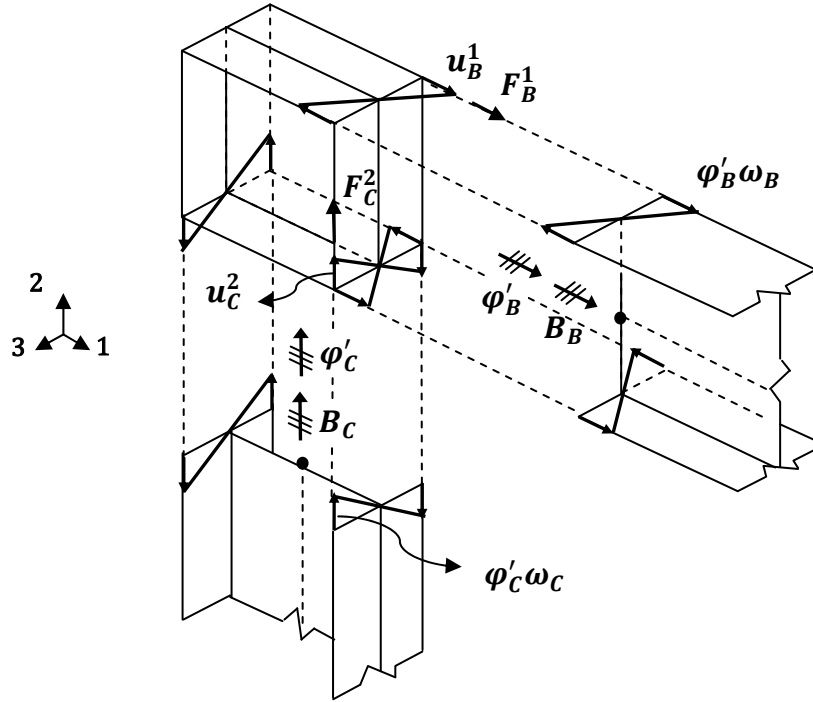


Figure 4-5: Warping compatibility of adjoining members

The stress resultants corresponding to the warping degrees of freedom ( $\phi_B'$ ,  $\phi_C'$ ) are bimoments ( $B_B, B_C$ ), as shown in Figure 4-5. Since a concentrated force in the longitudinal direction of a beam produces a bimoment equal to the force time the sectorial coordinate at the point of application of the force, the bimoments in the beam and column ( $B_B, B_C$ ) are related to the forces acting on the face of the joint ( $F_B^1, F_C^2$ ) through,

$$\mathbf{B} = \boldsymbol{\omega} \mathbf{F} \quad \text{where } \mathbf{B} = \begin{bmatrix} B_B \\ B_C \end{bmatrix} \quad 4-15$$

To obtain the relationship between the bimoments ( $\mathbf{B}$ ) and the warping degrees of freedom ( $\boldsymbol{\phi}'$ ), Equations 4-13 and 4-14 are substituted into Equation 4-15, whereby

$$\mathbf{B} = \mathbf{K}_{\boldsymbol{\phi}'} \boldsymbol{\phi}' \quad 4-16$$

where

$$\mathbf{K}_{\boldsymbol{\phi}'} = \boldsymbol{\omega} \mathbf{K}_u \boldsymbol{\omega} = \begin{bmatrix} \bar{K}_{BB} & \bar{K}_{BC} \\ \bar{K}_{CB} & \bar{K}_{CC} \end{bmatrix} \quad 4-17$$

The terms  $(\bar{K}_{BB}, \bar{K}_{BC} = \bar{K}_{CB}, \bar{K}_{CC})$  of the warping stiffness matrix  $(\mathbf{K}_{\varphi'})$  relating bimoments to warping degrees of freedom are readily obtained once the matrix  $\mathbf{K}_u$  has been obtained from the substructuring process and the sectorial coordinate matrix  $(\boldsymbol{\omega})$  has been obtained from a cross-section analysis.

In the particular case where the adjoining beam and column are doubly symmetric I-sections of the same width  $b$  and depth  $d$ , the sectorial coordinates are

$$\omega_B = \omega_C = \omega = \frac{1}{4}bh \quad 4-18$$

whereby

$$\boldsymbol{\omega} = \omega \begin{bmatrix} 1 & 0 \\ 0 & 1 \end{bmatrix} = \omega \mathbf{I} \quad 4-19$$

so that

$$\mathbf{K}_{\varphi'} = \omega^2 \mathbf{K}_u \quad 4-20$$

The stiffness Equation 4-16 relates the bimoments  $(\mathbf{B})$  at the ends of the adjoining beams to the warping degrees of freedom  $(\boldsymbol{\varphi}')$ . In principle, the stiffness terms could be incorporated directly into the global stiffness matrix for the frame. However, few finite element programs, including commercial programs, have a facility for such implementation. Hence, an alternative approach is used, in which the effect of joint warping stiffness is implemented in the beam finite element model by means of springs. Specifically, the model consists of using a combination of a spring and a linear constraint equation for each member connected to the joint.

For the particular angle box joint shown in Figure 4-4, two springs and two constraint equations are needed. To obtain the required linear constraint equations, the relation between bimoment and warping is written out in full,

$$\begin{bmatrix} B_B \\ B_C \end{bmatrix} = \begin{bmatrix} \bar{K}_{BB} & \bar{K}_{BC} \\ \bar{K}_{CB} & \bar{K}_{CC} \end{bmatrix} \begin{bmatrix} \varphi'_B \\ \varphi'_C \end{bmatrix} \quad 4-21$$

The first diagonal warping stiffness term is then nominated as a fixed value ( $\bar{K}_{BB}$ ) and the other terms are written as a fraction of that term, i.e.

$$\mathbf{K}_{\varphi'} = \begin{bmatrix} \bar{K}_{BB} & b_1 \bar{K}_{BB} \\ b_2 \bar{K}_{BB} & b_3 \bar{K}_{BB} \end{bmatrix} \quad b_1 = b_2 \quad 4-22$$

where  $b_1 = \bar{K}_{BC}/\bar{K}_{BB}$ ,  $b_2 = \bar{K}_{CB}/\bar{K}_{BB} = b_1$  and  $b_3 = \bar{K}_{CC}/\bar{K}_{BB}$ . Thus, the stiffness equations may be rewritten as,

$$\begin{cases} B_B = \bar{K}_{BB}(\varphi'_B + b_1 \varphi'_C) \\ B_C = \bar{K}_{BB}(b_2 \varphi'_B + b_3 \varphi'_C) \end{cases} \quad 4-23$$

or

$$\begin{cases} B_B = \bar{K}_{BB} \Phi_B \\ B_C = \bar{K}_{BB} \Phi_C \end{cases} \quad 4-24$$

where

$$\begin{cases} \Phi_B = \varphi'_B + b_1 \varphi'_C \\ \Phi_C = b_2 \varphi'_B + b_3 \varphi'_C \end{cases} \quad 4-25$$

Equation 4-24 describes a linear relationship between the bimoments and the new variables ( $\Phi_B, \Phi_C$ ). It may therefore be implemented in the finite element model using linear springs and constraint equations to define the spring deformations  $\Phi_B$  and  $\Phi_C$  as per Equation 4-25.

Keeping in mind that the frame should be modelled in such a way that separate nodes are used for the adjoining members at the joint and that these nodes are located at the perimeter of the joint, then, new “dummy” nodes are created near the ends of the adjoining elements and springs are attached to these nodes (Figure 4-6). It is obvious that the stiffness of all springs should be same and equal to  $\bar{K}_{BB}$ . The degrees of freedom corresponding to the springs are  $\Phi_B$  and  $\Phi_C$ . While the seventh degrees of freedom (warping) of the adjoining beams are partially transferred using the presented spring model, the other six degrees of freedom are transmitted directly between members connected to the joint. In this study, the joint is considered to be rigid with respect to

translation and rotation, and so rigid links are used to ensure compatibility of these six degrees of freedom (Figure 4-6).

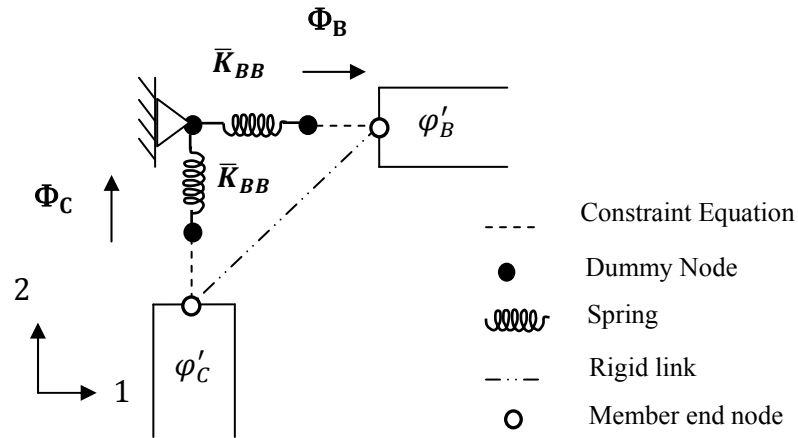


Figure 4-6: Joint spring model, 2D

#### 4.4.2 3D model

The proposed joint model was introduced in the previous section with reference to a simple 2D angle joint with two adjoining members. However, it applies equally to 3D joints with multiple adjoining members, as will be demonstrated in this section using an angle joint consisting of four members, three in same plan and one perpendicular to others (Figure 4-7). Following the same methodology, the warping deformations are first mapped to the substructure and after static condensation one longitudinal displacement is retained for each face which represents the warping degree of freedom for that connected face ( $u_{B_1}^1, u_{B_2}^3, u_{C_1}^2$  and  $u_{C_2}^2$ ).

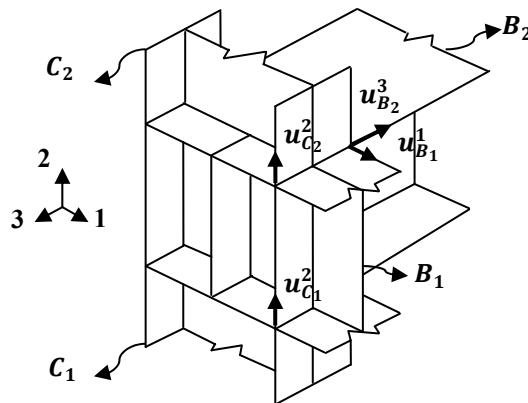


Figure 4-7: 3D corner joint

The relationship between force and longitudinal displacement of the joint can be written as

$$\begin{bmatrix} F_{B_1}^1 \\ F_{B_2}^3 \\ F_{C_1}^2 \\ F_{C_2}^2 \end{bmatrix} = \begin{bmatrix} K_{B_1B_1} & K_{B_1B_2} & K_{B_1C_1} & K_{B_1C_2} \\ K_{B_2B_1} & K_{B_2B_2} & K_{B_2C_1} & K_{B_2C_2} \\ K_{C_1B_1} & K_{C_1B_2} & K_{C_1C_1} & K_{C_1C_2} \\ K_{C_2B_1} & K_{C_2B_2} & K_{C_2C_1} & K_{C_2C_2} \end{bmatrix} \begin{bmatrix} u_{B_1}^1 \\ u_{B_2}^3 \\ u_{C_1}^2 \\ u_{C_2}^2 \end{bmatrix} \quad 4-26$$

To obtain the relationship between the bimoments and the warping degree of freedom, Equation 4-16 and Equation 4-17 apply in which the sectorial coordinate matrix now is defined as

$$\boldsymbol{\omega} = \begin{bmatrix} \omega_{B_1} & 0 & 0 & 0 \\ 0 & \omega_{B_2} & 0 & 0 \\ 0 & 0 & \omega_{C_1} & 0 \\ 0 & 0 & 0 & \omega_{C_2} \end{bmatrix} \quad 4-27$$

where  $(\omega_{B_1}, \omega_{B_2}, \omega_{C_1}, \omega_{C_2})$  are the sectorial coordinates of the points in the cross-sections where the displacements  $(u_{B_1}^1, u_{B_2}^3, u_{C_1}^2, u_{C_2}^2)$  are defined. Finally, the stiffness equations in terms of bimoments can be written as,

$$\begin{cases} B_{B_1} = \bar{K}_{B_1B_1} \Phi_{B_1} \\ B_{B_2} = \bar{K}_{B_1B_1} \Phi_{B_2} \\ B_{C_1} = \bar{K}_{B_1B_1} \Phi_{C_1} \\ B_{C_2} = \bar{K}_{B_1B_1} \Phi_{C_2} \end{cases} \quad 4-28$$

where,

$$\begin{cases} \Phi_{B_1} = \varphi'_{B_1} + b_1 \varphi'_{B_2} + b_2 \varphi'_{C_1} + b_3 \varphi'_{C_2} \\ \Phi_{B_2} = b_4 \varphi'_{B_1} + b_5 \varphi'_{B_2} + b_6 \varphi'_{C_1} + b_7 \varphi'_{C_2} \\ \Phi_{C_1} = b_8 \varphi'_{B_1} + b_9 \varphi'_{B_2} + b_{10} \varphi'_{C_1} + b_{11} \varphi'_{C_2} \\ \Phi_{C_2} = b_{12} \varphi'_{B_1} + b_{13} \varphi'_{B_2} + b_{14} \varphi'_{C_1} + b_{15} \varphi'_{C_2} \end{cases} \quad 4-29$$

In Equation 4-29, the constants  $(b_1, b_2, \text{etc.})$  are the ratios between stiffness terms of the  $\mathbf{K}_{\varphi'}$ -matrix, as obtained from Equation 4-17, and the reference stiffness  $(\bar{K}_{B_1B_1})$ , e.g.



$b_1 = \bar{K}_{B_1B_2}/\bar{K}_{B_1B_1}$ ,  $b_2 = \bar{K}_{B_1C_1}/\bar{K}_{B_1B_1}$ , etc. The warping stiffness matrix is symmetric so that  $b_1 = b_4$ ,  $b_2 = b_8$ , etc.

The 3D joint model, combining the linear springs and constraint equations expressed in Equations 4-28 and 4-29, respectively, is presented in Figure 4-8.

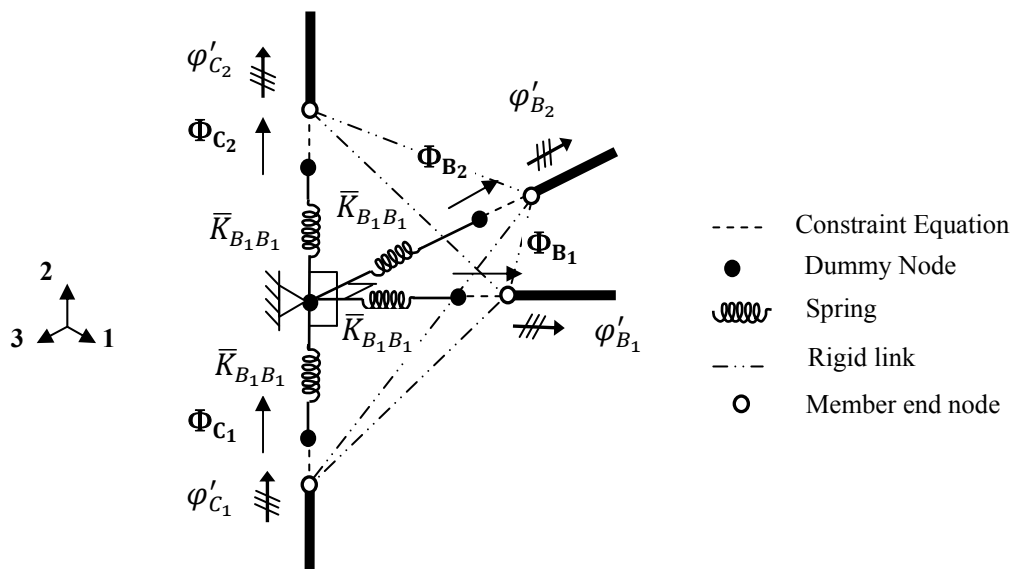


Figure 4-8: Joint spring model, 3D

## 4.5 Implementation of the model

ABAQUS (2009) is used in this study for creating numerical models, although the model is general and can be used in any FE software with the substructuring ability. The S4R shell element is used to model the joint as a substructure. The S4R element is a 4-node elements in which “R” stands for reduced integration. This element type is selected in preference to other element types, such as “solid” element, as the S4R shell element in ABAQUS features six degrees of freedom corresponding to three translations and three rotations at each node. Since the plate thicknesses are small compared to the other dimensions of the joint, thin shell theory is followed in which higher order effects on the stresses through the element’s thickness are ignored. To model beam elements, the ABAQUS B31OS beam element is selected which is a three dimensional element with 7

DOFs of which the seventh is warping. However, because there is no compatibility between the number of degrees of freedom in beam elements (7 DOFs) and shell elements (6 DOFs), no direct method is available to connect the warping degree of freedom of the beam to the joint model consisting of shell elements. However, the proposed joint model is capable to convert the 3D shell element joint model to a simple 2D system using linear spring.

In the first step, the substructure is modelled in the same way that any structural model may be created using shell elements. The \*EQUATION command in ABAQUS is then used to set the longitudinal displacements of corner nodes on each face of the joint in accordance with the sectorial coordinates of the nodes. For sections composed of three plate elements (e.g. I-sections), this requires three constraint equations for each face. Currently, substructure modelling is not supported by the ABAQUS/CAE pre-processing user interface; thus a PERL script was written to generate the joint model (PERL is a common programming language that can be run in most computer operating system). The joint itself is analysed using the ABAQUS \*SUBSTRUCTURE GENERATE command and the condensed stiffness matrix is generated using the \*SUBSTRUCTURE MATRIX OUPTPUT command. This produces the terms of the  $\mathbf{K}_u$  matrix (Equation 4-13). Two types joints (box joint and box joint with one diagonal stiffener) generated as substructure in ABAQUS using the script are presented in Figure 4-9. An example of a PERL script for creating a shell finite element model of the corner joint shown in Figure 4-4 and an ABAQUS input file for analysing the joint as a substructure can be found in Appendix B.

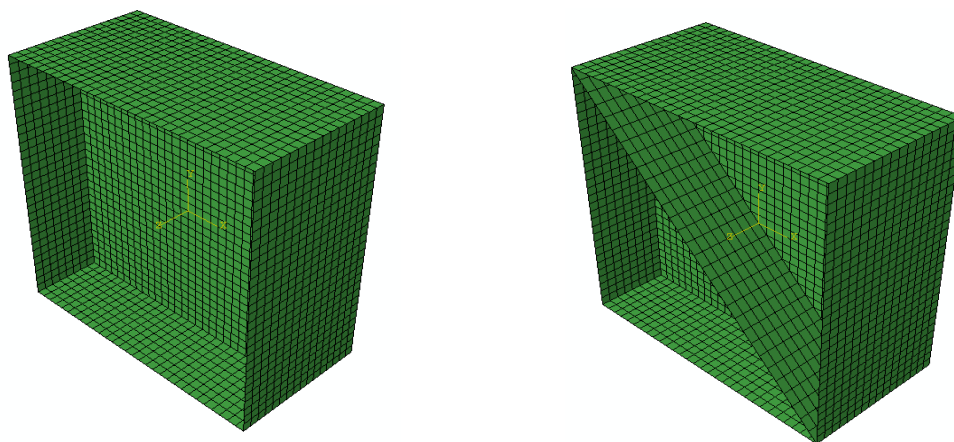


Figure 4-9: ABAQUS substructure (a) box joint (b) box joint with one diagonal stiffener

Once the warping stiffness matrix ( $\mathbf{K}_{\varphi'}$ ) is formulated using Equation 4-17, it can be applied to the beam finite element model. This is achieved by defining dummy nodes, which are independent of the nodes used to define the structure. Linear spring elements (SPRING2 element of the ABAQUS library) are connected to each pair of dummy nodes and for each spring element, one dummy node is fixed while the other is the degree of freedom of the element and is designated by  $\Phi$ . This spring degree of freedom is then related to the warping degrees of freedom ( $\varphi'$ ) of the adjoining members through a constraint equation (e.g. as per Equations 4-25 and 4-26), which is defined in ABAQUS using the \*EQUATION command. The translational and rotational degrees of freedom of the adjoining beams are transmitted directly and rigidly between members connected to the joint using “Beam” rigid links. The 2D and 3D joint models using ABAQUS are shown in Figure 4-10.

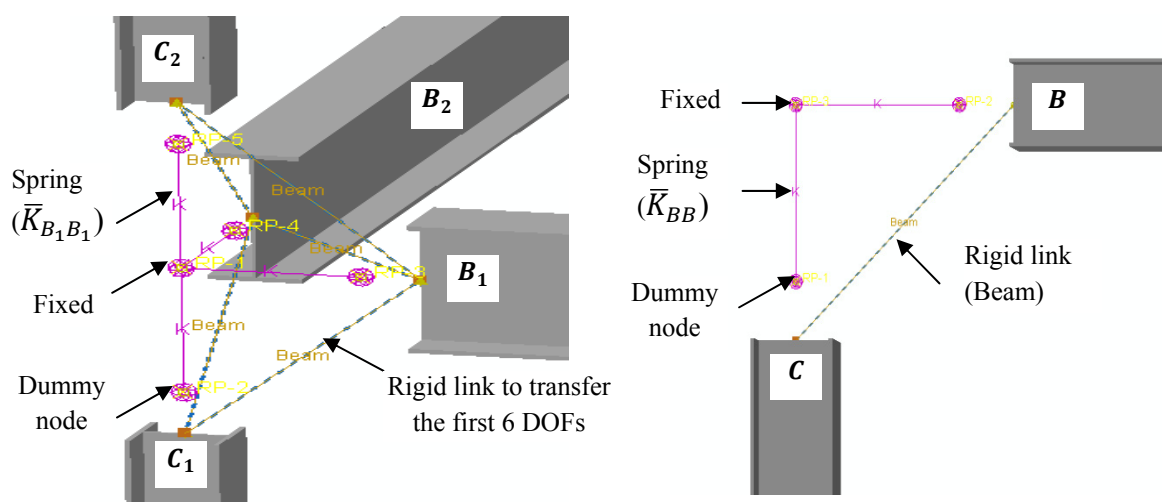


Figure 4-10: ABAQUS joint spring model, (a) 3D, (b) 2D

It should be mentioned that, as an alternative the substructure can be employed to the model as an element. The remaining DOFs of the substructure define its connectivity and can be linked to the adjacent beam and column nodes in the beam element model. The problem of this approach is that the substructure cannot be used with Eigen buckling analysis in ABAQUS. It is also possible to utilise the stiffness matrix as a “user element”. This method requires incorporating a user subroutine in which the elements are assembled manually and the reduced stiffness matrix is calculated in a closed form solution. This

method is more complex and requires a subroutine which must be written outside the ABAQUS. Thus, although both approaches provide same results, it was decided to model the joint using the combination of springs and constraint equations.

## 4.6 Verification and illustrative examples

In order to evaluate the performance and capabilities of the proposed joint model, three thin-walled planer steel frames as well as two space frames have been analysed using the model in conjunction with one-dimensional beam elements (B-FEA), and compared with results for the same frames obtained using 3D shell elements (S-FEA). To investigate the performance of proposed model, buckling and first order elastic analysis as well as second order inelastic analysis has been conducted using ABAQUS. All frames are made of steel I-sections with Elastic modulus ( $E$ ) equal to 200 GPa and Poisson's ratio equal to 0.3. In order to prevent the overall frame out-of-plane buckling of 2D frames, all frames are laterally restrained at the beam-column connections. For the shell element joint model, a lateral restraint is applied on a surface at the middle of the joint, (a surface rather than a node is restrained to avoid large local deformations as can result from applying a restraint at a single point) (see Figure 4-11). This method of applying boundary lateral restraint was verified by Yuan (2004). In the beam element model the top of the columns is restrained on the global Z-direction.

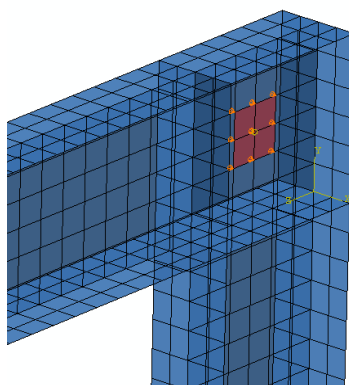


Figure 4-11: Out-of-plane restraint model in S-FEA

The column bases are fully fixed and to avoid any local deformations all cross-sections are chosen as compact. For this study, three dimensional beam elements with 7 DOFs per

node (B32OS) and S4R shell elements are used. The shell finite element analyses are based on discretisations of the flanges and webs into 4 and 6 elements respectively while the length of each element in the beam analyses is taken as 25 mm. The thicknesses of stiffeners added to the joints are taken as equal to the flange thickness of adjoining beams. For the nonlinear analysis, (i) the yield stress of all frames is taken as 320 MPa, (ii) the material is assumed to be linear perfectly-plastic, and (iii) the initial imperfection is modelled by scaling the first buckling mode by the scale factor of  $0.00123H$ , in which  $H$  is the total structural height (Shayan, Rasmussen et al. 2012). The detail of this model is presented in Chapter 5.

## 4.6.1 Planer Frames

### 4.6.1.1 L-Shape frame

The first study illustrates the elastic buckling behaviour as well as the nonlinear response of the L-shape steel frame shown in Figure 4-12, which has only one beam and one column meeting at the joint. In order to assess the application of the proposed model, three different types of joint have been considered: (a) box stiffened joint with web continuity, (b) box-stiffened joint with one diagonal stiffener and (c) box-stiffened joint with two diagonal stiffeners, as shown in Figure 4-12. The beam and column are made from 150UB14 section (Figure 4-12) and a vertical point load  $P$  equal to 1000 N is applied to the shear centre at the end of the beam. A sample ABAQUS indata file for analysing the frame using the B-FEA spring model with a box-stiffened joint (Figure 4-12 (a)) is presented in Appendix B.

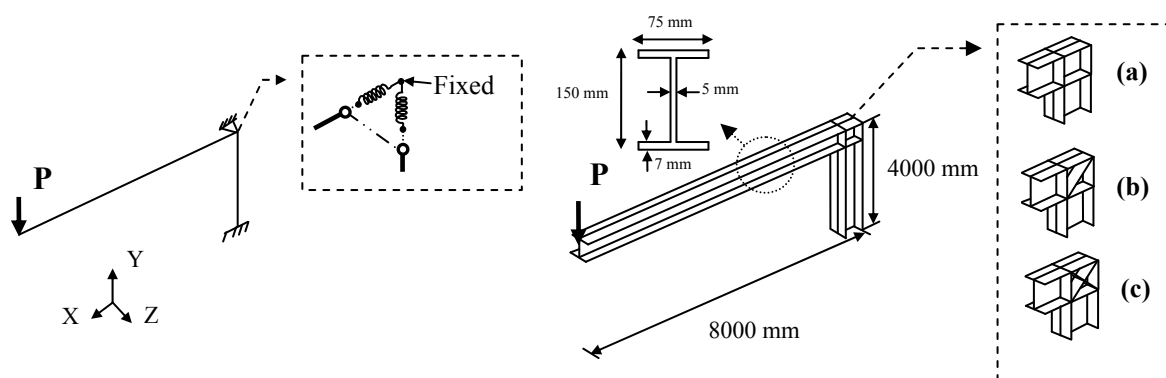


Figure 4-12: Configuration and dimension of L-shape plane frame

Table 4-2 shows the spring stiffness, the bimoments in the adjoining members at incipient buckling and the critical buckling loads obtained using the beam element (B-FEA) with spring joint model and the shell (S-FEA) element model for the three joint configurations. In addition, for comparison, the critical buckling loads are obtained using the constraint equation model introduced by Basaglia et al. (2010), referred to as “Equation” in Table 4-2.

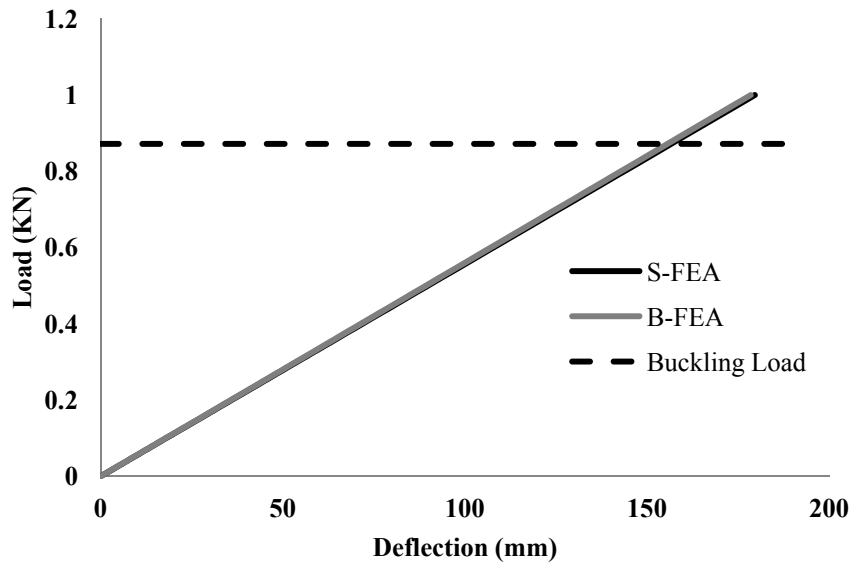
Table 4-2: Spring stiffness, bimoments and critical buckling loads of L-shape frame

Joint configuration	Spring Stiffness (N. mm <sup>3</sup> )	Bimoment (N. mm <sup>2</sup> )		Critical buckling load (N)			Error (%) (B-FEA (spring) and S-FEA)
	( $\bar{K}_{BB}$ )	Beam	Column	B-FEA (Equation)	B-FEA (Spring)	S-FEA	
Joint (a)	2.867E+12	860	-725	897	895	872	2.57%
Joint (b)	4.484E+12	1613	-250	972	937	920	1.80%
Joint (c)	6.200E+12	1727	-200	NA	948	931	1.79%

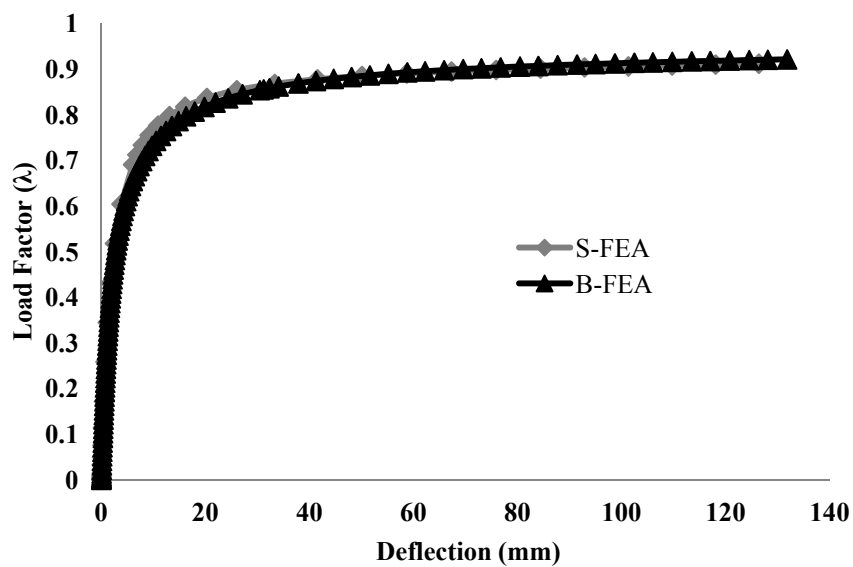
Based on the results in Table 4-2, it can be seen that the spring stiffness increases as stiffeners are added to the joint. The warping transmission is almost complete and inverse for the box joint (a) and almost prevented for the box joints with one and two diagonal stiffeners (b and c), as confirmed by Basaglia et al. (2010). Comparing the results of S-FEA and both types of B-FEA, it can be seen that for joints (a) and (b) the “spring” joint model can predict the critical buckling load more accurately than the “constraint equation” model.

The maximum discrepancy between the B-FEA using spring model and S-FEA model is 2.57%, indicating good accuracy. It is worth noticing that the joint configuration influences the critical buckling load and that by adding two stiffeners to the joint, the buckling load is increased by 6% compared to the frame with box-joint without diagonal stiffeners. Figure 4-13 (a) and (b) further illustrate that excellent agreement is achieved between the load versus out-of-plane tip-deflection curves of first-order elastic analysis and nonlinear analysis respectively, obtained using beam and shell element nonlinear analyses. The requirements and details of second-order analysis in ABAQUS are explained in Chapter 3. The joint stress contours at the ultimate load are presented in Figure 4-14 and clearly indicate that the joint is not yielded at the ultimate limit state. The maximum von Mises stress is 153.8 MPa which is less than half of the yield stress of 320

Mpa. The ultimate frame strength is 910 N which is almost equal to the critical buckling load. Hence, the frame fails in the frame fails elastically in a flexural-torsional buckling mode.



(a)



(b)

Figure 4-13: Load-deflection curve of L-shape planner frame (a) first-order elastic analysis, (b) nonlinear inelastic analysis

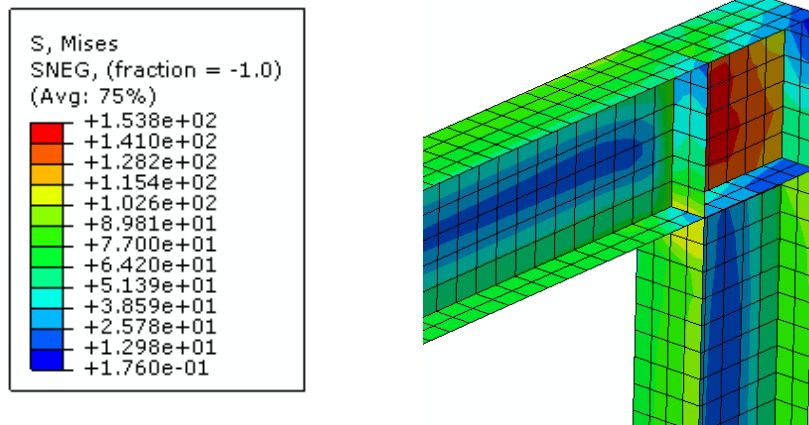


Figure 4-14: Joint stress contour for nonlinear analysis of L-shape planner frame

#### 4.6.1.2 One-bay, one -storey frame with an overhanging member

A portal frame with an overhanging member has been studied. In addition to the corner joint considered in the previous example, the frame features an intermediate joint which connects three members. This example has been chosen to show that the method is general and does not depend on the number of adjoining members or joints. The frame configuration and joint types can be seen in Figure 4-15. The same three joint types are considered as in the previous example, where the same type of joint (e.g. box-stiffened joint with web continuity) is assigned to both Joint 1 and 2. The frame is made from 150UB14 and the distributed load equal to 1 N/mm is applied along the length of both beams and the at shear centre.

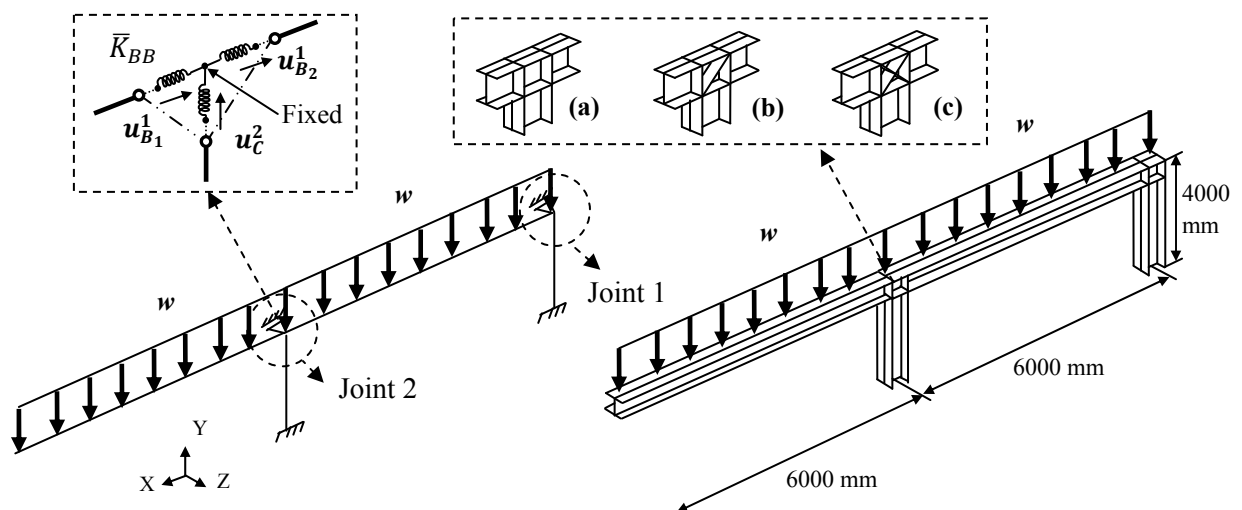


Figure 4-15: Configuration and dimension of plane portal frame with an overhanging member



The stiffness matrix for joint 2 with non-stiffened box-stiffened configuration obtained using the substructure analysis in ABAQUS is presented in Equation 4-30. As the size of the beams and column attached to the joint are the same, several stiffness matrix terms are equal (i.e.  $K_u(1, 1) = K_u(2, 2)$  and  $K_u(1, 3) = K_u(3, 2)$ , where columns 1, 2 and 3 of  $\mathbf{K}_u$  refer to  $u_{B_1}^1$ ,  $u_{B_2}^1$  and  $u_C^2$ , respectively).

$$\mathbf{K}_u = \begin{bmatrix} 440568 & -163044 & 251363 \\ -163044 & 440568 & 251363 \\ 251363 & 251363 & 523643 \end{bmatrix} \quad (\text{N. mm}^3) \quad 4-30$$

Using Equation 4-22, the warping stiffness matrix is determined and shown in Equation 4-31. The sectorial coordinate for this joint is  $2681 \text{ mm}^2$ .

$$\mathbf{K}_\varphi = \begin{bmatrix} 3.32E + 12 & -1.23E + 12 & 1.90E + 12 \\ -1.23E + 12 & 3.32E + 12 & 1.90E + 12 \\ 1.90E + 12 & 1.90E + 12 & 3.95E + 12 \end{bmatrix} \quad 4-31$$

As it is shown in Equation 4-22, the first diagonal stiffness term is considered as a fixed value ( $\bar{K}_{BB}$ ) and the other terms are written as a fraction of that fixed term. The warping stiffness matrix and a set of three constraint equations for joint 2 are shown in Equation 4-32 and Equation 4-33 respectively.

$$\mathbf{K}_\varphi = \begin{bmatrix} \bar{K}_{BB} & -0.37 \bar{K}_{BB} & 0.57 \bar{K}_{BB} \\ -0.37 \bar{K}_{BB} & \bar{K}_{BB} & 0.57 \bar{K}_{BB} \\ 0.57 \bar{K}_{BB} & 0.57 \bar{K}_{BB} & 1.188 \bar{K}_{BB} \end{bmatrix} \quad 4-32$$

The stiffness equations can be rewritten as

$$\begin{cases} \varphi'_{B_1} - 0.37 \varphi'_{B_2} + 0.57 \varphi'_C = \Phi_{B_1} \\ -0.37 \varphi'_{B_1} + \varphi'_{B_2} + 0.57 \varphi'_C = \Phi_{B_2} \\ 0.57 \varphi'_{B_1} + 0.57 \varphi'_{B_2} + 1.188 \varphi'_C = \Phi_{C_1} \end{cases} \quad 4-33$$

The warping stiffness ( $\bar{K}_{BB}$ ) and critical buckling loads are presented in Table 4-3 for the three Joint 2 configurations. Once again, excellent agreement is achieved between the critical buckling loads obtained from the beam finite element analysis using the spring joint model and the shell element analysis. The largest error is 1.08% which relates to the

box joint. Similar to the previous example, changing the joint configuration from a box joint to box joints with one and two diagonal stiffener increases the critical buckling load by 5% and 7% respectively. For all cases, the spring model more accurately predicts the elastic buckling behaviour compared to the constraint equation model (Basaglia et al. 2010).

Table 4-3: Spring stiffness of joint 2 and critical buckling loads of portal frame with an overhanging member

Joint configuration	Spring Stiffness (N.mm <sup>3</sup> )	Critical buckling load (N/mm)			Error (%) (B-FEA (spring) and S-FEA)
	( $\bar{K}_{BB}$ )	B-FEA (Equation)	B-FEA (Spring)	S-FEA	
Joint (a)	3.322E+12	939	922	912	1.08%
Joint (b)	5.038E+12	1031	969	960	0.93%
Joint (c)	6.269E+12	NA	990	983	0.71%

The load versus out-of-plane deflection curves obtained from nonlinear analyses of the frame with box joints is plotted in Figure 4-16, indicating excellent agreement between the shell and beam element analyses. The ultimate strength is 950 N/mm which is close to the elastic critical buckling load. It follows from the stress contours shown in Figure 4-17 that the failure is elastic.

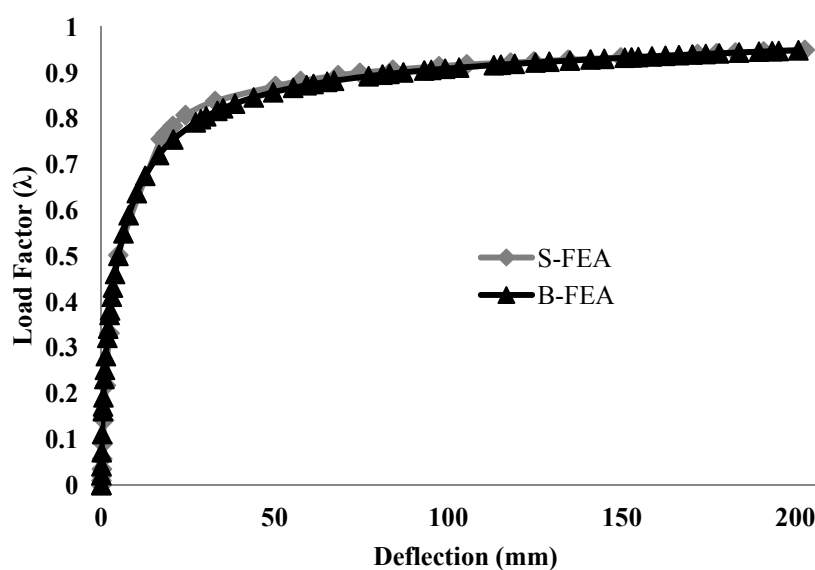


Figure 4-16: Nonlinear load-deflection response of one-bay, one storey frame with overhanging member

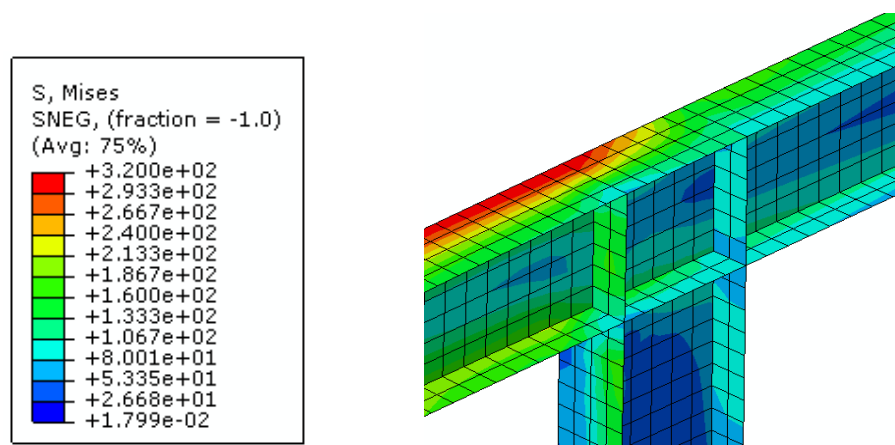


Figure 4-17: Joint stress contour for nonlinear analysis of one-bay, one-storey planner frame with overhanging member

#### 4.6.1.3 One-bay, two-story frame

A two-storey portal frame with box joint is analysed using both elastic buckling and nonlinear analysis. The frame configuration and loading are presented in Figure 4-18. The frame is made by 310UB40 and a distributed load ( $w$ ) equal to 67.5 N/mm is applied at shear centre. The elastic critical buckling load factor obtained using B-FEA and the presented spring model is 1.18, i.e. the critical buckling value of the applied load is 79.65 N/mm, while the frame buckling load corresponding to S-FEA is 76.95 N/mm. With the difference of 3.39 % and so again, the spring joint model fairly accurately predicts the effect of warping transmission through the joint in elastic buckling analyses.

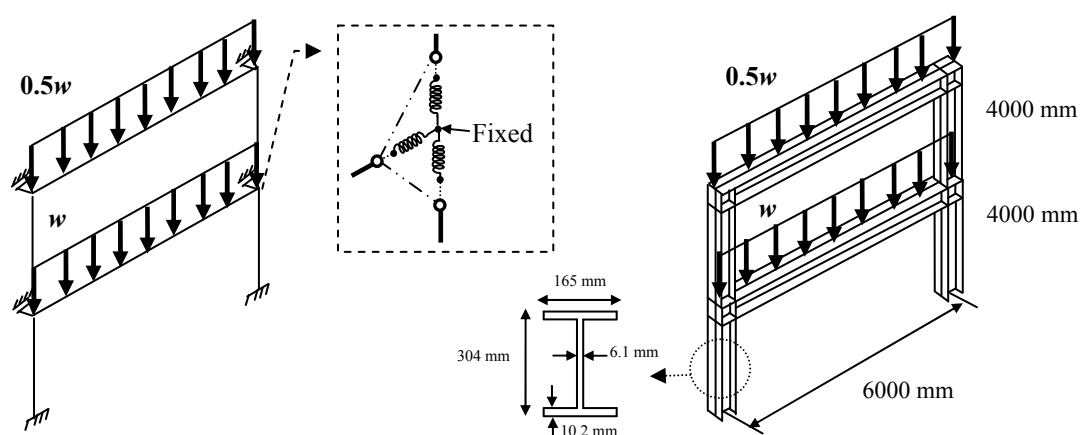


Figure 4-18: Configuration and dimension of two-storey plane portal frame

As the stress contour of nonlinear inelastic analysis shows, in this case the Joint 2 is yielded at the ultimate load (Figure 4-19).

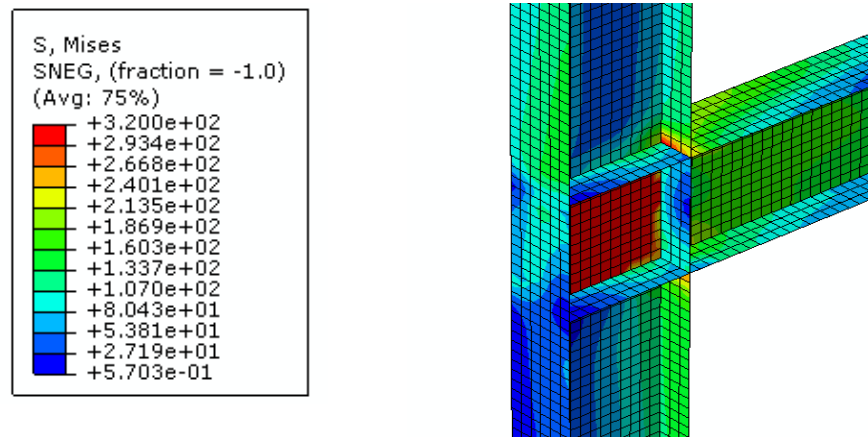


Figure 4-19: Joint stress contour for nonlinear analysis of one-bay, two-storey planner frame,  $f_y=320$  MPa

In the case of nonlinear analysis, the ultimate load factors obtained using B-FEA and S-FEA analyses are 0.96 and 0.82 respectively, as shown in Figure 4-20. It follows from the stress contours shown in Figure 4-21 that the joints are yielded in the ultimate limit state.

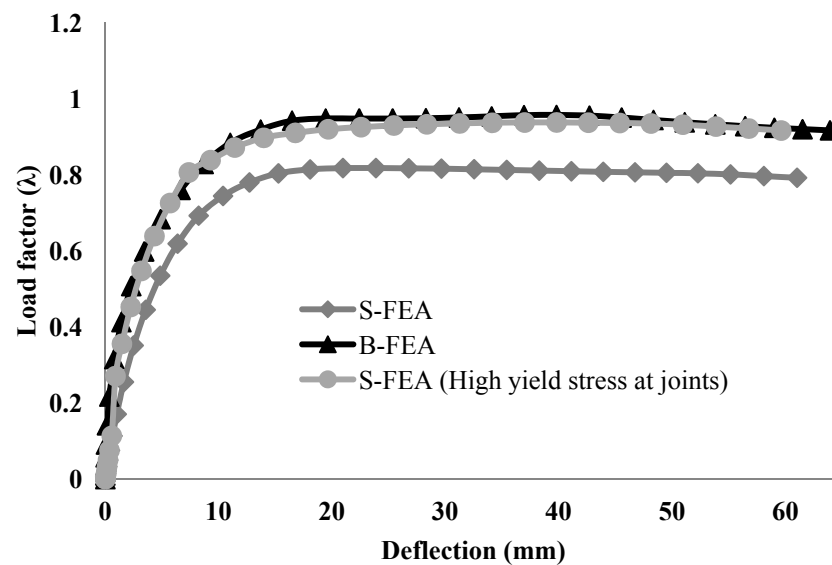


Figure 4-20: Nonlinear load-deflection response of one-bay, two-storey frame

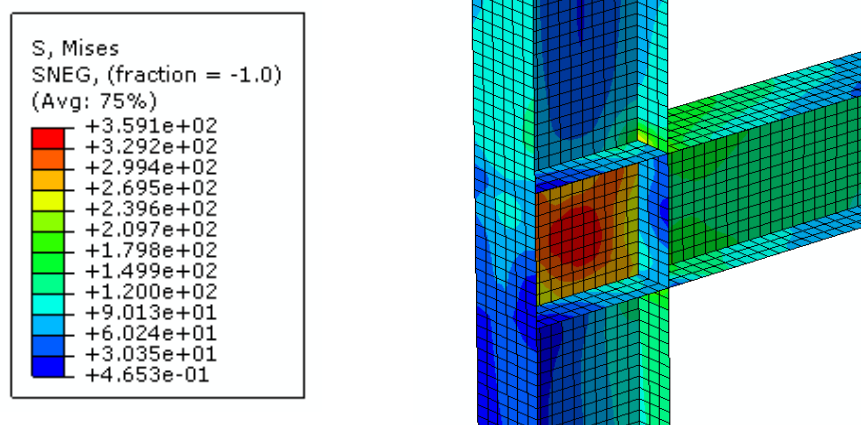


Figure 4-21: Joint stress contour for nonlinear analysis of one-bay, two-storey planner frame,  $f_y=450$  MPa

The discrepancy between the B-FEA and S-FEA nonlinear analysis results stems from the joint modelling which implicitly assumes elastic material behaviour, since the spring stiffness terms are obtained from a substructuring method that calls a linear-elastic analysis. Note that if the yield stress of the joints is increased to 450 MPa to prevent yielding at the joints, it can be seen from Figure 4-20 that the B-FEA and S-FEA analyses are in close agreement. It follows that the proposed model is accurate for nonlinear inelastic analysis as long as the joints remain elastic, but may become inaccurate when the frame strength is governed by yielding in the joints.

## 4.6.2 Space Frames

### 4.6.2.1 One-bay, one storey frame

Finally, two space frames have been analysed using beam and shell finite elements to evaluate the applicability of the proposed joint spring model to three dimensional frames with members adjoining in different planes. The first frame is a one-bay, one-storey frame with three transverse beams. All members have the same I-300×8 cross-sections with a flange width of 150 mm, web height between flange centrelines of 300 mm and uniform thickness of 8 mm, except for the two transverse end beams for which the flange width is 300 mm. The frame is subjected to five equal point loads  $P$  at the top of the

columns and the mid-span of the transverse beam at the centre. The loads are applied at the cross-section shear centre in S-FEA and at the top column nodes in B-FEA. The out-of-plane displacement along global X direction is restraint at all joints. The middle transverse beam cannot move along the global Z direction. While the lateral supports are located at the centre of the joints or at cross-section mid-web for transverse beam in shell finite element model, these restraints are applied at top of the columns in beam finite element model. All column bases are fully fixed.

The frame features two types of joint: (a) beam-column joint and (b) beam-beam joint. For both joint types the web of perpendicular member is continuous through the joint. Warping through the joints can be modelled by the use of three springs and three constraint equations in the beam finite element analysis. Figure 4-22 shows the frame configuration, loading and joint types of the space frame for both B-FEA and S-FEA.

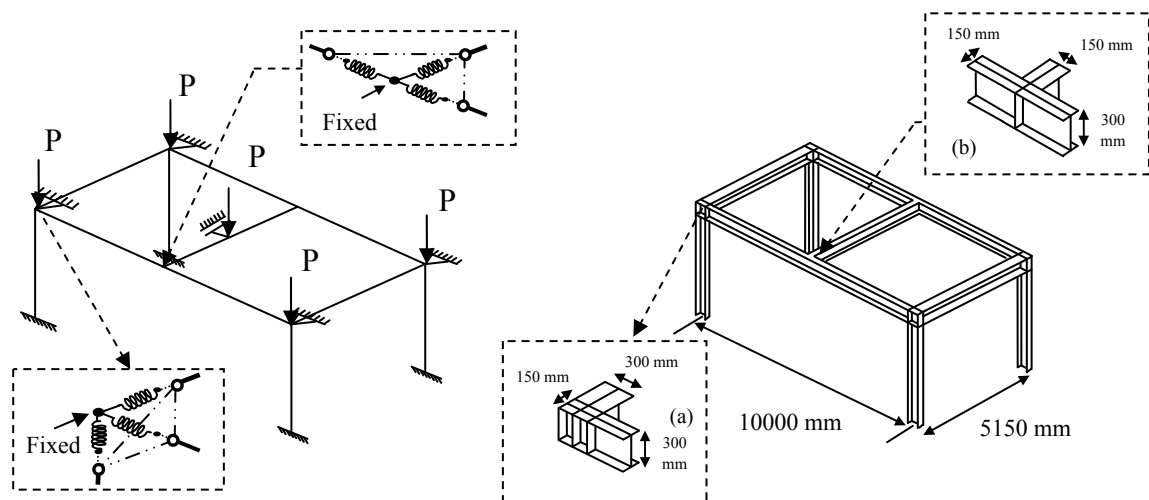


Figure 4-22: Configuration and joint types of the one-bay, one-storey space frame

The critical buckling loads from beam and shell finite element analysis are 350.3 kN and 342.8 kN respectively with the difference of 2.13%. Figure 4-23 compares the frame critical buckling mode configurations using the beam and shell finite element analyses and provides a clear coincidence between the buckling results. In this example, the beams incur significant flexural-torsional buckling deformations which cause pronounced warping of the joints, so the performance of the joint model is well tested.

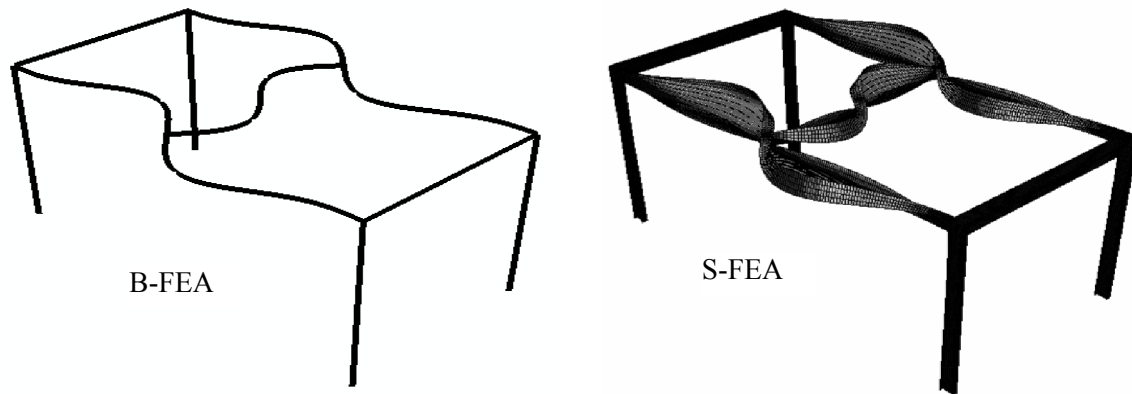


Figure 4-23: B-FEA and S-FEA critical buckling modes of the space frame with transverse beam

#### 4.6.2.2 One-bay, one storey frame

The second space frame is a one-bay, two-storey frame consisting of two different corner joints with three and four connecting members, as shown in Figure 4-24. This example is chosen to show that the model is applicable to any type of joint and does not depend on the number of adjoining members. To achieve a more general case compared to previous examples, while the connecting beams and columns have the same flange dimension, the beam depth is twice of the flange width. The cross-sections are still compact and their dimensions can be found Figure 4-24. Note that the columns have the same cross-section as do the beams in the  $X$ - and  $Z$ -directions. The loads are applied as uniform distributed load along the beams and all column bases are fully fixed. For S-FEA, the loads are applied at the beam shear centres. The critical buckling load obtained from of beam and shell analyses are 718.5 kN for 682.2 kN, results to the difference of 5%. It should be noted that, same as pervious example the joints indicate significant warping.

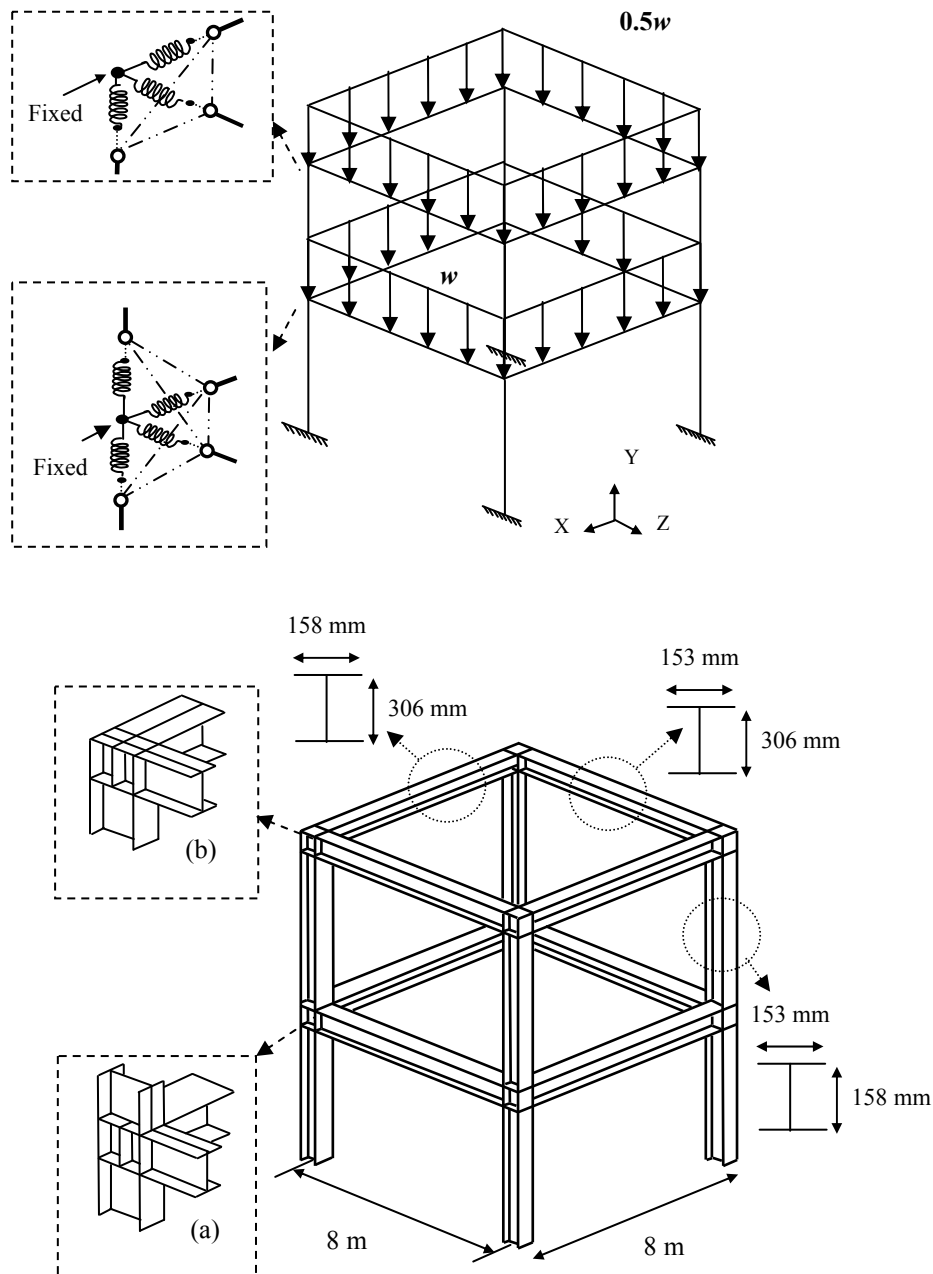


Figure 4-24: Configuration and joint types of the one-bay, two-storey space frame

The frame buckling shape includes the flexural torsional buckling of the first storey beams and perfectly matches for both analysis types (Figure 4-25).



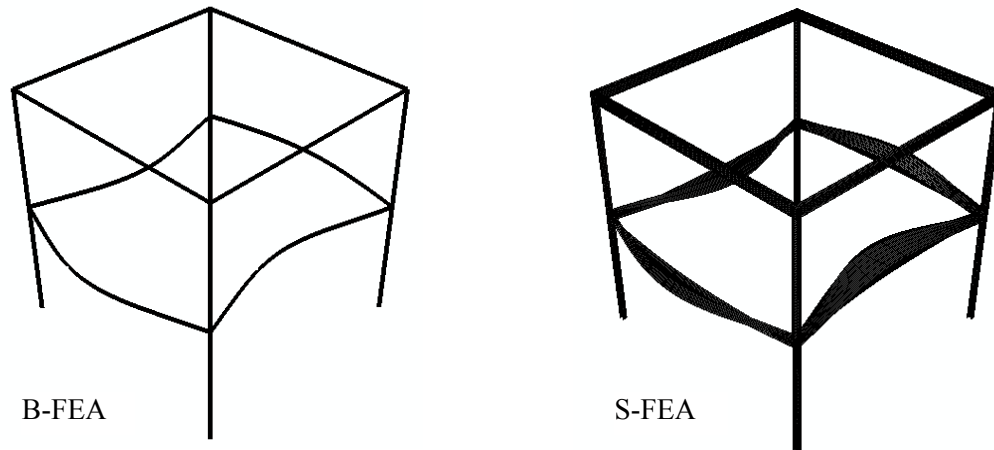


Figure 4-25: B-FEA and S-FEA critical buckling modes of the one-bay, two-storey space frame

## 4.7 Observations and remarks

The comparisons made in the analyses of 2D and 3D frames presented in Section 4.5 lead to the following remarks:

1. There is excellent agreement between the buckling results of all considered frames using beam finite element analysis with “spring” joint model and shell finite element analysis. All the current models for warping transmission including “linear constraint equation” proposed by Basaglia et al. (2010) assume fully prevented warping for diagonal-stiffened joint. This assumption is correct when the diagonal stiffener is thick enough to prevent warping. It was proved in the first example that even for the case of box-stiffened joint with two diagonal stiffeners there is still a portion of warping transmission though the joints and the assumption of fully prevented warping in diagonal/box-stiffened joint is conservative. The proposed model can predict the elastic behaviour of this type of joint more precisely.
2. Based on the first two examples, it can be seen that in all cases the spring joint model can predict the buckling loads more accurately compared to the constraint equation model. In addition, the suggested method can considerably reduce the number of degrees of freedom and computational expense in comparison with shell finite element analysis.

3. The study of different types of joints shows that the critical elastic buckling load is related to the joint configuration and progressively increases as the joint becomes stiffer. Stiffeners are effective in reducing distortion of the cross-section and so increase the resistance to warping and the critical buckling load.

4. The proposed joint model is based on a combination of linear springs and linear constraint equations, and as was shown in the verification examples it can accurately be applied in elastic buckling analyses. It can also be applied in nonlinear analyses as long as yielding does not occur in the joints. The substructuring technique adopted in this paper is based on a linear elastic analysis of the joint and so produces a linear spring model which cannot capture the effect of yielding.

5. It should be noticed that the model assumes the deformation imposed on the joint is a linear combination of extension, rotation, and warping modes of deformation. Consequently, if the connection between the adjoining member and the joint is such that the joint deformation will not be a combination of these modes, the joint model is unlikely to produce accurate results. This would typically occur if only a subset of plate elements of a cross-section were connected to the joint, e.g. if the bottom flange of a beam is rigidly connected to a column but the top flange is free.

6. The presented joint model is general and can readily be used for most typical joint configurations by means of substructuring techniques. Unlike most available methods for modelling joints, which apply to corner joints with only two adjoining members, the proposed model can be used regardless of the number of connected members, and applies equally to 2D and 3D frame structures.

## **4.8 Conclusion**

This chapter outlines an accurate joint model which can be incorporated into beam-based finite element analyses to consider the effect of warping and its transmission between the connected members. The proposed model is simple to implement into finite element using readily available beam and spring elements, and does not require the beam stiffness matrix to be modified or computationally costly shell finite element modelling to be

employed. In this method, the joint itself modelled as an assemblage of shell elements and analysed a priori as a substructure. By using static condensation, the substructuring technique produces a small stiffness matrix which can be converted to a warping stiffness matrix. The warping stiffness matrix components are applied as springs associated with a set of linear constraint equations.

The introduction of warping springs provides a simple and more accurate estimate of the joint warping stiffness in beam finite element analyses. The model is general and applicable to arbitrary 2D and 3D joint types. Different frames have been analysed using beam elements to evaluate the performance and capabilities of the proposed joint model. Excellent agreement has been achieved comparing the critical elastic buckling loads of the frames with the exact values obtained using shell finite element analysis. Finally, it is worthy to note that due to simple way of modelling, this approach can be used in all common applications in industry where designers look for fast and easy methods and avoid any implication in design methodologies.

# CHAPTER

## 5 .

# Modelling of initial geometric imperfections of steel structural frames

---

## 5.1 Introduction

Steel structural members and frames are not perfectly straight due to manufacturing and erection tolerances and always indicate imperfections to various degrees. In the early 1950s, large discrepancies were found between theoretical and experimental buckling loads of the steel structures. The discrepancies remained unexplained until the work of Koiter (1945) who understood that small unavoidable imperfections cause differences between theory and experiment. These discrepancies can be reduced by taking into account the effect of all imperfections to determine the load carrying capacity of a steel frame. In general, two types of geometrical imperfections should be taken into account: (i) the member out-of-straightness (bow imperfection) and (ii) the frame out-of-plumb (sway imperfection).

The initial geometric imperfections, which are a major factors contributing to the nonlinear behaviour of a steel structure, may have a significant effect on the strength and stability of the whole system (Rossow, Barney et al. 1967; Chebl and Neale 1984). The ultimate strength of a steel structure is sensitive to these imperfections and consequently, they need to be modelled accurately when determining the load carrying capacity of a steel frame by advanced structural analysis. In advanced analysis, the sway and bow imperfections are often chosen to be the worst case scenario to maximize the destabilizing effects under the applied loads. Nevertheless, the worst case scenario of imperfections may be overly conservative. In reality, both initial out-of-straightness and initial out-of-plumb are randomly distributed, and a rational modelling of geometric imperfections can only be achieved by using probabilistic methods. Although extensive research has been conducted on advanced analysis for steel structural systems (Beedle 1958; Clarke et al. 1992), a rational method of modelling initial geometric imperfection in advanced analysis has yet to be developed. The modelling of imperfections is more complex in the case of a structural system compared to a single member because not only the magnitude, but also the shape and direction of the imperfection of each member influence the structural response.

There are various ways to take geometric imperfection effects into account in the finite element analysis (FEA) of steel frames. The common approaches include: scaling of Eigen Buckling Modes (EBM), application of Notional Horizontal Forces (NHF), further reduction of member stiffness ( $E_t'$ ), and the direct and explicit modelling of Initial Geometric Imperfections (IGI) (Chan et al. 2005). These methods have been discussed in details in Chapter 2. The difficulty associated with most of the methods for modelling imperfections is that no information is provided about the direction of the imperfections. The designer has either to guess or solve for many possible combinations to find the worst case scenario, which for a real structure may be difficult to do. On the other hand, an incorrectly defined initial geometric imperfection may be beneficial to the system strength rather than being detrimental. In addition, the extension of these methods to three dimensional advanced analyses is unclear.

The present study is concerned with developing a new method for modelling initial geometric imperfections in second-order inelastic analyses as a linear superposition of a limited number of scaled buckling eigenmodes. The statistical data of initial geometric

imperfections are presented and probabilistic methods are employed to find a suitable number of buckling modes to be incorporated as well as the scaling factor for each buckling mode. For validation purposes, the performance of the proposed model is demonstrated by a number of case studies. The suggested procedure can be readily implemented into frame finite element analyses and extended to 3D models.

## **5.2 Statistical data for initial geometric imperfection**

The methods for modelling geometric imperfections can be classified as deterministic or random. For deterministic modelling, the maximum amplitude of an initial geometric imperfection is typically determined from a steel structural specification (Table 2-2). The pattern for the initial out-of-straightness is often assumed to be a half-sine wave and the frame out-of-plumb follows a linear pattern with all columns leaning in the same direction. In probabilistic modelling, the initial geometric imperfections (both shape and the magnitude) are treated as random variables. The probabilistic modelling requires statistical information for the geometric imperfection, such as distribution type, mean and standard deviation. Ideally, the probabilistic models should be established on the basis of sufficient experimental data.

### **5.2.1 Initial out-of-straightness**

Although a great number of experimental results on column strength can be found in the literature, very few studies report the detailed measurements of initial imperfections along the length of the member. Some of these measurements are back to 1960s and 1970s and published in form of research reports with no electronic recourses to easily access. In most studies, out-of-straightness is assumed to follow a half-sine shape and only the value for mid-span is reported which does not provide information about the contribution of higher order buckling modes with multiple half-waves. In this case only the magnitude of imperfection at mid-height can be modelled randomly while the shape of initial out-of-straightness is treated as deterministic. The statistical data for the non-dimensional out-of-straightness at mid-height of steel I-section members are summarized in Table 2-4. The presented results in this table show that a significant difference exists between measured

imperfections from different regions. It appears that on average, Japanese sections have smaller initial out-of-straightness compared to those from Europe or North America.

In this study, both the shape and magnitude are treated as random variables. Thus, detailed measurements of initial imperfections along the length of the member are required to obtain the statistics of initial out-of-straightness. The approach is based on the superposition of elastic buckling modes. For a member in compression the buckling modes are assumed to take the form of  $\sin(i\pi x)$  where  $i=1, 2, 3, \dots$  and  $x \in [0,1]$  is the non-dimensional coordinate measured along the length of the member ( $L$ ) (see Figure 5-1 for three buckling modes).

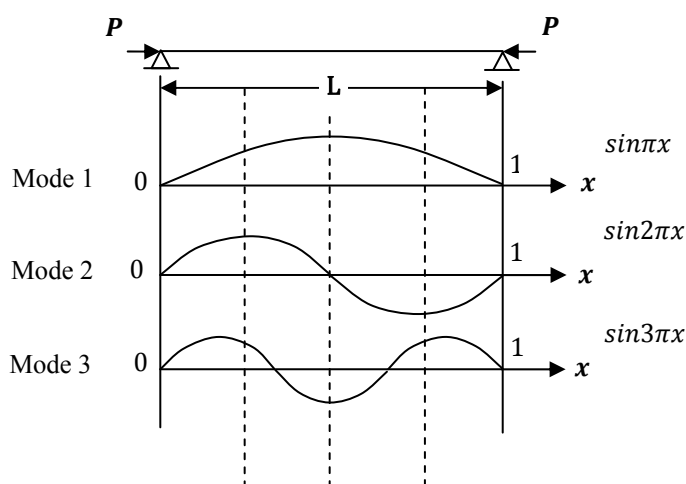


Figure 5-1: First three buckling modes of simply supported, axially loaded column

In general, the initial out-of-straightness of the member can be expressed in terms of a linear superposition of a given number of these eigen buckling modes:

$$d_x = \sum_{i=1}^m a_i \sin(i\pi x) \quad x \in [0,1] \quad 5-1$$

in which  $d_x$  is the initial out-of-straightness at location  $x$ ,  $a_i$  is the scale factor for the  $i$ th mode and  $m$  is the number of buckling modes included. In the following, it is assumed that a sample of  $N$  members is available and that for each member, the out-of-straightness at  $m$  locations along the length of member are measured.

This study is based on the initial out-of-straightness measurements of nine ( $N=9$ ) IPE 160 columns carried out at the University of Politecnico di Milano (C.E.A.C.M. 1966) and published by ECCS Committee 8.1 (Sfintesco 1970). The reported data comprises geometric imperfection measurements at mid-length and quarter points. First, the actual measurements are non-dimensionalised by dividing the measured imperfection by the length of the member (see Table 5-1).

Table 5-1: Measured initial out-of-straightness ( $d$ ) by Sfintesco (1970)

Sample No	$d_{0.25}$	$d_{0.50}$	$d_{0.75}$
1	0.000431	0.000507	0.000278
2	-0.00018	-0.00032	-0.0002
3	-7.27E-07	8.87E-05	0.000193
4	5.01E-05	-4.80E-05	-7.34E-05
5	-9.74E-05	-0.00031	-0.00025
6	-0.00011	-7.99E-05	-4.00E-05
7	-3.92E-05	1.45E-05	3.92E-05
8	-0.00016	-0.00022	-0.00022
9	-0.00026	-0.00023	-0.00036
$\mu( d )$	0.000148	0.000204	0.000183

As three readings of out-of-straightness are available for each sample, the out-of-straightness can be expressed as a linear combination of the first three buckling modes as shown in Figure 5-1. The scale factors, or contributions of each mode ( $a_i$ ,  $i=1, 2, 3$ ), can be determined by solving a set of three equations for each member (Equation 5-2) which is the expanded form of Equation 5-1.

$$\begin{cases} d_{0.25} = a_1 \sin \frac{\pi}{4} + a_2 \sin \frac{\pi}{2} + a_3 \sin \frac{3\pi}{4} \\ d_{0.50} = a_1 \sin \frac{\pi}{2} + a_2 \sin \pi + a_3 \sin \frac{3\pi}{2} \\ d_{0.75} = a_1 \sin \frac{3\pi}{4} + a_2 \sin \frac{3\pi}{2} + a_3 \sin \frac{9\pi}{4} \end{cases} \quad 5-2$$

Subsequently the statistical information of the scale factors  $a_1$ ,  $a_2$  and  $a_3$  (e.g. mean and coefficient of variation) can be obtained.

As shown in Table 5-1, the mean of the absolute values of measured out-of-straightness at mid-height, as reported by Sfintesco (1970), is equal to 0.000204 (1/4910), which appears



to be small compared to the mean provided by Fukumoto and Itoh (1983) based on 437 measurements and mean values obtained from other measurements around the world (Table 2-4). Thus, while the COVs of obtained scale factors remain unchanged (Table 5-2), the mean values are scaled up by a factor of 2.62 to match with the mean (1/1996) provided by Fukumoto and Itoh (1983) which appears to be a reliable representative value of initial out-of-straightness at member mid-might. The scale factor of 2.62 was obtained based on the fact that if the first three buckling modes are used to model the initial geometric imperfection of a single member, at mid-span only the first and the third modes contribute (see Figure 5-1). Therefore, the mean of the non-dimensional initial out-of-straightness at mid-span of a single member may be calculated as the difference between the mean of scale factors corresponding to mode one and three ( $\mu_{a_1} - \mu_{a_3}$ ), which is 0.00048 (1/2000) after scaling by factor of 2.62. The final statistical characteristics, i.e. mean ( $\mu$ ), standard deviation ( $\sigma$ ) and COV of the scale factors ( $a_i$ ,  $i=1, 2, 3$ ), are summarized in Table 5-3. The distribution of the scale factors, while based on a small number of data, was found to be approximately normal.

Table 5-2: Scale factors of the first three buckling modes

Sample No	$a_1$	$a_2$	$a_3$
1	0.000504	7.63E-05	2.86E-06
2	0.000294	1.02E-05	2.88E-05
3	0.000112	9.67E-05	2.35E-05
4	3.22E-05	6.18E-05	1.58E-05
5	0.000279	7.56E-05	3.47E-05
6	9.44E-05	3.71E-05	1.45E-05
7	7.27E-06	3.92E-05	7.27E-06
8	0.000246	2.91E-05	2.17E-05
9	0.000337	5.16E-05	0.000103
$\mu$	0.000212	5.31E-05	2.8E-05
COV	0.76771	0.511367	1.065306

Table 5-3: Statistic characteristics of scale factors

Statistics	$a_1$	$a_2$	$a_3$
Mean ( $\mu$ )	0.000556	0.000139	0.000073
COV	0.76771	0.511367	1.065306
Distribution	Normal	Normal	Normal

Using these statistics and combining the first three modes, random initial imperfection can be generated for different frame members. Since the absolute values of scale factors are considered to find the statistical characteristics, a random sign is generated and assigned to each scale factor. An example of randomly generated member out-of-straightness is presented in Figure 5-2.



Figure 5-2: Example of random shape of initial out-of-straightness for a simply-supported column

### 5.2.2 Initial out-of-plumb

The out-of-plumb can also be treated as a random variable and modelled as all columns leaning in same direction (Buonopane 2008) (Figure 5-3 (a)) or as each column leaning in its own direction (Lindner 1984 ; Lindner and Gietzelt 1984 ) (Figure 5-3 (b)).

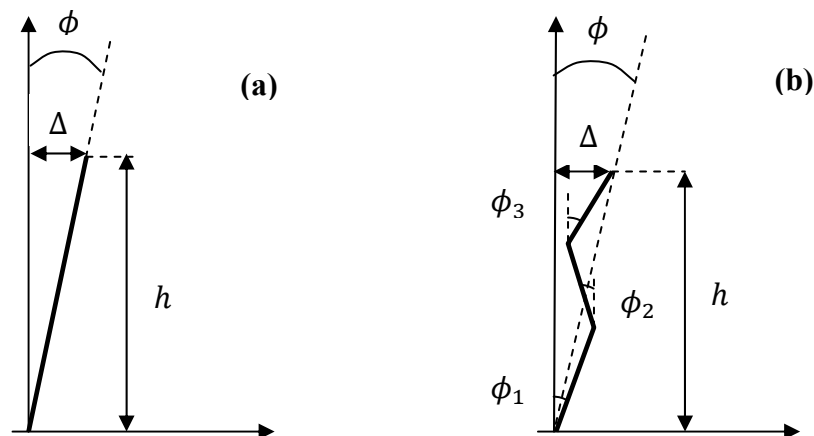


Figure 5-3: Initial out-of-plumb along the height (a) same direction (b) different direction

Horizontal displacements in both in-plane and out-of-plane directions of a multistorey steel frame has been reported by ECCS (1976) for the first, sixth and eleventh floor. Beaulieu and Adams (1978) measured the out-of-plumb,  $\Delta_o/L$ , of 916 columns in both directions and reported the mean as almost zero and the standard deviation as 0.00162. Extensive research in this area was undertaken by Linder (Lindner 1984 ; Lindner and Gietzelt 1984) who reported two groups of measurements from different buildings with different column heights. The first group of out-of-plumb measurements (approximately 725) were a second Canadian study by Beaulieu and Adams (1978) on two high rise buildings with a storey height of 3.6m. In the second group, the out-of-plumb of more than 900 German buildings with different heights between 3m and 125m were measured by Lindner and Gietzelt (1984 ). The mean and standard deviation of the total number of 1760 measurements recorded in Canada and Germany was  $\mu(\Delta_o/L)=0.0002$  and  $\sigma(\Delta_o/L)=0.000173$  respectively. The histogram of these data is presented in Figure 5-4 and appears to be normally distributed. Since these data are based on the measured out-of-plumb of existing structures in various parts of the world, they represent realistic values and are used in this study. It is assumed that all columns lean in a same direction and a single value of random out-of-plumb is applied to the whole frame.

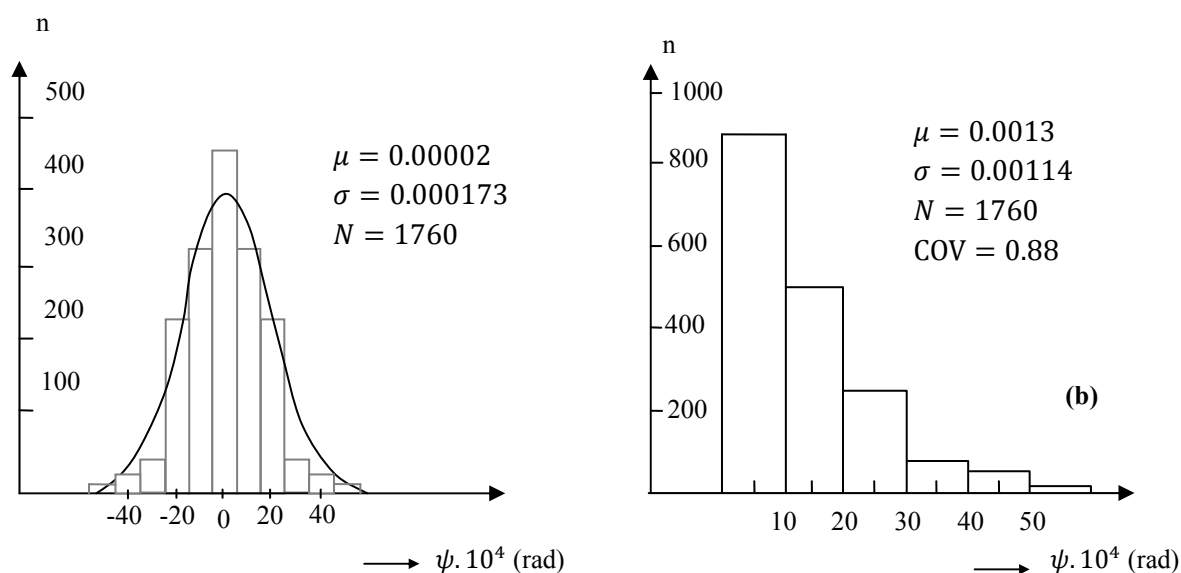


Figure 5-4: Out-of-plumb statistics reported by Lindner and Gietzelt (1984 ) (a) with sign (b) absolute

### **5.3 Initial geometric imperfection by linear combinations of eigenbuckling modes**

Since current methods for modeling initial geometric imperfections in advanced analysis are overly conservative and present difficulties such as guessing the worst direction of imperfection or manually offsetting node coordinates, a new procedure is introduced in this study. The method is based on the superposition of a limited number of eigenmodes which play the major role in triggering instability of the structure. Generally, when a structure reaches its critical load only the imperfection of those modes can influence the behaviour of the structure whose buckling load is close to the ultimate load (Rasmussen and Hancock 1988). If the buckling load of the first mode is not close to the ultimate load, this mode may not represent the critical shape of the initial imperfection. Thus, a combination of eigen buckling modes is a more appropriate approach.

For cold-formed steel members, studies have been carried out to model local and global perturbations in the geometry as a linear combination of buckling modes with scale factors calculated on the basis of experimental measurements (Rasmussen and Hancock 1988; Fang and Pekoz 2001; Zeinoddini and Schafer 2011; Zeinoddini and Schafer 2012). Theoretically, this methodology can also be applied to hot-rolled steel frames, provided we have the knowledge about how many elastic buckling modes to include and the scaling factor for each mode. A probabilistic framework is proposed here for determining a suitable number of buckling modes and their magnitudes for modeling initial geometric imperfections of steel frames.

#### **5.3.1 Amplitudes of eigenmodes**

In order to derive a general method for modelling imperfections as a superposition of scaled eigenmodes, the amplitude or the contribution of each mode needs to be determined. The general procedure for developing the scale factors can be summarised in seven essential steps:

(1) For each member of a given frame, a random member-of-straightness is generated as a superposition of three sine functions with 1, 2 and 3 half-waves and scale factors randomly determined using the statistical information presented in Table 5-3 is generated.

(2) An additional frame out-of-plumb is randomly generated according to the statistical information given in Figure 5-4.

(3) Steps 1 and 2 are repeated  $n$  times to create  $n$  frames with random geometric imperfections.

(4) For each frame, an elastic frame buckling analysis is performed to obtain the buckling shapes of the first  $m$  modes.

(5) Error minimization is then performed between the  $n$  randomly generated imperfect frames in Step 3 and the linear combination of  $m$  eigenmodes. This results in  $n$  values of scale factors for each mode, denoted by  $X_j^k$  ( $k=1, \dots, n$  and  $j=1, \dots, m$ ).

(6) The absolute values of the  $n$  scale factors are non-dimensionalised and their statistical characteristics are obtained. The mean values are denoted by  $\bar{x}_j$  ( $j=1, \dots, m$ ).

(7) Steps 1 to 6 are repeated for a range of frame layouts with different geometries and loading conditions. The mean values of the non-dimensionalised scale factors obtained from the different frame layouts are presented as the final values of the scale factors, denoted as  $SF_j$ , and can be implemented into advanced analysis to model initial geometric imperfections (both out-of-straightness and out-of-plumb).

Twenty braced frames and twenty-three unbraced frames were chosen in the present study to derive the scaling factors of buckling modes for modelling geometric imperfections. The frames were chosen to represent typical low-to-mid rise moment frames with regular and irregular configurations and were subjected to gravity loads. Detailed information about frame geometry, member sizes, and applied loads for the unbraced and braced frames can be found in Appendix C.1.1 and C.1.2., respectively.

Using the statistical characteristics obtained for initial out-of-straightness in Section 5.2.1, for each frame a sample of  $n$  ( $n=200$ ) sets of random scale factors ( $a_i, i=1, 2, 3$ ) are generated. Since the absolute values of scale factors are considered in finding the statistical characteristics, a random sign is generated and assigned to each scale factor. These values are subsequently substituted into Equation 5-1 to generate a sample of 200 random imperfections for each member of the frame. Additional random out-of-plumb imperfections are superimposed to the whole frame (Figure 5-4). Latin Hypercube Sampling (LHS), which is a highly efficient sampling method, is used to generate random variables. Figure 5-5 (a) shows a series of portal frames with random imperfections generated using the approach described in which  $\Delta_i^r$  represents the randomly generated imperfection at node  $i$  including both out-of-straightness and out-of-plumb.

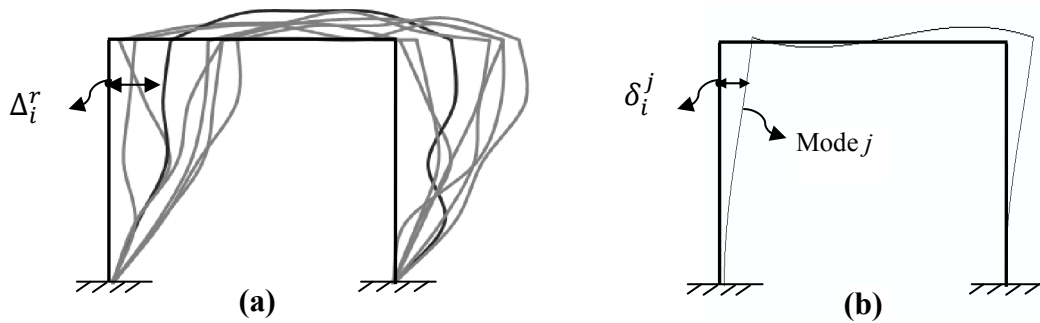


Figure 5-5: (a) Examples of randomly generated shapes of initial imperfection for a simple portal frame (b) Example of buckling mode ( $j$ ) for a simple portal frame

For each frame, an elastic frame buckling analysis is run using the FE software ABAQUS to obtain the buckling shapes for the first  $m$  elastic frame buckling modes. The scale factors ( $X_j^k, k=1,2,\dots,200$  and  $j=1,\dots,m$ ) are calculated using error minimization between the randomly generated shapes of imperfection and a linear combination of scaled buckling modes. The error for the  $k$ th frame is defined as:

$$Er^k = \sum_{i=1}^{no} (\Delta_i^k - (\sum_{j=1}^m X_j^k \delta_i^{kj}))^2 \quad 5-3$$

in which  $no$  is total number of frame nodes,  $\Delta_i^k$  is the randomly generated imperfection at node  $i$  of the  $k$ th frame,  $m$  is the number of modes included,  $X_j^k$  is the scale factor for

mode  $j$  corresponding to the  $k$ th frame, and  $\delta_i^{kj}$  is the deformation of node  $i$  in mode  $j$  corresponding to the  $k$ th frame (Figure 5-5 (b)). The scale factors for all braced and unbraced frames appear to be normally distributed. To enable application to steel frames in general, the scale factors are non-dimensionalised by dividing by  $H$  (total frame height) or  $L$  (member length) depending on whether the corresponding mode is a sway or a non-sway mode,  $x_j^k = X_j^k/(H, L)$ . In most FE software like ABAQUS the buckling eigenmodes are normalized such that the maximum displacement component is unity. In this study, sway modes are defined as those for which the maximum deformation (unity displacement) occurs at the top of the frame while those modes with maximum displacement occurring within the members are classified as non-sway (Figure 5-6).

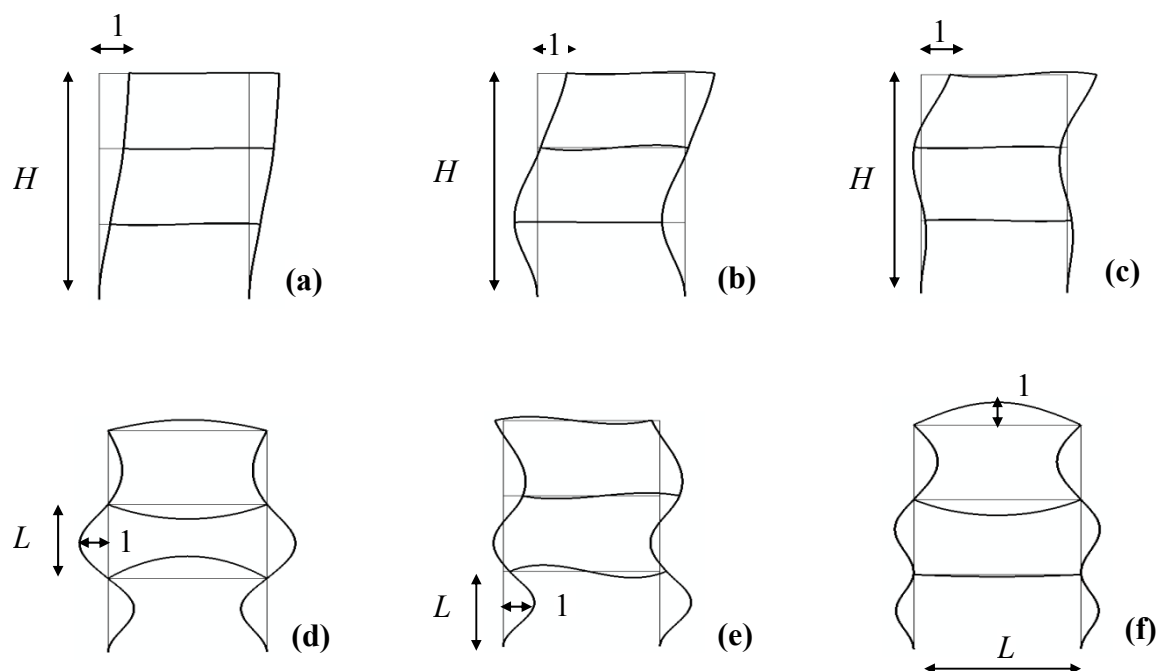


Figure 5-6: (a) Sway mode, (b) Sway mode, (c) Sway mode, (d) Non-sway mode, (e) Non-sway mode, (f) Non-sway mode

The average of the 200 non-dimensional scale factors  $x_j^k$  ( $k=1, \dots, 200$  and  $j=1, \dots, m$ ), called  $\bar{x}_j$ , is then calculated for the 20 braced frames and the 23 unbraced frames and presented in Table 5-4 and Table 5-5. Details of these scale factors including  $\bar{X}_j$ , buckling modes type (sway or non-sway) and  $\bar{x}_j$  for all unbraced and braced frames can be found in Appendix C.2.1 and C.2.2 respectively. These factors appear to be very similar for

different frames. To find a single value for the scale factor of each mode to be implemented into advanced analysis, the average of the  $\bar{x}_j$  values of 23 unbraced and 20 braced studied frames is calculated and denoted as  $SF_j$ .

Table 5-4: Scale factors of different buckling modes to model initial geometric imperfection, unbraced frames

No of modes	$SF_1$	$SF_2$	$SF_3$	$SF_4$	$SF_5$	$SF_6$	$SF_7$	$SF_8$	$SF_9$	$SF_{10}$
1	0.001228									
2	0.001225	0.000341								
3	0.001145	0.000296	0.000397							
4	0.001122	0.000260	0.000383	0.000383						
5	0.001105	0.000258	0.000394	0.000388	0.000358					
6	0.001087	0.000253	0.00039	0.000389	0.000337	0.000360				
7	0.001081	0.000244	0.000382	0.000392	0.000338	0.000350	0.000303			
8	0.001079	0.000243	0.000381	0.000376	0.000351	0.000356	0.000310	0.000317		
9	0.001069	0.000242	0.000371	0.000375	0.000345	0.000343	0.000322	0.000338	0.000376	
10	0.001072	0.000242	0.000367	0.000359	0.000340	0.000331	0.000311	0.000336	0.000363	0.000309

Table 5-5: Scale factors of different buckling modes to model initial geometric imperfection for braced frames

No of modes	$SF_1$	$SF_2$	$SF_3$	$SF_4$	$SF_5$	$SF_6$	$SF_7$	$SF_8$	$SF_9$	$SF_{10}$
1	0.000403									
2	0.000421	0.000376								
3	0.000414	0.000352	0.000324							
4	0.000409	0.000364	0.000318	0.000303						
5	0.000391	0.00037	0.000304	0.000302	0.000339					
6	0.00039	0.000367	0.000303	0.000294	0.000337	0.000262				
7	0.00038	0.00036	0.000282	0.000291	0.000342	0.000263	0.000348			
8	0.000376	0.000353	0.00028	0.000282	0.000333	0.000268	0.000343	0.000266		
9	0.000363	0.000348	0.000277	0.000278	0.000311	0.000267	0.000344	0.000269	0.000271	
10	0.000359	0.000344	0.000277	0.000277	0.000306	0.00025	0.000338	0.000254	0.000269	0.000211

Obviously, this average may vary depending on the considered frame configurations, applied loads and member cross-sections. However since in this study a wide range of low-to-mid-rise frame subjected to different load conditions are considered, the derived scale factors are deemed to be applicable to typical steel frames. To obtain the



contribution of each mode to the modelling of the imperfection, the average non-dimensional scale factors ( $SF_j$ ) can be normalized and expressed as the product of the proportion of each mode ( $P_j$ ) and a single factor ( $F$ ), which are shown in Table 5-6 for unbraced frames and Table 5-7 for braced frames, i.e.  $SF_j = P_j \times F$ , where  $P_j$  is normalized scale (participation) factor determined from Equation 5-4 and  $m$  is number of modes.

$$P_j = \frac{|SF_j|}{\sum_{j=1}^m |SF_j|} \quad 5-4$$

The imperfection amplitude ( $A_j$ ) to be incorporated into finite element analysis can be calculated as,

$$\begin{cases} A_j = P_j \times F \times H & \text{For sway modes} \\ A_j = P_j \times F \times L & \text{For non – sway modes} \end{cases} \quad 5-5$$

Based on the results provided in Table 5-6 and Table 5-7, it can be seen that the scale factors for different modes are very similar for braced frames where all buckling modes represent out-of-straightness while the scale factor of the first mode for unbraced frames, which represents out-of-plumb, is much higher than the scale factors for higher order modes. More details about the scale factors can be found in Appendix C.2.

Table 5-6: Proportion of each mode to model initial geometric imperfection, un-braced frames

No of modes	$P_1$	$P_2$	$P_3$	$P_4$	$P_5$	$P_6$	$P_7$	$P_8$	$P_9$	$P_{10}$	$F$
1	1										0.001228
2	0.782	0.218									0.001566
3	0.623	0.161	0.216								0.001838
4	0.522	0.121	0.178	0.178							0.002147
5	0.441	0.103	0.157	0.155	0.143						0.002504
6	0.386	0.090	0.138	0.138	0.120	0.128					0.002817
7	0.350	0.079	0.124	0.127	0.109	0.113	0.098				0.00309
8	0.316	0.071	0.112	0.110	0.103	0.104	0.091	0.093			0.003413
9	0.283	0.064	0.098	0.099	0.091	0.091	0.085	0.089	0.099		0.003782
10	0.266	0.060	0.091	0.089	0.084	0.082	0.077	0.083	0.090	0.077	0.004030

Table 5-7: Proportion of each mode to model initial geometric imperfection, braced frames

No of modes	$P_1$	$P_2$	$P_3$	$P_4$	$P_5$	$P_6$	$P_7$	$P_8$	$P_9$	$P_{10}$	$F$
1	1										0.001228
2	0.528	0.472									0.001566
3	0.380	0.323	0.297								0.001838
4	0.293	0.261	0.228	0.217							0.002147
5	0.229	0.217	0.178	0.177	0.199						0.002504
6	0.200	0.188	0.155	0.150	0.172	0.134					0.002817
7	0.168	0.159	0.124	0.129	0.151	0.116	0.154				0.003090
8	0.150	0.141	0.112	0.113	0.133	0.107	0.137	0.106			0.003413
9	0.133	0.128	0.102	0.102	0.114	0.098	0.126	0.099	0.099		0.003782
10	0.124	0.119	0.096	0.096	0.106	0.087	0.117	0.088	0.093	0.073	0.004030

The average of the COVs of the scale factors ( $SF_j$ ) for 23 unbraced and 20 braced frames are presented in Table 5-8 and Table 5-9, respectively. As it can be seen from these tables the values of COVs are quite similar for different buckling modes of both unbraced and braced frames. The COVs are of similar magnitude to those for out-of-plumb and member out-of-straightness, as shown in Figure 5-4 and Table 5-3 respectively. As will be shown in subsequent sections, despite the relatively large variance in imperfection magnitudes, the variance of the capacity of steel frames resulting from imperfections is a small fraction of the variance of the  $SF_j$  factors in Table 5-8 and Table 5-9.

Table 5-8: COVs of scale factors of different buckling modes, unbraced frames

No of modes	$COV_{SF_1}$	$COV_{SF_2}$	$COV_{SF_3}$	$COV_{SF_4}$	$COV_{SF_5}$	$COV_{SF_6}$	$COV_{SF_7}$	$COV_{SF_8}$	$COV_{SF_9}$	$COV_{SF_{10}}$
1	0.749									
2	0.752	0.790								
3	0.754	0.796	0.819							
4	0.754	0.828	0.814	0.806						
5	0.755	0.831	0.802	0.813	0.832					
6	0.753	0.832	0.787	0.811	0.835	0.805				
7	0.753	0.813	0.794	0.805	0.832	0.806	0.829			
8	0.754	0.804	0.793	0.803	0.815	0.801	0.826	0.827		
9	0.756	0.801	0.783	0.800	0.825	0.803	0.800	0.817	0.804	
10	0.755	0.799	0.791	0.801	0.826	0.810	0.799	0.809	0.817	0.802

Table 5-9: COVs of scale factors of different buckling modes, braced frames

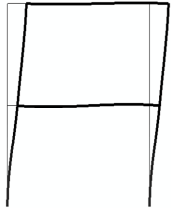
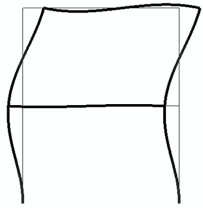
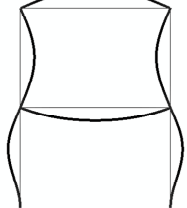
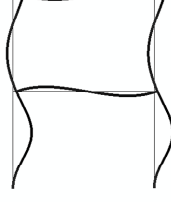
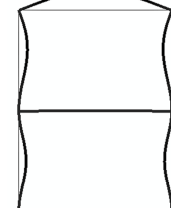
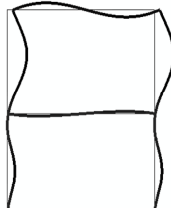
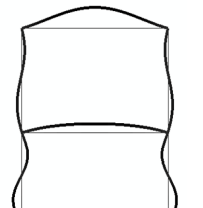
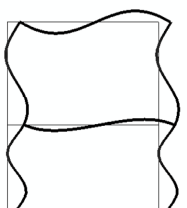
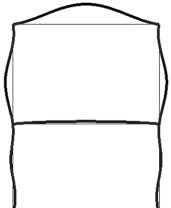
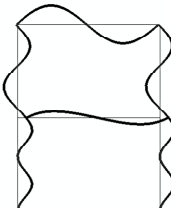
No of modes	$COV_{SF_1}$	$COV_{SF_2}$	$COV_{SF_3}$	$COV_{SF_4}$	$COV_{SF_5}$	$COV_{SF_6}$	$COV_{SF_7}$	$COV_{SF_8}$	$COV_{SF_9}$	$COV_{SF_{10}}$
1	0.868									
2	0.854	0.887								
3	0.803	0.901	0.846							
4	0.803	0.904	0.830	0.855						
5	0.812	0.892	0.830	0.852	0.832					
6	0.808	0.894	0.841	0.869	0.824	0.836				
7	0.816	0.899	0.839	0.867	0.788	0.838	0.804			
8	0.817	0.896	0.840	0.878	0.787	0.849	0.813	0.825		
9	0.821	0.900	0.844	0.874	0.788	0.836	0.786	0.822	0.827	
10	0.830	0.900	0.840	0.867	0.785	0.840	0.782	0.815	0.824	0.829

### 5.3.2 Number of eigenmodes

Evidently, the derived scale factors vary with the number of eigen buckling modes, which therefore needs to be determined. Theoretically, it is expected that greater accuracy will be achieved by combining more buckling modes but at the same time this number should be reasonable and optimal. It is obvious that the shape of buckling modes depends on the load, frame geometry and member cross-sections. It was observed that for most regular frames the first mode is a sway mode. Thus, if the initial geometric imperfection is modelled by scaling the first eigenmode, in most cases the initial out-of-straightness cannot modelled appropriately.

For example, Table 5-10 shows the first ten buckling modes for a 1-bay, 2-storey two dimensional frame subjected to gravity loads (Appendix C.1.1, Frame 9). The frame initial imperfection shapes considering two as well as ten scaled buckling modes are plotted in Figure 5-7. The scale factors are obtained by error minimization method using Equation 5-3. It can be seen that when considering only the first two modes, the out-of-straightness cannot be modelled appropriately and the imperfection shape does not match well with randomly generated initial imperfection. Using ten scaled modes can accurately modelled both out-of-plumb and out-of-straightness and perfectly matches with random shape of imperfection.

Table 5-10: First ten buckling modes of a 1-bay, 2-story frame (Appendix C.1.1)

Mode 1	Mode 2	Mode 3	Mode 4	Mode 5
				
Mode 6	Mode 7	Mode 8	Mode 9	Mode 10
				

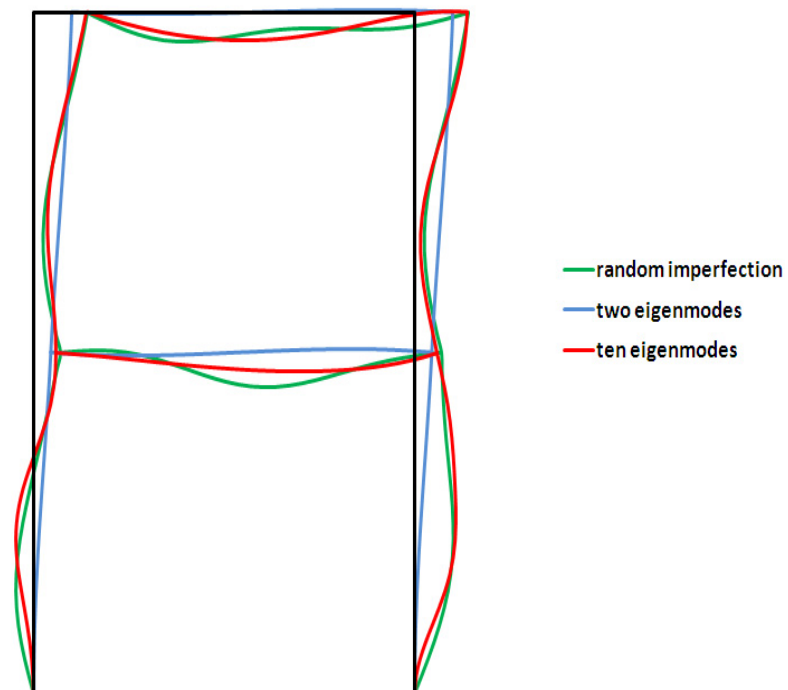


Figure 5-7: Comparison of randomly generated initial imperfection with imperfection modelled by scaling two and ten modes

To find the appropriate number of eigenmodes, three typical frames have been studied (Figure 5-8). For all frames, the span length is 6m while the storey height is 4m and the same between all levels. A total of 200 random geometric imperfections have been produced for each frame following the methodology presented in Section 5.3.1. The generated member and sway imperfections must then be multiplied by the member length ( $L$ ) and frame height ( $H$ ) respectively to obtain the actual magnitude, since the statistical characteristics in Table 5-3 and Figure 5-4 are non-dimensional. Those imperfect frames are then imported into ABAQUS and analysed under equal vertical loads ( $P=1000$  kN) applied at the top of each column thus providing the ultimate load factor of each frame ( $\lambda_{(actual)k}$ ,  $k = 1, \dots, 200$ ). The frames are two-dimensional and analysed using advanced analysis explained in Chapter 3. The material is modeled as elastic-perfectly plastic with the elastic modulus ( $E$ ) and yield stress equal to 200 GPa and 320 MPa respectively. All cross-sections are 150UB14 which is fully compact (Figure 5-4). Based on the mesh convergence study one element per 200 mm length is used for all members. So as to investigate the influence of imperfections on the frame ultimate strength as the only trigger of second-order effects, residual stress is not taken into account.

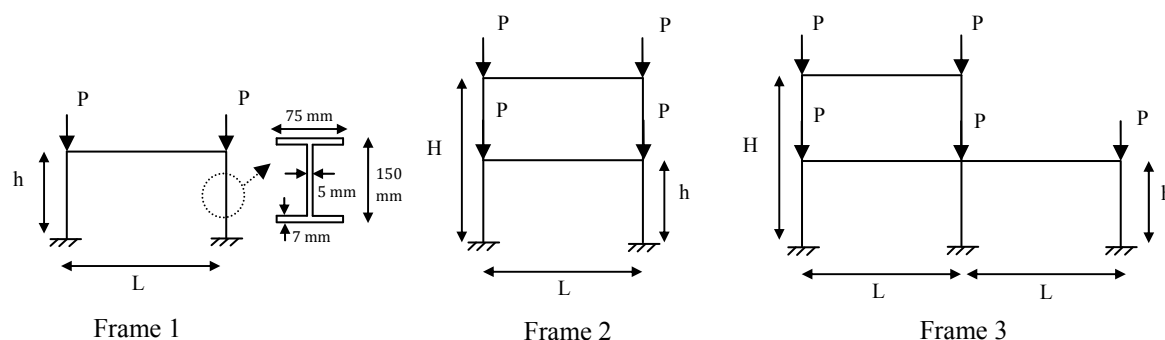


Figure 5-8: Steel frame layouts to determine the appropriate number of eigenmodes

Elastic buckling analyses are performed to obtain the buckling deformations of each frame for the first ten modes. Using Equation 5-3, a set of scale factors ( $X_j^k$ ,  $k=1, \dots, 200$  and  $j=1, \dots, m$ ) considering a finite number of buckling modes ( $m$ ) are evaluated for each frame by error minimization as explained before. Incorporating buckling modes scaled by these factors into finite element models, a second set of advanced analysis is carried out and the ultimate load factors are obtained ( $\lambda_{mk}$ ), where  $k$  refers to the  $k$ th imperfect

frame. Note that in this set of simulations, the frame is modeled with the perfect geometry and the imperfection is applied to the model as scaled eigenmodes using the \*IMPERFECTION option of ABAQUS.

To be able to compare the results of the three different frames, the ratio of  $\lambda_{mk}/\lambda_{(actual)k}$  is calculated in which  $\lambda_{mk}$  is the ultimate load factor of the  $k$ th frame considering the linear combination of  $m$  scaled modes and  $\lambda_{(actual)k}$  is the ultimate strength of frame  $k$  obtained from an advanced analysis of the frame with randomly generated imperfections. This ratio is called the “bias” for ease of reference. The mean and COV of the bias are plotted in Figure 5-9 and Figure 5-10 for the three frames. The values of absolute error are also calculated for all 200 frames of each type, as defined by Equation 5-6. The mean and maximum values of absolute error in percent (%) are plotted in Figure 5-11 and Figure 5-12.

$$Er^k = |1 - \lambda_{mk}/\lambda_{(actual)k}| \quad 5-6$$

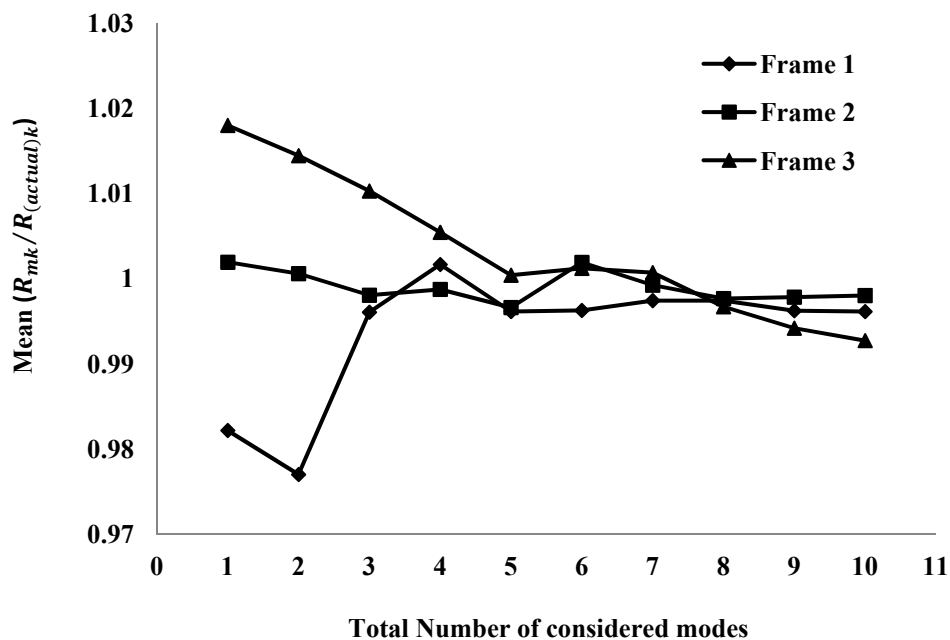


Figure 5-9: Mean value of bias for 200 simulations

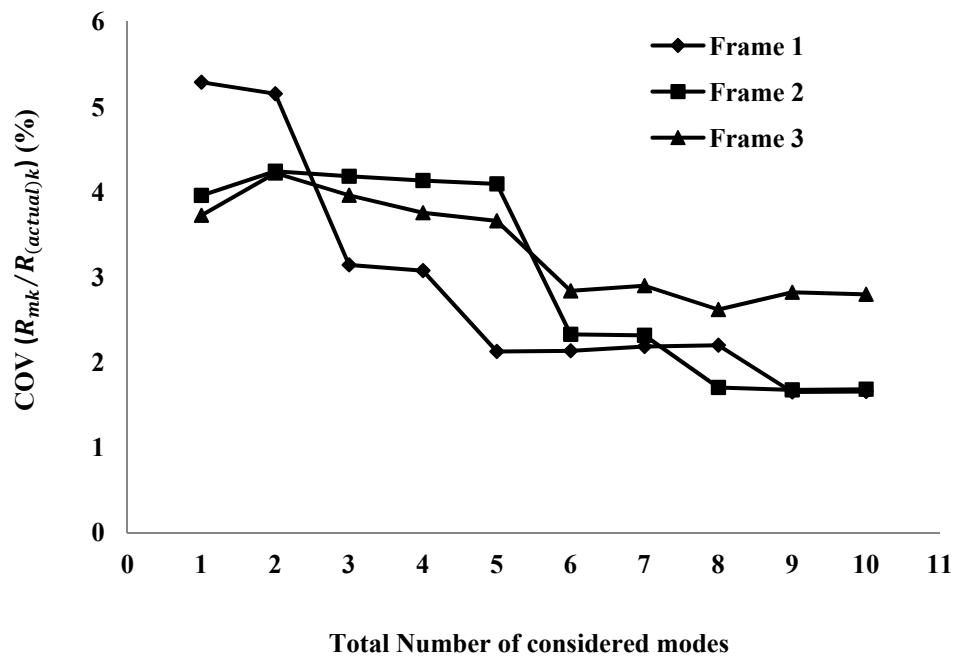


Figure 5-10: COV of bias for 200 simulations

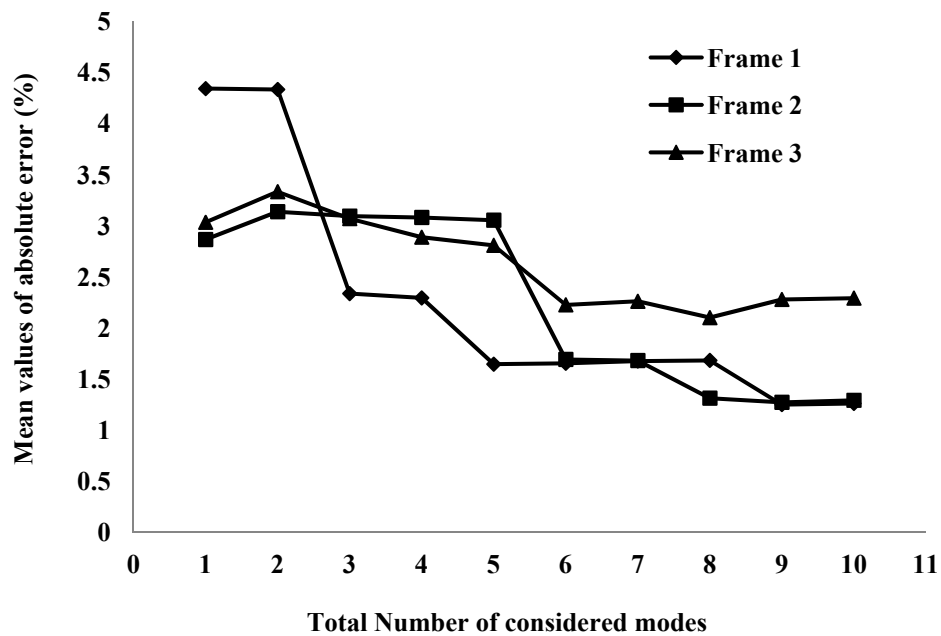


Figure 5-11: Mean of absolute error (%) for 200 simulations

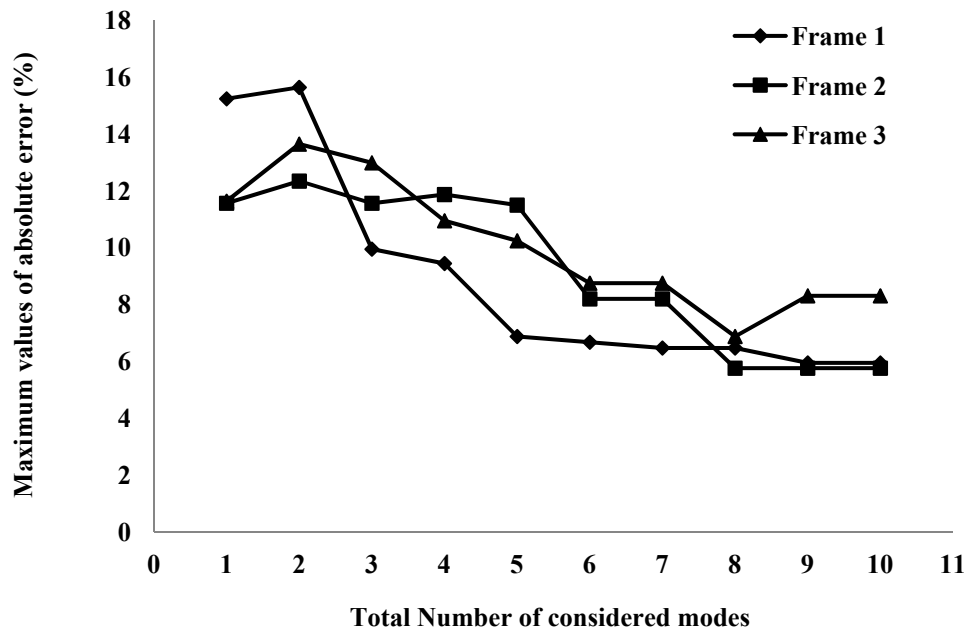


Figure 5-12: Maximum of absolute error (%) for 200 simulations

Based on this study, the following observations can be made:

(1) From Figure 5-9 it can be seen that by including an increasing number of modes the bias is approaching to unity for all considered frames and the discrepancy decreases. At the same time, the COV decreases from the average of 4.32% for all three frames when only one mode is included to 2.32% when including six modes. It is interesting to observe that although increasing the number of modes can provide better representation of the initial imperfection, including only the first mode does not result in significant error from the actual mean. For the case of including only the first mode, the mean values of bias for Frame 1 and Frame 3 are 0.982 and 1.017 respectively while the maximum COV is 5% (Frame 1).

(2) As could be expected, the mean and maximum values of absolute error reduce for all three frames by considering more modes (Figure 5-11 and Figure 5-12). It should be noticed that incorporating only the first mode can fairly accurately model the initial imperfection with the mean value of error less than 5%. The maximum value of error



among all 200 simulations is 15.2% considering only one mode, corresponding to Frame 1, and decreases to less than 10% for all frames when six modes are included.

(3) It appears that one, three and six are “good” numbers of eigenmodes to be used for modeling initial geometric imperfections. Using the first mode is easy and can produce reasonable results. There are noticeable reductions in the mean and maximum values of error in changing from 2 to 3 modes, which are about 46% and 36% respectively for Frame 1. Thus, three modes can be a better alternative compared to one mode. Although 10 modes have the smallest mean and maximum errors, little reduction in error is achieved by increasing the number of modes from six to ten. It can be concluded that six modes may predict the actual shape of imperfection and strength of a steel frame very accurately.

## 5.4 Verification and illustrative examples

The application of the proposed amplification factors ( $A_j$ ), is verified by means of a probabilistic approach. Different regular and irregular, braced and unbraced frames are studied. Advanced analysis is run for each frame considering first one, three and six eigenmodes to model initial geometric imperfections using the proposed amplitude factors provided in Table 5-4 and Table 5-5. The details of advanced analysis are explained in Chapter 3. The ultimate load factor for each frame is then obtained and denoted as  $\lambda_n^1$ ,  $\lambda_n^3$  and  $\lambda_n^6$ , considering one, three and six modes respectively. The load-deflection responses of unbraced and braced frames are presented in Appendix C.3.1 and C.3.2, respectively. These ultimate load factors are compared with the mean of the ultimate load factor of the 200 randomly generated shapes for each frame, denoted as  $\bar{\lambda}$ . The ultimate load factor distribution is found to be normal and plotted in Appendix C.4.1 and C.4.2.

### 5.4.1 Unbraced frames

A total of eight unbraced frames are chosen to investigate the effect of initial geometric imperfection on frame strength. Figure 5-13 shows the frame configurations and loadings. Four frames are adopted from the literature and represent more practical cases. The other

four are designed such that the column slenderness parameter ( $\lambda_c$ ) takes the value of unity for most columns, since this is the value for which the squash load and elastic buckling load coincide and produce the greatest sensitivity to initial imperfection (Clarke, Bridge et al. 1992). The column slenderness can be calculated as,

$$\lambda_c = (kL/\pi r)(\sqrt{f_y/E}) \quad 5-7$$

Material properties including elastic modulus and yield strength for different frames are summarized in Table 5-11.

Table 5-11: Material properties, un-braced frames

	F-UB 1	F-UB 2	F-UB 2	F-UB 4	F-UB 5	F-UB 6	F-UB 7	F-UB 8
Elastic modulus (GPa)	210	200	200	200	200	200	205	210
Yield stress (MPa)	300	320	320	320	250	320	235	275

The ultimate load factors ( $\lambda_n^1$ ,  $\lambda_n^3$  and  $\lambda_n^6$ ) of different frames using advanced analysis are presented in Table 5-12. These ultimate load factors are then compared with the mean of the ultimate load factor of the 200 randomly generated shapes for each frame ( $\bar{\lambda}$ ). The errors considering different number of modes are reported in Table 5-12 ( $Er^1$ ,  $Er^3$  and  $Er^6$ ). As could be expected, the values of absolute error reduce for most frames by considering more modes. Based on the presented results (Figure 5-14), it can be seen that the highest errors are related to those frames which are designed to have the column slenderness parameter equal to unity for most columns (F-UB 3 and F-UB 6). These frames fail by instability of the whole system. The maximum error is about 11.7% considering only one mode, corresponding to F-UB 6, and decreases to 9% when six modes are included. It appears that although considering six modes can reduce the error to be less than 10% for all frames, including only the first mode does not result in significant error from the actual mean, especially for more practical frames which are not very sensitive to the imperfections.

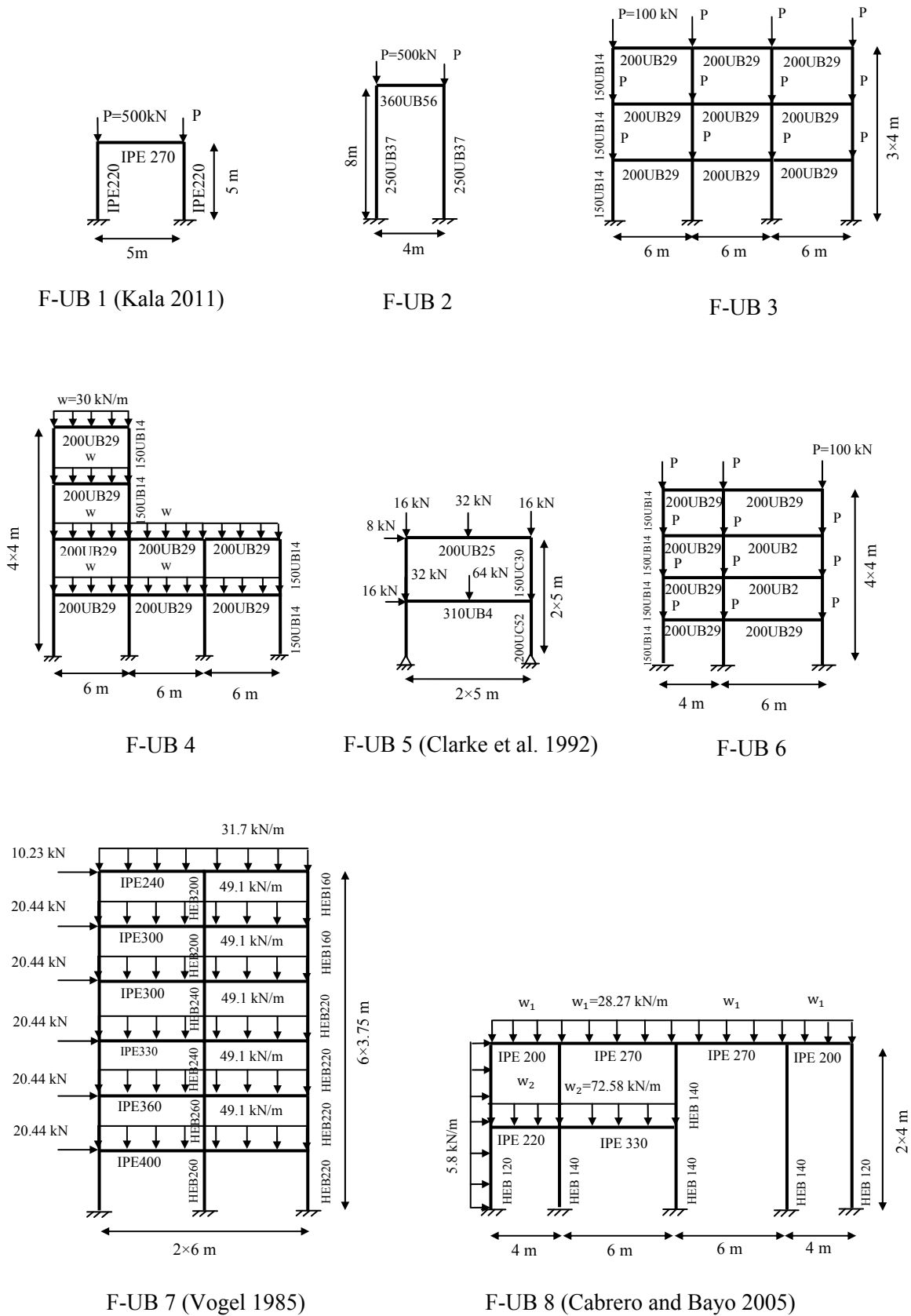


Figure 5-13: Steel frame layouts of verification examples, unbraced frames

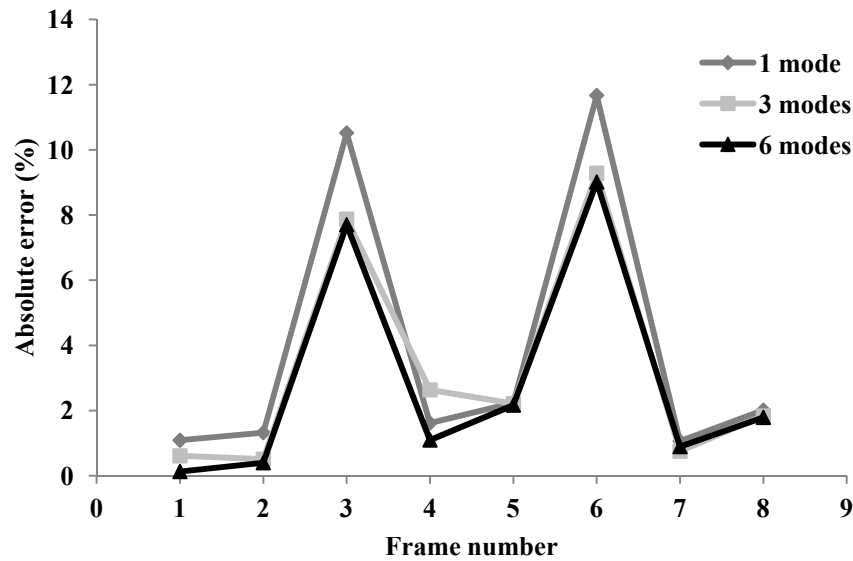


Figure 5-14: Absolute error (%) between  $\bar{\lambda}$  and  $\lambda_n^i$ , unbraced frame

To investigate the variation of the 200 simulations from the ultimate load factor using six modes ( $\lambda_n^6$ ), the ratio between the  $\lambda_k$ ,  $k = 1, \dots, 200$  and  $\lambda_n^6$  is calculated. The mean, COV, and maximum and minimum values of  $\lambda_k/\lambda_n^6$  are shown in Table 5-12 and represent the imperfection modelling error. This may be used to assess the reliability of ultimate strengths provided by advanced analysis. It be noticed that the mean values of  $\lambda_k/\lambda_n^6$  for all frames are around unity which shows that the proposed model by applying the scale factors provided in Table 5-4 can accurately predict the mean. The maximum COV is 8% corresponding to F-UB 2. It should be noted that although the COVs of the derived scale factors range between 75% and 85%, which indicates a large spread, this results in only 8% variation in the ultimate load factors. Again it can be observed that the highest values of COVs, approximately about 7% to 8 %, are associated with those frames which are sensitive to imperfections and fail by frame instability. In reality, it is most unlikely that all columns of a frame have a slenderness parameter of unity, so the statistics corresponding to these frames can be considered as upper bounds. For more practical frames the COV can decrease to as low as 0.3%.

The variation of the COV of the ratio between the ultimate loads ( $\lambda_k/\lambda_n^6$ ) when the column slenderness parameter is less than or greater than unity is also investigated in this study. The second frame (F-UB 2) with the highest COV is considered and redesigned with the values of column slenderness ( $\lambda_c$ ) equal to 0.88 and 1.37 respectively. The

member cross-sections and material properties can be found in Figure 5-15 and the simulation results are presented in Table 5-13. It can be concluded that from the results shown in Table 5-13 that changing the column slenderness from unity to 0.88 and 1.37 can decrease the COV to 6.3% and 5.4% respectively. This shows that when a diverse range of column slenderness values from unity are considered, the frame is less sensitive to imperfection. For most cases, using the imperfection amplitudes presented in Table 5-4, can provide excellent agreement between the finite element analysis of frames with actual random imperfection shapes and linear combination of eigenmodes, with the mean error less than 10%.

Table 5-12: Verification results, unbraced frames

	F-UB 1	F-UB 2	F-UB 2	F-UB 4	F-UB 5	F-UB 6	F-UB 7	F-UB 8
$\bar{\lambda}$	1.7702	2.339	1.598	1.326	1.311	1.1884	1.13	1.084
$\lambda_n^1$	1.7897	2.370	1.430	1.348	1.282	1.0497	1.118	1.062
$\lambda_n^3$	1.7811	2.351	1.472	1.362	1.282	1.0781	1.122	1.064
$\lambda_n^6$	1.7725	2.348	1.475	1.341	1.283	1.0813	1.120	1.065
$Er^1(\%)$	1.0896	1.321	10.52	1.617	2.235	11.671	1.062	2.011
$Er^3(\%)$	0.612	0.506	7.875	2.636	2.212	9.2814	0.752	1.836
$Er^6(\%)$	0.1298	0.400	7.700	1.096	2.166	9.0121	0.894	1.79
$\mu (\lambda_k/\lambda_n^6)$	0.9987	0.996	1.083	0.989	1.022	1.099	1.009	1.018
COV ( $\lambda_k/\lambda_n^6$ )	0.0432	0.0800	0.0702	0.0321	0.0031	0.0744	0.0133	0.0159
Min ( $\lambda_k/\lambda_n^6$ )	0.8782	0.8019	0.8851	0.9168	1.013	0.8765	0.9633	0.9745
Max ( $\lambda_k/\lambda_n^6$ )	1.0873	1.1725	1.2265	1.0534	1.0314	1.2692	1.0282	1.0679

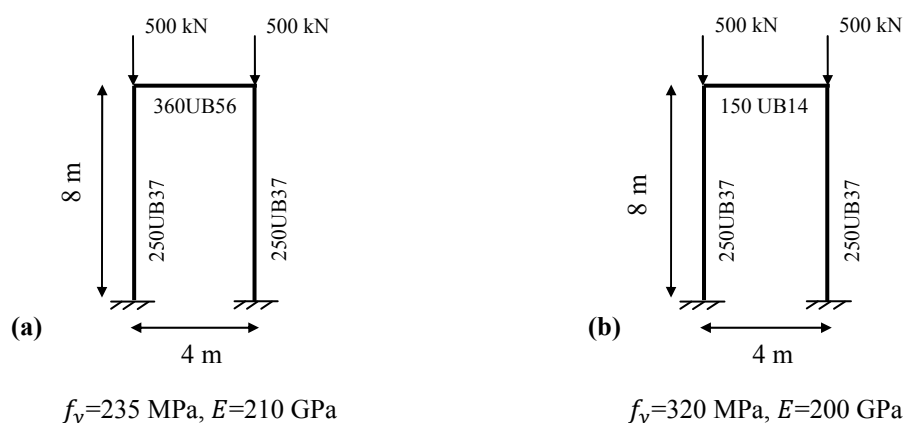


Figure 5-15: F-UB 2, (a) Column slenderness parameter  $\lambda_c = 0.88$  (b) Column slenderness parameter  $\lambda_c = 1.37$

Table 5-13: Simulation results for F-UB 2 different column slenderness

	$\lambda_c=0.88$	$\lambda_c=1$	$\lambda_c=1.37$
$\bar{\lambda}$	1.9348	2.33859	1.4392
$\lambda_n^6$	1.9278	2.34796	1.4389
$Er^6(\%)$	0.3617	0.40061	0.0206
$\mu (\lambda_k/\lambda_n^6)$	1.0036	0.99175	1.0002
COV ( $\lambda_k/\lambda_n^6$ )	0.063	0.08001	0.054
Min ( $\lambda_k/\lambda_n^6$ )	0.8355	0.80189	0.8709
Max ( $\lambda_k/\lambda_n^6$ )	1.1331	1.17246	1.0848

## 5.4.2 Braced frames

A total of eight regular and irregular braced frames are chosen to investigate the effect of initial geometric imperfection on frame strength. Figure 5-16 shows the frame configurations and loading. Four frames are adopted from the literature and represent practical cases. The braces are considered perfect without any initial geometric imperfections. To avoid those modes in which the braces buckle, in the buckling analyses (but not in the inelastic analyses) the braces are modelled by applying a lateral restraint at each storey level. The results of the simulations are summarised in Table 5-14.

Table 5-14: Verification results, braced frames

	F-B1	F-B 2	F-B 3	F-B 4	F-B 5	F-B 6	F-B 7	F-B 8
$\bar{\lambda}$	1.6257	1.119	1.088	1.327	1.183	1.1459	1.258	1.071
$\lambda_n^1$	1.6358	1.116	1.066	1.239	1.230	1.1716	1.1970	1.058
$\lambda_n^3$	1.6355	1.103	1.064	1.303	1.208	1.1671	1.2336	1.022
$\lambda_n^6$	1.6354	1.118	1.081	1.305	1.194	1.1669	1.2335	1.066
$Er^1(\%)$	0.6174	0.304	1.982	6.615	4.026	2.1915	4.893	1.199
$Er^3(\%)$	0.5992	1.413	2.184	1.853	2.166	1.8143	2.053	4.587
$Er^6(\%)$	0.5931	0.134	0.631	1.649	0.983	1.7975	1.999	0.517
$\mu (\lambda_k/\lambda_n^6)$	0.9941	1.001	1.006	1.017	0.9900	0.982	1.0200	1.005
COV ( $\lambda_k/\lambda_n^6$ )	0.0018	0.0093	0.0245	0.0127	0.0226	0.0144	0.0217	0.0247
Min ( $\lambda_k/\lambda_n^6$ )	0.9900	0.9758	0.9289	0.9896	0.9368	0.9465	1.0058	0.9128
Max ( $\lambda_k/\lambda_n^6$ )	0.9981	1.0160	1.0386	1.0889	1.0423	1.0057	1.0581	1.039

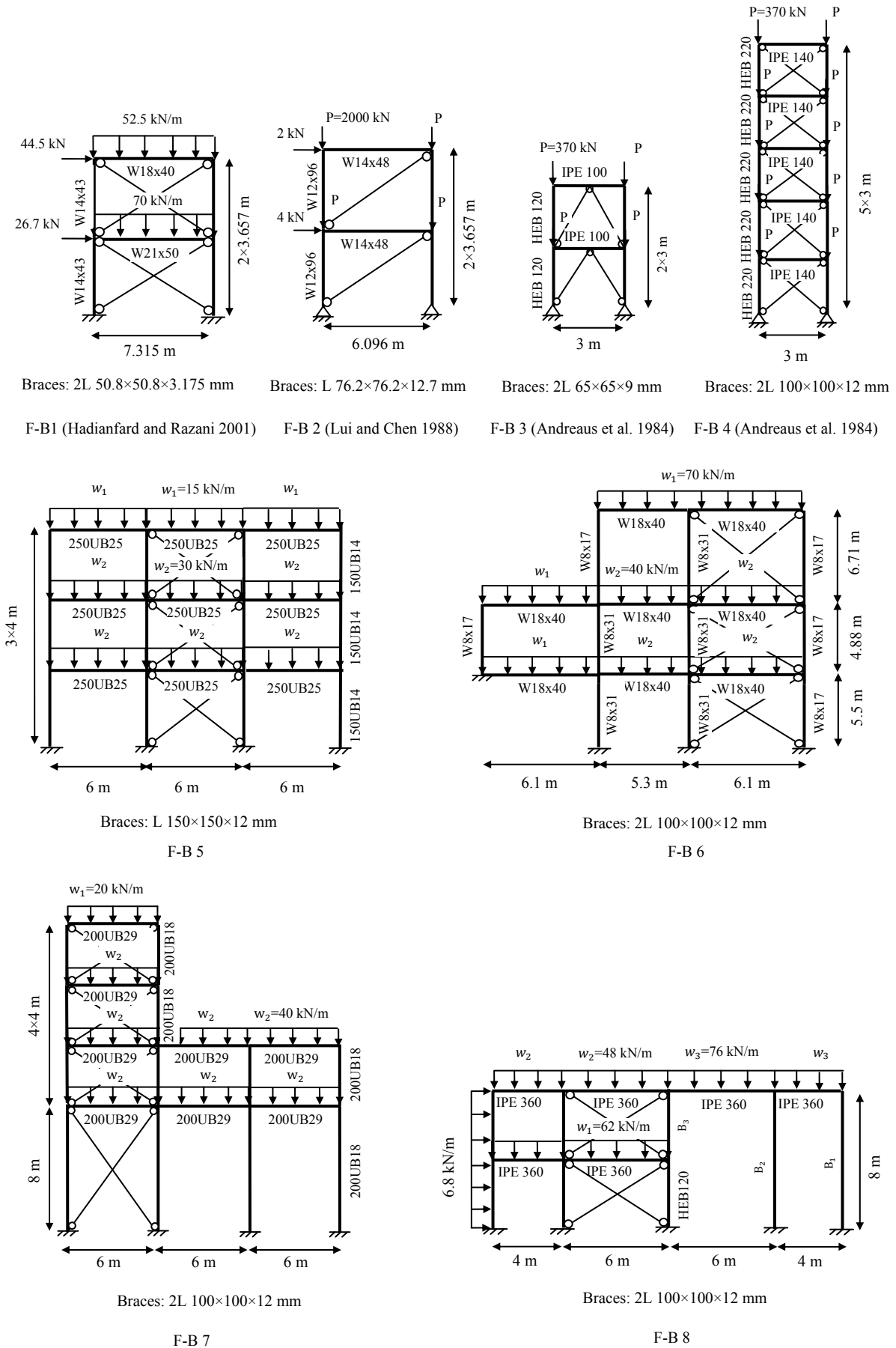


Figure 5-16: Steel frame layouts of verification examples, braced frames

The maximum error is about 6.6% considering only one mode, corresponding to F-B 4, and decreases to 1.65 % when six modes are included. Generally, the absolute values of error for these eight braced frames are lower than those for the set of eight unbraced frames discussed in Section 5.4.1. These errors are plotted in Figure 5-17 and are less than 5% for all frames incorporating six modes. The maximum COV of the ratio between the ultimate loads ( $\lambda_k/\lambda_n^6$ ) is 2.47% corresponding to F-B 8.

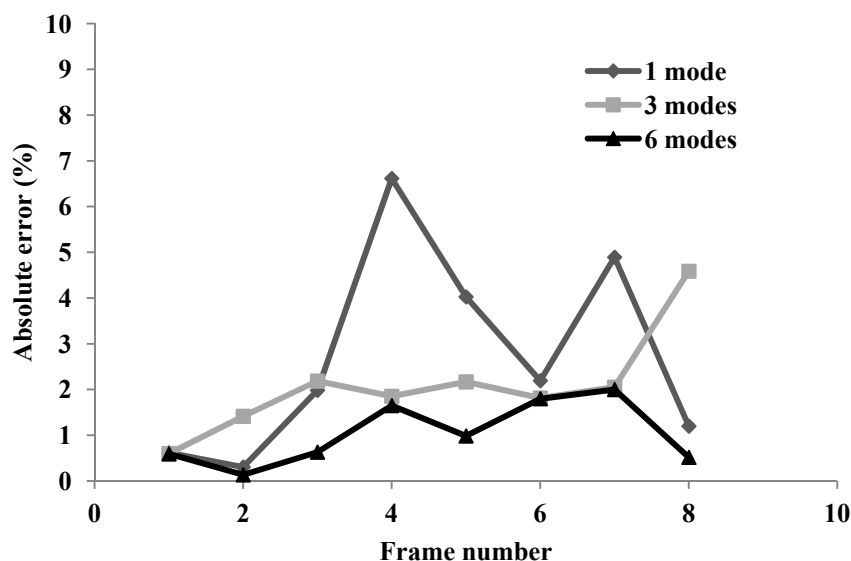


Figure 5-17: Absolute error (%) between  $\bar{\lambda}$  and  $\lambda_n^i$ , un-braced frame

As it can be seen in Table 5-14, for some frames considering only the first mode can predict the ultimate load more accurately than considering 3 modes. For these frames the ultimate limit state deformation is similar to the first buckling mode, and hence second order effects can be captured fairly accurately by scaling the first buckling mode. Conversely, the first two buckling modes are similar but tend to be in opposite directions, and so the inclusion of both modes reduces the effect of imperfections. Thus, only if the first buckling mode does not include the buckling of those columns which are participating in the failure of the frame, more modes are required to model the imperfection accurately. It can be concluded that for braced frames, although increasing the number of modes can provide a better representation of the initial imperfection, (i) including only the first mode does not result in significant error from the actual mean, and (ii) if multiple modes are to be included, including six modes is preferable to including three modes.



## 5.5 Conclusion

Initial geometric imperfections affect the nonlinear behaviour of structures and may have a considerable influence on the ultimate strength. Thus, imperfections need to be modeled appropriately in advanced structural analysis. There are several ways to model initial geometric imperfections which were discussed in this chapter. The difficulty associated with most of the methods for modelling imperfections is guessing the worst direction of the imperfection which is very difficult or impossible in large steel frames. All the common methods use the maximum magnitude of imperfections based on specifications (worst case scenario) which may be conservative in most situations.

This study outlines a convenient method for modelling initial geometric imperfections as a linear combination of scaled eigenmodes. The method is easy to implement into finite element analysis and obviates the difficulties of current methods such as offsetting nodes or guessing the worst imperfection shape. The study considers regular and irregular sway and braced planar frames. It may be extended to the 3D space frames. Based on the results of advanced analysis, the appropriate number and magnitudes of eigenmodes have been suggested in this study. It can be concluded that for unbraced frames although six buckling modes may predict the actual shape of imperfection more accurately, including only first three modes does not result in significant errors. The maximum modelling error is about 8%. For braced frames since in some cases the first two buckling modes are similar but in opposite directions, their effects may largely cancel out and three buckling modes may not be sufficient to model the imperfection accurately. Thus, for braced frames, including six modes is recommended. The associated maximum modelling error is about 2.5%. The recommended number of modes and rounded values of scaling factors to use for modelling imperfections of braced and unbraced frames are summarised in Table 5-15.

Table 5-15: Recommended proportions of each mode to model initial geometric imperfection

	Number of modes	$P_1$	$P_2$	$P_3$	$P_4$	$P_5$	$P_6$	$F$
Unbraced frames	3	0.60	0.20	0.20				0.002
	6	0.40	0.10	0.15	0.15	0.10	0.10	0.003
Braced frames	6	0.20	0.20	0.15	0.15	0.15	0.15	0.003

# CHAPTER

## 6 .

# Probabilistic modelling of residual stress in advanced analysis of steel frames

---

## 6.1 Introduction

Hot-rolled steel members are usually not initially stress free. The uneven rate of cooling after the rolling process creates a set of self-equilibrating initial stresses in the cross-section, called residual stress. This is particularly evident in the case of hot-rolled I-sections in which the flange and web intersections cool much slower than the flange tips or web centre. These internal longitudinal stresses are important for frames prone to instability, since they can cause premature yielding and consequently loss of stiffness, leading to reduced ultimate strength. Thus, when simulating the structural behaviour by means of advanced (second-order inelastic) analysis, (or GMNIA analysis), it is necessary to incorporate residual stress to achieve accurate results.

The actual residual stress profile is complex and depends on the material properties, cross-sectional geometry and the manufacturing and cooling processes. Since various

manufacturing techniques are used in different countries, essential differences can be found in the results of experimental measurements of the same type of profile. Extensive measurements of residual stresses have been conducted during the comprehensive study of column buckling over the last four decades (Huber and Beedle 1954; Beedle and Tall 1962; Jez-Gala 1962; Young 1975). Also, several residual stress distribution models have been developed based on experimental data measured in different parts of the world, e.g. Europe, Japan, Australia and North America. Three typical and commonly used residual stress patterns as well as two examples of measured data are presented in Figure 6-1.

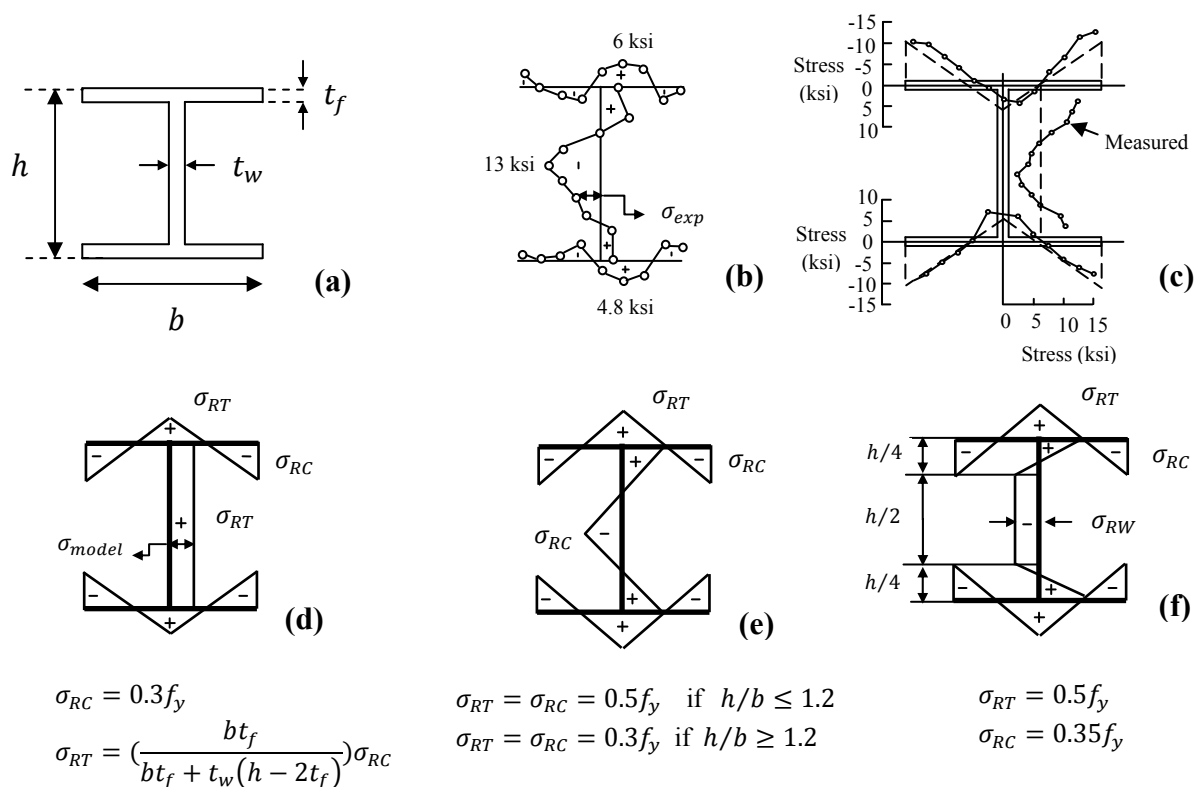


Figure 6-1: Residual stress patterns (a) Cross-sectional dimensions (b) Measured data (Beedle 1958) (c) Measured data (Chen and Sohal 1995) (d) Galambos and Ketter (1959) (e) ECCS (1976) (f) Bild and Trahair (1989)

The residual stress patterns presented in Figure 6-1 are generally implemented in the finite element analysis of steel structures by a deterministic scheme in which a specific pattern with nominal values of residual stress is used. However, since the magnitude and distribution of residual stress are not generally known with an absolute certainty and may vary from profile to profile, the longitudinal residual stress can be treated as a random

quantity in the advanced analysis of steel structures (Kala and Kala 2003; Buonopane 2008). Randomness in residual stress may have a significant influence on the strength and reliability of steel frames by increasing lateral deflections and thereby second-order effects as shown by Buonopane (2008). Thus, when investigating the behaviour of steel structures by means of a probabilistic approach, it is important to have proper statistical characteristics of such stresses.

Although several experimental works have been conducted to find the residual stress pattern of hot-rolled I-sections, few studies report the statistical characteristics of such data. The statistics of the residual stress at flange tips, flange centre and web centre are reported by Fukumoto and Itoh (1980) for hot-rolled steel I-sections (see Figure 6-2). Based on the provided statistics and distributions, the stresses at flange tips, flange to web junctions, and web centre can be randomly generated and used in advanced analysis. However there is no information about the residual stress pattern and how these stresses change along the flanges and web. Additionally, the correlation between these stresses has not been studied.

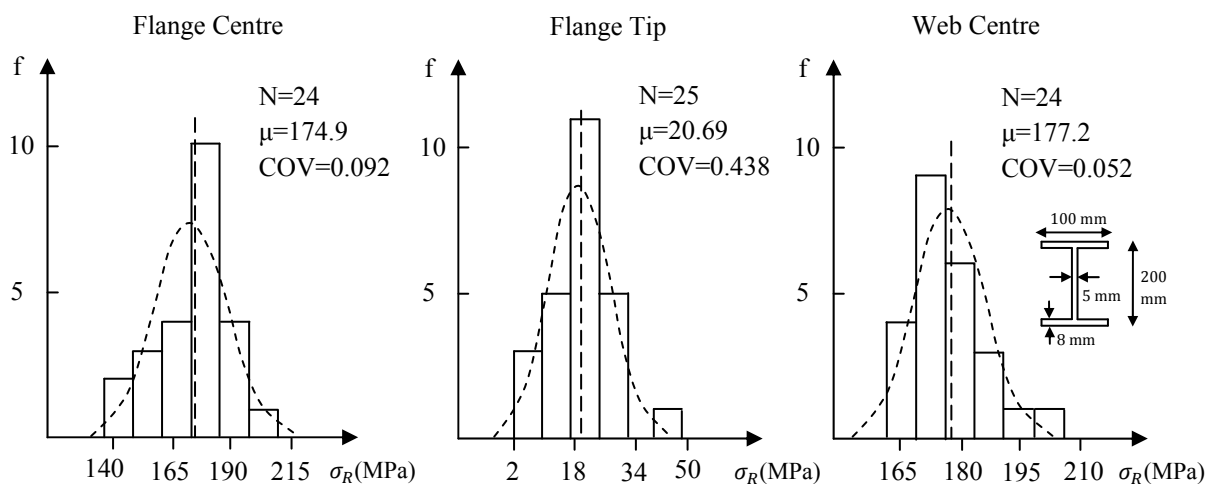


Figure 6-2: Residual stress statistics of reported by Fukumoto and Itoh (1980)

To overcome these limitations, a new approach is introduced in this paper to model residual stress as a random variable in advanced analysis of steel frames. This is achieved by fitting established residual stress patterns to experimental measurements obtained from literature. Additionally, the influence of different residual stress patterns on the ultimate strength and reliability of steel frames is investigated.

## 6.2 The proposed approach

The proposed approach to model the residual stress probabilistically is based on applying a random scale factor of  $X$  to each given residual stress pattern. To develop such a method and to find the statistics of the scale factors, detailed measurements of residual stresses for the entire cross-section is required. A total of 103 actual residual stress measurements, carried out in different parts of the world including Australia, north America, Japan and Europe, were obtained from the literature (selected references: (Beedle 1958; Heyman 1971; Kitipornchai 1973; Itoh 1984; Chen and Sohal 1995)). An investigation of the experimental data showed that the measured residual stress can be divided essentially into two groups, American sections (40 measurements) and sections from other regions (non-American sections) (63 measurements). While the American sections show tensile stress along the entire web, the sections from other parts of the world indicate tensile stress at web-to-flange junction changing to compressive stress at mid-web. The stress distributions in the flanges seem to be similar for all sections, i.e., compression at flange tips and tension at the web-to-flange junction. Based on these observations it is obvious that the Galambos and Ketter (1959) model is the best fit for American sections while the ECCS (1984) and Bild and Trahair (1989) models are better suited for non-American sections (see Figure 6-1 (d-e)). For ease of reference, these models are referred to as Galambos, ECCS and Trahair models respectively.

To determine the scale factors, firstly the measured residual stresses ( $\sigma_{exp}$ ) at  $i$  nodes distributed in each cross-section (Figure 6-1) are non-dimensionalised by dividing the stresses by the value of reported yield stress ( $f_y$ ). Then, the corresponding theoretical non-dimensional residual stresses ( $\sigma_{model}$ ) are calculated at the same points using the three models shown in Figure 6-1. Finally, the scale factors ( $X_{Galambos}$ ,  $X_{ECCS}$  and  $X_{Trahair}$ ), which minimize the error between the theoretical models and non-dimensionalised experimental measurements, are derived by error minimization. The error is defined as:

$$Error = \sum_{i=1}^n (X_j \sigma_{model}^i - \sigma_{exp}^i)^2 \quad 6-1$$

in which  $i$  refer to the  $i$ th measurement of the  $j$ th cross-section and  $n$  is the total number of measurements for  $j$ th cross-section. The error minimization is then performed (Equation 6-2) and the statistics (mean and COV) of scale factors ( $X_j, j=1,2,\dots$ ) for all profiles considered are obtained.

$$\partial Error / \partial X_j = 0 \quad 6-2$$

The statistical data and histograms of derived scale factors for the three residual stress distributions are presented in Table 6-1 and Figure 6-3 to Figure 6-5. A normal distribution is fitted to each histogram. More details about the scale factors can be found in Appendix D. The scale factors,  $X_{ECCS}$  and  $X_{Trahair}$ , are fitted to non-American sections while the scale factor  $X_{Galambos}$  is fitted to American sections.

Table 6-1: Statistics of scale factors

	$X_{ECCS}$	$X_{Trahair}$	$X_{Galambos}$
Mean ( $\mu_X$ )	1.047	0.965	1.064
COV	0.210	0.205	0.270

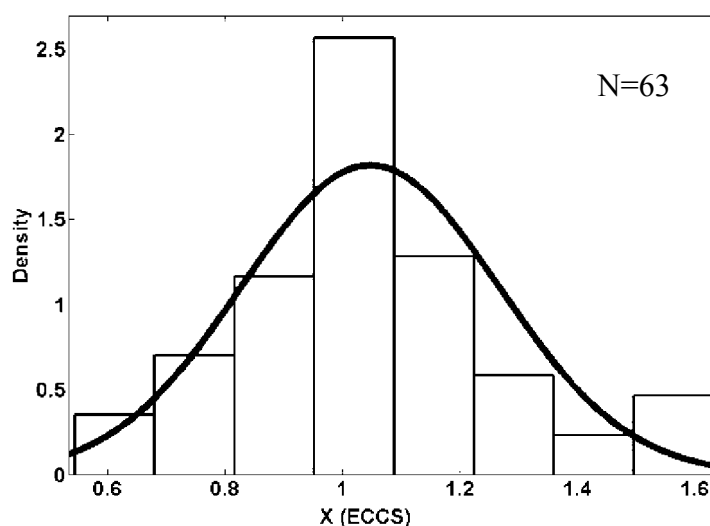


Figure 6-3: Histogram of scale factor for residual stress, ECCS model

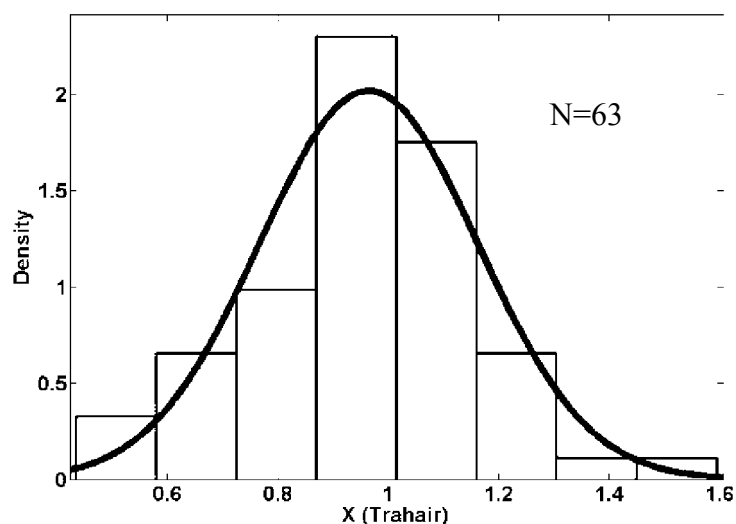


Figure 6-4: Histogram of scale factor for residual stress, Trahair model

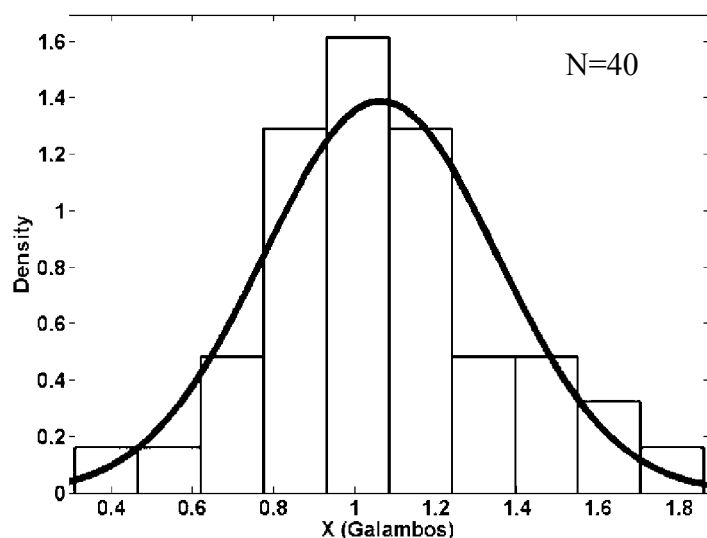


Figure 6-5: Histogram of scale factor for residual stress, Galambos model

### 6.3 Frame analysis

In order to study the effect of residual stress and its different patterns on the ultimate strength of steel structures, four planar steel frames are analysed by advanced analysis (see Figure 6-6) using both deterministic and probabilistic approaches. The first two frames are a 3-bay, 3-storey and a 2-bay, 4-storey frame with equal point loads applied at the top of each column. The geometry, material properties and cross-sections of these frames are chosen such that the column slenderness parameter  $\lambda_c = (kL/\pi r)(\sqrt{f_y/E})$ , where  $k$  is determined as per Section 4.6.3 of AS4100, approximately takes the value of

unity for most columns, since this is the value for which the squash load and elastic loads coincide and produce the greatest sensitivity to second-order effects (Clarke et al. 1992). In this case, the frames fail by column instability. The values of column slenderness for the most critical storeys are shown in Figure 6-6. Frames 3 and 4 are a two-storey irregular frame (Cabrero and Bayo 2005) and a six-storey frame (Vogel 1985) respectively with both lateral and vertical loads representing practical cases of steel frames. The column slenderness values range between 0.46 and 2.07 as can be seen from Figure 6-6. In all four frames, the columns and beams are bent about major axis.

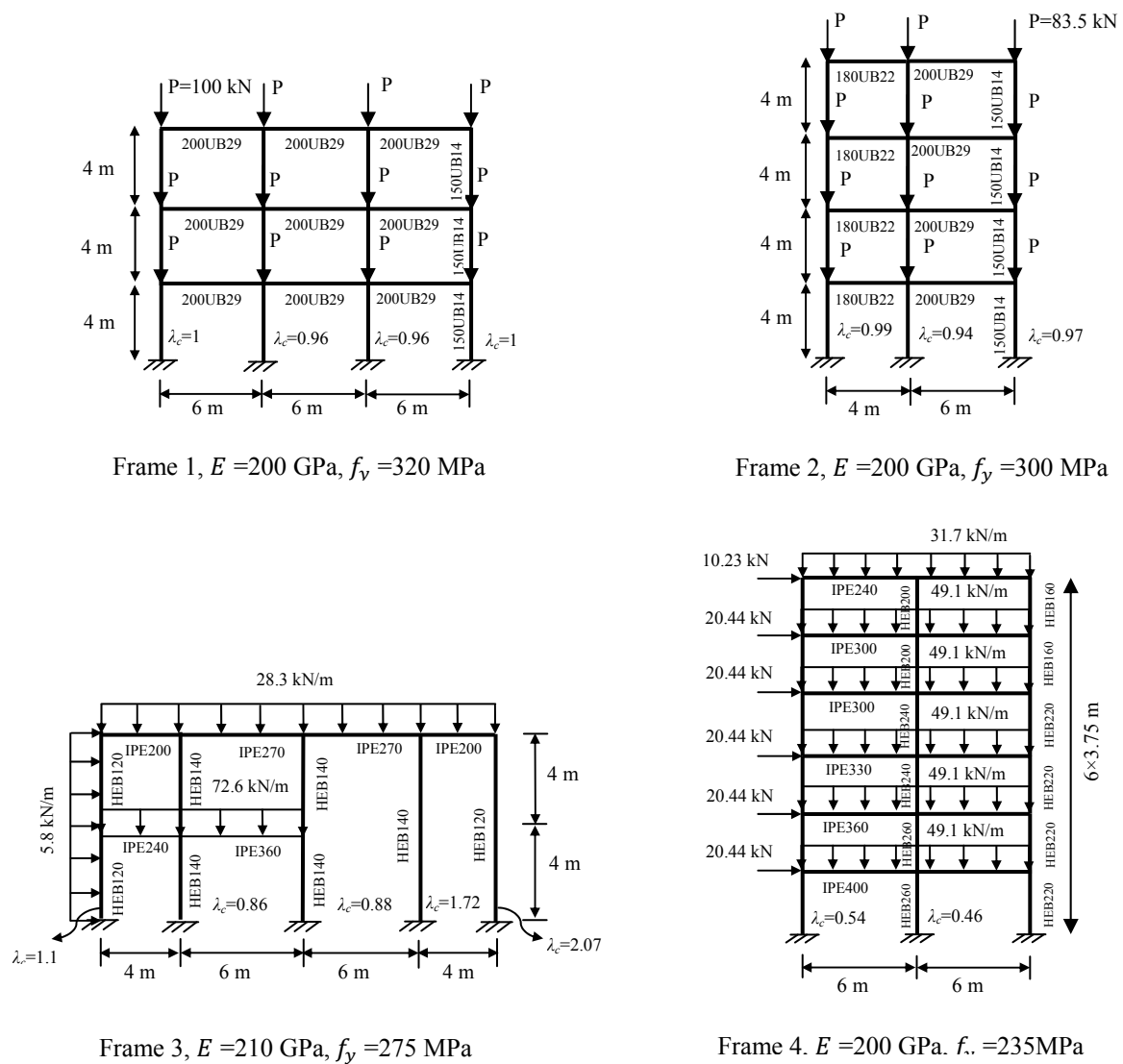


Figure 6-6: Steel frame layouts

For both deterministic and probabilistic studies, two-dimensional second order inelastic finite element (FE) models were developed using the commercial finite element software



ABAQUS (2009). To model material nonlinearity, a plastic-zone beam-column element was used to trace the spread of plasticity through the cross-section and along the member length. The arc-length technique was used to obtain the complete load-displacement response of the structure. The stress-strain response for the steel was modeled as elastic-perfectly-plastic. Column bases are fully fixed and the beam-column joints are modeled as rigid. Residual stresses are incorporated in the model as self-equilibrated initial stresses applied at ABAQUS default cross-sectional integration points. A separate FORTRAN subroutine was written to implement residual stress into the finite element models (Appendix A). Based on the mesh convergence study presented in Chapter 3, one element per 200 mm length is used for all members, resulting in typically 20-40 elements per member. All cross-sections are fully compact hot-rolled I-sections and the out-of-plane behavior is restrained (2D frames). Thus, local buckling and lateral-torsional buckling are not considered in this study. An initial geometric imperfection (mainly out-of-plumb) is applied to the model by scaling the first eigenmode using the scale factor presented in Chapter 5 for unbraced frames.

### 6.3.1 Deterministic study

A comprehensive study by ECCS (1997) was carried out to analyse the effect of possible variation of residual stress magnitude on the ultimate strength of a single column. In order to study the same effect on the ultimate strength of steel frames, five different magnitudes of scale factors ( $X$ ) within two standard deviations of the mean ( $\mu_X - 2\sigma_X$ ,  $\mu_X - \sigma_X$ ,  $\mu_X$ ,  $\mu_X + \sigma_X$ ,  $\mu_X + 2\sigma_X$ ) are chosen from the distributions provided in Table 6-1 and compared with the case of no residual stress. Since for the normal distribution about 95.45% of the values lie within 2 standard deviations of the mean, the range  $\mu_X - 2\sigma_X$ , to  $\mu_X + 2\sigma_X$  is a rough probability estimate of the total distribution. It can be observed from Table 6-1 that for all three residual stress models, the mean value can be accurately considered as unity. The scale factors of the ECCS and the Trahair models show a COV of 0.21 while the COV of Galambos model is equal to 0.27. To apply the same scale factor to different residual stress patterns, the COV of 0.2 is chosen for this deterministic study. Since both the ECCS and Trahair models have the same statistics and almost the same patterns, this study only focuses on the ECCS and the Galambos models. The ultimate load factors for all frames obtained by advanced analysis are listed in Table 6-2 and the percentage

difference between the load factors predicted using the ECCS and Galambos models is shown in Table 6.3.

Table 6-2: Ultimate load factors ( $\lambda$ )

	Frame 1		Frame 2		Frame 3		Frame 4	
Without residual stress	1.454		1.154		1.062		1.118	
	ECCS	Galambos	ECCS	Galambos	ECCS	Galambos	ECCS	Galambos
$X=0.6 (\mu_X-2\sigma_X)$	1.368	1.389	1.090	1.107	1.051	1.058	1.111	1.117
$X=0.8 (\mu_X-\sigma_X)$	1.339	1.369	1.065	1.091	1.046	1.055	1.109	1.113
$X=1 (\mu_X)$	1.307	1.348	1.040	1.075	1.038	1.053	1.100	1.112
$X=1.2 (\mu_X+\sigma_X)$	1.277	1.324	1.016	1.057	1.034	1.051	1.099	1.110
$X=1.4 (\mu_X+2\sigma_X)$	1.246	1.300	0.992	1.040	1.024	1.045	1.096	1.107

Table 6-3: The difference between ultimate load factors (%) by using ECCS and Galambos models

	Frame 1	Frame 2	Frame 3	Frame 4
$X=0.6 (\mu_X-2\sigma_X)$	1.51	1.60	0.67	0.54
$X=0.8 (\mu_X-\sigma_X)$	2.19	2.39	0.88	0.36
$X=1 (\mu_X)$	2.97	3.20	1.40	1.08
$X=1.2 (\mu_X+\sigma_X)$	3.55	3.92	1.57	0.99
$X=1.4 (\mu_X+2\sigma_X)$	4.15	4.69	2.13	0.99

The load-deflection response of all steel frames analysed by advanced analysis using the ECCS residual stress model with different scale factors are plotted in Figure 6-7 to Figure 6-10. The observation of the results is that for the first two frames (Figure 6-7 and Figure 6-8), which are most sensitive to second-order effects, increasing the scale factor from 0.6 to 1.4 (implying more than a doubling in the level of residual stress) can discernibly reduce the ultimate load factor while using the same range of residual stress barely changes the ultimate loads of the more practical Frames 3 and 4 (see Figure 6-9 and Figure 6-10). The reduction in ultimate load is about 9% for the first two frames using the ECCS model. It changes to 2.57% and 1.35% for Frame 3 and Frame 4 respectively. The

reduction in ultimate load is less severe when using the Galambos model, viz. 6.41%, 6.05%, 1.23% and 0.90% for frames 1 to 4 respectively.

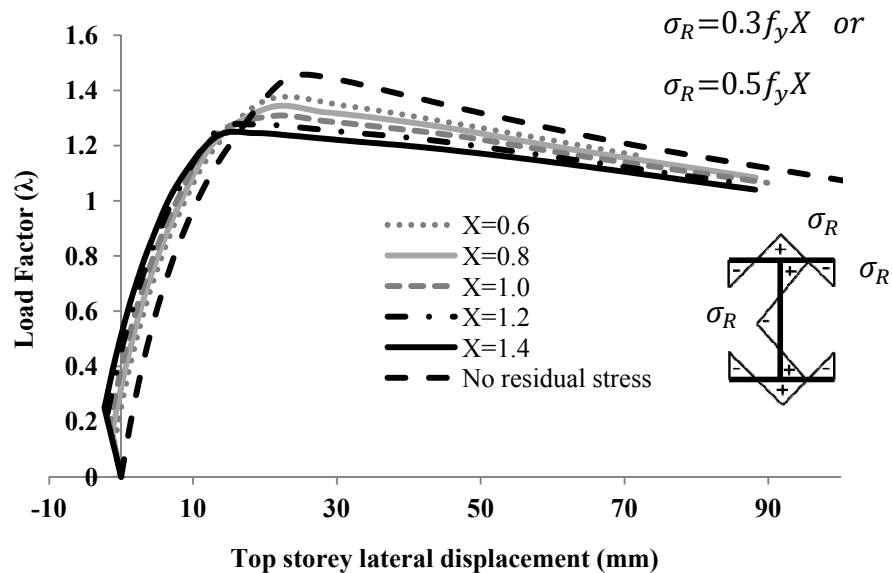


Figure 6-7: Load-deflection curve of Frame 1 with ECCS residual stress model

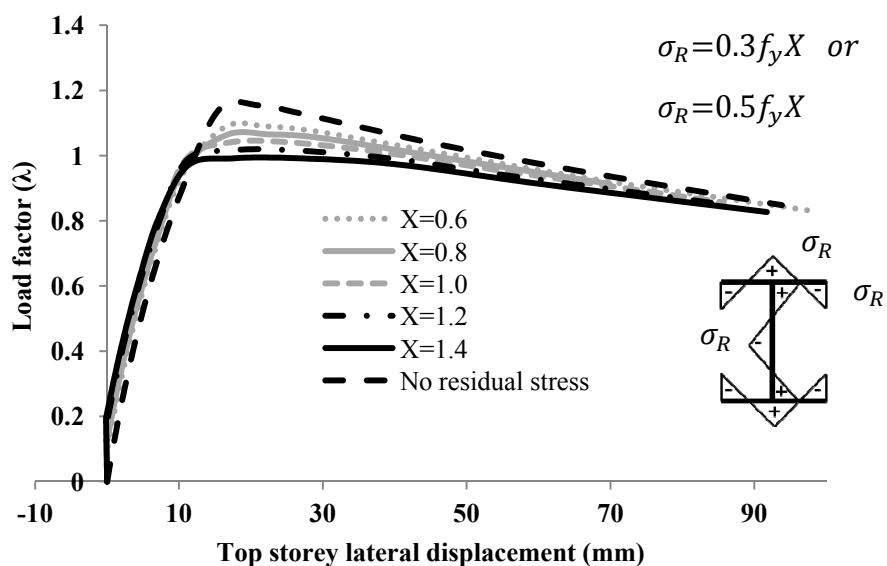


Figure 6-8: Load-deflection curve of Frame 2 with ECCS residual stress model

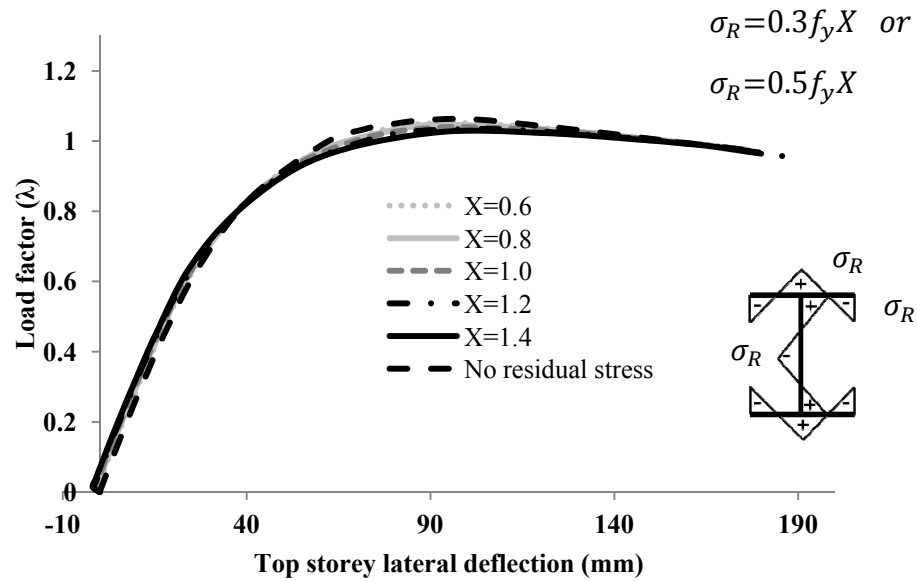


Figure 6-9: Load-deflection curve of Frame 3 with ECCS residual stress model

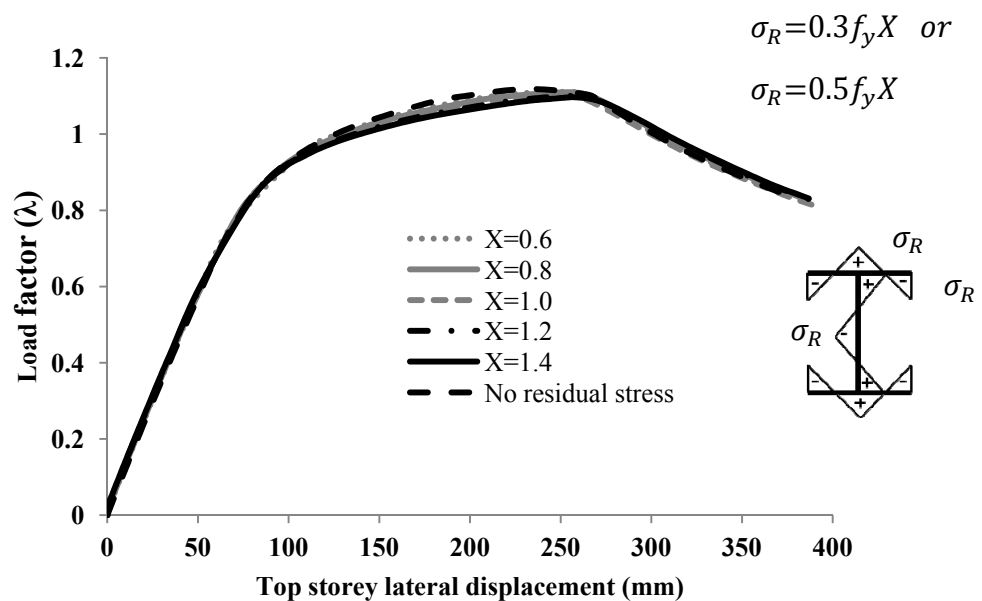


Figure 6-10: Load-deflection curve of Frame 4 with ECCS residual stress model

As mentioned before, the first two frames fail by instability of the first storey columns and the effect of incorporating residual stress on the ultimate load of the frame is comparable with what has been observed for a single column in the literature (ECCS (1976)). Figure 6-11 shows the effect of different levels of residual stress on the ultimate strength of a single column, as reported in the ECCS Manual (1976). Based on the results

provided in Table 6-2 for Frames 1 and 2, the ultimate load using the ECCS model shows a reduction of 14% when comparing the two cases of no residual stress and a scale factor of 1.4. For the scale factor of 1.4, the maximum flange tip stress is equal to  $0.3 \times 1.4 \times f_y = 0.42f_y$ . It can be seen from Figure 6-11 that by changing the maximum flange tip stress from zero (no residual stress) to  $0.4f_y$ , the column strength drops from 0.68 to 0.59 with the difference of 13.2% at a slenderness of one. This is similar to the reduction in strength of Frames 1 and 2 because the failure of these frames involve buckling of the lower storey of columns which were all designed to have a slenderness of unity. For Frames 3 and 4 which are more practical and fail by bending of both beams and columns, the difference between two discussed cases of no residual stress and scale factor of 1.4 reduces to 3.6% and 2% respectively. Thus, it can be concluded that although the variation in residual stress magnitude can have a significant effect on the ultimate strength of a single column with a slenderness of one, this effect is less severe in practical frames for which it is unlikely that all columns of the critical storey have a slenderness of unity.

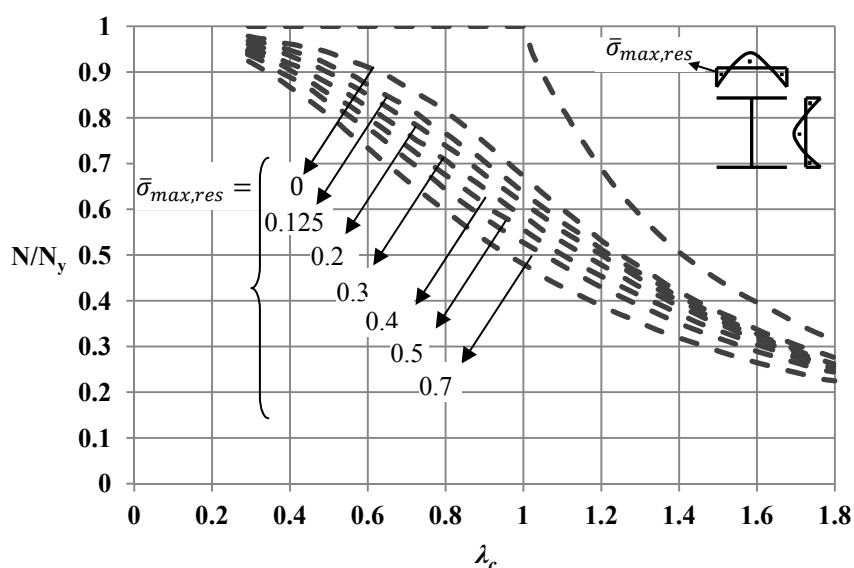


Figure 6-11: Column strength for different levels of residual stress, ECCS (1976)

In terms of the residual stress pattern, using the Galambos residual stress model with any magnitude of scale factor results in higher strength compared to the ECCS model (Table 6-2) with the maximum difference of 4.69%, which relates to Frame 2 and a scale factor of 1.4 (Table 6-3). This difference can be explained by comparing the residual stress patterns in Figures 6-1(d) and 6-1(e). While the ratio between tensile and compressive

residual stress ( $\sigma_{RT}/\sigma_{RC}$ ) is unity for the ECCS model, this ratio varies in the Galambos model depending on the cross-sections geometry. Since the residual stress is in equilibrium in the entire cross-section and the web is completely in tension in the Galambos model, this ratio is clearly less than one for this model. The mean value of the  $\sigma_{RT}/\sigma_{RC}$  ratio for the 40 American sections studied in Section 6.2 was found to be 0.62, which shows less tension in the Galambos model compared to the ECCS model. In the case of bending about the major axis, while less tension in the compression flange is detrimental, this is beneficial for the flange in tension and the net effect of changing the  $\sigma_{RT}/\sigma_{RC}$  ratio is negligible. However, for the web, less tension in the Galambos model implies less effect of residual stress and yielding at a later stage compared to the ECCS model. Thus, all frames indicate higher values of the frame ultimate load when using the Galambos model.

### 6.3.2 Probabilistic study

For all frames shown in Figure 6-6, 350 advanced structural analyses were performed with random levels of residual stress using the ECCS and Galambos models. For each simulation, the scale factor is randomly generated from the statistics provided in Table 6-1 using Latin Hypercube sampling (LHS). The yield stress is the same in all simulations for a given frame. It should be noticed that in this study only the magnitude of residual stress is treated as a random variable while the shape is kept unchanged. The scale factors are considered to be correlated between the members, implying that a single scale factor was generated and applied to all members of the frame. Table 6-4 presents the statistics (mean and COV) of the simulated ultimate strengths of the four frames taking into account the uncertainty in the magnitude of residual stress. The histograms of frame ultimate strengths for both residual stress models and the corresponding fitted normal distributions are shown in Figure 6-12 to Figure 6-15.

Table 6-4: Ultimate load factor statistics, using different pattern of residual stress

	Frame 1		Frame 2		Frame 3		Frame 4	
	ECCS	Galambos	ECCS	Galambos	ECCS	Galambos	ECCS	Galambos
Mean ( $\lambda$ )	1.307	1.348	1.040	1.075	1.038	1.053	1.100	1.112
COV ( $\lambda$ )	0.0246	0.0196	0.0234	0.0197	0.0057	0.0035	0.0066	0.0030

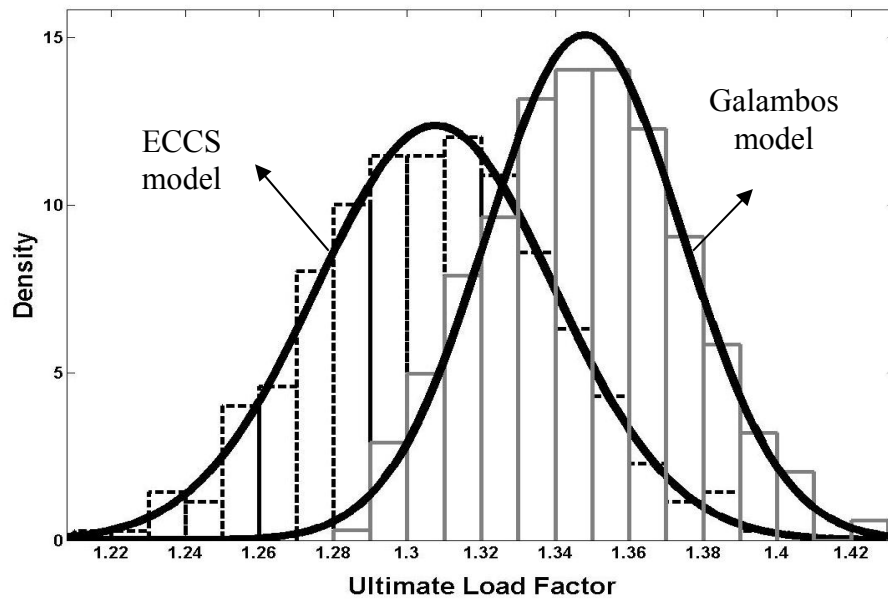


Figure 6-12: Histograms of ultimate frame strength for Frame 1 using ECCS and Galambos models

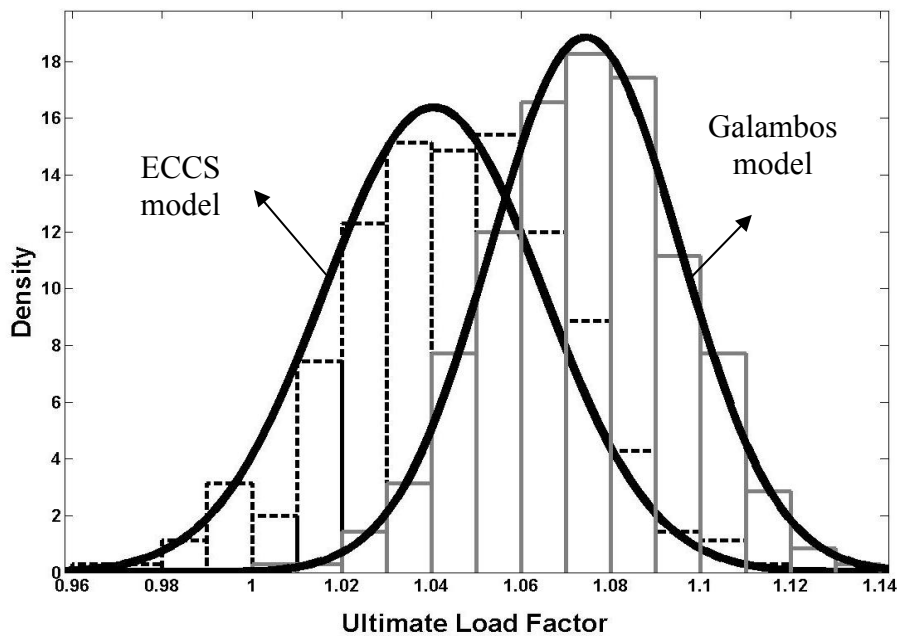


Figure 6-13: Histograms of ultimate frame strength for Frame 2 using ECCS and Galambos models

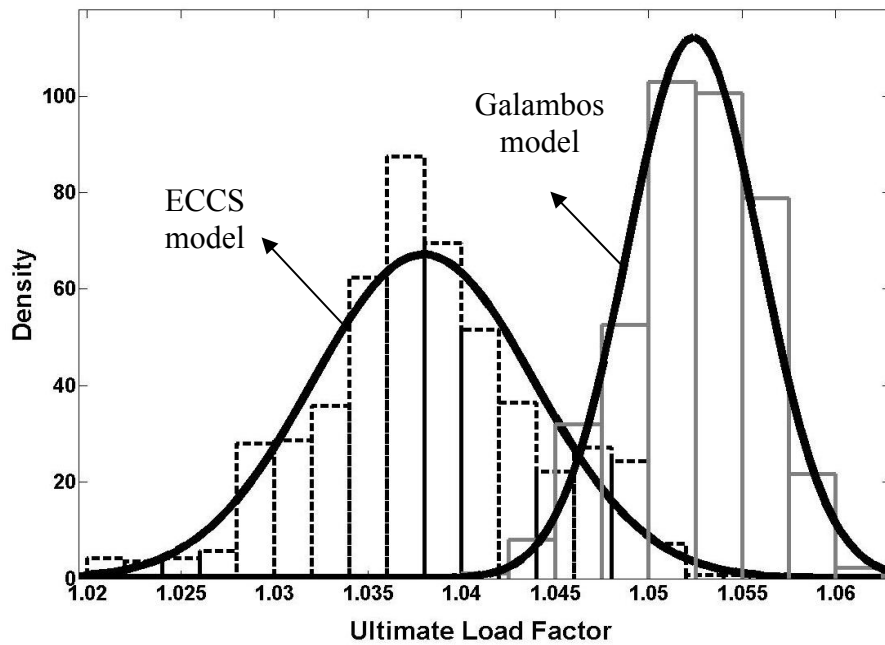


Figure 6-14: Histograms of ultimate frame strength for Frame 3 using ECCS and Galambos models

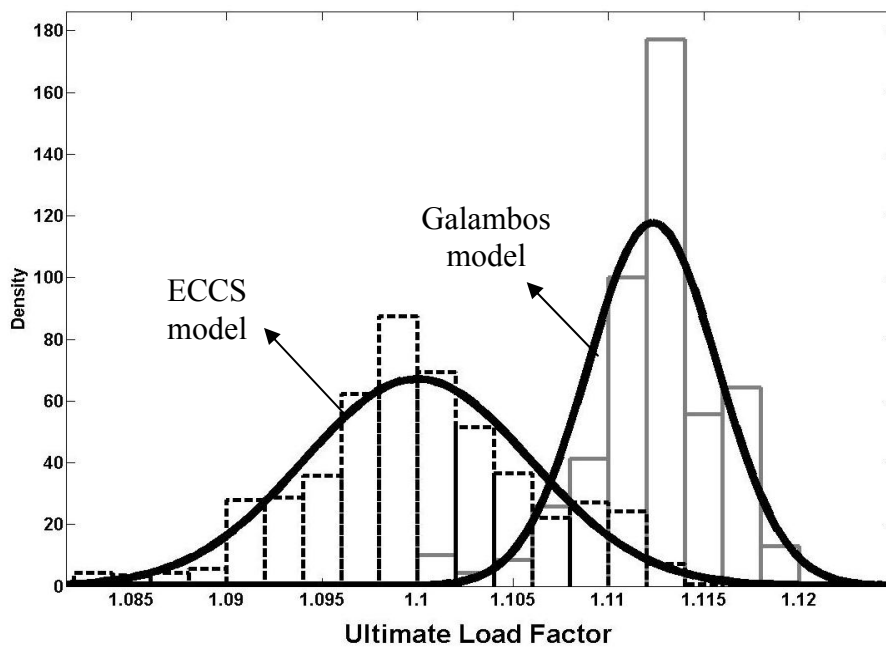


Figure 6-15: Histograms of ultimate frame strength for Frame 4 using ECCS and Galambos models



For all frames, using the Galambos model results in larger mean load factors compared to the ECCS model, which is consistent with the deterministic study presented in Section 6.3.1. It is interesting to see that although the COVs of the residual stress scale factors ( $X$ ) are quite large (approximately 20 % and 27 % for the ECCS and Galambos models respectively), these COVs result in the COVs of the ultimate strength of 2.5% and 2.3 % for Frame 1 and Frame 2 respectively using the ECCS model and 2% using the Galambos model for both frames. With the same residual stress statistics for Frame 3 and Frame 4, which are not as sensitive as the first two frames to second order effects, the COVs decrease to 0.57% and 0.66% using ECCS model and 0.35% and 0.3% using ECCS model respectively. It should be mentioned that similar to what was observed in the deterministic study, using the Galambos model results in less variation in the ultimate strength of steel frames (see Table 6-4)

## 6.4 Reliability analysis

The effect of random residual stress on the system reliability of steel frames using different residual stress pattern is evaluated in this study. The first two frames, which are most sensitive to second-order effects are selected. Since the randomness in yield stress has a significant influence on the residual stress magnitude, the yield stress is also modeled randomly, assuming a log-normal distribution with a mean of  $1.05f_{yn}$  and a COV of 0.1, where  $f_{yn}$  is the nominal yield stress (320 MPa for Frame 1 and 235 MPa for Frame 2) (Galambos and Ravindar 1978). The statistics of the residual stress scale factors for the different models can be found in Table 6-1. The yield stress is considered to be correlated between frame members which means a single random yield stress is assigned to all members of the frame. The frames are subjected to gravity loading using the load combination of  $1.2D_n+1.5L_n$  which is based on the Australian loading code (AS/NZS1170 2002) and in which  $D_n$  is the nominal dead load and  $L_n$  is the nominal live load. In this study it is assumed that the live and dead loads have the same magnitude ( $L_n/D_n=1$ ).

The system reliability index ( $\beta$ ) of these structures can be estimated using the First Order Reliability Method (FORM) (Nowak and Collins 2000), with the simple limit state function of  $G = R - D - L$ , in which  $R$  is the system resistance (or frame ultimate

strength),  $D$  is dead load and  $L$  is live load. For each frame, 350 nonlinear second-order inelastic analyses are conducted with random values of yield stress and residual stress scale factor. The dead load is assumed to be normally distributed with a mean value of  $1.05D_n$  and a COV of 0.1, while the live load is represented by an Extreme Type I distribution with a mean value of  $1.0L_n$  and a COV of 0.25 (Galambos, et al. (1982)). The histograms of the ultimate load factor for Frame 1 and Frame 2 are shown in Figure 6-16 and Figure 6-17, respectively and appear to be normally distributed. The statistics of the ultimate load factor are summarized in Table 6-5. Note that the frames were loaded by unfactored gravity loads  $\lambda(D+L)$  where  $\lambda$  is the load factor.

As it can be seen from Table 6-5, taking into account the effect of randomness in yield stress results in higher COV with the maximum value of 8.8% for Frame 1 using the ECCS model. This higher value of COV for the ultimate frame strength compared to the COV when only considering the scale factor as random variable (Section 6.3.2) is because of the high COV of the yield stress.

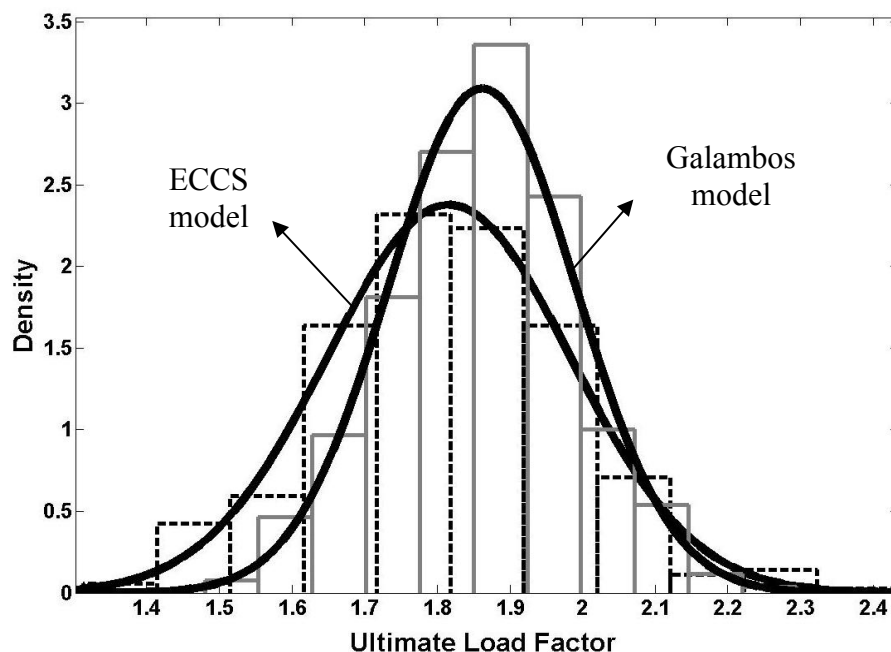


Figure 6-16: Histograms of ultimate frame strength using ECCS and Galambos models with both residual stress scale factors and yield stress as random variables, Frame 1

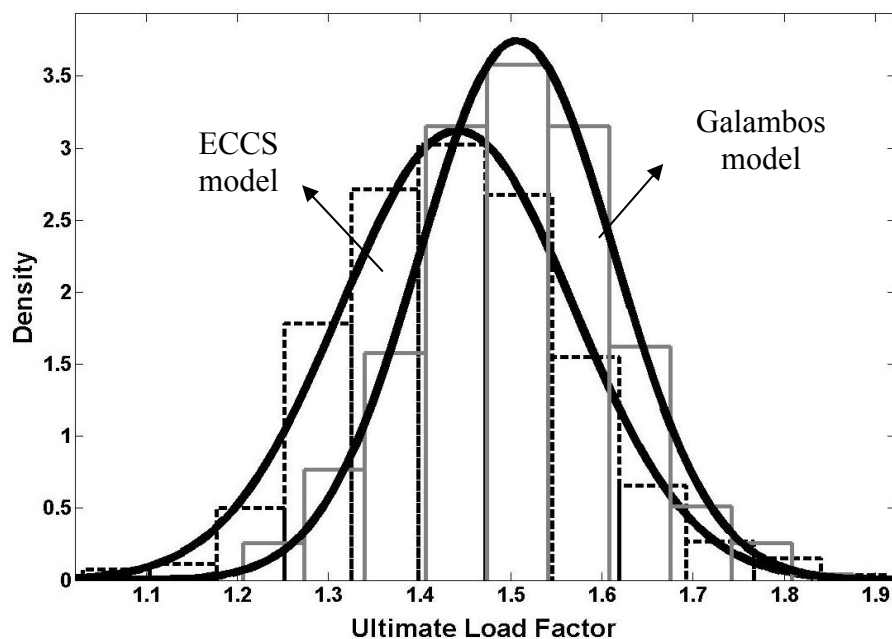


Figure 6-17: Histograms of ultimate frame strength using ECCS and Galambos models with both residual stress scale factors and yield stress as random variables, Frame 2

As was previously observed, using the Galambos model results in higher mean and less COV compared to the ECCS model, leading to higher values of reliability index when using the Galambos model compared to the ECCS model. Consequently, using the ECCS model is more conservative. The probability of failure of both frames using ECCS and Galambos models as well as reliability indices are shown in Table 6-5. Although the difference between probabilities of failure for Frame 1 and Frame 2 are 52% and 25% respectively, this difference drops to 6% and 9.2% when comparing the reliability indices. Based on this study, it can be concluded that the residual stress pattern influences the system reliability index depending on the sensitivity of the frame to second-order effects and needs to be chosen appropriately in the advanced analysis of steel structures.

Table 6-5: Ultimate load factor statistics and reliability index

	Frame 1		Frame 2	
	ECCS	Galambos	ECCS	Galambos
$\mu(\lambda)$	1.820	1.862	1.448	1.493
$COV(\lambda)$	0.0877	0.0743	0.0851	0.0740
$P_f$	$5.5 \times 10^{-4}$	$2.6 \times 10^{-4}$	$1.13 \times 10^{-2}$	$8.5 \times 10^{-3}$
$\beta$	3.26	3.47	2.16	2.38

## 6.5 Conclusion

Residual stress may have a significant impact on the strength and reliability of steel frames, depending on the sensitivity of the frame to second-order effects. Thus, residual stresses need to be modelled appropriately in advanced structural analysis.

Residual stress measurements available in the literature have been compiled in this paper, and scale factors that provide the best fit of common residual stress distributions to measured distributions have been determined by error minimisation. In conjunction with the residual stress distributions, the statistics for the scale factors present models for representing residual stress in probabilistic studies of the strength of steel frames. It was observed that the ECCS model is the best match to non-American sections while the Galambos model is better suited for American sections. Also, based on deterministic and probabilistic studies, it was concluded that using the ECCS residual stress model generally results in smaller values of ultimate load factor compared to the Galambos model. A reliability analysis showed that the corresponding change in reliability index could be as high as 9%.

The paper shows that although residual stresses can have significant impact on the strength of a single column, residual stresses generally have much less influence on the strength of a steel frame. The maximum influence of residual stress on the frame ultimate load occurs when the frame fails by instability of columns and decreases for the more practical situation where the frame fails by bending or buckling of both beams and columns. Only in the unlikely case, where all columns of the critical storey of a frame have a slenderness of close to unity, is the strength of a frame as affected by residual stress as a single column in the intermediate slenderness range. Similarly, the presented probabilistic study shows that although residual stresses indicate a relatively large COV (about 20%), the COV of the frame ultimate strength is much smaller with the maximum of 2.5%.

# CHAPTER

# 7 .

## System reliability-based design of steel frames by advanced analysis

---

### 7.1 Introduction

Steel structures are designed on a daily basis by structural engineers. The current process of design includes an analysis, which produce internal actions like moments and axial forces, followed by a design check to a steel structural Specifications to ensure that each member have adequate strength. While the types of analysis have changed from hand calculations to linear and more recently second order elastic analysis over the last four decades, the component-based approached (two-step design) has prevailed for longer than a century. In conventional steel design (component-based), members such as beams and columns are isolated from the structural system following analysis and designed individually based on the Load Resistance Factor Design (LRFD) equation,

$$\phi R_n \geq \sum \gamma_i Q_{ni} \quad 7-1$$

in which  $R_n$  is the member nominal capacity based on the steel design code and  $\sum \gamma_i Q_{ni}$  is the load effect in the corresponding member induced by applied nominal loads. In this approach, the interaction between the structural system and its members is only reflected indirectly through the use of effective length factor ( $k$ ) and is based on elastic analysis. This component-based approach cannot accurately capture the influence of the inelastic redistribution of internal forces subsequent to initial yielding. On the other hand, the interaction between members, especially in a large structural system, is too complex to be represented by the simple effective length factor approach (Chen and Kim 1997). Thus, the conventional design approach may not accurately predict the ultimate load-carrying capacity of the structural system or correctly represent the frame failure modes. Furthermore, capacity check of each individual frame component is a time consuming process.

Therefore, there are strong economic and safety reasons for developing a practical design method that can account for compatibility between the members and the whole system by use of advanced analysis (system-based design approach). The change of emphasis from individual member strengths to the overall structural behaviour promotes a more holistic approach and greater innovation in structural design, and is likely to become increasingly used by structural engineers as commercial software packages make geometric and material nonlinear analyses available.

“Advanced” second order inelastic analysis represents a new method in which analysis and design are performed in a single step. The proposed system strength check has the LRFD type format:

$$\varphi_s R_n \geq \sum \gamma_i Q_{ni} \quad 7-2$$

in which  $R_n$  is the nominal system strength predicted by advanced analysis and  $\varphi_s$  is the system resistance factor determined by reliability assessment. It is worth noticing that although Equation 7-2 has the same LRFD format as for members (Equation 7-1); it follows a different philosophy in that it is based on system performance. Since member failures are directly incorporated into advanced analysis, there is no need for a separate

member/section capacity check, provided a comparable or higher level of structural reliability is achieved by the analysis.

It should be noted that, among all main analysis methods, advanced analysis is best able to capture the behavioural characteristics and ultimate load carrying capacity of a structural system, taking into account system effects explicitly such as load redistribution subsequent to first yielding (see Figure 2-4). By using advanced analysis, the system failure mode becomes apparent and it is possible to consider the consequences of failure in the design process. This feature is especially important in the new paradigm of performance-based design. Ziemian et al. (1992), analysed a series of two-bay two-storey planar frames and a 22-storey 3D frame, and showed that design by advanced analysis could save about 12% of steel weight compared to design by the member-based AISC-LRFD specification.

The direct design-by-advanced-analysis method requires both an analysis procedure which considers the key factors influencing the frame ultimate strength and the availability of system resistance factors at the same time that consider the inherent uncertainty in structural load and system strength. The steel structural Specifications require the reliability of the system to be considered when advanced analysis is used but do not explain how this may be achieved. Traditionally, the issue of uncertainty and risk has been approached by calibrating resistance (reduction) factors for each type of member and applying these factors to the ultimate strength of each member composing the frame (Ellingwood 2000). To overcome the inherent shortcoming of the current member-based structural design process, a rational system reliability assessment is needed to accurately predict resistance factors to be applied to the entire system strength to account for potential risks arising from uncertainty, rather than to each component. In other words, while general guidelines are available for advanced analysis, one of the most important impediments to adopting a system-based design methodology in practical application is the lack of information about the system resistance factors. Probabilistic limit state design is based on the notion of a “target” reliability as a quantitative measure of structural safety (or probability of failure) and a basis for achieving a uniform performance in design (Ellingwood and Galambos 1982). The target reliability indices implied in current LRFD typically range between 2.25 for members and 3 (under gravity loads and combined gravity and wind) (AISC 1987). These target reliability indices were

established by calibration to the working stress design (Ellingwood et al. 1982). Selecting acceptable target reliability indices for structural systems is a difficult task because of the lack of research to inform the choice of such values. Target reliability values are usually selected by engineering judgment and/or assessing the reliability of existing structures.

This chapter outlines a novel framework for determining system resistance factors for different types of structural systems under various load combinations such as gravity and combined gravity and wind. This study is part of a research effort to develop the next generation of steel structural codes which most likely will be based on the direct design of structural systems by advanced analysis. The main objective of this chapter is to examine the structural reliability of a wide range of 2D low-to-mid-rise moment resisting frames and find appropriate system resistance factors by means of a probabilistic approach. Monte Carlo types of simulations are conducted for a series of moment-resisting (sway) frames and braced frames including regular and irregular configurations subject to different load combinations. The reliability assessment and the system-based failure criteria are explained.

Additionally, the effect of correlation in member yield strength on the ultimate strength of the frame and subsequently on the system resistance factor has been examined by comparing three cases of uncorrelated, partially correlated, and fully correlated. Based on the simulation results, a First Order Reliability Method (FORM) analysis is performed to determine relationships between the system reliability and the system resistance factor. Finally, an appropriate target reliability is selected based on the reliability assessment of existing structures and conclusions are drawn about the resistance factors required for the proposed level of reliability for any type of frame. Design examples are provided to (i) demonstrate the application of the proposed system-based design method and (ii) show the benefits it provides by comparing the results obtained with those obtained using current member-based design specifications. The study presented in this thesis is limited to two-dimensional frames and hence, spatial behavior including lateral-torsional buckling is not considered.



## 7.2 Methodology

The procedure for developing a system reliability-based design format for steel frames can be summarized in five essential steps:

(1) A series of low-to-mid-rise sway and braced steel frames are selected and designed to an existing member-based specification (here chosen as AS4100 (1998)) as a starting point. Various load combinations e.g. gravity (dead and live load) and combined gravity and wind are considered.

(2) Different system resistance factors ( $\varphi_s$ ) between 0.6 and 1 are assumed for each frame and the frames are then designed by advanced analysis to satisfy the limit state equation presented in Equation 7-2 (system-based design). For frames under gravity loading this can be achieved by adjusting either the cross-sections or the loads. In the former choice, for each specific value of  $\varphi_s$ , new combinations of cross-sections are selected to satisfy the limit state equation while the total applied load remains constant (referred to as Cross-Section Scaling Method (CSM) in this paper). The second choice is based on changing loads for different values of  $\varphi_s$  to satisfy Equation 7-2 while the cross-sections remain unchanged (referred to as Load Scaling Method (LSM)). It should be noted that for frames under combined gravity and wind loads, since the loads represent different events in different directions, it is not possible to scale these loads simultaneously. Thus, only CSM is applicable. The merits of these two approaches will be discussed subsequently.

(3) For all designed frames, Monte Carlo simulations are performed in a “pushdown” ultimate limit state analysis (for frames under gravity loading) or “pushover” analysis (for frames subjected to gravity and wind loading) to develop a probabilistic model (distribution type, mean and standard deviation) for the system strength, considering the randomness in material and geometric properties.

(4) Using the statistics for the frame ultimate strength ( $R$ ) in Step 3, and the probabilistic models for loads, the reliability index ( $\beta$ ) can be determined for all frames by first order reliability analysis (FORM) (Melchers 1999). Note that determining the limit state probability of the frame directly through Monte Carlo simulation would require an

unmanageable number of frame analyses. The reliability index relates to the structural failure probability by  $P_f = \Phi(-\beta)$ , where  $P_f$  is the probability of failure and  $\Phi()$  is the standard normal distribution function. Different load ratios are considered e.g. live to dead load ratios ( $L_n/D_n$ ) for frames under gravity loading as well as wind to gravity load ratios ( $W_n/(L_n + D_n)$ ) for frames subject to gravity and lateral loads.

(5) For different frames with different failure modes, the relationships between  $\beta$  (reliability index) and  $\varphi_s$  (system resistance factor) are plotted whereby  $\varphi_s$  can be obtained for different levels of target reliability.

### 7.3 Structural framing system

A series of nine 2D steel frames, which represents the typical low-to-mid rise steel building inventory, consisting of regular and irregular geometries of moment-resisting (sway) frames as well as braced frames, has been selected as a basis for the present study. Figure 7-1 shows the geometry, support conditions and loading patterns. Various load combinations are applied to the frames which are explained in Section 7.3.1.

Two-dimensional second-order inelastic FE models are developed as a nominal model using ABAQUS (2009) based on the modeling concept developed in Chapter 3. The model accounts for all material and geometrical nonlinearities. To model material nonlinearity, a 2D plastic-zone beam-column element is used to trace the spread of plasticity through the cross-section and along the member length. In tracking the nonlinear load-deflection response, the element geometry in each load increment is updated whereby second-order effects are captured. The material is modeled as elastic-perfectly-plastic and the effect of strain hardening is ignored as discussed in Section 3.7. Residual stress is modeled as a self-equilibrating initial stress using the ECCS model (1984) (Section 3.5). Initial geometric imperfections are modeled as a linear superposition of the first six elastic buckling modes. In this study, all beams and columns are bent about major axis. Details about this method and appropriate scale factors for each buckling mode can be found in Chapter 5.

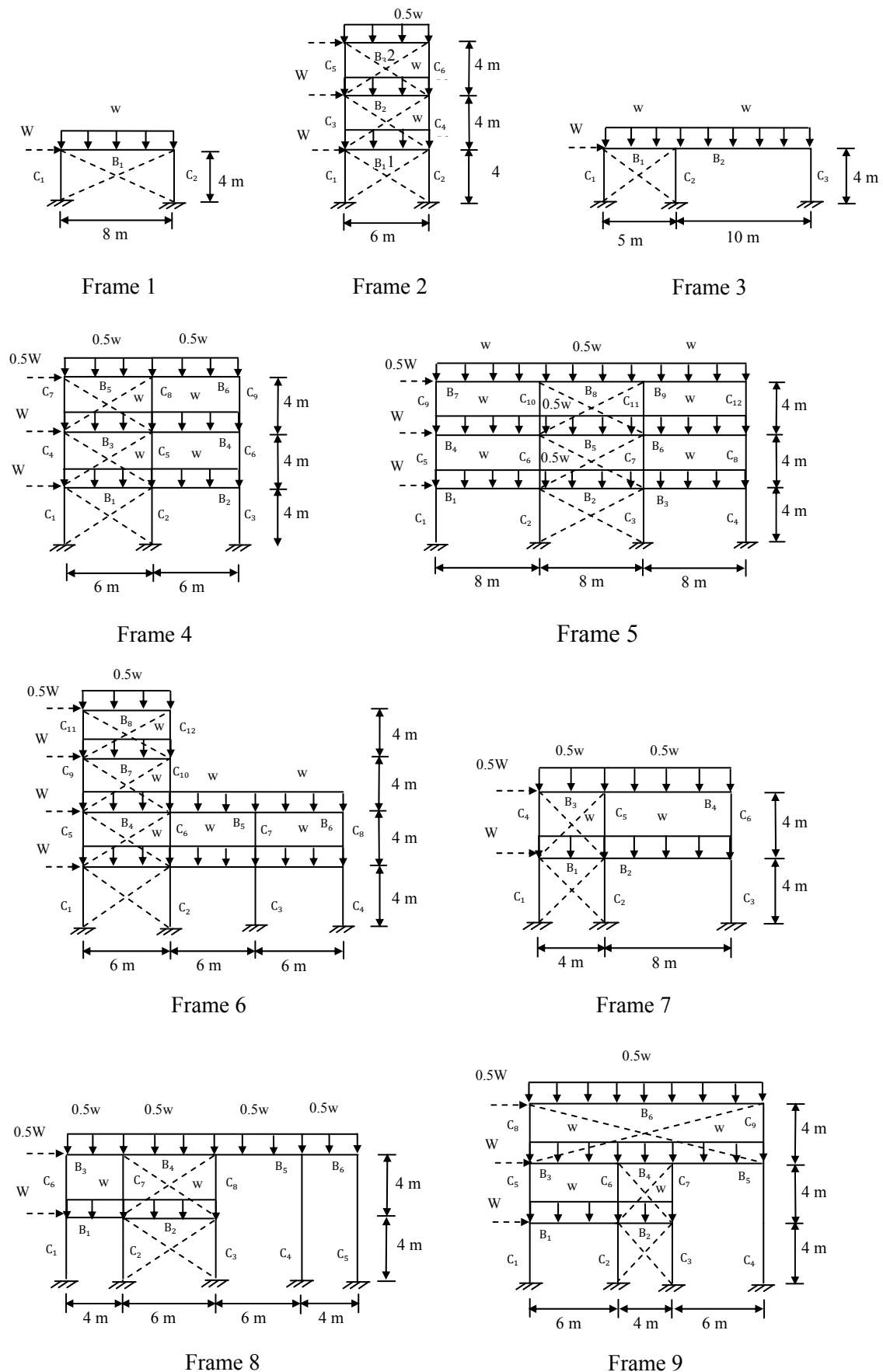


Figure 7-1: Layouts for steel framing system

A mesh convergence study is performed in Chapter 3 and suggesting one element per 200 mm length be used for all members, resulting in typically 20-40 elements per member. All column bases are fully fixed. The beam-column connections are modeled as rigid for sway frames while both rigid and hinged joints are considered for braced frames. The influence of connection stiffness on the frame ultimate strength and its failure mode is ignored in this study. The brace members are chosen from equal angles sections in a way that the failure does not occur in the braces. All cross-sections are fully compact hot-rolled I-sections and the out-of-plane behavior is restrained by applying a full lateral restraint to all frame members (2D frames). Thus, local buckling and lateral-torsional buckling are not considered in this study. The nominal ultimate strength for each frame is evaluated based on the nominal material and geometric properties. It should be noted that the nominal model is the model intended to be used for practical design.

### 7.3.1 Loading

The load combinations being considered in this study are (i) gravity (dead plus occupancy live load) (ii) gravity plus wind. The sway frames are subjected to both load cases while for braced frames only the former load combination is considered. The frames are designed according to ASCE Standard 7-05 (2006), load criteria. Frames controlled by gravity loading are designed for the load combination of  $1.2D_n+1.6L_n$ , in which  $D_n$  represents dead load and  $L_n$  live load. For frames subjected to lateral and gravity loads, the load combination of  $1.2D_n+0.5L_n+1.6W_n$  is used where  $W_n$  is the wind load. These load combinations are selected since the load statistical characteristics used for this study are based on the same American data as that used for the ASCE Standard. It should be noted that  $1.6W_n$  in ASCE 7-05 based on a wind speed with a 50 years mean recurrence interval (MRI), is approximately equal to  $1.0W_n$  in ASCE 7-10, in which the wind speed is based on a 700 years MRI. Hence the results would be the same for frames designed by the more recent ASCE standard.

The total gravity load is applied as a uniformly distributed load (UDL) along the beam lengths. To calculate the gravity load, typical office live load equal to 2.4 kPa, floor construction dead load of 4.4 to 5 kPa and the frame spacing of 6 to 8 m are used, according to the American code AISC360-10 (2010). Based on these values the total

nominal gravity load (dead plus live loads) is assumed to be  $w=48$  kN/m. For frames under gravity loading, the nominal dead and live loads are assumed to have the same magnitude ( $L_n/D_n=1$ ). For the gravity plus wind load case, the live to dead load ratio of 2 (i.e.  $L_n/D_n=2$ ) and the wind to gravity load ratio of 0.1 (i.e.  $W_n/(D_n+L_n)=0.1$ ) are considered. It should be noted that in this study, the frames are subjected to factored loads (i.e.  $1.2D_n+1.6L_n$  and  $1.2D_n+0.5L_n+1.6W_n$ ) when designed based on the Specifications and unfactored load (i.e.  $D+L$  and  $D+L+W$ ) when it comes to the simulations.

### 7.3.2 System failure criterion

In the simple plastic theory, the ultimate strength of a frame is reached when there are enough plastic hinges developed to create a statically unstable mechanism. Various failure mechanisms can be developed depending upon whether the frame is made of a strong beam and weak column combination or a strong column and weak beam combination (Figure 7-2).

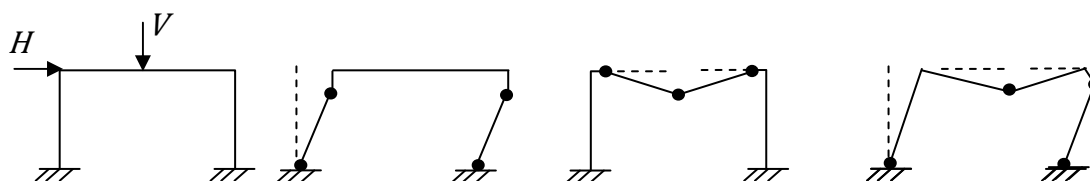


Figure 7-2: Various failure mechanisms

Since complete plastic hinges do not develop in the frame when plastic zone analysis is used, failure occurs when yielding spreads sufficiently through the member cross-section and along the member length. Figure 7-3 schematically shows the representation of a moment-curvature relationship for an I-section subjected to pure bending. Although the material may be modeled as elastic-perfectly-plastic, the moment-curvature relationship shows a smooth transition from the elastic part to fully plastic. This is due to gradual yielding of the section from extreme fibers with higher stresses compared to interior fibers. The gradual yielding of the section results in the gradual formation of plastic hinges. Thus, while the cross-section is completely plastic at point (a) in Figure 7-3 using plastic hinge method, the corresponding point using plastic zone analysis (point (b)) has not reached full plastification. However, to simulate the exact same concept of plastic

hinge in using the plastic zone method, point (b) is considered as fully yielded in this study. Consequently, it is necessary to find the percentage of yielding of the cross-sectional area at point (b).

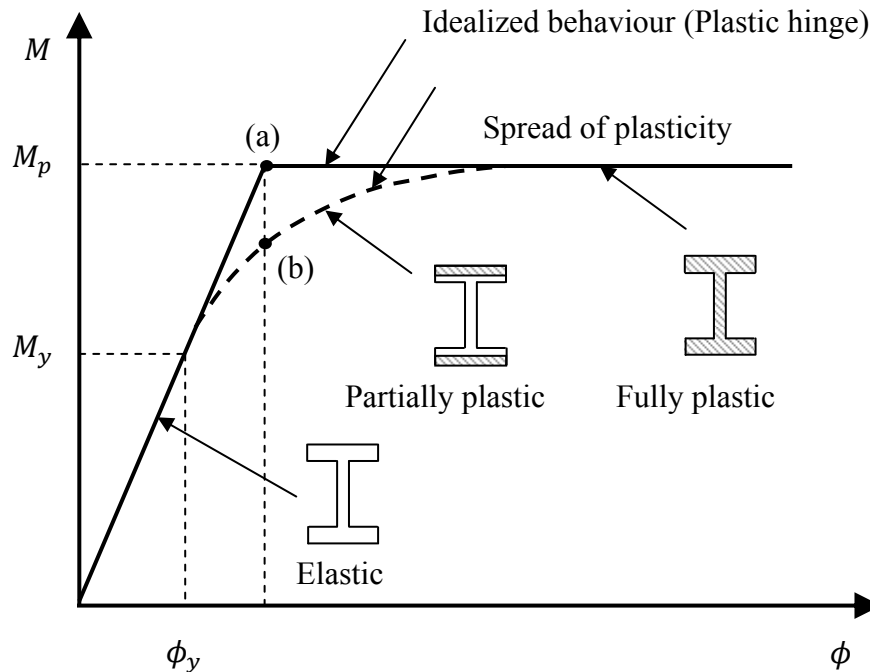


Figure 7-3: Schematic moment-curvature relationship of an I-section (Kim and Chen 1996)

For this purpose a simply supported beam with a point load at mid-span is considered and analysed using the second-order plastic zone method. The beam is made from 150UB14 with the yield stress of 320 MPa and elastic modulus of 200 GPa.

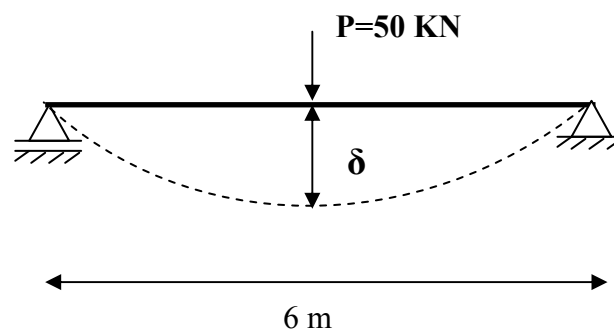


Figure 7-4: Simply supported beam used to define yielding criterion

The load-deflection responses comparing the plastic hinge and plastic zone analyses are presented in Figure 7-5. As it can be seen from the figure, for the deflection in which a hinge is developed at beam mid-span using the idealized plastic hinge method (point (a)), about 76% of the cross-section area is yielded using plastic zone method (point (b)). Therefore, based on this result, in this study if any beam or column is yielded in more than 75% of the cross-section area, it is categorized as fully yielded.

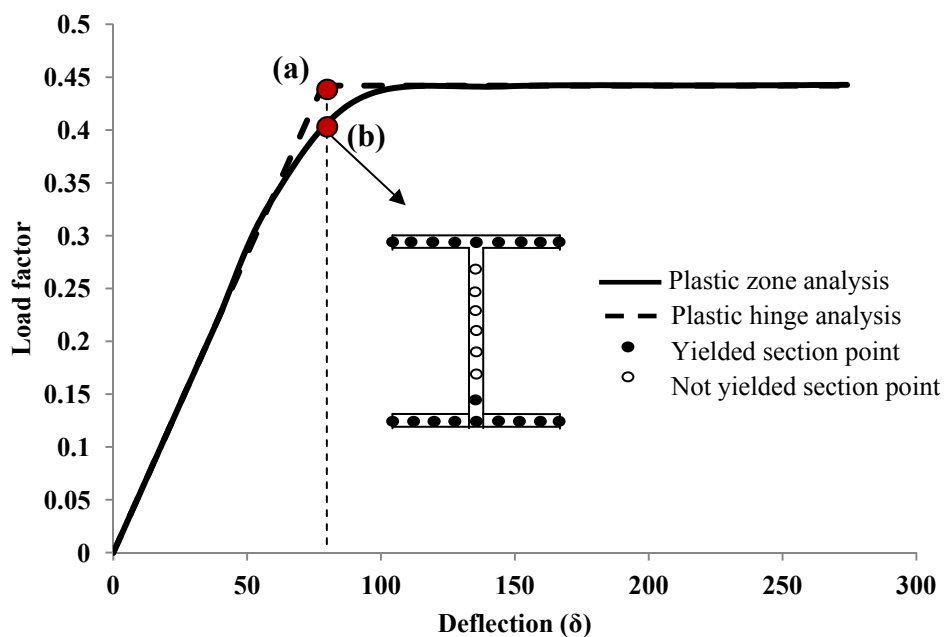


Figure 7-5: Load-deflection curve of simply supported beam used to define the yielding criteria

As mentioned by Galambos (1990), the structural system generally does not fail when one element fails. Rather, different combinations of element failures may take place to reach the point at which the failure of the entire structural system occurs. Therefore, it is important to consider different system failure modes. Beams as well as columns can be fully or partially yielded and the combination of these failures is considered. If any beam or column is fully yielded (more than 75% of the cross-section area), the failure mode is referred to as BFY (beam fully yielded) or CFY (column fully yielded) in this study. If the yield ratio in any beam or column is less than 75%, the failure mode is referred to as beam partially yielded (BPY) and column partially yielded (CPY) respectively. The frames are categorized in this way regardless of the number of fully or partially yielded

members. For example a specific frame with 2 fully yielded beams or 3 fully yielded beams does not result in different failure modes and is categorized as BFY for both models. Different combinations of these failure modes are considered in this study to evaluate the influence of system failure mode on the frame ultimate strength statistics and consequently system resistance factors. Two examples of frame failure modes are presented in Figure 7-6 in which the portion of yielded cross-sectional area is shown in percentage for all elements. The ultimate capacity of the frame is defined as the maximum point on the load-displacement curve (Section 3.6), or the load causing a storey drift of 5%, whichever comes first.

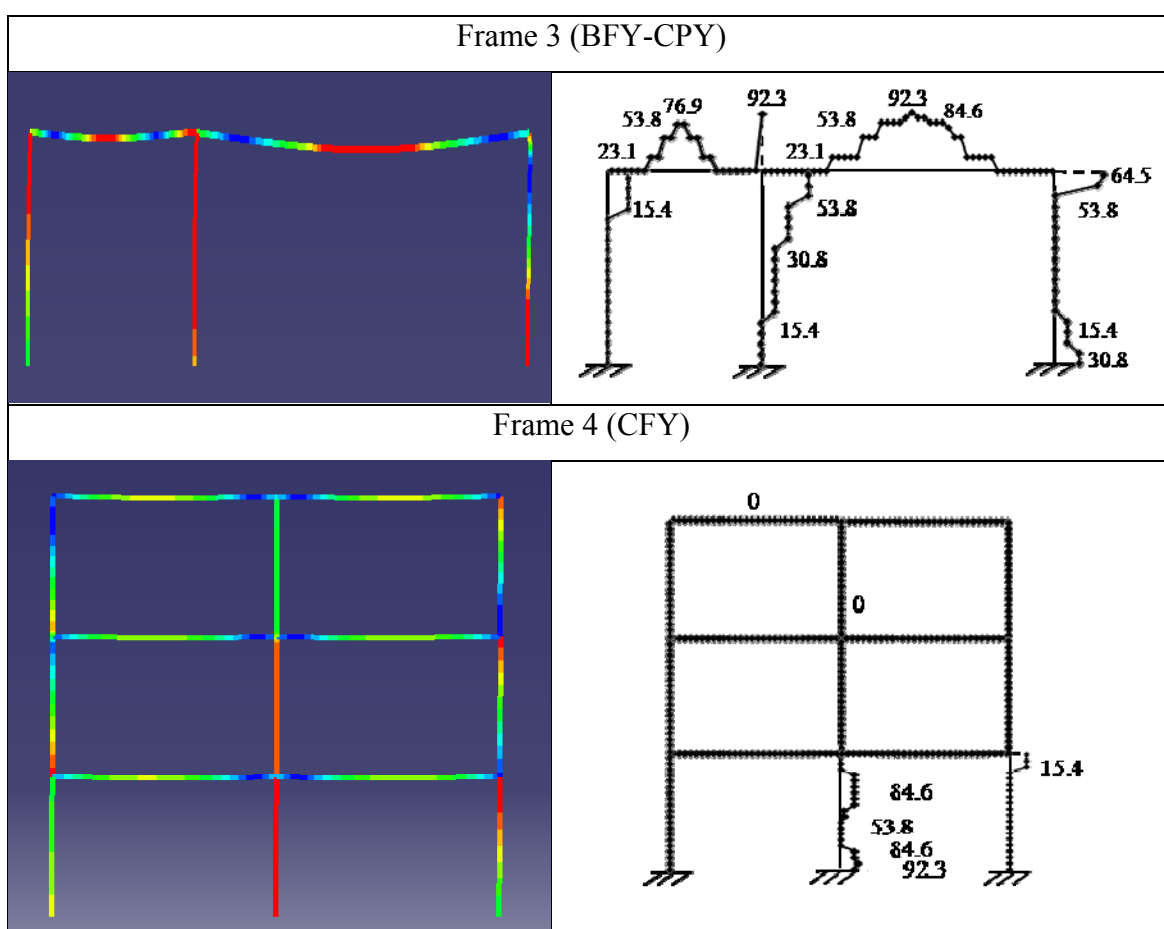


Figure 7-6: Examples of frames failure modes

## 7.4 Probabilistic analysis

The use of probabilistic methods in code development is traced back to 1940's and the concept of what is known today as the classical reliability theory was developed within



the period of 1940's to mid-1960's (Ellingwood 1994 ). Subsequent improvements can be summarised as the development of First-Order Reliability Method (FORM) and defining reliability index ( $\beta$ ) rather than the probability of failure ( $P_f$ ) as the quantitative measure of safety. In developing a probabilistic-based design code one of the major steps is the modelling and quantification of various sources of uncertainty due to inherent variability in material and structural properties, modelling and prediction, and measurement.

Various simulation techniques such as direct Monte Carlo, Latin Hypercube Sampling and importance sampling are available to determine the uncertainty in frame strength among which Latin Hypercube Sampling (LHS) is used in this research. Compared to direct random sampling, LHS requires fewer samples to achieve similar accuracy. The advantages of this method have been discussed in details in Chapter 2. In the present study, 350 advanced analyses were performed for a given frame using randomly generated values of yield stress, elastic modulus, cross-sectional geometry, member and frame initial geometric imperfection and residual stress, as described in the following sections. A MATLAB script is written to generate the random variables and subsequently 350 ABAQUS input files (.inp) for each frame. An example of these scripts can be found in Appendix E.13. Once developed the input files, they are run in batch mode using a supercomputer. The load-deflection curves are plotted automatically using a MATLAB script to find those cases with convergence problem and discard them in determining the statistics of ultimate strength. An example of these load-deflection curves is presented in Figure 7-7.

For frames controlled by gravity loading, the dead and live loads are not treated as random variables in the simulation since the purpose is to determine the probability distribution of the frame capacity. Randomness in loads will be taken into account subsequently in determining the probability of frame failure and the frame reliability index. The main restriction of this simplified method is that the increase in gravity load is proportional on all floors and in all bays. For frames under gravity and wind loading, the gravity loads are modelled as random variables in the simulations while the nominal value of unfactored wind load is applied to the frame. Similar to the gravity load case, the randomness in wind load is considered subsequently when the reliability analysis is conducted.

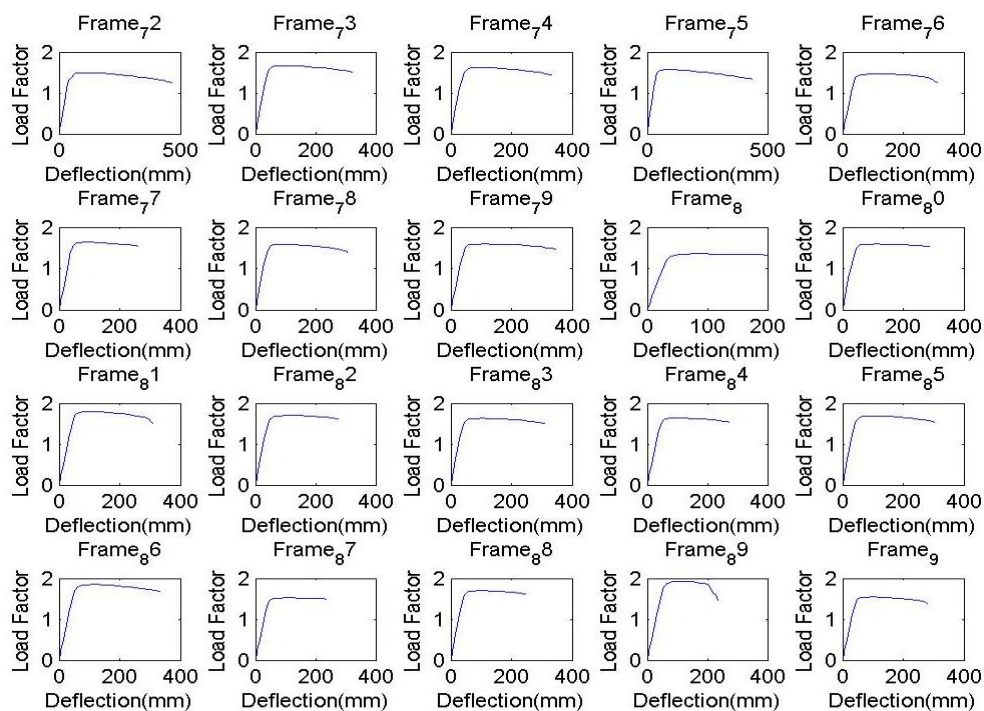


Figure 7-7: Example of plotted load-deflection curves using MALTB script to check the convergence

### 7.4.1 Uncertainties in steel structures

Various sources of uncertainty exist in steel structures which can influence the load-carrying capacity of a structure. These uncertainties arise as a result of errors associated with measurement devices, construction tolerances, human errors, and changes occurring to certain parameters over time. The inevitable consequence of the inherent uncertainties is the risk that a structure completely fails or cannot attain its intended performance. Basically, although it is impossible to completely eliminate the risk, it must be managed by engineers when developing the structural design standards. One of the most important steps in this regard is considering all sources of uncertainty as random variables when deriving the system resistance factors.

The basic random variables considered in this study are: yield stress ( $f_y$ ), residual stress ( $\sigma_R$ ), elastic modulus ( $E$ ), cross-sectional dimensions such as flange width ( $b_f$ ), web height ( $h$ ), and flange and web thickness ( $t_f$  and  $t_w$ ), member out-of-straightness ( $\delta$ ) and frame out-of-plumb ( $\Delta$ ). Recommended statistical data in the literature for these random

variables is summarized in Table 7-1. The summary of statistic characteristics of both initial out-of-straightness and out-of-plumb can be found in Table 2-4 and Table 2-5. Strain hardening and its randomness were not taken into account in this study since its influence on the frame strength appeared to be negligible (Section 7.9). Perfectly-correlated yield stress and Young's modulus for all frame members are used in which one random yield stress value  $f_y$  is generated and assigned to all beams and columns.

Table 7-1: Statistical characteristics of random variable obtained from the literature

	Reference	Number of Samples	Mean	COV	Distribution
Elastic modulus ( $E$ )	(Galambos and Ravindra 1978)	-	$E_n$	0.0600	Log-normal
	(Itoh 1984)	96	$1.0085 E_n$	0.0256	Normal
	(Fukumoto and Itoh 1983)	1665	$0.999 E_n$	0.0450	Lognormal
	(Kala 2009)	-	$E_n$	0.0600	Normal
	(Beck and Dória 2008)	-	$E_n$	0.0300	Log-normal
	(Buonopane 2008)	-	$0.993 E_n$	0.0340	Normal
Yield stress ( $f_y$ )	(Galambos and Ravindra 1978)	-	$1.05 f_{yn}$	0.1000	-
	(Itoh 1984)	50	$1.07 f_{yn}$	0.0300	Normal
	(Buonopane 2008)	-	$1.01 f_{yn}$	0.0600	Normal
	(Beck and Dória 2008)	-	$1.05 f_{yn}$	0.0700	Lognormal
	(Ellingwood 1996)	-	$1.05 f_{yn}$	0.1100	Lognormal
	(Fukumoto and Itoh 1983)	222	$1.24 f_{yn}$	0.0136	Normal
	(Kala 2009)	371	$1.21 f_{yn}$	0.0565	Normal
Area ( $A$ )	(Strating and Vos 1973)	189	$1.0186 A$	0.0396	Normal
	(Bjorhovde 1972)	-	$1 A$	0.0600	Normal
	(Fukumoto and Itoh 1983)	-	$1.01 A$	0.0340	Normal
	(Kala 2009)	371	$1.025 A$	0.0324	Normal
	(Itoh 1984)	75	$0.98 A$	0.0113	Normal
Strain hardening ( $E_{sh}$ )	(Galambos and Ravindra 1978)	-	4100 MPa	0.2500	-
	(Fukumoto and Itoh 1983)	1665	3726.5 MPa	0.2890	Normal
Residual stress (Flange tip)	(Itoh 1984)	24	174.9 MPa	0.0920	Normal
Residual stress (Flange centre)	(Itoh 1984)	25	20.69 MPa	0.4380	Normal
Residual stress (web centre)	(Itoh 1984)	24	17.72 MPa	0.0520	Normal

### 7.4.1.1 Variability in yield stress and elastic modulus

Due to uncertainty in manufacturing process, steel members usually show variation in yield stress which often has a significant influence on the load-carrying capacity of the frame system. In this study, the yield stress is modeled by a lognormal distribution with the mean of  $1.05f_{yn}$  and a coefficient of variation (COV) of 0.1, as presented by Galambos and Ravindra (1978)<sup>1</sup>. Here,  $f_{yn}$  represents the nominal yield stress, taken as 320 MPa. The modulus of elasticity is modeled as a normally distributed variable with a mean equal to the nominal value (200 GPa) and a COV of 6% (Galambos and Ravindar 1978).

### 7.4.1.2 Variability in cross-section dimensions

The uncertainty in manufacturing environment, results in different section dimensions and therefore variation in cross-sectional area. Section properties are statistically evaluated by Melchers et al. (2004) based on the experimental measurement of 369 hot-rolled I-sections. The statistical data for the cross-section dimensions shown in Figure 7-8 are listed in Table 7-2 as the ratio of the real dimension obtained from the measurement of cross-section geometry to the nominal dimension. Correlations observed between section parameters can be found in Table 7-3.

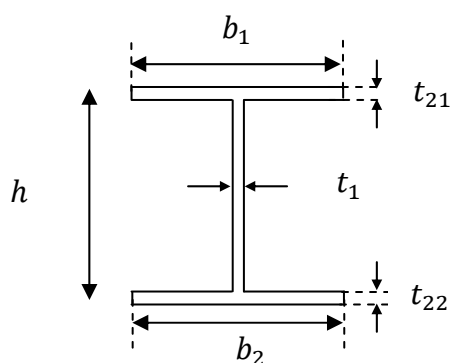


Figure 7-8: Cross-section dimensions

<sup>1</sup> These steel properties are based on tests of steels that were manufactured in the 1960's. Recent studies of steel properties for modern grades of steel have indicated that the COV may be somewhat less because most steel is manufactured from recycled materials using better controlled processes. These differences are not believed to have a significant impact on the results presented herein.

Using the statistics in Table 7-2 and the correlation matrix in Table 7-3, the mean and COV of member cross-section area can be found as  $1.025A$  and  $0.032$ , respectively which is comparable to the statistical data reported in the literature (Strating and Vos 1973; Fukumoto and Itoh 1983). These mean and COV are based on generating 10000 random cross-section dimensions considering the correlation matrix using a MATLAB script and subsequently calculating the cross-sectional area.

Table 7-2: Statistical result for cross-section dimensions

Thickness	Mean/Nominal	Standard deviation of Mean/Nominal
Section depth ( $h$ )	1.001	0.00443
Section width ( $b_1$ )	1.012	0.01026
Section width ( $b_2$ )	1.015	0.00961
Web thickness ( $t_1$ )	1.055	0.04182
Flange thickness ( $t_{21}$ )	0.988	0.04357
Flange thickness ( $t_{22}$ )	0.988	0.04803

Table 7-3: Correlation matrix for cross-section dimensions

	$h$	$b_1$	$b_2$	$t_1$	$t_{21}$	$t_{22}$
$h$	1	-0.0068	0.0534	0.0399	-0.0686	-0.0989
$b_1$	-0.0068	1	0.6227	-0.2142	-0.2681	-0.1456
$b_2$	0.0534	0.6227	1	-0.2132	-0.1596	-0.0423
$t_1$	0.0399	-0.2142	-0.2132	1	0.2368	0.2451
$t_{21}$	0.0686	-0.2681	-0.1596	0.2368	1	0.7634
$t_{22}$	0.0989	-0.1456	0.0423	0.2451	0.7634	1

### 7.4.1.3 Variability in initial geometric imperfection

Steel structural members are not perfectly straight due to manufacturing and erection tolerances. The frame ultimate strength is susceptible to these initial geometric imperfections and thereby second-order effects ( $P - \delta$  and  $P - \Delta$ ). In this study, both the out-of-straightness (member imperfection) and the out-of-plumb (frame imperfection) are incorporated as random variables in the FE model. The modelling of these geometric imperfections is based on the method proposed in Chapter 5. To model initial out-of-straightness the actual non-dimensionalised measured imperfections were extracted into

first three buckling modes (Figure 5-1) and the mean ( $\mu$ ), standard deviation ( $\sigma$ ) and coefficient of variation (COV) of the different modal amplitudes ( $a_1, a_2, a_3$ ) were determined (Table 5-2). More details of this method can be found in Chapter 5.

Using the statistics shown in Table 5-2, the random shape of each member imperfection is determined by generating a random scale factor for each mode, assigning a random sign to each mode and combining the modes. The random sway imperfection (out-of-plumb) for the frame as a whole is generated using the statistics provided by Lindner (1984) (Figure 2-26 (a)).

#### **7.4.1.4 Variability in residual stress**

Hot-rolled steel members usually have significant residual stresses due to uneven rate of cooling after the rolling process. These stresses may vary considerably from profile to profile due to different method of manufacturing and cross-sectional properties and needs to be treated as a random variable in determining the ultimate strength of the frame. Randomness in residual stress can have a significant impact on the strength and reliability of steel frames by increasing lateral deflections and thereby second-order effects.

In this study, the residual stress is modelled using the ECCS model (1984) (Figure 6-1). The variability of residual stresses is taken into account based on the model developed in Chapter 6. A scale factor ( $X$ ) was applied to the ECCS residual stress pattern and subsequently an error minimization was performed to minimize the error between theoretical model and experimental measurements. The scale factors seemed to be normally distributed with a mean of  $1.047X$  and COV of 0.21. The residual stress is assumed to be constant along the length of a member and perfectly correlated among the members of a frame.

### **7.5 Sensitivity analysis**

Analysing the dependency of the system behaviour on the input quantities is often necessary to determine which parameters have the greatest effect on the studied output. Generally, the objective of the sensitivity analysis is to evaluate how the variations in

model output can be influenced by variations of input parameters. This enables the dominant random quantities, which must be paid special attention in probabilistic analysis, to be determined. Sensitivity analyses can be categorized as deterministic or stochastic. The deterministic sensitivity analysis, also referred as “what-if-analysis”, is based on a parametric study which investigates the influence of changing selected input variables on the output results. Although this kind of study provides a quick overview of the model behaviour, it is not able to capture the whole spectrum of the possible cases. The stochastic sensitivity analysis results in more advanced information about the influence of input parameters by modelling them as random variables.

One of the most well-known methods of probabilistic sensitivity analysis is a variance-based technique, referred to as the analysis of variance (ANOVA), which is used to determine whether there is a statistical association between an output and one or more inputs (Krishnaiah 1981). The method is based on Sobol’s decomposition theory (Sobol 1993) which defines the first order sensitivity index ( $S_i$ ) for the load-carrying capacity of a structural system as,

$$S_i = \frac{\sigma_{Ri}^2}{\sigma_R^2} \quad 7-3$$

in which  $\sigma_{Ri}$  is the standard deviation of frame ultimate strength, assuming all input quantities except the  $i$ th one are deterministic and  $\sigma_R$  is the standard deviation of frame ultimate strength when all input quantities are modeled randomly.

To perform the sensitivity analysis, Frame 4 with the failure mode of BFY-CPY corresponding to  $\varphi_s=0.74$  is chosen. The member cross-sections can be found in Appendix E.1 and all random variables presented in Section 7.4.1 are considered. The standard deviation of ultimate strength when there is only one random variable in each simulation sets and the sensitivity indices ( $S_i$ ) are summarized in Table 7-4. The standard deviation of frame ultimate strength when considering all random variables ( $\sigma_R$ ) is 0.19.

Table 7-4: Results of sensitivity analysis of Frame 4 corresponding to  $\phi_s=0.74$  with BFY-CPY as failure mode

Random quantities	Standard deviation ( $\sigma_{Ri}$ )	$S_i$ (%)
Yield stress ( $f_y$ )	0.1834	93.21
Cross-section area ( $A$ )	0.0488	6.605
Initial geometric imperfection	0.0131	0.477
Residual stress ( $X$ )	0.0038	0.039
Young's modulus ( $E$ )	0.0053	0.078

As it is expected, since the failure mode is beam yielding, the yield stress has the greatest influence with the sensitivity index of 93.21%, followed by cross-section area and initial geometric imperfection. For this particular case, residual stress and Young's modulus have almost negligible effect on the frame ultimate strength statistics. To obtain a more physical sense about the contribution of these random variables, the ultimate load factor distribution when all random variables are taken into account is compared with the cases with only random yield stress, cross-section area and initial imperfection in Figure 7-9, Figure 7-10 and Figure 7-11, respectively.

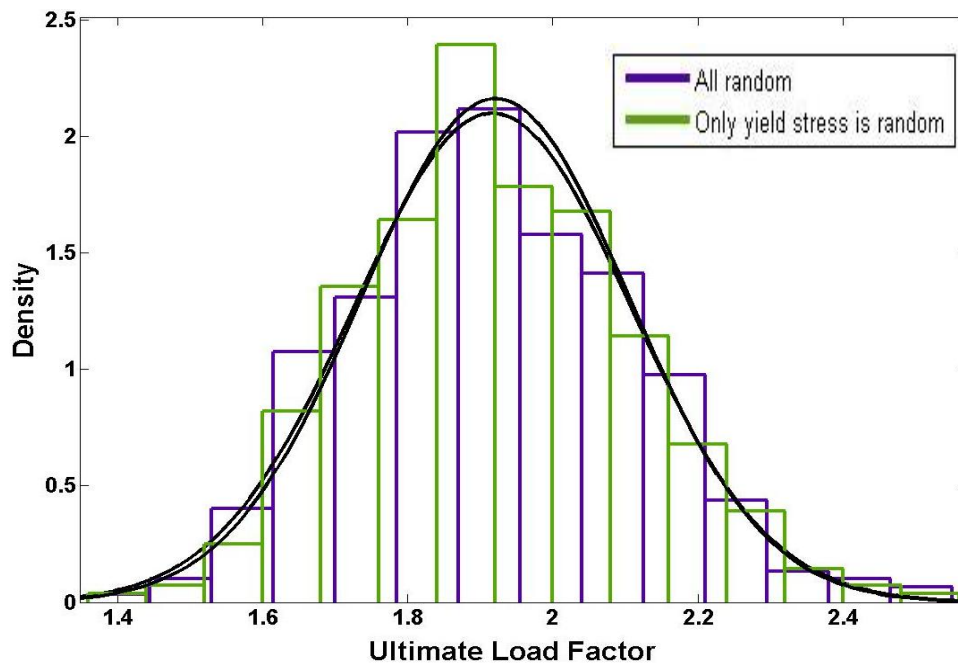


Figure 7-9: Comparison between ultimate load distributions with all random variables and with only yield stress as random, Frame 4



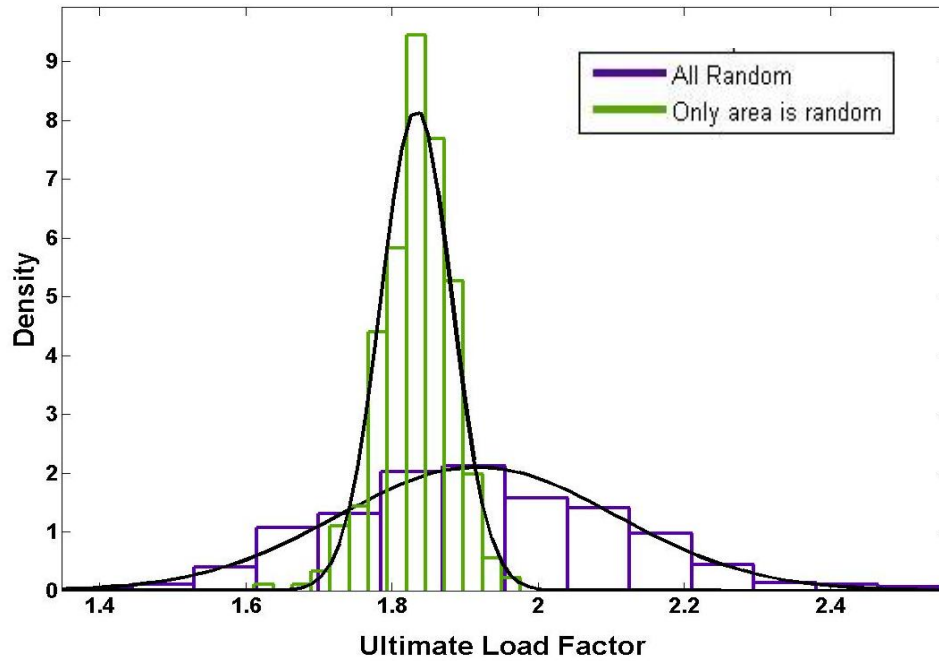


Figure 7-10: Comparison between ultimate load distributions with all random variables and with only cross-section area as random, Frame 4

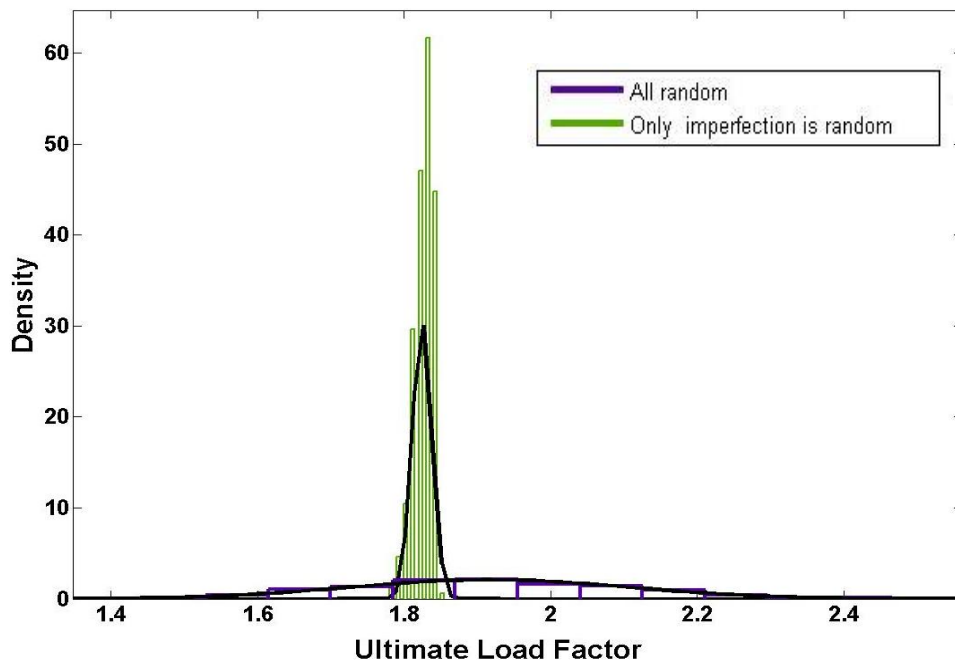


Figure 7-11: Comparison between ultimate load distributions with all random variables and with only cross-section area as random, Frame 4

It should be noted that the sensitivity analysis provided in this section is only an example and generally the actual contribution of each random variable to the frame ultimate strength depends on the frame failure mode. For example, for this particular frame the effect of randomness in residual stress appears to be negligible. However, as it was discussed in Chapter 6, if the frame is sensitive to the second-order effects and fails by instability, residual stress may have a significant impact on the strength and reliability of the frame. Thus, since different failure modes are considered in this study, it was decided to model all key parameters as random variables, regardless whether they have significant influence on the ultimate strength or not.

## 7.6 System reliability and model uncertainty

The probability of failure ( $P_f$ ) of the structure is defined as:

$$P_f = P(G(X) \leq 0) = \int \dots \int_{G(X) \leq 0} f_X(x) dx \quad 7-4$$

in which  $P_f$  is the probability of failure of the structure,  $X = (X_1, \dots, X_n)$  is the  $n$ -dimensional vector of random variables such as applied load and structural system resistance,  $f_X(x)$  is the joint probability density function for  $X$ ,  $G(X)$  is the limit state function such that  $G(X) \leq 0$  defines the unsafe (failure) region. In other word, the probability of failure is the probability that  $R < Q$ , in which  $Q$  (the load effect) and  $R$  (the structural resistance) are statistically independent. This can be expressed as a single frequency distribution curve which combines the uncertainties in  $R$  and  $Q$  by dividing the expression  $R < Q$  by  $Q$  and show the result logarithmically (AISC 1987). Thus, the failure condition is expressed as

$$G = \ln(R/Q) \leq 0 \quad 7-5$$

The first-order reliability index ( $\beta$ ) is defined as the mean ( $\mu$ ) divided by the standard deviation ( $\sigma$ ) of the limit function  $G$ ,

$$\beta = \frac{\mu_R - \mu_Q}{\sqrt{\sigma_R^2 + \sigma_Q^2}} \quad 7-6$$

Using small-variance approximations (Ellingwood, Galambos et al. 1980) the reliability index ( $\beta$ ) can be written as

$$\beta = \frac{\ln(\mu_R/\mu_Q)}{\sqrt{V_R^2 + V_Q^2}} \quad 7-7$$

in which  $V_R$  and  $V_Q$  are the coefficients of variation (COV) of resistance and load, respectively. Equation 7-7 may be rearranged as Equation 7-8 to obtain the separate means of load and resistance.

$$\mu_R = \exp(\beta \sqrt{V_R^2 + V_Q^2}) \mu_Q \quad 7-8$$

The below substitution can be made to simplify the equation (AISC 1987):

$$\sqrt{V_R^2 + V_Q^2} \approx V_Q + \alpha V_R \quad 7-9$$

Substituting Equation 7-9 into Equation 7-8 and rearranging leads to:

$$\exp(-\alpha\beta V_R) \mu_R = \exp(\beta V_Q) \mu_Q \quad 7-10$$

For the development of the current LRFD specification the resistance ( $R$ ) in Equation 7-10 refers to “true” resistance which is related to the nominal resistant ( $R_n$ ) through the Equation 7-11, in which  $P$  is the variation due to the method of analysis,  $M$  is the variation in material strength and  $F$  is the variation in fabrication.

$$R = P \cdot M \cdot F \cdot R_n \quad 7-11$$

Following the same concept the “true” load can be defined as

$$Q = A.B.C.Q_n \quad 7-12$$

where  $A$  is the variation in load,  $B$  is the variation due to the method of applying loads,  $C$  is the variation due to the method of analysis and  $Q_n$  is the nominal load. While the Monte Carlo type simulation considers the inherent uncertainty in basic variables as explained in Section 7.4, the factors ( $A, B, C, P, M$  and  $F$ ) account for uncertainties arising from simplifications and assumptions in the modeling and must be taken into account as random variables for the structural reliability analysis. Solving the Equation 7-11 and Equation 7-12 for means and standard deviations and substituting into Equation 7-10 results in:

$$\exp\left(-\alpha\beta\sqrt{V_P^2 + V_M^2 + V_F^2}\right)\mu_p\mu_M\mu_F R_n = \exp\left(\beta\sqrt{V_A^2 + V_B^2 + V_C^2}\right)\mu_A\mu_B\mu_C Q_n \quad 7-13$$

This equation is now in the LRFD format shown as

$$\phi R_n = \gamma Q_n \quad 7-14$$

For frames under gravity loading, the Equation 7-14 can be written as

$$\phi R_n = 1.2D_n + 1.6L_n \quad 7-15$$

In this equation,  $D_n$  and  $L_n$  are the nominal dead and live loads respectively, applied to the structure. The system reliability index ( $\beta$ ) can be estimated using the first order reliability method (FORM) (Melchers 1999), with the simple limit state function of  $G = R - D - L$ , in which  $R$  is system resistance or frame ultimate strength,  $D$  is dead load and  $L$  is live load. Using Equation 7-15, the limit state can be written in terms of the nominal loads, resistance and partial factors as:

$$\frac{R}{R_n} \times \left( \frac{1.2 + 1.6 (L_n/D_n)}{\phi_s} \right) - \frac{D}{D_n} - \frac{L}{L_n} \times \frac{L_n}{D_n} = 0 \quad 7-16$$

The first order reliability method (FORM) permits the actual distributions of the random variables to be taken into account (Melchers 1999). The mean-to-nominal strength ( $\bar{R}/R_n$ ) (bias) statistics are determined from the frame simulations while the statistics of loads can be obtained from the literature. Dead load is assumed to be normally distributed with a mean-to-nominal value ( $\bar{D}/D_n$ ) of 1.05 and a COV of 0.1, and live load is presented by Extreme Type I distribution with a mean-to-nominal value ( $\bar{L}/L_n$ ) of 1.0 and a COV of 0.25 (Galambos et al. 1982). The term  $L_n/D_n$  in Equation 7-16 indicates the nominal live to dead load ratio.

For frames subject to gravity and wind loading, the limit state function is defined as  $G = R - W$  in which  $R$  is the system resistance in terms of lateral load capacity and  $W$  is the wind load. To determine the system resistance statistics ( $R$ ), the dead load and the “arbitrary-point-in-time” live load ( $L_{apt}$ ) are applied as random variables. The load combination is based on Turkstra’s rule (Turkstra and Madsen 1980), which assumes that the maximum combined load effect occurs when one load attains its maximum value while other load(s) are at their arbitrary point-in-time values. The wind load is assumed to have Extreme Type I distribution with the mean and COV equal to  $0.96 W_n$  and 0.37 respectively. The arbitrary-point-in-time live load is modeled by a Gamma distribution with mean-to-nominal ratio ( $L_{apt}/L_n$ ) equal to 0.25 and COV of 0.6 (Galambos et al. 1982).

## **7.7 Simulation results to determine appropriate system resistance factors**

Following the procedure described in Section 7.2, all frames in Figure 7-1 subject to gravity and gravity plus wind loading were first designed according to the Australian steel structures standard (AS4100 1998) using the commercial software of Microstran (2004). It should be noted that the member cross-sections are designed in a way to be practical and not changing in each storey. Those frame were then modelled using ABAQUS and analysed by advanced analysis, explained in Chapter 3, to obtain the ultimate load factor ( $\lambda_n$ ), defined as the ratio of frame strength to total applied load. The frame ultimate strength ( $R_n$ ) may be determined as the product of total applied load ( $\sum \gamma_i Q_{ni}$ ) and the

ultimate load factor ( $\lambda_n$ ). By substituting this expression ( $\lambda_n \sum \gamma_i Q_{ni}$ ) for  $R_n$  into the design equation (Equation 7-2), the total load can be eliminated from both sides of the equation and the system resistance factor ( $\varphi_s$ ) may thus be determined as  $\varphi_s = 1/\lambda_n$ .

### 7.7.1 Proposed methods to plot $\beta - \varphi_s$ curves

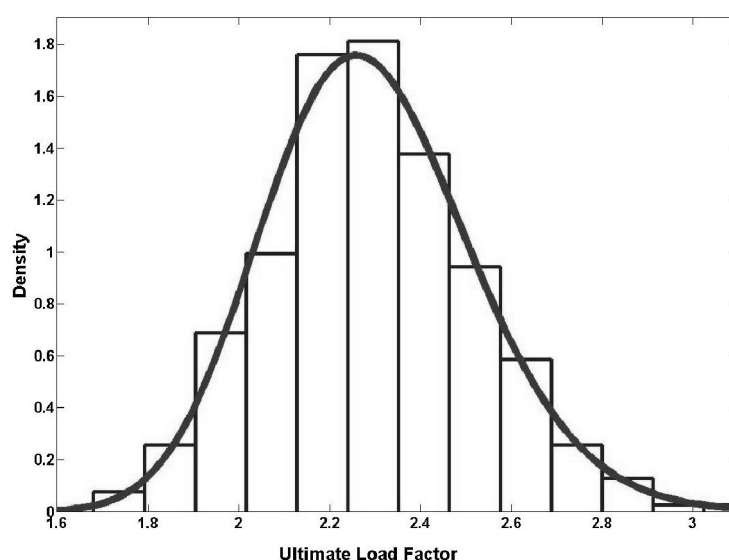
As mentioned in Section 7.2, to plot  $\beta$  (reliability index) versus  $\varphi_s$  for structural frames, two approaches are utilized. Frame 5 which is a three-bay, three-storey frame under gravity is selected as an example to describe these methods.

#### 7.7.1.1 Cross-Section Scaling Method (CSM)

In the first approach, the cross-sections obtained from designing the frame to an existing code are adjusted to achieve different ultimate load factors ( $\lambda_n$ ), and thus different resistance factors ( $\varphi_s$ ), making sure that frames with different  $\varphi_s$  fail in the same mode as the frame designed to the code. For example, for frame (Frame 5) designed to AS4100 (AS4100 1998), under factored gravity loads, the failure mode is BFY-CPY (beam(s) fully yielded and column(s) partially yielded), the ultimate load factor obtained using advanced analysis is  $\lambda_n=1.46$ , and hence the corresponding resistance factor is 0.68 ( $\varphi_s = 1/\lambda_n$ ). The cross-sections of selected members are then changed to create a new frame and the ultimate load factor ( $\lambda_n$ ) is obtained using advanced analysis, thus producing a new resistance factor  $\varphi_s = 1/\lambda_n$ . This process is repeated to generate a range of  $\varphi_s$ -values for different frames with the same layout and failure mode. Table 7-5 details the cross-sections and corresponding  $\varphi_s$ -values. Monte Carlo simulation is then conducted for the different frames, accounting for all uncertainties as discussed in Section 7.4, and the statistics (frequency distribution, mean and COV) of the ultimate load factors ( $\lambda$ ) are determined. The frame strength statistics are summarized in Table 7-5. Note that for these simulations the mean and nominal values are based on applying unfactored nominal loads ( $D_n + L_n$ ) to the structure. A lognormal distribution is fitted to the histogram of frame strength. An example of the frame ultimate load factor histogram for the frame assigned to  $\varphi_s = 0.63$  is shown in Figure 7-12.

Table 7-5: System-based design of Frame 5 under gravity loading ( $L_n/D_n=1$ )

$\varphi_s$	Members (see Figure 7-1)	Section	$\lambda_n$ (factored loads)	Mean ( $\bar{\lambda}$ )	COV	$\lambda_n$ (unfactored loads)	$\bar{\lambda}/\lambda_n$ (unfactored load)
0.63	$C_1, C_4, C_5, C_8, C_9, C_{12}$ $C_2, C_3, C_6, C_7$ $C_{10}, C_{11}$ $B_1, B_3, B_4, B_6, B_7, B_9$ $B_2, B_5, B_8$	250UC72 200UC59 150UC30 460UB74 360UB56	1.58	2.292	0.100	2.143	1.07
0.68	$C_1, C_4, C_5, C_8, C_9, C_{12}$ $C_2, C_3, C_6, C_7$ $C_{10}, C_{11}$ $B_1, B_3, B_4, B_6, B_7, B_9$ $B_2, B_5, B_8$	250UC72 200UC59 150UC30 460UB67 360UB50	1.46	2.089	0.101	1.959	1.07
0.74	$C_1, C_4, C_5, C_8, C_9, C_{12}$ $C_2, C_3, C_6, C_7$ $C_{10}, C_{11}$ $B_1, B_3, B_4, B_6, B_7, B_9$ $B_2, B_5, B_8$	200UC59 200UC59 150UC30 460UB67 360UB50	1.36	1.959	0.100	1.832	1.07
0.85	$C_1, C_4, C_5, C_8, C_9, C_{12}$ $C_2, C_3, C_6, C_7$ $C_{10}, C_{11}$ $B_1, B_3, B_4, B_6, B_7, B_9$ $B_2, B_5, B_8$	250UC72 200UC59 150UC30 360UB56 360UB50	1.18	1.692	0.102	1.593	1.06
0.96	$C_1, C_4, C_5, C_8, C_9, C_{12}$ $C_2, C_3, C_6, C_7$ $C_{10}, C_{11}$ $B_1, B_3, B_4, B_6, B_7, B_9$ $B_2, B_5, B_8$	250UC72 200UC59 150UC30 360UB50 310UB40	1.04	1.483	0.100	1.399	1.06

Figure 7-12: Histogram of ultimate load factor for Frame 5 subjected to gravity with BFY-CPY failure mode for  $\varphi_s=0.63$  ( $L_n/D_n=1$ )

Using first order reliability analysis (FORM), the reliability index ( $\beta$ ) corresponding to any value of  $\phi_s$  can be calculated by assuming different load ratios ( $L_n/D_n$ ) in Equation 7-16. Figure 7-13 shows the system reliability indices ( $\beta$ ) versus  $\phi_s$  for Frame 5. Four values of reliability indices are considered, i.e.  $\beta = 2.5, 2.75, 3$  and  $3.5$ , and the related system resistance factors are determined using Figure 7-13 for different live to dead load ratios, as summarized in Table 7-6.

To find a single resistance factor for the frame which does not depend on the specific load ratio, a weight is assigned to each load ratio, representing the relative likelihood of different load situations (Galambos et al. 1982). Thus, the final system resistance factors can be calculated based on Equation 7-17 in which  $w_i$  is the weight assigned to a given load ratio and  $\phi_{si}$  is the system resistance factor for this specific load ratio. These weight-averaged resistance factors are summarized in Table 7-6.

$$\phi_s = (\sum w_i \times \phi_{si})/100 \quad 7-17$$

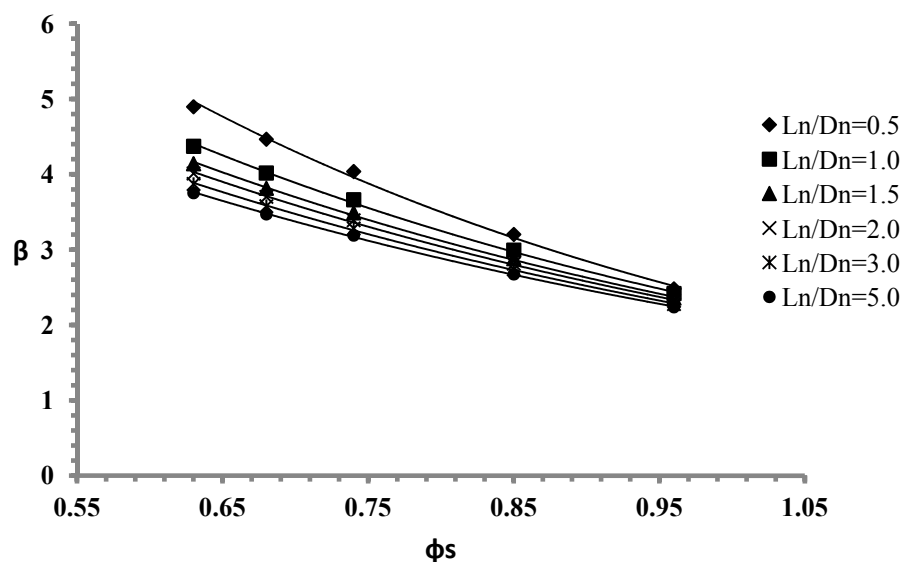


Figure 7-13:  $\beta$  vs.  $\phi_s$  for Frame 5 using CSM



Table 7-6: System resistance factors ( $\varphi_s$ ) for Frame 5 for different reliability levels, CSM

$L_n/D_n$	Weight (%)	$\varphi_s$			
		$\beta = 2.5$	$\beta = 2.75$	$\beta = 3$	$\beta = 3.5$
0.5	10	0.96	0.92	0.87	0.80
1.0	20	0.95	0.89	0.84	0.76
1.5	25	0.93	0.87	0.82	0.73
2.0	35	0.92	0.86	0.81	0.72
3.0	7	0.90	0.85	0.79	0.70
5.0	3	0.89	0.83	0.77	0.68
Final value of $\varphi_s$		0.93	0.87	0.82	0.73

### 7.7.1.2 Load Scaling Method (LSM)

An alternative method for developing plots of the reliability indices ( $\beta$ ) versus system resistance factor ( $\varphi_s$ ) is to keep the frame cross-sections unchanged and achieve different system resistance factors for a specific frame by changing the total applied load. In this method, each frame is first designed to a code and analysed using advanced analysis, and the corresponding system resistance factor ( $\varphi_s = 1/\lambda_n$ ) is determined. Then, the total applied loads on the frame are scaled to obtain different values of  $\varphi_s$ . Because the frame is the same in every case and only the loads are changed, the mean-to-nominal value of frame strength ( $\bar{R}/R_n$ ) remains the same for different frames related to different  $\varphi_s$ . In this case, there is no need to run simulations for every value of  $\varphi_s$  as only the ratio of mean-to-nominal strength is important in Equation 7-16. The Monte Carlo simulation is run for one frame with a specific failure mode and the statistics of the mean bias ( $\bar{R}/R_n$ ) is obtained. Then by assuming different values of  $\varphi_s$  in Equation 7-16, relative reliability indices ( $\beta$ ) are determined. This method is faster as it needs fewer simulations to plot the  $\beta - \varphi_s$  curves compared to CSM. Figure 7-14 shows the reliability index versus system resistance factor for the frame with BFY-CPY as failure mode.

The final values of  $\varphi_s$  obtained from the graph are summarized in Table 7-7. A comparison of the results shown in Table 7-7 reveals that both methods give essentially the same system resistance factors  $\varphi_s$  for various reliability levels. Therefore, as the load

scaling method (LMS) requires fewer simulations to generate the  $\beta$ - $\phi$  curves, this method is used in this study for frames under gravity loading.

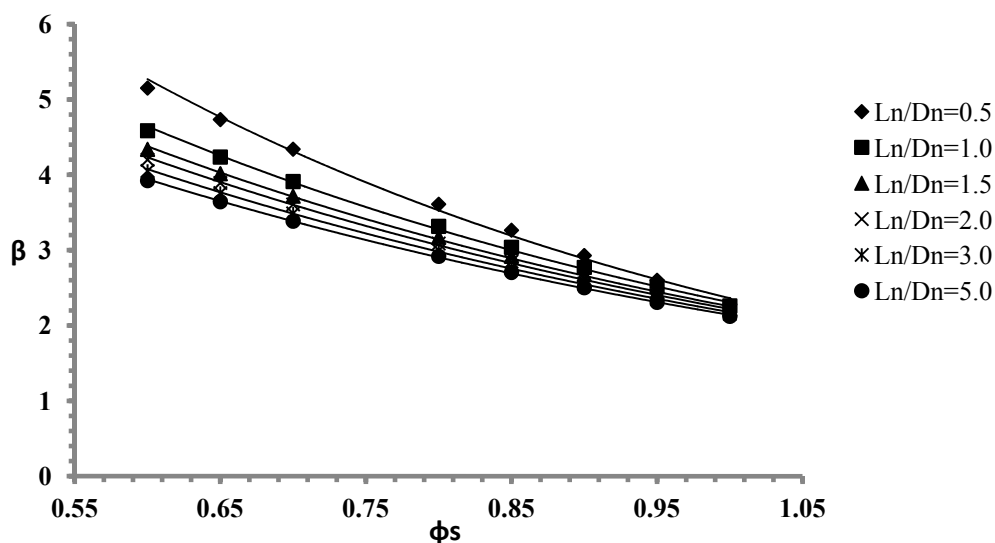


Figure 7-14:  $\beta$  vs.  $\phi_s$  for Frame 5 using LSM

Table 7-7: System resistance factors ( $\phi_s$ ) for Frame 5 for different reliability levels, LSM

$L_n/D_n$	Weight (%)	$\phi_s$			
		$\beta = 2.5$	$\beta = 2.75$	$\beta = 3$	$\beta = 3.5$
0.5	10	0.97	0.93	0.88	0.80
1.0	20	0.95	0.89	0.85	0.76
1.5	25	0.93	0.87	0.82	0.74
2.0	35	0.93	0.87	0.82	0.73
3.0	7	0.90	0.86	0.80	0.70
5.0	3	0.90	0.84	0.78	0.68
Final value of $\phi_s$		0.93	0.87	0.82	0.73

## 7.7.2 Simulation results for sway frames under gravity loading

### 7.7.2.1 Ziemian's frames

The eight frames designed by Ziemian (1990) using advanced analysis are considered in this study. The system reliability of these frames were previously evaluated by Buonopane and Schafer (2006). The geometry, support conditions and applied loads for

the frames are shown in Figure 7-15. Detailed information including member sizes are provided by Buonopane and Schafer (2006). Columns were subdivided into eight elements and beams into sixteen elements using 2D beam elements in ABAQUS. All random variables discussed in Section 7.4 are considered in the frame simulations here reported.

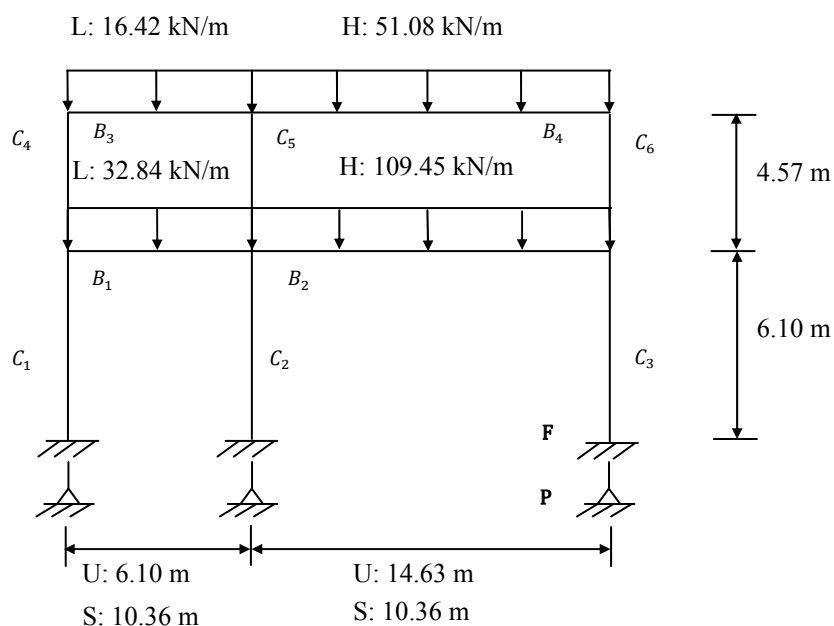


Figure 7-15: Loads and dimensions of Ziemian's frames

To determine the reliability index ( $\beta$ ) of this structure, Equation 7-7 was used by (Buonopane and Schafer 2006) which is based on First Order Second Moment (FOSM) theory (Nowak and Collins 2000). The statistics of frame ultimate strength ( $R$ ) are presented in Table 7-8. It should be noticed that the mean values of ultimate strength ( $\bar{R}$ ) are based on unfactored gravity loads. The total load ( $Q$ ) has the mean of  $1.026Q_n$  and the COV of 0.1 as reported by Buonopane and Schafer (2006). Note that the distribution of total gravity load was obtained in that paper by combining the Extreme Type I distribution for live load with the mean equal to  $L_n$  and COV of 0.1 and the normally distributed dead load with the mean of  $1.05D_n$  and COV of 0.1. The reliability indices, obtained based on Equation 7-7 and these statistic, are summarized in Table 7-8.

A more accurate alternative to find the reliability index is to use the First Order Reliability Method (FORM), as presented in Section 7.6. In using this method, the limit

state is taken as  $R - Q = 0$ , and the COV of the total load ( $Q$ ) is updated to 0.132. Note that in this study, to generate the total load ( $Q$ ), the COV of live load is assumed to be 0.25, as reported in most research studies (Galambos, Ellingwood et al. 1982; Beck and Doria 2008), instead of 0.1 as used in (2006). The dead load, live load as well as total load are presented in Figure 7-16. A lognormal distribution is fitted to the total load histogram.

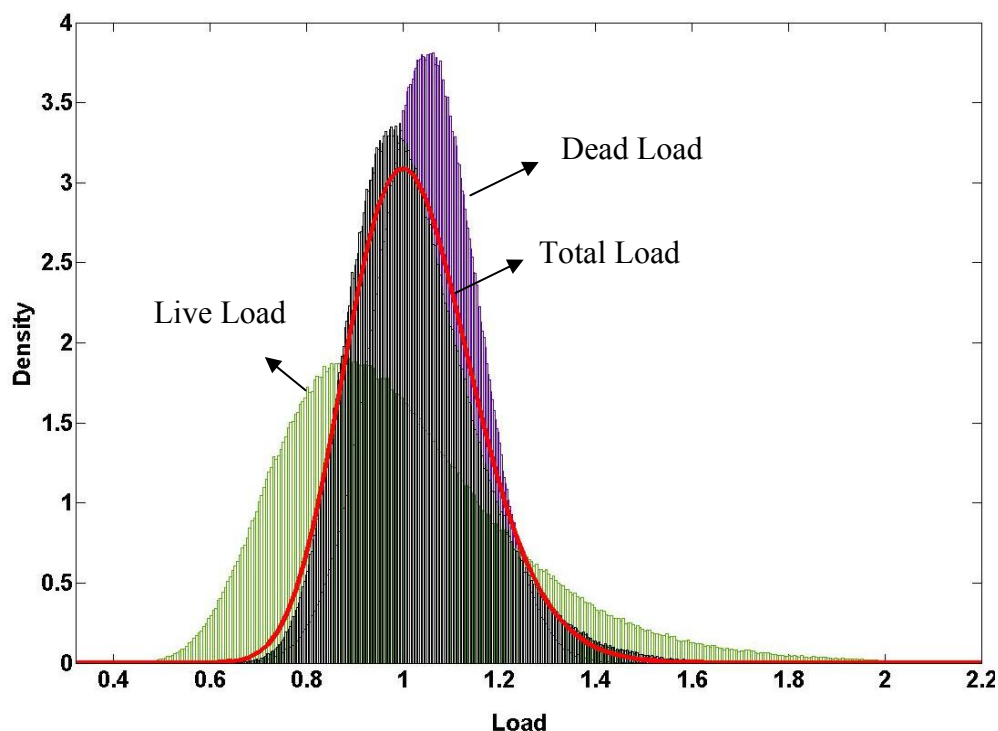


Figure 7-16: Gravity load distribution

Based on these statistics for the total load, the reliability index ( $\beta$ ) can be determined (Table 7-8). More accurately, instead of combining dead and live load to generate the total load, the limit state of  $R - D - L = 0$  can be considered and the corresponding reliability indices ( $\beta$ ) and system resistance factors ( $\varphi_s$ ) can be calculated according to the methodology developed in Section 7.2. The results for  $\beta$  and  $\varphi_s$  are presented in Table 7-8. Note that to design the frames using advanced analysis, (Ziemian 1990) incorporated resistance factors by scaling the yield surface by the factor of 0.9. The resistance factors ( $\varphi_s$ ) presented in Table 7-8 are close to 0.9, and thus consistent with Ziemian's results.

Table 7-8: Statistic characteristics for Ziemian's frames (Ziemian 1990)

Frame	Mean ( $\bar{R}$ )	Bias ( $\bar{R}/R_n$ )	COV	$\varphi_s$ ( $1/\lambda_n$ )	Reliability index ( $\beta$ ) using Equation 7-7	Reliability index ( $\beta$ ) using FORM and limit state of $R - Q$	Reliability index ( $\beta$ ) using FORM and limit state of $R - D - L$
UP50HA	1.582	1.037	0.094	0.92	3.16	2.66	2.48
UP50LA	1.653	1.067	0.099	0.90	3.39	2.86	2.65
UF50HA	1.646	1.058	0.100	0.90	3.34	2.85	2.62
UF50LA	1.708	1.039	0.102	0.85	3.57	3.04	2.77
SP50HA	1.646	1.069	0.087	0.92	3.57	3.09	2.73
SP50LA	1.666	1.073	0.098	0.90	3.46	2.92	2.69
SF50HA	1.758	1.077	0.098	0.86	3.85	3.20	2.93
SF50LA	1.655	1.069	0.100	0.90	3.38	2.87	2.63
Average value of $\beta$					3.47	2.94	2.70

Using the load scaling method (LSM) with the mean and COV values of the bias terms ( $\bar{R}/R_n$ ) presented in Table 7-8, the system resistance factors ( $\varphi_s$ ) can be determined for all Ziemian's frames assuming different values of reliability index ( $\beta$ ), as shown in Table 7-9.

Table 7-9: System resistance factors ( $\varphi_s$ ) for frames designed by Ziemian (1990)

Frame	Failure modes	$\varphi_s$			
		$\beta = 2.5$	$\beta = 2.75$	$\beta = 3$	$\beta = 3.5$
UP50HA	BFY-CPY	0.92	0.87	0.82	0.73
UP50LA	BFY-CPY	0.91	0.85	0.80	0.72
UF50HA	BFY-CPY	0.95	0.89	0.84	0.74
UF50LA	BFY-CPY	0.94	0.88	0.83	0.74
SP50HA	BFY-CPY	0.96	0.9	0.85	0.76
SP50LA	BFY-CPY	0.93	0.88	0.83	0.73
SF50HA	BFY-CFY	0.94	0.89	0.83	0.74
SF50LA	BFY-CPY	0.94	0.88	0.83	0.74
Average value of $\varphi_s$		0.94	0.88	0.83	0.738

The mean value of system resistance factor ( $\varphi_s$ ) for Ziemian's frames corresponding to a target reliability of 3 is equal to 0.83, which is less than the mean value of 0.88 reported by Buonopane and Schafer (2006) for the same frames. The incorporation of additional

random variables (including residual stress, elastic modulus and initial geometric imperfections) in this study leads to larger values of COVs and therefore smaller  $\varphi_s$  for the same target reliability. Moreover, Equation 7-18 was used in (2006) to determine the value of  $\varphi_s$ . Being based on First Order Second Moment theory, the equation may overestimate the prediction of system resistance factor ( $\varphi_s$ ).

$$\varphi_s = (\bar{R}/R_n)exp(-0.55\beta V_R) \quad 7-18$$

### 7.7.2.2 Proposed sway frames

The nine steel frames presented in Figure 7-1 and designed to AS4100 (1998) are considered in this study to obtain the system resistance factors using the Load Scaling Method (LSM). The member cross-sections, the ultimate load factors and the ultimate failure modes are presented in Table 7-10 . The characteristics of these frames as well as the final values of  $\varphi_s$  are summarized in Table 7-11 for four target reliability levels. Different failure modes are considered for each frame to study the influence of the ultimate failure mode on the system resistance factors. The COVs of the frame strengths are in range of 0.093 to 0.106 and the ratio of mean-to-nominal strength varies between 1.02 and 1.12. A goodness-of-fit test (Kolmogorov-Smirnov (K-S)) (Haldar and Mahadevan 2000) were performed on the ultimate strength simulation results and the log-normal distribution was found to provide the best fit.

Based on the results presented in Table 7-11, it can be seen that for common rigid jointed moment frames under gravity load, the system resistance factors for specific target reliabilities are quite similar, despite the differences in frame configuration (regular or irregular) and frame failure modes (BFY-CPY, CFY, etc). For the reliability index of 2.5, the value of  $\varphi_s$  ranges between 0.89 and 0.98. These system resistance factors decrease to be between 0.69 and 0.77 when the target reliability increases to 3.5. The average value of  $\varphi_s$  is 0.93 for a reliability index of 2.5, which is close to the common member resistance factor of 0.9 for ductile limit states in the AISC Specification. Figure 7-17 and Figure 7-18 illustrate the relationship between reliability index and system resistance factor for two selected frames.

Table 7-10: Sway frames under gravity loading design based on AS4100

Frame	Members	Section	$\lambda_n$	Failure mode
Frame 1	$C_1, C_2$ $B_1$	200UC59 460 UB74	1.32	BFY-CPY
Frame 2	$C_1$ to $C_6$ $B_1, B_2$ $B_3$	250UB37 310UB40 250UB31	1.39	BFY-CPY
Frame 3	$C_1, C_3$ $C_2$ $B_1$ $B_2$	460UB74 460UB67 410UB59 530UB92	1.63	BFY-CPY
Frame 4	$C_1, C_3, C_4, C_6$ $C_2, C_5$ $C_7, C_8, C_9$ $B_1$ to $B_4$ $B_5, B_6$	200UB25 250UB37 200UB22 360UB56 250UB37	1.26	CFY
Frame 5	$C_1, C_4, C_5, C_8, C_9, C_{12}$ $C_2, C_3, C_6, C_7$ $C_{10}, C_{11}$ $B_1, B_3, B_4, B_6, B_7, B_9$ $B_2, B_5, B_8$	250UC72 200UC59 150UC30 460UB67 360UB50	1.45	BFY-CPY
Frame 6	$C_1$ to $C_8$ $C_9, C_{10}$ $C_{11}, C_{12}$ $B_1$ to $B_6$ $B_7$ $B_8$	250UB37 250UB31 200UB29 360UB56 310UB40 200UB29	1.28	BFY-CPY
Frame 7	$C_1, C_4$ $C_2$ $C_3, C_5, C_6$ $B_1, B_4$ $B_2$ $B_3$	150UB14 310UB40 250UB37 310UB46 460UB67 200UB29	1.55	BFY-CPY
Frame 8	$C_1, C_5, C_6$ $C_2, C_3$ $C_4$ $C_7, C_8$ $B_1$ $B_2$ $B_3, B_6$ $B_4, B_5$	150UB14 250UB37 180UB18 200UB22 310UB40 360UB50 200UB29 250UB37	1.69	BFY-CPY
Frame 9	$C_1, C_4, C_5, C_8, C_9$ $C_2, C_3, C_6, C_7$ $B_1$ $B_2, B_4$ $B_3, B_5$ $B_6$	530UB92 200UB25 310UB46 250UB37 410UB53 610UB125	1.43	BPY-CPY

Table 7-11: System resistance factors ( $\varphi_s$ ), bias factors and COVs of sway frames under gravity loads

Frame	Failure mode	$\bar{R}/R_n$	COV	$\varphi_s$			
				$\beta = 2.5$	$\beta = 2.75$	$\beta = 3$	$\beta = 3.5$
Frame 1	BFY-CPY	1.07	0.103	0.93	0.87	0.82	0.73
Frame 2	BFY-CPY	1.03	0.100	0.89	0.84	0.79	0.71
	Instability	1.10	0.097	0.96	0.90	0.85	0.76
	BPY-CPY	1.10	0.093	0.97	0.91	0.86	0.76
Frame 3	BFY-CPY	1.07	0.102	0.93	0.87	0.82	0.74
	BPY-CFY	1.06	0.104	0.93	0.87	0.81	0.72
	BPY-CPY	1.02	0.105	0.89	0.83	0.78	0.69
Frame 4	BFY-CPY	1.07	0.102	0.96	0.89	0.83	0.73
	CFY	1.07	0.103	0.94	0.88	0.83	0.74
	BPY-CFY	1.07	0.105	0.94	0.88	0.83	0.73
Frame 5	BFY-CPY	1.07	0.101	0.93	0.87	0.82	0.73
	CFY	1.12	0.102	0.98	0.93	0.87	0.77
	BPY-CFY	1.11	0.101	0.94	0.89	0.84	0.76
Frame 6	BFY-CPY	1.06	0.101	0.91	0.86	0.81	0.73
	BPY-CFY	1.08	0.104	0.94	0.88	0.83	0.74
Frame 7	BFY-CPY	1.06	0.099	0.92	0.87	0.82	0.74
	CFY	1.04	0.095	0.92	0.86	0.81	0.72
	BPY-CPY	1.04	0.095	0.92	0.86	0.81	0.72
Frame 8	BFY-CPY	1.06	0.102	0.92	0.87	0.82	0.73
	BPY-CFY	1.07	0.102	0.93	0.88	0.83	0.74
	BPY-CPY	1.06	0.101	0.94	0.88	0.83	0.73
Frame 9	BFY-CPY	1.06	0.106	0.91	0.86	0.81	0.73
	BPY-CPY	1.07	0.103	0.96	0.89	0.84	0.74
	BFY-CFY	1.09	0.103	0.91	0.85	0.8	0.71
Average value of $\varphi_s$				0.93	0.87	0.82	0.73



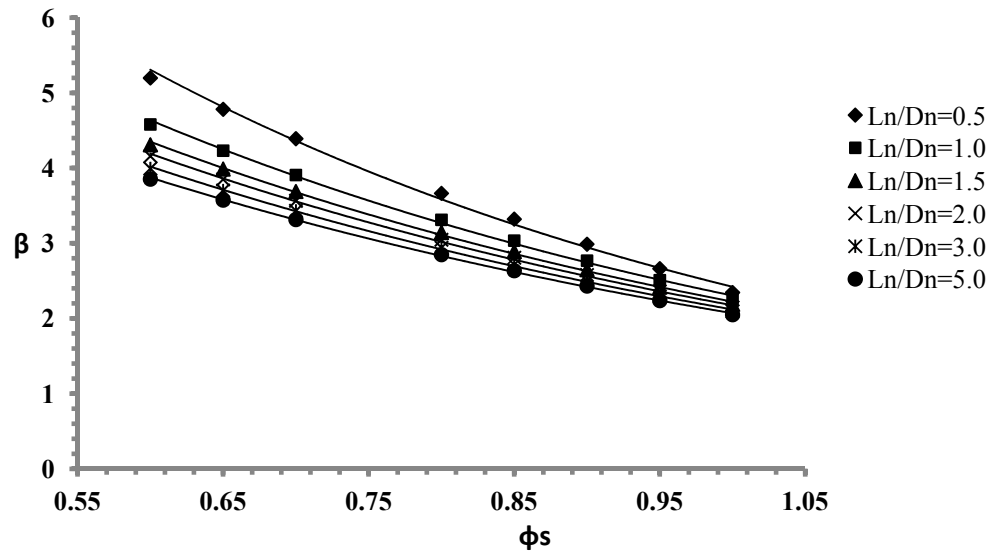


Figure 7-17:  $\beta$  vs.  $\phi_s$  curves for Frame 5 under gravity loading using LSM with BPY-CFY failure mode

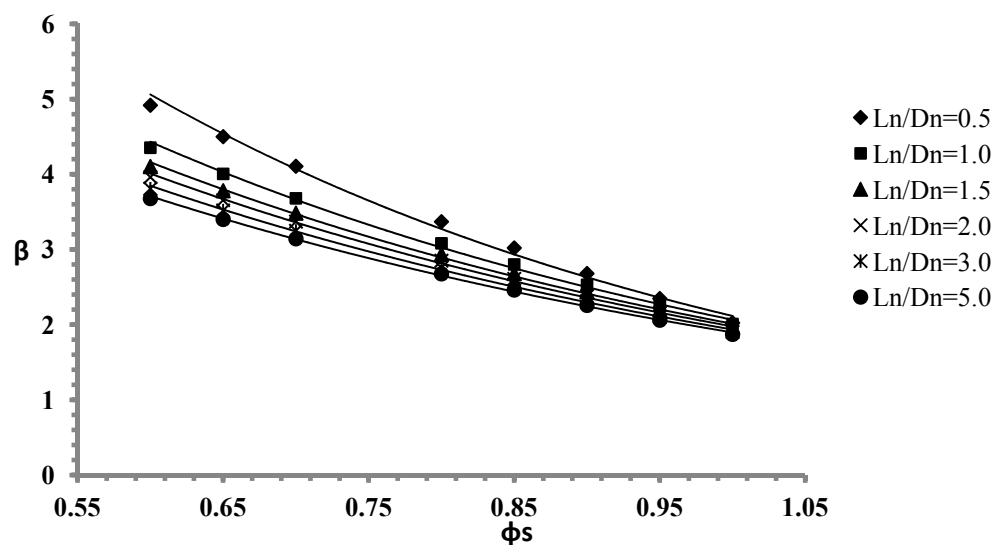


Figure 7-18:  $\beta$  vs.  $\phi_s$  curves for Frame 7 under gravity loading using LSM with CFY failure mode

### 7.7.3 Verification of FORM against Direct Monte-Carlo for frames under gravity

The direct Monte-Carlo technique is a tool for reliability prediction and it is very useful when the system complexity makes the use of approximation methods such as FOSM and FORM unreliable. However, this method suffers from poor computational efficiency and

large number of simulations is needed to achieve an estimate of probability of failure with sufficient accuracy. Since direct Monte-Carlo is a not practical tool, FORM, which is one the most reliable approximation method, is used in this study. The performance of FORM in predicting reliability index is verified against direct Monte-Carlo by comparing the results of both methods for Frame 2 subject to gravity with BFY-CPY as a failure mode.

In direct Monte-Carlo simulations, for each frame related to each value of  $\varphi_s$ , 10000 simulations were first run and the probability of failure was obtained as ( $P_f = n/N$ ) in which  $n$  is the number of frames that failed ( $\lambda_n < 1$ ) and  $N$  is the total number of simulations. Consequently, the reliability index can be determined as

$$\beta = -\Phi^{-1}(P_f) \quad 7-19$$

where  $\Phi^{-1}$  denotes the inverse of the standard normal distribution function. The reliability index is then plotted versus the number of simulations to observe the convergence rate (see Figure 7-19). If the reliability index does not converge within 10000 simulations, further simulations are conducted until the convergence is achieved.

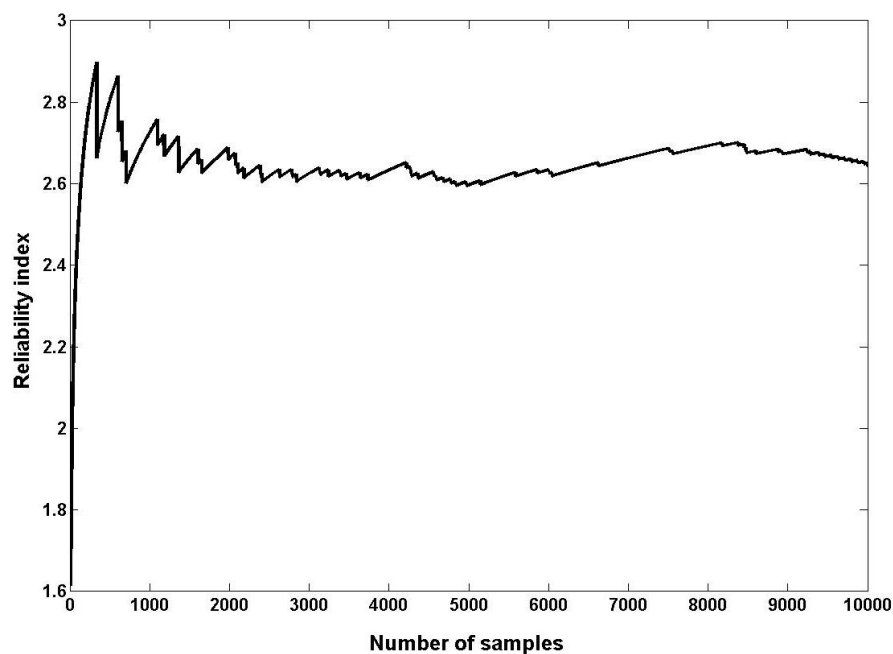


Figure 7-19: Estimate of reliability index by direct Monte Carlo simulation, Frame 2 corresponding to live to dead load ratio of 5 and  $\varphi_s=0.85$

The live to dead load ratios of 1.5 and 5 are considered in this study. The  $\beta - \varphi_s$  curve is plotted in Figure 7-21.

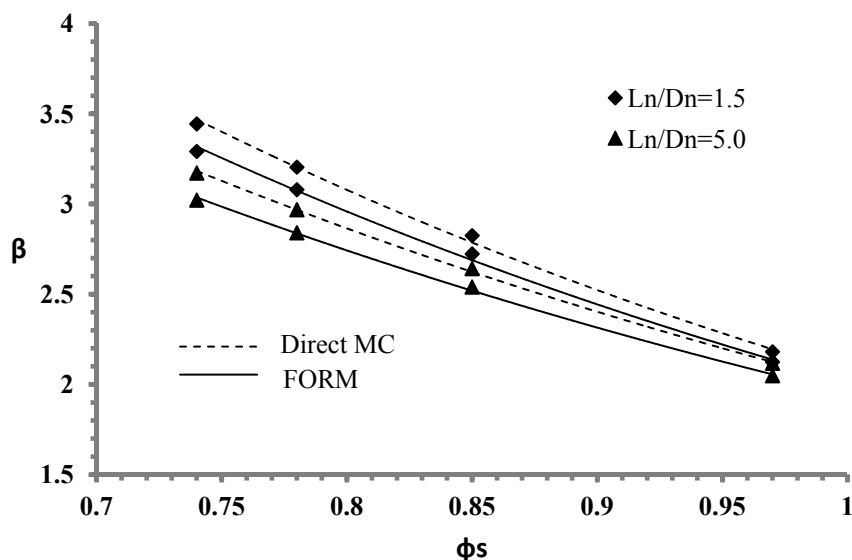


Figure 7-20:  $\beta$  vs.  $\varphi_s$  for Frame 2 (BFY-CPY) subject to gravity loading, using FORM and direct MC simulation

Table 7-12 presents the reliability indices and errors in percentage for both FORM and direct Monte-Carlo. As it can be seen, the reliability indices result from FORM are slightly less than those by MC method with the maximum difference of 4.73%. Since the less value of reliability index leads to higher value of  $\varphi_s$ , by using FORM the derived system reliability indices are in the conservative side. For all cases the error is less than 5% which indicates that direct Monte-Carlo can be replaced by FORM with acceptable accuracy.

Table 7-12: Comparison of reliability indices resulting from FORM and direct MC simulation methods for Frame 2 under gravity

$\varphi_s$	$L_n/D_n=1.5$			$L_n/D_n=5.0$		
	$\beta$ (FORM)	$\beta$ (MC)	Error (%)	$\beta$ (FORM)	$\beta$ (MC)	Error (%)
0.74	3.291	3.443	4.43	3.021	3.171	4.73
0.78	3.079	3.204	3.89	2.84	2.968	4.32
0.85	2.723	2.824	3.59	2.539	2.642	3.87
0.97	2.124	2.181	2.6	2.048	2.118	3.29

#### 7.7.4 Simulation results for frames under gravity plus wind loading

As mentioned in Section 7.3.1, the load combination of  $1.2D_n+0.5L_n+1.6W_n$  including both gravity and wind loads is considered for this study. Since it is not possible to scale the gravity and wind loads simultaneously, only the Cross-Section Scaling Method (CSM) is applicable for this load combination.

First, the frames in Figure 7-1 are designed based on AS4100 (1998) for the live to dead load ratio of 2 ( $L_n/D_n= 2$ ), which is assigned the largest weight in Table 7-6, and the wind to gravity ratio of 0.1 ( $W_n/(L_n + D_n)) =0.1$ , which is the most common case for Australian buildings based on the calculation of wind loads for different regions (AS/NZS1170 2002). The member cross-sections, the ultimate load factors and the ultimate failure modes are presented in Table 7-14. The cross-sections of the members are then changed to obtain different values of resistance factors. As an example, the detailed results of Frame 5 are presented in Table 7-13. The failure mode of this frame is BFY-CFY with the resistance factor of 0.42 ( $\phi_s = 1/\lambda_n$ ).

To determine the ultimate load factor for frames subject to gravity and wind, the analysis is carried out in two separate steps. In the first step, the randomly generated gravity loads are applied to the frame and a static pushdown analysis is performed. Once the deformed shape of the frame under gravity loading is obtained and the gravity loads are in position, a static lateral pushover analysis is conducted by increasing the nominal wind load by the factor  $\lambda$  until failure occurs at  $\lambda_n$ . By repeating this procedure in Monte Carlo simulations, the distribution of lateral load capacity ( $\lambda_n$ ) is obtained. It should be mentioned that the distribution thus obtained is based on the unfactored gravity loads ( $D_n + L_n$ ) and nominal wind loads. The ultimate lateral load capacity distributions, determined by Monte-Carlo type simulations, are close to log-normal for all frames. As an example, the statistics as well as ultimate load distribution for Frame 5 are summarized in Table 7-13 and Figure 7-21, respectively. The details of simulation results for other frames can be found in Appendix E.

The procedure here outlined is simplified by the fact that randomness of wind (lateral) load is not taken into account directly in simulations. The randomness is considered

separately in the FORM analysis. The performance of this simplified method is evaluated by comparing the reliability analysis results of the method with those obtained from direct Monte Carlo (MC) simulations for Frame 5 as an example.

Table 7-13: System-based design of Frame 5 under gravity plus wind loading, BFY-CFY ( $L_n/D_n=2$ ,  $W_n/(L_n + D_n)=0.1$ )

$\varphi_s$	Members	Section	$\lambda_n$ (factored load)	Mean ( $\bar{\lambda}$ ) (unfactored load)	COV
0.69	$C_1, C_4, C_5, C_8, C_9, C_{12}$ $C_2, C_3, C_6, C_7$ $C_{10}, C_{11}$ $B_1, B_3, B_4, B_6, B_7, B_9$ $B_2, B_5, B_8$	460UB74 360UB50 250UB31 460UB74 360UB56	1.45	2.691	0.116
0.82	$C_1, C_4, C_5, C_8, C_9, C_{12}$ $C_2, C_3, C_6, C_7$ $C_{10}, C_{11}$ $B_1, B_3, B_4, B_6, B_7, B_9$ $B_2, B_5, B_8$	460UB67 310UB46 250UB25 460UB74 360UB56	1.21	2.379	0.123
0.89	$C_1, C_4,$ $C_5, C_8, C_9, C_{12}$ $C_2, C_3, C_6, C_7$ $C_{10}, C_{11}$ $B_1, B_3, B_4, B_6, B_7, B_9$ $B_2, B_5, B_8$	460UB67 360UB56 310UB40 250UB25 460UB82 360UB56	1.13	2.149	0.120
1.04	$C_1, C_4, C_5, C_8, C_9, C_{12}$ $C_2, C_3, C_6, C_7$ $C_{10}, C_{11}$ $B_1, B_3, B_4, B_6, B_7, B_9$ $B_2, B_5, B_8$	360UB50 360UB50 250UB25 460UB67 360UB50	0.96	1.935	0.128

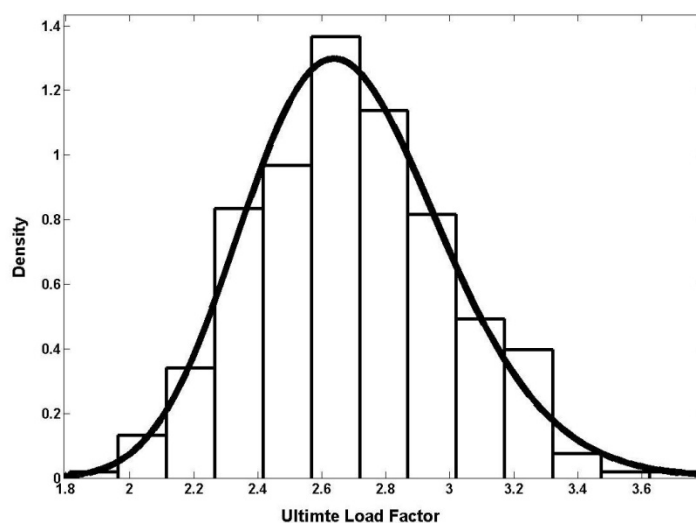


Figure 7-21: Histogram of ultimate load factor for Frame 5 subjected to gravity plus wind with BFY-CFY for  $\varphi_s = 0.69$  ( $L_n/D_n=2$ ,  $W_n/(L_n + D_n)=0.1$ )

Table 7-14: Sway frames under gravity plus wind loading design based on AS4100

Frame	Members	Section	$\lambda_n$	Failure mode
Frame 1	$C_1, C_3$ $B_1$	200UB29 610UB101	1.45	CFY
Frame 2	$C_1, C_2$ $C_3, C_4, C_5, C_6$ $B_1$ $B_2$ $B_3$	410UB53 360UB44 410UB53 310UB46 250UB31	2.13	BFY-CFY
Frame 3	$C_1$ $C_2$ $C_3$ $B_1$ $B_2$	150UB14 200UB29 310UB40 250UB37 460UB82	1.59	BFY-CFY
Frame 4	$C_1, C_3, C_4, C_6, C_7, C_8, C_9$ $C_2$ $C_5$ $B_1$ to $B_4$ $B_5, B_6$	250UB25 610UB113 410UB53 460UB74 460UB67	1.23	BFY-CFY
Frame 5	$C_1, C_5, C_6, C_7, C_8$ $C_2, C_3, C_4, B_2, B_5, B_8$ $C_9, C_{12}$ $C_{10}, C_{11}$ $B_1, B_3, B_4, B_6, B_7, B_9$	460UB67 530UB82 310UB40 250UB37 610UB113	2.37	BFY-CFY
Frame 6	$C_1$ to $C_{12}$ $B_1, B_2, B_4, B_6, B_7$ $B_3, B_6, B_8$	460UB67 460UB74 360UB56	2.26	BFY-CFY
Frame 7	$C_1, C_4$ $C_2, B_2$ $C_3$ $C_5, B_3$ $C_6$ $B_1$ $B_4$	150UB14 460UB74 460UB67 200UB22 310UB32 310UB40 310UB46	2.22	BFY-CFY
Frame 8	$C_1$ $C_2$ $C_3, C_4$ $C_5, C_8, B_3, B_6$ $C_6$ $C_7$ $B_1, B_2$ $B_4, B_5$	180UB18 360UB44 250UB37 200UB22 150UB14 180UB22 310UB40 250UB31	1.58	BFY-CFY
Frame 9	$C_1, C_4, C_5, C_8, C_9$ $C_2, C_3, C_6, C_7$ $B_1$ $B_2, B_4$ $B_3, B_5$ $B_6$	460UB82 360UB56 310UB40 200UB22 360UB50 610UB125	2.27	BFY-CFY

A direct Monte Carlo (MC) simulation was conducted in which both gravity and wind loads were modelled as random variables. Four different wind to gravity load ratios of 0.05, 0.1, 0.15 and 0.25 are considered in this study (see Figure 7-22). These ratios are selected to cover a typical range of wind to gravity load ratios for different regions in Australia and existing frames in the literature. The reliability indices versus the system resistance factors are plotted for different load ratios in Figure 7-22 using both direct Monte Carlo (MC) simulation and the first order reliability method.

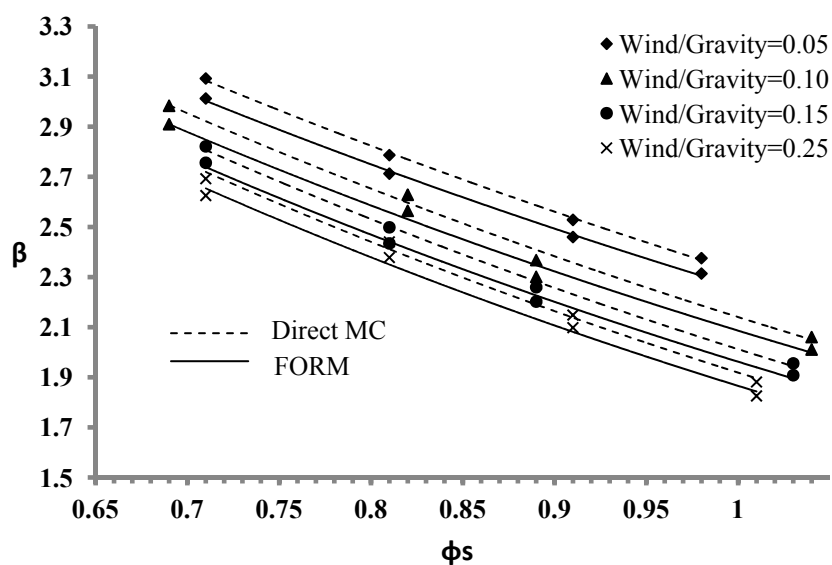


Figure 7-22:  $\beta$  vs.  $\phi_s$  for Frame 5 subject to gravity and wind loading, using FORM and direct MC simulation

Table 7-15 compares the reliability indices resulting from the two simulation methods and shows the percentage error of the FORM analysis. As it can be seen from the results, the Monte Carlo simulations result in higher values of reliability index for all frames corresponding to different system resistance factors and load ratios. The average and maximum errors are 2.55% and 2.97% respectively which shows the simplified method can predict the reliability of the structure accurately to within 3%.

By assigning weights to different load ratios, the final values of system resistance factors for different reliability levels are determined and summarized in Table 7-16 using both simulation methods. The weights, which represent the likelihood of different wind to gravity loads ratios, are based on observations from existing frames and the authors'

engineering judgments. Once again, it is clear that the system resistance factors obtained from direct MC simulations are higher than those predicted by the simplified FORM. However, since the simplified method needs fewer simulations and the error is negligible, this method is used in the study to obtain the system resistance factors for frames under gravity and wind loads.

Table 7-15: Comparison of reliability indices resulting from FORM and direct MC simulation methods for Frame 5 subjected to gravity plus wind

$W_n/(L_n + D_n)$	$\varphi_s$	$\beta$ (FORM)	$\beta$ (MC)	Error (%)
0.05	0.71	3.013	3.093	2.59
	0.81	2.713	2.787	2.64
	0.91	2.460	2.529	2.71
	0.98	2.314	2.376	2.59
0.10	0.69	2.910	2.984	2.47
	0.82	2.565	2.629	2.45
	0.89	2.301	2.368	2.81
	1.04	2.012	2.061	2.40
0.15	0.71	2.757	2.822	2.32
	0.81	2.435	2.499	2.57
	0.89	2.203	2.260	2.54
	1.03	1.909	1.956	2.41
0.25	0.71	2.626	2.693	2.50
	0.81	2.378	2.441	2.56
	0.91	2.099	2.149	2.34
	1.01	1.826	1.882	2.97

Table 7-16: System resistance factor ( $\varphi_s$ ) for Frame 5 subjected to wind plus gravity for different reliability levels using FORM and MC

$W_n/(L_n + D_n)$	Weight (%)	FORM ( $\varphi_s$ )			MC ( $\varphi_s$ )		
		$\beta = 2.5$	$\beta = 2.75$	$\beta = 3$	$\beta = 2.5$	$\beta = 2.75$	$\beta = 3$
0.5	15	0.90	0.78	0.68	0.92	0.83	0.74
1.0	40	0.83	0.73	0.65	0.86	0.76	0.68
1.5	35	0.79	0.71	0.63	0.81	0.73	0.65
2.0	10	0.76	0.68	0.60	0.78	0.70	0.63
Final value of $\varphi_s$		0.82	0.73	0.64	0.84	0.75	0.67



Using the simplified FORM method, the final values of system resistance factors for various reliability levels are presented in Table 7-17 for all proposed frames in Figure 7-1.

Table 7-17: System resistance factors ( $\varphi_s$ ) for sway frames subject to gravity and wind loading

Frame	Failure modes	$\varphi_s$		
		$\beta = 2.5$	$\beta = 2.75$	$\beta = 3$
Frame 1	CFY	0.79	0.71	0.64
Frame 2	BFY- CFY	0.80	0.72	0.66
Frame 3	BFY- CFY	0.79	0.71	0.63
Frame 4	BFY- CFY	0.77	0.68	0.60
Frame 5	BFY- CFY	0.82	0.73	0.65
Frame 6	BFY- CFY	0.80	0.73	0.65
Frame 7	BFY- CFY	0.79	0.72	0.66
Frame 8	BFY- CFY	0.79	0.72	0.65
Frame 9	BFY- CFY	0.79	0.68	0.59
Average value of $\varphi_s$		0.79	0.71	0.64

For the reliability index of 2.5, the system resistance factors vary between 0.77 to 0.82 while these values change to 0.59 and 0.66 for the target reliability index of 3. As it can be seen from the results, generally, the system resistance factors for gravity and wind loading are lower than the values obtained for the same frames subject to gravity loading for a given reliability index. However, the suggested values (Ellingwood et al. 1980) of reliability indices for members subjected to gravity and gravity plus wind loading are 3 and 2.5 respectively.

Comparing the results of Table 7-11 and Table 7-17 for  $\beta$ -values of 3 and 2.5 respectively, the corresponding values of  $\varphi_s$  are 0.82 and 0.79 respectively, and so are close enough and consistent. The reliability index ( $\beta$ ) versus system resistance factor ( $\varphi_s$ ) curves are plotted in Figure 7-23 and Figure 7-24 for two selected frames using FORM and considering four different wind to gravity load ratios.

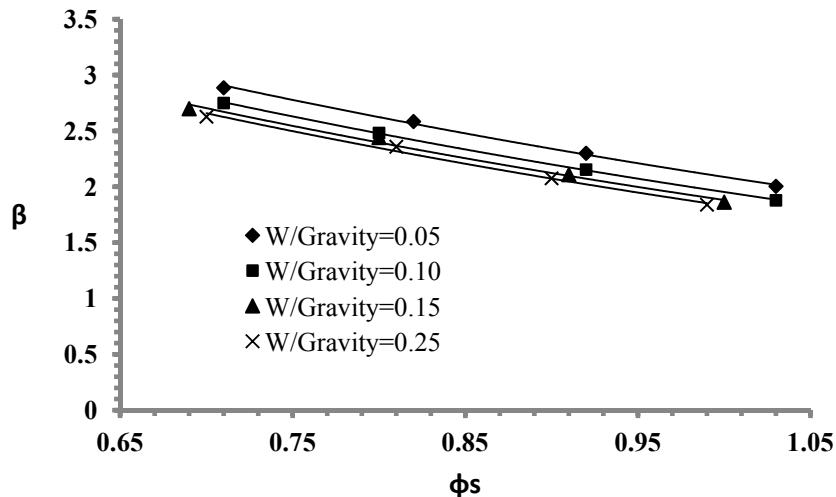


Figure 7-23:  $\beta$  vs.  $\phi_s$  curves for Frame 3 subject to gravity and wind loading using CSM with BFY-CFY failure mode

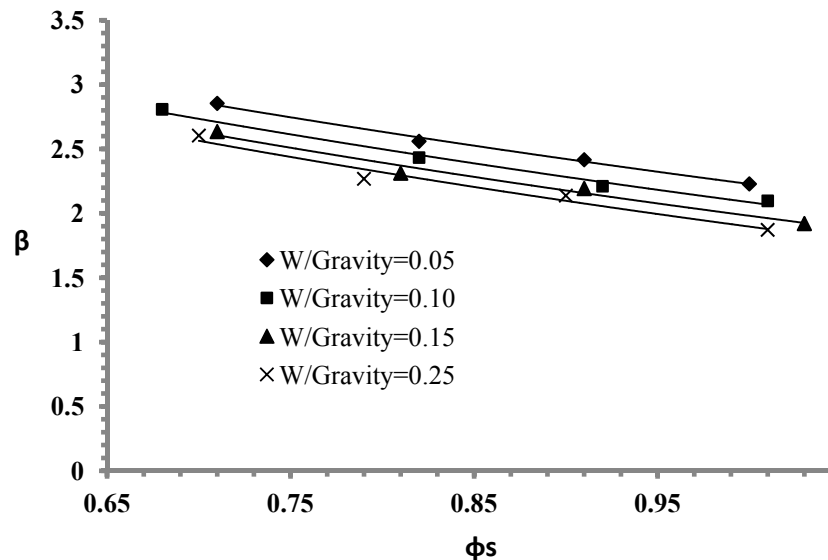


Figure 7-24:  $\beta$  vs.  $\phi_s$  curves for Frame 8 subject to gravity and wind loading using CSM with BFY-CFY failure mode

### 7.7.5 Simulation results for braced frames under gravity loading

Although it is common practice to design the connections in braced frames as cost-effective hinged connections, rigid connections may result in smaller beam sizes because the negative moments transferred from beams to columns usually lead to smaller positive moments near the mid-spans of beams. In high-rise braced frames, the space between building floors is costly and hence in some situations, rigid beam-column connections are

used in braced frame construction. Accordingly, for the braced frames shown in Figure 7-1, both hinged and rigid beam-column connections are considered. The X-bracing system is selected for simplicity as it was ascertained that the layout of the bracing system does not affect ultimate strength of the frame. The frames are designed only for gravity loading since the gravity plus wind combination is not governing for these frames. The design and the probabilistic procedure to determine system resistance factors are the same as those for sway frames under gravity loading. The reliability indices versus system resistance factors for Frame 3 with hinged joint and Frame 6 with rigid joint are plotted in Figure 7-25 and Figure 7-26, respectively.

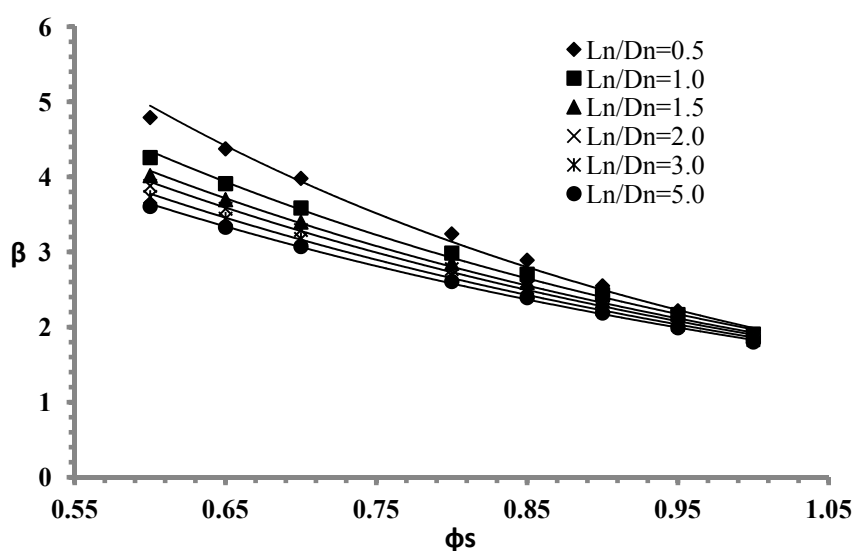


Figure 7-25:  $\beta$  vs.  $\phi_s$  curves for Frame 3 (braced) with hinged joints with BFY-CFY failure mode

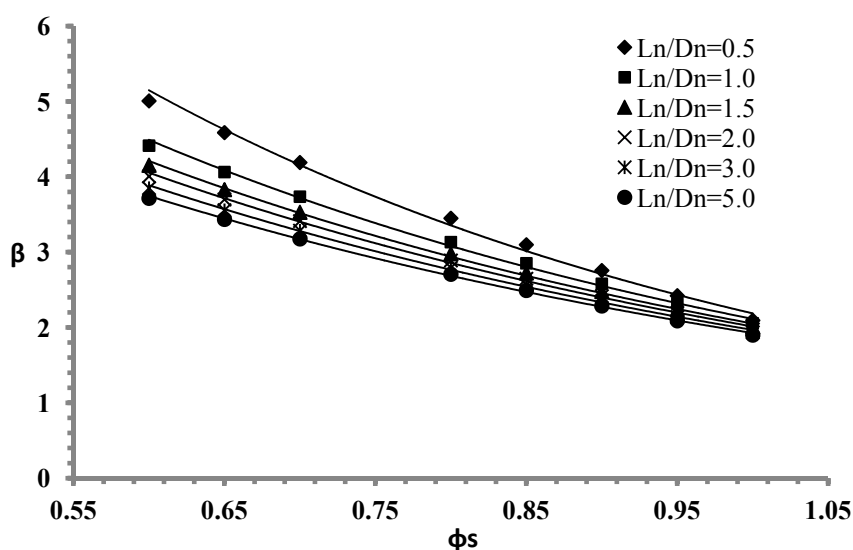


Figure 7-26:  $\beta$  vs.  $\phi_s$  curves for Frame 6 (braced) with rigid joints with CFY failure mode

The simulation results (bias and COV) as well values of  $\varphi_s$  are summarized in Table 7-18 and Table 7-19 for hinged and rigid jointed frames respectively. The cross-sections of the beams and columns are chosen in a way to achieve different failure modes, while the brace members are designed not to fail. The brace members are modeled as straight without any initial geometric imperfection as they were mainly engaged when acting in tension.

Table 7-18: System resistance factors ( $\varphi_s$ ), Bias factors and COVs of braced frames with hinged connections

Frame	Failure mode	$\bar{R}/R_n$	COV	$\varphi_s$			
				$\beta = 2.5$	$\beta = 2.75$	$\beta = 3$	$\beta = 3.5$
Frame 2	CFY	1.04	0.096	0.91	0.86	0.81	0.72
	CFY-BFY	1.05	0.095	0.92	0.87	0.82	0.73
	CFY-BPY	1.04	0.101	0.90	0.85	0.80	0.71
Frame 3	CFY-BPY	1.05	0.105	0.91	0.86	0.81	0.72
	CFY-BFY	1.04	0.107	0.90	0.85	0.80	0.71
Frame 4	CFY	1.04	0.098	0.91	0.86	0.81	0.72
	CFY-BFY	1.05	0.102	0.92	0.86	0.81	0.72
	CFY-BPY	1.05	0.097	0.92	0.87	0.82	0.73
Frame 5	CFY	1.07	0.104	0.93	0.88	0.83	0.73
	CFY-BFY	1.06	0.102	0.93	0.87	0.82	0.73
	CFY-BPY	1.06	0.104	0.93	0.87	0.82	0.73
Frame 6	CFY	1.01	0.100	0.88	0.83	0.78	0.70
	CFY-BFY	1.01	0.101	0.96	0.90	0.84	0.75
	CFY-BPY	1.02	0.100	0.89	0.84	0.79	0.70
Frame 7	CFY	1.02	0.097	0.89	0.84	0.79	0.71
	CFY-BFY	1.04	0.092	0.92	0.86	0.81	0.73
	CFY-BPY	1.04	0.105	0.90	0.84	0.80	0.71
Frame 8	CFY	1.11	0.101	0.97	0.91	0.86	0.76
	CFY-BFY	1.10	0.106	0.96	0.90	0.85	0.75
	CFY-BPY	1.06	0.099	0.93	0.87	0.82	0.73
Frame 9	CFY-BFY	1.01	0.095	0.88	0.83	0.78	0.70
Average value of $\varphi_s$				0.92	0.86	0.81	0.72

Table 7-19: System resistance factors ( $\varphi_s$ ), Bias factors and COVs of braced frames with rigid connections

Frame	Failure mode	$\bar{R}/R_n$	COV	$\varphi_s$			
				$\beta = 2.5$	$\beta = 2.75$	$\beta = 3$	$\beta = 3.5$
Frame 2	CFY	1.066	0.097	0.94	0.88	0.83	0.74
	CPY-BFY	1.088	0.112	0.94	0.88	0.83	0.74
	CFY-BPY	1.070	0.096	0.94	0.88	0.83	0.74
Frame 3	CFY-BPY	1.010	0.118	0.86	0.81	0.76	0.68
	CFY-BFY	1.010	0.102	0.87	0.82	0.78	0.69
Frame 4	CFY	1.050	0.101	0.92	0.86	0.81	0.72
	CFY-BFY	1.052	0.098	0.92	0.87	0.82	0.73
	CFY-BPY	1.028	0.103	0.92	0.87	0.82	0.73
Frame 5	CFY	1.055	0.106	0.91	0.86	0.81	0.72
	CFY-BFY	1.058	0.096	0.93	0.87	0.82	0.73
	CFY-BPY	1.061	0.099	0.93	0.87	0.82	0.73
Frame 6	CFY	1.065	0.099	0.93	0.88	0.83	0.73
	CFY-BFY	1.054	0.103	0.92	0.86	0.81	0.72
	CFY-BPY	1.063	0.106	0.92	0.87	0.82	0.73
Frame 7	CFY	1.010	0.093	0.89	0.84	0.79	0.70
	CPY-BFY-CB	1.042	0.091	0.92	0.86	0.81	0.73
	CPY-BPY-CB	1.068	0.085	0.95	0.89	0.84	0.75
Frame 8	CFY	1.061	0.102	0.93	0.87	0.82	0.73
	CPY-BFY	1.060	0.099	0.93	0.87	0.82	0.73
	CFY-BPY	1.063	0.103	0.91	0.86	0.81	0.72
Frame 9	CFY-BFY	1.016	0.095	0.89	0.84	0.79	0.71
Average value of $\varphi_s$				0.92	0.86	0.81	0.72

To determine more failure modes including buckling of columns for both hinged and rigid joints, the first storey column heights of frames presented in Figure 7-1 are changed to 10m and the simulations with random variables are conducted. The detailed information of these frames can be found in Appendix E. The simulation results for these frames are summarized in Table 7-20 and Table 7-21.

As it can be seen from Table 7-18 to Table 7-21, the reliability assessment of hinged and rigid jointed braced frames results in almost the same resistance factors and hence the resistance factor values for a given reliability index do not depend on the joint type and failure mode. Furthermore, comparing the results for braced frames with those for sway

frames under gravity loading shows that the system resistance factors are essentially independent of the frame system type. Although those frames with long columns (10m) which fail by column buckling indicate less COVs, the final resistance factors are almost the same as those for other frames. These frames might not be practical but have been analysed in this thesis to show that the derived resistance factors are not dependent on the frame configuration.

Table 7-20: System resistance factors ( $\phi_s$ ), Bias factors and COVs of braced frames with hinged connections and long columns

Frame	Failure mode	$\bar{R}/R_n$	COV	$\phi_s$			
				$\beta = 2.5$	$\beta = 2.75$	$\beta = 3$	$\beta = 3.5$
Frame 2	CPY-BFY-CB	1.041	0.073	0.94	0.88	0.83	0.74
Frame 3	CPY-BFY-CB	1.069	0.089	0.95	0.89	0.84	0.75
Frame 4	CFY-BFY-CB	1.074	0.081	0.96	0.90	0.85	0.76
Frame 5	CFY-BPY-CB	1.018	0.090	0.90	0.84	0.80	0.71
Frame 6	CFY-BPY-CB	1.002	0.094	0.88	0.83	0.78	0.70
Frame 7	CPY-CB	1.030	0.079	0.92	0.87	0.82	0.73
Frame 8	CPY-CB	1.027	0.071	0.92	0.87	0.82	0.73
Frame 9	CPY-BPY-CB	1.022	0.072	0.92	0.86	0.82	0.73
Average value of $\phi_s$				0.92	0.87	0.82	0.73

Table 7-21: System resistance factors ( $\phi_s$ ), Bias factors and COVs of braced frames with rigid connections and long columns

Frame	Failure mode	$\bar{R}/R_n$	COV	$\phi_s$			
				$\beta = 2.5$	$\beta = 2.75$	$\beta = 3$	$\beta = 3.5$
Frame 2	CPY-BFY-CB	1.036	0.087	0.92	0.86	0.81	0.73
Frame 3	CPY-BFY-CB	1.052	0.093	0.93	0.87	0.82	0.73
Frame 4	CFY-BFY-CB	1.034	0.081	0.92	0.87	0.82	0.73
Frame 5	CPY-BPY-CB	1.063	0.099	0.93	0.88	0.82	0.73
Frame 6	CFY -CB	1.025	0.099	0.89	0.84	0.79	0.71
Frame 8	CPY-CB	1.007	0.067	0.91	0.85	0.81	0.72
Frame 9	CFY-BPY-CB	1.015	0.077	0.91	0.85	0.81	0.72
Average value of $\phi_s$				0.92	0.86	0.81	0.72

## 7.8 Effect of member yield stress correlation on the system resistance factor

As discussed in Section 7.4, randomness in yield strength has a significant influence on the frame strength as it has the largest COV among all relevant steel properties. Generally, three cases of correlation of yield stress among members are considered, viz. perfectly-correlated, uncorrelated and partially-correlated. The results presented in previous sections for all load combinations are based on the assumption of perfectly-correlated yield stress for all frame members in which one random value of yield stress ( $f_y$ ) is generated and assigned to all beams and columns. The perfectly correlated case is of interest because of its similarity to deterministic analysis where all members are assigned a single yield stress equal to the nominal yield stress (Buonopane and Schafer 2006). In practice this might be an unrealistic assumption since each member can have different yield stress due to different manufacturing conditions. To investigate the effect of yield stress correlation on the system resistance factor ( $\phi_s$ ), the uncorrelated and partially-correlated cases are studied for four of the frames shown in Figure 7-1 under gravity loading. In the former case, different values of randomly generated  $f_y$  are assigned to each beam and column, while in the later case, one random value of  $f_y$  is assigned to all beams and a different random value is assigned to all columns. Statistical characteristics such as bias ( $\bar{R}/R_n$ ) and COV are summarized in Table 7-22 for the three different cases of yield stress correlation.

Table 7-22: Statistical characteristics of frame strength for different yield stress correlations

Frame	Failure mode	$\bar{R}/R_n$			COV		
		Correlated	Partially-correlated	Un-correlated	Correlated	Partially-correlated	Un-correlated
Frame 4	BFY-CPY	1.07	1.07	1.06	0.102	0.087	0.076
Frame 6	BPY-CFY	1.08	1.08	1.07	0.104	0.100	0.094
Frame 7	BFY-CPY	1.06	1.05	1.04	0.099	0.081	0.073
Frame 9	BPY-CPY	1.07	1.06	1.05	0.103	0.092	0.083

Based on the results presented in Table 7-22, it can be concluded that (i) frames with uncorrelated  $f_y$  have a slightly lower ratio of mean to nominal strength ( $\bar{R}/R_n$ ) compared

to the perfectly-correlated and partially-correlated cases, and (ii) the COV drops significantly when the correlation decreases between the members.

Using these statistical characteristics in the FORM reliability framework detailed in the companion paper,  $\beta$ - $\phi$  curves are generated for the four frames and the corresponding system resistance factors for different reliability levels are obtained for different correlation types, as summarized in Table 7-23. The results show that although different types of yield stress correlation result in different values of  $\bar{R}/R_n$  and COV, the final values of system resistance factors ( $\phi_s$ ) for different levels of reliability ( $\beta$ ) do not change significantly. Consequently, using the assumption of perfectly-correlated yield stress to determine system resistance factors is satisfactory.

Table 7-23: System resistance factor ( $\phi_s$ ) for different yield stress correlations

Frame	Failure mode	Correlation type	$\beta = 2.5$	$\beta = 2.75$	$\beta = 3$	$\beta = 3.5$
Frame 4	BFY-CPY	Correlated	0.96	0.89	0.83	0.73
		Partially correlated	0.98	0.91	0.84	0.75
		Uncorrelated	0.98	0.91	0.84	0.75
Frame 6	BPY-CFY	Correlated	0.94	0.88	0.83	0.74
		Partially correlated	0.94	0.88	0.83	0.74
		Uncorrelated	0.96	0.89	0.83	0.74
Frame 7	BFY-CPY	Correlated	0.92	0.87	0.82	0.74
		Partially correlated	0.92	0.87	0.82	0.75
		Uncorrelated	0.93	0.88	0.83	0.75
Frame 9	BPY-CPY	Correlated	0.96	0.89	0.84	0.74
		Partially correlated	0.96	0.89	0.84	0.74
		Uncorrelated	0.97	0.90	0.84	0.74

## 7.9 Effect of strain hardening on the system resistance factor

The effect of strain hardening on the nominal frame ultimate strength was discussed in Chapter 3 and appeared to be negligible. In this section, the influence of strain hardening on the statistics of the ultimate strength and system resistance factor is investigated. Frame 2 subjected to gravity loading with the failure mode of BFY-CPY is selected as an example for this study. The two cases of with and without strain hardening is considered.



The hardening modulus ( $E_{st}$ ) is modelled as a normally distributed random variable with the mean of 4100 MPa and COV of 0.25 as recommended by Galambos and Ravindra (1978) (see Table 7-1). For the case of elastic-perfectly plastic material, two different methods of defining the ultimate strength are compared. The first method is choosing the ultimate strength as maximum point of the load-displacement curve while the second method is defining the ultimate strength as the load at which the slope of load-displacement curve becomes less than 5% of its initial value. The second method is used for the case with strain hardening.

The statistical data of the frame ultimate strength ( $R$ ) corresponding to different resistance factors ( $\phi_s$ ) for the live to dead load ratio of 1 ( $L_n/D_n=1$ ) are summarized in Table 7-24. Using these statistics the  $\beta - \phi_s$  curves are plotted and presented in Figure 7-27 to Figure 7-29. Although the mean values of ultimate strength in Table 7-24 are different, the mean-to-nominal values ( $\bar{R}/R_n$ ) are almost the same. Since only the ratio ( $\bar{R}/R_n$ ) is important in the reliability calculation (Equation 7-16), the  $\beta - \phi_s$  curves and final values of system resistance factors for different reliability levels are essentially identical (Table 7-25). Therefore, material strain hardening is ignored in this study and the maximum load in load-displacement curve is selected as the frame ultimate strength.

Table 7-24: Comparison of frame ultimate strength statistical data of Frame 2 with and without considering strain hardening

$\phi_s$	Mean ( $\bar{R}$ )			COV			$\bar{R}/R_n$		
	Elastic-Perfectly Plastic		With strain hardening	Elastic-Perfectly Plastic		With strain hardening	Elastic-Perfectly Plastic		With strain hardening
	5% of initial slop	Max	5% of initial slop	5% of initial slop	Max	5% of initial slop	5% of initial slop	Max	5% of initial slop
0.60	2.31	2.36	2.42	0.103	0.102	0.101	1.03	1.03	1.04
0.71	2.04	2.05	2.06	0.102	0.097	0.102	1.03	1.02	1.03
0.74	1.93	1.95	1.96	0.108	0.101	0.105	1.04	1.02	1.03
0.78	1.82	1.84	1.84	0.103	0.100	0.102	1.03	1.02	1.04
0.85	1.69	1.70	1.69	0.101	0.099	0.104	1.03	1.02	1.04
0.97	1.58	1.51	1.59	0.105	0.104	0.100	1.03	1.02	1.03

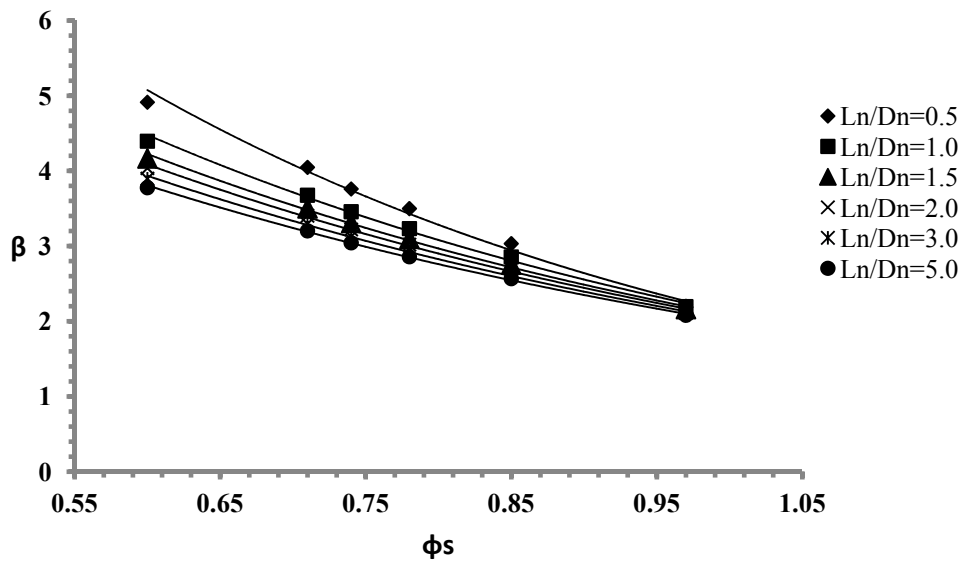


Figure 7-27:  $\beta$  vs.  $\phi_s$  curves for Frame 2 under gravity with elastic-perfectly plastic material and 5% of initial slope criteria for choosing ultimate strength

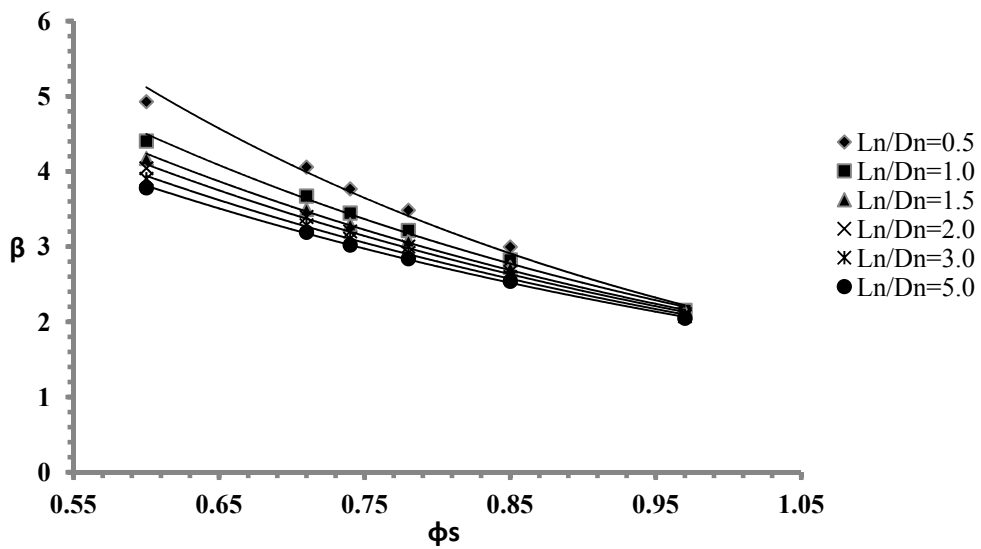


Figure 7-28:  $\beta$  vs.  $\phi_s$  curves for Frame 2 under gravity with elastic-perfectly plastic material and maximum criteria for choosing ultimate strength

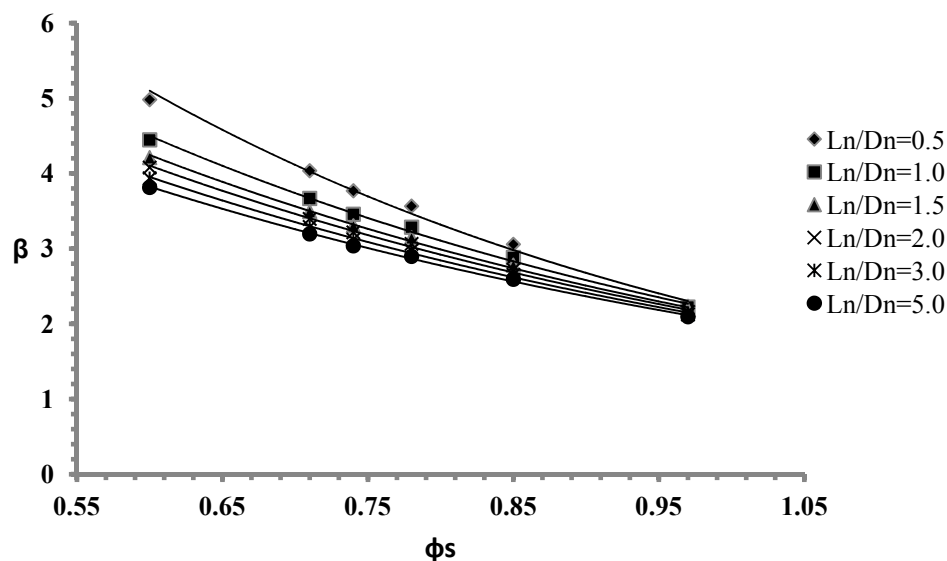


Figure 7-29:  $\beta$  vs.  $\varphi_s$  curves for Frame 2 under gravity with material with strain hardening and 5% of initial slope criteria for choosing ultimate strength

Table 7-25: Comparison of system resistance factors ( $\varphi_s$ ) of Frame 2 with and without considering strain hardening

Frame	Method of choosing the ultimate load	$\varphi_s$			
		$\beta = 2.5$	$\beta = 2.75$	$\beta = 3$	$\beta = 3.5$
Frame 2	Elastic-perfectly plastic (5% of initial slope)	0.90	0.84	0.79	0.71
	Elastic-perfectly plastic (max)	0.89	0.84	0.79	0.71
	With strain hardening (5% of initial slope)	0.90	0.85	0.80	0.71

## 7.10 Target reliability and design example

The values of system resistance factors ( $\varphi_s$ ) for different frame types under different load combinations are presented in this study for four target reliability levels. However, to use the system-based approach in practical design, a specific value of acceptable target reliability and corresponding system resistance factors are needed. The value of target reliability varies from one situation to another depending on factors such as the cause of failure, the failure mode, and the consequences of failure. In the AISC Specification, the target reliability indices for steel members range between 2.5 and 3 (Ellingwood et al. 1980). Generally, the reliability of redundant structural systems is higher than the

reliability of a single member. The difference, however, is unknown and depends on many factors. Available approaches for determining appropriate levels of target reliability include, (i) calibration to existing design practice (Ellingwood, Galambos et al. 1980), (ii) comparison of risks of system failure to other societal risks and (iii) minimization of lifecycle costs. The first approach is deemed the most suitable and is used in this study. It requires evaluating the system failure probability (or reliability index) using a system reliability assessment method for frames designed to current standards. The reliability level obtained from this calibration is then synthesized with the reliability indices obtained for the same frames when designed by advanced analysis so as to determine the value of resistance factor ( $\phi_s$ ) that provides consistent levels of reliability.

The total of sixteen steel frames under gravity load designed by Ziemian (1990) are considered in this study. Half of these frames are designed based on advanced analysis and the reliability indices ( $\beta$ ) of those frames are listed in last column of Table 7-8. The other half are designed based on a combination of a 2<sup>nd</sup> order elastic analysis and the AISC360-10 Specification (2010), referred to as “Elastic-LRFD design method”. The corresponding reliability indices are determined using the probabilistic approach explained in the companion paper, and presented in Table 7-26. In addition, the reliability indices of the nine frames presented in Figure 7-1, which are designed to AS4100, are determined and shown in Table 7-26.

Based on the results shown in Table 7-8 and Table 7-26 the average values of reliability are 2.70 and 3.50 for frames designed based on advanced analysis and Elastic-LRFD respectively. When a structure is designed based on Elastic-LRFD, the failure criterion is the formation of the first plastic hinge. Hence, the Elastic-LRFD design method only partially considers the effect of member failure on the system safety, and does not consider inelastic interaction and load redistribution between members as it is implicit that the whole structure fails when the first member fails. The Elastic-LRFD method of design leads to higher levels of reliability compared to those based on design by advanced analysis. It should be noticed that the reliability values determined in this study for those frames designed using Elastic-LRFD are system reliabilities as they are based on the overall strength of the frame, not on the failure of an individual member.

Since existing frames designed using Elastic-LRFD are performing well but at the same time advanced analysis more accurately models the behavior of steel frames and thus intrinsically offers greater reliability, based on authors' engineering judgment the value of  $\beta=3$  is proposed as a suitable target reliability index for steel frames under the gravity loads. It follows from Table 7-11, 6-15, 6-16 and 6-17 that the corresponding system resistance factor ( $\phi_s$ ) may be chosen as 0.8. This value ( $\phi_s=0.8$ ) applies to braced and unbraced, regular and irregular 2D steel frames subjected to gravity loads. To be consistent with the existing LRFD philosophy, the system-resistance factors should not be dependent on the applied load combination. Therefore, it is proposed that the same resistance factor of 0.8 be used for frames under gravity plus wind loading, which according to Table 7-17 implies a target reliability of 2.5. Note that a similar differentiation is made in current member-based design where the target reliability index for members subject to gravity loading is 2.6 according to the AISC360-10 (2010) Specification, while it is 2.25 for members subjected to gravity and wind loading.

Table 7-26: Reliability indices ( $\beta$ ) for frames designed by Elastic-LRFD

Frame	Mean ( $\bar{R}$ )	COV	Reliability Index ( $\beta$ )	Failure Mode
UP50HE	1.857	0.095	3.21	BFY-CPY
UP50LE	1.938	0.100	3.35	BFY-CFY
UF50HE	1.927	0.100	3.32	BFY-CPY
UF50LE	2.010	0.099	3.52	BFY-CPY
SP50HE	1.955	0.096	3.43	BPY-CFY
SP50LE	2.636	0.106	4.63	BFY-CPY
SF50HE	1.909	0.017	3.22	BFY-CPY
SF50LE	2.221	0.098	3.22	BFY-CPY
Frame 1	1.922	0.104	3.28	BFY-CPY
Frame 2	1.999	0.101	3.47	BFY-CPY
Frame 3	2.208	0.103	3.93	BFY-CPY
Frame 4	1.841	0.104	3.09	CFY
Frame 5	2.089	0.101	3.66	BFY-CPY
Frame 6	1.832	0.100	3.11	BFY-CPY
Frame 7	2.159	0.100	3.80	BFY-CPY
Frame 8	2.026	0.099	3.55	BFY-CPY
Frame 9	2.076	0.103	3.60	BPY-CPY
average value of $\beta$			3.50	

To demonstrate the implications of using the proposed design-by-advanced-analysis method on member sizes and total steel weight, a design example is presented which uses the nominal model and advanced (second-order inelastic) analysis explained in the companion paper and the system resistance factor ( $\phi_s=0.8$ ) developed in the present paper. Table 7-27 compares the member-based design to AS4100 and the system-based design using advanced analysis for Frame 6 under gravity loading. To achieve an optimum design, in both methods, the smallest possible member cross-sections are chosen, (although it is acknowledged that in practical design, the member cross-sections in a multi-storey frame would not change in each storey). As shown in Table 7-27, design by advanced analysis leads to a lighter steel frame (14.6% less steel in this particular case). More detailed worked examples can be found in Appendix E.

Table 7-27: Comparison of member-based and system-based design of Frame 6

Design method	Members	Sections	$\lambda_n$	Failure	Steel weight (kg)
Member-based design (AS4100)	$C_1, B_7$ $C_2$ $C_3, B_6$ $C_4, C_7$ to $C_{10}$ $C_5, B_4, B_5$ $C_6, B_1, B_2, B_3$ $C_{11}, C_{12}$ $B_8$	410UB59 460UB74 360UB56 250UB37 410UB53 360UB50 250UB31 310UB40	1.87	BFY-CPY	4676.6
System-based design (proposed method)	$C_1, C_2$ $C_3, C_6$ $C_4, C_7, C_8$ $C_5$ $C_9$ to $C_{12}, B_8$ $B_1$ to $B_6$ $B_7$	360UB56 310UB46 250UB37 360UB50 250UB31 310UB40 410UB53	1.25	BFY-CPY	3994.4

## 7.11 Conclusions

Advanced analysis, which is permitted by most of the existing steel specifications, can simplify the design process by capturing the system behavior directly and obviating the need for individual member/connection capacity checks to a structural standard. With the significant advances in and availability of advanced structural analysis software, the behavior of a complex structural system can now be determined accurately for design purposes. This chapter details a research methodology for determining system resistance

factors for the direct design of steel frames by advanced (or inelastic) analysis. The methodology consists of combining a geometric and material advanced analysis method with a probabilistic approach considering the inherent uncertainties in the ultimate strength of a frame by modeling yield stress, elastic modulus, cross-sectional properties, member and frame initial geometric imperfections and residual stress as random variables. A rigorous statistical assessment of the system strength of a wide range of mid-to-low-rise two-dimensional structural frames and derives system resistance factors to be used in conjunction with advanced structural analysis are presented in this study. The model frames represent the current steel building inventory in Australia, consisting of regular and irregular geometries of moment resisting and braced frames. Various load combinations as well as different failure modes are considered for each frame and the system strength distribution and its statistical characteristics are obtained. The resistance factor  $\varphi_s$  versus reliability index ( $\beta$ ) is then plotted for each frame using the probabilistic approach developed in this study. The simulation results show that although different frames with various geometries and configurations are analysed, the COVs and mean-to-nominal ratios of ultimate strength are quite similar and do not depend on the frame or joint types. Moreover, the system resistance statistics of different frames failing in different failure modes are quite similar, leading to similar values of system resistance factors ( $\varphi_s$ ). The target reliability is evaluated based on the simulation results of 25 frames designed by both Elastic-LRFD and advanced analysis. Based on the simulation results and engineering judgment, the target reliability index of 3 for frames under gravity loading and 2.5 for frames subject to gravity plus wind loading are selected. Subsequently, the system resistance factor to be implemented into system-based design is determined as  $\varphi_s=0.80$  for 2D low-to-mid-rise steel frames. A moment resisting frame under gravity loading was designed as an example using the proposed system resistance factor to show that the system-based design procedure leads to a lighter structural system compared to member-based design to existing specifications. In addition, by using the design-by-analysis approach and derived system resistance factors, the designer stands to benefit from a more reliable design method and shortened design time as there is no need for separate member/section capacity checks. The method also clearly shows the failure mode of the frame and readily allows the designer to consider the consequences of failure.

# CHAPTER

## 8 .

# Conclusion

---

### **8.1 Summary**

Advanced analysis is now permitted by many steel structural specifications and is likely to become the next generation design tool for steel frames. At the same time, there is an increasing tendency towards of designing a structure as a whole system rather the combination of its components. However, before the direct design of steel structures by advanced analysis is fully adopted as a practical tool by the engineering profession several limitations must be overcome.

This thesis provides comprehensive studies towards the system-based design of steel structures by advanced geometric and material nonlinear analysis. Using Monte-Carlo probability modelling, the statistical characteristics of frame strength were obtained for a diverse range of low-to-mid rise two dimensional steel frames. In this, all parameters affecting the frame ultimate strength were modelled randomly including cross-section geometry, material yield stress and elastic modulus, residual stress and initial geometric



imperfection. A comprehensive literature review indicated that while the statistical data of most random variables can readily be obtained from the literature, modelling initial geometric imperfection and residual stress stochastically have not been stated clearly in the literature. A new approach to model initial geometric imperfection in advanced analysis was proposed which is based on scaling elastic buckling modes. In addition, a new perspective about the probabilistic modelling of residual stress using commonly used residual stress patterns was introduced. Having produced statistical models for initial geometric imperfection and residual stress, more than 100000 advanced analyses were run and the frequency of strength were plotted for any particular type of structures. Subsequently, a first-order reliability method was used to estimate the system resistance factors, leading to the formulation of a direct design method which obviates tedious check of member strength to a specification.

Additionally, a new model is developed in this study for transmitting warping through the joints of steel members. Although this research is based on advanced analysis of two-dimensional frames in which the out-of-plane behaviour is ignored, this method can be used in future studies of 3D space frames.

## **8.2 Remarks**

The following is a summary of the conclusions drawn from this research project as stated at the end of Chapters 2 to 7:

A comprehensive literature review on most common analysis methods and reliability analyses is presented in Chapter 2. The key findings are summarized as follows:

- a) Among all analysis methods, advanced analysis is best able to capture the behavioural characteristics and ultimate load carrying capacity of a structural system, taking into account system effects explicitly.
- b) Many codes for steel structures allow the use of advanced material and geometric analysis. However, there is no rational way to account for the risk arising from

uncertainties in load and strength in a steel frame. Consequently, appropriate system resistance factors need to be determined.

- c) One of the most important parameters affecting the frame ultimate strength is initial geometric imperfections. Most commonly used methods model the imperfection to be the worst case scenario to maximize the destabilizing effects under the applied loads. Nevertheless, the worst case scenario of imperfections may be overly conservative. In addition, the difficulty associated with most of these methods is that no information is provided about the direction of the imperfections. The designer has either to guess or solve for many possible combinations to find the worst scenario, which for a real structure may be a difficult task.
- d) A few models can be found in the literature for the partial transmission of warping at joints when using beam finite element analysis. Despite the simplicity of all proposed methods, they are limited to specific kinds of joints and cannot be extended to 3D space frames.
- e) Latin-Hypercube sampling is a very efficient technique for estimating mean values and standard deviations compared to Direct Monte-Carlo method. Among all approximation methods, first-order reliability method is considered to be one of the most reliable computational methods.

In Chapter 3, nonlinear finite element analysis models for steel frames are developed. The main features are as follows:

- a) Details about element selection, material properties, residual stress and structural collapse state are summarized. The finite element model is calibrated against frames from the literature and an excellent agreement achieved.
- b) The effect of strain hardening on the ultimate frame strength is evaluated and appears to be negligible when a (5%) stiffness limit state is included.

- c) Mesh sensitivity analysis is conducted. It was concluded that beam finite element analysis of ABAQUS is very sensitive to the mesh size. However, after reaching a specific size, decreasing the mesh size further does not change the ultimate load factor. The global element size of 200 mm was chosen.

In Chapter 4, a new joint model is developed for the transmission of warping through a joint. The main remarks are as follows:

- a) The proposed joint model is simple to implement into finite element models, using readily available beam and spring elements, and does not require the beam stiffness matrix to be modified or computationally costly shell finite element modelling to be employed. It is also general and can be applied equally to 2D and 3D frames regardless of the number and direction of connected members. The model lends itself to common steel frame design applications in industry where designers look for fast and convenient methods of analysis.
- b) The proposed joint model is based on a combination of linear springs and linear constraint equations, and as was shown in the verification examples it can be applied accurately in elastic buckling analysis. It can also be applied accurately in nonlinear analyses as long as yielding does not occur in the joints.
- c) All previous models for warping transmission including “linear constraint equations”, as proposed by (Basaglia, Camotim et al. 2010), assume fully prevented warping for diagonal-stiffened joints. It was shown by verification examples that even for this case there is still a degree of warping transmission through the joints which the proposed model can accurately predict.

In Chapter 5, a convenient approach is introduced to model initial geometric imperfection by linear combination of scaled buckling modes. The main important features are as follows:

- a) The study recommends appropriate numbers of elastic buckling modes and the values of scale factors for each mode through a probabilistic approach. It transpired that one, three and six are “good” numbers of eigenmodes to be used

for modelling imperfections. Using the first mode is easy and can lead to reasonable results but six modes may predict the actual shape of imperfection very accurately.

- b) To verify the application of the proposed scale factors, the frame ultimate strengths obtained using these factors are compared with the mean of the ultimate strengths of 200 frames with randomly generated shape, considering eight braced and eight unbraced frame layouts. Excellent agreement was achieved when considering six modes to represent the imperfection.

In Chapter 6, a new perspective for probabilistic modelling of residual stress is proposed. The main observations are:

- a) Randomness in residual stress may have a significant impact on the strength and reliability of steel frames, especially for those frames which are very sensitive to second-order effects and fail by instability. Different patterns of residual stress result in different ultimate frame strengths.
- b) Regarding the reliability index, using different residual stress patterns can lead to significant differences. Thus, the residual stress patterns need to be chosen thoughtfully in the advanced analysis of steel structures.

In Chapter 7, the effect of uncertainties in material properties, initial geometric imperfection and residual stress on the ultimate strength of steel structural systems are studied. The Chapter presents a reliability analysis of a wide range of steel frames to determine appropriate system resistance factors which can be used in system-based design of steel structures by advanced analysis. Some important remarks about this study are as follows:

- a) A set of system resistance factors,  $\varphi_s$ , are obtained for a various 2D sway and braced frames under different load combinations including gravity and gravity plus wind loading, considering different levels of system reliability.

- b) Probabilistic assessments of frame ultimate strength indicated that the statistical characteristics (e.g. mean and COV) of the strength and consequently the values of system resistance factors do not depend on the particular frame failure mode.
- c) The system resistance factors also do not appear to be sensitive to whether or not a frame system is braced or unbraced, regular or irregular; or what kind of load combination is used. As a result, the system resistance factors gathered from all frame structure types and load combinations are remarkably consistent. This is a positive result from the structural designer's viewpoint, obviating the need to apply different resistance factors to different types of frames and/or loading.
- d) The effect of strain hardening on the frame ultimate strength statistics is evaluated and appears to be negligible. In addition, the influence of members yield strength correlation on the system resistance factor is studied. It was concluded that although various types of yield stress correlation resulted in different values of COV, the final value of system resistance factors does not change significantly. Thus, the perfectly-correlated yield stress is considered in this study.
- e) The application of FORM to predict the system reliability index was verified against direct Monte-Carlo for frames subjected to both gravity loading and combined gravity and wind loading. By having errors less than 5% between the reliability indices predicted by the two methods, it was concluded that FORM is sufficiently accurate to predict the reliability index and is used in this study.
- f) To recommend an appropriate value of target reliability for a redundant structural system, a total of 25 frames are studied. The results indicated that the average target reliabilities are 2.7 and 3.5 for frames designed based on advanced analysis and Elastic-LRFD respectively. Based on engineering judgement, the values of 3 and 2.5 are chosen as final target reliability indices for steel frames under gravity loads and gravity plus wind loads, respectively.
- g) Using these target reliability indices ( $\beta$ ), the recommended value of system resistance factor ( $\phi_s$ ) for system-based design was determined as 0.8 for 2D braced and unbraced frames under gravity and combined gravity and wind loads.

- h) To show the accuracy and reliability of the proposed direct design method, a design example is presented which relies on the second-order inelastic analysis explained in Chapter 3 and the derived system resistance factor of 0.8. The results indicate that while advanced analysis can be used effectively to design steel structures, it leads to lighter frames (14.6% lighter for the studied case).
- i) As it was mentioned in this chapter, the cross-sectioned are assumed to be compact and hence their ductility is deemed adequate in terms of general yielding and straining. Nevertheless, locations with highly localised stress, such as at connections and/or the points with large concentrated applied forces may require separate check on strain demand.

### **8.3 Recommendation for future research**

The following are recommendations for future research in the area of this study:

- a) The research presented in this thesis is based on two-dimensional frames with full lateral restraint in which the cross-sections are fully compact. Therefore, the effect of lateral-torsional buckling and local buckling is ignored in this study. The same methodology can be used to perform the statistical assessment of the system strength for 3D frames and frames with slender cross-sections. The appropriate system resistance factors for these types of frames still needs to be determined.
- b) In this study the connections are modelled as rigid and the influence of connection stiffness on the frame ultimate strength and its failure mode is ignored. Frames with semi-rigid connections should be studied and the parameters defining moment-rotation curves of typical connections need to be modelled randomly in the probabilistic assessment of frame strength. While substantial research is available on the modelling and design of semi-rigid connections, the statistical characteristics should be obtained by carrying out experimental tests on common steel joints.

- c) The system resistance factors derived in this study are based on simplified FORM. The gravity loads are modelled as deterministic values in simulations and randomness in loads is taken into account later in determining the probability of failure using FORM. The only restriction of this method is that the increase in gravity load is proportional on all floors and in all bays. Further research is needed to determine the effect of load variations between floors and bays.
- d) The frames in this study are subjected to gravity loading and combined gravity and wind loads. More load combinations including snow and earthquake can be considered and corresponding system resistance factors can be derived, although these load combinations are generally not governing in Australia.
- e) This study only focuses on 2D steel frames subject to major-axis bending. System behaviour of frames with members oriented for minor-axis bending must be investigated. In this case partial yielding accentuated by the presence of residual stresses can have a significant impact on the frame behaviour (Ziemian and Miller 1997) and the residual stress results presented in Chapter 6 may be somewhat different although this might have a small impact on the resistance factors presented in Chapter 7.
- f) Despite the presence of step-by-step structural guidelines, it has been observed that the most spectacular structural failures occur as a result of human errors rather than the uncertainties in loads and strengths which can be measured statistically (Ellingwood 1994). This error cannot be taken into account by adjusting the load and resistance factors. Current structural reliability methods do not address this problem and further research is needed to find a way to take this kind of error into account.
- g) The proposed model for transmission of warping through the joints of steel frames is based on linear springs and is only valid if the joints remain elastic under applied load. Further research is needed to extend the model to when yielding occurs at the joint.

---

## References

- ABAQUS (2009). "Version 6.8." Karlsson & Sorensen, Hibbit, USA.
- ABAQUS/STANDARD (2009). User's manual version 6.8. Hibbit, USA: Karlsson & Sorensen.
- AISC360-10 (2010). "Specification for structural steel buildings." American Institute of Steel Construction (AISC), Chicago, Illinois.
- AISC (1987). "Specification for the design, fabrication and erection of structural steel buildings." American Institute of Steel Construction, Chicago.
- AISC (1994). "Load and resistance factor design specification." 2nd ed. Chicago: AISC.
- Al-Mashary, F. and W. F. Chen (1991). "Simplified second-order inelastic analysis for steel frames." *Journal of Structural Engineer* **69**(23): 395-399.
- Al-Rasby, S. N. (1991). "Solution techniques in nonlinear structural analysis." *Computer and Structures* **40**(4): 985-993.
- Alpsten, G. A. (1968). "Thermal residual stresses in hot-rolled steel members." Fritz Engineering Laboratory, Report No.337.3, Lehigh University, Bethlehem, Pennsylvania.
- Alvarenga, A. R. and R. A. M. Silveira (2009). "Second-order plastic-zone analysis of steel frames – Part II: effects of initial geometric imperfection and residual stress." *Latin American Journal of Solids and Structures* **6**(4): 323 – 342.
- Alvarez, R. J. and C. Birnstiel (1969). "Inelastic analysis of multistory multibay frame." *Journal of Structural Division* **95**(11): 2477-2503.
- Andreaus, U., P. D'Asdia and F. Iannozzi (1984). "On the Optimal Choice of the Shape of Antiseismic Bracing Systems." W.C.E.E., San Francisco, U.S.A., Luglio: 459-466.
- ANSI/AISC360-05 (2005). "Specification for Structural Steel Buildings." American Institute of Steel Construction, Chicago.
- ANSYS (2000). "Reference manual." ANSYS Inc, Release 5.6, Canonsburg, PA, USA.
- Argyris, J. H. (1965). "Continua and Discontinua." First Conference on Matrix Methods in Structural Mechanics. OH, Wright-Patterson Air Force Base: 11-189.
- AS4100 (1998). "Australian Steel Structures Standard." Sydney, NSW 2001, Australia.
- AS/NZS1170 (2002). "Structural Design Actions." Standards Australia, Homebush (NSW), Australia.
- ASCE7-05 (2006). "Minimum design loads for buildings and other structures." ASCE, Reston, VA.
- Attalla, M. R., G. G. Deierlein and W. McGuire (1994). "Spread of plasticity: quasi-plastic- hinge approach." *Journal of Structural Engineering, ASCE* **120**(8): 2451-2473.
- Austin, W. S., S. Yegian and T. P. Tung (1957). "Lateral buckling of elastically end restrained I-beams." *Transactions, ASCE* **122**: 374–388.
- Avery, P. (1998). "Advanced Analysis of Steel Frame Structures Comprising Non-compact Sections." PhD thesis, School of Civil Engineering, Queensland University of Technology.
- Baigent, A. H. and G. J. Hancock (1982). "Structural analysis of assemblages of thin-walled members." *Engineering Structures* **4**(3): 207-216.
- Baker, M. J. (1969). "Variations in material properties and flexural behaviour of certain UB's." Research Report, Imperial Collage, London.



- Barsan, G. M. and C. G. Chiorean (1999). "Computer program for large deflection elasto-plastic analysis of semi-rigid steel frameworks." *Journal of Computers and Structures* **72**: 699-711.
- Basaglia, C., D. Camotim and N. Silvestre (2009). "GBT-based local, distortional and global buckling analysis of thin-walled steel frames." *Thin-Walled Structures* **47**(11): 1246-1264.
- Basaglia, C., D. Camotim and N. Silvestre (2010). "Kinematic models to simulate the torsion warping transmission at thin-walled steel frame joints." *Steel & Composite Structures- Proceeding of the 4th International Conference*. Sydney, Australia.
- Bazant, Z. P. and M. El Nimeiri (1973). "Large-deflection spatial buckling of thin walled beams and frames." *Journal of Engineering Mechanics Division* **99**(EM6): 1259-1281.
- Beaulieu, D. and P. F. Adams (1977). "A Statistical Approach to the Problem of Stability Related to Structural Out-Of-Plumb." *International Colloquium on Stability of Structures under Static and Dynamic Loads*, Washington, D.C., May 17-19: 114-121.
- Beaulieu, D. and P. F. Adams (1978). "The results of a survey on structural out-of-plumbs." *Canadian Journal of Civil Engineering* **5**(4): 462-470.
- Beck, A. T. and A. S. Doria (2008). "Reliability Analysis of I-Section Steel Columns Designed According to New Brazilian Building Codes." *Journal of the Brazilian Society of Mechanical Sciences and Engineering* **30**(2): 152-159.
- Beedle, L. S. (1958). "Plastic Design of Steel Frames." New York, John Wiley and Sons, Inc. .
- Beedle, L. S. and L. Tall (1962). "Basic column strength." *Transactions of the ASCE* **127**: 138-179.
- Beerman, H. J. (1980). "Warping torsion in commercial vehicle frames, taking into consideration flexible joints." *International Journal of Vehicle Design* **1**(5): 397-414.
- Bild, S. and N. S. Trahair (1989). "In-plane strengths of steel columns and beam columns." *Journal of Constructional Steel Research* **13**(1): 1-22.
- Bjorhovde, R. (1972). "Deterministic and Probabilistic Approaches to the Strength of Steel Columns." Ph.D. thesis, Lehigh University, Bethlehem.
- Blandford, G. E. (1990). "Thin-walled space frame analysis with geometric and flexible connection nonlinearities." *Computers & Structures* **35**(5): 609-617.
- BS5950-1 (2003). *Structural Use of Steelwork in Buildings, Part 1: Code of Practice for Design*. British Standards Institution, London.
- Buonopane, S. G. (2008). "Strength and Reliability of Steel Frames with Random Properties." *Journal of Structural Engineering, ASCE* **134**(2): 337-344.
- Buonopane, S. G. and B. W. Schafer (2006). "Reliability of Steel Frames Designed with Advanced Analysis." *Journal of Structural Engineering* **132**(2): 267-276.
- Buonopane, S. G. and B. W. Schafer (2006). "Reliability of steel frames designed with advanced analysis." *Journal of structural engineering-ASCE* **132**(2): 267-276.
- C.E.A.C.M. (1966). "Laboratory report, Commission 8, ." Politecnico di Milano, Istituto di Scienza delle Costruzioni, Laboratorio Prove Materiali.
- Cabrero, J. M. and E. Bayo (2005). "Development of practical design methods for steel structures with semi-rigid connections." *Engineering Structures* **27**: 1125-1137.
- Camotim, D., C. Basaglia and N. Silvestre (2010). "GBT buckling analysis of thin-walled steel frames: A state-of-the-art report." *Thin-Walled Structures* **48**(10-11): 726-743.

- CAN/CAS-S16 (1994). "Limit states design of steel structures." CAN/CAS-S16.1-M94. Canadian Standards Association.
- Chai, H., M. Mascagni, and T. Warnock (2005). "On the optimal Halton sequence." *Mathematics and Computers in Simulation* **70**: 9-21.
- Chan, S. L., H. Y. Huang and L. X. Fang (2005). "Advanced analysis of imperfect portal frames with semirigid base connections." *Journal of Engineering Mechanics* **131**(6): 633-640.
- Chandramouli, S., S. T. Wang and G. E. Blandford (1994). "Stability response of flexibly connected cold-formed steel space frames." *Thin-Walled Structures* **18**(4): 333-346.
- Chaudhary, A. B. (1982). "Generalized stiffness matrix for thin-walled beams." *Journal of the Structural Division, ASCE* **108** (3): 559-577.
- Chebl, C. and K. W. Neale (1984). "A finite element method for elastic-plastic beams and columns at large deflections." *Computers & Structures* **18**(2): 255-261.
- Chen, W. F. (2000). "Practical Analysis for Semi-Rigid Frame Design." Singapore, World Scientific.
- Chen, W. F. (2000). "Structural Stability: From Theory to Practice." *Engineering Structures* **22**(2): 116-122.
- Chen, W. F. and S. E. Kim (1997). "LRFD Steel Design Using Advanced Analysis." CRC Press, Boca Raton, Florida.
- Chen, W. F. and S. E. Kim (1997). "LRFD steel design using advanced analysis." Florida, CRC Press: Boca Raton.
- Chen, W. F., S. E. Kim and S. H. Choi (2001). "Practical second-order inelastic analysis for threedimensional steel frames." *Steel Structures* **1**: 213–223.
- Chen, W. F. and I. Sohal (1995). "Plastic design and second-order analysis of steel frames." New York, Springer-Verlag.
- Chen, W. F. and S. Toma (1994). "Advanced Analysis of Steel Frames : Theory, Software, and Applications." Boca Raton, Florida, CRC Press.
- Chu, K. H. and R. H. Rampetsreiter (1972). "Large deflection buckling of space frames." *Journal of the Structural Division, ASCE* **98**(12): 2701–2722.
- Clarke, M. J., R. Q. Bridge, G. J. Hancock and N. S. Trahair (1992). "Advanced analysis of steel building frames." *Journal of Constructional Steel Research* **23**(1-3): 1-29.
- Crisfield, M. A. (1981). "A fast incremental/iterative solution procedure that handles snap-through." *Computer and Structures* **13**(1): 55–62.
- Dai, H. Z. and W. Wang (2009). "Application of low-discrepancy sampling method in structural reliability analysis." *Jornal of Structural Safety* **31**: 55-64.
- Deierlein, G. G., Y. Zhao and W. McGuire (1991). "A discrete model for gradual plastification and nonlinear connection response in three-dimensional framed structures." Lehigh University, Bethlehem, Annual Technical Session Proceeding, SSRC: 423-432.
- Dibley, J. and J. S. Sowter (1967). "Tests on laterally unsupported beams of steel to BS 15." BISRA Open Report No. FE/E/31.
- DIN18800-2 (1990). *Stahlbauten, Stabilitätsfälle, Knicken von Stäben und Stabwerken.*
- Dinno, K. S. and S. S. Gill (1964). "The plastic torsion of I-sections with warping restraint." *International Journal of Mechanical Sciences* **6** (1): 27-43.
- Dinno, K. S. and W. Merchant (1965). "A procedure for calculating the plastic collapse of I-sections under bending and torsion." *Journal of Structural Engineering* **43** 219-221.
- Dux, P. F. and S. Kitipornchai (1983). "Inelastic beam buckling experiments." *Journal of Construction Steel Research* **3**(1).

- ECCS (1976). "ECCS Manual on the Stability of Steel Structures." 2nd ed., European Convention for Constructional Steelwork, Brussels, Belgium.
- ECCS (1984). "Ultimate limit state calculation of sway frames with rigid joints." European Convention for Constructional Steelwork, Technical Committee 8 – Structural Stability Technical Working Group 8.2 – System Publication No. 33.
- ECCS (1991). "Essentials of Eurocode 3 design manual for steel structures in building." ECCS Advisory Committee 5 (no. 65).
- El-Zanaty, M., D. W. Murray and R. Bjorhovde (1980). "Inelastic behaviour of multi-storey frames." Edmonton, Alberta, Canada, University of Alberta, **No.83**.
- Ellingwood, B. and T. V. Galambos (1982). "Probability-based criteria for structural design." *Journal of Structural Safety* **1**: 15-26.
- Ellingwood, B. R. (1994). "Probability-based codified design: past accomplishments and future challenges." *Structural Safety* **13**: 159-176.
- Ellingwood, B. R. (1996). "Reliability-based condition assessment and LRFD for existing structures " *Structural Safety* **18**(2/3): 67-80.
- Ellingwood, B. R. (2000). "LRFD: implementing structural reliability in professional practice." *Journal of Engineering Structures* **22**: 106-115.
- Ellingwood, B. R. and T. V. Galambos (1982). "Probability-based criteria for structural design." *Journal of Structural Safety* **1**(1): 15-26.
- Ellingwood, B. R., T. V. Galambos, J. G. MacGregor and C. A. Cornell (1980). "Development of a probability based load criterion for American National Standard A58—Building code requirements for minimum design loads in buildings and other structures. " Washington, D.C., National Bureau of Standards.
- Ellingwood, B. R., T. V. Galambos, J. G. MacGregor and C. A. Cornell (1982). "Probability-based load criteria: load factors and load combinations." *Journal of Structural Division, ASCE* **108**(5): 978–997.
- Epstein, M. and D. W. Murray (1976). "Three-dimensional large deformation analysis of thin walled beams." *International Journal of Solids and Structures* **12**(12): 867-876.
- Ettouney, M. M. and J. B. Kirby (1981). "Warping restraint in three-dimensional frames." *Journal of the Structural Division, ASCE* **107**(ST8): 1643–1656.
- Eurocode3 (2003). "Design of Steel Structure, Part 1-1 : General Rules and Rules for Buildings Commission of European Communities." Brussels.
- Eurocode3 (2005). "EN 1993 : Design of Steel Structures." European Committee for Standardization, Brussels.
- Fafard, M. and B. Massicotte (1993). "Geometrical interpretation of the arc-length method." *Computer and Structures* **46**(4): 603-615.
- Fang, Y. and T. Pekoz (2001). "Design of cold-formed steel plain channels." School of Civil and Environmental Engineering Report, Cornell University.
- Frangopol, D. M. and F. Moses (1994). Reliability-based structural optimization. *Advances in Design Optimization*. Chapman-Hall, London: 492–570.
- Fraser, W. B. and B. Budiansky (1969). "The Buckling of a Column with Random Initial Deflections." *Journal of Applied Mechanics, ASME* **36**(2): 233-240.
- Fukumoto, Y. and Y. Itoh (1980). "Strength variation of laterally unsupported beams." *Journal of the Structural Division, ASCE* **106**(ST1): 165-181.
- Fukumoto, Y. and Y. Itoh (1983). "Evaluation of multiple column curves using the experimental data-base approach." *Journal of Constructional Steel Research* **3**(3): 2-19.
- Galambos, T. V. (1990). "System reliability and structural design " *Journal of Structural Safety* **7**(2-4): 101-108.

- Galambos, T. V. (1990). "System reliability and structural design." *Structural Safety*, Elsevier **7**: 101-108.
- Galambos, T. V., B. R. Ellingwood, J. G. MacGregor and C. A. Cornell (1982). "Probability Based Load Criteria : Assessment of Current Design Practice." *Journal of Structural Division, ASCE* **108**(5): 959-977.
- Galambos, T. V. and R. L. Ketter (1959). "Columns under combined bending and thrust." *Journal of Engineering Mechanics Division, ASCE* **85**: 1-30.
- Galambos, T. V. and M. K. Ravindra (1978). "Properties of steel for use in LRFD." *Journal of the Structural Division, ASCE* **104**(9): 1459-1468.
- GB50205 (2001). "Code for Acceptance of Construction Quality of Steel structures." China Planning Press, China (in Chinese).
- Gozum, A. T. and A. W. Huber (1955). "Material properties, residual stresses and column strength." Fritz Engineering Laboratory, Report No.220 A.14, Lehigh University, Bethlehem, Pennsylvania.
- Gu, J. X. and S. L. Chan (2005). "Second-order analysis and design of steel structures allowing for member and frame imperfections." *International Journal for Numerical Methods in Engineering* **62**(5): 601-615.
- Hadianfard, M. A. and R. Razani (2001). "Effects of semi-rigid behavior of connections in the reliability of steel frames." *Structural Safety* **25**: 123-138.
- Hajjar, J. F. (1997). "Effective length and notional load approaches for assessing frame stability: Implications for American steel." Technical report, Task Committee on Effective Length of the Technical Committee on Load and Resistance Factor Design of the Technical Division of the Structural Engineering Institute of the American Society of Civil Engineers, Reston.
- Haldar, A. and S. Mahadevan (2000). "Probability, Reliability, and Statistical Method in Engineering Design." New York, John Wiley & Sons.
- Han, T. Y. and J. F. Abel (1984). "Substructure condensation using modified decomposition." *International Journal for Numerical Methods in Engineering* **20**: 1959-1964.
- Hartmann, A. J. and W. H. Munse (1966). "Flexural-torsional buckling of planar frames." *Journal of the Structural Division, ASCE* **92**(EM2): 37-59.
- Hasofer, A. M. and N. C. Lind (1974). "Exact and invariant second-moment code format." *Journal of Engineering Mechanics Division, ASCE* **100**: 111-121.
- Heyman, J. (1971). "Plastic Design of Frames -2. Applications" Cambridge University Press.
- HKC (2005). "Code of Practice for the Structural Use of steel" Building Department, The Government of the Hong Kong Special Administrative Region.
- Horne, M. (1985). "Frame Instability and the Plastic Design of Rigid Frames." *Steel Framed Structures - Stability and Strength*. R. Narayanan. London, Elsevier Applied Science: 1-29.
- Huber, A. W. and L. S. Beedle (1954). "Residual stress and the compressive strength of steel." *Welding Journal Research Supplement* **33**(12): 589-615.
- Huber, A. W. and R. L. Ketter (1952). "Experimental results of the influence of residual stress on column strength." Fritz Engineering Laboratory, Report No.220A.6, Lehigh University, Bethlehem, Pennsylvania.
- Iman, R. L. and W. J. Conover (1982). "A distribution-free approach to inducing rank correlation among input variables, Communications in Statistics Part B." *Simulation and Computation* **11**(3): 311-334.
- Itoh, Y. (1984). "Ultimate Strength Variations of Structural Steel Members." PhD Thesis, Nagoya, Nagoya University.

- Jez-Gala, C. (1962). "Residual stresses in rolled I-sections." *Proceedings of the Institution of Civil Engineering* **23**(3): 361-378.
- Jiang, X. M., H. Chen and J. Y. R. Liew (2002). "Spread-of-plasticity analysis of three-dimensional steel frames." *Journal of Constructional Steel Research* **58**(2): 193-212.
- Kala, Z. (2003). "The influence of initial curvature of the axis upon the member ultimate strength." *Journal of Structural Mechanics* **36**(1): 3-14.
- Kala, Z. (2005). "Fuzzy Sets Theory in Comparison with Stochastic Methods to Analyse Nonlinear Behaviour of a Steel Member under Compression." *Journal Nonlinear Analysis: Modelling and Control* **10**(1): 65-75.
- Kala, Z. (2007). "Fuzzy-Random Analysis of Steel Structures." *Engineering Mechanics* **14**(1): 199-210.
- Kala, Z. (2007). "Fuzzy Probability Methods in Applications to Reliability Analysis of Eurocode Rules for Steel Structure Design." *Engineering Mechanics* **14**(5): 359-370.
- Kala, Z. (2007). "Stability problems of steel structures in the presence of stochastic and fuzzy uncertainty." *Thin-Walled Structures* **45**(10-11): 861-865.
- Kala, Z. (2009). "Sensitivity assessment of steel members under compression." *Engineering Structures* **31**(6): 1344-1348.
- Kala, Z. (2011). "Sensitivity analysis of steel plane frames with initial imperfections." *Engineering Structures* **33**: 2342-2349.
- Kala, Z. and J. Kala (2003). "The Statistical Correlation of Material Characteristics—Experimental and Theoretical Results of Hot-Rolled Steel Beam." *International Conference on Metal Structures, Miskolc, Hungary*.
- Kanchanalai, T. (1977). "The design and behaviour of beam-columns in unbraced steel frames" *Civil Engineering/Structures Research Lab, University of Texas, Austin*.
- Kao, R. (1974). "A comparison of Newton- Raphson methods and incremental procedures for geometrically nonlinear analysis." *Computers and Structures* **4**: 1091-1097.
- Ketter, R. L. (1958). "the influence of residual stresses on the strength of structural members." *Welding Research Council Bulletin* **44**.
- Kim, S. E. (1996). "Practical Advanced Analysis for Steel Frame Design." Ph.D. Thesis, Purdue University, West Lafayette, IN.
- Kim, S. E. and W. F. Chen (1996). "Practical Advanced Analysis for Braced Steel Frame Design." *Journal of Structural Engineering, ASCE* **122**(11): 1266-1274.
- Kim, S. E. and W. F. Chen (1996). "Practical Advanced Analysis for Unbraced Steel Frame Design." *Journal of Structural Engineering, ASCE* **122**(11): 1259-1265.
- Kim, S. E. and W. F. Chen (1999). *An Innovative Design For Steel Frame Using Advanced Analysis*. Boca Raton, CRC Press.
- Kim, S. E., Y. Kim and S. H. Choi (2001). "Nonlinear analysis of 3-D steel frames." *Thin-Walled Structures* **39**(6): 445-461.
- Kim, S. E. and D. H. Lee (2002). "Second-order distributed plasticity analysis of space steel frames." *Engineering Structures* **24**: 735–744.
- Kim, S. E., J. S. Lee, S. H. Choi and C. S. Kim (2004). "Practical second-order inelastic analysis for steel frames subjected to distributed load." *Engineering structures* **26**: 51-61.
- Kim, S. E., C. M. Uang and S. H. Choi and K. Y. An (2006). "Practical advanced analysis of steel frames considering lateral-torsional buckling." *Thin-Walled Structures* **44** 709–720.
- King, W. S. and W. F. Chen (1994). "Practical second-order inelastic analysis of semirigid frames." *Journal of Structural Engineering, ASCE* **120**(7): 2156-2175.

- King, W. S., D. W. White and W. F. Chen (1992). "Second-Order Inelastic Analysis Methods for Steel Frame Design." *Journal of Structural Engineering*, ASCE **118**(2): 408-428.
- Kitipornchai, S. (1973). "Stability of steel structures." PhD Thesis, the University of Sydney
- Kitipornchai, S. and N. S. Trahair (1971). "Elastic lateral buckling of stepped I-Beams." *Journal of the Structural Division*, ASCE **97**(10): 2535-2548.
- Koiter, W. T. (1945). "On the Stability of Elastic Equilibrium." Thesis, Polytechnic Institute Delft, NASA TTF-10833.
- Kounadis, A. N. and A. F. Economou (1984). "The Effects of Initial Curvature and Other Parameters on the Nonlinear Buckling of Simple Frames." *Journal of Structural Mechanics* **12**(1): 27-42.
- Krahula, J. L. (1967). "Analysis of bent and twisted bars using the finite element method." *AIAA Jnl* **5**: 1194-1197.
- Krajcinovic, D. (1969). "A consistent discrete elements technique for thin-walled assemblages." *International Journal of Solids and Structures* **5**(7): 639-662.
- Krenk, S. and L. Damkilde (1991). "Warping of joints in I-beam assemblages." *Journal of Engineering Mechanics Division* **117**(11): 2457-2474.
- Krishnaiah, P. R. (1981). *Analysis of Variance*, Elsevier Science & Technology Books.
- Ku, C. K. and L. Tall (1966). "A Pilot Study on the Strength of 5Ni-Cr-Mo-V Steel Columns." Fritz Engineering Laboratory Report, No. 290.12, Lehigh University, Bethlehem, Pennsylvania.
- Lay, M. G. and R. Ward (1969). "Residual stresses in steel structures." *Journal of Australian Institute of Steel Construction* **3**: 2-21.
- Li, J. J. and G. Q. Li (2004). "Reliability-based integrated design of steel portal frames with tapered members." *Journal of Structural Safety* **26**(2): 221-239.
- Li, Y. and E. M. Lui (1995). "A simplified plastic zone method for frame analysis." *Microcomputers in Civil Engineering* **10**: 51-62.
- Liew, J. Y. R. (1992). "Advanced analysis for frame design" PhD thesis, Purdue University, West Lafayette.
- Liew, J. Y. R., H. Chen, N. E. Shanmugam and W. F. Chen (2000). "Improved nonlinear plastic hinge analysis of space frame structures." *Engineering Structures* **22**(10): 1324-1338.
- Liew, J. Y. R. and L. K. Tang (1998). "Nonlinear Refined Plastic Hinge analysis of Space Frame Structures" Report No. CE 027/98, School of Civil Engineering, National University of Singapore.
- Liew, J. Y. R., D. W. White and W. F. Chen (1993a). "Second-Order Refined Plastic Hinge Analysis for Frame Design: Part 1." *Journal of Structural Engineering*, ASCE **119**(11): 3196-3216.
- Liew, J. Y. R., D. W. White and W. F. Chen (1994). "Notional-load plastic-hinge method for frame design." *Journal of Structural Engineering*, ASCE **120**(5): 1434-1454.
- Lim, L. C. and L. W. Lu (1970). "Behavior of structural subassemblages with laterally unsupported columns." Fritz Engineering Laboratory, Report No.329.3, Lehigh University, Bethlehem, Pennsylvania.
- Lindner, J. (1984). "Ungewollte Schiefstellungen von Stahlstützen (Unavoidable Out-of-plumb of Steel Columns)." 12th IABSE Congress, Vancouver, BC: 669-676 (in German).
- Lindner, J. (1984). "Ungewollte Schiefstellungen von Stahlstützen (Unavoidable out-of-plumb of steel columns) (in German)." *Schlussbericht zum 12. IVBH Kongreß Vancouver, Zürich*.

- Lindner, J. and R. Gietzelt (1983 ). "Imperfektionen mehrgeschossiger Stahlstützen (Stützenschiefstellungen). (imperfections for multistorey steel columns – out-of-plumb) (in German)." Schlussbericht zum Forschungsvorhaben IV/1-81/299 des Instituts für Bautechnik Berlin, Institut für Baukonstruktionen und Festigkeit, internal report, TU Berlin.
- Lindner, J. and R. Gietzelt (1984). "Imperfektionsannahmen für Stützenschiefstellungen (assumptions for imperfections for out-of-plumb of columns) (in German)." Stahlbau 53 , Heft 4: 97-102.
- Lui, E. M. and W. F. Chen (1988). "Behavior of braced and unbraced semi-rigid frames " Journal of Solids Structures **24**(9): 893-913.
- LUSAS (1998). "LUSAS." User manual version 12.2, FEA Ltd., UK.
- Mahendran, M. (2007). Applications of Finite Element Analysis in Structural Engineering. Proceedings International Conference on Computer Aided Engineering, Chennai, India.
- Marek, P. and V. Křivý (2006) "Probabilistic reliability assessment of a steel frame applying the SBRA method." 3rd ASRANet International Colloquium Glasgow, U.K.: 10-12.
- Marek, P. and V. Křivý (2010). "How to Assess the Safety of a Steel Frame Using Probabilistic SBRA Method." Mechanical Structures and Foundation Engineering, International Scientific Conference MSFE, Ostrava.
- Mas, E. and C. Massonet (1966). "European column research." Acier-Stahl-Steel: 385.
- Masarira, A. (2002). "The effect of joints on the stability behaviour of steel frame beams." Journal of Constructional Steel Research **58**(10): 1375-1390.
- McGuire, W., R. H. Gallagher and R. D. Ziemian (2000). "Matrix structural analysis." Wiley, 2nd Ed., New York.
- McKay, M. D., W. J. Conover and R. J. Beckman (1979). "A comparison of three methods for selecting values of input variables in the analysis of output from a computer code." Technometrics **21**(2): 239-245.
- Melcher, J., Z. Kala, M. Holicky, M. Fajkus and L. Rozlivka (2004). "Design characteristics of structural steels based on statistical analysis of metallurgical products." Journal of Constructional Steel Research **60**: 795-808.
- Melchers, R. E. (1999). Structural reliability analysis and prediction. West Sussex, England, John Wiley & Sons.
- Microstran (2004). Version 8.0, Engineering Systems Pty Ltd, New South Wales, Australia.
- Morrell, P. J. B., J. R. Riddington F. A. Ali and H. A. Hamid (1996). "Influence of joint detail on the flexural/torsional interaction of thin-walled structures." Thin-Walled Structures **24**(2): 97-111.
- NAF-NIDA (2001). "Software for nonlinear integrated design and analysis for framed structures, User's manual, Department of Civil and Structural Engineering, Hong Kong Polytechnic University."
- NASTRAN, P. (1998). "Reference Manual, Version 2001, MSC Software, Los Angeles, USA."
- Nethercot, D. A. (2000). "Frame Structures: Global Performance, Static and Stability Behaviour - General Report." Journal of Constructional Steel Research **55**(1-3): 109-124.
- Nishino, F. and L. Tall (1970). "Experimental investigation of the strength of T-1 steel columns." Fritz Engineering Laboratory Report, No. 290.9, Lehigh University ,Bethlehem, Pennsylvania.
- Nowak, A. S. and K. R. Collins (2000). "Reliability of Structures." McGraw-Hill, Boston.

- Ofner, R. (2003). "Buckling check of members and frame based on numerical simulations".
- Ojalvo, M. and R. S. Chambers (1977). "Effect of warping restraints on I-beam buckling." *Journal of the Structural Division, ASCE* **103** (ST12): 2351–2360.
- Olsson, A. M. J. and G. E. Sandberg (2002). "On Latin hypercube sampling for stochastic finite element analysis." *Journal of Engineering Mechanics* **128**(1): 121–125.
- Omishore, A. (2010). "Sensitivity analysis of structures, problems and applications." in *Proceeding of the 6th WSEAS International Conference on Applied and Theoretical Mechanics (MECHANICS '10)*, Athens (Greece): 120-125.
- Omishore, A. and Z. Kala (2009). "Reliability Analysis of Steel Structures with Imperfections." *Nordic Steel Construction Conference*. Malmo, Švédsko: 540-545.
- Orbiso, J. G. (1982). "Nonlinear Static Analysis of Three-Dimensional Steel Frames." PhD thesis, Ithaca, New York, Cornell University.
- Papadrakakis, M. and V. Papadopoulos (1995). "A computationally efficient method for the limit elasto plastic analysis of space frames." *Journal of Computational Mechanics* **16**(2): 132–141.
- Pebesma, E. J. and G. B. M. Heuvelink (1999). "Latin hypercube sampling of Gaussian random fields." *Technometrics* **41**(4): 303-312.
- Rackwitz, R. and B. Fiessler (1978). "Structural reliability under combined load sequence." *Computers & Structures* **9**(5): 489–494.
- Rajasekaran, S. and D. W. Murray (1973). "Finite element solutions of inelastic beam equations." *Journal of the Structural Division, ASCE* **99**(12): 2423-2438.
- Rasmussen, K. J. R. and G. J. Hancock (1988). "Geometric imperfections in plated structures subject to interaction between buckling modes." *Thin-walled Structures* **6**: 433-452.
- Raviprakash, A. V., B. Prabu and N. Alagumurthi (2010). "Mean value first order second moment analysis of buckling of axially loaded thin plates with random geometrical imperfections." *International Journal of Engineering, Science and Technology* **2**(4): 150-162.
- Razzaq, Z. and T. V. Galambos (1979). "Biaxial bending of beams with or without torsion." *Journal of the Structural Division, ASCE* **105** (ST11): 2145-2162.
- Renton, J. D. (1962). "Stability of space frames by computer." *Journal of the Structural Division, ASCE* **88** (ST4): 81–103.
- Renton, J. D. (1974). *On the transmission of non-uniform torsion through joints*. Oxford University, Department of Engineering Science.
- Riks, E. (1979). "An incremental approach to the solution of snapping and buckling problems." *International Journal of Solids and Structures* **15**: 529-551.
- Roorda, J. (1974). "The Random Nature of Column Failure." *Journal of Structural Mechanics*.
- Rossow, E. C., G. B. Barney and S. L. Lee (1967). "Eccentrically Loaded Steel Columns with Initial Curvatures." *Journal of the Structural Division, ASCE* **93**(ST2): 339-358.
- Sabir, B. and A. C. Lock (1972). *The Application of Finite Elements to the Large-deflection Geometrically Nonlinear Behavior of Cylindrical Shells*. Proceedings of International Conference on Variational Mechanics. Southampton University, Session VII.
- Sfintesco, D. (1970). "Fondement experimental des courbes Europeennes de flambement (in French)." *Journal of Construction Métallique*(3): 5-12.



- Sharman, P. G. (1985). "Analysis of structures with thin-walled open sections." *International Journal of Mechanical Sciences* **27**(10): 665–667.
- Shayan, S., K. J. R. Rasmussen and H. Zhang (2012). "On the modelling of geometric imperfections of steel structural members and frames." *The Seventh International Conference on Advances in Steel Structures (ICASS)*. China, Nanjing.
- Shayan, S., K. J. R. Rasmussen and H. Zhang (2014). "System-based design provisions for 2D steel frames by advanced analysis." *Research Report*, The University of Sydney, Sydney, Australia.
- Sheninger, E. L. and L. W. Lu (1968). "Experiments on non-sway structural subassemblages." *Fritz Engineering Laboratory, Report No. 273.62*, Lehigh University, Bethlehem, Pennsylvania.
- Sivakumar Babu, G. L. and B. M. Basha (2008). "Optimum design of cantilever retaining walls using target reliability approach." *International Journal of Geomechanics* **8**(4): 240-252.
- Smith-Pardo, J. P. and J. D. Aristizábal-Ochoa (1999). "Buckling Reversals of Axially Restrained Imperfect Beam-Column." *Journal of Engineering Mechanics* **125**(4): 401-409.
- Sobol, I. M. (1993). "Sensitivity estimates for nonlinear mathematical models." *Mathematical Modeling and Computational Experiment* **1**(4): 407-414.
- Sohal, I. S., L. Duan and W. F. Chen (1989). "Design interaction equations for steel members." *Journal of Structural Engineering, ASCE* **15**(7): 1650-1665.
- Sousaa, C. A. G. and P. M. Pimentab (2010). "A new parameter to arc-length method in nonlinear structural analysis." *Mecánica Computacion*: 1841-1848.
- Strand7 (2009). "Strand 7 release 2.4.1 manual " Strand 7 Pty. Ltd.
- Strating, J. and H. Vos (1973). "Computer simulation of the E.C.C.S. buckling curves using a Monte-Carlo method." *HERON* **19**(2).
- Strating, J. and H. Vos (1973). "Computer Simulation of the ECCS Buckling Curve Using a Monte-Carlo Method." *Heron* **19**(2).
- Surovek-Maleck, A. E. and D. W. White (2004). "Alternative Approaches for Elastic Analysis and Design of Steel Frames. I: Overview." *Journal of Structural Engineering, ASCE* **130**(8): 1186-1196.
- Surovek, A. E. (ed.) (2012), "Guidelines for the use of Direct Second-Order Inelastic Analysis in Steel Frame Design", Report of the Special Project Committee on Advanced Analysis, Technical Committee on Compression and Flexural Members of the Structural Engineering Institute of ASCE, Reston, VA.
- Szalai, J. and F. Papp (2005). "A new residual stress distribution for hot-rolled I-shaped sections." *Journal of Constructional Steel Research* **61**: 845–861.
- Tall, L. (1964). "Recent developments in study of column behaviour." *Journal of the Institute of Engineers Australia* **36**(12).
- Tebedge, N., W. F. Chen and L. Tall (1972). "Experimental Studies on Column Strength of European Heavy Shapes " *Fritz Engineering Laboratory Report, No. 351.7*, Lehigh University, Bethlehem, Pennsylvania.
- Tebedge, N., P. Marek and L. Tall (1969). "Column Testing Procedure." *Fritz Engineering Laboratory Report, No. 351.1*, Lehigh University, Bethlehem, Pennsylvania.
- Tebedge, N. and L. Tall (1973). "Linear stability analysis of beam- columns." *Journal of the Structural Division, ASCE*, **99** (ST12): 24-39.
- Teng, J. G. and Y. F. Luo (1998). "A user-controlled arc-length method for convergence to predefined deformation states." *Communications in Numerical Methods in Engineering* **51**(1): 51–58.

- Timoshenko, S. P. (1905). Bull. Polyt. Inst. St. Petersburg.
- Timoshenko, S. P. and J. M. Gere (1961). Theory of Elastic Stability. New York, McGraw-Hill.
- Toma, S. and W. F. Chen (1992). "European calibration frames for second-order inelastic analysis." *Engineering Structures* **14**(1): 7-14.
- Toma, S. and W. F. Chen (1994). "Calibration Frames for Second-Order Inelastic Analysis in Japan." *Journal of Constructional Steel Research* **28** 51-77.
- Toma, S., W. F. Chen and D. W. White (1993). "A selection of calibration frames in North America for second-order inelastic analysis." *Engineering Structures* **17**(2): 104-112.
- Tomonaga, K. (1971). "Actually Measured Errors in Fabrication of Kasumigaseki Building." 3rd Regional Conference Proceedings, Tokyo, Japan.
- Tong, G. S., X. X. Yan and L. Zhang (2005). "Warping and bimoment transmission through diagonally stiffened beam-to-column joints." *Journal of Constructional Steel Research* **61**(6): 749-763.
- Trahair, N. S. (1966). "Elastic stability of I-beam elements in rigid-jointed structures." *Journal of the Institution of Engineers* **38**: 171-180.
- Trahair, N. S. (1968). "Elastic stability of propped cantilevers." *Institution of Engineers, Australia, Civil Engineering Transactions* **CE10**(1): 94-100.
- Trahair, N. S. (1969). "Elastic Stability of continuous beams." *Journal of the Structural Division, ASCE* **101**(7): 1497-1516.
- Turkstra, C. J. and H. O. Madsen (1980). "Load combinations in codified structural design." *Journal of Structural Division, ASCE* **106**(ST12): 2527-2543.
- Vacharajittiphan, P. and N. S. Trahair (1974). "Warping and distortion at I-section Joints." *Journal of the Structural Division, ASCE* **100**(ST3): 547-564.
- Vacharajittiphan, P. and N. S. Trahair (1975). "Analysis of lateral buckling in plane frames." *Journal of the Structural Division, ASCE* **101**(7): 1497-1516.
- Vlasov, V. Z. (1939). "Twisting, stability and vibrations of thin-walled members." *Journal of Applied Mathematics and Mechanics* **3**(1).
- Vlasov, V. Z. (1961). "Thin-walled elastic beams." Israel Program for Scientific Translations, Ltd, Jerusalem, Israel.
- Vogel, U. (1985). "Calibrating frames." *Stahlbau* **54**: 295-311.
- Wagner, H. (1936). "Torsion and Buckling of Open Sections." 25th Anniversary Publication, Technische Hochschule, Danzig: 1904-1929.
- Ward, R. F. (1966). "Internal stresses and notch ductility determination of Group 1 commissioned universal sections." BHP Co. Ltd. Report No. QR14.
- Ward, R. F. (1967). "Comparison of BHP manufactured universal sections with competitors." BHP Co. Ltd. Report No. QR20.
- Wempner, G. A. (1971). "Discrete approximation related to nonlinear theories of solids." *International Journal of Solids and Structures* **7**: 1581-1599.
- White, D. W. (1985). "Material and geometric nonlinear analysis of local planar behavior in steel frames using iterative computer graphics." M.S. Thesis, Cornell University, Ithaca, NY.
- White, D. W. and W. F. Chen (1993). "Plastic hinge based methods for advanced analysis and design of steel frames-an assessment of the state of the art" Structural Stability Research Council.
- White, D. W., J. Y. R. Liew and W. F. Chen (1991a). second-order inelastic analysis for frame design: a report to SSRC task group 29 on recent research and perceived state-of-the-art. West Lafayette, Purdue University: 116.

- White, D. W., A. E. Surovek, B. N. Alemdar, C. J. Chang and Y. D. Kim (2006). "Stability Analysis and Design of Steel Building Frames Using the 2005 AISC Specification." *International Journal of Steel Structures*, KSSC: 71-91.
- Wong, M. B. and E. Tin-Loi (1990). "Geometrically Nonlinear Analysis of Elastic Framed Structures." *Computers & Structures* **34**(4): 633-640.
- Xu, L. and X. H. Wang (2008). "Storey-based column effective length factors with accounting for initial geometric imperfections." *Engineering Structures* **30**(12): 3434-3444.
- Yang, Y. B. and W. McGuire (1984). "A procedure for analysing space frames with partial warping restraint." *International Journal for Numerical Methods in Engineering* **20**: 1377-1390.
- Yoo, C. H. (1980). "Bimoment contribution to stability of thin-walled assemblages." *Computers & Structures* **11**(5): 465-471.
- Young, B. W. (1975). "Residual stresses in hot rolled members." *IABSE Reports of the Working Commissions* **23**: 25-38.
- Yuan, Z. (2004). "Advanced Analysis of Steel Frame Structures Subjected to Lateral Torsional Buckling Effects" PhD thesis, Queensland University of Technology.
- Zeinoddini, V. M. and B. W. Schafer (2011). "Global Imperfections and Dimensional Variations in Cold-Formed Steel Members." *Journal of Structural Stability and Dynamics* **11**(5): 829-854.
- Zeinoddini, V. M. and B. W. Schafer (2012). "Simulation of geometric imperfections in cold-formed steel members using spectral representation approach." *Thin-Walled Structures* **60**: 105-117.
- Zhang, L., W. H. Tang and C. W. W. Ng (2001). "Reliability of axially loaded driven pile groups." *Journal of Geotechnical and Geo-Environmental Engineering* **127**(12): 1051-1060.
- Zhang, Y., L. Jin, Y. Shao and J. Zhao (2010). "Practical advanced design considering random distribution of initial geometric imperfections." *Advances in Structural Engineering* **14**(3): 379-389.
- Zhang, Y., J. Zhao and W. Zhang (2008). "Parametric Studies on Inter-Column Brace Forces." *Advances in Structural Engineering* **11**(3): 293-303.
- Ziemian, R. D. (1990). "Advanced methods of inelastic analysis in the limit states design of steel structures." PhD thesis, Cornell University.
- Ziemian, R.D. and A. R. Miller (1997). "Inelastic Analysis and Design: Frames with Members in Minor-Axis Bending." *Journal of Structural Engineering*, ASCE, **123** (2): 151-157.
- Ziemian, R. D. and W. McGuire (2002). "Modified tangent modulus approach, a contribution to plastic hinge analysis." *Journal of Structural Engineering*, ASCE **128**(10): 1301-1307.
- Ziemian, R. D., W. McGuire and G. G. Deierlein (1992a). "Inelastic limit states design: part I, planar frame studies." *Journal of Structural Engineering*, ASCE **118**(9): 2532-2549.
- Ziemian, R. D., W. McGuire and G. G. Deierlein (1992b). "Inelastic limit states design: Part II, Three-dimensional frame study." *Journal of Structural Engineering*, ASCE **118**(9): 2550-2568.
- Zienkiewicz, O. C. (1971). "Incremental Displacement in Non-linear Analysis." *International Journal for Numerical Methods in Engineering* **3**: 587-588.

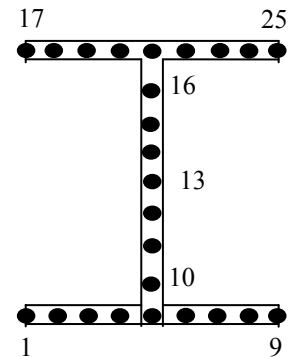
# Appendix A. Residual stress subroutine

---

```

SUBROUTINE SIGINI (SIGMA, COORDS, NTENS, NCRDS, NOEL, NPT, LAYER,
1 KSPT, LREBAR, NAMES)
C
INCLUDE 'ABA_PARAM.INC'
C
REAL FY
DIMENSION SIGMA (NTENS), COORDS (NCRDS)
CHARACTER NAMES (2) * 80
C RESIDUAL STRESS DISTRIBUTION
FY=320
FR=0.3*FY
IF (KSPT.LE.5) THEN
SIGMA (1)=-FR+FLOAT (KSPT-1) * (FR/2)
ENDIF
IF (KSPT.GT.5.AND.KSPT.LE.9) THEN
SIGMA (1)=FR-FLOAT (KSPT-5) * (FR/2)
ENDIF
IF (KSPT.GT.9.AND.KSPT.LE.13) THEN
SIGMA (1)=FR-FLOAT (KSPT-9) * (FR/2)
ENDIF
IF (KSPT.GT.13.AND.KSPT.LE.16) THEN
SIGMA (1)=-FR+FLOAT (KSPT-13) * (FR/2)
ENDIF
IF (KSPT.GE.17.AND.KSPT.LE.21) THEN
SIGMA (1)=-FR+FLOAT (KSPT-17) * (FR/2)
ENDIF
IF (KSPT.GT.21.AND.KSPT.LE.25) THEN
SIGMA (1)=FR-FLOAT (KSPT-5) * (FR/2)
ENDIF
C
RETURN
END

```



# Appendix

## B.

### Warping torsion

---

As it was mentioned in Chapter 4 currently ABAQUS/CAE pre-processing user interface does not support substructure modelling. It means that it is not possible to analyse the substructure directly in ABAQUS user interface and the analysis can be done only by creating a text file as an input file. Since it is difficult to form this text file manually every time when the dimensions change, a PERL script was made to do it automatically. The program in Section B.1 is an example for a corner box joint with diagonal stiffener using 150UB14 cross-section. It is obvious that this code can be modified easily to generate any other joint types. The ABAQUS input file (.inp file) generated from this script is presented in Section B.2. A sample ABAQUS input file of a frame using beam finite elements and consisting spring joint models is presented in Section B.3.

#### **B.1. Example of a PERL script for creating a shell finite element model of the corner box-stiffened joint shown in Figure 4-4**

```
#!/usr/local/bin/perl
open (MYFILE, '> diagonal_stiffener _150_ UB _14.txt');
# Define substructure element for box joint
# Element number for library
$ElemeNum = 200;
# Required inputs for "box" type joint
# Centre to centre depth of beam, thickness of horizontal plates
$depthb = 150 - 7;
$thik1 = 7;
# Centre to centre width of column, thickness of vertical plates
$depthc = 150 - 7;
$thik2 = 7;
# web thickness
$webt = 5;
# full width of joint
$width = 75;
```

```

# Width by number of elements
$nelem = 16;
# This part writes the substructure element(s)
print MYFILE"*HEADING\n This is a superstructure for a box type
joint\n";
# define geometry for joint
# The centre of the element is nominally at 0,0,0
$nelemup = int($depthb/$width * $nelem);
if (($nelemup % 2) == 1) {$nelemup++;}
$nelemfr = int($depthc/$width * $nelem);
if (($nelemfr % 2) == 1) {$nelemfr++;}
$nodenum = 1;
# Generate all nodes for joint
$dx = $depthc/$nelemfr;
$dy = $depthb/$nelemup;
$dz = $width/$nelem;
print MYFILE"*NODE\n";
for ($h=0; $h<=$nelemfr; $h++) {
  $x = ($h - $nelemfr/2)*$dx;
  for ($i=0; $i<=$nelemup; $i++) {
    $y = $dy*( $i - $nelemup/2);
    for ($j=0; $j<=$nelem; $j++) {
      $z = $dz*( $nelem/2 - $j);
      print MYFILE $nodenum,",", $x,",", $y,",", $z,"\n";
    }
  }
  # Flag corner nodes
  if ($h == 0) {
    if ((( $j==0) || ( $j == $nelem) ) && (( $i==0) || ( $i ==
      $nelemup))) {
      if (( $j==0) && ( $i==0)) {
        $nodea = $nodenum;
      } elsif (( $j==0) && ( $i==$nelemup)) {
        $nodec = $nodenum;
      } elsif (( $j==$nelem) && ( $i==0)) {
        $nodeb = $nodenum;
      } else {
        $noded = $nodenum;
      }
    }
  }
  } elsif ($h == $nelemfr) {
    if ((( $j==0) || ( $j == $nelem) ) && (( $i==0) || ( $i ==
      $nelemup))) {
      if (( $j==0) && ( $i==0)) {
        $nodee = $nodenum;
      } elsif (( $j==0) && ( $i==$nelemup)) {
        $nodeg = $nodenum;
      } elsif (( $j==$nelem) && ( $i==0)) {
        $nodef = $nodenum;
      } else {
        $nodeh = $nodenum;
      }
    }
  }
  } elsif (( $x == 0) && ( $y == 0) && ( $z == 0)) {
    $cntrnode = $nodenum;
  }
}
$nodenum++;

```

```

}
}
}
# Nodes for "back" plate
print MYFILE"*NSET, NSET=NODEA\n ".$nodea."\n";
print MYFILE"*NSET, NSET=NODEB\n ".$nodeb."\n";
print MYFILE"*NSET, NSET=NODEC\n ".$nodec."\n";
print MYFILE"*NSET, NSET=NODED\n ".$noded."\n";
print MYFILE"*NSET, NSET=FACEBA\n
" . (($nelemup/2)*($nelem+1)+$nelem/2+1) . "\n";
# Nodes for "front" plate
print MYFILE"*NSET, NSET=NODEE\n ".$nodee."\n";
print MYFILE"*NSET, NSET=NODEF\n ".$nodef."\n";
print MYFILE"*NSET, NSET=NODEG\n ".$nodeg."\n";
print MYFILE"*NSET, NSET=NODEH\n ".$nodeh."\n";
print MYFILE"*NSET, NSET=FACEFR\n
" . (($nelemup/2)*($nelem+1)+$nelem/2+1+($nelem+1)*($nelemup+1)*$nelemfr) . "\n";
print MYFILE"*NSET, NSET=FACETP\n
" . ($cntrnode+($nelemup/2)*($nelem+1)) . "\n";
print MYFILE"*NSET, NSET=FACEBO\n ".$cntrnode-
($nelemup/2)*($nelem+1) . "\n";
# Node for "centre"
print MYFILE"*NSET, NSET=CENTRE\n ".$cntrnode."\n";
# set up elements
print MYFILE"*ELEMENT, TYPE=S4R, ELSET=BACK\n";
$elem=1;
for ($n=0; $n<$nelemup; $n++) {
for ($m=1; $m<=$nelem; $m++) {
print
MYFILE $elem.", ".$n*($nelem+1)+$m.", ".$n*($nelem+1)+$m+1.", ".
(($n+1)*($nelem+1)+$m+1).", ".$n*($nelem+1)+$m)."\n";
$elem++;
}
}
print MYFILE "*ELEMENT, TYPE=S4R, ELSET=FRONT\n";
$offset = ($nelem+1)*($nelemup+1)*$nelemfr;
for ($n=0; $n<$nelemup; $n++) {
for ($m=1; $m<=$nelem; $m++) {
print MYFILE
$elem.", ".$n*($nelem+1)+$m+$offset.", ".$n*($nelem+1)+$m+1+$offset).", ".
(($n+1)*($nelem+1)+$m+1+$offset).", ".$n*($nelem+1)+$m
+$offset)."\n";
$elem++;
}
}
#
print MYFILE"*ELEMENT, TYPE=S4R, ELSET=TOP\n";
$offset = ($nelem+1)*($nelemup);
for ($n=0; $n<$nelemfr; $n++) {
for ($m=1; $m<=$nelem; $m++) {
print MYFILE $elem.", ".
($offset+$m+$n*($nelem+1)*($nelemup+1)).", ".
($offset+$m+1+$n*($nelem+1)*($nelemup+1)).", ".
($offset+$m+1+($n+1)*($nelem+1)*($nelemup+1)).", ".
($offset+$m+($n+1)*($nelem+1)*($nelemup+1))."\n";
}
}

```

```

$elem++;
}
}
print MYFILE"*ELEMENT, TYPE=S4R, ELSET=BOTTOM\n";
$offset = 0;
for ($n=0; $n<$nelemfr; $n++) {
for ($m=1; $m<=$nelem; $m++) {
print MYFILE $elem.",".
($offset+$m+$n*($nelem+1)*($nelemup+1)).",".
($offset+$m+1+$n*($nelem+1)*($nelemup+1)).",".
($offset+$m+1+($n+1)*($nelem+1)*($nelemup+1)).",".
($offset+$m+($n+1)*($nelem+1)*($nelemup+1))."\n";
$elem++;
}
}
print MYFILE"*ELEMENT, TYPE=S4R, ELSET=WEB\n";
$offset = int($nelem / 2)+1;
for ($n=0; $n<$nelemfr; $n++) {
for ($m=0; $m<$nelemup; $m++) {
print MYFILE$elem.",".
($offset + $m*($nelem+1) +
$n*($nelem+1)*($nelemup+1)).",".
($offset + ($m+1)*($nelem+1) +
$n*($nelem+1)*($nelemup+1)).",".
($offset + ($m+1)*($nelem+1) +
($n+1)*($nelem+1)*($nelemup+1)).",".
($offset + ($m)*($nelem+1) +
($n+1)*($nelem+1)*($nelemup+1))."\n";
$elem++;
}
}
print MYFILE"*ELEMENT, TYPE=S4R, ELSET=STIFFENER\n";
for ($n=$nelemup; $n>0; $n--) {
for ($m=1; $m<=$nelem; $m++) {
print MYFILE $elem.",".
($n*($nelem+1)+$m+($nelemup-$n)*($nelemup+1)*($nelem+1)).",".
($n*($nelem+1)+$m+1+($nelemup-$n)*($nelemup+1)*($nelem+1)).",".
(($n-1)*($nelem+1)+$m+1+($nelemup-$n+1)*($nelemup+1)*($nelem+1)).",".
(($n-1)*($nelem+1)+$m+($nelemup-$n+1)*($nelemup+1)*($nelem+1))."\n";
$elem++;
}
}
print MYFILE"*SHELL SECTION, ELSET=BACK, MATERIAL=STEEL1\n";
print MYFILE$thik2,"\n";
print MYFILE"*SHELL SECTION, ELSET=FRONT, MATERIAL=STEEL1\n";
print MYFILE$thik2,"\n";
print MYFILE"*SHELL SECTION, ELSET=TOP, MATERIAL=STEEL1\n";
print MYFILE$thik1,"\n";
print MYFILE"*SHELL SECTION, ELSET=BOTTOM, MATERIAL=STEEL1\n";
print MYFILE$thik1,"\n";
print MYFILE"*SHELL SECTION, ELSET=WEB, MATERIAL=STEEL1\n";
print MYFILE$webt,"\n";
print MYFILE"*SHELL SECTION, ELSET=STIFFENER, MATERIAL=STEEL1\n";
print MYFILE$thik2,"\n";
print MYFILE"*MATERIAL, NAME=STEEL1\n";

```



```
print MYFILE"*ELASTIC\n 200E3, 0.3\n";
print MYFILE"*DENSITY\n 7.7E-9\n";
# Constraints
print MYFILE"*EQUATION\n";
print MYFILE"* Back face\n";
print MYFILE"2\n";
print MYFILE"NODEC, 1, 1, NODEA, 1, 1\n";
print MYFILE"2\n";
print MYFILE"NODEA, 1, 1, NODEB, 1, 1\n";
print MYFILE"2\n";
print MYFILE"NODEB, 1, 1, NODED, 1, 1\n";
print MYFILE"* Front face\n";
print MYFILE"2\n";
print MYFILE"NODEG, 1, 1, NODEE, 1, 1\n";
print MYFILE"2\n";
print MYFILE"NODEE, 1, 1, NODEF, 1, 1\n";
print MYFILE"2\n";
print MYFILE"NODEF, 1, 1, NODEH, 1, 1\n";
print MYFILE"* Top face\n";
print MYFILE"2\n";
print MYFILE"NODEC, 2, 1, NODED, 2, 1\n";
print MYFILE"2\n";
print MYFILE"NODED, 2, 1, NODEH, 2, 1\n";
print MYFILE"2\n";
print MYFILE"NODEH, 2, 1, NODEG, 2, 1\n";
print MYFILE"* Bottom face\n";
print MYFILE"2\n";
print MYFILE"NODEA, 2, 1, NODEB, 2, 1\n";
print MYFILE"2\n";
print MYFILE"NODEB, 2, 1, NODEF, 2, 1\n";
print MYFILE"2\n";
print MYFILE"NODEF, 2, 1, NODEE, 2, 1\n";
# Generate element
print MYFILE"*STEP\n";
# Note that type is of format Zn where 0<n<10000
printf MYFILE"*SUBSTRUCTURE GENERATE, TYPE=Z%d, OVERWRITE,
RECOVERY
MATRIX=YES\n", $ElemeNum;
print MYFILE"*RETAINED NODAL DOFS, SORTED=NO\n";
# Lines to generate dof's - NodeNumber, dof_start, dof_end
print MYFILE" ".$nodeh.", ".1".\n";
print MYFILE" ".$nodee.", ".2".\n";
# End of definition
print MYFILE"*SUBSTRUCTURE MATRIX OUTPUT, OUTPUT FILE=USER DEFINED,
FILE NAME= UB_150_14_one_stiffener, STIFFNESS=YES\n";
print MYFILE"*END STEP\n";
close (MYFILE);
```

---

**B.2. An ABAQUS input file for analysing the joint shown in Figure 4-4 as a substructure**

```
*Heading
*Preprint, echo=NO, model=NO, history=NO, contact=NO
*Part, name=frame
*End Part
** ASSEMBLY
*Assembly, name=Assembly
*Instance, name=Part-1-1, part=Part-1
*Node
*Include,INPUT=Node.inp
*Element, type=B32OS
*Include,INPUT=Element.inp
** Section: Ub_150_14 Profile: UB_150_14
*Beam Section, elset=_PickedSet2, material=Material-1, temperature=GRADIENTS,
section=l
75., 150., 75., 75., 7., 7., 5.
0.,0.,-1.
*End Instance
*Element, type=CONN3D2
6, Part-1-1.4, Part-1-1.5
7, Part-1-1.7, Part-1-1.4
8, Part-1-1.8, Part-1-1.2
*Connector Section, elset=Wire-1-Set-1
Beam,
*Nset, nset=rp1
1,
*Nset, nset=rp2
2,
*Nset, nset=rp3
3,
*Nset, nset=rp4
4,
*Nset, nset=rp5
5,
*Nset, nset=rp6
6,
*Nset, nset=rp7
7,
*Nset, nset=base, instance=Part-1-1
1, 3
*Nset, nset=Wire-1-Set-1, instance=Part-1-1
2, 4, 5, 7, 8
*Nset, nset=end_beam, instance=Part-1-1
400
*Elset, elset=Wire-1-Set-1, generate
6, 8, 1
*Nset, nset=beam_left, instance=Part-1-1
8,
*Nset, nset=column_left, instance=Part-1-1
2,
*Nset, nset=mid_beam_right, instance=Part-1-1
```

```
5,
*Nset, nset=mid_beam_left, instance=Part-1-1
7,
*Nset, nset=mid_column, instance=Part-1-1
4,
** Constraint: Constraint-1
*Equation
3
rp2, 1, -1.
beam_left, 7, 1.
column_left, 7, 0.9057
** Constraint: Constraint-2
*Equation
3
rp1, 2, -1.
beam_left, 7, 0.9057
column_left, 7, 1.
** Constraint: Constraint-3
*Equation
4
rp6, 1, -1.
mid_beam_left, 7, 1.
mid_beam_right, 7, -0.37
mid_column, 7, 0.57
** Constraint: Constraint-4
*Equation
4
rp5, 1, -1.
mid_beam_left, 7, -0.37
mid_beam_right, 7, 1.
mid_column, 7, 0.57
** Constraint: Constraint-5
*Equation
4
rp4, 2, -1.
mid_beam_left, 7, 0.57
mid_beam_right, 7, 0.57
mid_column, 7, 1.188
*Element, type=Spring2, elset=kbb_left-spring
1, 3, 2
*Spring, elset=kbb_left-spring
1, 1
2.867e+12
*Element, type=Spring2, elset=kcc_left-spring
2, 3, 1
*Spring, elset=kcc_left-spring
2, 2
2.867e+12
*Element, type=Spring2, elset=mid_kb1-spring
3, 7, 5
*Spring, elset=mid_kb1-spring
1, 1
3.322e+12
*Element, type=Spring2, elset=mid_kb2-spring
4, 7, 6
```

```

*Spring, elset=mid_kb2-spring
1, 1
3.322e+12
*Element, type=Spring2, elset=mid_kc-spring
5, 7, 4
*Spring, elset=mid_kc-spring
2, 2
3.322e+12
*End Assembly
**
** MATERIALS
**
*Material, name=Material-1
*Elastic
200000., 0.3
*Plastic
320.,0.
** -----
** STEP: buckling
*Step, name=buckling, perturbation
*Buckle
3, , 6, 30
** BOUNDARY CONDITIONS
** Name: BC-1 Type: Displacement/Rotation
*Boundary, op=NEW, load case=1
base, 1, 1
base, 2, 2
base, 3, 3
base, 4, 4
base, 5, 5
base, 6, 6
*Boundary, op=NEW, load case=2
base, 1, 1
base, 2, 2
base, 3, 3
base, 4, 4
base, 5, 5
base, 6, 6
** Name: BC-2 Type: Displacement/Rotation
*Boundary, op=NEW, load case=1
column_left, 3, 3
*Boundary, op=NEW, load case=2
column_left, 3, 3
*Boundary, op=NEW, load case=1
mid_column, 3, 3
*Boundary, op=NEW, load case=2
mid_column, 3, 3
** Name: BC-3 Type: Displacement/Rotation
*Boundary, op=NEW, load case=1
rp3, 1, 1
rp3, 2, 2
rp3, 3, 3
*Boundary, op=NEW, load case=2
rp3, 1, 1
rp3, 2, 2

```

```
rp3, 3, 3
*Boundary, op=NEW, load case=1
rp7, 1, 1
rp7, 2, 2
rp7, 3, 3
*Boundary, op=NEW, load case=2
rp7, 1, 1
rp7, 2, 2
rp7, 3, 3
** LOADS
** Name: Load-1  Type: Line load
*Dload
end_beam, PY, -1.
** OUTPUT REQUESTS
*Restart, write, frequency=0
** FIELD OUTPUT: F-Output-1
*Output, field, variable=PRESELECT
*NODE FILE, GLOBAL=YES
U
*End Step
```

### B.3. A sample ABAQUS indata file for analysing planar L-shape frame using the B- FEA spring model with a box-stiffened joint

```
*Heading
** Job name: beam_box_joint_buckling Model name: beam_box_joint_buckling
*Preprint, echo=NO, model=NO, history=NO, contact=NO
*Part, name=Part-1
*End Part
** ASSEMBLY
*Assembly, name=Assembly
*Instance, name=Part-1-1, part=Part-1
*Node
*Include,INPUT=Node.inp
*Element, type=B31OS
*Include,INPUT=Element.inp
*Nset, nset=_PickedSet2, internal, generate
  1, 476, 1
*Elset, elset=_PickedSet2, internal, generate
  1, 474, 1
*Nset, nset=_PickedSet3, internal, generate
  1, 476, 1
*Elset, elset=_PickedSet3, internal, generate
  1, 474, 1
*Nset, nset=_PickedSet4, internal, generate
  1, 476, 1
*Elset, elset=_PickedSet4, internal, generate
  1, 474, 1
** Section: UB_150_14 Profile: UB_150_14
*Beam Section, elset=_PickedSet2, material=Material-1, temperature=GRADIENTS,
section=l
75., 150., 75., 7., 7., 5.
0.,0.,-1.
*End Instance
**
*Node
  1,      0.,    3927.75,      0.
*Node
  2,    0.75,    3928.5,      0.
*Node
  3,      0.,    3928.5,      0.
*Element, type=CONN3D2
3, Part-1-1.2, Part-1-1.3
*Connector Section, elset=_PickedSet12
Beam,
*Nset, nset=Wire-1-Set-1, instance=Part-1-1
2, 3
*Elset, elset=Wire-1-Set-1
3,
*Elset, elset=_PickedSet12, internal
3,
*Nset, nset=rp1
1,
*Nset, nset=rp2
```

```
2,
*Nset, nset=rp3
3,
*Nset, nset=_PickedSet24, internal, instance=Part-1-1
1,
*Nset, nset=_PickedSet25, internal
3,
*Nset, nset=_PickedSet26, internal, instance=Part-1-1
2,
*Nset, nset=_PickedSet27, internal, instance=Part-1-1
4,
*Nset, nset=beam, instance=Part-1-1
3,
*Nset, nset=column, instance=Part-1-1
2,
*Elset, elset=ele_beam, instance=Part-1-1
158,
*Elset, elset=ele_col, instance=Part-1-1
157,
** Constraint: Constraint-1
*Equation
3
rp2, 1, -1.
beam, 7, 1.
column, 7, 0.9057
** Constraint: Constraint-2
*Equation
3
column, 2, -1.
beam, 7, 0.9057
column, 7, 1.
*Element, type=Spring2, elset=kbb-spring
1, 3, 2
*Spring, elset=kbb-spring
1, 1
2.867e+12
*Element, type=Spring2, elset=kcc-spring
2, 3, 1
*Spring, elset=kcc-spring
2, 2
2.867e+12
*End Assembly
**
** MATERIALS
**
*Material, name=Material-1
*Elastic
200000., 0.3
** -----
**
** STEP: buckle
**
*Step, name=buckle, perturbation
*Buckle
3, , 6, 30
```

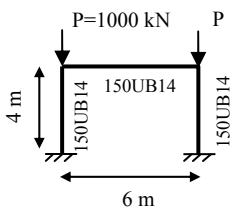
```
**  
** BOUNDARY CONDITIONS  
**  
** Name: BC-1 Type: Displacement/Rotation  
*Boundary, op=NEW, load case=1  
_PickedSet24, 1, 1  
_PickedSet24, 2, 2  
_PickedSet24, 3, 3  
_PickedSet24, 4, 4  
_PickedSet24, 5, 5  
_PickedSet24, 6, 6  
*Boundary, op=NEW, load case=2  
_PickedSet24, 1, 1  
_PickedSet24, 2, 2  
_PickedSet24, 3, 3  
_PickedSet24, 4, 4  
_PickedSet24, 5, 5  
_PickedSet24, 6, 6  
** Name: BC-2 Type: Displacement/Rotation  
*Boundary, op=NEW, load case=1  
_PickedSet25, 1, 1  
_PickedSet25, 2, 2  
_PickedSet25, 3, 3  
*Boundary, op=NEW, load case=2  
_PickedSet25, 1, 1  
_PickedSet25, 2, 2  
_PickedSet25, 3, 3  
** Name: BC-3 Type: Displacement/Rotation  
*Boundary, op=NEW, load case=1  
_PickedSet26, 1, 1  
_PickedSet26, 3, 3  
*Boundary, op=NEW, load case=2  
_PickedSet26, 1, 1  
_PickedSet26, 3, 3  
**  
** LOADS  
**  
** Name: Load-1 Type: Concentrated force  
*Cload  
_PickedSet27, 2, -1000.  
**  
** OUTPUT REQUESTS  
**  
*Restart, write, frequency=0  
**  
** FIELD OUTPUT: F-Output-1  
**  
*Output, field, variable=PRESELECT  
*NODE FILE, GLOBAL=YES  
U  
*End Step
```



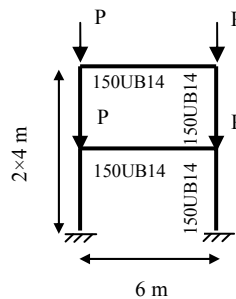
# Appendix C. Initial geometric imperfection

## C.1. Frame layouts to find the amplitude of eigen buckling modes

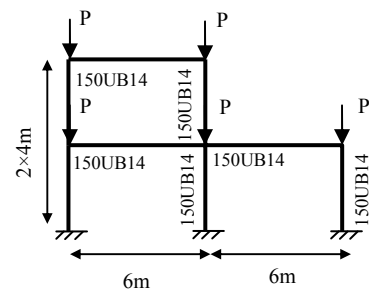
### C.1.1. Unbraced frames



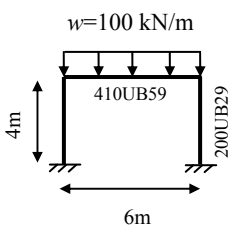
Frame 1



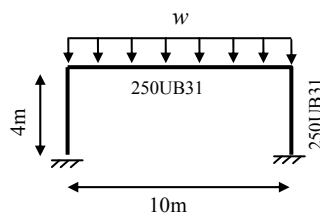
Frame 2



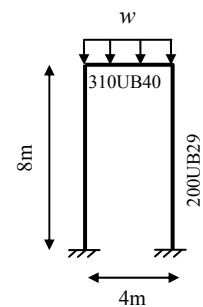
Frame 3



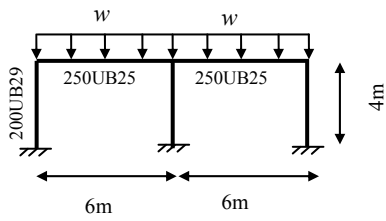
Frame 4



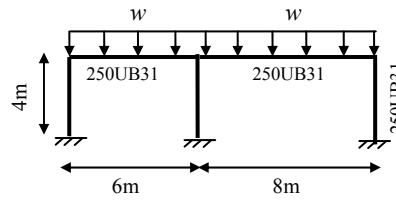
Frame 5



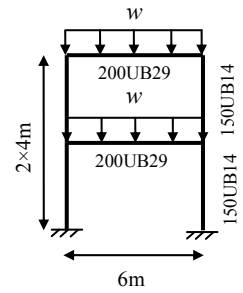
Frame 6



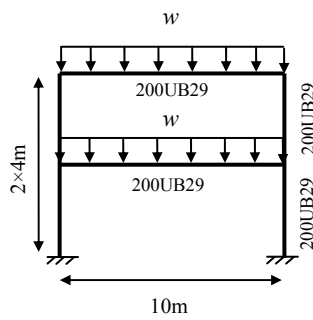
Frame 7



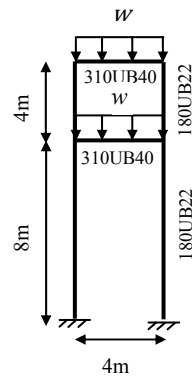
Frame 8



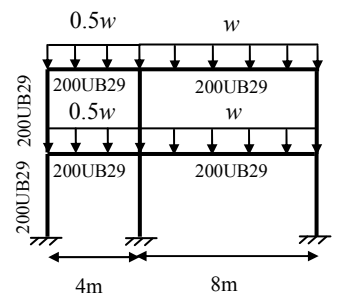
Frame 9



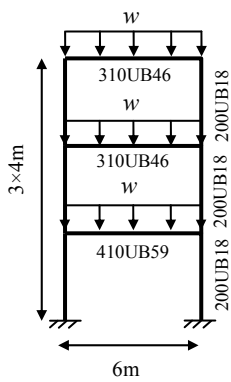
Frame 10



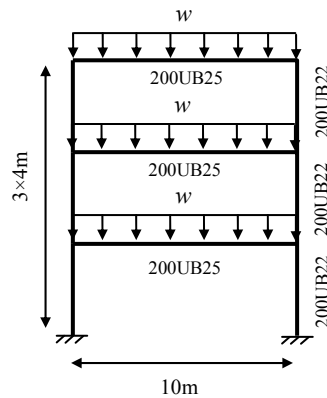
Frame 11



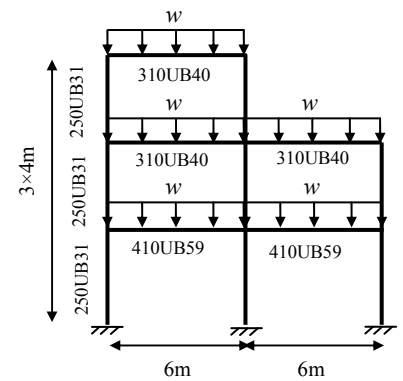
Frame 12



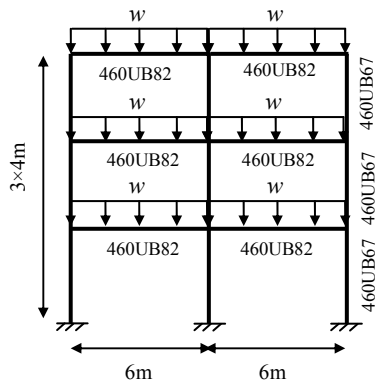
Frame 13



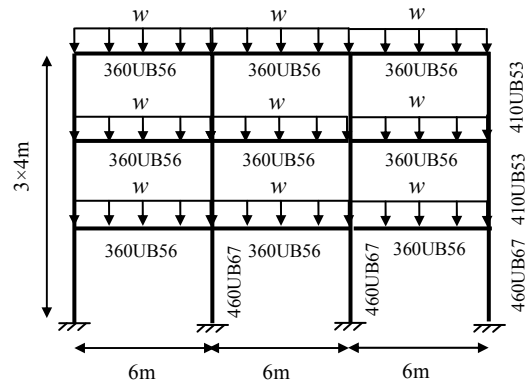
Frame 14



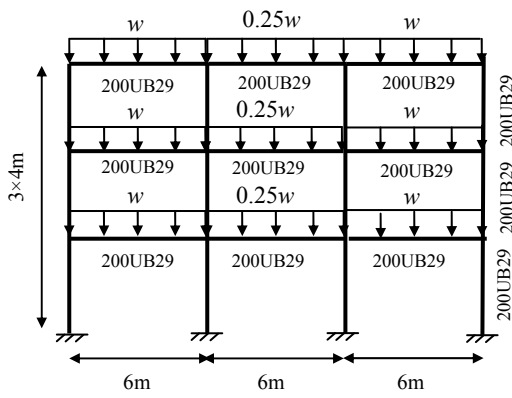
Frame 15



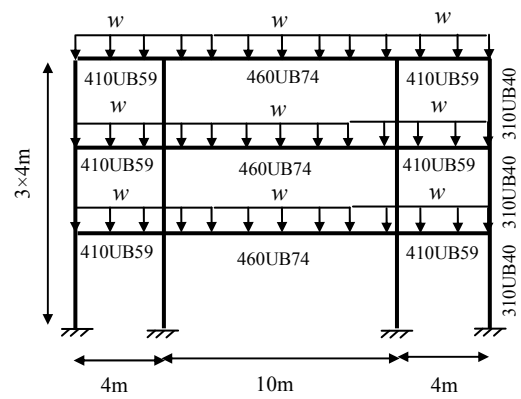
Frame 16



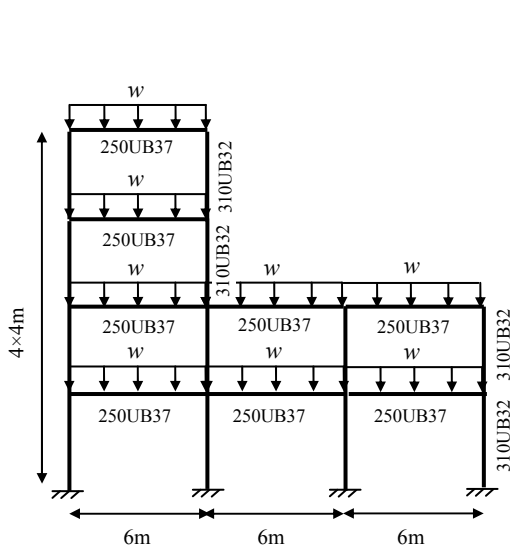
Frame 17



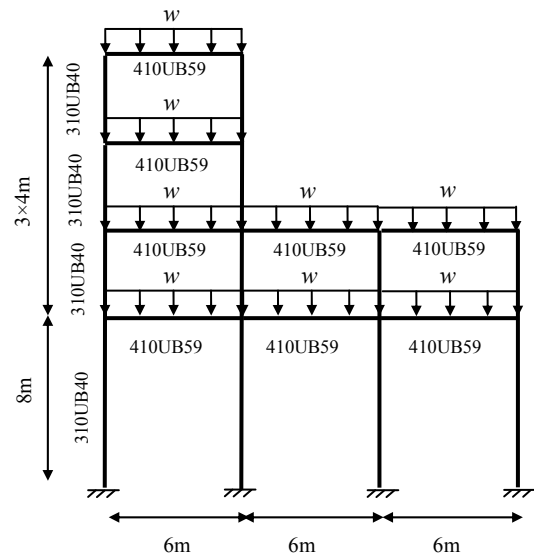
Frame 18



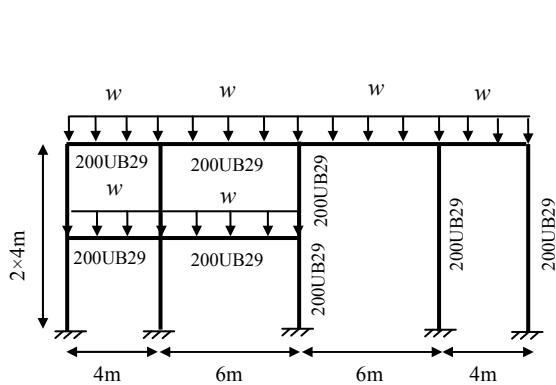
Frame 19



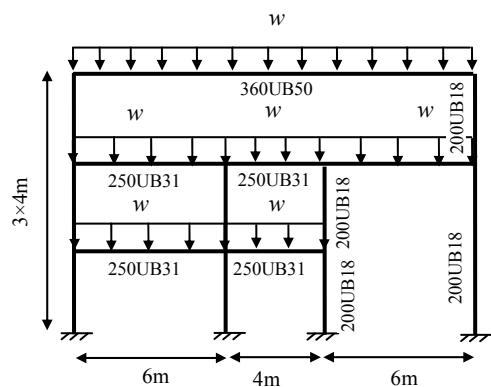
Frame 20



Frame 21



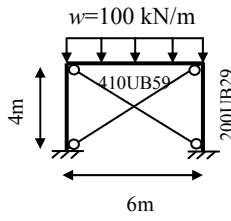
Frame 22



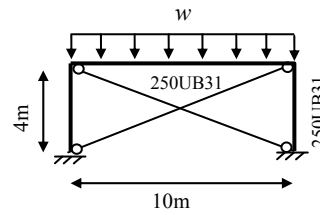
Frame 23

Figure C.1: Unbraced frame layouts to obtain the scale factors of initial geometric imperfection

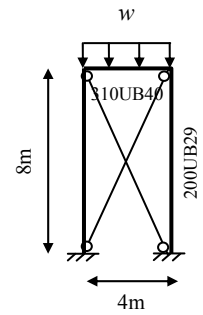
C.1.2. Braced frames



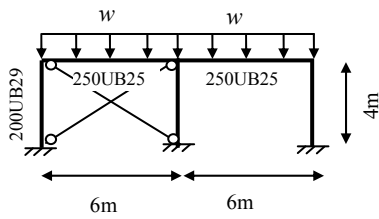
Frame 1



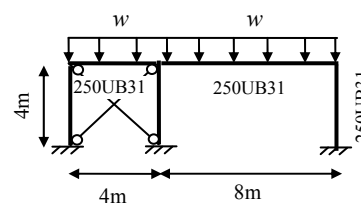
Frame 2



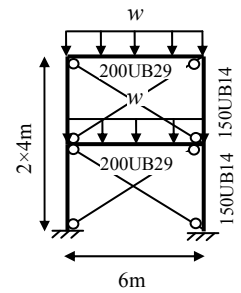
Frame 3



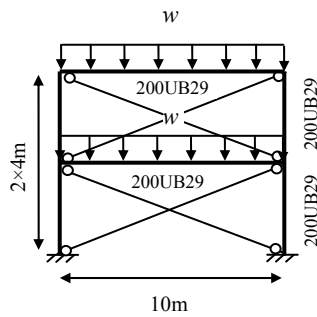
Frame 4



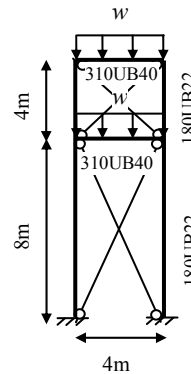
Frame 5



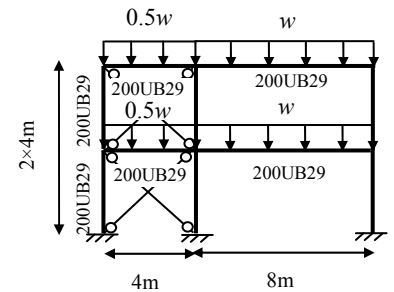
Frame 6



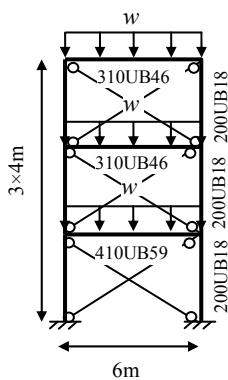
Frame 7



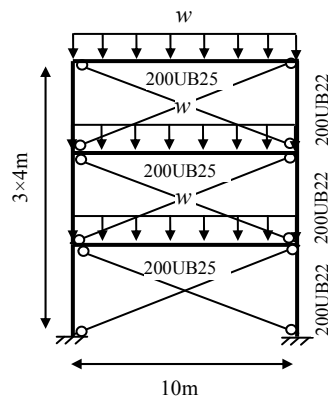
Frame 8



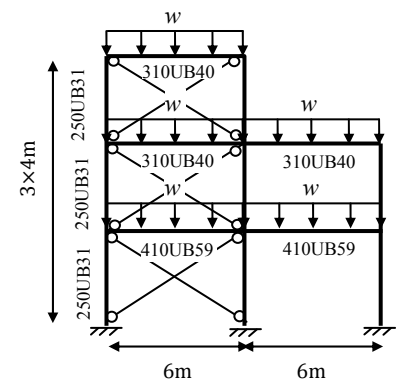
Frame 9



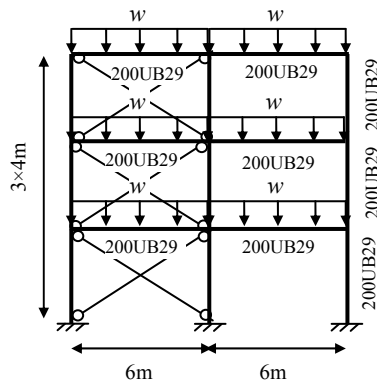
Frame 10



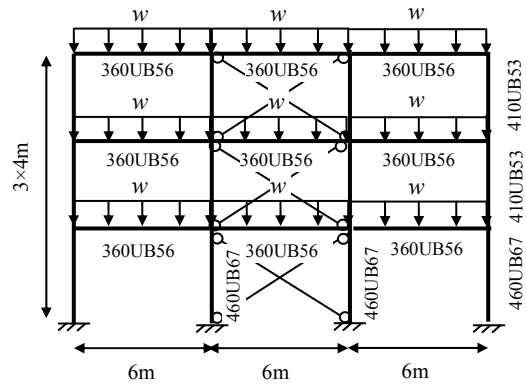
Frame 11



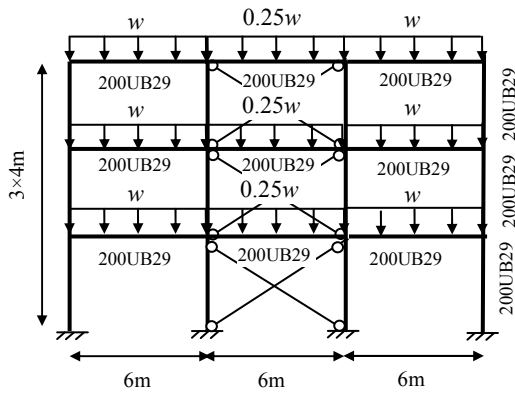
Frame 12



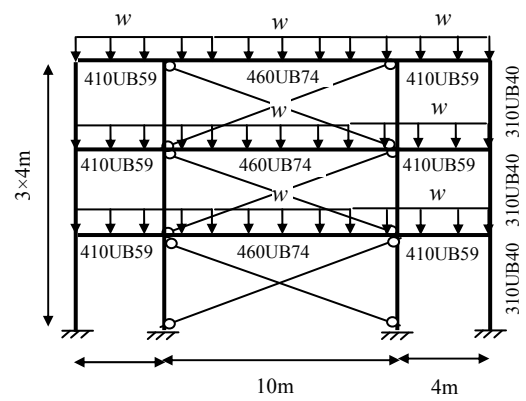
Frame 13



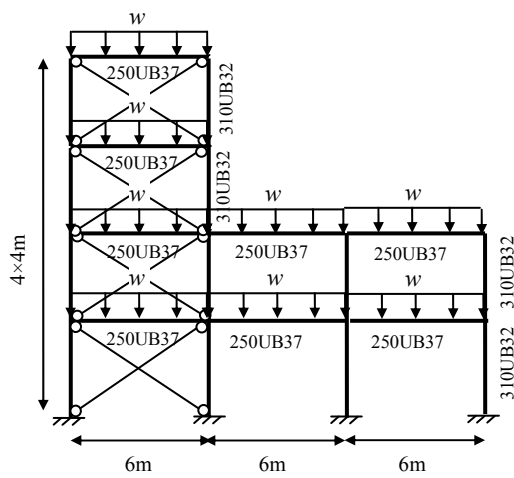
Frame 14



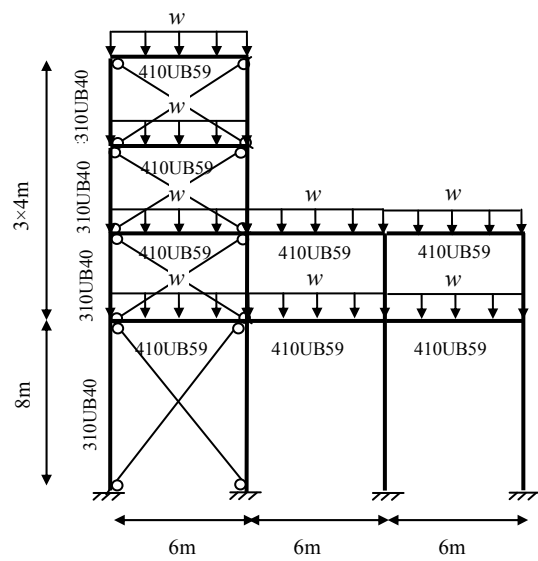
Frame 15



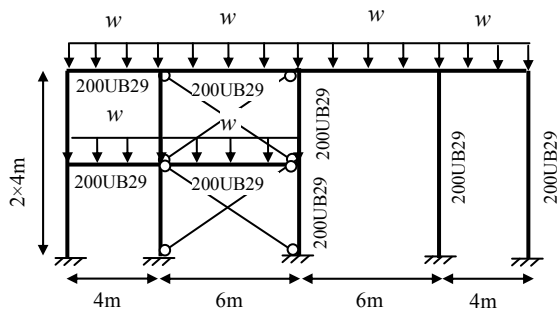
Frame 16



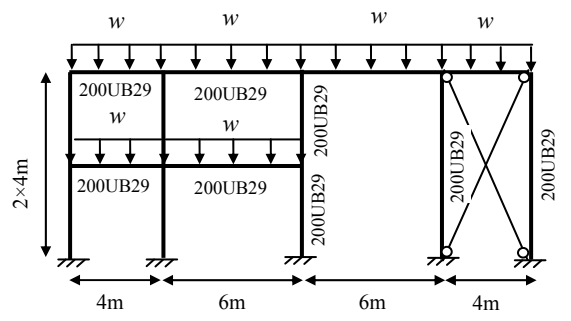
Frame 17



Frame 18



Frame 19



Frame 20

Figure C.2: Braced frame layouts to obtain the scale factors of initial geometric imperfection

## C.2. Scale factors

The scale factors to model initial geometric imperfection are presented for 23 unbraced frames in Section C.2.1 and 20 braced frames in Section C.2.2. The actual mean scale factors obtained from error minimization ( $\bar{x}_j$ ), total frame heights ( $H$ ) or member lengths ( $L$ ) depending on whether the buckling mode is sway or non-sway, and the non-dimensional scale factors  $\bar{x}_j = \bar{X}_j / (H \text{ or } L)$  are summarized in following sections.

### C.2.1. Unbraced frames

Table C.1: Mean scale factors from error minimization between unbraced frames with randomly generated imperfection and first ABAQUS eigenmode

	$\bar{X}_1$
Frame 1	5.93503
Frame 2	10.9230
Frame 3	11.1711
Frame 4	5.96198
Frame 5	5.13613
Frame 6	11.0993
Frame 7	5.53935
Frame 8	5.48724
Frame 9	10.5848
Frame 10	11.2489
Frame 11	11.7056
Frame 12	10.3389
Frame 13	14.7967
Frame 14	15.4969
Frame 15	13.5867
Frame 16	14.1582
Frame 17	13.9720
Frame 18	13.9639
Frame 19	13.7307
Frame 20	17.2727
Frame 21	14.4838
Frame 22	10.4975
Frame 23	8.00430

Table C.2: Mean scale factors from error minimization between unbraced frames with randomly generated imperfection and first two ABAQUS eigenmodes

	$\bar{X}_1$	$\bar{X}_2$
Frame 1	5.935030	2.180784
Frame 2	10.93620	1.739270
Frame 3	11.19936	1.633143
Frame 4	5.961983	1.919224
Frame 5	5.136126	6.233305
Frame 6	11.09929	2.660094
Frame 7	5.650072	1.866370
Frame 8	5.593071	2.172916
Frame 9	10.59075	0.668041
Frame 10	10.70699	1.410163
Frame 11	11.81686	3.201295
Frame 12	10.30497	1.732491
Frame 13	14.69312	0.917720
Frame 14	15.50694	0.874841
Frame 15	13.08227	1.756590
Frame 16	13.90128	1.139665
Frame 17	13.56629	0.474975
Frame 18	13.54447	1.416517
Frame 19	13.08901	1.763988
Frame 20	15.34375	4.984623
Frame 21	14.27006	8.806922
Frame 22	10.44615	2.142178
Frame 23	11.12476	7.416430

Table C.3: Mean scale factors from error minimization between unbraced frames with randomly generated imperfection and first three ABAQUS eigenmodes

	$\bar{X}_1$	$\bar{X}_2$	$\bar{X}_3$
Frame 1	4.67837	2.180784	2.113619
Frame 2	10.9362	1.739270	1.970385
Frame 3	11.1380	1.632252	2.126346
Frame 4	4.77731	1.928724	1.791716
Frame 5	4.52032	6.233305	1.905821
Frame 6	9.93856	2.660094	3.24661
Frame 7	4.99746	1.996015	3.018464
Frame 8	5.23822	1.592967	1.708469
Frame 9	10.5908	0.668041	0.769300
Frame 10	10.7070	1.410163	5.945970
Frame 11	11.8169	3.201295	2.547636
Frame 12	10.3198	1.182164	2.494371
Frame 13	14.2817	0.887216	2.606970
Frame 14	15.2860	1.036091	1.610221
Frame 15	12.7455	1.433272	1.103898
Frame 16	13.6037	0.967146	0.752970
Frame 17	13.2396	0.290197	2.658149
Frame 18	13.2215	0.798077	2.784182
Frame 19	13.0890	1.763989	1.152793
Frame 20	15.3183	3.592395	2.739214
Frame 21	13.7324	7.836998	8.323518
Frame 22	10.4576	1.518611	3.516646
Frame 23	5.13697	3.808523	10.95999



Table C.4: Mean scale factors from error minimization between unbraced frames with randomly generated imperfection and first four ABAQUS eigenmodes

	$\bar{X}_1$	$\bar{X}_2$	$\bar{X}_3$	$\bar{X}_4$
Frame 1	4.67837	1.790049	2.113603	2.183971
Frame 2	10.7602	1.123276	1.970386	2.863638
Frame 3	11.1081	1.237527	2.203936	2.746760
Frame 4	4.77731	1.608726	1.791716	3.306674
Frame 5	4.52032	6.192759	1.905821	1.288963
Frame 6	9.93856	2.630999	3.246610	1.057469
Frame 7	4.99746	1.996015	3.018464	1.612736
Frame 8	5.21817	1.608096	1.680288	1.588678
Frame 9	10.4552	0.446867	1.076493	1.347844
Frame 10	10.7151	1.410163	5.945970	0.913037
Frame 11	9.43423	2.874348	2.547636	6.456606
Frame 12	10.3282	1.024938	2.627075	3.575889
Frame 13	14.2817	0.887216	2.606970	0.856299
Frame 14	15.2860	1.036091	1.610221	5.379716
Frame 15	12.7807	1.140771	1.240851	3.091877
Frame 16	13.5695	0.696654	0.812317	2.596075
Frame 17	13.2396	0.290197	2.658149	1.070446
Frame 18	13.2215	0.798077	2.784182	1.080595
Frame 19	12.6859	1.372977	1.152791	0.588981
Frame 20	15.3333	3.562240	2.733197	1.511949
Frame 21	8.78399	5.00423	4.992441	4.808890
Frame 22	10.4396	1.518465	3.530988	1.628480
Frame 23	5.13665	3.800838	10.95002	1.620598

Table C.5: Mean scale factors from error minimization between unbraced frames with randomly generated imperfection and first five ABAQUS eigenmodes

	$\bar{X}_1$	$\bar{X}_2$	$\bar{X}_3$	$\bar{X}_4$	$\bar{X}_5$
Frame 1	4.61194	1.790057	2.001812	2.183971	0.93453904
Frame 2	10.7602	1.123278	2.205748	2.863639	2.47377542
Frame 3	11.1163	1.240526	2.601582	2.764694	2.70019217
Frame 4	4.69337	1.608726	1.786661	3.306674	0.81943102
Frame 5	3.91651	6.192759	2.106588	1.288963	1.06713506
Frame 6	9.70680	2.630999	2.653062	1.057469	1.78341428
Frame 7	4.97129	1.992992	3.234010	1.612736	1.13122724
Frame 8	5.00593	1.623833	1.788308	1.588485	2.53114836
Frame 9	10.4552	0.446867	1.312408	1.347844	1.95257066
Frame 10	10.7151	1.410163	6.169270	0.913037	6.69984747
Frame 11	9.43423	2.874348	2.544035	6.456606	0.90960837
Frame 12	10.2871	0.934760	2.937501	3.022905	3.43262880
Frame 13	14.1302	0.834843	2.615920	0.851299	1.17019493
Frame 14	15.2860	1.036091	1.610221	5.655530	5.59233615
Frame 15	12.7742	1.175530	1.372296	3.372884	1.79898766
Frame 16	13.4157	0.767467	0.932401	2.673204	1.91761417
Frame 17	13.2944	0.276855	2.690188	1.070446	1.22109774
Frame 18	13.2236	0.789237	2.783896	1.080595	1.15003319
Frame 19	12.8163	0.960141	1.152784	0.484534	2.13562378
Frame 20	15.3951	3.520123	2.383811	1.574640	1.89809560
Frame 21	6.94791	5.039160	4.925425	5.424730	5.57463401
Frame 22	10.4373	1.516495	3.555427	1.634820	1.48399541
Frame 23	5.19689	3.888087	10.43373	1.860802	2.18479195

Table C.6: Mean scale factors from error minimization between unbraced frames with randomly generated imperfection and first six ABAQUS eigenmodes

	$\bar{X}_1$	$\bar{X}_2$	$\bar{X}_3$	$\bar{X}_4$	$\bar{X}_5$	$\bar{X}_6$
Frame 1	4.61194	1.634845	2.001817	1.553605	0.93453735	2.122691034
Frame 2	10.2007	1.029824	2.205748	3.097732	2.47377538	2.907115135
Frame 3	10.5227	1.162343	2.578745	3.183134	2.69789276	3.649266029
Frame 4	4.69337	1.520940	1.786661	3.007290	0.81943102	1.479928521
Frame 5	3.91651	5.671772	2.106588	1.356756	1.06713506	1.775103276
Frame 6	9.70680	2.549141	2.653062	1.055409	1.78341432	0.861852810
Frame 7	4.65447	2.090186	3.018726	1.612736	0.66972534	2.892405799
Frame 8	4.99938	1.672795	1.782893	1.768024	2.61231319	1.444605376
Frame 9	9.99207	0.417799	1.312408	1.443259	1.95257067	1.437872406
Frame 10	10.7151	1.410163	5.670998	0.913037	6.84330443	1.754108924
Frame 11	9.34595	2.892487	2.544035	6.414011	0.90960837	1.027337330
Frame 12	9.77275	0.952487	2.672332	3.293893	2.92080330	2.588055286
Frame 13	14.1302	0.834842	2.615920	0.946588	1.17019523	1.148773130
Frame 14	14.7220	1.031496	1.667523	5.655530	5.59233613	1.338563286
Frame 15	12.7986	1.159523	1.364023	3.508565	1.84808348	1.518535217
Frame 16	13.4157	0.767467	0.932401	2.673204	1.91761377	1.183015592
Frame 17	13.2944	0.276851	2.690189	1.208658	1.22109776	1.286579264
Frame 18	13.2236	0.789237	2.783896	1.116237	1.15003313	1.079034178
Frame 19	12.8163	0.960221	1.412947	0.484887	2.13732055	1.308520693
Frame 20	15.3373	3.654458	2.325593	1.637584	2.01070434	7.664675108
Frame 21	7.61064	4.971248	4.847143	4.120506	2.63479404	13.94627107
Frame 22	9.97746	1.497942	3.545182	1.665301	1.48776859	2.368735129
Frame 23	5.32867	3.888046	10.23412	1.896470	2.40809601	3.928523706

Table C.7: Mean scale factors from error minimization between unbraced frames with randomly generated imperfection and first seven ABAQUS eigenmodes

	$\bar{X}_1$	$\bar{X}_2$	$\bar{X}_3$	$\bar{X}_4$	$\bar{X}_5$	$\bar{X}_6$	$\bar{X}_7$
Frame 1	4.54705	1.634846	1.726964	1.553604	0.936031	2.122692	0.668891
Frame 2	10.2007	1.029824	2.302738	3.097731	3.102628	2.907116	2.490162
Frame 3	10.6065	1.042932	2.572432	3.181880	2.700463	3.460685	3.707246
Frame 4	4.73998	1.552094	1.369037	3.007289	0.839971	1.479930	0.815454
Frame 5	3.90666	5.671772	2.08205	1.356756	1.048656	1.775103	0.473881
Frame 6	9.51425	2.549141	2.619602	1.055409	1.536747	0.861853	1.031168
Frame 7	4.68210	2.000253	3.072095	1.612736	0.671022	1.974320	1.820828
Frame 8	4.94183	1.628162	1.782016	1.648239	2.585881	1.201116	0.512325
Frame 9	9.99207	0.417798	1.272890	1.443259	1.761589	1.437872	2.258831
Frame 10	10.2241	0.837348	5.670998	1.317599	6.843304	1.754109	1.895399
Frame 11	9.34595	2.892487	2.551628	6.414011	0.873160	1.027337	1.888106
Frame 12	9.85813	1.012700	2.546040	3.294885	2.719500	2.771439	2.239569
Frame 13	13.9607	0.486917	2.558290	0.996588	1.287817	1.148773	1.154577
Frame 14	14.7774	1.020478	1.519466	5.655529	5.592336	1.377559	0.844520
Frame 15	12.3106	1.241139	1.352949	3.198235	1.816480	1.456685	2.062555
Frame 16	13.4694	0.754125	0.972560	2.568874	1.764300	1.183016	1.187192
Frame 17	13.1022	0.290825	2.733098	1.208658	1.251016	1.286580	1.486673
Frame 18	13.1382	0.833130	2.783914	1.116236	1.134320	1.079034	1.299517
Frame 19	12.6210	1.022022	1.412027	0.536079	2.110953	1.308190	1.219931
Frame 20	15.3553	3.654149	2.339714	1.670625	2.251048	7.728155	1.159402
Frame 21	8.16113	4.978886	4.820287	3.928581	2.597055	13.54658	1.907575
Frame 22	9.96012	1.511706	3.550901	1.787342	1.458531	2.344223	1.828453
Frame 23	5.19665	3.848522	10.22412	1.876993	2.350829	3.856991	1.798143

Table C.8: Mean scale factors from error minimization between unbraced frames with randomly generated imperfection and first eight ABAQUS eigenmodes

	$\bar{X}_1$	$\bar{X}_2$	$\bar{X}_3$	$\bar{X}_4$	$\bar{X}_5$	$\bar{X}_6$	$\bar{X}_7$	$\bar{X}_8$
Frame 1	4.547	1.6215	1.7270	0.8673	0.9360	1.5179	0.6689	1.6642
Frame 2	10.304	0.8830	2.3027	2.9958	3.1026	3.0107	2.4902	0.9019
Frame 3	10.589	1.0373	2.6717	3.2088	3.0769	3.4644	3.7000	2.2048
Frame 4	4.7400	1.4560	1.3690	3.0871	0.8400	1.5637	0.8155	1.1162
Frame 5	3.9067	5.6192	2.0821	1.3100	1.0487	1.8223	0.4739	0.4438
Frame 6	9.5142	2.5052	2.6196	0.8470	1.5367	0.8524	1.0312	0.9490
Frame 7	4.6821	2.0003	3.0721	1.2709	0.6710	1.9716	1.8208	1.9716
Frame 8	4.9508	0.5967	1.7869	1.6885	2.6440	1.3589	0.5484	1.4462
Frame 9	9.9347	0.3936	1.7279	1.4035	1.7616	1.5015	2.2588	0.5605
Frame 10	10.224	0.8373	5.6679	1.3176	6.8526	1.8634	1.8954	1.0494
Frame 11	9.3265	2.8293	2.5516	6.2678	0.8732	1.0175	0.8761	0.9145
Frame 12	9.5927	1.1364	2.4589	3.1904	2.7657	3.3167	2.9272	3.5828
Frame 13	13.961	0.4869	2.5583	0.9886	1.2878	1.8763	1.1546	1.6281
Frame 14	14.777	1.0205	1.5195	5.5993	6.8081	1.3776	0.8445	3.6986
Frame 15	12.369	1.2428	1.3671	3.1682	1.8643	1.5007	2.3355	1.7163
Frame 16	13.383	0.7648	0.9527	2.2971	1.8847	1.1830	1.2047	2.3775
Frame 17	13.102	0.2908	2.7331	1.2343	1.2510	1.2840	1.4867	1.6680
Frame 18	13.138	0.8331	2.7839	1.1325	1.1343	1.0771	1.2995	1.0335
Frame 19	12.621	1.0221	1.4039	0.5368	2.1110	1.7208	1.2210	2.6688
Frame 20	15.352	3.6818	2.3054	1.6549	2.3381	7.6992	1.1619	1.6562
Frame 21	8.2962	5.1088	4.8340	3.8560	2.5426	13.874	1.8693	1.7728
Frame 22	9.8549	1.5585	3.5419	1.7739	1.6172	2.3325	1.8467	2.5049
Frame 23	5.0166	3.7123	9.8789	1.8644	2.2137	3.8368	1.7984	0.6960

Table C.9: Mean scale factors from error minimization between unbraced frames with randomly generated imperfection and first nine ABAQUS eigenmodes

	$\bar{X}_1$	$\bar{X}_2$	$\bar{X}_3$	$\bar{X}_4$	$\bar{X}_5$	$\bar{X}_6$	$\bar{X}_7$	$\bar{X}_8$	$\bar{X}_9$
Frame 1	4.5891	1.6215	1.7337	0.8673	0.7308	1.5179	0.6470	1.6642	0.4521
Frame 2	10.304	0.8830	2.3805	2.9958	3.2476	3.0107	2.4716	0.9019	2.4533
Frame 3	10.747	1.1926	2.6726	3.1649	3.0779	3.5105	3.7052	2.2006	1.4388
Frame 4	4.6678	1.4560	1.4012	3.0871	0.6882	1.5637	0.9231	1.1162	0.6549
Frame 5	4.0488	5.6192	1.8134	1.3100	0.9433	1.8223	0.5964	0.4438	0.5946
Frame 6	9.4939	2.5052	2.5588	0.8470	1.4850	0.8524	0.8960	0.9490	0.5525
Frame 7	4.6669	1.9609	2.6166	1.2709	0.6384	1.9141	1.9150	1.9716	0.5791
Frame 8	4.5636	1.5880	1.7768	1.7928	2.5772	1.3686	0.6244	1.2298	5.2160
Frame 9	9.9347	0.3936	1.2840	1.4035	1.7280	1.5015	2.9594	0.5605	3.4506
Frame 10	10.106	0.8275	5.6679	1.3124	6.8526	1.8635	1.9626	1.0494	0.9190
Frame 11	9.3265	2.8293	2.4144	6.2678	0.7987	1.0175	1.6400	0.9145	1.2378
Frame 12	9.6275	1.1009	2.4281	3.1589	2.7743	2.8557	3.5269	3.3069	1.9101
Frame 13	13.646	0.4873	2.4533	0.9886	1.2616	1.1884	1.2865	1.6281	1.2602
Frame 14	14.043	0.6347	1.4631	5.5993	6.8080	1.3763	1.2717	3.6986	1.6461
Frame 15	12.375	1.2508	1.3844	3.1268	1.8105	1.3860	2.3391	1.7142	1.9249
Frame 16	13.250	0.9164	0.9523	2.2808	1.8867	1.1830	1.1455	3.2460	1.8892
Frame 17	13.121	0.2888	2.7673	1.2343	1.1836	1.2840	1.3964	1.6688	1.3663
Frame 18	13.163	0.8567	2.7840	1.1325	1.1438	1.0771	1.2870	1.0335	1.3887
Frame 19	12.621	1.0216	1.0084	0.5360	2.1127	1.1883	1.2214	4.0960	3.6961
Frame 20	15.136	3.8088	2.1814	1.6664	2.3377	8.6087	1.1163	1.6476	1.3654
Frame 21	7.6542	5.1089	4.8517	3.3521	2.5216	12.191	1.9035	1.6120	5.9967
Frame 22	9.8274	1.5501	3.4520	1.7691	1.6196	1.9155	1.8523	2.4959	4.9411
Frame 23	5.004	3.7040	9.8822	1.8562	2.2066	3.8884	1.8031	0.6768	5.7766

Table C.10: Mean scale factors from error minimization between unbraced frames with randomly generated imperfection and first ten ABAQUS eigenmodes

	$\bar{X}_1$	$\bar{X}_2$	$\bar{X}_3$	$\bar{X}_4$	$\bar{X}_5$	$\bar{X}_6$	$\bar{X}_7$	$\bar{X}_8$	$\bar{X}_9$	$\bar{X}_{10}$
Frame 1	4.5891	1.6627	1.7337	0.8449	0.7308	0.8776	0.6470	1.3512	0.4521	1.4320
Frame 2	10.285	0.9345	2.3805	2.8679	3.2476	3.0132	2.4716	1.0424	2.4533	0.6380
Frame 3	10.739	1.1922	2.7502	3.1658	3.1593	3.5111	3.7249	2.2065	1.4451	2.5588
Frame 4	4.6678	1.4481	1.4012	2.6126	0.6882	1.7148	0.9231	1.0321	0.6549	0.6963
Frame 5	4.0488	5.4361	1.8134	1.3282	0.9433	1.7814	0.5964	0.4904	0.5946	0.4619
Frame 6	9.4939	2.5485	2.5588	0.8477	1.4850	0.6903	0.8960	0.8580	0.5525	0.7709
Frame 7	4.7486	1.9618	2.5627	1.2709	0.5634	2.2084	1.7386	1.9716	0.5616	1.3392
Frame 8	4.5713	1.5726	1.6127	1.4526	2.5020	1.3747	0.4820	1.1742	4.2881	2.9283
Frame 9	9.9461	0.4290	1.2841	1.3105	1.7240	1.4535	2.9594	0.5797	3.4507	0.3740
Frame 10	10.394	0.9110	5.6679	1.2347	6.8526	1.8635	1.7565	1.0494	0.9276	1.7951
Frame 11	9.1975	2.8316	2.4144	6.0619	0.7987	0.8407	1.6400	0.9733	1.2378	1.2970
Frame 12	9.6235	0.8648	1.8630	3.1200	2.8657	2.4150	1.4884	2.7339	1.0528	5.3648
Frame 13	13.646	0.4873	2.4533	0.9248	1.2616	1.1441	1.2864	2.0324	1.2603	1.9492
Frame 14	14.043	0.6347	1.4631	5.5593	5.5643	1.3763	1.2717	2.9362	1.6461	2.3402
Frame 15	12.331	1.4688	1.3880	3.1539	1.8006	1.3918	2.7721	1.7562	1.9357	2.1265
Frame 16	13.250	0.9161	0.9523	2.2808	1.8867	1.1927	1.1453	3.2460	1.8888	1.2001
Frame 17	13.121	0.2888	2.7672	1.1821	1.1835	1.3131	1.3963	1.6680	1.3662	0.8647
Frame 18	13.163	0.8568	2.7840	1.1244	1.1438	1.0742	1.2870	0.9727	1.3887	1.0520
Frame 19	12.467	1.0372	1.0086	0.6425	2.1116	1.1882	1.3890	4.0960	3.6961	3.6509
Frame 20	15.176	3.8152	2.1782	1.6496	2.2670	8.6723	1.1596	1.6291	1.3474	1.7417
Frame 21	8.0488	5.0194	4.8203	3.0645	2.5301	10.710	1.6390	1.8986	5.5448	3.3169
Frame 22	9.8288	1.5556	3.4103	1.7239	1.6125	1.8836	1.7382	2.6379	4.9821	1.5905
Frame 23	5.0046	3.7040	9.8758	1.9740	2.2243	3.8486	1.8014	0.6765	5.4246	1.5923

Table C.11: Total frame heights or member lengths depending on the eigenmode type

	<i>H</i> or <i>L</i> (mm)									
	Mode 1	Mode 2	Mode 3	Mode 4	Mode 5	Mode 6	Mode 7	Mode 8	Mode 9	Mode 10
Frame 1	4000	4000	4000	4000	4000	4000	4000	4000	4000	4000
Frame 2	8000	8000	4000	4000	4000	4000	4000	4000	4000	4000
Frame 3	8000	8000	4000	4000	4000	4000	4000	4000	4000	4000
Frame 4	4000	4000	4000	6000	4000	6000	4000	6000	4000	6000
Frame 5	4000	10000	10000	10000	10000	10000	4000	10000	10000	10000
Frame 6	8000	8000	8000	8000	8000	8000	8000	8000	8000	8000
Frame 7	4000	4000	6000	4000	4000	6000	6000	6000	4000	6000
Frame 8	4000	4000	4000	4000	8000	8000	4000	8000	8000	8000
Frame 9	8000	8000	4000	4000	4000	4000	6000	4000	6000	4000
Frame 10	8000	4000	10000	4000	10000	10000	10000	10000	4000	10000
Frame 11	12000	8000	8000	12000	8000	8000	8000	8000	4000	4000
Frame 12	8000	8000	8000	8000	8000	8000	8000	8000	8000	8000
Frame 13	12000	12000	12000	4000	4000	4000	4000	4000	4000	4000
Frame 14	12000	12000	12000	10000	10000	4000	10000	4000	10000	10000
Frame 15	12000	12000	4000	12000	4000	4000	4000	4000	4000	4000
Frame 16	12000	12000	4000	12000	4000	4000	4000	4000	4000	4000
Frame 17	12000	4000	12000	4000	4000	4000	4000	6000	4000	4000
Frame 18	12000	12000	12000	4000	4000	4000	4000	4000	4000	4000
Frame 19	12000	12000	4000	4000	12000	4000	4000	4000	4000	10000
Frame 20	16000	16000	16000	4000	16000	16000	4000	4000	4000	4000
Frame 21	20000	8000	8000	8000	8000	20000	8000	8000	8000	8000
Frame 22	8000	8000	8000	4000	4000	8000	4000	4000	8000	8000
Frame 23	12000	8000	12000	4000	16000	16000	16000	4000	16000	4000

Table C.12: Mean non-dimensional scale factors from error minimization between unbraced frames with randomly generated imperfection and first ABAQUS eigenmodes

	$\bar{x}_1$
Frame 1	0.001484
Frame 2	0.001365
Frame 3	0.001396
Frame 4	0.001490
Frame 5	0.001284
Frame 6	0.001387
Frame 7	0.001385
Frame 8	0.001372
Frame 9	0.001323
Frame 10	0.001406
Frame 11	0.000975
Frame 12	0.001292
Frame 13	0.001233
Frame 14	0.001291
Frame 15	0.001132
Frame 16	0.001180
Frame 17	0.001164
Frame 18	0.001164
Frame 19	0.001144
Frame 20	0.001080
Frame 21	0.000724
Frame 22	0.001312
Frame 23	0.000667
Average	0.001228

Table C.13: Mean non-dimensional scale factors from error minimization between unbraced frames with randomly generated imperfection and first two ABAQUS eigenmodes

	$\bar{x}_1$	$\bar{x}_2$
Frame 1	0.001484	0.0005452
Frame 2	0.001367	0.0002174
Frame 3	0.001400	0.0002041
Frame 4	0.001490	0.0004798
Frame 5	0.001284	0.0006233
Frame 6	0.001387	0.0003325
Frame 7	0.001413	0.0004666
Frame 8	0.001398	0.0005429
Frame 9	0.001324	8.351E-05
Frame 10	0.001338	0.0003525
Frame 11	0.000985	0.0004002
Frame 12	0.001288	0.0002166
Frame 13	0.001224	7.648E-05
Frame 14	0.001292	7.29E-05
Frame 15	0.001090	0.0001464
Frame 16	0.001158	9.497E-05
Frame 17	0.001131	0.0001185
Frame 18	0.001129	0.0001180
Frame 19	0.001091	0.0001470
Frame 20	0.000959	0.0003115
Frame 21	0.000714	0.0011009
Frame 22	0.001306	0.0002678
Frame 23	0.000927	0.0009270
Average	0.001225	0.0003410

Table C.14: Mean non-dimensional scale factors from error minimization between unbraced frames with randomly generated imperfection and first three ABAQUS eigenmodes

	$\bar{x}_1$	$\bar{x}_2$	$\bar{x}_3$
Frame 1	0.001170	0.000545	0.000528
Frame 2	0.001367	0.000217	0.000493
Frame 3	0.001392	0.000204	0.000532
Frame 4	0.001194	0.000480	0.000448
Frame 5	0.001130	0.000623	0.000191
Frame 6	0.001242	0.000333	0.000406
Frame 7	0.001249	0.000499	0.000503
Frame 8	0.001310	0.000398	0.000427
Frame 9	0.001324	8.35E-05	0.000269
Frame 10	0.001338	0.000353	0.000595
Frame 11	0.000985	0.000400	0.000318
Frame 12	0.001290	0.000148	0.000312
Frame 13	0.001190	7.39E-05	0.000217
Frame 14	0.001274	8.63E-05	0.000134
Frame 15	0.001062	0.000119	0.000275
Frame 16	0.001134	8.06E-05	0.000188
Frame 17	0.001103	7.25E-05	0.000222
Frame 18	0.001102	6.65E-05	0.000232
Frame 19	0.001091	0.000147	0.000288
Frame 20	0.000957	0.000225	0.000171
Frame 21	0.000687	0.000980	0.001040
Frame 22	0.001307	0.000190	0.000440
Frame 23	0.000428	0.000476	0.000913
Average	0.001145	0.000296	0.000397

Table C.15: Mean non-dimensional scale factors from error minimization between unbraced frames with randomly generated imperfection and first four ABAQUS eigenmodes

	$\bar{x}_1$	$\bar{x}_2$	$\bar{x}_3$	$\bar{x}_4$
Frame 1	0.001170	0.000448	0.000528	0.000546
Frame 2	0.001345	0.000140	0.000493	0.000716
Frame 3	0.001389	0.000155	0.000551	0.000687
Frame 4	0.001194	0.000402	0.000448	0.000551
Frame 5	0.001130	0.000619	0.000191	0.000129
Frame 6	0.001242	0.000329	0.000406	0.000132
Frame 7	0.001249	0.000499	0.000503	0.000403
Frame 8	0.001305	0.000402	0.000420	0.000397
Frame 9	0.001307	5.59E-05	0.000269	0.000337
Frame 10	0.001339	0.000353	0.000595	0.000228
Frame 11	0.000786	0.000359	0.000318	0.000538
Frame 12	0.001291	0.000128	0.000328	0.000447
Frame 13	0.001190	7.39E-05	0.000217	0.000214
Frame 14	0.001274	8.63E-05	0.000134	0.000538
Frame 15	0.001065	9.51E-05	0.000310	0.000258
Frame 16	0.001131	5.81E-05	0.000203	0.000216
Frame 17	0.001103	7.25E-05	0.000222	0.000268
Frame 18	0.001102	6.65E-05	0.000232	0.000270
Frame 19	0.001057	0.000114	0.000288	0.000147
Frame 20	0.000958	0.000223	0.000171	0.000378
Frame 21	0.000439	0.000626	0.000624	0.000601
Frame 22	0.001305	0.000190	0.000441	0.000407
Frame 23	0.000428	0.000475	0.000913	0.000405
Average	0.001122	0.000260	0.000383	0.000383

Table C.16: Mean non-dimensional scale factors from error minimization between unbraced frames with randomly generated imperfection and first five ABAQUS eigenmodes

	$\bar{x}_1$	$\bar{x}_2$	$\bar{x}_3$	$\bar{x}_4$	$\bar{x}_5$
Frame 1	0.001153	0.000448	0.000500	0.000546	0.000234
Frame 2	0.001345	0.000140	0.000551	0.000716	0.000618
Frame 3	0.001390	0.000155	0.000650	0.000691	0.000675
Frame 4	0.001173	0.000402	0.000447	0.000551	0.000205
Frame 5	0.000979	0.000619	0.000211	0.000129	0.000107
Frame 6	0.001213	0.000329	0.000332	0.000132	0.000223
Frame 7	0.001243	0.000498	0.000539	0.000403	0.000283
Frame 8	0.001251	0.000405	0.000447	0.000395	0.000316
Frame 9	0.001307	5.59E-05	0.000328	0.000337	0.000488
Frame 10	0.001339	0.000353	0.000617	0.000228	0.000670
Frame 11	0.000786	0.000359	0.000318	0.000538	0.000114
Frame 12	0.001286	0.000117	0.000367	0.000378	0.000429
Frame 13	0.001178	6.96E-05	0.000218	0.000214	0.000293
Frame 14	0.001274	8.63E-05	0.000134	0.000566	0.000559
Frame 15	0.001065	9.8E-05	0.000343	0.000281	0.000450
Frame 16	0.001118	6.4E-05	0.000233	0.000223	0.000479
Frame 17	0.001108	6.92E-05	0.000224	0.000268	0.000305
Frame 18	0.001102	6.58E-05	0.000232	0.000270	0.000288
Frame 19	0.001068	8E-05	0.000288	0.000121	0.000178
Frame 20	0.000962	0.000220	0.000149	0.000394	0.000119
Frame 21	0.000347	0.000630	0.000616	0.000678	0.000697
Frame 22	0.001305	0.000190	0.000444	0.000409	0.000371
Frame 23	0.000433	0.000486	0.000869	0.000465	0.000137
Average	0.001105	0.000258	0.000394	0.000388	0.000358

Table C.17: Mean non-dimensional scale factors from error minimization between unbraced frames with randomly generated imperfection and first six ABAQUS eigenmodes

	$\bar{x}_1$	$\bar{x}_2$	$\bar{x}_3$	$\bar{x}_4$	$\bar{x}_5$	$\bar{x}_6$
Frame 1	0.001153	0.000409	0.000500	0.000388	0.000234	0.000531
Frame 2	0.001275	0.000129	0.000551	0.000774	0.000618	0.000727
Frame 3	0.001315	0.000145	0.000645	0.000796	0.000674	0.000912
Frame 4	0.001173	0.000375	0.000447	0.000501	0.000205	0.000247
Frame 5	0.000979	0.000567	0.000211	0.000136	0.000107	0.000178
Frame 6	0.001213	0.000319	0.000332	0.000132	0.000223	0.000108
Frame 7	0.001164	0.000523	0.000503	0.000403	0.000167	0.000482
Frame 8	0.001250	0.000418	0.000445	0.000442	0.000327	0.000181
Frame 9	0.001249	5.22E-05	0.000328	0.000361	0.000488	0.000359
Frame 10	0.001339	0.000353	0.000567	0.000228	0.000684	0.000175
Frame 11	0.000779	0.000362	0.000318	0.000535	0.000114	0.000128
Frame 12	0.001222	0.000119	0.000334	0.000412	0.000365	0.000324
Frame 13	0.001178	6.96E-05	0.000218	0.000249	0.000293	0.000287
Frame 14	0.001227	8.6E-05	0.000139	0.000566	0.000559	0.000335
Frame 15	0.001067	9.66E-05	0.000341	0.000292	0.000462	0.000380
Frame 16	0.001118	6.4E-05	0.000233	0.000223	0.000479	0.000296
Frame 17	0.001108	6.92E-05	0.000224	0.000302	0.000305	0.000322
Frame 18	0.001102	6.58E-05	0.000232	0.000279	0.000288	0.000270
Frame 19	0.001068	8E-05	0.000353	0.000121	0.000178	0.000327
Frame 20	0.000959	0.000228	0.000145	0.000409	0.000126	0.000479
Frame 21	0.000381	0.000621	0.000606	0.000515	0.000329	0.000697
Frame 22	0.001247	0.000187	0.000443	0.000416	0.000372	0.000296
Frame 23	0.000444	0.000486	0.000853	0.000474	0.000151	0.000245
Average	0.001087	0.000253	0.000390	0.000389	0.000337	0.000360

Table C.18: Mean non-dimensional scale factors from error minimization between unbraced frames with randomly generated imperfection and first seven ABAQUS eigenmodes

	$\bar{x}_1$	$\bar{x}_2$	$\bar{x}_3$	$\bar{x}_4$	$\bar{x}_5$	$\bar{x}_6$	$\bar{x}_7$
Frame 1	0.001137	0.000409	0.000432	0.000388	0.000234	0.000531	0.000167
Frame 2	0.001275	0.000129	0.000576	0.000774	0.000776	0.000727	0.000623
Frame 3	0.001326	0.000130	0.000643	0.000795	0.000675	0.000865	0.000927
Frame 4	0.001185	0.000375	0.000342	0.000501	0.000210	0.000247	0.000204
Frame 5	0.000977	0.000567	0.000208	0.000136	0.000105	0.000178	0.000118
Frame 6	0.001189	0.000319	0.000327	0.000132	0.000192	0.000108	0.000129
Frame 7	0.001171	0.000500	0.000512	0.000403	0.000168	0.000329	0.000303
Frame 8	0.001235	0.000405	0.000445	0.000412	0.000323	0.000150	0.000128
Frame 9	0.001249	5.22E-05	0.000318	0.000361	0.000440	0.000359	0.000376
Frame 10	0.001278	0.000209	0.000567	0.000329	0.000684	0.000175	0.000190
Frame 11	0.000779	0.000362	0.000319	0.000535	0.000109	0.000128	0.000235
Frame 12	0.001232	0.000127	0.000318	0.000412	0.000340	0.000346	0.000280
Frame 13	0.001163	4.06E-05	0.000213	0.000249	0.000322	0.000287	0.000289
Frame 14	0.001231	8.5E-05	0.000127	0.000566	0.000559	0.000344	8.45E-05
Frame 15	0.001026	0.000103	0.000338	0.000267	0.000454	0.000364	0.000516
Frame 16	0.001122	6.28E-05	0.000243	0.000214	0.000441	0.000296	0.000297
Frame 17	0.001092	7.27E-05	0.000228	0.000302	0.000313	0.000322	0.000372
Frame 18	0.001095	6.94E-05	0.000232	0.000279	0.000284	0.000270	0.000325
Frame 19	0.001052	8.52E-05	0.000353	0.000134	0.000176	0.000327	0.000305
Frame 20	0.00096	0.000228	0.000146	0.000418	0.000141	0.000483	0.000290
Frame 21	0.000408	0.000622	0.000603	0.000491	0.000325	0.000677	0.000238
Frame 22	0.001245	0.000189	0.000444	0.000447	0.000365	0.000293	0.000457
Frame 23	0.000433	0.000481	0.000852	0.000469	0.000147	0.000241	0.000112
Average	0.001081	0.000244	0.000382	0.000392	0.000338	0.000350	0.000303

Table C.19: Mean non-dimensional scale factors from error minimization between unbraced frames with randomly generated imperfection and first eight ABAQUS eigenmodes

	$\bar{x}_1$	$\bar{x}_2$	$\bar{x}_3$	$\bar{x}_4$	$\bar{x}_5$	$\bar{x}_6$	$\bar{x}_7$	$\bar{x}_8$
Frame 1	0.001137	0.000405	0.000432	0.000217	0.000234	0.0003795	0.0001672	0.000416
Frame 2	0.001288	0.000110	0.000576	0.000749	0.000776	0.0007527	0.0006225	0.000225
Frame 3	0.001324	0.000130	0.000668	0.000802	0.000769	0.0008661	0.0009250	0.000551
Frame 4	0.001185	0.000364	0.000342	0.000515	0.000210	0.0002606	0.0002039	0.000186
Frame 5	0.000977	0.000562	0.000208	0.000131	0.000105	0.0001822	0.0001185	4.44E-05
Frame 6	0.001189	0.000313	0.000327	0.000106	0.000192	0.0001066	0.0001289	0.000119
Frame 7	0.001171	0.000500	0.000512	0.000318	0.000168	0.0003286	0.0003035	0.000329
Frame 8	0.001238	0.000399	0.000445	0.000422	0.000330	0.0001699	0.0001371	0.000181
Frame 9	0.001242	4.92E-05	0.000318	0.000351	0.000440	0.0003754	0.0003765	0.000140
Frame 10	0.001278	0.000209	0.000567	0.000329	0.000685	0.0001863	0.0001895	0.000105
Frame 11	0.000777	0.000354	0.000319	0.000522	0.000109	0.0001272	0.0002345	0.000114
Frame 12	0.001199	0.000142	0.000307	0.000399	0.000346	0.0004146	0.0003659	0.000448
Frame 13	0.001163	4.06E-05	0.000213	0.000247	0.000322	0.0002969	0.0002886	0.000407
Frame 14	0.001231	8.5E-05	0.000127	0.000560	0.000681	0.0003444	8.445E-05	0.000370
Frame 15	0.001031	0.000104	0.000340	0.000264	0.000466	0.0003752	0.0005839	0.000429
Frame 16	0.001115	6.37E-05	0.000238	0.000191	0.000471	0.0002958	0.0003012	0.000594
Frame 17	0.001092	7.27E-05	0.000228	0.000309	0.000313	0.0003210	0.0003717	0.000278
Frame 18	0.001095	6.94E-05	0.000232	0.000283	0.000284	0.0002693	0.0003249	0.000258
Frame 19	0.001052	8.52E-05	0.000350	0.000134	0.000176	0.0004302	0.0003053	0.000667
Frame 20	0.000959	0.00023	0.000144	0.000414	0.000146	0.0004812	0.0002905	0.000414
Frame 21	0.000415	0.000639	0.000604	0.000482	0.000318	0.0006937	0.0002337	0.000222
Frame 22	0.001232	0.000195	0.000443	0.000443	0.000404	0.0002916	0.0004617	0.000626
Frame 23	0.000418	0.000464	0.000823	0.000466	0.000138	0.0002398	0.0001124	0.000174
Average	0.001079	0.000243	0.000381	0.000376	0.000351	0.0003560	0.0003100	0.000317



Table C.20: Mean non-dimensional scale factors from error minimization between unbraced frames with randomly generated imperfection and first nine ABAQUS eigenmodes

	$\bar{x}_1$	$\bar{x}_2$	$\bar{x}_3$	$\bar{x}_4$	$\bar{x}_5$	$\bar{x}_6$	$\bar{x}_7$	$\bar{x}_8$	$\bar{x}_9$
Frame 1	0.001147	0.000405	0.000433	0.000217	0.000183	0.000379	0.000162	0.000416	0.000113
Frame 2	0.001288	0.000110	0.000595	0.000749	0.000812	0.000753	0.000618	0.000225	0.000613
Frame 3	0.001343	0.000149	0.000668	0.000791	0.000769	0.000878	0.000926	0.000550	0.000360
Frame 4	0.001167	0.000364	0.000350	0.000515	0.000172	0.000261	0.000231	0.000186	0.000164
Frame 5	0.001012	0.000562	0.000181	0.000131	9.43E-05	0.000182	0.000149	4.44E-05	5.95E-05
Frame 6	0.001187	0.000313	0.000320	0.000106	0.000186	0.000107	0.000112	0.000119	6.91E-05
Frame 7	0.001167	0.000490	0.000436	0.000318	0.000160	0.000319	0.000319	0.000329	0.000145
Frame 8	0.001141	0.000397	0.000444	0.000448	0.000322	0.000171	0.000156	0.000154	0.000652
Frame 9	0.001242	4.92E-05	0.000321	0.000351	0.000432	0.000375	0.000493	0.000140	0.000575
Frame 10	0.001263	0.000207	0.000567	0.000328	0.000685	0.000186	0.000196	0.000105	0.000230
Frame 11	0.000777	0.000354	0.000302	0.000522	9.98E-05	0.000127	0.000205	0.000114	0.000309
Frame 12	0.001203	0.000138	0.000304	0.000395	0.000347	0.000357	0.000441	0.000413	0.000239
Frame 13	0.001137	4.06E-05	0.000204	0.000247	0.000315	0.000297	0.000322	0.000407	0.000315
Frame 14	0.001170	5.29E-05	0.000122	0.000560	0.000681	0.000344	0.000127	0.000370	0.000165
Frame 15	0.001031	0.000104	0.000346	0.000261	0.000453	0.000346	0.000585	0.000429	0.000481
Frame 16	0.001104	7.64E-05	0.000238	0.000190	0.000472	0.000296	0.000286	0.000811	0.000472
Frame 17	0.001093	7.22E-05	0.000231	0.000309	0.000296	0.000321	0.000349	0.000278	0.000342
Frame 18	0.001097	7.14E-05	0.000232	0.000283	0.000286	0.000269	0.000322	0.000258	0.000347
Frame 19	0.001052	8.51E-05	0.000252	0.000134	0.000176	0.000297	0.000305	0.001024	0.000924
Frame 20	0.000946	0.000238	0.000136	0.000417	0.000146	0.000538	0.000279	0.000412	0.000341
Frame 21	0.000383	0.000639	0.000606	0.000441	0.000315	0.000605	0.000238	0.000202	0.000750
Frame 22	0.001228	0.000194	0.000431	0.000442	0.000405	0.000239	0.000463	0.000624	0.000618
Frame 23	0.000417	0.000463	0.000824	0.000464	0.000138	0.000243	0.000113	0.000169	0.000361
Average	0.001069	0.000242	0.000371	0.000375	0.000345	0.000343	0.000322	0.000338	0.000376

Table C.21: Mean non-dimensional scale factors from error minimization between unbraced frames with randomly generated imperfection and first ten ABAQUS eigenmodes

	$\bar{x}_1$	$\bar{x}_2$	$\bar{x}_3$	$\bar{x}_4$	$\bar{x}_5$	$\bar{x}_6$	$\bar{x}_7$	$\bar{x}_8$	$\bar{x}_9$	$\bar{x}_{10}$
Frame 1	0.001147	0.000416	0.000433	0.000211	0.000183	0.000219	0.000162	0.000338	0.000113	0.000358
Frame 2	0.001286	0.000117	0.000595	0.000717	0.000812	0.000753	0.000618	0.000261	0.000613	0.000159
Frame 3	0.001342	0.000149	0.000688	0.000791	0.000790	0.000878	0.000931	0.000552	0.000361	0.000640
Frame 4	0.001167	0.000362	0.000350	0.000435	0.000172	0.000286	0.000231	0.000172	0.000164	0.000116
Frame 5	0.001012	0.000544	0.000181	0.000133	9.43E-05	0.000178	0.000149	4.9E-05	5.95E-05	4.62E-05
Frame 6	0.001187	0.000319	0.000320	0.000106	0.000186	8.63E-05	0.000112	0.000107	6.91E-05	9.64E-05
Frame 7	0.001187	0.000490	0.000427	0.000318	0.000141	0.000368	0.000290	0.000329	0.000140	0.000223
Frame 8	0.001143	0.000393	0.000403	0.000363	0.000313	0.000172	0.000120	0.000147	0.000536	0.000366
Frame 9	0.001243	5.36E-05	0.000321	0.000328	0.000431	0.000363	0.000493	0.000145	0.000575	9.35E-05
Frame 10	0.001299	0.000228	0.000567	0.000309	0.000685	0.000186	0.000176	0.000105	0.000232	0.000180
Frame 11	0.000766	0.000354	0.000302	0.000505	9.98E-05	0.000105	0.000205	0.000122	0.000309	0.000324
Frame 12	0.001203	0.000108	0.000233	0.000390	0.000358	0.000302	0.000186	0.000342	0.000132	0.000671
Frame 13	0.001137	4.06E-05	0.000204	0.000231	0.000315	0.000286	0.000322	0.000508	0.000315	0.000475
Frame 14	0.001170	5.29E-05	0.000122	0.000556	0.000556	0.000344	0.000127	0.000294	0.000165	0.000234
Frame 15	0.001028	0.000122	0.000347	0.000263	0.000450	0.000348	0.000693	0.000439	0.000484	0.000532
Frame 16	0.001104	7.63E-05	0.000238	0.000190	0.000472	0.000298	0.000286	0.000811	0.000472	0.000300
Frame 17	0.001093	7.22E-05	0.000231	0.000296	0.000296	0.000328	0.000349	0.000278	0.000342	0.000216
Frame 18	0.001097	7.14E-05	0.000232	0.000281	0.000286	0.000269	0.000322	0.000243	0.000347	0.000263
Frame 19	0.001039	8.64E-05	0.000252	0.000135	0.000176	0.000297	0.000347	0.001024	0.000924	0.000365
Frame 20	0.000948	0.000238	0.000136	0.000412	0.000142	0.000542	0.000290	0.000407	0.000337	0.000435
Frame 21	0.000402	0.000627	0.000603	0.000383	0.000316	0.000535	0.000205	0.000237	0.000693	0.000415
Frame 22	0.001229	0.000194	0.000426	0.000431	0.000403	0.000235	0.000435	0.000659	0.000623	0.000199
Frame 23	0.000417	0.000463	0.000823	0.000475	0.000139	0.000240	0.000113	0.000169	0.000339	0.000398
Average	0.001072	0.000242	0.000367	0.000359	0.000340	0.000331	0.000311	0.000336	0.000363	0.000309

### C.2.2. Braced frames

Table C.22: Mean scale factors from error minimization between braced frames with randomly generated imperfection and first ABAQUS eigenmode

	$\bar{X}_1$
Frame 1	1.374100
Frame 2	5.053025
Frame 3	2.806508
Frame 4	2.497376
Frame 5	2.190420
Frame 6	0.826440
Frame 7	2.855212
Frame 8	2.672531
Frame 9	2.180871
Frame 10	0.952075
Frame 11	5.587761
Frame 12	1.774369
Frame 13	1.604464
Frame 14	1.185454
Frame 15	1.094544
Frame 16	1.184860
Frame 17	1.633737
Frame 18	5.131378
Frame 19	0.891541
Frame 20	5.018140

Table C.23: Mean scale factors from error minimization between braced frames with randomly generated imperfection and first two ABAQUS eigenmodes

	$\bar{X}_1$	$\bar{X}_2$
Frame 1	1.3769900	1.250833
Frame 2	5.0530246	1.191313
Frame 3	2.8065082	2.461037
Frame 4	2.4077761	1.486670
Frame 5	1.7882561	1.408226
Frame 6	2.3842520	2.819226
Frame 7	2.8552118	0.883084
Frame 8	2.6728484	2.696828
Frame 9	1.9388566	2.458285
Frame 10	0.9520298	1.035279
Frame 11	6.2340318	5.136739
Frame 12	1.9690022	1.467801
Frame 13	1.7828720	1.890237
Frame 14	1.1854800	1.199456
Frame 15	1.0945312	1.135524
Frame 16	1.1846130	1.057299
Frame 17	1.6850980	1.495410
Frame 18	5.1147839	4.951066
Frame 19	0.8076180	4.895951
Frame 20	5.0214855	1.456579

Table C.24: Mean scale factors from error minimization between braced frames with randomly generated imperfection and first three ABAQUS eigenmodes

	$\bar{X}_1$	$\bar{X}_2$	$\bar{X}_3$
Frame 1	1.160949	1.2508325	1.3633530
Frame 2	3.282959	1.1913133	3.8803945
Frame 3	2.765991	2.4610371	1.1700148
Frame 4	2.407776	1.4866696	1.4733338
Frame 5	1.721342	1.4886500	1.3207250
Frame 6	1.096560	0.9839089	1.3720957
Frame 7	4.545151	0.8830844	5.0265044
Frame 8	2.673427	2.6970402	0.9257400
Frame 9	2.448631	1.9773129	3.6472103
Frame 10	1.044989	1.0351586	1.0081960
Frame 11	6.232757	5.1379481	0.8615220
Frame 12	2.051700	1.5257756	1.5265163
Frame 13	1.693270	1.9367011	1.0359517
Frame 14	1.295000	1.1994704	1.2585136
Frame 15	1.115182	1.1356971	1.2272982
Frame 16	1.384931	1.0574986	1.2329450
Frame 17	1.853985	1.5043283	1.6845035
Frame 18	5.160717	4.9430393	2.1441410
Frame 19	0.806172	4.8968118	1.4446000
Frame 20	5.021517	1.4608238	1.5928883

Table C.25: Mean scale factors from error minimization between braced frames with randomly generated imperfection and first four ABAQUS eigenmodes

	$\bar{X}_1$	$\bar{X}_2$	$\bar{X}_3$	$\bar{X}_4$
Frame 1	1.166949	1.2361516	1.3642251	0.6842910
Frame 2	3.282959	1.1849651	3.8803945	1.0413288
Frame 3	2.765991	2.4718913	1.1700148	0.6792979
Frame 4	2.388007	1.8752275	1.4733338	1.6377452
Frame 5	1.664433	1.5410122	1.3821640	2.5056843
Frame 6	1.645756	1.0636137	1.3721026	1.3376578
Frame 7	4.545151	1.0623735	5.0265044	1.2753031
Frame 8	2.673007	2.6997227	0.9256152	0.7188581
Frame 9	2.247206	2.5431939	3.0372079	3.7671035
Frame 10	1.044002	1.1153604	1.0080302	1.1344319
Frame 11	6.231279	5.1377460	0.9240552	0.9898691
Frame 12	1.928001	1.5488813	1.5191047	1.0243441
Frame 13	1.693182	1.9362799	1.0356677	1.1818910
Frame 14	1.295011	1.2229777	1.2585690	1.3420997
Frame 15	1.112952	1.0852218	1.2272315	1.0666513
Frame 16	1.384432	1.1253047	1.2324354	1.2541984
Frame 17	1.844089	1.4842300	1.6744050	1.9506714
Frame 18	5.155063	4.9337140	1.5220177	5.0781245
Frame 19	0.805767	4.8972092	1.4560059	1.6230044
Frame 20	5.032339	1.4607460	1.5905389	1.8218468

Table C.26: Mean scale factors from error minimization between braced frames with randomly generated imperfection and first five ABAQUS eigenmodes

	$\bar{X}_1$	$\bar{X}_2$	$\bar{X}_3$	$\bar{X}_4$	$\bar{X}_5$
Frame 1	0.964295	1.2361516	1.0123216	0.6842911	2.031923
Frame 2	2.688174	1.1849651	2.8279263	1.0413288	3.420252
Frame 3	2.669232	2.4718913	1.1680109	0.6792979	0.444521
Frame 4	2.252491	1.4428527	1.4733339	1.2240346	1.345672
Frame 5	1.708185	1.5841600	1.4640516	2.3400551	0.772454
Frame 6	1.024568	1.0636137	1.2040820	1.3376578	1.828508
Frame 7	2.879907	1.0623735	3.7306806	1.2753031	4.053778
Frame 8	2.751926	2.6997358	0.9038116	0.7189305	1.924001
Frame 9	2.063649	2.4132882	2.7547507	4.5542843	1.954662
Frame 10	1.024425	1.1155588	1.0724133	1.1342326	1.792332
Frame 11	6.210344	6.6135344	0.9246944	0.9893122	3.687032
Frame 12	1.913995	1.5391873	1.5035928	1.0926092	1.504239
Frame 13	1.684324	1.8640788	1.0441721	1.1818119	1.768202
Frame 14	1.293551	1.2199145	1.2732656	1.3431333	1.292130
Frame 15	1.214183	1.0854040	1.2140660	1.0656467	1.239003
Frame 16	1.408201	1.1242073	1.6564529	1.2552970	2.588003
Frame 17	1.825239	1.6011433	1.6986627	1.9554294	1.522952
Frame 18	5.170333	4.9622802	1.4834475	5.0459048	1.470137
Frame 19	0.804163	4.9014683	1.4578294	1.6034100	1.715721
Frame 20	5.044574	1.5519809	1.5667599	1.7898594	1.749353

Table C.27: Mean scale factors from error minimization between braced frames with randomly generated imperfection and first six ABAQUS eigenmodes

	$\bar{X}_1$	$\bar{X}_2$	$\bar{X}_3$	$\bar{X}_4$	$\bar{X}_5$	$\bar{X}_6$
Frame 1	0.963245	1.2565052	1.0124313	0.6658601	2.031923	0.4694944
Frame 2	2.688174	1.1048397	2.8279263	0.8336152	3.420252	0.3262422
Frame 3	2.669232	2.3318075	1.1680109	0.6650878	0.443210	0.8869784
Frame 4	2.226038	1.2413511	1.4733432	1.1171136	1.003831	1.0359121
Frame 5	1.723247	1.6284132	1.3881533	2.1376575	0.684412	0.3420204
Frame 6	1.538568	1.0431827	1.2041020	1.3260620	1.828508	0.5499782
Frame 7	2.879907	1.0609519	3.7306806	1.2991558	4.053778	0.8606104
Frame 8	2.752388	2.7330499	0.9038454	0.7168258	1.928095	0.8695000
Frame 9	2.077817	2.4339515	2.8053896	3.9290086	1.693105	3.3974511
Frame 10	1.024311	1.1066129	1.0724202	1.2040390	1.792249	0.9065094
Frame 11	6.210344	6.6131959	0.9422269	1.2328537	3.686952	1.5649888
Frame 12	1.945780	1.5192028	1.3918376	1.0840099	1.517386	1.8622415
Frame 13	1.659952	1.8547210	1.0446506	1.1818664	2.220151	2.3508059
Frame 14	1.292462	1.1680330	1.2747908	1.3299861	1.291622	1.2145837
Frame 15	1.214189	1.1814200	1.2135985	1.0673292	1.239003	1.4644092
Frame 16	1.403014	1.1353401	1.6563315	1.3109966	2.584213	0.8984756
Frame 17	1.780184	1.6094304	1.6853397	1.9466088	1.511599	1.2841900
Frame 18	5.043005	4.9711753	1.3683451	4.8772041	1.450487	1.6700361
Frame 19	0.792078	4.8977170	1.5458793	1.5940288	1.687251	1.8426484
Frame 20	5.045470	1.5160068	1.6136304	1.7747740	1.753541	1.8872237

Table C.28: Mean scale factors from error minimization between braced frames with randomly generated imperfection and first seven ABAQUS eigenmodes

	$\bar{X}_1$	$\bar{X}_2$	$\bar{X}_3$	$\bar{X}_4$	$\bar{X}_5$	$\bar{X}_6$	$\bar{X}_7$
Frame 1	0.956231	1.2565053	0.6128984	0.6658606	1.582178	0.4694944	1.3686069
Frame 2	2.686555	1.1048392	1.6737476	0.8336163	2.549458	0.3268480	2.3926675
Frame 3	2.635283	2.3318075	0.9930332	0.6650878	0.436441	0.8869785	0.4248441
Frame 4	2.226038	1.2413554	1.3666281	1.1171091	1.003828	1.0359127	1.3709014
Frame 5	1.712132	1.6042055	1.4027038	2.0221631	0.732053	0.4083227	0.5722211
Frame 6	1.485330	1.0431827	1.1927535	1.3260635	1.561184	0.5499781	1.6806668
Frame 7	3.044075	1.0609519	3.4648545	1.2991556	3.633419	0.8606117	3.3516640
Frame 8	2.552690	2.7329275	0.8036131	0.7170532	1.800010	0.8698373	1.1204237
Frame 9	2.081612	2.3746643	2.7597026	3.8574515	1.995502	3.5928833	2.6738163
Frame 10	0.972919	1.1061759	1.0364207	1.2061458	2.042389	0.9058343	1.8324779
Frame 11	5.992594	5.3484319	0.9421013	1.2328202	2.847452	1.5691732	2.4500366
Frame 12	1.912300	1.5202990	1.4017458	1.1329111	1.514888	1.8448330	1.5161733
Frame 13	1.661781	1.8591018	1.0754686	1.1823787	2.121033	2.0293302	1.3850386
Frame 14	1.204741	1.1680373	1.3249578	1.3290528	1.292730	1.2145708	0.8209344
Frame 15	1.205674	1.1815840	1.2036343	1.0735775	1.222414	1.4648667	1.1481598
Frame 16	0.943560	1.1343735	1.1361933	1.2910588	3.908241	0.8790204	3.8361191
Frame 17	1.755982	1.6057451	1.6783395	1.9580656	1.630443	1.5211962	1.1160291
Frame 18	5.040610	5.0162487	1.3686656	4.8858840	1.319965	1.6412420	5.0068604
Frame 19	0.800803	4.9114004	1.5226554	1.6340872	1.677755	1.8361647	1.9269451
Frame 20	5.095390	1.5156792	1.6172421	1.3684807	1.724679	1.8787698	5.0619022

Table C.29: Mean scale factors from error minimization between braced frames with randomly generated imperfection and first eight ABAQUS eigenmodes

	$\bar{X}_1$	$\bar{X}_2$	$\bar{X}_3$	$\bar{X}_4$	$\bar{X}_5$	$\bar{X}_6$	$\bar{X}_7$	$\bar{X}_8$
Frame 1	0.956362	1.232643	0.612498	0.502179	1.582177	0.431352	1.368606	0.511296
Frame 2	2.686555	1.092101	1.673750	0.532859	2.549457	0.246440	2.392668	0.721679
Frame 3	2.635283	2.328075	0.993033	0.615342	0.436941	0.870255	0.424895	0.132208
Frame 4	2.179606	0.920954	1.366624	1.128751	0.894815	1.203984	1.370903	0.721929
Frame 5	1.704321	1.468536	1.332149	2.009003	0.727530	0.371167	0.528257	0.592311
Frame 6	0.992110	1.043642	1.192353	1.329906	1.561185	0.561639	1.680667	0.359721
Frame 7	3.044075	1.030819	3.464854	1.316456	3.633420	0.771192	3.351664	0.689044
Frame 8	2.552702	2.564426	0.803691	0.647939	1.800088	0.773686	1.120529	2.441364
Frame 9	1.847405	2.430543	2.678112	3.637619	1.508573	5.007233	2.266182	4.350538
Frame 10	0.972367	1.082086	1.036305	1.206011	2.041081	0.660640	1.836168	1.180742
Frame 11	5.992882	5.351195	0.942009	1.249375	2.846343	1.643122	2.451114	0.836944
Frame 12	1.982131	1.520372	1.402576	0.968332	1.489859	1.815115	1.408046	1.944074
Frame 13	1.662145	1.859357	1.082953	1.201494	2.116280	2.041073	1.419787	1.154762
Frame 14	1.204404	1.143987	1.326335	1.310364	1.292202	1.214521	0.824011	1.011254
Frame 15	1.205665	1.183128	1.206479	1.124784	1.223563	1.373722	1.147057	1.147650
Frame 16	0.942522	1.126541	1.136905	1.290755	3.908921	0.841535	3.844123	1.129930
Frame 17	1.746580	1.605264	1.608855	1.983088	1.638572	1.521267	1.124440	2.059754
Frame 18	4.944397	5.017574	1.361178	4.865107	1.319513	1.540124	4.975486	1.383677
Frame 19	0.797417	4.875271	1.522970	1.633123	1.432881	1.795165	1.860359	5.105035
Frame 20	5.079102	1.482247	1.627476	1.358117	1.663740	2.237677	5.032270	1.800515

Table C.30: Mean scale factors from error minimization between braced frames with randomly generated imperfection and first nine ABAQUS eigenmodes

	$\bar{X}_1$	$\bar{X}_2$	$\bar{X}_3$	$\bar{X}_4$	$\bar{X}_5$	$\bar{X}_6$	$\bar{X}_7$	$\bar{X}_8$	$\bar{X}_9$
Frame 1	0.96405	1.23267	0.59601	0.50222	0.97162	0.43136	1.16292	0.51130	1.21675
Frame 2	2.67403	1.09210	1.60470	0.53286	1.51753	0.24641	1.98110	0.72165	2.09180
Frame 3	2.66627	2.32808	0.99270	0.61534	0.34043	0.87026	0.39492	0.13322	0.32321
Frame 4	2.23071	0.89884	1.36661	1.12138	0.58242	1.11671	1.37090	0.59982	0.75646
Frame 5	1.66644	1.46189	1.26447	1.65641	0.78121	0.44810	0.45120	0.59630	3.34448
Frame 6	0.14411	1.04364	1.28009	1.32995	1.37669	0.56164	1.56260	0.35971	1.76794
Frame 7	1.76393	1.03082	3.70306	1.31646	2.87453	0.77120	2.83077	0.68904	3.53041
Frame 8	2.54848	2.56436	0.73906	0.64799	1.77632	0.77369	1.12591	2.44288	0.63018
Frame 9	1.76127	2.49843	2.65977	3.61107	1.42087	4.94410	1.90859	5.19259	2.01655
Frame 10	0.98824	1.08374	1.02240	1.20183	2.03665	0.66188	1.84160	1.18077	1.51227
Frame 11	5.95555	4.67215	0.94199	1.24846	2.68701	1.64335	3.27474	0.83946	2.40199
Frame 12	2.04769	1.49858	1.40157	0.85600	1.49273	1.79299	1.74270	1.94826	1.87072
Frame 13	1.66813	1.82772	1.11745	1.20275	2.01519	1.94455	1.55223	1.15662	1.19234
Frame 14	1.16300	1.14358	1.31359	1.31118	1.28274	1.21445	1.15880	1.01176	2.42425
Frame 15	1.14507	1.18346	1.21002	1.12480	1.25517	1.37281	1.09968	1.14683	1.22193
Frame 16	0.92803	1.12676	1.02838	1.28608	3.90419	0.84120	3.95520	1.12895	6.24286
Frame 17	1.74265	1.59622	1.60979	1.98080	1.63166	1.59906	1.73383	2.05693	1.21125
Frame 18	4.61211	5.01353	1.26453	4.87035	1.30460	1.62919	4.77799	1.40468	1.44100
Frame 19	0.84375	4.77428	1.46296	1.63446	1.39745	1.72938	2.05726	4.97949	1.48306
Frame 20	4.89835	1.47790	1.62820	1.34344	1.66383	2.24270	4.38782	1.81490	1.94613

Table C.31: Mean scale factors from error minimization between braced frames with randomly generated imperfection and first ten ABAQUS eigenmodes

	$\bar{X}_1$	$\bar{X}_2$	$\bar{X}_3$	$\bar{X}_4$	$\bar{X}_5$	$\bar{X}_6$	$\bar{X}_7$	$\bar{X}_8$	$\bar{X}_9$	$\bar{X}_{10}$
Frame 1	0.96356	1.26777	0.63010	0.50054	0.97160	0.32099	1.16293	0.46084	1.21678	0.32708
Frame 2	2.67403	1.10856	1.60469	0.52287	1.51753	0.16430	1.98112	0.58836	2.09177	0.63528
Frame 3	2.66627	2.30342	0.99270	0.61248	0.34023	0.78405	0.39644	0.12840	0.33213	0.27910
Frame 4	2.18340	0.79675	1.36694	1.13106	0.57024	0.88332	1.37089	0.44112	0.62553	0.64677
Frame 5	1.64425	1.40600	1.24116	1.70788	0.76332	0.44340	0.44100	0.52443	3.28824	4.64000
Frame 6	1.11824	1.00239	1.91721	1.25225	1.37670	0.57046	1.56260	0.37269	1.76793	0.56757
Frame 7	1.76392	1.01629	3.70303	1.32046	2.87453	0.71375	2.83081	0.59685	3.53041	0.91518
Frame 8	2.54841	2.56299	0.73915	0.61477	1.76358	0.73792	1.12590	1.76701	0.62992	0.83946
Frame 9	1.74774	2.37476	2.64876	3.67316	1.42027	4.82100	1.86978	5.17377	1.93115	1.43438
Frame 10	1.10011	1.09288	1.04019	1.19242	2.04130	0.66121	1.84042	1.14198	1.52621	0.51767
Frame 11	5.95051	4.67400	0.94811	1.24952	2.68839	1.65552	3.27210	0.90612	2.40177	1.07410
Frame 12	1.90102	1.51609	1.41333	0.80242	1.43327	1.76961	1.56113	1.84311	1.80919	2.04015
Frame 13	1.56816	1.89613	1.11161	1.20249	1.74846	1.64893	1.40219	1.14749	1.14873	1.35815
Frame 14	1.16247	1.14378	1.31278	1.31108	1.28429	1.20019	1.16122	0.90638	1.44416	2.16146
Frame 15	1.14507	1.13771	1.21029	1.12569	1.25552	1.40965	1.10157	1.09120	1.22300	0.94687
Frame 16	0.92370	1.12615	1.04104	1.27734	3.92132	0.78880	3.96022	1.22938	6.24347	0.44057
Frame 17	1.74814	1.59422	1.61951	1.97685	1.55853	1.40470	1.00089	2.14804	1.27175	1.12322
Frame 18	4.58886	4.91791	1.28920	4.88672	1.28614	1.56149	4.66906	1.41869	1.43685	2.56883
Frame 19	0.86578	4.47265	1.43726	1.63427	1.39198	1.72050	2.12660	4.65206	1.56702	1.78620
Frame 20	4.88206	1.47768	1.64788	1.33561	1.73790	2.00358	4.37502	1.54309	1.95124	1.04387

Table C.32: Total frame heights or member lengths depending on the eigenmode type

	<i>H</i> or <i>L</i> (mm)									
	Mode 1	Mode 2	Mode 3	Mode 4	Mode 5	Mode 6	Mode 7	Mode 8	Mode 9	Mode 10
Frame 1	4000	4000	4000	4000	6000	4000	6000	4000	6000	4000
Frame 2	10000	4000	10000	4000	10000	4000	10000	10000	10000	10000
Frame 3	8000	8000	8000	8000	4000	8000	4000	4000	4000	8000
Frame 4	4000	6000	4000	4000	6000	6000	6000	4000	6000	6000
Frame 5	4000	4000	4000	8000	4000	4000	4000	4000	8000	8000
Frame 6	4000	4000	4000	4000	6000	4000	6000	4000	6000	4000
Frame 7	10000	4000	10000	4000	10000	4000	10000	10000	10000	4000
Frame 8	8000	8000	8000	8000	8000	8000	4000	8000	4000	4000
Frame 9	4000	8000	8000	8000	4000	8000	8000	8000	8000	8000
Frame 10	4000	4000	4000	4000	4000	4000	4000	4000	4000	4000
Frame 11	10000	10000	4000	10000	10000	10000	10000	10000	10000	10000
Frame 12	4000	4000	4000	4000	4000	4000	4000	4000	6000	6000
Frame 13	4000	4000	4000	4000	4000	4000	6000	4000	4000	6000
Frame 14	4000	4000	4000	4000	4000	4000	4000	4000	4000	6000
Frame 15	6000	4000	4000	4000	4000	4000	4000	4000	6000	4000
Frame 16	4000	4000	4000	4000	4000	4000	4000	4000	10000	4000
Frame 17	4000	4000	4000	4000	4000	4000	4000	4000	4000	4000
Frame 18	8000	8000	8000	8000	8000	8000	8000	8000	8000	8000
Frame 19	4000	8000	4000	4000	8000	4000	4000	8000	8000	8000
Frame 20	6000	4000	4000	8000	4000	4000	8000	4000	8000	4000

Table C.33: Mean non-dimensional scale factors from error minimization between braced frames with randomly generated imperfection and first ABAQUS eigenmode

	$\bar{x}_1$
Frame 1	0.0003435
Frame 2	0.0005053
Frame 3	0.0003508
Frame 4	0.0006243
Frame 5	0.0005476
Frame 6	0.0002066
Frame 7	0.0002855
Frame 8	0.0003341
Frame 9	0.0005452
Frame 10	0.000238
Frame 11	0.0005588
Frame 12	0.0004436
Frame 13	0.0004011
Frame 14	0.0002964
Frame 15	0.0001824
Frame 16	0.0002962
Frame 17	0.0004084
Frame 18	0.0006414
Frame 19	0.0002229
Frame 20	0.0006273
Average	0.000403

Table C.34: Mean non-dimensional scale factors from error minimization between braced frames with randomly generated imperfection and first two ABAQUS eigenmodes

	$\bar{x}_1$	$\bar{x}_2$
Frame 1	0.000344	0.000313
Frame 2	0.000505	0.000298
Frame 3	0.000351	0.000308
Frame 4	0.000602	0.000248
Frame 5	0.000447	0.000352
Frame 6	0.000596	0.000705
Frame 7	0.000286	0.000221
Frame 8	0.000334	0.000337
Frame 9	0.000485	0.000307
Frame 10	0.000238	0.000259
Frame 11	0.000623	0.000514
Frame 12	0.000492	0.000367
Frame 13	0.000446	0.000473
Frame 14	0.000296	0.000300
Frame 15	0.000182	0.000284
Frame 16	0.000296	0.000264
Frame 17	0.000421	0.000374
Frame 18	0.000639	0.000619
Frame 19	0.000202	0.000612
Frame 20	0.000628	0.000364
Average	0.000421	0.000376

Table C.35: Mean non-dimensional scale factors from error minimization between braced frames with randomly generated imperfection and first three ABAQUS eigenmodes

	$\bar{x}_1$	$\bar{x}_2$	$\bar{x}_3$
Frame 1	0.000290	0.000313	0.000340
Frame 2	0.000328	0.000298	0.000388
Frame 3	0.000346	0.000308	0.000146
Frame 4	0.000602	0.000248	0.000368
Frame 5	0.000430	0.000370	0.000330
Frame 6	0.000274	0.000246	0.000343
Frame 7	0.000455	0.000221	0.000503
Frame 8	0.000334	0.000337	0.000116
Frame 9	0.000612	0.000247	0.000456
Frame 10	0.000261	0.000259	0.000252
Frame 11	0.000623	0.000514	0.000215
Frame 12	0.000513	0.000381	0.000382
Frame 13	0.000423	0.000484	0.000259
Frame 14	0.000324	0.000300	0.000315
Frame 15	0.000186	0.000284	0.000307
Frame 16	0.000346	0.000264	0.000308
Frame 17	0.000463	0.000376	0.000421
Frame 18	0.000645	0.000618	0.000268
Frame 19	0.000202	0.000612	0.000361
Frame 20	0.000628	0.000365	0.000398
Average	0.000414	0.000352	0.000324



Table C.36: Mean non-dimensional scale factors from error minimization between braced frames with randomly generated imperfection and first four ABAQUS eigenmodes

	$\bar{x}_1$	$\bar{x}_2$	$\bar{x}_3$	$\bar{x}_4$
Frame 1	0.000290	0.000309	0.000340	0.000171
Frame 2	0.000328	0.000296	0.000388	0.000260
Frame 3	0.000346	0.000309	0.000146	8.49E-05
Frame 4	0.000597	0.000313	0.000368	0.000409
Frame 5	0.000415	0.000385	0.000345	0.000313
Frame 6	0.000274	0.000266	0.000343	0.000334
Frame 7	0.000455	0.000266	0.000503	0.000319
Frame 8	0.000334	0.000337	0.000116	8.99E-05
Frame 9	0.000562	0.000318	0.000380	0.000471
Frame 10	0.000261	0.000279	0.000252	0.000284
Frame 11	0.000623	0.000514	0.000231	9.9E-05
Frame 12	0.000482	0.000387	0.000380	0.000256
Frame 13	0.000423	0.000484	0.000259	0.000295
Frame 14	0.000324	0.000306	0.000315	0.000336
Frame 15	0.000185	0.000271	0.000307	0.000267
Frame 16	0.000346	0.000281	0.000308	0.000314
Frame 17	0.000461	0.000371	0.000419	0.000488
Frame 18	0.000644	0.000617	0.000190	0.000635
Frame 19	0.000201	0.000612	0.000364	0.000406
Frame 20	0.000629	0.000365	0.000398	0.000228
Average	0.000409	0.000364	0.000318	0.000303

Table C.37: Mean non-dimensional scale factors from error minimization between braced frames with randomly generated imperfection and first five ABAQUS eigenmodes

	$\bar{x}_1$	$\bar{x}_2$	$\bar{x}_3$	$\bar{x}_4$	$\bar{x}_5$
Frame 1	0.000240	0.000309	0.000253	0.000171	0.000339
Frame 2	0.000269	0.000296	0.000283	0.000260	0.000342
Frame 3	0.000334	0.000309	0.000146	8.49E-05	0.000110
Frame 4	0.000563	0.000240	0.000368	0.000306	0.000224
Frame 5	0.000427	0.000396	0.000365	0.000293	0.000193
Frame 6	0.000256	0.000266	0.000301	0.000334	0.000305
Frame 7	0.000288	0.000266	0.000373	0.000319	0.000405
Frame 8	0.000344	0.000337	0.000113	8.99E-05	0.000240
Frame 9	0.000516	0.000302	0.000344	0.000569	0.000489
Frame 10	0.000256	0.000279	0.000268	0.000284	0.000448
Frame 11	0.000621	0.000661	0.000231	9.89E-05	0.000369
Frame 12	0.000478	0.000385	0.000376	0.000273	0.000376
Frame 13	0.000421	0.000466	0.000261	0.000295	0.000442
Frame 14	0.000323	0.000305	0.000318	0.000336	0.000323
Frame 15	0.000202	0.000271	0.000304	0.000266	0.000310
Frame 16	0.000352	0.000281	0.000414	0.000314	0.000647
Frame 17	0.000456	0.000400	0.000425	0.000489	0.000381
Frame 18	0.000646	0.000620	0.000185	0.000631	0.000184
Frame 19	0.000201	0.000613	0.000364	0.000401	0.000214
Frame 20	0.000631	0.000388	0.000392	0.000224	0.000437
Average	0.000391	0.000370	0.000304	0.000302	0.000339

Table C.38: Mean non-dimensional scale factors from error minimization between braced frames with randomly generated imperfection and first six ABAQUS eigenmodes

	$\bar{x}_1$	$\bar{x}_2$	$\bar{x}_3$	$\bar{x}_4$	$\bar{x}_5$	$\bar{x}_6$
Frame 1	0.000240	0.000314	0.000253	0.000166	0.000339	0.000117
Frame 2	0.000269	0.000276	0.000283	0.000208	0.000342	8.15E-05
Frame 3	0.000334	0.000291	0.000146	8.31E-05	0.000110	0.000111
Frame 4	0.000557	0.000207	0.000368	0.000279	0.000167	0.000173
Frame 5	0.000430	0.000407	0.000347	0.000267	0.000170	8.57E-05
Frame 6	0.000256	0.000261	0.000301	0.000332	0.000305	0.000137
Frame 7	0.000288	0.000265	0.000373	0.000325	0.000405	0.000215
Frame 8	0.000344	0.000342	0.000113	8.96E-05	0.000240	0.000109
Frame 9	0.000519	0.000304	0.000351	0.000491	0.000423	0.000425
Frame 10	0.000256	0.000277	0.000268	0.000301	0.000448	0.000227
Frame 11	0.000621	0.000661	0.000236	0.000123	0.000369	0.000156
Frame 12	0.000486	0.000380	0.000348	0.000271	0.000379	0.000466
Frame 13	0.000415	0.000464	0.000261	0.000295	0.000555	0.000588
Frame 14	0.000323	0.000292	0.000319	0.000332	0.000323	0.000304
Frame 15	0.000202	0.000295	0.000303	0.000267	0.000310	0.000366
Frame 16	0.000350	0.000284	0.000414	0.000328	0.000646	0.000225
Frame 17	0.000445	0.000402	0.000421	0.000487	0.000378	0.000321
Frame 18	0.000630	0.000621	0.000171	0.000610	0.000181	0.000209
Frame 19	0.000198	0.000612	0.000386	0.000399	0.000211	0.000461
Frame 20	0.000631	0.000379	0.000403	0.000222	0.000438	0.000472
Average	0.000390	0.000367	0.000303	0.000294	0.000337	0.000262

Table C.39: Mean non-dimensional scale factors from error minimization between braced frames with randomly generated imperfection and first seven ABAQUS eigenmodes

	$\bar{x}_1$	$\bar{x}_2$	$\bar{x}_3$	$\bar{x}_4$	$\bar{x}_5$	$\bar{x}_6$	$\bar{x}_7$
Frame 1	0.000239	0.000314	0.000153	0.000166	0.000264	0.000117	0.000228
Frame 2	0.000269	0.000276	0.000167	0.000208	0.000255	8.15E-05	0.000239
Frame 3	0.000329	0.000291	0.000124	8.31E-05	0.000109	0.000111	0.000106
Frame 4	0.000557	0.000207	0.000342	0.000279	0.000167	0.000173	0.000228
Frame 5	0.000428	0.000401	0.000350	0.000253	0.000183	0.000102	0.000143
Frame 6	0.000248	0.000261	0.000298	0.000332	0.000260	0.000137	0.000280
Frame 7	0.000304	0.000265	0.000346	0.000325	0.000363	0.000215	0.000335
Frame 8	0.000319	0.000342	0.000100	8.96E-05	0.000225	0.000109	0.000280
Frame 9	0.000520	0.000297	0.000345	0.000482	0.000499	0.000449	0.000334
Frame 10	0.000243	0.000277	0.000259	0.000302	0.000510	0.000226	0.000458
Frame 11	0.000599	0.000535	0.000236	0.000123	0.000285	0.000157	0.000245
Frame 12	0.000478	0.000380	0.000350	0.000283	0.000379	0.000461	0.000379
Frame 13	0.000415	0.000465	0.000269	0.000296	0.000530	0.000507	0.000231
Frame 14	0.000301	0.000292	0.000331	0.000332	0.000323	0.000304	0.000205
Frame 15	0.000201	0.000295	0.000301	0.000268	0.000306	0.000366	0.000287
Frame 16	0.000235	0.000284	0.000284	0.000323	0.000977	0.000220	0.000959
Frame 17	0.000439	0.000401	0.000420	0.000490	0.000408	0.000380	0.000279
Frame 18	0.000630	0.000627	0.000171	0.000611	0.000165	0.000205	0.000626
Frame 19	0.000200	0.000614	0.000381	0.000409	0.000210	0.000459	0.000482
Frame 20	0.000637	0.000379	0.000404	0.000171	0.000431	0.000470	0.000633
Average	0.000380	0.000360	0.000282	0.000291	0.000342	0.000263	0.000348

Table C.40: Mean non-dimensional scale factors from error minimization between braced frames with randomly generated imperfection and first eight ABAQUS eigenmodes

	$\bar{x}_1$	$\bar{x}_2$	$\bar{x}_3$	$\bar{x}_4$	$\bar{x}_5$	$\bar{x}_6$	$\bar{x}_7$	$\bar{x}_8$
Frame 1	0.000239	0.000308	0.000153	0.000126	0.000264	0.0001078	0.000228	0.000128
Frame 2	0.000269	0.000273	0.000167	0.000133	0.000255	6.161E-05	0.000239	7.22E-05
Frame 3	0.000329	0.000291	0.000124	7.69E-05	0.000109	0.0001088	0.000106	3.33E-05
Frame 4	0.000545	0.000153	0.000342	0.000282	0.000149	0.0002007	0.000228	0.00018
Frame 5	0.000426	0.000367	0.000333	0.000251	0.000180	9.265E-05	0.000132	0.000148
Frame 6	0.000248	0.000261	0.000298	0.000332	0.000260	0.0001404	0.000280	8.99E-05
Frame 7	0.000304	0.000258	0.000346	0.000329	0.000363	0.0001928	0.000335	6.89E-05
Frame 8	0.000319	0.000321	0.000100	8.1E-05	0.000225	9.671E-05	0.000280	0.000305
Frame 9	0.000462	0.000304	0.000335	0.000455	0.000377	0.0006259	0.000283	0.000544
Frame 10	0.000243	0.000271	0.000259	0.000302	0.000510	0.0001652	0.000459	0.000295
Frame 11	0.000599	0.000535	0.000236	0.000125	0.000285	0.0001643	0.000245	8.37E-05
Frame 12	0.000496	0.000380	0.000351	0.000242	0.000372	0.0004538	0.000352	0.000486
Frame 13	0.000416	0.000465	0.000271	0.000300	0.000529	0.0005103	0.000237	0.000289
Frame 14	0.000301	0.000286	0.000332	0.000328	0.000323	0.0003036	0.000206	0.000253
Frame 15	0.000201	0.000296	0.000302	0.000281	0.000306	0.0003434	0.000287	0.000287
Frame 16	0.000235	0.000282	0.000284	0.000323	0.000977	0.0002104	0.000960	0.000282
Frame 17	0.000437	0.000401	0.000402	0.000496	0.000410	0.0003803	0.000281	0.000515
Frame 18	0.000618	0.000627	0.00017	0.000608	0.000165	0.0001925	0.000622	0.000173
Frame 19	0.000199	0.000609	0.000381	0.000408	0.000179	0.0004488	0.000465	0.000638
Frame 20	0.000635	0.000371	0.000407	0.000170	0.000416	0.0005594	0.000629	0.000450
Average	0.000376	0.000353	0.000280	0.000282	0.000333	0.0002680	0.000343	0.000266

Table C.41: Mean non-dimensional scale factors from error minimization between braced frames with randomly generated imperfection and first nine ABAQUS eigenmodes

	$\bar{x}_1$	$\bar{x}_2$	$\bar{x}_3$	$\bar{x}_4$	$\bar{x}_5$	$\bar{x}_6$	$\bar{x}_7$	$\bar{x}_8$	$\bar{x}_9$
Frame 1	0.000241	0.000308	0.000149	0.000126	0.000162	0.000108	0.0001938	0.000128	0.000203
Frame 2	0.000267	0.000273	0.000160	0.000133	0.000152	6.16E-05	0.0001981	7.22E-05	0.000209
Frame 3	0.000333	0.000291	0.000124	7.69E-05	8.51E-05	0.000109	9.873E-05	3.33E-05	8.33E-05
Frame 4	0.000558	0.00015	0.000342	0.000280	9.71E-05	0.000186	0.0002285	0.00015	0.000126
Frame 5	0.000416	0.000365	0.000316	0.000207	0.000195	0.000112	0.0001128	0.000149	0.000418
Frame 6	0.000186	0.000261	0.00032	0.000332	0.000229	0.000140	0.0002604	8.99E-05	0.000295
Frame 7	0.000176	0.000258	0.00037	0.000329	0.000287	0.000193	0.0002831	6.89E-05	0.000353
Frame 8	0.000319	0.000321	9.24E-05	8.1E-05	0.000222	9.67E-05	0.0002815	0.000305	0.000158
Frame 9	0.000440	0.000312	0.000332	0.000451	0.000355	0.000618	0.0002386	0.000649	0.000252
Frame 10	0.000247	0.000271	0.000255	0.000300	0.000509	0.000165	0.0004604	0.000295	0.000378
Frame 11	0.000596	0.000467	0.000235	0.000125	0.000269	0.000164	0.0003275	8.39E-05	0.000240
Frame 12	0.000512	0.000375	0.000350	0.000214	0.000373	0.000448	0.0004355	0.000487	0.000312
Frame 13	0.000417	0.000457	0.000279	0.000301	0.000504	0.000486	0.0002587	0.000289	0.000298
Frame 14	0.000291	0.000286	0.000328	0.000328	0.000321	0.000304	0.0002897	0.000253	0.000356
Frame 15	0.000191	0.000296	0.000303	0.000281	0.000314	0.000343	0.0002749	0.000287	0.000204
Frame 16	0.000232	0.000282	0.000257	0.000322	0.000976	0.000210	0.0009888	0.000282	0.000624
Frame 17	0.000436	0.000399	0.000402	0.000495	0.000408	0.000400	0.0002890	0.000514	0.000303
Frame 18	0.000577	0.000627	0.000158	0.000609	0.000163	0.000204	0.0005972	0.000176	0.00018
Frame 19	0.000211	0.000597	0.000366	0.000409	0.000175	0.000432	0.0005143	0.000622	0.000185
Frame 20	0.000612	0.000369	0.000407	0.000168	0.000416	0.000561	0.0005485	0.000454	0.000243
Average	0.000363	0.000348	0.000277	0.000278	0.000311	0.000267	0.000344	0.000269	0.000271

Table C.42: Mean non-dimensional scale factors from error minimization between braced frames with randomly generated imperfection and first ten ABAQUS eigenmodes

	$\bar{x}_1$	$\bar{x}_2$	$\bar{x}_3$	$\bar{x}_4$	$\bar{x}_5$	$\bar{x}_6$	$\bar{x}_7$	$\bar{x}_8$	$\bar{x}_9$	$\bar{x}_{10}$
Frame 1	0.00024	0.00032	0.00015	0.00013	0.00016	8E-05	0.00019	0.00012	0.00020	8.2E-05
Frame 2	0.00027	0.00028	0.00016	0.00013	0.00015	4.1E-05	0.0002	5.9E-05	0.00021	6.4E-05
Frame 3	0.00033	0.00029	0.00012	7.7E-05	8.5E-05	9.8E-05	9.9E-05	3.2E-05	8.3E-05	3.5E-05
Frame 4	0.00055	0.00013	0.00034	0.00028	9.5E-05	0.00015	0.00023	0.00011	0.00010	0.00011
Frame 5	0.00041	0.00035	0.00031	0.00021	0.00019	0.00011	0.00011	0.00013	0.00041	0.00058
Frame 6	0.00019	0.00025	0.00032	0.00031	0.00023	0.00014	0.00026	9.3E-05	0.00029	0.00014
Frame 7	0.00018	0.00025	0.00037	0.00033	0.00029	0.00018	0.00028	6E-05	0.00035	0.00023
Frame 8	0.00032	0.00032	9.2E-05	7.7E-05	0.00022	9.2E-05	0.00028	0.00022	0.00016	0.00021
Frame 9	0.00044	0.00030	0.00033	0.00046	0.00036	0.0006	0.00023	0.00065	0.00024	0.00018
Frame 10	0.00025	0.00027	0.00026	0.00030	0.00051	0.00017	0.00046	0.00029	0.00038	0.00013
Frame 11	0.00060	0.00047	0.00024	0.00012	0.00027	0.00017	0.00033	9.1E-05	0.00024	0.00011
Frame 12	0.00048	0.00038	0.00035	0.00020	0.00036	0.00044	0.00039	0.00046	0.00030	0.00034
Frame 13	0.00039	0.00047	0.00028	0.00030	0.00044	0.00041	0.00023	0.00029	0.00029	0.00023
Frame 14	0.00029	0.00029	0.00033	0.00033	0.00032	0.00030	0.00029	0.00023	0.00036	0.00036
Frame 15	0.00019	0.00028	0.00030	0.00028	0.00031	0.00035	0.00028	0.00027	0.00020	0.00024
Frame 16	0.00023	0.00028	0.00026	0.00032	0.00098	0.00020	0.00099	0.00031	0.00062	0.00011
Frame 17	0.00044	0.00040	0.00040	0.00049	0.00039	0.00035	0.00025	0.00054	0.00032	0.00028
Frame 18	0.00057	0.00061	0.00016	0.00061	0.00016	0.00020	0.00058	0.00018	0.00018	0.00032
Frame 19	0.00022	0.00056	0.00036	0.00041	0.00017	0.00043	0.00053	0.00058	0.00020	0.00022
Frame 20	0.00061	0.00037	0.00041	0.00017	0.00043	0.0005	0.00055	0.00039	0.00024	0.00026
Average	0.00036	0.00034	0.00028	0.00028	0.00031	0.00025	0.00034	0.00025	0.00027	0.00021

### C.3. Load-deflection response of frames for verification examples

#### C.3.1. Unbraced frames

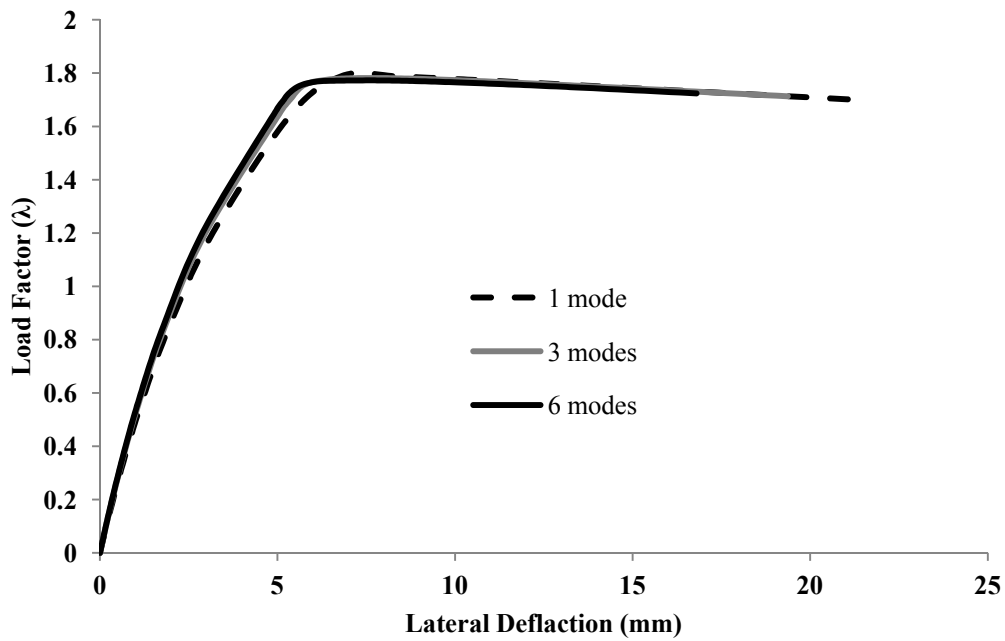


Figure C.3: Load-deflection response of F-UB1

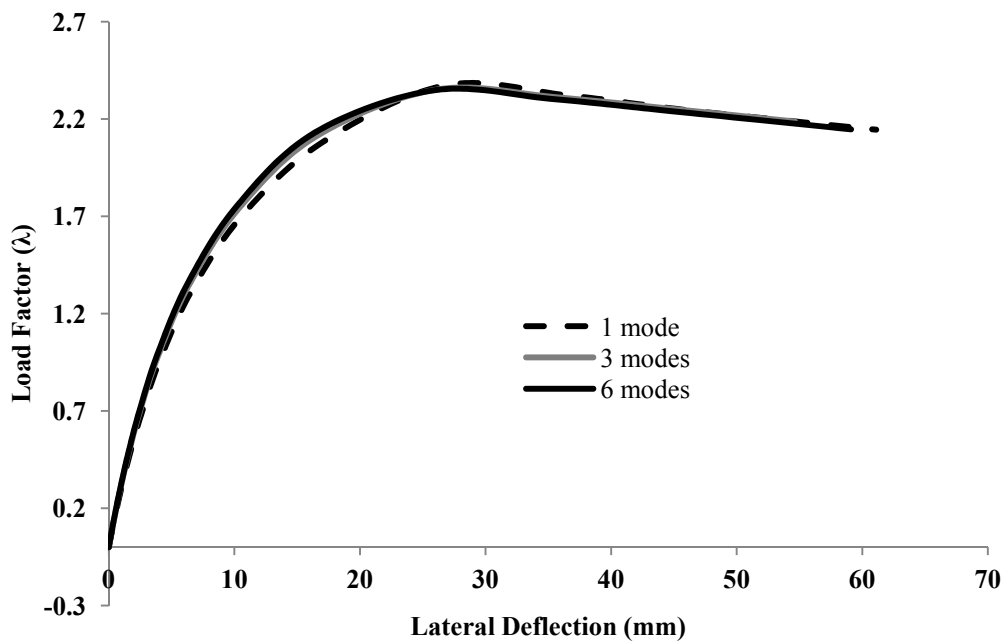


Figure C.4: Load-deflection response of F-UB2

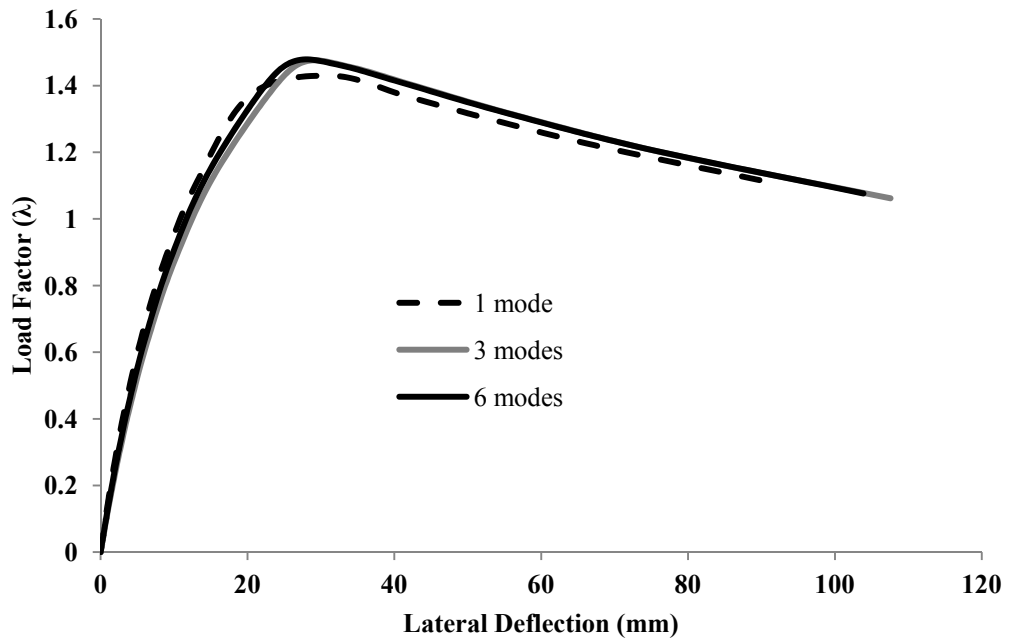


Figure C.5: Load-deflection response of F-UB3

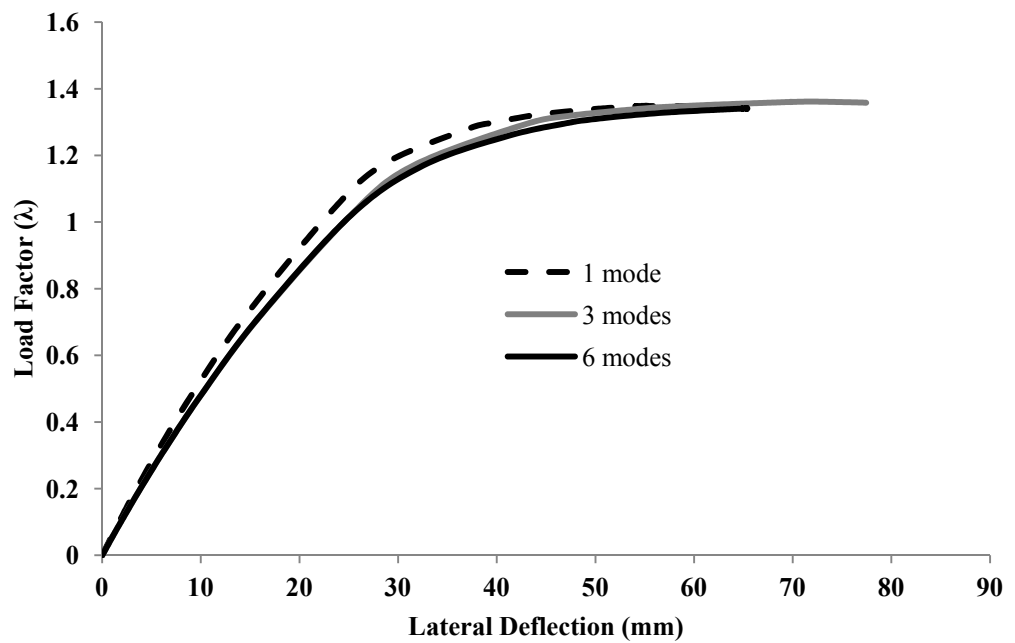


Figure C.6: Load-deflection response of F-UB4

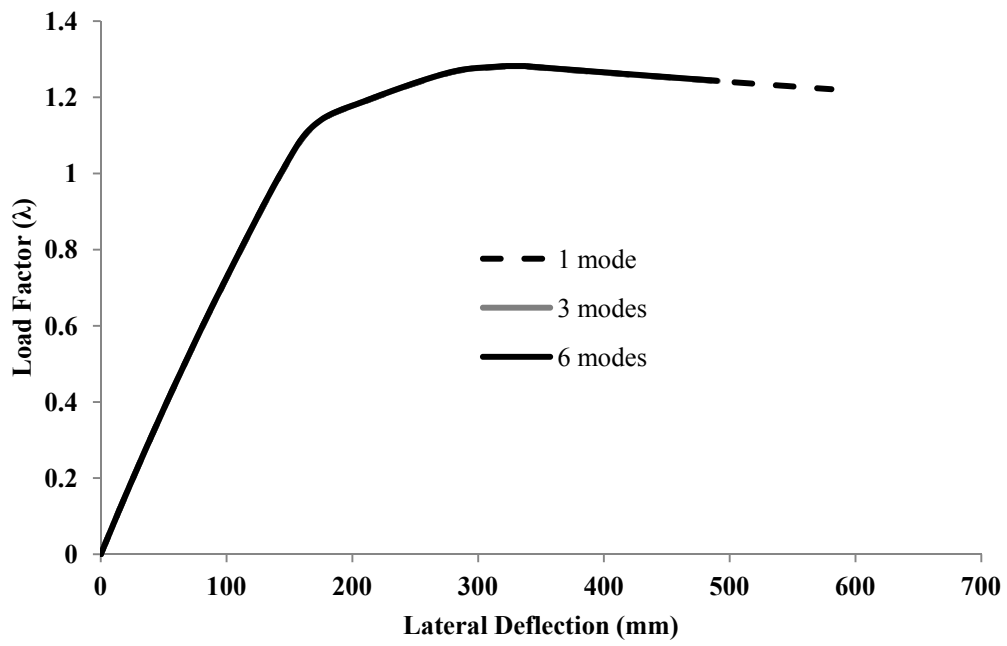


Figure C.7: Load-deflection response of F-UB5

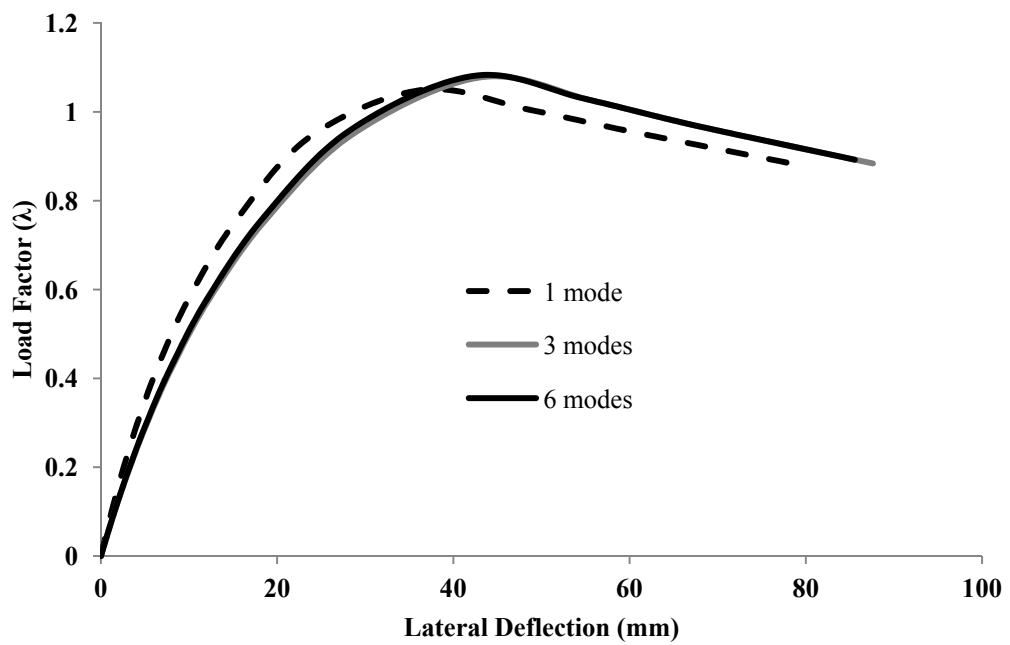


Figure C.8: Load-deflection response of F-UB6

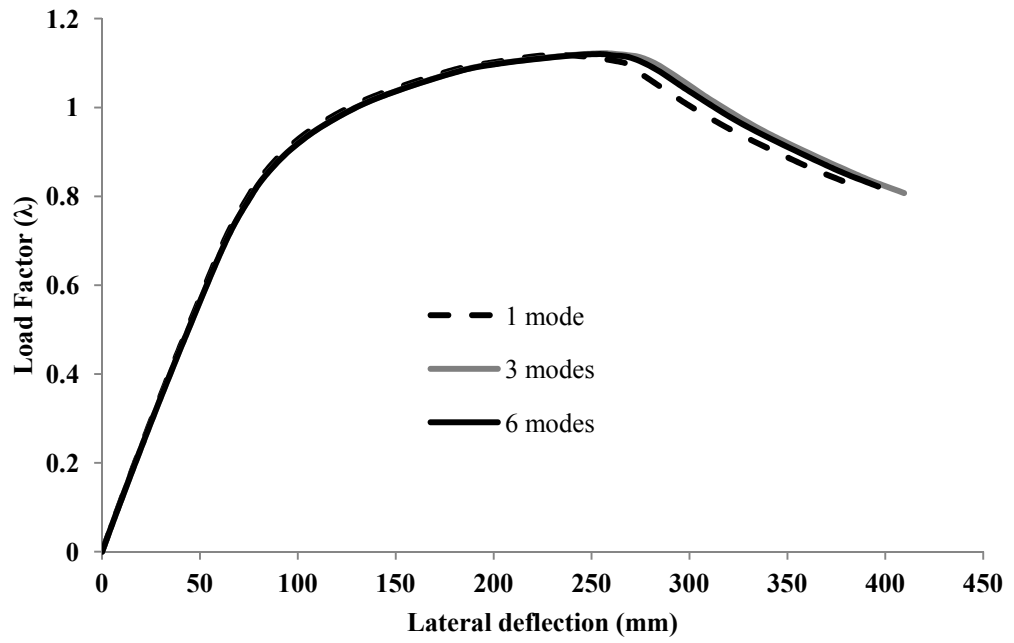


Figure C.9: Load-deflection response of F-UB7

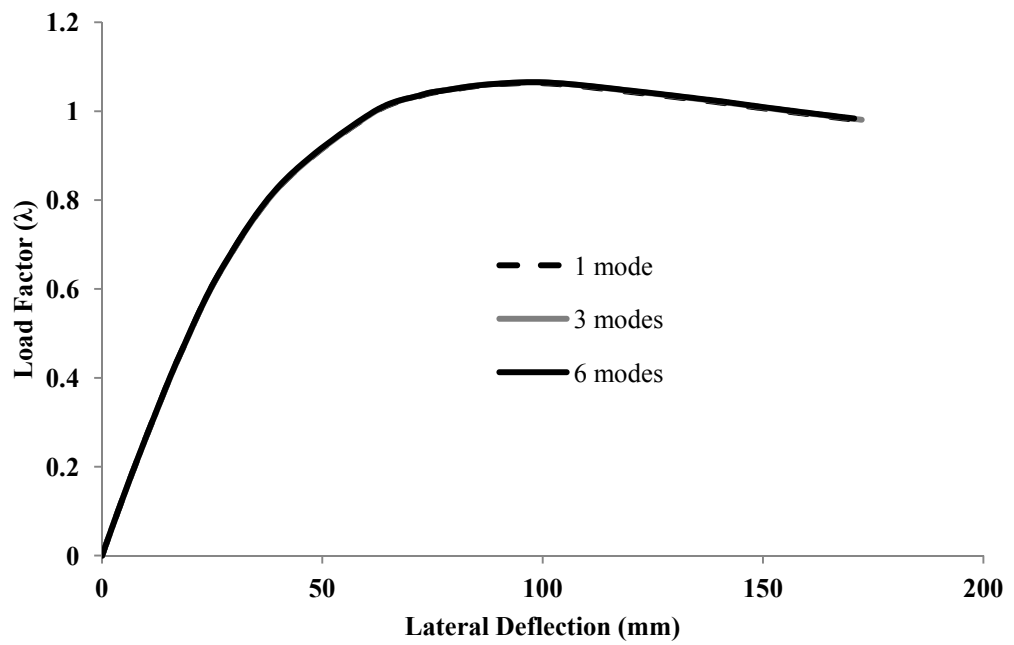


Figure C.10: Load-deflection response of F-UB8



### C.3.2. Braced frames

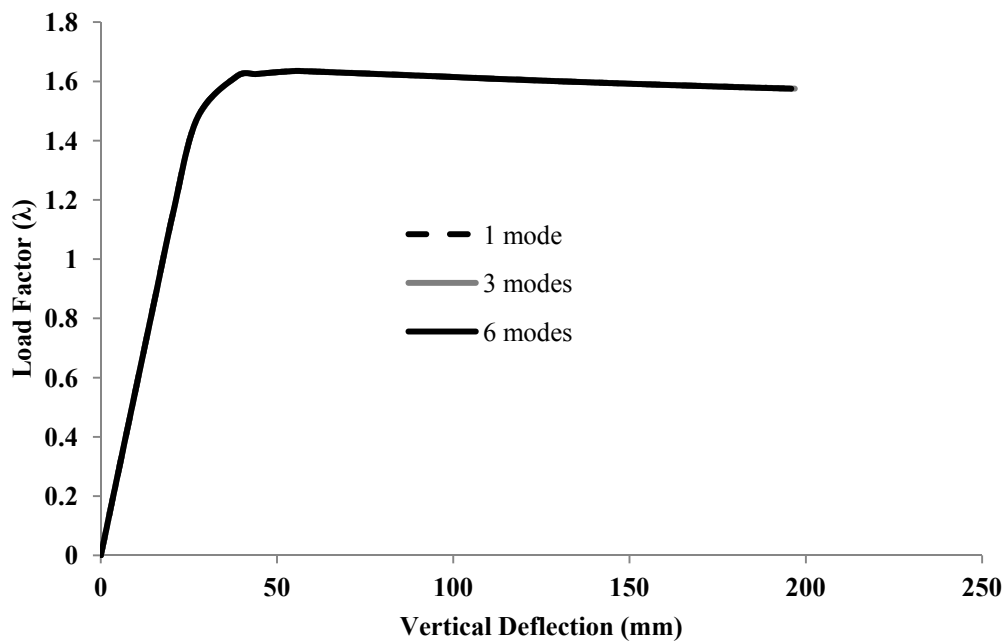


Figure C.11: Load-deflection response of F-B1

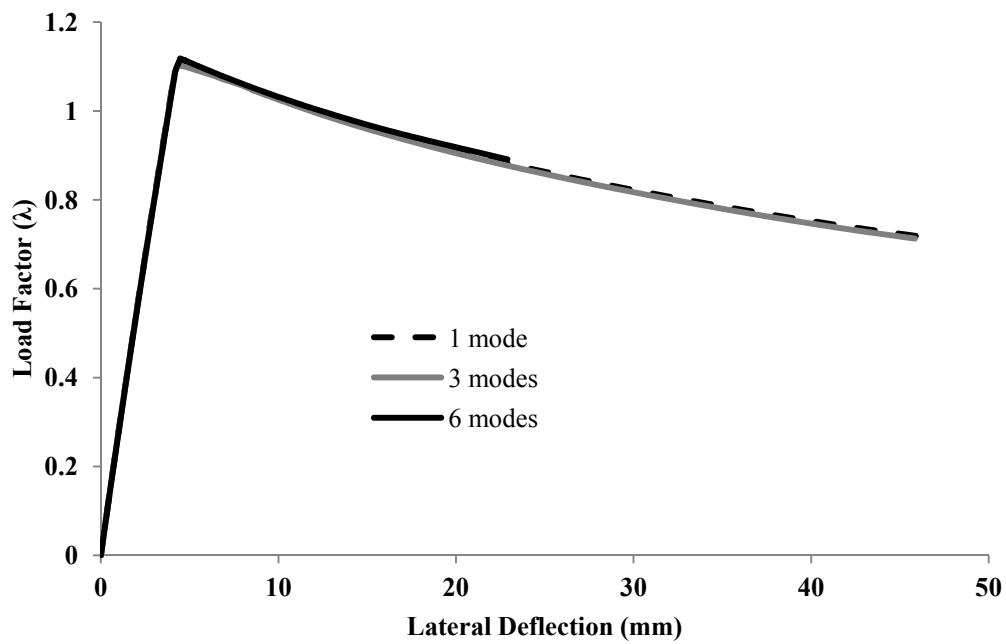


Figure C.12: Load-deflection response of F-B2

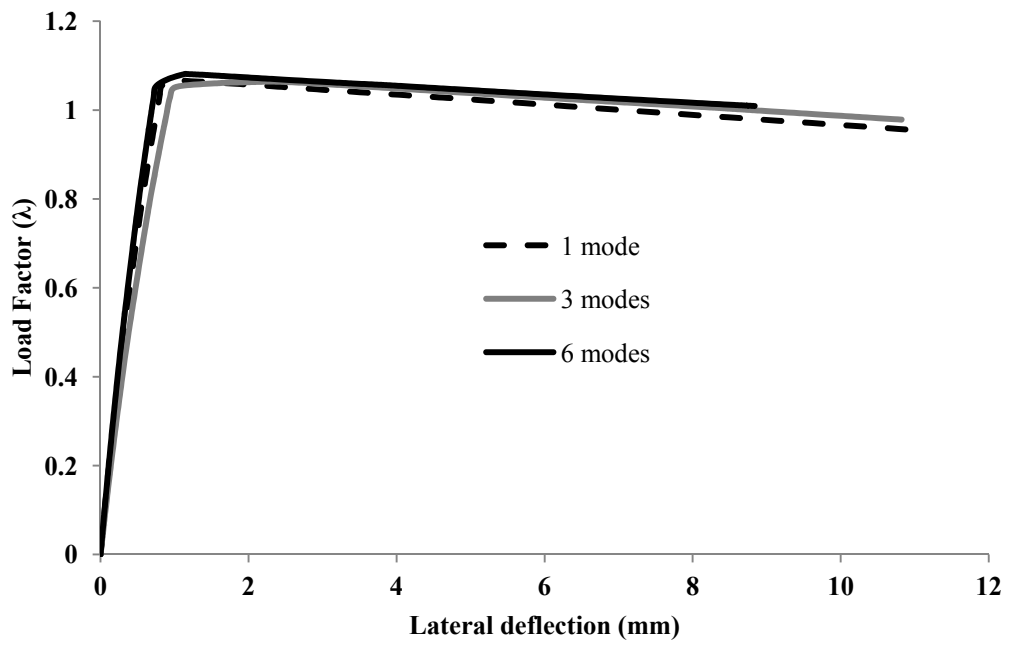


Figure C.13: Load-deflection response of F-B3

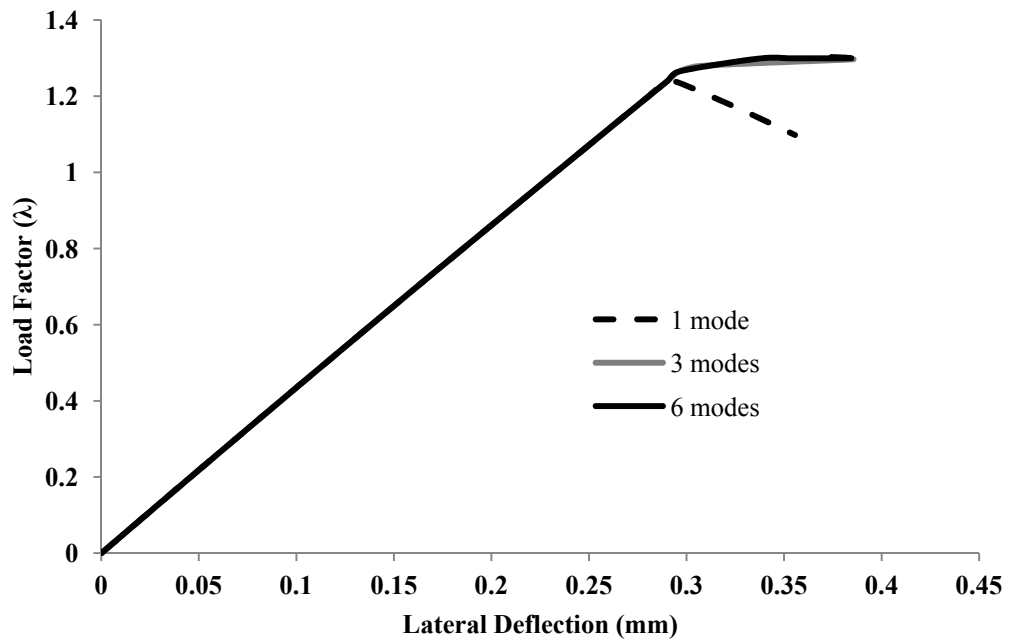


Figure C.14: Load-deflection response of F-B4

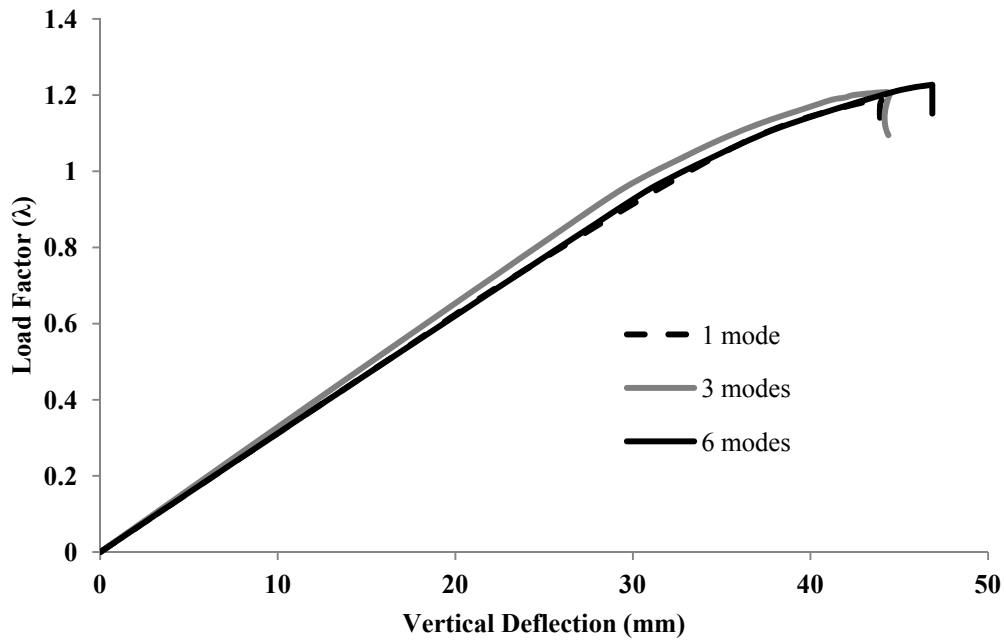


Figure C.15: Load-deflection response of F-B5

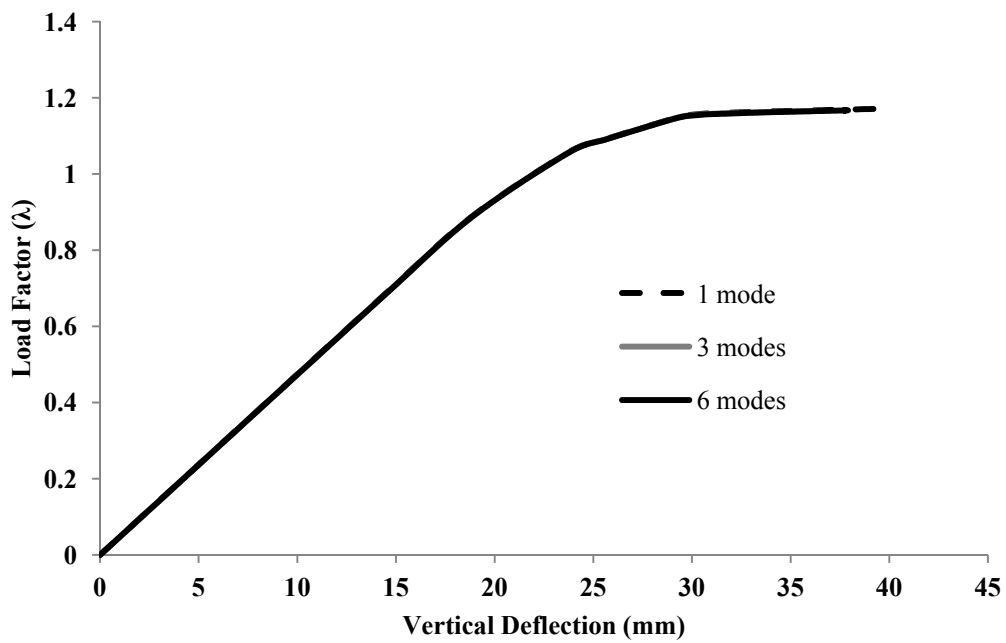


Figure C.16: Load-deflection response of F-B6

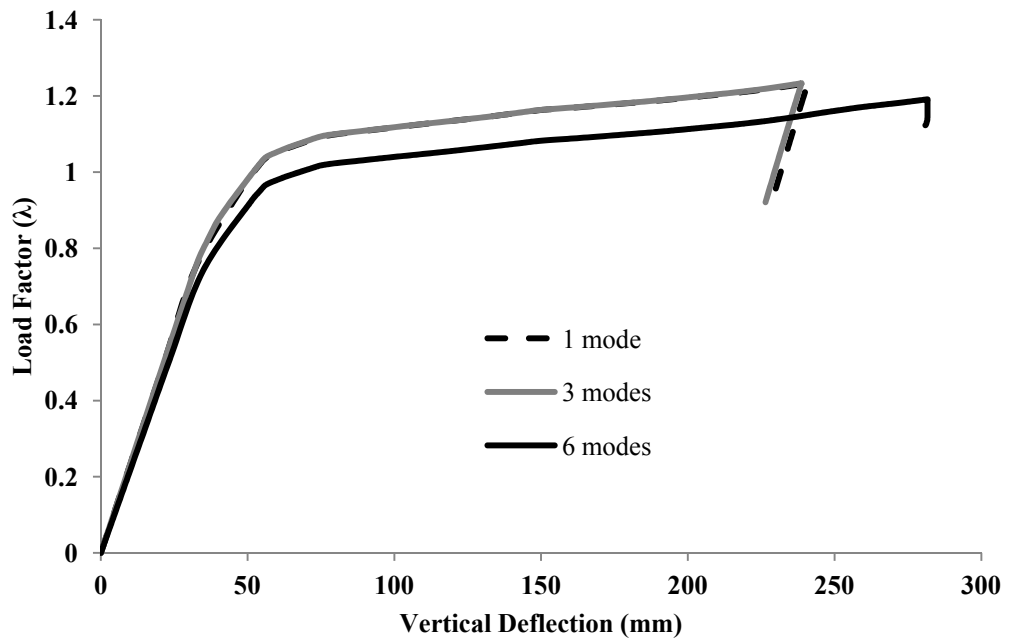


Figure C.17: Load-deflection response of F-B7

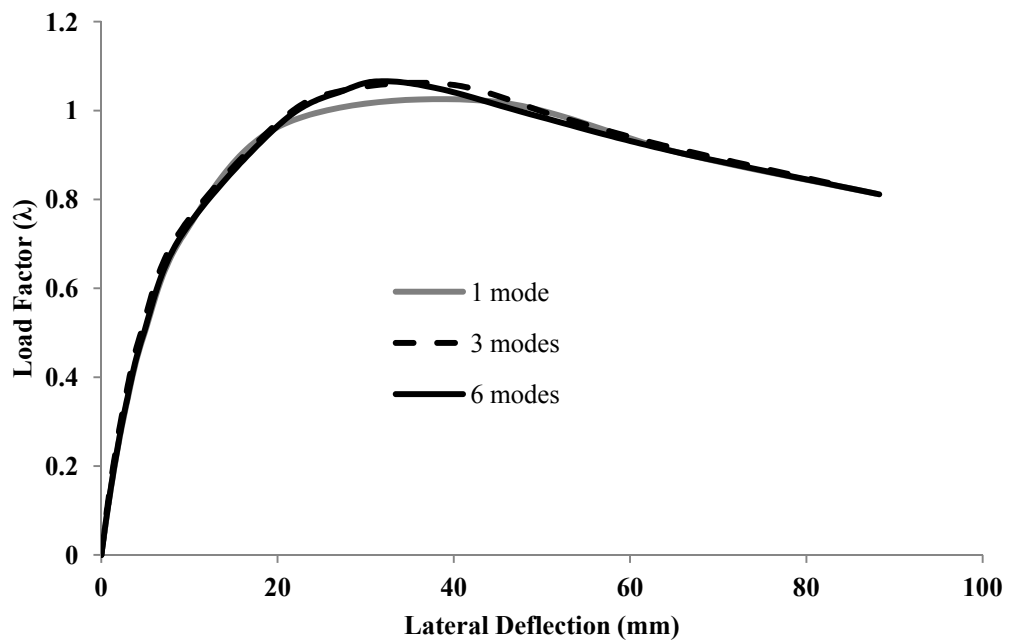


Figure C.18: Load-deflection response of F-B8

## C.4. Ultimate strength distributions of frames for verification examples

### C.4.1 Unbraced frames

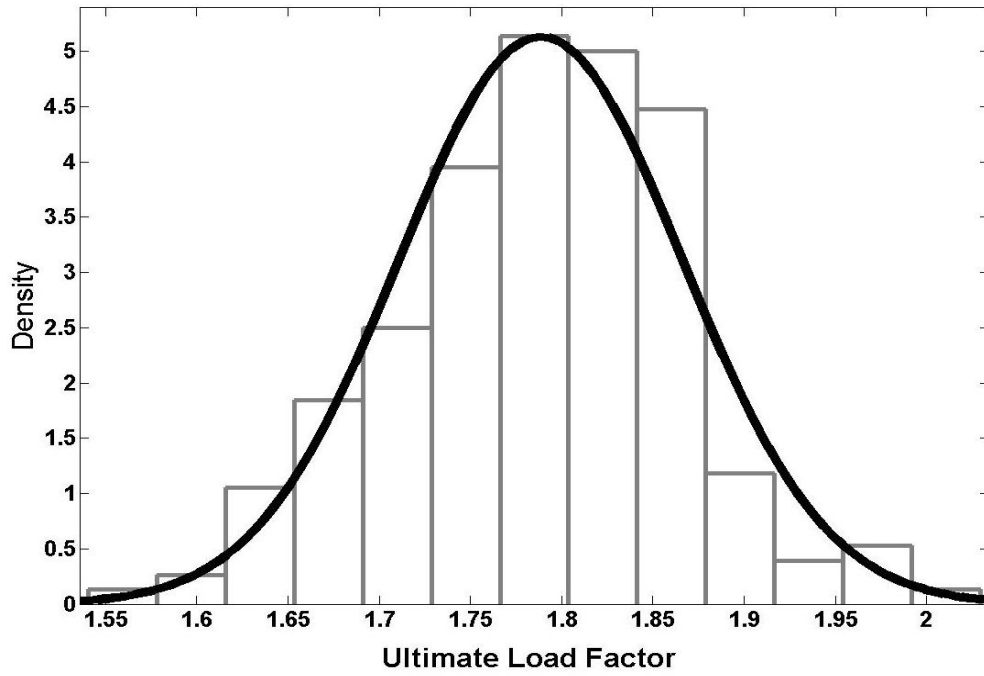


Figure C.19: Histogram of ultimate load factor, F-UB1

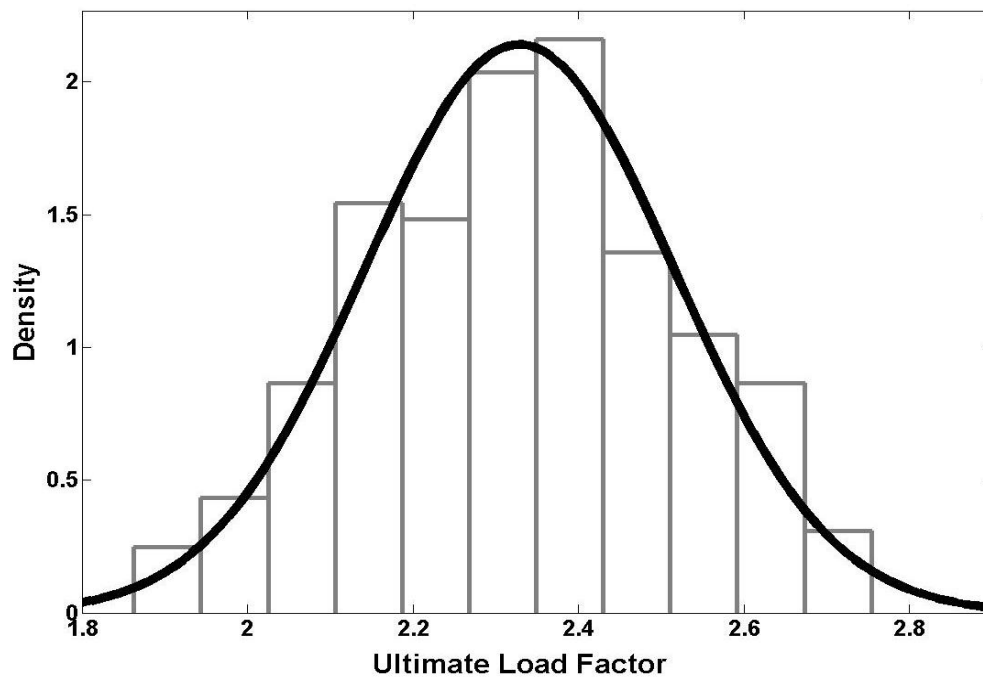


Figure C.20: Histogram of ultimate load factor, F-UB2

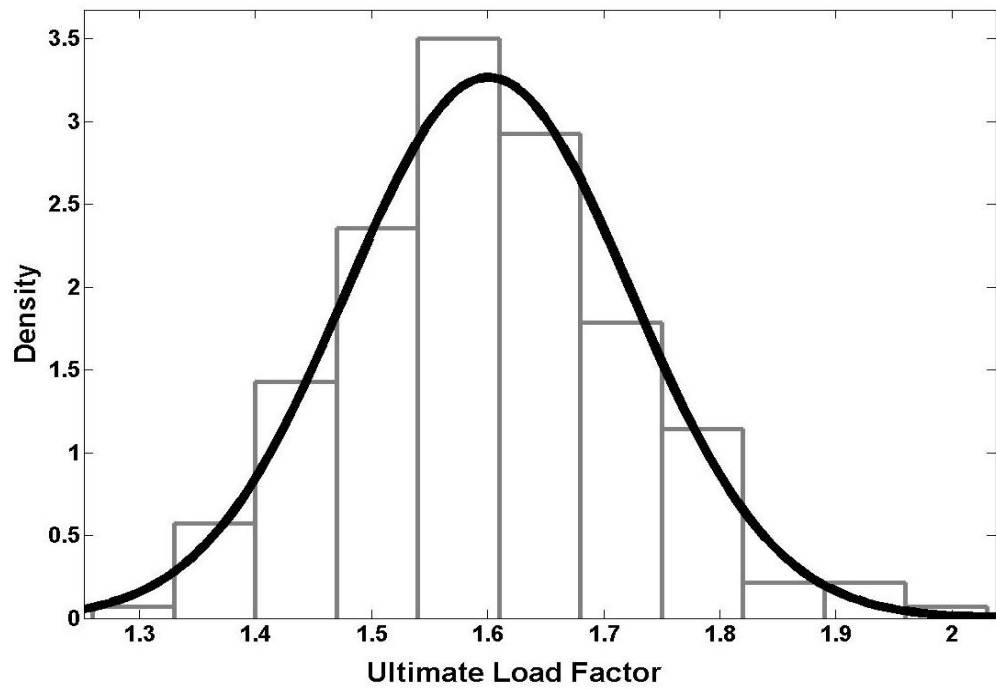


Figure C.21: Histogram of ultimate load factor, F-UB3

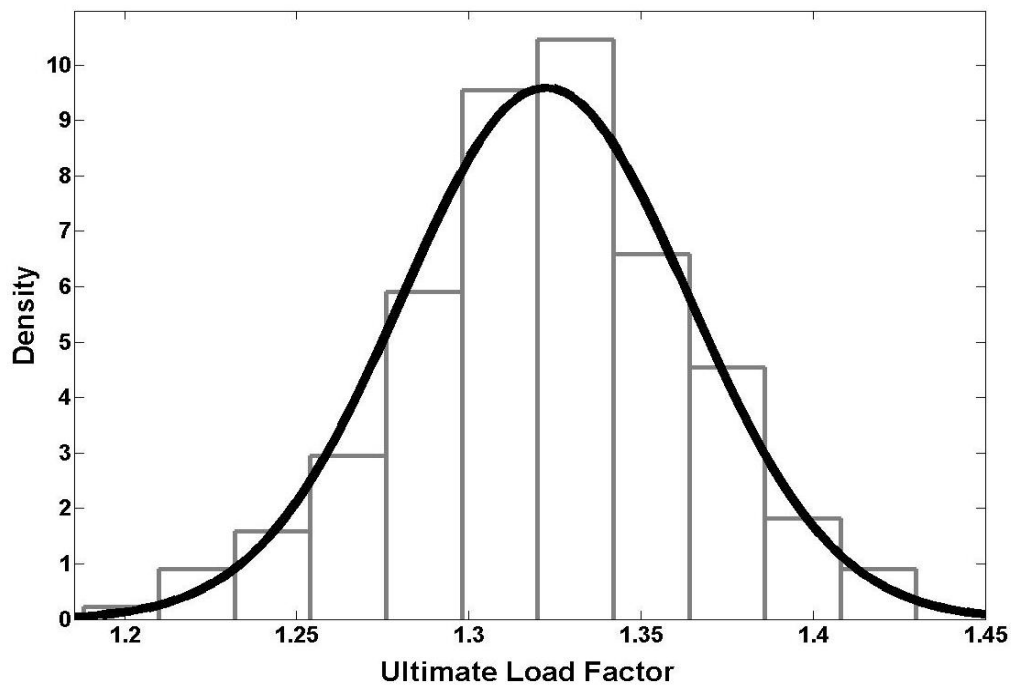


Figure C.22: Histogram of ultimate load factor, F-UB4

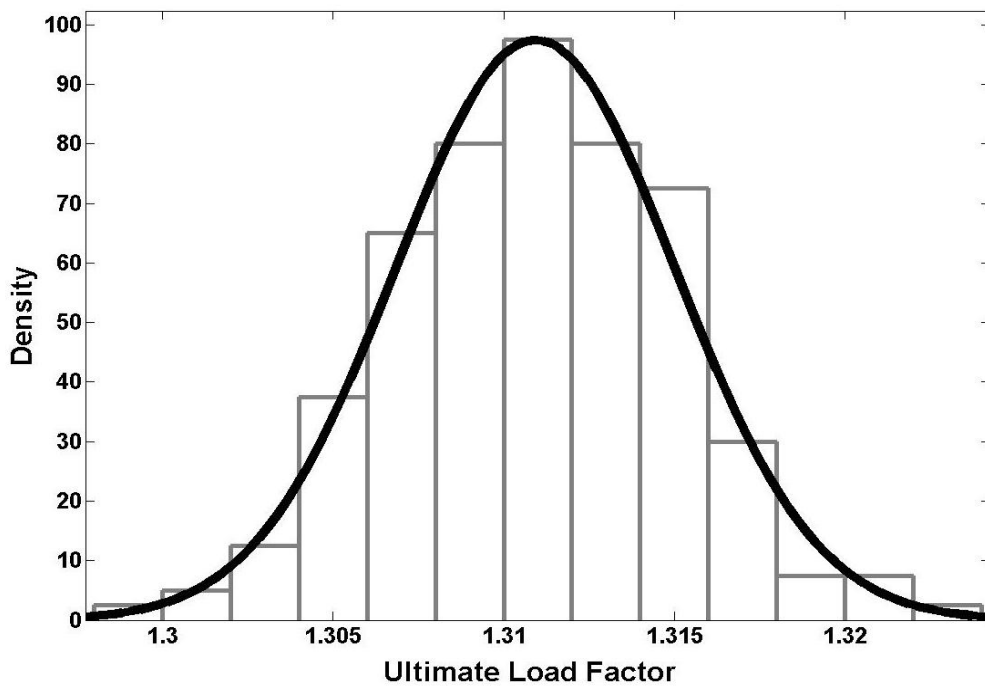


Figure C.23: Histogram of ultimate load factor, F-UB5

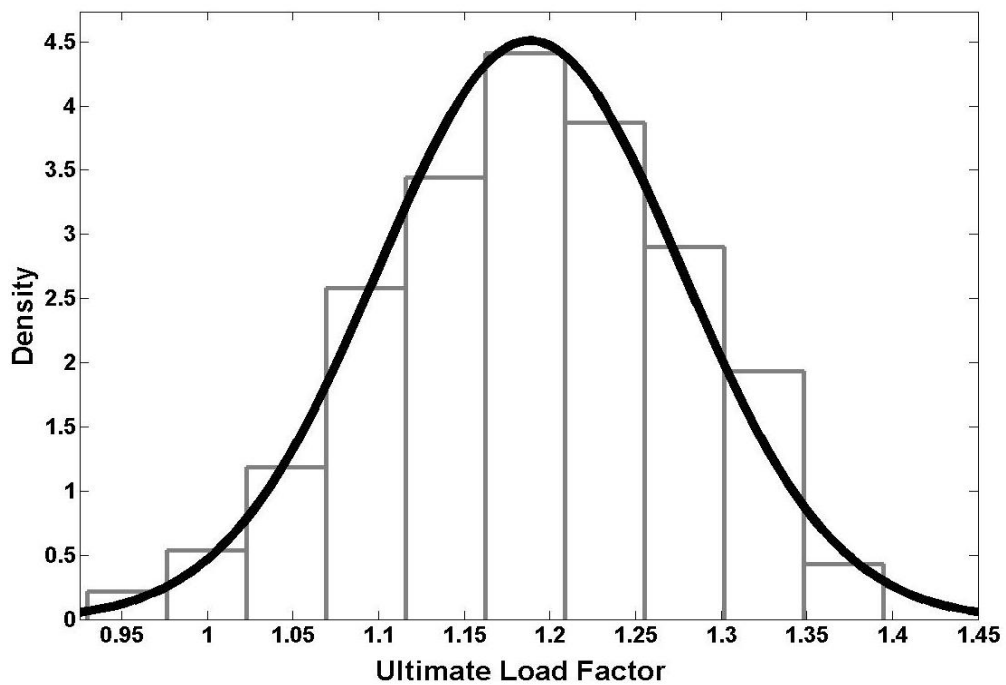


Figure C.24: Histogram of ultimate load factor, F-UB6

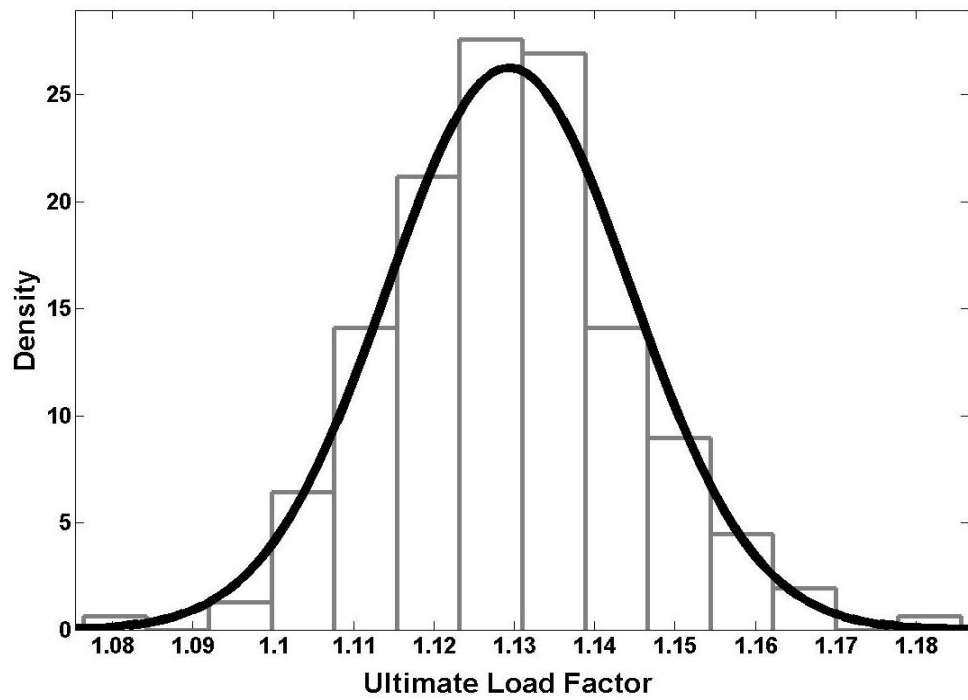


Figure C.25: Histogram of ultimate load factor, F-UB7

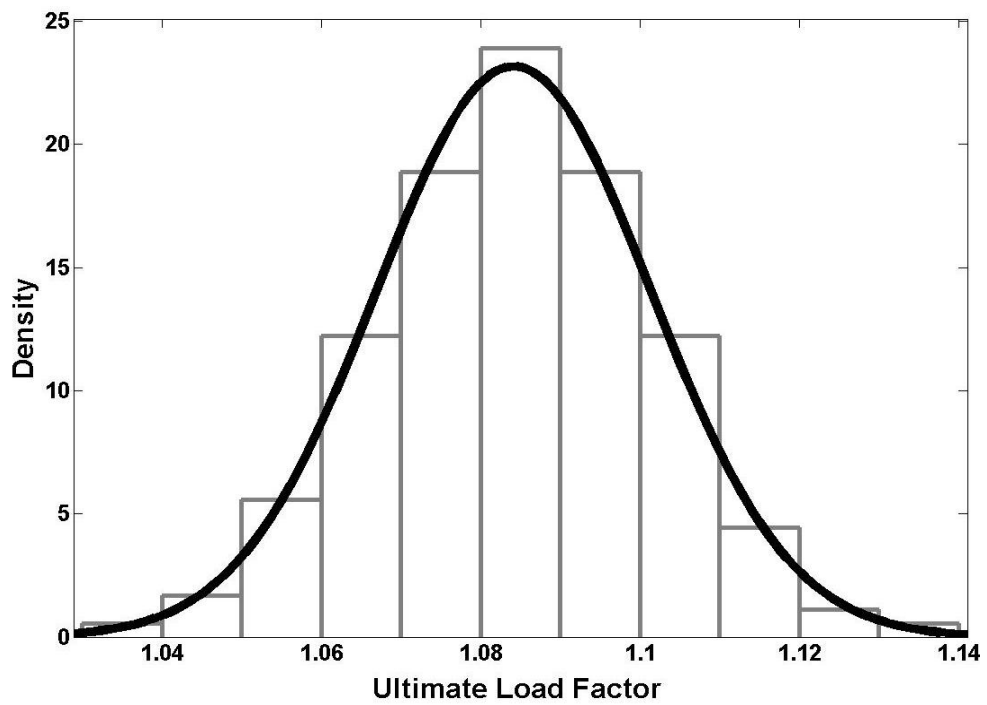


Figure C.26: Histogram of ultimate load factor, F-UB8



**C.4.2. Braced frames**

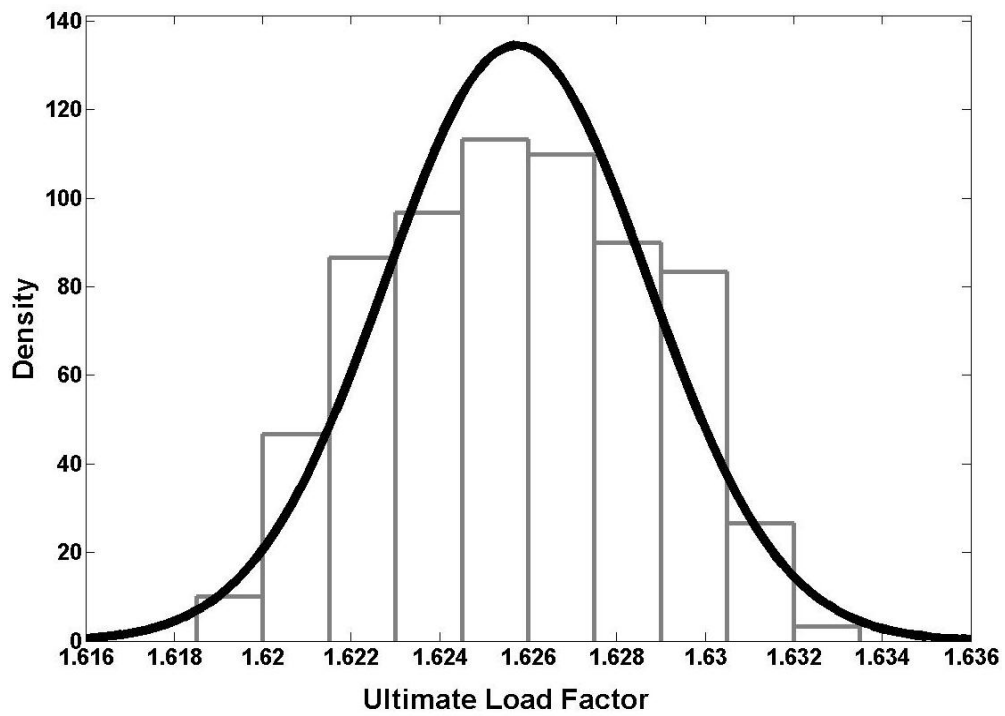


Figure C.27: Histogram of ultimate load factor, F-B1

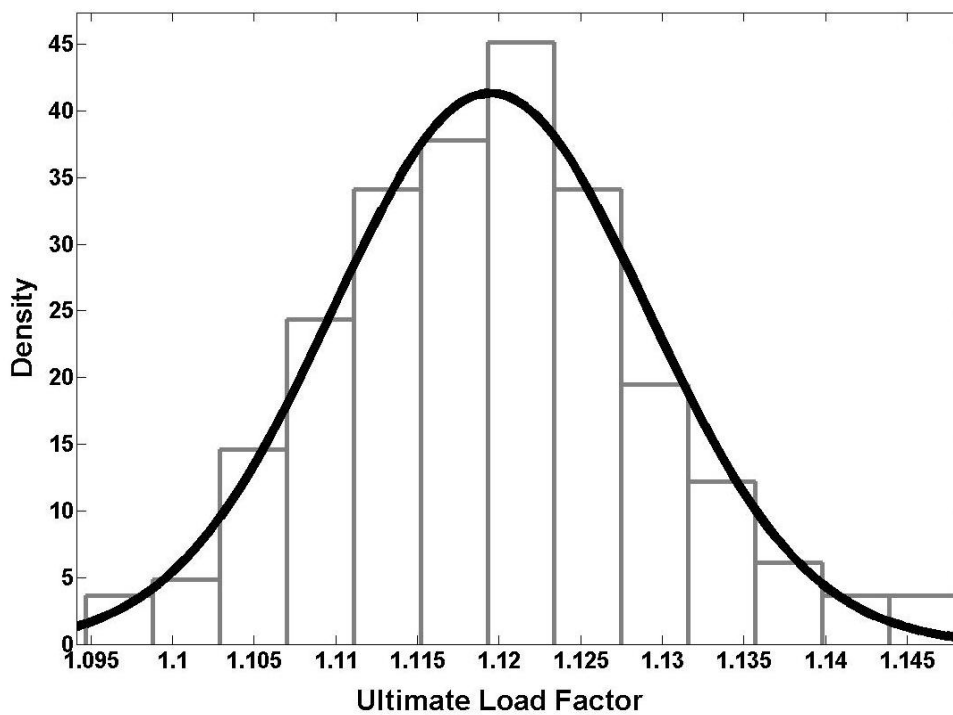


Figure C.28: Histogram of ultimate load factor, F-B2

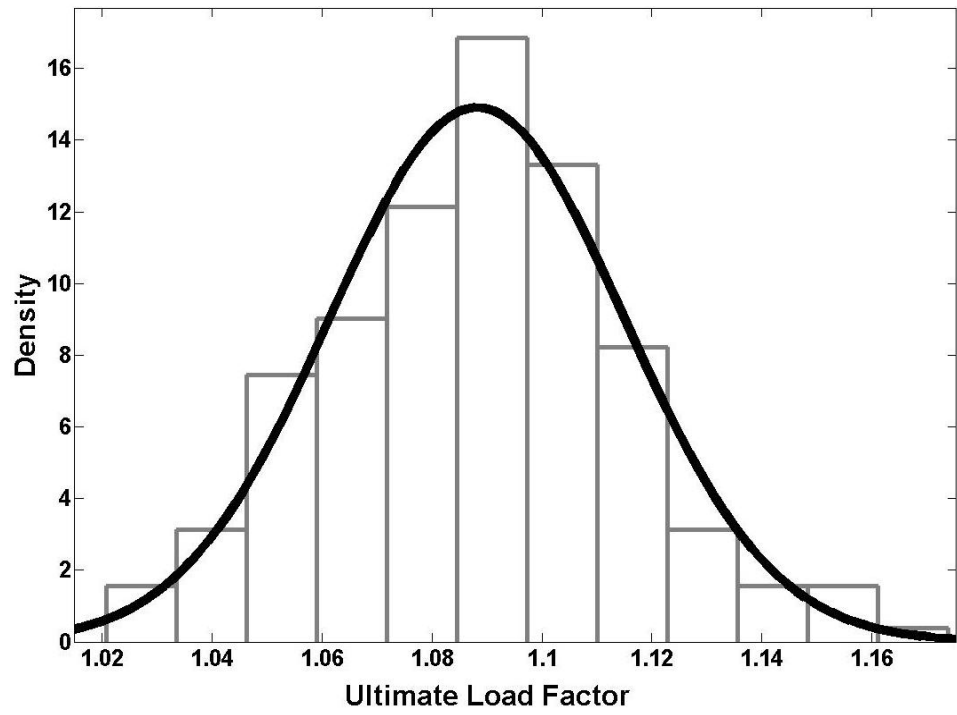


Figure C.29: Histogram of ultimate load factor, F-B3

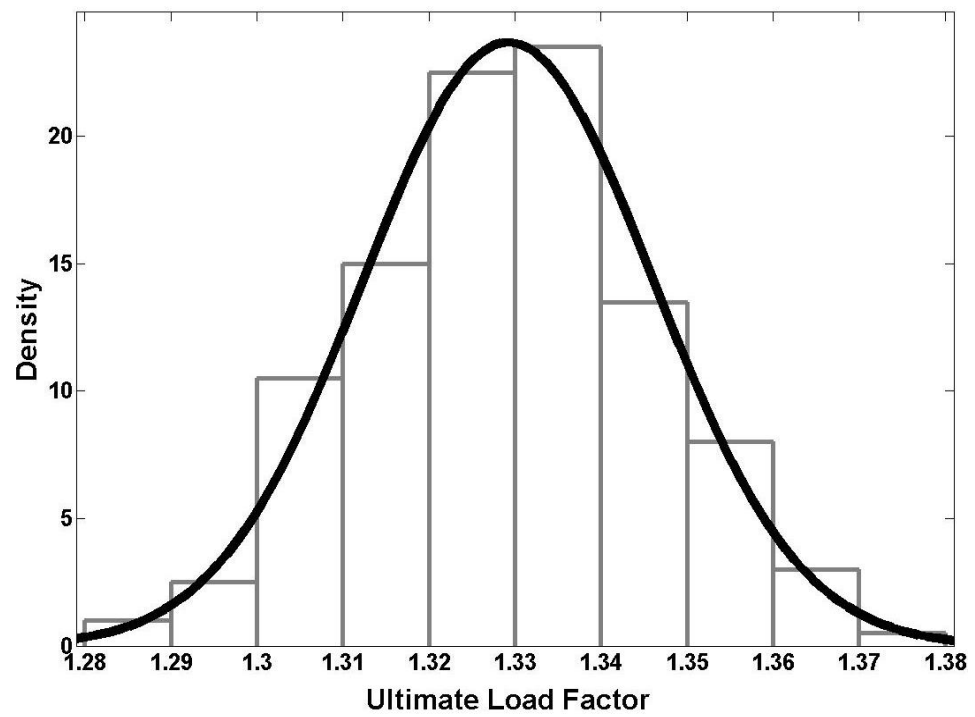


Figure C.30: Histogram of ultimate load factor, F-B4

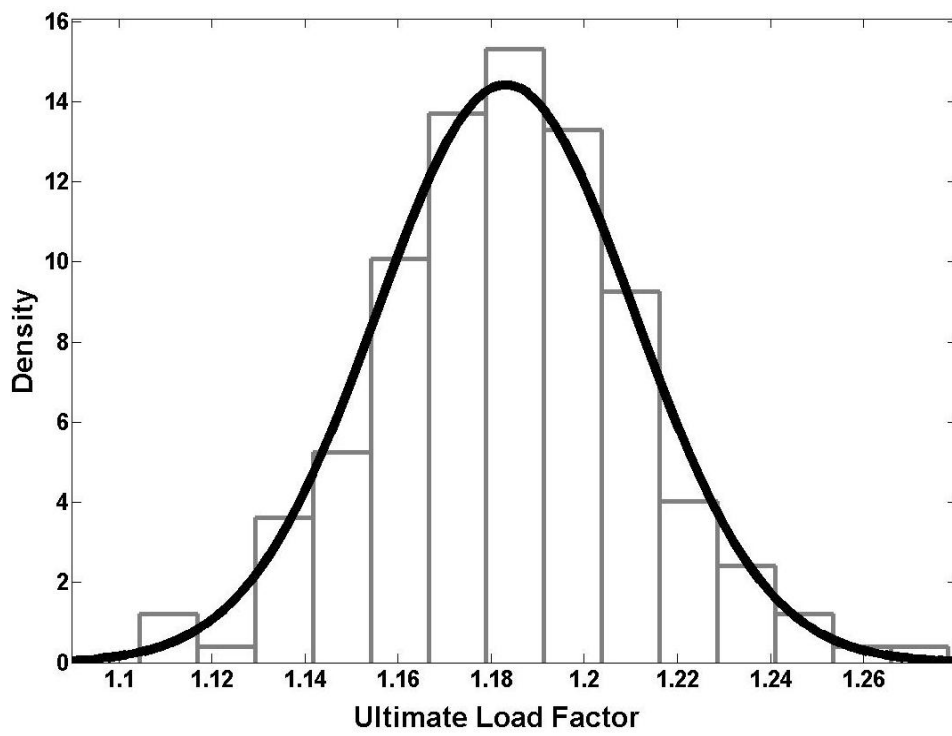


Figure C.31: Histogram of ultimate load factor, F-B5

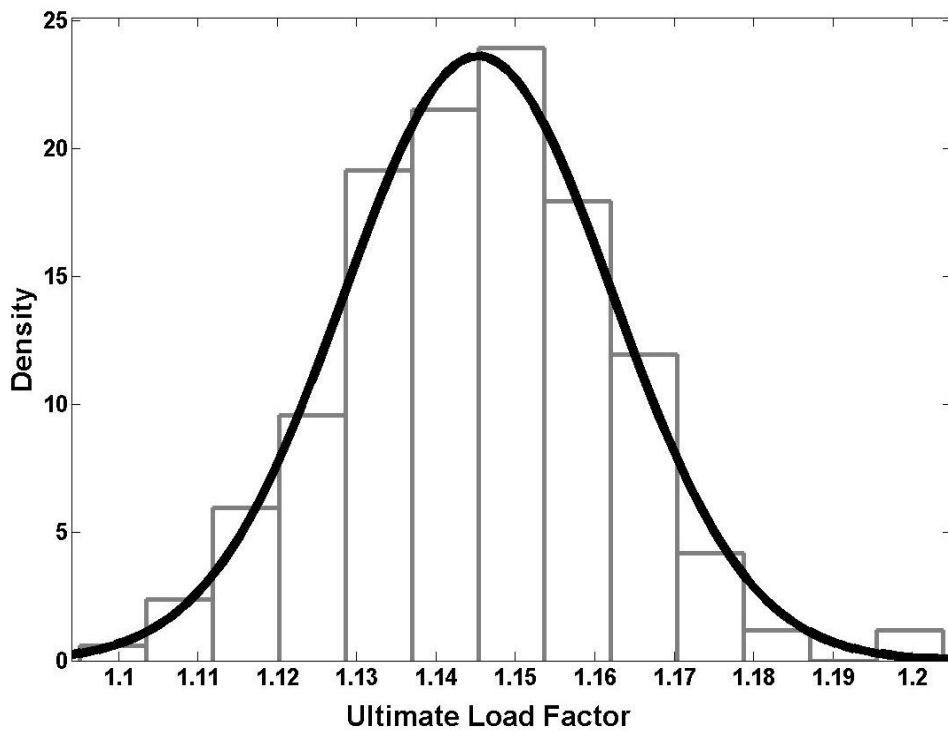


Figure C.32: Histogram of ultimate load factor, F-B6

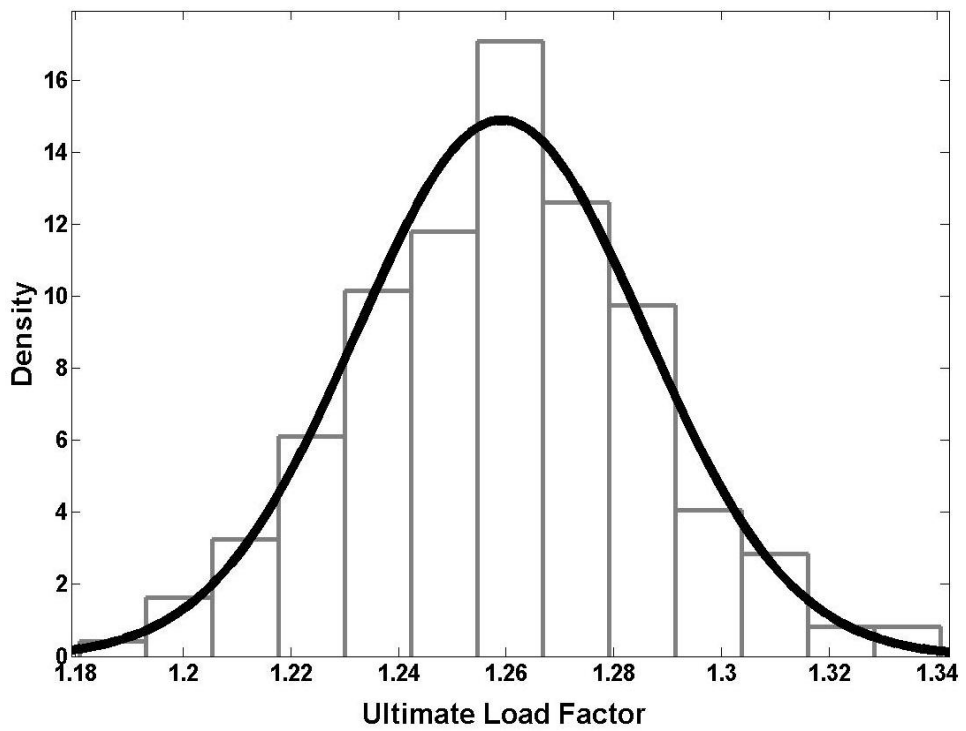


Figure C.33: Histogram of ultimate load factor, F-B7

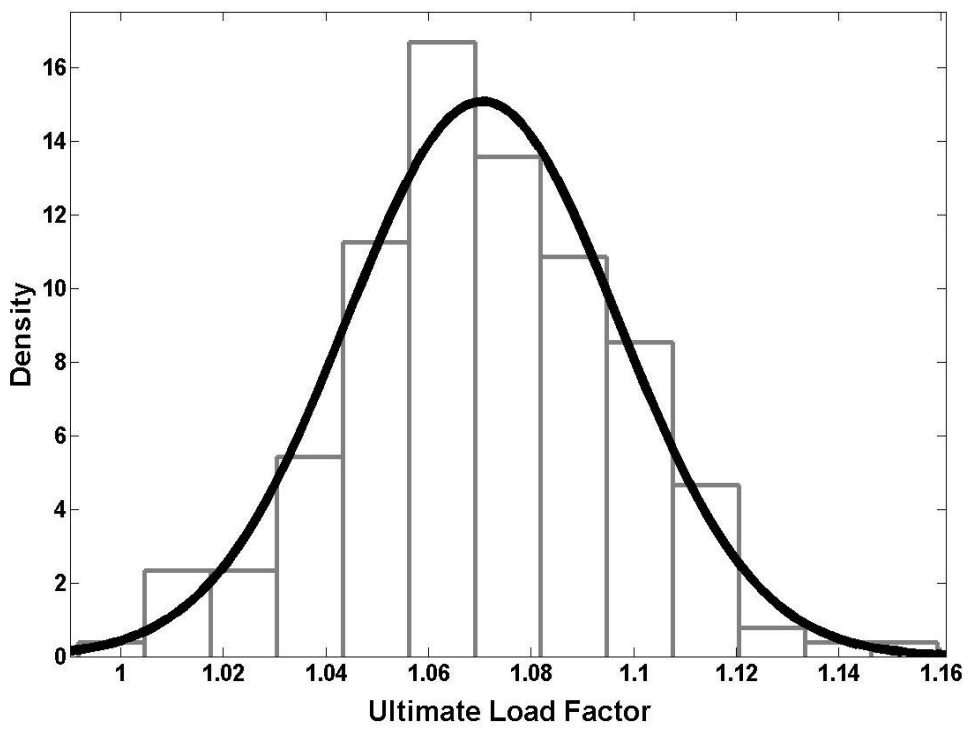


Figure C.34: Histogram of ultimate load factor, F-B8

# Appendix D.

## Scale factors for residual stress

### D.1. Non-American sections

Table D.1: Scale factors for residual stress (Non-American sections)

No	Section	Origin	X-ECCS	X-Trahair	Reference
1	12W50	Europe	0.83815	0.6660125	(Gozum and Huber 1955)
2	8W40	Europe	0.753479	1.0554975	(Alpsten 1968)
3	12W65	Europe	0.925149	1.1370431	(Gozum and Huber 1955)
4	6x6	Europe	0.750927	0.8419998	(Jez-Gala 1962)
5	8x8	Europe	0.677607	0.7071933	(Jez-Gala 1962)
6	10x10	Europe	1.231571	1.4861505	(Jez-Gala 1962)
7	12x12	Europe	0.900186	1.1466224	(Jez-Gala 1962)
8	10UB29	Australia	0.796032	0.7306041	(Kitipornchai 1973)
9	250UB37	Australia	0.729395	0.6508165	(Dux and Kitipornchai 1983)
10	IPE200	Europe	0.951944	0.8084236	(Alpsten 1968)
11	12W31	Europe	1.415932	1.2432115	(Alpsten 1968)
12	14W43	Europe	1.120918	1.1450123	(Alpsten 1968)
13	HE360B	Europe	0.843987	0.560116	(Alpsten 1968)
14	HE360B	Europe	0.997573	0.7270142	(Alpsten 1968)
15	10UB29	Europe	1.232335	0.9428995	(Kitipornchai 1973)
16	100x200	Japan	1.032581	0.9609233	(Itoh 1984)
17	100x200	Japan	1.037803	1.0124147	(Itoh 1984)
18	100x200	Japan	1.029109	0.9766988	(Itoh 1984)
19	100x200	Japan	1.048646	0.9924209	(Itoh 1984)
20	100x200	Japan	1.0413	0.996669	(Itoh 1984)
21	100x200	Japan	0.989858	0.9682622	(Itoh 1984)
22	100x200	Japan	1.157223	1.019415	(Itoh 1984)
23	100x200	Japan	1.20347	1.1201236	(Itoh 1984)
24	100x200	Japan	1.057353	0.9899618	(Itoh 1984)
25	100x200	Japan	1.014464	1.000185	(Itoh 1984)

No	Section	Origin	X-ECCS	X-Trahair	Reference
26	100x200	Japan	1.100639	1.0403658	(Itoh 1984)
27	100x200	Japan	1.035086	0.9840363	(Itoh 1984)
28	100x200	Japan	1.077879	1.0392011	(Itoh 1984)
29	100x200	Japan	1.101172	1.0273264	(Itoh 1984)
30	100x200	Japan	1.021682	0.98656	(Itoh 1984)
31	100x200	Japan	1.159615	1.0546657	(Itoh 1984)
32	100x200	Japan	1.074236	1.0388837	(Itoh 1984)
33	100x200	Japan	1.087168	1.0216596	(Itoh 1984)
34	100x200	Japan	1.049075	1.0057415	(Itoh 1984)
35	100x200	Japan	1.098468	1.0633304	(Itoh 1984)
36	100x200	Japan	0.977903	0.9646948	(Itoh 1984)
37	100x200	Japan	1.002502	0.9811087	(Itoh 1984)
38	100x200	Japan	1.099042	1.0140788	(Itoh 1984)
39	100x200	Japan	1.023796	0.9523933	(Itoh 1984)
40	100x200	Japan	0.982248	0.9248678	(Itoh 1984)
41	12x6.5x27	Australia	0.798519	0.5503916	(Ward 1967)
42	12x6.5x27	Japan	0.881481	0.655478	(Ward 1967)
43	16x7x50	Australia	1.047407	0.8374986	(Ward 1967)
44	16x7x50	Japan	1.232593	0.9484246	(Ward 1967)
45	27x10x102	Australia	1.179259	0.9172657	(Ward 1967)
46	27x10x102	UK	1.531852	1.180874	(Ward 1967)
47	12x6.5x31	Australia	1.574815	1.1533006	(Ward 1966)
48	16x7x50	Australia	1.573333	1.1875222	(Ward 1966)
49	16x7x50	Australia	1.318519	0.9804413	(Ward 1966)
50	10x10x69	Australia	0.929778	1.2098077	(Ward 1966)
51	12x12x190	Australia	0.912889	1.1324806	(Ward 1966)
52	27x10x102	Australia	1.552593	1.1889898	(Ward 1966)
53	12x5x25	UK	1.268148	0.9616001	(Dibley and Sowter 1967)
54	IPE200	Belgium	1.022222	0.6873107	(Mas and Massonet 1966)
55	6x6x20	UK	0.624	0.8391847	(Jez-Gala 1962)
56	8x8x31	UK	0.623111	0.8275004	(Jez-Gala 1962)
57	10x10x49	UK	1.104	1.4458901	(Jez-Gala 1962)
58	12x12x92	UK	0.887111	1.1194853	(Jez-Gala 1962)
59	12x5x32	UK	0.72	0.5119755	(Baker 1969)
60	12x5x32	UK	1.136296	0.8369749	(Baker 1969)
61	12x5x32	UK	1.077037	0.7876618	(Baker 1969)
62	18x7.5x66	UK	1.493333	1.173727	(Baker 1969)
63	18x7.5x66	UK	0.82963	0.6547366	(Baker 1969)

**D.2. American sections**

Table D.2: Scale factors for residual stress (American sections)

No	Section	Origin	X-Galambos	Reference
1	8W24	USA	1.08437018	(Lim and Lu 1970)
2	8W35	USA	1.49755878	(Lim and Lu 1970)
3	8W24	USA	1.045168233	(Lim and Lu 1970)
4	8W67	USA	1.263682101	(Sheninger and Lu 1968)
5	8W67	USA	1.192368038	(Sheninger and Lu 1968)
6	8W31	USA	1.050712194	(Gozum and Huber 1955)
7	8W31	USA	1.257637489	(Gozum and Huber 1955)
8	8W31	USA	0.900477007	(Gozum and Huber 1955)
9	8W31	USA	0.840912013	(Gozum and Huber 1955)
10	4W13	USA	0.894843522	(Gozum and Huber 1955)
11	8W24	USA	1.444896099	(Gozum and Huber 1955)
12	8W67	USA	1.133878502	(Gozum and Huber 1955)
13	8W31	USA	0.847280698	(Lay and Ward 1969)
14	8W31	USA	0.969909196	(Huber and Ketter 1952)
15	HEM 340	USA	1.14548029	(Tebedge, Chen et al. 1972)
16	HEM 340	USA	1.672376665	(Tebedge, Chen et al. 1972)
17	12W161	USA	0.731948924	(Tebedge, Chen et al. 1972)
18	12W161	USA	0.739305705	(Tebedge, Chen et al. 1972)
19	HEM340	USA	1.17232629	(Tebedge, Chen et al. 1972)
20	HEM340	USA	1.33312302	(Tebedge, Chen et al. 1972)
21	HEM340	USA	1.015118395	(Tebedge, Chen et al. 1972)
22	HEM340	USA	1.433037812	(Tebedge, Chen et al. 1972)
23	12W50	USA	0.517618943	(Ketter 1958)
24	12W65	USA	1.578462798	(Ketter 1958)
25	14W426	USA	1.735231577	(Ketter 1958)
26	14W13	USA	1.064837842	(Ketter 1958)
27	8W24	USA	0.68423856	(Ketter 1958)
28	8W31	USA	1.119602019	(Ketter 1958)
29	8W67	USA	0.411810299	(Ketter 1958)
30	14W43	USA	1.111135762	(Ketter 1958)
31	36W150	USA	0.812269787	(Ketter 1958)
32	4W13	USA	0.983484755	(Tall 1964)
33	8W31	USA	0.901544112	(Tall 1964)
34	12W65	USA	0.993743858	(Tall 1964)
35	14W426	USA	1.141753017	(Tall 1964)
36	8W31	USA	0.978554811	(Huber and Beedle 1954)
37	8W31	USA	0.83045669	(Huber and Beedle 1954)
38	8W31	USA	0.859570795	(Huber and Beedle 1954)
39	8W31	USA	1.165826324	(Huber and Beedle 1954)
40	8W67	USA	0.997911737	(Alpsten 1968)

# Appendix E. System-based design

---

## E.1. System-based design of sway frames under gravity, CSM

Table E.1: System-based design of Frame 1 (sway) under gravity loading using CSM,  
BFY-CPY

$\varphi_s$	Members (see Figure 7.1)	Section	$\lambda_n$ (factored loads)	Mean ( $\bar{\lambda}$ )	COV	$\lambda_n$ (unfactored loads)	$\bar{\lambda}/\lambda_n$ (unfactored load)
0.64	$C_1, C_2$ $B_1$	200UC59 530UB82	1.554	2.250	0.103	2.098	1.07
0.75	$C_1, C_2$ $B_1$	200UC59 460UB74	1.320	1.922	0.104	1.796	1.07
0.88	$C_1, C_2$ $B_1$	200UC46 460UB67	1.132	1.633	0.104	1.528	1.07
0.94	$C_1, C_2$ $B_1$	200UC59 410UB59	1.066	1.539	0.103	1.439	1.07
1.04	$C_1, C_2$ $B_1$	200UC59 360UB56	0.961	1.380	0.102	1.297	1.06



Table E.2: System-based design of Frame 2 (sway) under gravity loading using CSM,  
BFY-CPY

$\varphi_s$	Members (see Figure 7.1)	Section	$\lambda_n$ (factored loads)	Mean ( $\bar{\lambda}$ )	COV	$\lambda_n$ (unfactored loads)	$\bar{\lambda}/\lambda_n$ (unfactored load)
0.60	$C_1, C_2, C_3, C_4$ $C_5, C_6$ $B_1, B_2$ $B_3$	310UB46 250UB37 310UB46 250UB37	1.681	2.359	0.102	2.29	1.03
0.71	$C_1, C_2, C_3, C_4$ $C_5, C_6$ $B_1, B_2$ $B_3$	310UB32 250UB25 310UB46 250UB37	1.402	2.052	0.097	2.006	1.023
0.74	$C_1, C_2, C_3, C_4$ $C_5, C_6$ $B_1, B_2$ $B_3$	250UB31 250UB31 310UB46 250UB31	1.353	1.951	0.101	1.913	1.020
0.78	$C_1, C_2, C_3, C_4$ $C_5, C_6$ $B_1, B_2$ $B_3$	250UB31 250UB31 310UB40 250UB25	1.280	1.840	0.100	1.804	1.020
0.85	$C_1, C_2, C_3, C_4$ $C_5, C_6$ $B_1, B_2$ $B_3$	310UB46 200UB25 310UB40 200UB29	1.179	1.700	0.099	1.667	1.020
0.91	$C_1, C_2, C_3, C_4$ $C_5, C_6$ $B_1, B_2$ $B_3$	200UB29 200UB18 310UB40 250UB37	1.099	1.589	0.100	1.519	1.046
0.97	$C_1, C_2, C_3, C_4$ $C_5, C_6$ $B_1, B_2$ $B_3$	250UB31 250UB31 310UB32 250UB25	1.032	1.506	0.104	1.476	1.020

Table E.3: System-based design of Frame 2 (sway) under gravity loading using CSM,  
Instability

$\varphi_s$	Members (see Figure 7.1)	Section	$\lambda_n$ (factored loads)	Mean ( $\bar{\lambda}$ )	COV	$\lambda_n$ (unfactored loads)	$\bar{\lambda}/\lambda_n$ (unfactored load)
0.67	$C_1, C_2$ $C_3, C_4$ $C_5, C_6$ $B_1, B_2$ $B_3$	200UB25 200UB25 200UB18 460UB67 310UB46	1.486	2.208	0.095	2.02	1.093
0.79	$C_1, C_2$ $C_3, C_4$ $C_5, C_6$ $B_1, B_2$ $B_3$	180UB22 180UB18 180UB18 460UB67 310UB46	1.260	1.867	0.091	1.698	1.104
0.90	$C_1, C_2$ $C_3, C_4$ $C_5, C_6$ $B_1, B_2$ $B_3$	180UB18 180UB18 180UB18 460UB67 310UB46	1.108	1.587	0.094	1.492	1.064
1.08	$C_1, C_2$ $C_3, C_4$ $C_5, C_6$ $B_1, B_2$ $B_3$	180UB16 180UB16 180UB16 460UB67 310UB46	0.930	1.414	0.098	1.261	1.122

Table E.4: System-based design of Frame 2 (sway) under gravity loading using CSM,  
BPY-CPY

$\varphi_s$	Members (see Figure 7.1)	Section	$\lambda_n$ (factored loads)	Mean ( $\bar{\lambda}$ )	COV	$\lambda_n$ (unfactored loads)	$\bar{\lambda}/\lambda_n$ (unfactored load)
0.57	$C_1, C_2, C_3, C_4, C_5, C_6$ $B_1, B_2$ $B_3$	200UB29 460UB74 310UB46	1.767	2.602	0.093	2.382	1.092
0.68	$C_1, C_2, C_3, C_4, C_5, C_6$ $B_1, B_2$ $B_3$	200UB25 460UB67 310UB46	1.499	2.219	0.093	2.024	1.097
0.87	$C_1, C_2, C_3, C_4, C_5, C_6$ $B_1, B_2$ $B_3$	180UB22 360UB56 310UB46	1.145	1.672	0.091	1.546	1.081
0.96	$C_1, C_2, C_3, C_4, C_5, C_6$ $B_1, B_2$ $B_3$	180UB18 410UB53 310UB46	1.042	1.547	0.094	1.41	1.098
1.01	$C_1, C_2, C_3, C_4, C_5, C_6$ $B_1, B_2$ $B_3$	200UB18 360UB56 310UB46	0.992	1.485	0.094	1.344	1.105

Table E.5: System-based design of Frame 3 (sway) under gravity loading using CSM,  
BFY-CPY

$\varphi_s$	Members (see Figure 7.1)	Section	$\lambda_n$ (factored loads)	Mean ( $\bar{\lambda}$ )	COV	$\lambda_n$ (unfactored loads)	$\bar{\lambda}/\lambda_n$ (unfactored load)
0.66	$C_1, C_2, C_3$ $B_1$ $B_2$	360UB56 250UB37 610UB31	1.510	2.181	0.101	2.038	1.070
0.76	$C_1, C_2, C_3$ $B_1$ $B_2$	360UB56 250UB31 530UB92	1.307	1.879	0.104	1.762	1.066
0.83	$C_1, C_2, C_3$ $B_1$ $B_2$	360UB56 250UB31 530UB82	1.194	1.728	0.095	1.613	1.072
0.96	$C_1, C_2, C_3$ $B_1$ $B_2$	250UB25 250UB31 530UB92	1.045	1.506	0.106	1.411	1.067
1.04	$C_1, C_2, C_3$ $B_1$ $B_2$	200UB29 200UB29 530UB92	0.960	1.386	0.105	1.298	1.068

Table E.6: System-based design of Frame 3 (sway) under gravity loading using CSM,  
BPY-CFY

$\varphi_s$	Members (see Figure 7.1)	Section	$\lambda_n$ (factored loads)	Mean ( $\bar{\lambda}$ )	COV	$\lambda_n$ (unfactored loads)	$\bar{\lambda}/\lambda_n$ (unfactored load)
0.63	$C_1, C_3$ $C_2$ $B_1$ $B_2$	460UB74 180UB22 360UB56 610UB125	1.593	2.237	0.105	2.154	1.039
0.79	$C_1, C_3$ $C_2$ $B_1$ $B_2$	460UB74 200UB18 360UB56 610UB125	1.271	1.817	0.106	1.715	1.06
0.83	$C_1, C_3$ $C_2$ $B_1$ $B_2$	310UB46 200UB18 360UB56 610UB125	1.203	1.700	0.104	1.625	1.046
0.89	$C_1, C_3$ $C_2$ $B_1$ $B_2$	460UB74 180UB16 360UB56 610UB125	1.124	1.618	0.102	1.516	1.067
1.02	$C_1, C_3$ $C_2$ $B_1$ $B_2$	460UB74 150UB14 360UB56 610UB125	0.977	1.410	0.102	1.319	1.069

Table E.7: System-based design of Frame 3 (sway) under gravity loading using CSM,  
BPY-CPY

$\varphi_s$	Members (see Figure 7.1)	Section	$\lambda_n$ (factored loads)	Mean ( $\bar{\lambda}$ )	COV	$\lambda_n$ (unfactored loads)	$\bar{\lambda}/\lambda_n$ (unfactored load)
0.63	$C_1, C_2, C_3$ $B_1$ $B_2$	200UB25 460UB74 610UB125	1.579	2.192	0.112	2.183	1.004
0.71	$C_1, C_2, C_3$ $B_1$ $B_2$	200UB22 460UB67 610UB113	1.398	1.941	0.103	1.894	1.025
0.85	$C_1, C_2, C_3$ $B_1$ $B_2$	200UB18 360UB56 610UB125	1.171	1.612	0.107	1.580	1.02
0.92	$C_1, C_2, C_3$ $B_1$ $B_2$	180UB18 460UB74 610UB125	1.080	1.539	0.103	1.490	1.033
1.01	$C_1, C_3$ $C_2$ $B_1$ $B_2$	180UB16 180UB18 460UB67 610UB125	0.986	1.376	0.102	1.331	1.034

Table E.8: System-based design of Frame 4 (sway) under gravity loading using CSM,  
BFY-CPY

$\varphi_s$	Members (see Figure 7.1)	Section	$\lambda_n$ (factored loads)	Mean ( $\bar{\lambda}$ )	COV	$\lambda_n$ (unfactored loads)	$\bar{\lambda}/\lambda_n$ (unfactored load)
0.63	$C_1$ to $C_9$ $B_1$ to $B_4$ $B_5, B_6$	310UB46 310UB46 250UB31	1.590	2.294	0.102	2.156	1.064
0.74	$C_1$ to $C_9$ $B_1$ to $B_4$ $B_5, B_6$	250UB37 310UB40 200UB29	1.341	1.879	0.099	1.819	1.033
0.83	$C_1, C_3, C_4, C_6$ $C_2, C_5$ $C_7, C_8, C_9$ $B_1$ to $B_4$ $B_5, B_6$	250UB25 250UB37 250UB25 310UB40 200UB29	1.204	1.728	0.098	1.628	1.062
0.92	$C_1$ to $C_9$ $B_1$ to $B_4$ $B_5, B_6$	250UB37 250UB37 200UB29	1.078	1.556	0.101	1.456	1.069
1.04	$C_1, C_2, C_3$ $C_4$ to $C_9$ $B_1$ to $B_4$ $B_5, B_6$	310UB40 250UB37 250UB31 200UB29	0.963	1.369	0.110	1.198	1.143

Table E.9: System-based design of Frame 4 (sway) under gravity loading using CSM, CFY

$\varphi_s$	Members (see Figure 7.1)	Section	$\lambda_n$ (factored loads)	Mean ( $\bar{\lambda}$ )	COV	$\lambda_n$ (unfactored loads)	$\bar{\lambda}/\lambda_n$ (unfactored load)
0.67	$C_1$ to $C_9$ $B_1$ to $B_4$ $B_5, B_6$	310UB40 460UB67 310UB40	1.493	2.156	0.101	2.017	1.069
0.75	$C_1$ to $C_9$ $B_1$ to $B_4$ $B_5, B_6$	250UB37 460UB67 310UB40	1.335	1.93	0.103	1.803	1.070
0.79	$C_1$ to $C_9$ $B_1$ to $B_4$ $B_5, B_6$	310UB32 460UB67 310UB40	1.260	1.841	0.104	1.721	1.070
0.89	$C_1$ to $C_9$ $B_1$ to $B_4$ $B_5, B_6$	250UB31 460UB67 310UB40	1.117	1.620	0.103	1.508	1.075
0.97	$C_1$ to $C_9$ $B_1$ to $B_4$ $B_5, B_6$	200UB29 460UB67 310UB40	1.031	1.490	0.104	1.392	1.070

Table E.10: System-based design of Frame 4 (sway) under gravity loading using CSM,  
BPY-CFY

$\varphi_s$	Members (see Figure 7.1)	Section	$\lambda_n$ (factored loads)	Mean ( $\bar{\lambda}$ )	COV	$\lambda_n$ (unfactored loads)	$\bar{\lambda}/\lambda_n$ (unfactored load)
0.66	$C_1$ to $C_9$ $B_1$ to $B_4$ $B_5, B_6$	310UB40 460UB67 250UB37	1.050	2.168	0.105	2.02	1.073
0.73	$C_1$ to $C_9$ $B_1$ to $B_4$ $B_5, B_6$	250UB37 360UB56 250UB31	1.365	1.98	0.106	1.843	1.075
0.87	$C_1$ to $C_9$ $B_1$ to $B_4$ $B_5, B_6$	250UB31 360UB56 250UB25	1.145	1.655	0.105	1.546	1.071
0.95	$C_1$ to $C_9$ $B_1$ to $B_4$ $B_5, B_6$	200UB29 360UB56 250UB25	1.050	1.521	0.105	1.418	1.073

Table E.11: System-based design of Frame 5 (sway) under gravity loading using CSM,  
BFY-CPY

$\varphi_s$	Members (see Figure 7.1)	Section	$\lambda_n$ (factored loads)	Mean ( $\bar{\lambda}$ )	COV	$\lambda_n$ (unfactored loads)	$\bar{\lambda}/\lambda_n$ (unfactored load)
0.63	$C_1, C_4, C_5, C_8, C_9, C_{12}$ $C_2, C_3, C_6, C_7$ $C_{10}, C_{11}$ $B_1, B_4, B_7$ $B_2, B_5, B_8$ $B_3, B_6, B_9$	250UC72 200UC59 150UC30 460UB74 360UB56 460UB74	1.588	2.292	0.100	2.143	1.069
0.68	$C_1, C_4, C_5, C_8, C_9, C_{12}$ $C_2, C_3, C_6, C_7$ $C_{10}, C_{11}$ $B_1, B_4, B_7$ $B_2, B_5, B_8$ $B_3, B_6, B_9$	250UC72 200UC59 150UC30 460UB67 360UB50 460UB67	1.451	2.089	0.101	1.959	1.066
0.74	$C_1, C_4, C_5, C_8, C_9, C_{12}$ $C_2, C_3, C_6, C_7$ $C_{10}, C_{11}$ $B_1, B_4, B_7$ $B_2, B_5, B_8$ $B_3, B_6, B_9$	200UC59 200UC59 150UC30 460UB67 360UB50 460UB67	1.357	1.959	0.100	1.833	1.069
0.85	$C_1, C_4, C_5, C_8, C_9, C_{12}$ $C_2, C_3, C_6, C_7$ $C_{10}, C_{11}$ $B_1, B_4, B_7$ $B_2, B_5, B_8$ $B_3, B_6, B_9$	250UC72 200UC59 150UC30 360UB56 360UB50 360UB56	1.179	1.692	0.102	1.593	1.062
0.96	$C_1, C_4, C_5, C_8, C_9, C_{12}$ $C_2, C_3, C_6, C_7$ $C_{10}, C_{11}$ $B_1, B_4, B_7$ $B_2, B_5, B_8$ $B_3, B_6, B_9$	250UC72 200UC59 150UC30 360UB50 310UB40 360UB50	1.036	1.483	0.100	1.399	1.060

Table E.12: System-based design of Frame 5 (sway) under gravity loading using CSM, CFY

$\varphi_s$	Members (see Figure 7.1)	Section	$\lambda_n$ (factored loads)	Mean ( $\bar{\lambda}$ )	COV	$\lambda_n$ (unfactored loads)	$\bar{\lambda}/\lambda_n$ (unfactored load)
0.58	$C_1, C_4, C_5, C_8, C_9, C_{12}$ $C_2, C_3, C_6, C_7, C_{10}, C_{11}$ $B_1, B_4, B_7$ $B_2, B_5, B_8$ $B_3, B_6, B_9$	250UC72 200UC59 610UB113 460UB67 610UB113	1.732	2.634	0.103	2.339	1.126
0.72	$C_1, C_4, C_5, C_8, C_9, C_{12}$ $C_2, C_3, C_6, C_7, C_{10}, C_{11}$ $B_1, B_4, B_7$ $B_2, B_5, B_8$ $B_3, B_6, B_9$	310UC96 200UC46 530UB92 460UB67 530UB92	1.382	2.123	0.104	1.867	1.137
0.92	$C_1, C_4, C_5, C_8, C_9, C_{12}$ $C_2, C_3, C_6, C_7, C_{10}, C_{11}$ $B_1, B_4, B_7$ $B_2, B_5, B_8$ $B_3, B_6, B_9$	310UC158 150UC37 610UB113 460UB67 610UB113	1.093	1.639	0.101	1.473	1.113
1.12	$C_1, C_4, C_5, C_8, C_9, C_{12}$ $C_2, C_3, C_6, C_7, C_{10}, C_{11}$ $B_1, B_4, B_7$ $B_2, B_5, B_8$ $B_3, B_6, B_9$	310UC96 150UC30 460UB74 360UB56 460UB74	0.891	1.394	0.100	1.203	1.159

Table E.13: System-based design of Frame 5 (sway) under gravity loading using CSM,  
BPY-CFY

$\varphi_s$	Members (see Figure 7.1)	Section	$\lambda_n$ (factored loads)	Mean ( $\bar{\lambda}$ )	COV	$\lambda_n$ (unfactored loads)	$\bar{\lambda}/\lambda_n$ (unfactored load)
0.59	$C_1$ to $C_{11}$ $B_1, B_4, B_7$ $B_2, B_5, B_8$ $B_3, B_6, B_9$	200UC59 610UB101 360UB56 610UB101	1.687	2.621	0.102	2.279	1.150
0.75	$C_1, C_4, C_5, C_8, C_9, C_{12}$ $C_2, C_3, C_6, C_7, C_{10}, C_{11}$ $B_1, B_4, B_7$ $B_2, B_5, B_8$ $B_3, B_6, B_9$	200UC59 200UC46 530UB92 360UB56 530UB92	1.328	1.991	0.102	1.797	1.108
0.79	$C_1$ to $C_{11}$ $B_1, B_4, B_7$ $B_2, B_5, B_8$ $B_3, B_6, B_9$	200UC46 460UB74 360UB56 460UB74	1.271	1.875	0.103	1.715	1.093
0.95	$C_1, C_4, C_5, C_8, C_9, C_{12}$ $C_2, C_3, C_6, C_7, C_{10}, C_{11}$ $B_1, B_4, B_7$ $B_2, B_5, B_8$ $B_3, B_6, B_9$	200UC59 150UC37 460UB74 360UB56 460UB74	1.053	1.504	0.098	1.418	1.060

Table E.14: System-based design of Frame 6 (sway) under gravity loading using CSM,  
BFY-CPY

$\varphi_s$	Members (see Figure 7.1)	Section	$\lambda_n$ (factored loads)	Mean ( $\bar{\lambda}$ )	COV	$\lambda_n$ (unfactored loads)	$\bar{\lambda}/\lambda_n$ (unfactored load)
0.63	$C_1, C_4, C_5, C_8$ $C_9, C_{10}, C_{11}, C_{12}$ $C_2, C_3, C_6, C_7$ $B_1$ to $B_6$ $B_7$ $B_8$	250UB31 250UB31 360UB50 360UB50 360UB50 250UB37	1.582	2.292	0.101	2.136	1.073
0.73	$C_1, C_4, C_5, C_8$ $C_9, C_{10}, C_{11}, C_{12}$ $C_2, C_3, C_6, C_7$ $B_1$ to $B_6$ $B_7$ $B_8$	250UB31 250UB31 360UB44 310UB46 310UB46 250UB37	1.369	1.967	0.103	1.847	1.065
0.82	$C_1, C_4, C_5, C_8$ $C_9, C_{10}, C_{11}, C_{12}$ $C_2, C_3, C_6, C_7$ $B_1$ to $B_6$ $B_7$ $B_8$	200UB25 200UB25 310UB40 310UB46 310UB46 250UB31	1.224	1.763	0.099	1.653	1.067
0.88	$C_1, C_4, C_5, C_8$ $C_9, C_{10}, C_{11}, C_{12}$ $C_2, C_3, C_6, C_7$ $B_1$ to $B_6$ $B_7$ $B_8$	200UB25 200UB25 310UB40 310UB40 310UB40 200UB29	1.131	1.580	0.102	1.527	1.035
1.02	$C_1, C_4, C_5, C_8$ $C_9, C_{10}, C_{11}, C_{12}$ $C_2, C_3, C_6, C_7$ $B_1$ to $B_6$ $B_7$ $B_8$	200UB25 200UB25 310UB40 310UB40 250UB31 200UB29	0.979	1.381	0.102	1.323	1.044



Table E.15: System-based design of Frame 6 (sway) under gravity loading using CSM,  
BPY-CFY

$\varphi_s$	Members (see Figure 7.1)	Section	$\lambda_n$ (factored loads)	Mean ( $\bar{\lambda}$ )	COV	$\lambda_n$ (unfactored loads)	$\bar{\lambda}/\lambda_n$ (unfactored load)
0.63	$C_1$ to $C_8$ $C_9, C_{10}$ $C_{11}, C_{12}$ $B_1$ to $B_6$ $B_7$ $B_8$	250UB31 250UB31 360UB50 360UB50 360UB50 250UB37	1.576	2.288	0.105	2.127	1.076
0.71	$C_1$ to $C_8$ $C_9, C_{10}$ $C_{11}, C_{12}$ $B_1$ to $B_6$ $B_7$ $B_8$	250UB31 250UB31 360UB44 310UB46 310UB46 250UB37	1.407	2.06	0.104	1.900	1.084
0.78	$C_1$ to $C_8$ $C_9, C_{10}$ $C_{11}, C_{12}$ $B_1$ to $B_6$ $B_7$ $B_8$	200UB25 200UB25 310UB40 310UB46 310UB46 250UB31	1.273	1.87	0.103	1.719	1.088
0.93	$C_1$ to $C_8$ $C_9, C_{10}$ $C_{11}, C_{12}$ $B_1$ to $B_6$ $B_7$ $B_8$	200UB25 200UB25 310UB40 310UB40 310UB40 200UB29	1.071	1.535	0.103	1.446	1.062

Table E.16: System-based design of Frame 7 (sway) under gravity loading using CSM,  
BFY-CPY

$\varphi_s$	Members (see Figure 7.1)	Section	$\lambda_n$ (factored loads)	Mean ( $\bar{\lambda}$ )	COV	$\lambda_n$ (unfactored loads)	$\bar{\lambda}/\lambda_n$ (unfactored load)
0.64	$C_1, C_4$ $C_2$ $C_3, C_5, C_6$ $B_1, B_4$ $B_2$ $B_3$	150UB14 310UB40 250UB37 310UB46 460UB67 200UB29	1.550	2.201	0.100	2.093	1.052
0.75	$C_1, C_4$ $C_2$ $C_3, C_5, C_6$ $B_1, B_4$ $B_2$ $B_3$	150UB14 310UB40 250UB37 310UB46 410UB59 200UB29	1.338	1.945	0.099	1.806	1.077
0.82	$C_1, C_4$ $C_2$ $C_3, C_5, C_6$ $B_1, B_4$ $B_2$ $B_3$	150UB14 310UB40 250UB37 310UB46 360UB56 200UB29	1.213	1.745	0.099	1.653	1.056
0.90	$C_1, C_4$ $C_2$ $C_3, C_5, C_6$ $B_1, B_4$ $B_2$ $B_3$	150UB14 310UB40 250UB37 310UB32 410UB57 200UB29	1.100	1.580	0.097	1.486	1.064
0.98	$C_1, C_4$ $C_2$ $C_3, C_5, C_6$ $B_1, B_4$ $B_2$ $B_3$	150UB14 310UB40 250UB37 310UB32 310UB46 200UB29	1.015	1.426	0.100	1.371	1.040

Table E.17: System-based design of Frame 7 (sway) under gravity loading using CSM, CFY

$\varphi_s$	Members (see Figure 7.1)	Section	$\lambda_n$ (factored loads)	Mean ( $\bar{\lambda}$ )	COV	$\lambda_n$ (unfactored loads)	$\bar{\lambda}/\lambda_n$ (unfactored load)
0.63	$C_1, C_2, C_3$ $C_4, C_5, C_6$ $B_1$ to $B_4$	200UB29 200UB18 610UB125	1.579	2.212	0.092	2.131	1.038
0.74	$C_1, C_2, C_3$ $C_4, C_5, C_6$ $B_1$ to $B_4$	200UB25 200UB18 610UB125	1.353	1.919	0.097	1.822	1.053
0.84	$C_1, C_2, C_3$ $C_4, C_5, C_6$ $B_1$ to $B_4$	180UB18 180UB18 610UB125	1.184	1.642	0.092	1.597	1.028
1.01	$C_1, C_2, C_3$ $C_4, C_5, C_6$ $B_1$ to $B_4$	200UB18 200UB18 610UB125	0.990	1.415	0.097	1.336	1.059

Table E.18: System-based design of Frame 7 (sway) under gravity loading using CSM,  
BPY-CPY

$\varphi_s$	Members (see Figure 7.1)	Section	$\lambda_n$ (factored loads)	Mean ( $\bar{\lambda}$ )	COV	$\lambda_n$ (unfactored loads)	$\bar{\lambda}/\lambda_n$ (unfactored load)
0.65	$C_1$ to $C_6$ $B_1, B_3, B_4$ $B_2$	200UB29 360UB56 530UB92	1.549	2.159	0.097	2.073	1.041
0.72	$C_1, C_3, C_4, C_6$ $C_2, C_5$ $B_1, B_3, B_4$ $B_2$	250UB31 200UB25 360UB56 530UB92	1.394	1.936	0.100	1.879	1.030
0.79	$C_1$ to $C_6$ $B_1, B_3, B_4$ $B_2$	200UB25 360UB56 460UB74	1.264	1.748	0.093	1.709	1.023
0.95	$C_1$ to $C_6$ $B_1, B_3, B_4$ $B_2$	180UB18 360UB56 460UB74	1.056	1.496	0.094	1.426	1.049

Table E.19: System-based design of Frame 8 (sway) under gravity loading using CSM,  
BFY-CPY

$\phi_s$	Members (see Figure 7.1)	Section	$\lambda_n$ (factored loads)	Mean ( $\bar{\lambda}$ )	COV	$\lambda_n$ (unfactored loads)	$\bar{\lambda}/\lambda_n$ (unfactored load)
0.59	$C_1, C_5, C_6$ $C_2, C_3$ $C_4$ $C_7, C_8$ $B_1$ $B_2$ $B_3, B_6$ $B_4, B_5$	150UB14 250UB37 180UB18 200UB22 310UB40 360UB50 200UB29 250UB37	1.696	2.442	0.099	2.289	1.067
0.69	$C_1, C_5, C_6$ $C_2, C_3$ $C_4$ $C_7, C_8$ $B_1$ $B_2$ $B_3, B_6$ $B_4, B_5$	150UB14 250UB37 180UB18 200UB22 310UB32 310UB46 200UB25 250UB31	1.453	2.097	0.103	1.962	1.069
0.76	$C_1, C_5, C_6$ $C_2, C_3$ $C_4$ $C_7, C_8$ $B_1$ $B_2$ $B_3, B_6$ $B_4, B_5$	150UB14 250UB37 180UB18 200UB22 310UB32 310UB40 200UB25 250UB31	1.317	1.895	0.103	1.776	1.067
0.86	$C_1, C_5, C_6$ $C_2, C_3$ $C_4$ $C_7, C_8$ $B_1$ $B_2$ $B_3, B_6$ $B_4, B_5$	150UB14 250UB37 180UB18 200UB22 310UB32 310UB40 200UB25 200UB25	1.160	1.662	0.102	1.576	1.055
0.96	$C_1, C_5, C_6$ $C_2, C_3$ $C_4$ $C_7, C_8$ $B_1$ $B_2$ $B_3, B_6$ $B_4, B_5$	150UB14 250UB37 180UB18 200UB22 250UB37 310UB40 200UB18 200UB22	1.038	1.472	0.102	1.402	1.050

Table E.20: System-based design of Frame 8 (sway) under gravity loading using CSM,  
BPY-CFY

$\varphi_s$	Members (see Figure 7.1)	Section	$\lambda_n$ (factored loads)	Mean ( $\bar{\lambda}$ )	COV	$\lambda_n$ (unfactored loads)	$\bar{\lambda}/\lambda_n$ (unfactored load)
0.62	$C_1, C_4, C_5, C_6$ $C_2, C_3, C_7, C_8$ $B_1, B_3, B_6$ $B_2$ $B_4, B_5$	310UB40 180UB18 250UB37 460UB67 310UB46	1.610	2.311	0.102	2.157	1.071
0.79	$C_1, C_4, C_5, C_6$ $C_2, C_3, C_7, C_8$ $B_1, B_3, B_6$ $B_2$ $B_4, B_5$	310UB40 150UB18 250UB37 460UB67 310UB46	1.272	1.800	0.101	1.653	1.089
0.88	$C_1, C_4, C_5, C_6$ $C_2, C_3, C_7, C_8$ $B_1, B_3, B_6$ $B_2$ $B_4, B_5$	310UB40 180UB16 250UB37 460UB67 310UB46	1.133	1.619	0.103	1.508	1.074
0.94	$C_1, C_4, C_5, C_6$ $C_2, C_3$ $C_7, C_8$ $B_1, B_3, B_6$ $B_2$ $B_4, B_5$	310UB40 180UB16 150UB14 250UB37 360UB50 310UB46	1.063	1.552	0.102	1.465	1.06
1.04	$C_1, C_4, C_5, C_6$ $C_2, C_3, C_7, C_8$ $B_1, B_3, B_6$ $B_2$ $B_4, B_5$	310UB40 150UB14 250UB37 360UB50 310UB46	0.966	1.388	0.101	1.290	1.076

Table E.21: System-based design of Frame 8 (sway) under gravity loading using CSM,  
BPY-CPY

$\varphi_s$	Members (see Figure 7.1)	Section	$\lambda_n$ (factored loads)	Mean ( $\bar{\lambda}$ )	COV	$\lambda_n$ (unfactored loads)	$\bar{\lambda}/\lambda_n$ (unfactored load)
0.64	$C_1$ to $C_8$ $B_1, B_3, B_6$ $B_2$ $B_4, B_5$	180UB18 250UB37 460UB67 310UB46	1.553	2.253	0.105	2.098	1.074
0.83	$C_1$ to $C_8$ $B_1, B_3, B_6$ $B_2$ $B_4, B_5$	200UB18 250UB37 360UB56 310UB46	1.204	1.721	0.105	1.627	1.058
0.96	$C_1$ to $C_8$ $B_1, B_3, B_6$ $B_2$ $B_4, B_5$	180UB16 250UB37 360UB56 310UB46	1.038	1.504	0.099	1.393	1.080
1.09	$C_1$ to $C_8$ $B_1, B_3, B_6$ $B_2$ $B_4, B_5$	150UB14 250UB37 360UB50 310UB46	0.914	1.275	0.095	1.230	1.036

Table E.22: System-based design of Frame 9 (sway) under gravity loading using CSM,  
BFY-CPY

$\varphi_s$	Members (see Figure 7.1)	Section	$\lambda_n$ (factored loads)	Mean ( $\bar{\lambda}$ )	COV	$\lambda_n$ (unfactored loads)	$\bar{\lambda}/\lambda_n$ (unfactored load)
0.62	$C_1, C_4, C_5, C_8, C_9$ $C_2, C_3, C_6, C_7$ $B_1$ $B_2, B_4$ $B_3, B_5$ $B_6$	530UB92 250UB37 310UB46 250UB31 410UB53 610UB113	1.606	2.315	0.101	2.169	1.067
0.75	$C_1, C_4, C_5, C_8, C_9$ $C_2, C_3, C_6, C_7$ $B_1$ $B_2, B_4$ $B_3, B_5$ $B_6$	530UB92 200UB25 310UB46 250UB31 410UB53 530UB92	1.340	1.930	0.100	1.808	1.067
0.87	$C_1, C_4, C_5, C_8, C_9$ $C_2, C_3, C_6, C_7$ $B_1$ $B_2, B_4$ $B_3, B_5$ $B_6$	530UB92 250UB37 310UB32 250UB31 310UB40 530UB92	1.137	1.615	0.109	1.535	1.052
0.92	$C_1, C_4, C_5, C_8, C_9$ $C_2, C_3, C_6, C_7$ $B_1$ $B_2, B_4$ $B_3, B_5$ $B_6$	530UB92 250UB37 310UB40 200UB22 310UB32 530UB82	1.086	1.531	0.107	1.496	1.023
1.03	$C_1, C_4, C_5, C_8, C_9$ $C_2, C_3, C_6, C_7$ $B_1$ $B_2, B_4$ $B_3, B_5$ $B_6$	530UB92 250UB37 250UB31 250UB31 250UB31 530UB92	0.974	1.411	0.114	1.316	1.072

Table E.23: System-based design of Frame 9 (sway) under gravity loading using CSM,  
BPY-CPY

$\varphi_s$	Members (see Figure 7.1)	Section	$\lambda_n$ (factored loads)	Mean ( $\bar{\lambda}$ )	COV	$\lambda_n$ (unfactored loads)	$\bar{\lambda}/\lambda_n$ (unfactored load)
0.60	$C_1, C_4, C_5, C_8, C_9$ $C_2, C_3, C_6, C_7$ $B_1$ $B_2, B_4$ $B_3, B_5$ $B_6$	530UB92 200UB29 360UB50 250UB37 410UB53 610UB125	1.652	2.425	0.101	2.295	1.057
0.69	$C_1, C_4, C_5, C_8, C_9$ $C_2, C_3, C_6, C_7$ $B_1$ $B_2, B_4$ $B_3, B_5$ $B_6$	530UB92 200UB25 310UB46 250UB37 410UB53 610UB125	1.437	2.076	0.103	1.94	1.070
0.79	$C_1, C_4, C_5, C_8, C_9$ $C_2, C_3, C_6, C_7$ $B_1$ $B_2, B_4$ $B_3, B_5$ $B_6$	530UB92 200UB22 310UB46 250UB37 410UB53 610UB125	1.271	1.876	0.103	1.717	1.093
0.84	$C_1, C_4, C_5, C_8, C_9$ $C_2, C_3, C_6, C_7$ $B_1$ $B_2, B_4$ $B_3, B_5$ $B_6$	530UB82 180UB18 310UB40 250UB37 410UB53 530UB92	1.196	1.739	0.104	1.625	1.070
0.99	$C_1, C_4, C_5, C_8, C_9$ $C_2, C_3, C_6, C_7$ $B_1$ $B_2, B_4$ $B_3, B_5$ $B_6$	530UB92 200UB18 310UB40 250UB37 410UB53 530UB92	1.007	1.495	0.104	1.359	1.100



Table E.24: System-based design of Frame 9 (sway) under gravity loading using CSM,  
BFY-CFY

$\varphi_s$	Members (see Figure 7.1)	Section	$\lambda_n$ (factored loads)	Mean ( $\bar{\lambda}$ )	COV	$\lambda_n$ (unfactored loads)	$\bar{\lambda}/\lambda_n$ (unfactored load)
0.60	$C_1, C_4, C_5, C_8, C_9$ $C_2, C_3, C_6, C_7$ $B_1$ $B_2, B_4$ $B_3, B_5$ $B_6$	360UB56 250UB37 360UB56 250UB37 360UB56 610UB125	1.661	2.359	0.102	2.290	1.030
0.79	$C_1, C_4, C_5, C_8, C_9$ $C_2, C_3, C_6, C_7$ $B_1$ $B_2, B_4$ $B_3, B_5$ $B_6$	360UB56 200UB22 360UB56 250UB37 360UB56 610UB125	1.263	1.840	0.100	1.804	1.020
0.84	$C_1, C_4, C_5, C_8, C_9$ $C_2, C_3, C_6, C_7$ $B_1$ $B_2, B_4$ $B_3, B_5$ $B_6$	310UB40 180UB18 310UB46 250UB37 360UB56 610UB125	1.193	1.700	0.099	1.667	1.020
0.89	$C_1, C_4, C_5, C_8, C_9$ $C_2, C_3, C_6, C_7$ $B_1$ $B_2, B_4$ $B_3, B_5$ $B_6$	310UB40 180UB22 310UB46 250UB37 360UB56 610UB113	1.121	1.589	0.100	1.519	1.046

## E.2. System-based design of sway frames under gravity plus wind, CSM

Table E.25: System-based design of Frame 1 under gravity and wind loading,

$$W_n/(D_n + L_n)=0.05, \text{ CFY}$$

$\varphi_s$	Members (see Figure 7.1)	Section	$\lambda_n$ (factored loads)	Mean ( $\bar{\lambda}$ )	COV
0.69	$C_1, C_2$ $B_1$	180UB22 360UB56	1.439	2.883	0.123
0.81	$C_1, C_2$ $B_1$	200UB18 360UB56	1.238	2.528	0.142
0.90	$C_1, C_2$ $B_1$	180UB18 360UB56	1.114	2.300	0.144
0.99	$C_1$ $C_2$ $B_1$	180UB16 180UB18 360UB56	1.013	2.043	0.141

Table E.26: System-based design of Frame 1 under gravity and wind loading,

$$W_n/(D_n + L_n)=0.10, \text{ CFY}$$

$\varphi_s$	Members (see Figure 7.1)	Section	$\lambda_n$ (factored loads)	Mean ( $\bar{\lambda}$ )	COV
0.71	$C_1, C_2$ $B_1$	200UB29 460UB74	1.416	2.568	0.118
0.77	$C_1, C_2$ $B_1$	250UB25 360UB56	1.306	2.403	0.120
0.90	$C_1, C_2$ $B_1$	200UB25 460UB67	1.114	2.063	0.119
1.05	$C_1, C_2$ $B_1$	200UB22 460UB67	0.953	1.809	0.122

Table E.27: System-based design of Frame 1 under gravity and wind loading,

$$W_n/(D_n + L_n)=0.15, \text{ CFY}$$

$\varphi_s$	Members (see Figure 7.1)	Section	$\lambda_n$ (factored loads)	Mean ( $\bar{\lambda}$ )	COV
0.69	$C_1, C_2$ $B_1$	310UB32 460UB74	1.453	2.504	0.111
0.82	$C_1, C_2$ $B_1$	250UB31 460UB74	1.226	2.205	0.112
0.92	$C_1, C_2$ $B_1$	200UB29 460UB74	1.087	1.998	0.118
1.01	$C_1, C_2$ $B_1$	200UB25 460UB74	0.988	1.814	0.110

Table E.28: System-based design of Frame 1 under gravity and wind loading,  
 $W_n/(D_n + L_n)=0.25$ , CFY

$\varphi_s$	Members (see Figure 7.1)	Section	$\lambda_n$ (factored loads)	Mean ( $\bar{\lambda}$ )	COV
0.71	$C_1, C_2$ $B_1$	310UB46 460UB74	1.417	2.282	0.107
0.81	$C_1$ $C_2$ $B_1$	310UB40 310UB46 360UB56	1.238	2.173	0.112
0.89	$C_1$ $C_2$ $B_1$	310UB32 310UB46 360UB56	1.124	1.933	0.110
1.02	$C_1$ $C_2$ $B_1$	250UB31 310UB40 460UB74	0.978	1.735	0.107

Table E.29: System-based design of Frame 2 under gravity and wind loading,  
 $W_n/(D_n + L_n)=0.05$ , BFY-CFY

$\varphi_s$	Members (see Figure 7.1)	Section	$\lambda_n$ (factored loads)	Mean ( $\bar{\lambda}$ )	COV
0.71	$C_1$ $C_2$ $C_3, C_4, C_5, C_6$ $B_1$ $B_2$ $B_3$	200UB29 250UB31 200UB22 310UB46 310UB32 200UB25	1.417	2.766	0.125
0.83	$C_1, C_2$ $C_3, C_4, C_5, C_6$ $B_1$ $B_2$ $B_3$	200UB29 200UB25 310UB46 310UB40 200UB25	1.211	2.437	0.130
0.88	$C_1$ $C_2$ $C_3, C_4, C_5, C_6$ $B_1$ $B_2$ $B_3$	200UB29 250UB25 200UB25 310UB40 310UB32 200UB25	1.141	2.365	0.131
1.00	$C_1$ $C_2$ $C_3, C_4, C_5, C_6$ $B_1$ $B_2$ $B_3$	200UB22 200UB29 200UB18 310UB40 310UB32 200UB25	1.004	2.018	0.147

Table E.30: System-based design of Frame 2 under gravity and wind loading,  
 $W_n/(D_n + L_n)=0.10$ , BFY-CFY

$\varphi_s$	Members (see Figure 7.1)	Section	$\lambda_n$ (factored loads)	Mean ( $\bar{\lambda}$ )	COV
0.68	$C_1, C_2$ $C_3, C_4, C_5, C_6$ $B_1$ $B_2$ $B_3$	310UB40 250UB31 410UB59 310UB46 200UB29	1.478	2.652	0.114
0.84	$C_1$ $C_2$ $C_3, C_4, C_5, C_6$ $B_1$ $B_2$ $B_3$	250UB37 310UB40 250UB25 360UB56 310UB46 200UB29	1.189	2.193	0.115
0.92	$C_1, C_2$ $C_3, C_4, C_5, C_6$ $B_1$ $B_2$ $B_3$	250UB37 250UB25 360UB56 310UB46 200UB29	1.111	2.011	0.122
1.02	$C_1$ $C_2$ $C_3, C_4, C_5, C_6$ $B_1$ $B_2$ $B_3$	250UB31 250UB37 200UB29 360UB56 310UB46 200UB29	0.981	1.827	0.113

Table E.31: System-based design of Frame 2 under gravity and wind loading,  
 $W_n/(D_n + L_n)=0.15$ , BFY-CFY

$\varphi_s$	Members (see Figure 7.1)	Section	$\lambda_n$ (factored loads)	Mean ( $\bar{\lambda}$ )	COV
0.70	$C_1$ $C_2$ $C_3, C_4, C_5, C_6$ $B_1$ $B_2$ $B_3$	310UB46 360UB56 310UB46 460UB67 360UB50 250UB31	1.429	2.531	0.108
0.82	$C_1$ $C_2$ $C_3, C_4, C_5, C_6$ $B_1$ $B_2$ $B_3$	310UB46 360UB44 310UB40 460UB67 360UB50 250UB31	1.216	2.162	0.107
0.91	$C_1$ $C_2$ $C_3, C_4, C_5, C_6$ $B_1$ $B_2$ $B_3$	310UB40 310UB46 250UB37 460UB67 360UB50 250UB31	1.096	1.940	0.107
0.99	$C_1, C_2$ $C_3, C_4, C_5, C_6$ $B_1$ $B_2$ $B_3$	310UB40 250UB31 410UB59 310UB46 200UB29	1.012	1.778	0.114

Table E.32: System-based design of Frame 2 under gravity and wind loading,

$$W_n/(D_n + L_n)=0.25, \text{BFY-CFY}$$

$\varphi_s$	Members (see Figure 7.1)	Section	$\lambda_n$ (factored loads)	Mean ( $\bar{\lambda}$ )	COV
0.69	$C_1, C_2$ $C_3, C_4, C_5, C_6$ $B_1$ $B_2$ $B_3$	460UB74 360UB56 460UB82 410UB59 250UB37	1.444	2.415	0.102
0.80	$C_1$ $C_2$ $C_3, C_4, C_5, C_6$ $B_1$ $B_2$ $B_3$	360UB56 460UB67 360UB56 460UB82 410UB59 250UB37	1.247	2.114	0.108
0.88	$C_1, C_2$ $C_3, C_4, C_5, C_6$ $B_1$ $B_2$ $B_3$	410UB59 310UB46 460UB74 360UB56 250UB31	1.142	1.896	0.104
0.99	$C_1, C_2$ $C_3, C_4, C_5, C_6$ $B_1$ $B_2$ $B_3$	360UB56 310UB46 460UB74 360UB56 250UB31	1.007	1.707	0.106

Table E.33: System-based design of Frame 3 under gravity and wind loading,

$$W_n/(D_n + L_n)=0.05, \text{BFY-CFY}$$

$\varphi_s$	Members (see Figure 7.1)	Section	$\lambda_n$ (factored loads)	Mean ( $\bar{\lambda}$ )	COV
0.71	$C_1, C_2$ $C_3$ $B_1$ $B_2$	180UB16 200UB25 310UB40 310UB46	1.410	2.682	0.122
0.82	$C_1, C_2$ $C_3$ $B_1$ $B_2$	180UB18 200UB18 310UB40 310UB46	1.226	2.395	0.122
0.92	$C_1, C_2$ $C_3$ $B_1$ $B_2$	180UB16 200UB18 310UB40 310UB46	1.087	2.168	0.132
1.03	$C_1, C_2$ $C_3$ $B_1$ $B_2$	180UB16 180UB16 310UB40 310UB46	0.970	1.934	0.130

Table E.34: System-based design of Frame 3 under gravity and wind loading,  
 $W_n/(D_n + L_n)=0.10$ , BFY-CFY

$\varphi_s$	Members (see Figure 7.1)	Section	$\lambda_n$ (factored loads)	Mean ( $\bar{\lambda}$ )	COV
0.71	$C_1$ $C_2$ $C_3$ $B_1$ $B_2$	180UB22 200UB25 250UB37 310UB40 310UB46	1.410	2.533	0.115
0.80	$C_1$ $C_2$ $C_3$ $B_1$ $B_2$	180UB22 200UB25 250UB31 310UB40 310UB46	1.252	2.288	0.112
0.92	$C_1$ $C_2$ $C_3$ $B_1$ $B_2$	180UB22 200UB25 250UB25 310UB40 310UB46	1.088	2.024	0.113
1.03	$C_1$ $C_2$ $C_3$ $B_1$ $B_2$	180UB22 180UB22 250UB25 250UB37 310UB46	0.971	1.829	0.118

Table E.35: System-based design of Frame 3 under gravity and wind loading,  
 $W_n/(D_n + L_n)=0.15$ , BFY-CFY

$\varphi_s$	Members (see Figure 7.1)	Section	$\lambda_n$ (factored loads)	Mean ( $\bar{\lambda}$ )	COV
0.69	$C_1$ $C_2$ $C_3$ $B_1$ $B_2$	180UB22 310UB32 310UB46 310UB40 310UB46	1.439	2.471	0.107
0.80	$C_1$ $C_2$ $C_3$ $B_1$ $B_2$	180UB22 250UB31 310UB40 310UB40 310UB46	1.254	2.256	0.114
0.91	$C_1$ $C_2$ $C_3$ $B_1$ $B_2$	180UB22 200UB25 310UB40 310UB40 310UB46	1.103	1.987	0.112
1.00	$C_1$ $C_2$ $C_3$ $B_1$ $B_2$	180UB22 200UB29 250UB37 310UB46 310UB46	1.002	1.810	0.111



Table E.36: System-based design of Frame 3 under gravity and wind loading,  
 $W_n/(D_n + L_n)=0.25$ , BFY-CFY

$\varphi_s$	Members (see Figure 7.1)	Section	$\lambda_n$ (factored loads)	Mean ( $\bar{\lambda}$ )	COV
0.70	$C_1$ $C_2$ $C_3$ $B_1$ $B_2$	200UB25 360UB50 360UB56 360UB56 530UB92	1.427	2.402	0.105
0.81	$C_1$ $C_2$ $C_3$ $B_1$ $B_2$	200UB25 310UB40 360UB56 360UB50 460UB74	1.240	2.175	0.106
0.90	$C_1$ $C_2$ $C_3$ $B_1$ $B_2$	180UB22 310UB40 360UB50 310UB46 460UB67	1.111	1.956	0.106
0.99	$C_1$ $C_2$ $C_3$ $B_1$ $B_2$	180UB22 250UB37 360UB50 310UB46 460UB67	1.015	1.790	0.106

Table E.37: System-based design of Frame 4 under gravity and wind loading,  
 $W_n/(D_n + L_n)=0.05$ , BFY-CFY

$\varphi_s$	Members (see Figure 7.1)	Section	$\lambda_n$ (factored loads)	Mean ( $\bar{\lambda}$ )	COV
0.71	$C_1, C_3, C_4, C_6, C_7, C_8, C_9$ $C_2$ $C_5$ $B_1, B_3$ $B_2, B_4$ $B_5, B_6$	200UB22 360UB56 250UB31 310UB46 250UB37 200UB22	1.405	2.634	0.140
0.81	$C_1, C_3, C_4, C_6, C_7, C_8, C_9$ $C_2$ $C_5$ $B_1, B_3$ $B_2, B_4$ $B_5, B_6$	200UB18 360UB50 310UB40 360UB50 250UB37 200UB22	1.234	2.346	0.133
0.89	$C_1, C_3, C_4, C_6, C_7, C_8, C_9$ $C_2$ $C_5$ $B_1, B_3$ $B_2, B_4$ $B_5, B_6$	200UB18 360UB50 250UB37 310UB46 250UB37 200UB29	1.130	2.230	0.149
0.94	$C_1, C_3, C_4, C_6, C_7, C_8, C_9$ $C_2$ $C_5$ $B_1, B_3$ $B_2, B_4$ $B_5, B_6$	180UB18 360UB50 250UB37 310UB46 250UB37 200UB22	1.064	2.135	0.142

Table E.38: System-based design of Frame 4 under gravity and wind loading,  
 $W_n/(D_n + L_n)=0.10$ , BFY-CFY

$\varphi_s$	Members (see Figure 7.1)	Section	$\lambda_n$ (factored loads)	Mean ( $\bar{\lambda}$ )	COV
0.71	$C_1, C_3, C_4, C_6, C_7, C_8, C_9$ $C_2$ $C_5$ $B_1, B_3$ $B_2, B_4$ $B_5, B_6$	310UB40 410UB59 360UB50 410UB59 310UB40 250UB31	1.399	2.467	0.118
0.80	$C_1, C_3, C_4, C_6, C_7, C_8, C_9$ $C_2$ $C_5$ $B_1, B_3$ $B_2, B_4$ $B_5, B_6$	250UB37 410UB59 360UB50 410UB59 310UB46 250UB31	1.248	2.284	0.120
0.88	$C_1, C_3, C_4, C_6, C_7, C_8, C_9$ $C_2$ $C_5$ $B_1, B_3$ $B_2, B_4$ $B_5, B_6$	250UB31 410UB59 360UB50 410UB59 360UB50 250UB31	1.135	2.093	0.118
0.99	$C_1, C_3, C_4, C_6, C_7, C_8, C_9$ $C_2$ $C_5$ $B_1, B_3$ $B_2, B_4$ $B_5, B_6$	200UB29 410UB59 360UB50 410UB59 360UB50 250UB31	1.006	1.900	0.117

Table E.39: System-based design of Frame 4 under gravity and wind loading,  
 $W_n/(D_n + L_n)=0.15$ , BFY-CFY

$\varphi_s$	Members (see Figure 7.1)	Section	$\lambda_n$ (factored loads)	Mean ( $\bar{\lambda}$ )	COV
0.71	$C_1, C_3, C_4, C_6$ $C_2$ $C_5$ $C_7, C_8, C_9$ $B_1, B_3$ $B_2, B_4$ $B_5, B_6$	360UB56 460UB67 360UB56 360UB50 460UB67 360UB56 250UB31	1.409	2.380	0.109
0.80	$C_1, C_3, C_4, C_6$ $C_2$ $C_5$ $C_7, C_8, C_9$ $B_1, B_3$ $B_2, B_4$ $B_5, B_6$	360UB56 410UB59 360UB50 310UB46 410UB59 360UB50 250UB31	1.256	2.258	0.114
0.87	$C_1, C_3, C_4, C_6, C_7, C_8, C_9$ $C_2$ $C_5$ $B_1, B_3$ $B_2, B_4$ $B_5, B_6$	360UB50 410UB59 360UB50 410UB59 310UB46 250UB31	1.145	2.083	0.116
1.00	$C_1, C_3, C_4, C_6, C_7, C_8, C_9$ $C_2$ $C_5$ $B_1, B_3$ $B_2, B_4$ $B_5, B_6$	310UB46 410UB59 360UB50 410UB59 310UB40 250UB31	1.001	1.826	0.113

Table E.40: System-based design of Frame 4 under gravity and wind loading,

$$W_n/(D_n + L_n)=0.25, \text{BFY-CFY}$$

$\varphi_s$	Members (see Figure 7.1)	Section	$\lambda_n$ (factored loads)	Mean ( $\bar{\lambda}$ )	COV
0.71	$C_1, C_3, C_4, C_6$ $C_2$ $C_5$ $C_7, C_8, C_9$ $B_1, B_3$ $B_2, B_4$ $B_5, B_6$	410UB59 610UB101 310UB46 250UB37 530UB92 460UB82 360UB50	1.408	2.288	0.102
0.81	$C_1, C_3, C_4, C_6$ $C_2$ $C_5$ $C_7, C_8, C_9$ $B_1, B_3$ $B_2, B_4$ $B_5, B_6$	360UB56 610UB101 310UB46 250UB31 530UB82 410UB59 310UB46	1.227	2.154	0.102
0.91	$C_1, C_3, C_4, C_6$ $C_2$ $C_5$ $C_7, C_8, C_9$ $B_1, B_3$ $B_2, B_4$ $B_5, B_6$	360UB50 610UB101 310UB46 250UB31 530UB82 410UB59 310UB46	1.099	1.936	0.106
1.02	$C_1, C_3, C_4, C_6$ $C_2$ $C_5$ $C_7, C_8, C_9$ $B_1, B_3$ $B_2, B_4$ $B_5, B_6$	310UB46 610UB101 310UB46 250UB31 530UB82 410UB59 310UB46	0.993	1.752	0.102

Table E.41: System-based design of Frame 5 under gravity and wind loading,

$$W_n/(D_n + L_n)=0.05, \text{BFY-CFY}$$

$\varphi_s$	Members (see Figure 7.1)	Section	$\lambda_n$ (factored loads)	Mean ( $\bar{\lambda}$ )	COV
0.71	$C_1, C_4, C_5, C_8, C_9, C_{12}$ $C_2, C_3, C_6, C_7$ $C_{10}, C_{11}$ $B_1, B_3, B_4, B_6, B_7, B_9$ $B_2, B_5, B_8$	360UB56 310UB32 200UB29 460UB67 360UB50	1.414	2.863	0.140
0.81	$C_1, C_4, C_5, C_8, C_9, C_{12}$ $C_2, C_3, C_6, C_7$ $C_{10}, C_{11}$ $B_1, B_3, B_4, B_6, B_7, B_9$ $B_2, B_5, B_8$	360UB50 250UB37 200UB29 360UB56 360UB50	1.238	2.572	0.146
0.91	$C_1, C_4, C_5, C_8, C_9, C_{12}$ $C_2, C_3, C_6, C_7$ $C_{10}, C_{11}$ $B_1, B_3, B_4, B_6, B_7, B_9$ $B_2, B_5, B_8$	360UB50 250UB31 200UB29 360UB56 360UB50	1.094	2.339	0.149
0.98	$C_1, C_4, C_5, C_8, C_9, C_{12}$ $C_2, C_3, C_6, C_7$ $C_{10}, C_{11}$ $B_1, B_3, B_4, B_6, B_7, B_9$ $B_2, B_5, B_8$	310UB46 250UB37 200UB29 360UB50 310UB40	1.016	2.202	0.147

Table E.42: System-based design of Frame 5 under gravity and wind loading,  
 $W_n/(D_n + L_n)=0.10$ , BFY-CFY

$\varphi_s$	Members (see Figure 7.1)	Section	$\lambda_n$ (factored loads)	Mean ( $\bar{\lambda}$ )	COV
0.69	$C_1, C_4, C_5, C_8, C_9, C_{12}$ $C_2, C_3, C_6, C_7$ $C_{10}, C_{11}$ $B_1, B_3, B_4, B_6, B_7, B_9$ $B_2, B_5, B_8$	460UB74 360UB50 250UB31 460UB74 360UB56	1.450	2.691	0.116
0.82	$C_1, C_4, C_5, C_8, C_9, C_{12}$ $C_2, C_3, C_6, C_7$ $C_{10}, C_{11}$ $B_1, B_3, B_4, B_6, B_7, B_9$ $B_2, B_5, B_8$	460UB67 310UB46 250UB25 460UB74 360UB56	1.215	2.379	0.123
0.89	$C_1, C_4$ $C_5, C_8, C_9, C_{12}$ $C_2, C_3, C_6, C_7$ $C_{10}, C_{11}$ $B_1, B_3, B_4, B_6, B_7, B_9$ $B_2, B_5, B_8$	460UB67 360UB56 310UB40 250UB25 460UB82 360UB56	1.127	2.149	0.120
1.04	$C_1, C_4, C_5, C_8, C_9, C_{12}$ $C_2, C_3, C_6, C_7$ $C_{10}, C_{11}$ $B_1, B_3, B_4, B_6, B_7, B_9$ $B_2, B_5, B_8$	360UB50 360UB50 250UB25 460UB67 360UB50	0.961	1.935	0.128

Table E.43: System-based design of Frame 5 under gravity and wind loading,  
 $W_n/(D_n + L_n)=0.15$ , BFY-CFY

$\phi_s$	Members (see Figure 7.1)	Section	$\lambda_n$ (factored loads)	Mean ( $\bar{\lambda}$ )	COV
0.71	$C_1, C_4, C_5, C_8, C_9, C_{12}$ $C_2, C_3, C_6, C_7$ $C_{10}, C_{11}$ $B_1, B_3, B_4, B_6, B_7, B_9$ $B_2, B_5, B_8$	460UB82 460UB74 250UB37 460UB82 360UB56	1.399	2.533	0.112
0.81	$C_1, C_4, C_5, C_8, C_9, C_{12}$ $C_2, C_3, C_6, C_7$ $C_{10}, C_{11}$ $B_1, B_3, B_4, B_6, B_7, B_9$ $B_2, B_5, B_8$	460UB74 460UB67 250UB31 460UB74 360UB56	1.231	2.249	0.113
0.89	$C_1, C_4$ $C_5, C_8, C_9, C_{12}$ $C_2, C_3, C_6, C_7$ $C_{10}, C_{11}$ $B_1, B_3, B_4, B_6, B_7, B_9$ $B_2, B_5, B_8$	460UB67 360UB56 460UB67 250UB31 460UB67 360UB50	1.122	2.064	0.116
1.03	$C_1, C_4, C_5, C_8, C_9, C_{12}$ $C_2, C_3, C_6, C_7$ $C_{10}, C_{11}$ $B_1, B_3, B_4, B_6, B_7, B_9$ $B_2, B_5, B_8$	460UB74 360UB50 250UB31 460UB74 360UB56	0.967	1.849	0.118



Table E.44: System-based design of Frame 5 under gravity and wind loading,

$$W_n/(D_n + L_n)=0.25, \text{BFY-CFY}$$

$\varphi_s$	Members (see Figure 7.1)	Section	$\lambda_n$ (factored loads)	Mean ( $\bar{\lambda}$ )	COV
0.71	$C_1, C_4, C_5, C_8, C_9, C_{12}$ $C_2, C_3, C_6, C_7$ $C_{10}, C_{11}$ $B_1, B_3, B_4, B_6, B_7, B_9$ $B_2, B_5, B_8$	610UB101 610UB101 310UB46 530UB92 460UB67	1.401	2.400	0.105
0.81	$C_1, C_4, C_5, C_8, C_9, C_{12}$ $C_2, C_3, C_6, C_7$ $C_{10}, C_{11}$ $B_1, B_3, B_4, B_6, B_7, B_9$ $B_2, B_5, B_8$	610UB101 530UB82 310UB46 530UB92 460UB67	1.227	2.192	0.107
0.91	$C_1, C_4, C_5, C_8, C_9, C_{12}$ $C_2, C_3, C_6, C_7$ $C_{10}, C_{11}$ $B_1, B_3, B_4, B_6, B_7, B_9$ $B_2, B_5, B_8$	530UB82 530UB92 310UB46 530UB92 460UB67	1.104	1.976	0.109
1.01	$C_1, C_4, C_5, C_8, C_9, C_{12}$ $C_2, C_3, C_6, C_7$ $C_{10}, C_{11}$ $B_1, B_3, B_4, B_6, B_7, B_9$ $B_2, B_5, B_8$	530UB92 460UB74 310UB46 530UB92 460UB67	0.994	1.783	0.108

Table E.45: System-based design of Frame 6 under gravity and wind loading,

$$W_n/(D_n + L_n)=0.05, \text{BFY-CFY}$$

$\varphi_s$	Members (see Figure 7.1)	Section	$\lambda_n$ (factored loads)	Mean ( $\bar{\lambda}$ )	COV
0.70	$C_1, C_5, C_9, C_{11}, C_{12}$ $C_2, C_3, C_4, C_6, C_7, C_8, C_{10}$ $B_1, B_2, B_4, B_5, B_7$ $B_3, B_6, B_8$	200UB25 310UB40 360UB56 310UB40	1.431	2.804	0.123
0.80	$C_1$ to $C_{12}$ $B_1, B_2, B_4, B_5, B_7$ $B_3, B_6, B_8$	250UB37 360UB56 310UB40	1.258	2.521	0.128
0.87	$C_1$ to $C_{12}$ $B_1, B_2, B_4, B_5, B_7$ $B_3, B_6, B_8$	310UB32 360UB56 310UB40	1.153	2.363	0.140
1.06	$C_1$ to $C_{12}$ $B_1, B_2, B_4, B_5, B_7$ $B_3, B_6, B_8$	250UB31 360UB56 310UB40	0.943	1.982	0.154

Table E.46: System-based design of Frame 6 under gravity and wind loading,

$$W_n/(D_n + L_n)=0.10, \text{BFY-CFY}$$

$\varphi_s$	Members (see Figure 7.1)	Section	$\lambda_n$ (factored loads)	Mean ( $\bar{\lambda}$ )	COV
0.72	$C_1$ to $C_{12}$ $B_1, B_2, B_4, B_5, B_7$ $B_3, B_6, B_8$	360UB50 460UB67 360UB56	1.380	2.556	0.116
0.80	$C_1, C_5, C_9, C_{11}, C_{12}$ $C_2, C_3, C_4, C_6, C_7, C_8, C_{10}$ $B_1, B_2, B_4, B_5, B_7$ $B_3, B_6, B_8$	360UB44 360UB50 360UB56 310UB40	1.249	2.327	0.114
0.91	$C_1$ to $C_{12}$ $B_1, B_2, B_4, B_5, B_7$ $B_3, B_6, B_8$	360UB44 360UB56 310UB40	1.102	2.077	0.121
1.00	$C_1$ to $C_{12}$ $B_1, B_2, B_4, B_5, B_7$ $B_3, B_6, B_8$	310UB46 360UB56 310UB32	0.995	1.891	0.124

Table E.47: System-based design of Frame 6 under gravity and wind loading,

$$W_n/(D_n + L_n)=0.15, \text{BFY-CFY}$$

$\varphi_s$	Members (see Figure 7.1)	Section	$\lambda_n$ (factored loads)	Mean ( $\bar{\lambda}$ )	COV
0.68	$C_1$ to $C_{12}$ $B_1, B_2, B_4, B_5, B_7$ $B_3, B_6, B_8$	460UB67 460UB74 310UB46	1.471	2.628	0.119
0.80	$C_1$ to $C_{12}$ $B_1, B_2, B_4, B_5, B_7$ $B_3, B_6, B_8$	410UB59 460UB67 360UB50	1.245	2.254	0.110
0.88	$C_1, C_5, C_9, C_{11}, C_{12}$ $C_2, C_3, C_4, C_6, C_7, C_8, C_{10}$ $B_1, B_2, B_4, B_5, B_7$ $B_3, B_6, B_8$	360UB50 410UB59 460UB67 310UB40	1.139	2.062	0.113
0.98	$C_1$ to $C_{12}$ $B_1, B_2, B_4, B_5, B_7$ $B_3, B_6, B_8$	360UB56 460UB67 310UB40	1.021	1.866	0.112

Table E.48: System-based design of Frame 6 under gravity and wind loading,  
 $W_n/(D_n + L_n)=0.25$ , BFY-CFY

$\phi_s$	Members (see Figure 7.1)	Section	$\lambda_n$ (factored loads)	Mean ( $\bar{\lambda}$ )	COV
0.69	$C_1$ to $C_{12}$ $B_1, B_2, B_4, B_5, B_7$ $B_3, B_6, B_8$	530UB92 530UB82 460UB74	1.439	2.510	0.102
0.81	$C_1$ to $C_{12}$ $B_1, B_2, B_4, B_5, B_7$ $B_3, B_6, B_8$	530UB92 460UB74 410UB59	1.240	2.159	0.102
0.90	$C_1$ to $C_{12}$ $B_1, B_2, B_4, B_5, B_7$ $B_3, B_6, B_8$	460UB82 460UB74 410UB59	1.109	1.937	0.104
0.99	$C_1$ to $C_{12}$ $B_1, B_2, B_4, B_5, B_7$ $B_3, B_6, B_8$	460UB74 460UB74 360UB56	1.011	1.791	0.109

Table E.49: System-based design of Frame 7 under gravity and wind loading,

$$W_n/(D_n + L_n)=0.05, \text{BFY-CFY}$$

$\phi_s$	Members (see Figure 7.1)	Section	$\lambda_n$ (factored loads)	Mean ( $\bar{\lambda}$ )	COV
0.71	$C_1, C_4$ $C_2$ $C_3$ $C_5$ $C_6$ $B_1, B_4$ $B_2$ $B_3$	180UB16 310UB40 250UB37 200UB22 200UB18 250UB37 360UB50 200UB22	1.414	2.746	0.122
0.81	$C_1, C_4$ $C_2, C_3$ $C_5$ $C_6$ $B_1, B_4$ $B_2$ $B_3$	180UB16 250UB37 200UB22 200UB18 250UB37 360UB50 200UB22	1.236	2.386	0.126
0.91	$C_1, C_4$ $C_2$ $C_3$ $C_5$ $C_6$ $B_1, B_4$ $B_2$ $B_3$	180UB16 250UB37 250UB31 200UB22 200UB18 250UB37 360UB50 200UB22	1.097	2.161	0.123
1.03	$C_1, C_4$ $C_2, C_3$ $C_5$ $C_6$ $B_1, B_4$ $B_2$ $B_3$	180UB16 250UB31 200UB22 200UB18 250UB37 360UB50 200UB22	0.971	1.936	0.128

Table E.50: System-based design of Frame 7 under gravity and wind loading,  
 $W_n/(D_n + L_n)=0.10$ , BFY-CFY

$\varphi_s$	Members (see Figure 7.1)	Section	$\lambda_n$ (factored loads)	Mean ( $\bar{\lambda}$ )	COV
0.70	$C_1$ $C_2$ $C_3$ $C_4, C_6$ $C_5$ $B_1, B_4$ $B_2$ $B_3$	250UB25 360UB56 360UB50 200UB25 200UB29 310UB40 360UB56 200UB25	1.435	2.624	0.111
0.81	$C_1, C_5$ $C_2$ $C_3$ $C_4, C_6$ $B_1, B_4$ $B_2$ $B_3$	200UB29 360UB50 310UB46 200UB25 310UB40 360UB56 200UB25	1.227	2.259	0.111
0.90	$C_1, C_5$ $C_2, C_3$ $C_4, C_6$ $B_1, B_4$ $B_2$ $B_3$	200UB29 310UB46 200UB25 310UB40 360UB56 200UB25	1.112	2.040	0.114
1.00	$C_1, C_4, C_6$ $C_2$ $C_3$ $C_5$ $B_1, B_4$ $B_2$ $B_3$	200UB25 310UB46 310UB40 200UB29 310UB40 360UB56 200UB25	0.997	1.838	0.115

Table E.51: System-based design of Frame 7 under gravity and wind loading,  
 $W_n/(D_n + L_n)=0.15$ , BFY-CFY

$\varphi_s$	Members (see Figure 7.1)	Section	$\lambda_n$ (factored loads)	Mean ( $\bar{\lambda}$ )	COV
0.71	$C_1, C_5$ $C_2$ $C_3$ $C_4, C_6$ $B_1$ $B_2$ $B_3$ $B_4$	250UB31 460UB67 410UB59 250UB25 360UB50 460UB67 200UB29 310UB46	1.408	2.512	0.108
0.81	$C_1$ $C_2, C_3$ $C_4, C_6$ $C_5$ $B_1, B_4$ $B_2$ $B_3$	250UB31 410UB59 200UB29 250UB25 310UB46 410UB59 200UB29	1.232	2.210	0.110
0.89	$C_1$ $C_2$ $C_3$ $C_4, C_6$ $C_5$ $B_1$ $B_2$ $B_3$ $B_4$	250UB25 410UB59 360UB56 200UB25 200UB29 310UB46 410UB59 200UB25 310UB40	1.120	1.988	0.107
1.02	$C_1$ $C_2$ $C_3$ $C_4, C_6$ $C_5$ $B_1$ $B_2$ $B_3$ $B_4$	250UB25 360UB56 360UB50 200UB25 200UB29 310UB46 410UB59 200UB25 310UB40	0.977	1.762	0.112

Table E.52: System-based design of Frame 7 under gravity and wind loading,  
 $W_n/(D_n + L_n)=0.25$ , BFY-CFY

$\varphi_s$	Members (see Figure 7.1)	Section	$\lambda_n$ (factored loads)	Mean ( $\bar{\lambda}$ )	COV
0.70	$C_1$ $C_2$ $C_3$ $C_4, C_6$ $C_5$ $B_1$ $B_2$ $B_3$ $B_4$	360UB50 530UB92 460UB82 250UB37 310UB40 460UB67 460UB82 360UB56 410UB59	1.408	0.106	0.106
0.81	$C_1$ $C_2$ $C_3$ $C_4, C_6$ $C_5$ $B_1$ $B_2$ $B_3$ $B_4$	360UB50 460UB82 460UB74 250UB37 310UB40 460UB67 460UB82 360UB56 410UB59	1.241	0.106	0.106
0.92	$C_1$ $C_2$ $C_3$ $C_4, C_6$ $C_5$ $B_1$ $B_2$ $B_3$ $B_4$	310UB46 460UB74 460UB67 250UB31 360UB50 460UB67 460UB82 360UB56 410UB59	1.083	0.107	0.107
1.00	$C_1$ $C_2$ $C_3$ $C_4, C_6$ $C_5$ $B_1$ $B_2$ $B_3$ $B_4$	310UB46 460UB67 460UB67 250UB31 250UB37 460UB74 530UB92 410UB59 460UB67	1.001	0.107	0.107

Table E.53: System-based design of Frame 8 under gravity and wind loading,

$$W_n/(D_n + L_n)=0.05, \text{BFY-CFY}$$

$\varphi_s$	Members (see Figure 7.1)	Section	$\lambda_n$ (factored loads)	Mean ( $\bar{\lambda}$ )	COV
0.69	$C_1, C_6$ $C_2, C_3$ $C_4$ $C_5$ $C_7, C_8$ $B_1, B_2$ $B_3, B_6$ $B_4, B_5$	180UB16 200UB29 200UB22 200UB18 180UB18 310UB40 200UB22 250UB25	1.460	2.744	0.118
0.81	$C_1, C_6$ $C_2$ $C_3$ $C_4, C_5$ $C_7, C_8$ $B_1, B_2$ $B_3, B_6$ $B_4, B_5$	180UB16 200UB29 200UB22 200UB18 180UB18 310UB40 200UB22 250UB25	1.235	2.364	0.116
0.90	$C_1, C_6$ $C_2$ $C_3$ $C_4$ $C_5$ $C_7, C_8$ $B_1, B_2$ $B_3, B_6$ $B_4, B_5$	180UB16 200UB25 200UB22 200UB18 180UB18 180UB18 310UB40 200UB22 250UB25	1.105	2.113	0.122
1.02	$C_1, C_6$ $C_2$ $C_3, C_4$ $C_5$ $C_7, C_8$ $B_1, B_2$ $B_3, B_6$ $B_4, B_5$	150UB18 200UB25 200UB18 180UB18 180UB16 310UB40 200UB22 250UB25	0.981	1.899	0.127



Table E.54: System-based design of Frame 8 under gravity and wind loading,  
 $W_n/(D_n + L_n)=0.10$ , BFY-CFY

$\varphi_s$	Members (see Figure 7.1)	Section	$\lambda_n$ (factored loads)	Mean ( $\bar{\lambda}$ )	COV
0.69	$C_1, C_6$ $C_2$ $C_3$ $C_4$ $C_5$ $C_7, C_8$ $B_1, B_2$ $B_3, B_6$ $B_4, B_5$	200UB22 310UB40 250UB37 250UB31 200UB29 200UB18 310UB46 200UB29 250UB25	1.452	2.639	0.109
0.81	$C_1, C_6$ $C_2, C_3$ $C_4$ $C_5$ $C_7, C_8$ $B_1, B_2$ $B_3, B_6$ $B_4, B_5$	200UB18 250UB37 250UB31 200UB29 200UB18 310UB46 200UB29 250UB25	1.236	2.289	0.109
0.90	$C_1, C_6$ $C_2$ $C_3$ $C_4$ $C_5$ $C_7, C_8$ $B_1, B_2$ $B_3, B_6$ $B_4, B_5$	200UB18 250UB37 250UB31 250UB25 200UB29 200UB18 310UB46 200UB29 250UB25	1.113	2.051	0.112
1.00	$C_1, C_6$ $C_2, C_3$ $C_4, C_5$ $C_7, C_8$ $B_1, B_2$ $B_3, B_6$ $B_4, B_5$	200UB18 250UB31 200UB29 200UB18 310UB46 200UB29 250UB25	1.004	1.880	0.118

Table E.55: System-based design of Frame 8 under gravity and wind loading,

$$W_n/(D_n + L_n)=0.15, \text{BFY-CFY}$$

$\varphi_s$	Members (see Figure 7.1)	Section	$\lambda_n$ (factored loads)	Mean ( $\bar{\lambda}$ )	COV
0.70	$C_1, C_6$ $C_2, C_3, C_4$ $C_5$ $C_7, C_8$ $B_1, B_2$ $B_3, B_6$ $B_4, B_5$	200UB29 310UB46 310UB40 250UB25 360UB50 250UB25 250UB37	1.426	2.549	0.110
0.82	$C_1, C_6$ $C_2$ $C_3, C_4$ $C_5$ $C_7, C_8$ $B_1, B_2$ $B_3, B_6$ $B_4, B_5$	200UB22 310UB46 310UB40 250UB25 200UB22 360UB50 250UB25 250UB37	1.217	2.190	0.110
0.92	$C_1, C_6$ $C_2, C_3$ $C_4$ $C_5$ $C_7, C_8$ $B_1, B_2$ $B_3, B_6$ $B_4, B_5$	200UB22 310UB40 250UB37 200UB29 200UB22 360UB50 250UB25 250UB37	1.089	1.978	0.112
1.03	$C_1, C_6$ $C_2$ $C_3$ $C_4$ $C_5$ $C_7, C_8$ $B_1, B_2$ $B_3, B_6$ $B_4, B_5$	200UB22 310UB40 250UB37 250UB31 200UB29 200UB18 360UB50 250UB25 250UB37	0.969	1.760	0.111

Table E.56: System-based design of Frame 8 under gravity and wind loading,  
 $W_n/(D_n + L_n)=0.25$ , BFY-CFY

$\varphi_s$	Members (see Figure 7.1)	Section	$\lambda_n$ (factored loads)	Mean ( $\bar{\lambda}$ )	COV
0.69	$C_1, C_6$ $C_2, C_3$ $C_4$ $C_5$ $C_7, C_8$ $B_1, B_2$ $B_3, B_6$ $B_4, B_5$	310UB40 410UB59 360UB50 310UB40 200UB29 460UB74 310UB46 410UB59	1.456	2.514	0.109
0.80	$C_1, C_6$ $C_2, C_3$ $C_4, C_5$ $C_7, C_8$ $B_1, B_2$ $B_3, B_6$ $B_4, B_5$	310UB40 360UB56 310UB40 250UB31 460UB74 310UB46 410UB59	1.246	2.151	0.109
0.89	$C_1, C_6$ $C_2, C_3$ $C_4, C_5$ $C_7, C_8$ $B_1, B_2$ $B_3, B_6$ $B_4, B_5$	250UB37 360UB56 250UB37 200UB29 460UB74 310UB46 410UB59	1.127	1.950	0.105
1.01	$C_1, C_6$ $C_2$ $C_3$ $C_4$ $C_5$ $C_7, C_8$ $B_1, B_2$ $B_3, B_6$ $B_4, B_5$	250UB25 360UB56 360UB50 250UB37 250UB31 200UB29 460UB74 310UB46 410UB59	0.984	1.736	0.107

Table E.57: System-based design of Frame 9 under gravity and wind loading,  
 $W_n/(D_n + L_n)=0.05$ , BFY-CFY

$\varphi_s$	Members (see Figure 7.1)	Section	$\lambda_n$ (factored loads)	Mean ( $\bar{\lambda}$ )	COV
0.71	$C_1, C_4, C_5, C_8, C_9$ $C_2, C_3, C_6, C_7$ $B_1$ $B_2, B_4$ $B_3, B_5$ $B_6$	310UB40 200UB22 360UB50 310UB32 360UB56 610UB125	1.410	2.679	0.133
0.82	$C_1, C_4, C_5, C_8, C_9$ $C_2$ $C_3, C_6, C_7$ $B_1$ $B_2, B_4$ $B_3, B_5$ $B_6$	250UB37 200UB29 200UB25 360UB50 310UB32 360UB56 610UB125	1.222	2.380	0.126
0.91	$C_1, C_4, C_5, C_8, C_9$ $C_2$ $C_3, C_6, C_7$ $B_1$ $B_2, B_4$ $B_3, B_5$ $B_6$	310UB32 200UB29 200UB22 360UB50 310UB32 360UB56 610UB125	1.101	2.272	0.135
1.00	$C_1, C_4, C_5, C_8, C_9$ $C_2$ $C_3, C_6, C_7$ $B_1$ $B_2, B_4$ $B_3, B_5$ $B_6$	250UB37 200UB25 200UB22 360UB50 310UB32 360UB56 610UB125	1.001	2.106	0.130

Table E.58: System-based design of Frame 9 under gravity and wind loading,  
 $W_n/(D_n + L_n)=0.10$ , BFY-CFY

$\varphi_s$	Members (see Figure 7.1)	Section	$\lambda_n$ (factored loads)	Mean ( $\bar{\lambda}$ )	COV
0.68	$C_1, C_4, C_5, C_8, C_9$ $C_2$ $C_3, C_6, C_7$ $B_1$ $B_2, B_4$ $B_3, B_5$ $B_6$	360UB56 310UB40 250UB37 460UB74 360UB56 460UB82 610UB125	1.464	2.573	0.108
0.82	$C_1, C_4, C_5, C_8, C_9$ $C_2, C_3, C_6, C_7$ $B_1$ $B_2, B_4$ $B_3, B_5$ $B_6$	360UB56 250UB31 460UB74 360UB56 460UB82 610UB125	1.223	2.244	0.111
0.92	$C_1, C_4, C_5, C_8, C_9$ $C_2, C_3, C_6, C_7$ $B_1$ $B_2, B_4$ $B_3, B_5$ $B_6$	360UB56 200UB29 360UB56 310UB40 460UB67 610UB125	1.085	2.074	0.118
1.01	$C_1, C_4, C_5, C_8, C_9$ $C_2$ $C_3, C_6, C_7$ $B_1$ $B_2, B_4$ $B_3, B_5$ $B_6$	360UB50 250UB31 200UB29 360UB56 310UB40 460UB67 610UB125	0.993	1.980	0.113

Table E.59: System-based design of Frame 9 under gravity and wind loading,

$$W_n/(D_n + L_n)=0.15, \text{BFY-CFY}$$

$\phi_s$	Members (see Figure 7.1)	Section	$\lambda_n$ (factored loads)	Mean ( $\bar{\lambda}$ )	COV
0.71	$C_1, C_4, C_5, C_8, C_9$ $C_2$ $C_3, C_6, C_7$ $B_1$ $B_2, B_4$ $B_3, B_5$ $B_6$	410UB59 360UB56 360UB50 460UB82 410UB59 530UB92 610UB125	1.409	2.411	0.106
0.81	$C_1, C_4, C_5, C_8, C_9$ $C_2$ $C_3, C_6, C_7$ $B_1$ $B_2, B_4$ $B_3, B_5$ $B_6$	410UB59 360UB50 310UB40 460UB82 410UB59 530UB92 610UB125	1.230	2.140	0.108
0.91	$C_1, C_4, C_5, C_8, C_9$ $C_2, C_3, C_6, C_7$ $B_1$ $B_2, B_4$ $B_3, B_5$ $B_6$	410UB59 310UB40 460UB74 360UB56 460UB82 610UB125	1.102	2.045	0.107
1.03	$C_1, C_4, C_5, C_8, C_9$ $C_2, C_3, C_6, C_7$ $B_1$ $B_2, B_4$ $B_3, B_5$ $B_6$	360UB56 310UB40 460UB74 360UB56 460UB82 610UB125	0.967	1.850	0.110

Table E.60: System-based design of Frame 9 under gravity and wind loading,  
 $W_n/(D_n + L_n)=0.25$ , BFY-CFY

$\varphi_s$	Members (see Figure 7.1)	Section	$\lambda_n$ (factored loads)	Mean ( $\bar{\lambda}$ )	COV
0.70	$C_1, C_4, C_5, C_8, C_9$ $C_2, C_3, C_6, C_7$ $B_1$ $B_2, B_4$ $B_3, B_5$ $B_6$	460UB82 460UB74 530UB92 460UB74 610UB113 610UB125	1.431	2.283	0.106
0.79	$C_1, C_4, C_5, C_8, C_9$ $C_2, C_3, C_6, C_7$ $B_1$ $B_2, B_4$ $B_3, B_5$ $B_6$	460UB74 460UB67 530UB92 460UB74 610UB113 610UB125	1.260	2.003	0.107
0.90	$C_1, C_4, C_5, C_8, C_9$ $C_2, C_3, C_6, C_7$ $B_1$ $B_2, B_4$ $B_3, B_5$ $B_6$	460UB74 410UB59 530UB92 460UB74 610UB113 610UB125	1.108	1.904	0.108
1.01	$C_1, C_4, C_5, C_8, C_9$ $C_2$ $C_3, C_6, C_7$ $B_1$ $B_2, B_4$ $B_3, B_5$ $B_6$	460UB67 410UB59 360UB56 530UB92 460UB74 610UB113 610UB125	0.991	1.713	0.107

### E.3. System-based design of hinged joint braced frames under gravity, LSM

Table E.61: System-based design of Frame 2 (braced, hinged joint) under gravity loading using LSM

Failure mode	Members (see Figure 7.1)	Section	$\lambda_n$ (factored loads)	Mean ( $\bar{\lambda}$ )	COV	$\lambda_n$ (unfactored loads)	$\bar{\lambda}/\lambda_n$ (unfactored load)
CFY	$C_1$ to $C_6$ $B_1, B_2$ $B_3$ Braces	150UB14 460UB82 410UB59 L100×100×10	1.241	1.740	0.096	1.674	1.039
CFY-BFY	$C_1$ to $C_6$ $B_1, B_2$ $B_3$ Braces	150UB14 410UB59 410UB59 L100×100×10	1.218	1.733	0.095	1.651	1.049
CFY-BPY	$C_1$ to $C_6$ $B_1, B_2$ $B_3$ Braces	150UB14 460UB82 360UB44 L100×100×10	1.235	1.739	0.101	1.676	1.037
CPY-BFY-CB	$C_1$ to $C_6$ $B_1, B_2$ $B_3$ Braces(first storey) Braces (top storey)	150UB14 460UB67 360UB56 L200×200×13 L100×100×10	1.537	2.161	0.073	2.075	1.041

Table E.62: System-based design of Frame 3 (braced, hinged joint) under gravity loading using LSM

Failure mode	Members (see Figure 7.1)	Section	$\lambda_n$ (factored loads)	Mean ( $\bar{\lambda}$ )	COV	$\lambda_n$ (unfactored loads)	$\bar{\lambda}/\lambda_n$ (unfactored load)
CFY-BPY	$C_1$ to $C_3$ $B_1$ $B_2$ Braces	150UB14 410UB59 610UB125 L100×100×10	1.193	1.688	0.105	1.604	1.053
CFY-BFY	$C_1$ to $C_3$ $B_1$ $B_2$ Braces	150UB14 360UB56 610UB113 L100×100×10	1.197	1.685	0.107	1.616	1.043
CPY-BFY-CB	$C_1$ to $C_3$ $B_1$ $B_2$ Braces	180UB18 410UB59 610UB125 L200×200×13	1.306	1.764	0.089	1.651	1.069



Table E.63: System-based design of Frame 4 (braced, hinged joint) under gravity loading using LSM

Failure mode	Members (see Figure 7.1)	Section	$\lambda_n$ (factored loads)	Mean ( $\bar{\lambda}$ )	COV	$\lambda_n$ (unfactored loads)	$\bar{\lambda}/\lambda_n$ (unfactored load)
CFY	$C_1, C_2, C_3$ $C_4$ to $C_9$ $B_1, B_2, B_3, B_4$ $B_5, B_6$ Braces	200UB29 180UB18 530UB82 360UB56 L100×100×10	1.231	1.729	0.098	1.662	1.041
CFY-BFY	$C_1, C_2, C_3$ $C_4$ to $C_9$ $B_1, B_2, B_3, B_4$ $B_5, B_6$ Braces	200UB29 150UB18 410UB59 310UB46 L100×100×10	1.208	1.711	0.102	1.631	1.049
CFY-BPY	$C_1, C_2, C_3$ $C_4$ to $C_9$ $B_1, B_2, B_3, B_4$ $B_5, B_6$ Braces	200UB29 150UB18 460UB74 360UB56 L100×100×10	1.211	1.720	0.097	1.633	1.054
CFY-BFY-CB	$C_1$ to $C_9$ $B_1, B_2, B_3, B_4$ $B_5, B_6$ Braces(first storey) Braces (top storey)	180UB18 410UB59 360UB56 L200×200×26 L200×200×13	1.219	1.765	0.081	1.644	1.074

Table E.64: System-based design of Frame 5 (braced, hinged joint) under gravity loading using LSM

Failure mode	Members (see Figure 7.1)	Section	$\lambda_n$ (factored loads)	Mean ( $\bar{\lambda}$ )	COV	$\lambda_n$ (unfactored loads)	$\bar{\lambda}/\lambda_n$ (unfactored load)
CFY	$C_1, C_4$ $C_2, C_3$ $C_5$ to $C_{12}$ $B_1, B_4, B_7$ $B_2, B_5, B_8$ $B_3, B_6, B_9$ Braces	200UB29 250UB31 200UB29 610UB125 460UB74 610UB125 L90×90×10	1.055	1.527	0.104	1.426	1.071
CFY-BFY	$C_1, C_4$ $C_2, C_3$ $C_5$ to $C_{12}$ $B_1, B_4, B_7$ $B_2, B_5, B_8$ $B_3, B_6, B_9$ Braces	250UB25 360UB56 200UB29 530UB82 360UB56 530UB82 L90×90×10	1.201	1.719	0.102	1.621	1.061
CFY-BPY	$C_1, C_4$ $C_2, C_3$ $C_5$ to $C_{12}$ $B_1, B_4, B_7$ $B_2, B_5, B_8$ $B_3, B_6, B_9$ Braces	250UB25 360UB56 200UB29 610UB101 410UB59 610UB101 L90×90×10	1.228	1.763	0.104	1.658	1.063
CFY-BPY-CB	$C_1, C_4$ $C_2, C_3$ $C_5$ to $C_{12}$ $B_1, B_4, B_7$ $B_2, B_5, B_8$ $B_3, B_6, B_9$ Braces(first storey) Braces (top storey)	200UB29 200UB18 200UB29 610UB101 460UB74 610UB101 L200×200×26 L150×150×16	1.255	1.725	0.090	1.695	1.018

Table E.65: System-based design of Frame 6 (braced, hinged joint) under gravity loading using LSM

Failure mode	Members (see Figure 7.1)	Section	$\lambda_n$ (factored loads)	Mean ( $\bar{\lambda}$ )	COV	$\lambda_n$ (unfactored loads)	$\bar{\lambda}/\lambda_n$ (unfactored load)
CFY	$C_1, C_4, C_5, C_8$ $C_9, C_{10}, C_{11}, C_{12}$ $C_2, C_3, C_6, C_7$ $B_1$ to $B_7$ $B_8$ Braces	180UB18 180UB18 200UB29 610UB101 360UB56 L100×100×10	1.159	1.585	0.100	1.564	1.013
CFY-BFY	$C_1, C_4, C_5, C_8$ $C_9, C_{10}, C_{11}, C_{12}$ $C_2, C_3, C_6, C_7$ $B_1$ to $B_7$ $B_8$ Braces	180UB18 180UB18 200UB29 410UB59 310UB46 L100×100×10	1.157	1.578	0.101	1.562	1.010
CFY-BPY	$C_1, C_4, C_5, C_8$ $C_9, C_{10}, C_{11}, C_{12}$ $C_2, C_3, C_6, C_7$ $B_1$ to $B_7$ $B_8$ Braces	180UB18 180UB18 200UB29 460UB74 310UB46 L100×100×10	1.148	1.581	0.100	1.550	1.020
CFY-BPY-CB	$C_1, C_4$ $C_2, C_3$ $C_5$ to $C_{12}$ $B_1$ to $B_7$ $B_8$ Braces	200UB18 200UB29 200UB18 460UB74 360UB56 L200×200×26	1.255	1.733	0.094	1.729	1.002

Table E.66: System-based design of Frame 7 (braced, hinged joint) under gravity loading using LSM

Failure mode	Members (see Figure 7.1)	Section	$\lambda_n$ (factored loads)	Mean ( $\bar{\lambda}$ )	COV	$\lambda_n$ (unfactored loads)	$\bar{\lambda}/\lambda_n$ (unfactored load)
CFY	$C_1$ to $C_6$ $B_1, B_4,$ $B_2$ $B_3$ Braces	150UB14 460UB74 610UB125 360UB56 L125×125×10	1.193	1.638	0.097	1.609	1.018
CFY-BFY	$C_1$ to $C_6$ $B_1, B_4,$ $B_2$ $B_3$ Braces	150UB14 410UB59 530UB82 310UB40 L125×125×10	1.190	1.672	0.092	1.604	1.042
CFY-BPY	$C_1$ to $C_6$ $B_1, B_4,$ $B_2$ $B_3$ Braces	150UB14 460UB67 610UB101 310UB40 L125×125×10	1.252	1.761	0.105	1.699	1.036
CPY-CB	$C_1$ to $C_6$ $B_1, B_4,$ $B_2$ $B_3$ Braces(first storey) Braces (top storey)	150UB18 530UB82 610UB125 360UB56 L200×200×26 L150×150×16	1.215	1.687	0.079	1.638	0.079

Table E.67: System-based design of Frame 8 (braced, hinged joint) under gravity loading  
using LSM

Failure mode	Members (see Figure 7.1)	Section	$\lambda_n$ (factored loads)	Mean ( $\bar{\lambda}$ )	COV	$\lambda_n$ (unfactored loads)	$\bar{\lambda}/\lambda_n$ (unfactored load)
CFY	$C_1$ to $C_8$ $B_1, B_4, B_5$ $B_2$ $B_3, B_6$ Braces	150UB14 460UB67 610UB125 360UB56 L125×125×10	1.214	1.811	0.101	1.639	1.105
CFY-BFY	$C_1$ to $C_8$ $B_1, B_4, B_5$ $B_2$ $B_3, B_6$ Braces	150UB14 310UB46 410UB59 250UB37 L125×125×10	1.208	1.804	0.106	1.635	1.103
CFY-BPY	$C_1$ to $C_6$ $B_1, B_4, B_5$ $B_2$ $B_3, B_6$ Braces	150UB14 310UB46 460UB74 250UB37 L100×100×10	1.213	1.735	0.099	1.638	1.059
CPY-CB	$C_1$ to $C_6$ $B_1, B_4, B_5$ $B_2$ $B_3, B_6$ Braces	180UB18 460UB67 610UB101 360UB56 L150×150×16	1.389	1.926	0.071	1.876	1.027

Table E.68: System-based design of Frame 9 (braced, hinged joint) under gravity loading  
using LSM

Failure mode	Members (see Figure 7.1)	Section	$\lambda_n$ (factored loads)	Mean ( $\bar{\lambda}$ )	COV	$\lambda_n$ (unfactored loads)	$\bar{\lambda}/\lambda_n$ (unfactored load)
CFY-BFY	$C_1, C_2, C_3$ $C_4$ $C_5, C_6, C_7$ $C_8, C_9$ $B_1, B_3, B_5$ $B_2, B_4$ $B_6$ Braces(first two storeys) Braces (top storey)	250UB25 150UB18 250UB25 150UB18 610UB101 460UB74 610UB125 L100×100×10 L200×200×13	1.192	1.619	0.095	1.610	1.005
CPY-BPY-CB	$C_1, C_2, C_3$ $C_4$ $C_5, C_6, C_7$ $C_8, C_9$ $B_1, B_3, B_5$ $B_2, B_4$ $B_6$ Braces(first two storeys) Braces (top storey)	250UB25 180UB22 250UB25 180UB22 610UB101 460UB74 610UB125 L200×200×26 L150×150×16	0.956	1.321	0.072	1.292	1.022

### E.4. System-based design of rigid joint braced frames under gravity, LSM

Table E.69: System-based design of Frame 2 (braced, rigid joint) under gravity loading using LSM

Failure mode	Members (see Figure 7.1)	Section	$\lambda_n$ (factored loads)	Mean ( $\bar{\lambda}$ )	COV	$\lambda_n$ (unfactored loads)	$\bar{\lambda}/\lambda_n$ (unfactored load)
CFY	$C_1$ to $C_6$ $B_1, B_2$ $B_3$ Braces	150UB14 460UB74 360UB50 L100×100×10	1.171	1.683	0.097	1.579	1.066
CPY-BFY	$C_1, C_2$ $C_3, C_4, C_5, C_6$ $B_1, B_2, B_3$ Braces	150UB18 150UB14 410UB59 L150×150×16	1.342	1.998	0.112	1.836	1.088
CFY-BPY	$C_1$ to $C_6$ $B_1, B_2$ $B_3$ Braces	150UB14 460UB74 310UB46 L100×100×10	1.171	1.688	0.096	1.578	1.070
CPY-BFY-CB	$C_1$ to $C_6$ $B_1, B_2, B_3$ Braces (first storey) Braces (top storey)	150UB14 360UB56 L150×150×16 L100×100×10	1.297	1.793	0.087	1.731	1.036

Table E.70: System-based design of Frame 3 (braced, rigid joint) under gravity loading using LSM

Failure mode	Members (see Figure 7.1)	Section	$\lambda_n$ (factored loads)	Mean ( $\bar{\lambda}$ )	COV	$\lambda_n$ (unfactored loads)	$\bar{\lambda}/\lambda_n$ (unfactored load)
CFY-BPY	$C_1$ to $C_3$ $B_1$ $B_2$ Braces	150UB14 310UB40 610UB125 L150×150×16	1.214	1.839	0.118	1.822	1.010
CFY-BFY	$C_1$ to $C_3$ $B_1$ $B_2$ Braces	150UB14 250UB37 610UB113 L150×150×16	1.161	1.688	0.102	1.677	1.010
CPY-BFY-CB	$C_1$ to $C_3$ $B_1$ $B_2$ Braces	150UB18 410UB59 530UB92 L200×200×13	1.108	1.575	0.093	1.496	1.052

Table E.71: System-based design of Frame 4 (braced, rigid joint) under gravity loading using LSM

Failure mode	Members (see Figure 7.1)	Section	$\lambda_n$ (factored loads)	Mean ( $\bar{\lambda}$ )	COV	$\lambda_n$ (unfactored loads)	$\bar{\lambda}/\lambda_n$ (unfactored load)
CFY	$C_1, C_2, C_3$ $C_4$ to $C_9$ $B_1, B_2, B_3, B_4$ $B_5, B_6$ Braces	200UB29 180UB18 460UB74 360UB50 L100×100×10	1.068	1.514	1.050	1.442	0.101
CFY-BFY	$C_1, C_2, C_3$ $C_4$ to $C_9$ $B_1, B_2, B_3, B_4$ $B_5, B_6$ Braces	200UB29 150UB18 310UB40 250UB31 L100×100×10	1.081	1.531	1.052	1.455	0.098
CFY-BPY	$C_1, C_2, C_3$ $C_4$ to $C_9$ $B_1, B_2, B_3, B_4$ $B_5, B_6$ Braces	200UB29 180UB18 360UB56 250UB37 L100×100×10	1.097	1.522	1.028	1.480	0.103
CFY-BFY-CB	$C_1$ to $C_9$ $B_1, B_2, B_3, B_4$ $B_5, B_6$ Braces (first storey) Braces (top storey)	180UB18 310UB46 250UB31 L200×200×26 L200×200×13	1.081	1.503	0.081	1.453	1.034

Table E.72: System-based design of Frame 5 (braced, rigid joint) under gravity loading  
using LSM

Failure mode	Members (see Figure 7.1)	Section	$\lambda_n$ (factored loads)	Mean ( $\bar{\lambda}$ )	COV	$\lambda_n$ (unfactored loads)	$\bar{\lambda}/\lambda_n$ (unfactored load)
CFY	$C_1, C_4$ $C_2, C_3$ $C_5$ to $C_{12}$ $B_1, B_4, B_7$ $B_2, B_5, B_8$ $B_3, B_6, B_9$ Braces	250UB31 250UB37 250UB31 610UB101 360UB56 610UB101 L100×100×10	1.165	1.678	0.106	1.591	1.055
CFY- BFY	$C_1, C_4$ $C_2, C_3$ $C_5$ to $C_{12}$ $B_1, B_4, B_7$ $B_2, B_5, B_8$ $B_3, B_6, B_9$ Braces	250UB25 310UB46 200UB29 460UB67 310UB32 460UB67 L90×90×10	1.135	1.603	0.096	1.515	1.058
CFY- BPY	$C_1, C_4$ $C_2, C_3$ $C_5$ to $C_{12}$ $B_1, B_4, B_7$ $B_2, B_5, B_8$ $B_3, B_6, B_9$ Braces	250UB25 360UB56 200UB29 460UB74 310UB46 460UB74 L90×90×10	1.196	1.712	0.099	1.613	1.061
CPY- BPY-CB	$C_1$ to $C_{12}$ $B_1, B_4, B_7$ $B_2, B_5, B_8$ $B_3, B_6, B_9$ Braces(first storey) Braces (top storey)	200UB29 460UB74 410UB59 460UB74 L200×200×26 L150×150×16	1.192	1.711	0.099	1.609	1.063



Table E.73: System-based design of Frame 6 (braced, rigid joint) under gravity loading using LSM

Failure mode	Members (see Figure 7.1)	Section	$\lambda_n$ (factored loads)	Mean ( $\bar{\lambda}$ )	COV	$\lambda_n$ (unfactored loads)	$\bar{\lambda}/\lambda_n$ (unfactored load)
CFY	$C_1, C_4, C_5, C_8$ $C_9, C_{10}, C_{11}, C_{12}$ $C_2, C_3, C_6, C_7$ $B_1$ to $B_7$ $B_8$ Braces	180UB18 180UB18 200UB29 460UB67 310UB46 L100×100×10	1.074	1.544	0.099	1.450	1.065
CFY-BFY	$C_1, C_4, C_5, C_8$ $C_9, C_{10}, C_{11}, C_{12}$ $C_2, C_3, C_6, C_7$ $B_1$ to $B_7$ $B_8$ Braces	180UB18 180UB18 200UB29 310UB46 250UB31 L100×100×10	1.071	1.531	0.103	1.453	1.054
CFY-BPY	$C_1, C_4, C_5, C_8$ $C_9, C_{10}, C_{11}, C_{12}$ $C_2, C_3, C_6, C_7$ $B_1$ to $B_7$ $B_8$ Braces	180UB18 180UB18 200UB29 410UB59 310UB32 L100×100×10	1.077	1.545	0.106	1.454	1.063
CFY-CB	$C_1, C_4, C_5, C_8$ $C_9, C_{10}, C_{11}, C_{12}$ $C_2, C_3, C_6, C_7$ $B_1$ to $B_7$ $B_8$ Braces	200UB18 200UB18 200UB29 460UB67 360UB56 L200×200×26	1.264	1.744	0.099	1.708	1.025

Table E.74: System-based design of Frame 7 (braced, rigid joint) under gravity loading using LSM

Failure mode	Members (see Figure 7.1)	Section	$\lambda_n$ (factored loads)	Mean ( $\bar{\lambda}$ )	COV	$\lambda_n$ (unfactored loads)	$\bar{\lambda}/\lambda_n$ (unfactored load)
CFY	$C_1, C_2, C_3$ $C_4, C_5, C_6$ $B_1$ $B_2$ $B_3$ $B_4$ Braces	150UB18 150UB14 410UB59 610UB125 310UB40 460UB67 L125×125×10	1.217	1.662	0.093	1.647	1.010
CPY-BFY-CB	$C_1$ to $C_6$ $B_1, B_4,$ $B_2$ $B_3$ Braces	150UB18 360UB56 460UB74 310UB32 L150×150×16	1.303	1.835	0.091	1.760	1.042
CPY-BPY-CB	$C_1$ to $C_6$ $B_1, B_4,$ $B_2$ $B_3$ Braces	150UB14 410UB59 460UB67 310UB46 L150×150×16	1.076	1.550	0.085	1.452	1.068

Table E.75: System-based design of Frame 8 (braced, rigid joint) under gravity loading using LSM

Failure mode	Members (see Figure 7.1)	Section	$\lambda_n$ (factored loads)	Mean ( $\bar{\lambda}$ )	COV	$\lambda_n$ (unfactored loads)	$\bar{\lambda}/\lambda_n$ (unfactored load)
CFY	$C_1$ to $C_8$ $B_1, B_4, B_5$ $B_2$ $B_3, B_6$ Braces	150UB14 360UB56 460UB74 310UB40 L100×100×10	1.060	1.520	0.102	1.432	1.061
CPY-BFY	$C_1$ to $C_8$ $B_1, B_4, B_5$ $B_2$ $B_3, B_6$ Braces	150UB14 250UB25 310UB46 200UB29 L150×150×16	1.061	1.689	0.099	1.593	1.060
CFY-BPY	$C_1, C_4, C_5, C_6, C_7, C_8$ $C_2, C_3$ $B_1, B_4, B_5$ $B_2$ $B_3, B_6$ Braces	150UB14 150UB18 310UB32 410UB59 250UB25 L100×100×10	1.341	1.928	0.103	1.813	1.063
CPY-CB	$C_1$ to $C_8$ $B_1, B_4, B_5$ $B_2$ $B_3, B_6$ Braces (first storey) Braces (top storey)	150UB14 410UB59 460UB67 310UB40 L200×200×26 L150×150×16	1.404	1.941	0.067	1.927	1.007

Table E.76: System-based design of Frame 9 (braced, rigid joint) under gravity loading  
using LSM

Failure mode	Members (see Figure 7.1)	Section	$\lambda_n$ (factored loads)	Mean ( $\bar{\lambda}$ )	COV	$\lambda_n$ (unfactored loads)	$\bar{\lambda}/\lambda_n$ (unfactored load)
CFY- BFY	$C_1, C_2, C_3$ $C_4$ $C_5, C_6, C_7$ $C_8, C_9$ $B_1, B_3, B_5$ $B_2, B_4$ $B_6$ Braces(first two storeys) Braces (top storey)	250UB25 150UB18 250UB25 150UB18 460UB74 360UB56 610UB125 L100×100×10 L200×200×26	1.289	1.764	0.095	1.736	1.016
CFY- BPY- CB	$C_1, C_2, C_3$ $C_4$ $C_5, C_6, C_7$ $C_8, C_9$ $B_1, B_3, B_5$ $B_2, B_4$ $B_6$ Braces(first & third storeys) Braces (top storey)	250UB25 180UB22 250UB25 180UB22 530UB82 460UB67 610UB125 L200×200×26 L200×200×26	1.165	1.596	0.077	1.572	1.015

**E.5. Selected histograms of ultimate load factors, sway frames under gravity loads**

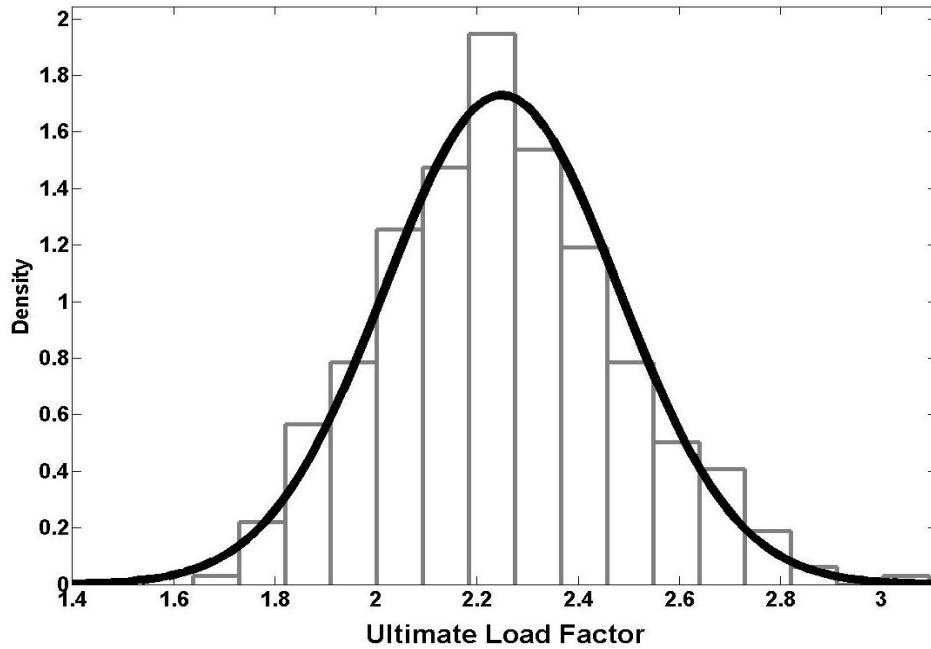


Figure E.1. Histogram of ultimate load factor, Frame 1, BFY-CPY,  $\varphi_s=0.64$

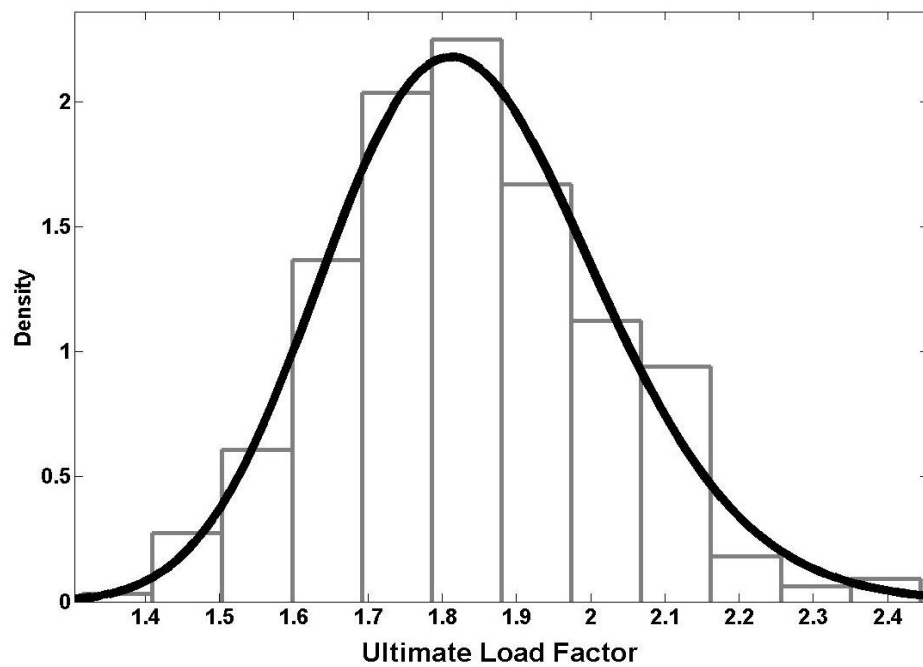


Figure E.2. Histogram of ultimate load factor, Frame 2, BFY-CPY,  $\varphi_s=0.78$

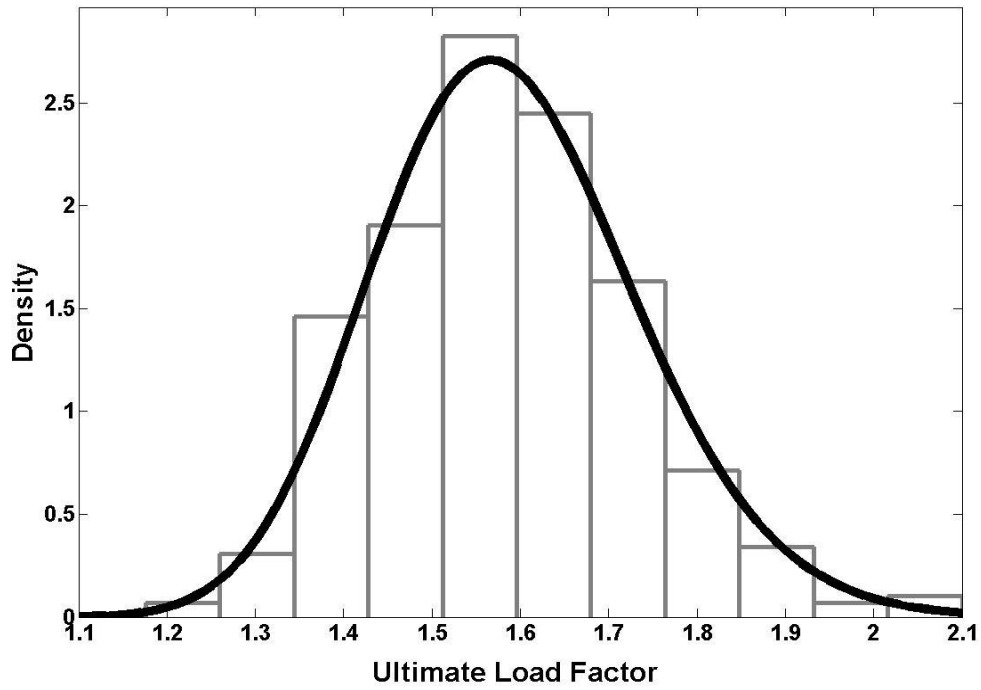


Figure E.3. Histogram of ultimate load factor, Frame 2, Instability,  $\varphi_s=0.90$

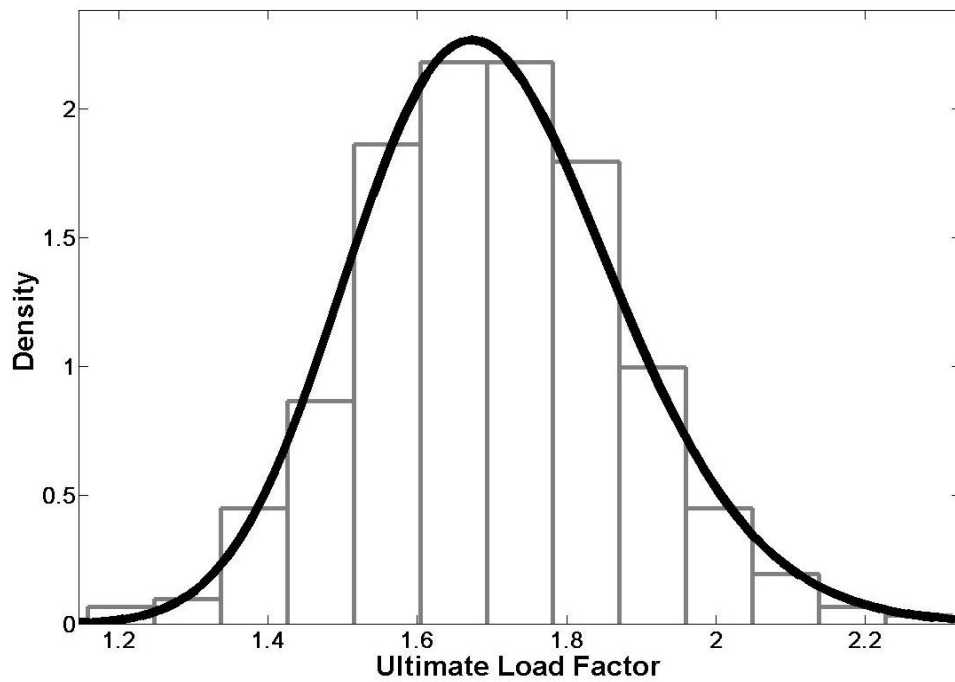


Figure E.4. Histogram of ultimate load factor, Frame 3, BPY-CFY,  $\varphi_s=0.83$

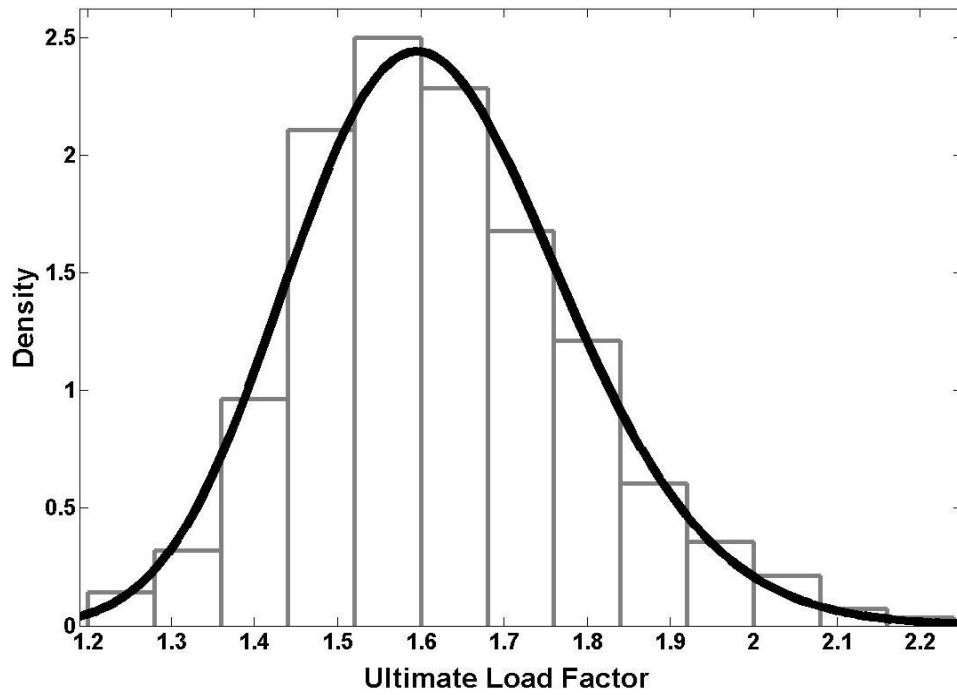


Figure E.5. Histogram of ultimate load factor, Frame 4, CFY,  $\varphi_s=0.89$

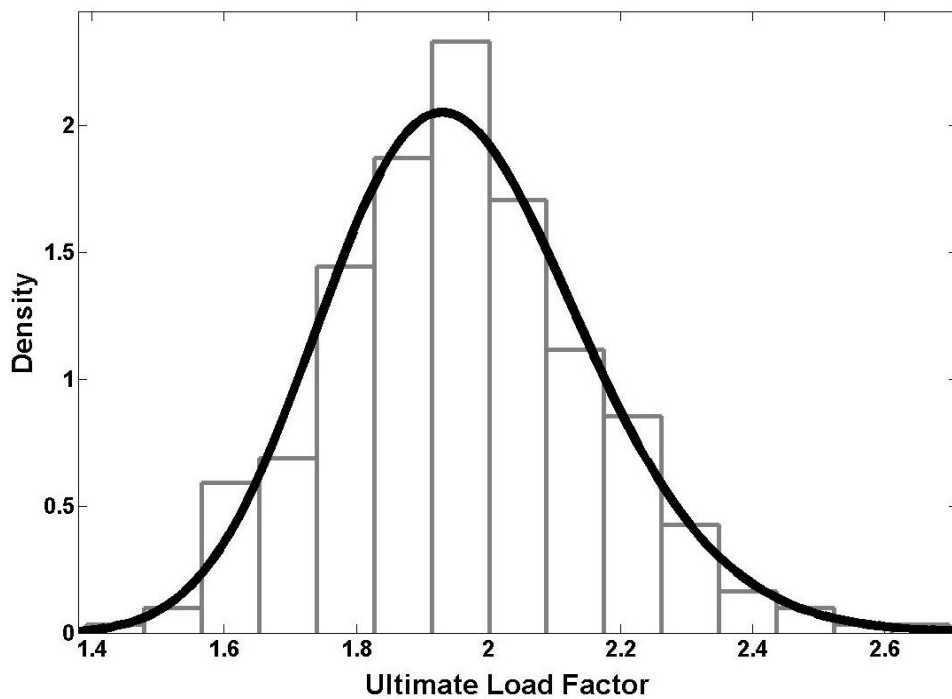


Figure E.6. Histogram of ultimate load factor, Frame 5, BFY-CPY,  $\varphi_s=0.74$

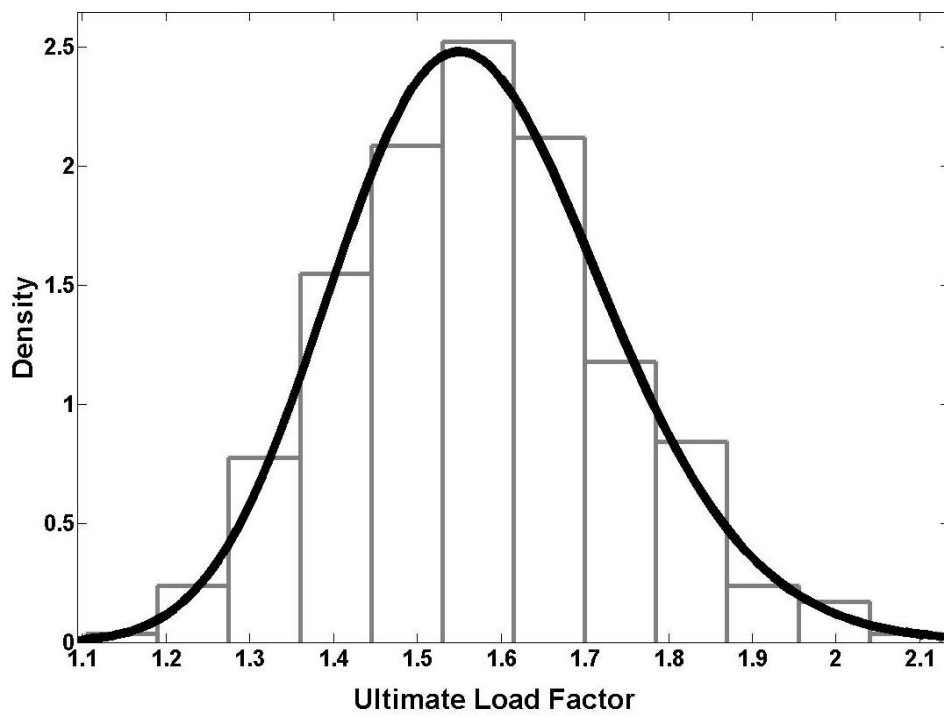


Figure E.7. Histogram of ultimate load factor, Frame 6, BPY-CFY,  $\varphi_s=0.93$

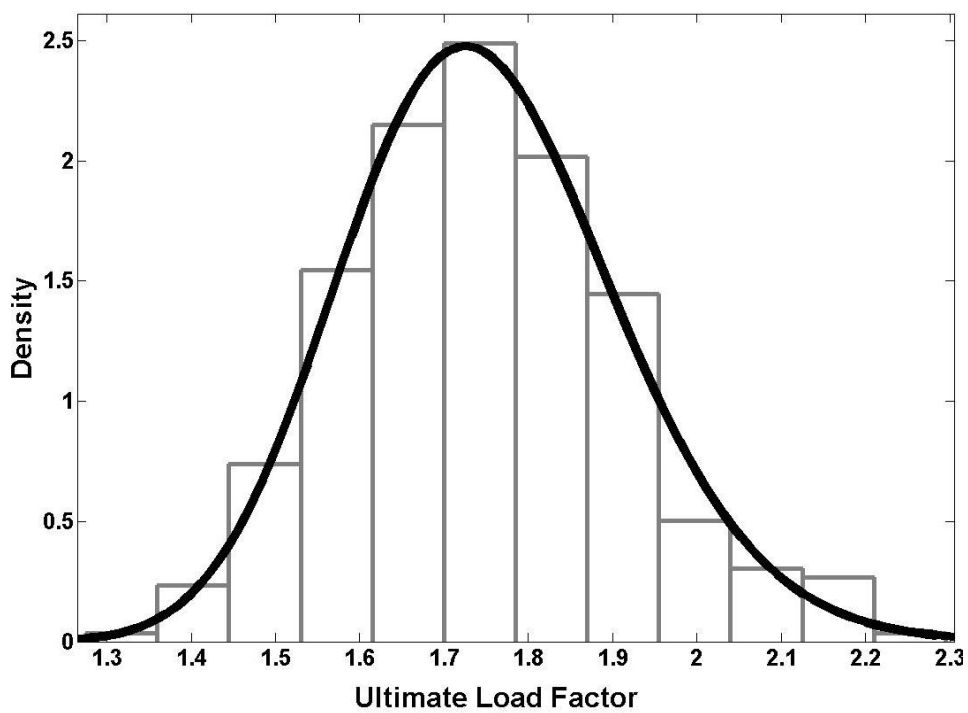


Figure E.8. Histogram of ultimate load factor, Frame 7, BPY-CPY,  $\varphi_s=0.79$

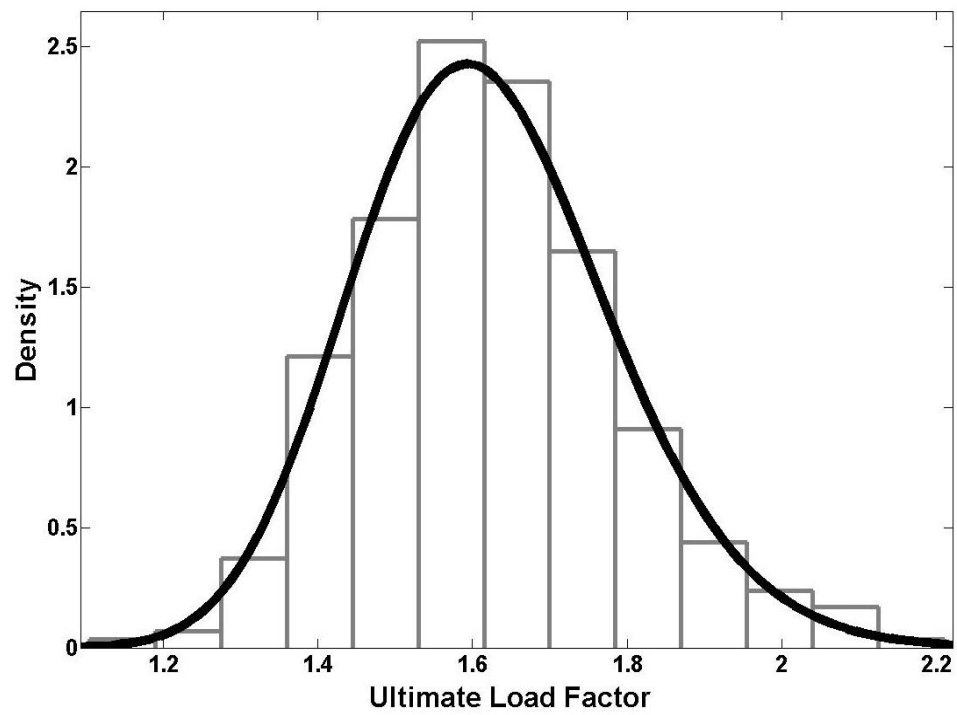


Figure E.9. Histogram of ultimate load factor, Frame 8, BPY-CFY,  $\varphi_s=0.88$

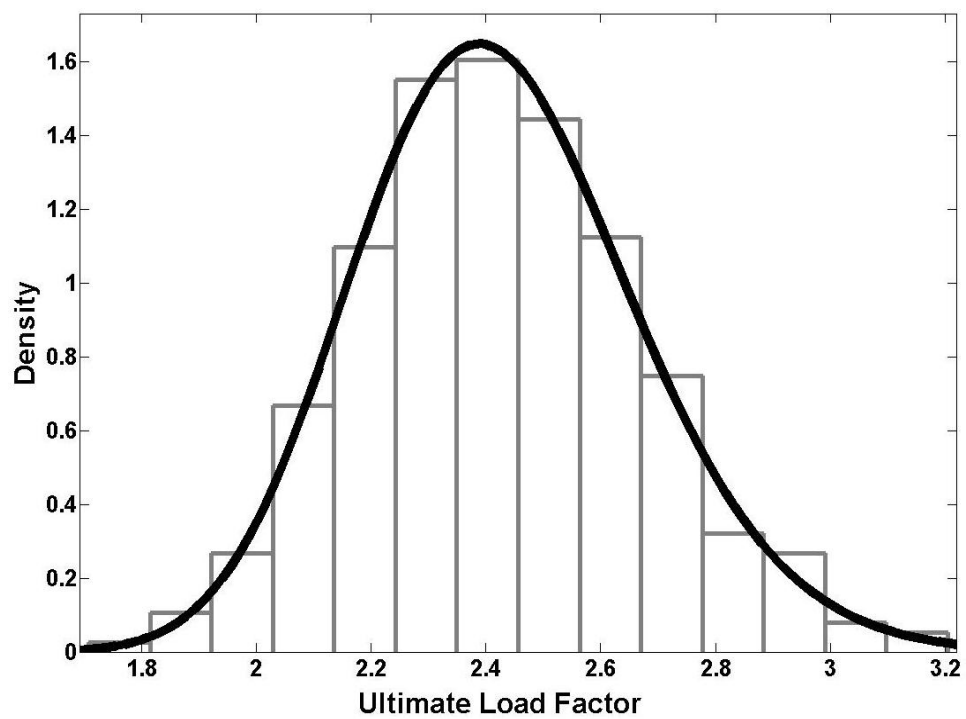


Figure E.10. Histogram of ultimate load factor, Frame 9, BPY-CPY,  $\varphi_s=0.60$



### E.6. Selected histograms of ultimate load factors, sway frames under gravity plus wind loads

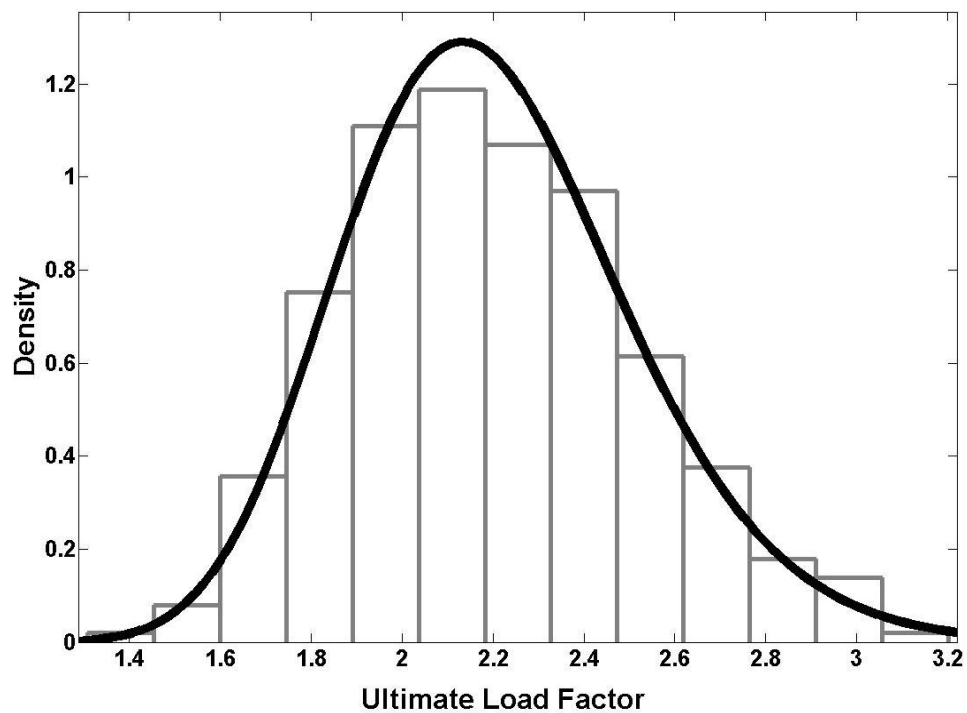


Figure E.11. Histogram of ultimate load factor, Frame 1,  $W_n/(D_n + L_n)=0.05$ ,  $\varphi_s=0.90$

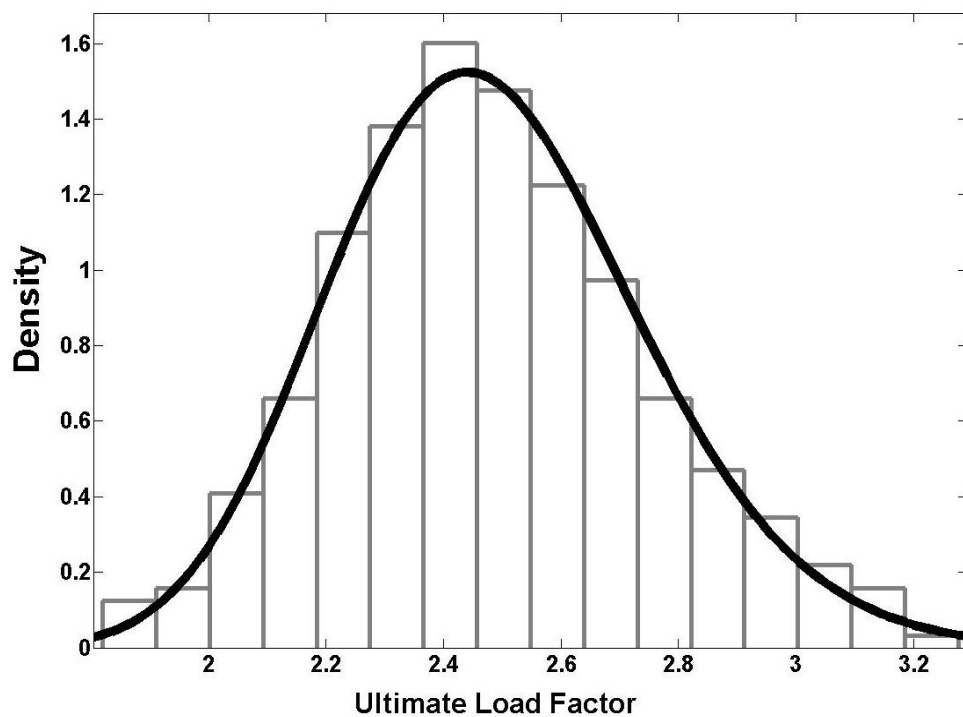


Figure E.12. Histogram of ultimate load factor, Frame 1,  $W_n/(D_n + L_n)=0.25$ ,  $\varphi_s=0.71$

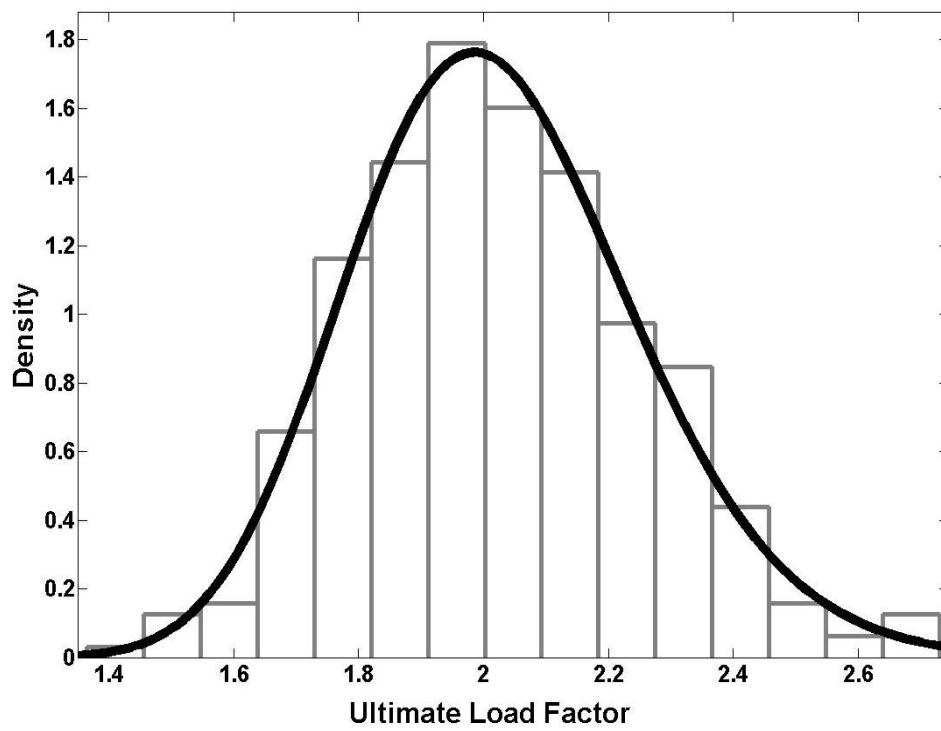


Figure E.13. Histogram of ultimate load factor, Frame 3,  $W_n/(D_n + L_n)=0.10$ ,  $\varphi_s=0.92$

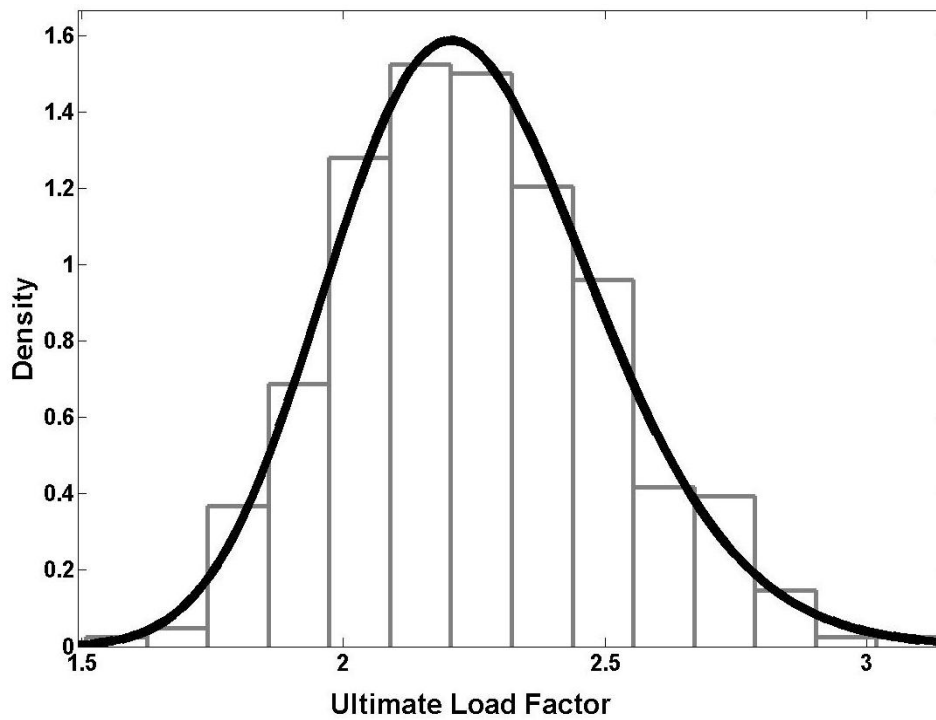


Figure E.14. Histogram of ultimate load factor, Frame 5,  $W_n/(D_n + L_n)=0.15$ ,  $\varphi_s=0.81$

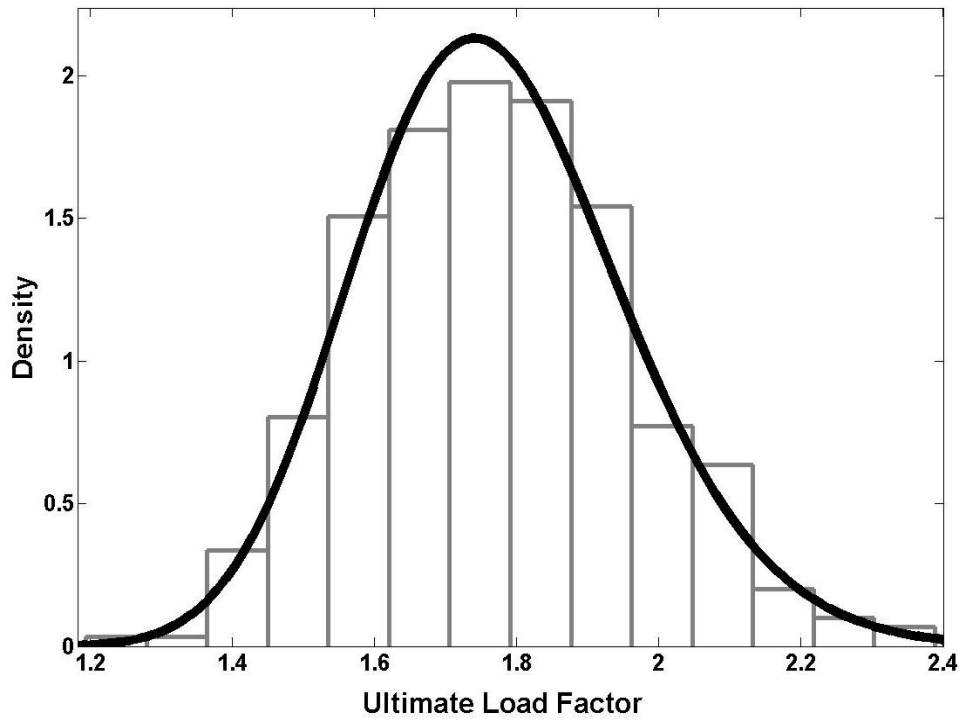


Figure E.15. Histogram of ultimate load factor, Frame 7,  $W_n/(D_n + L_n)=0.25$ ,  $\phi_s=1.00$

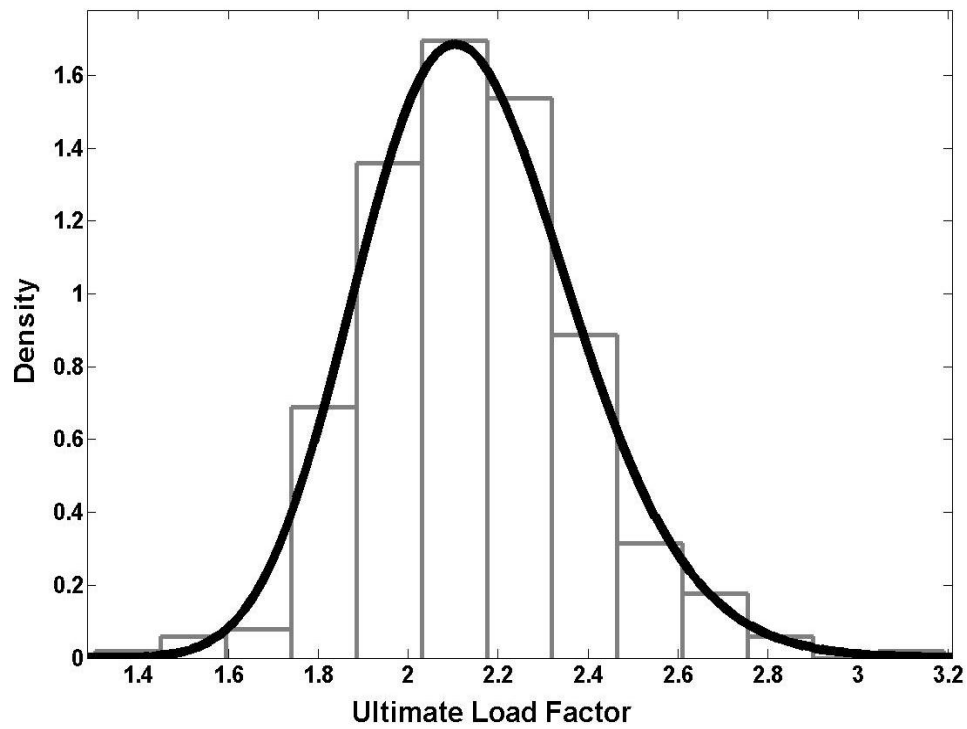


Figure E.16. Histogram of ultimate load factor, Frame 9,  $W_n/(D_n + L_n)=0.10$ ,  $\phi_s=0.82$

**E.7. Selected histograms of ultimate load factors, hinged joint braced frames under gravity loads**

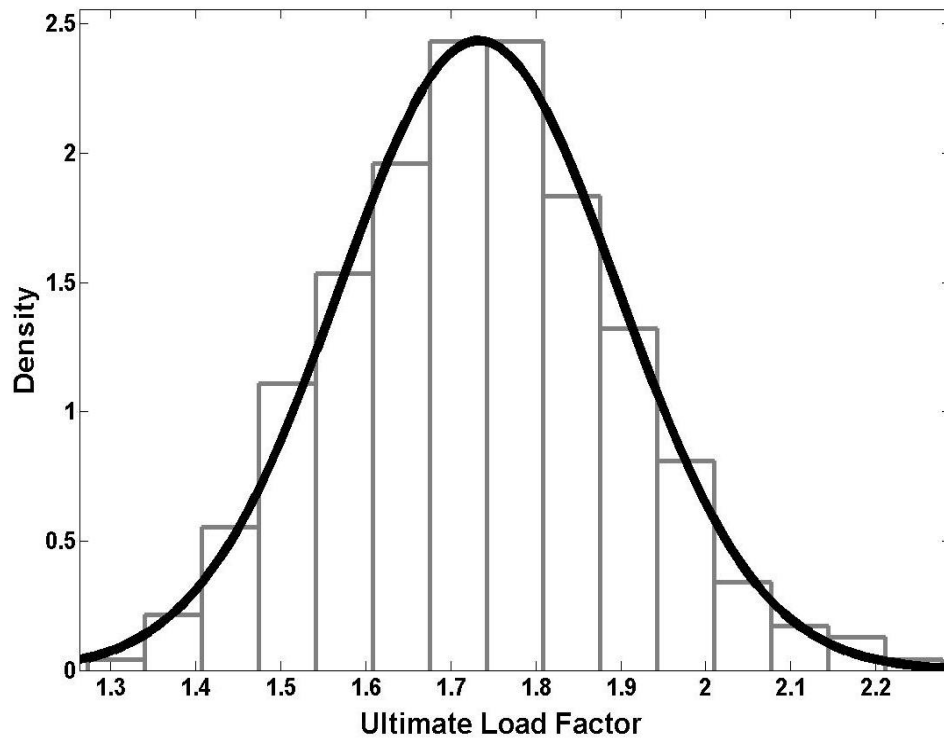


Figure E.17. Histogram of ultimate load factor, Frame 2, BFY-CFY,  $\varphi_s=0.82$

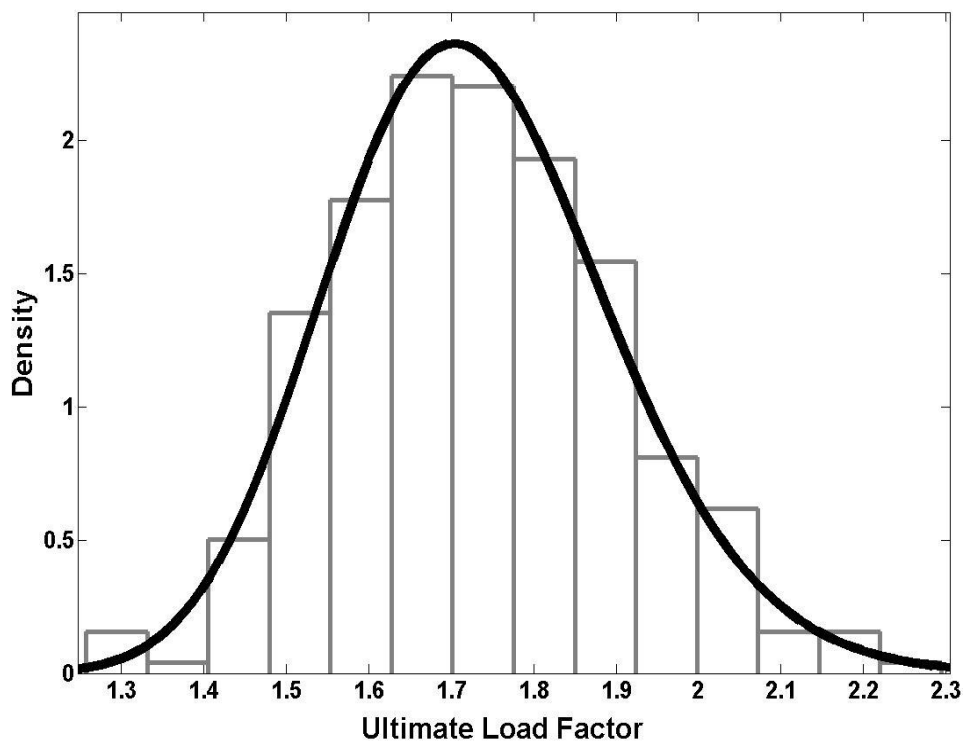


Figure E.18. Histogram of ultimate load factor, Frame 4, CFY,  $\varphi_s=0.81$

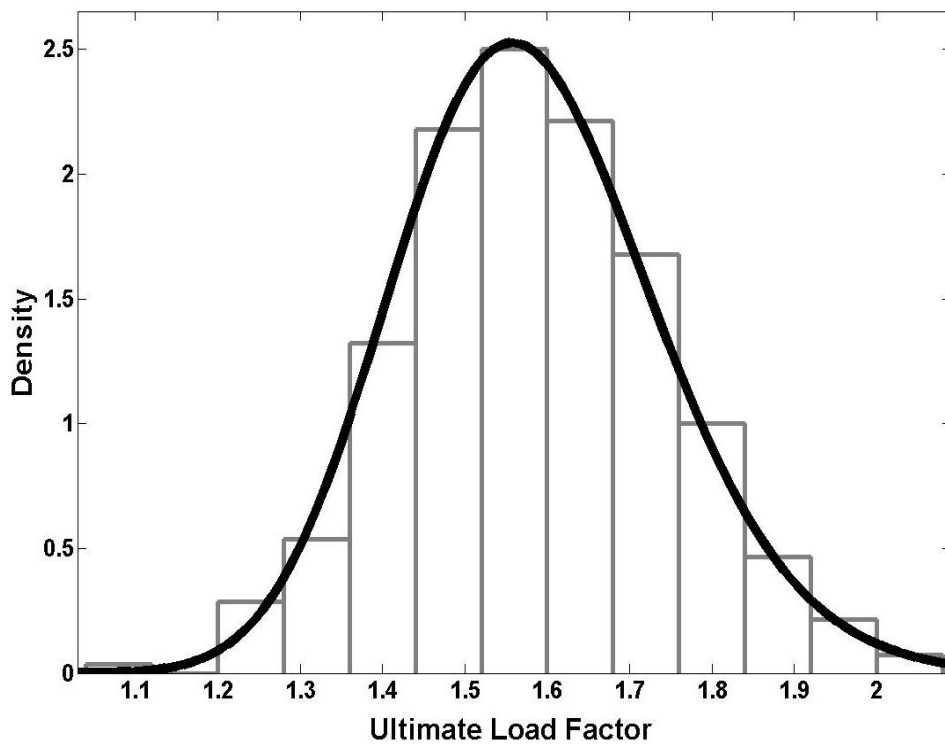


Figure E.19. Histogram of ultimate load factor, Frame 6, CFY-BPY,  $\varphi_s=0.87$

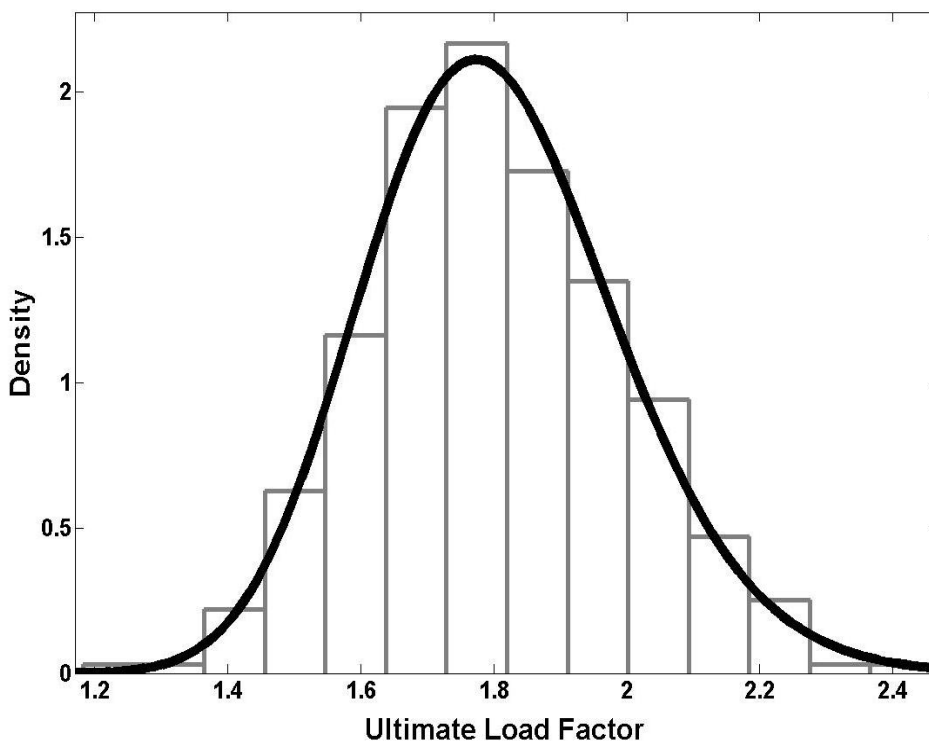


Figure E.20. Histogram of ultimate load factor, Frame 8, CFY-BFY,  $\varphi_s=0.83$

**E.8. Selected histograms of ultimate load factors, rigid joint braced frames under gravity loads**

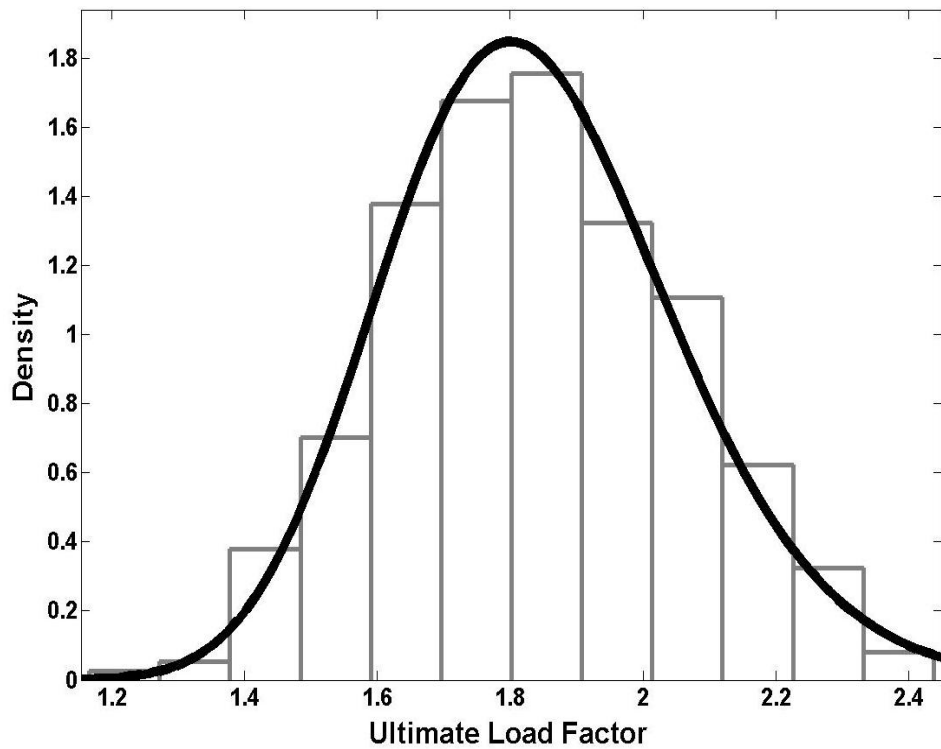


Figure E.21. Histogram of ultimate load factor, Frame 3, CFY-BPY,  $\varphi_s=0.82$

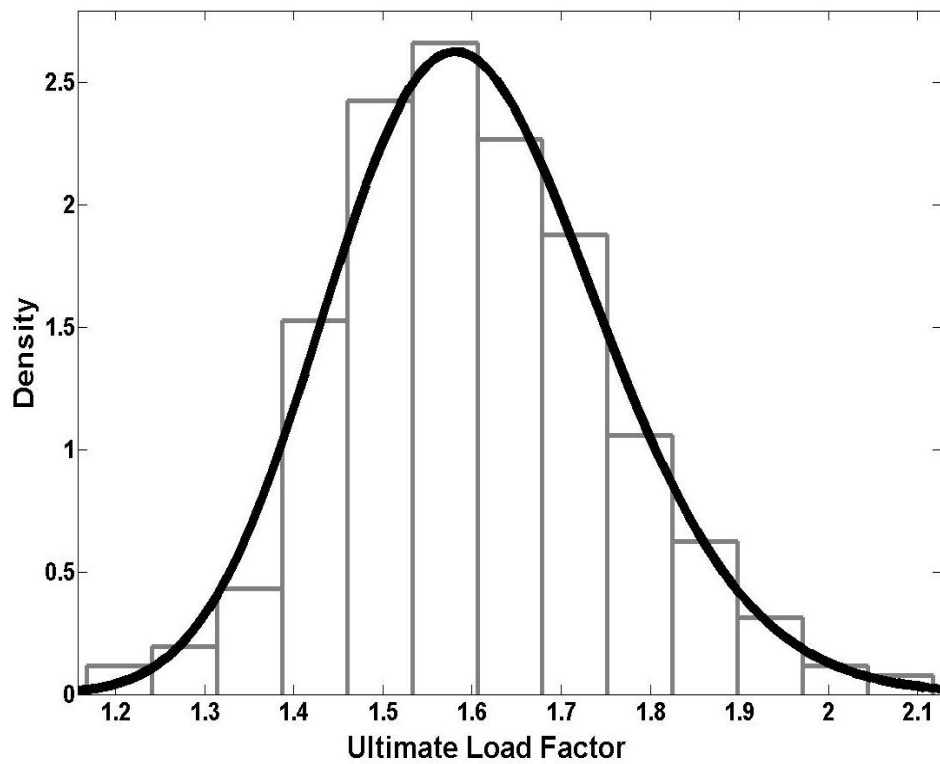


Figure E.22. Histogram of ultimate load factor, Frame 5, CFY-BFY,  $\varphi_s=0.88$

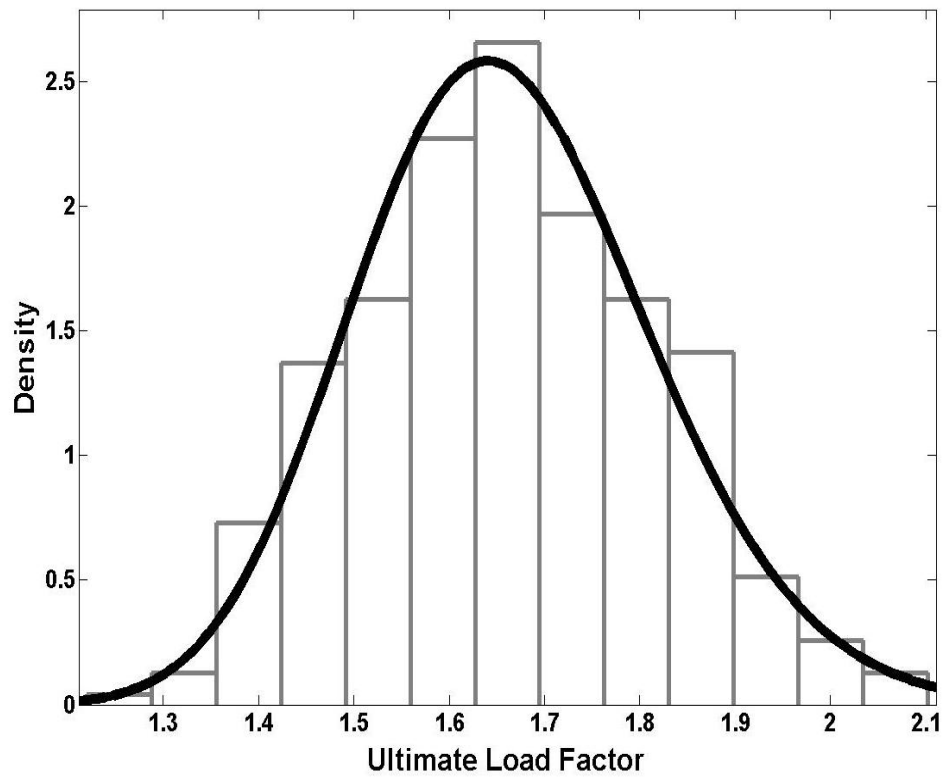


Figure E.23. Histogram of ultimate load factor, Frame 7, CFY,  $\varphi_s=0.82$

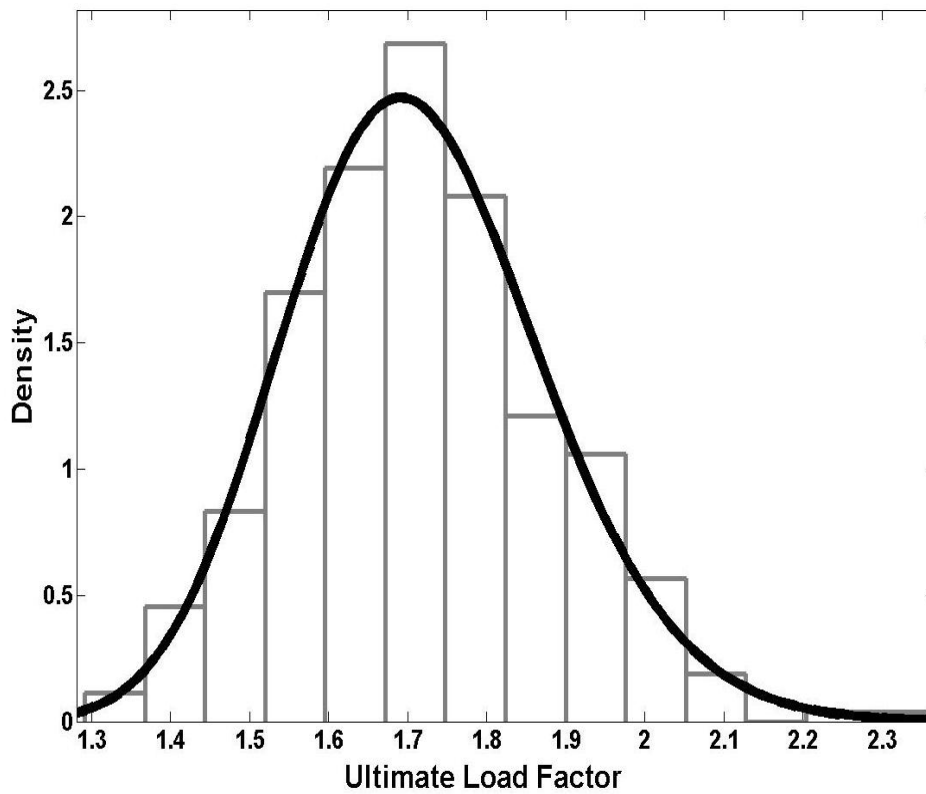


Figure E.24. Histogram of ultimate load factor, Frame 9, CFY-BFY,  $\varphi_s=0.78$

**E.9. Selected  $\beta - \varphi_s$  plots, sway frames under gravity loads**

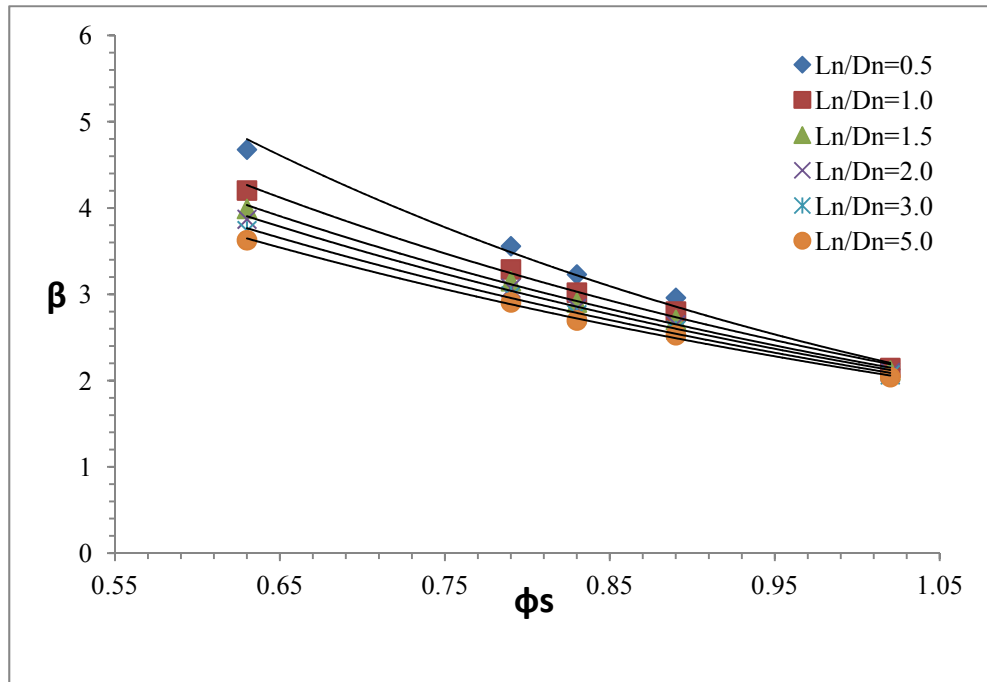


Figure E.25.  $\beta$  vs.  $\varphi_s$  curve, Frame 3, BPY-CFY

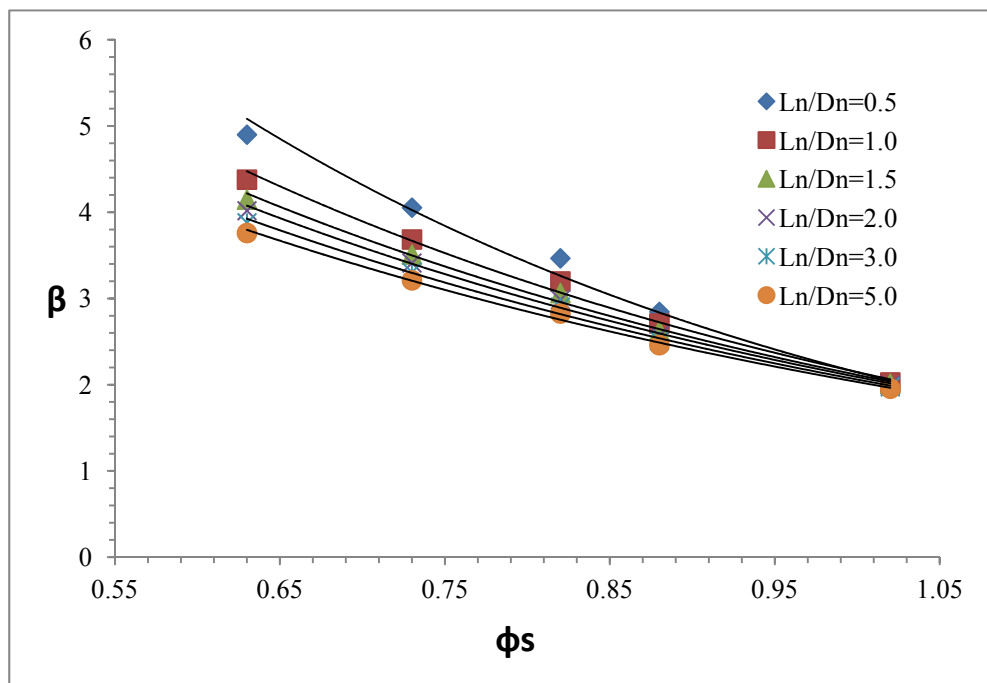


Figure E.26.  $\beta$  vs.  $\varphi_s$  curve, Frame 6, BFY-CFY



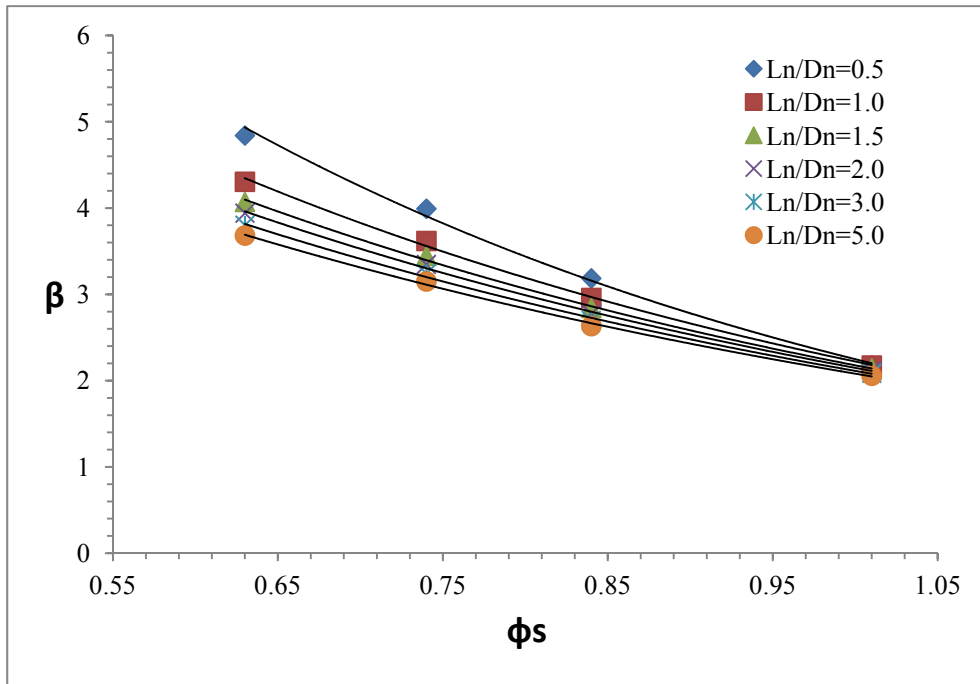


Figure E.27.  $\beta$  vs.  $\phi_s$  curve, Frame 7, CFY

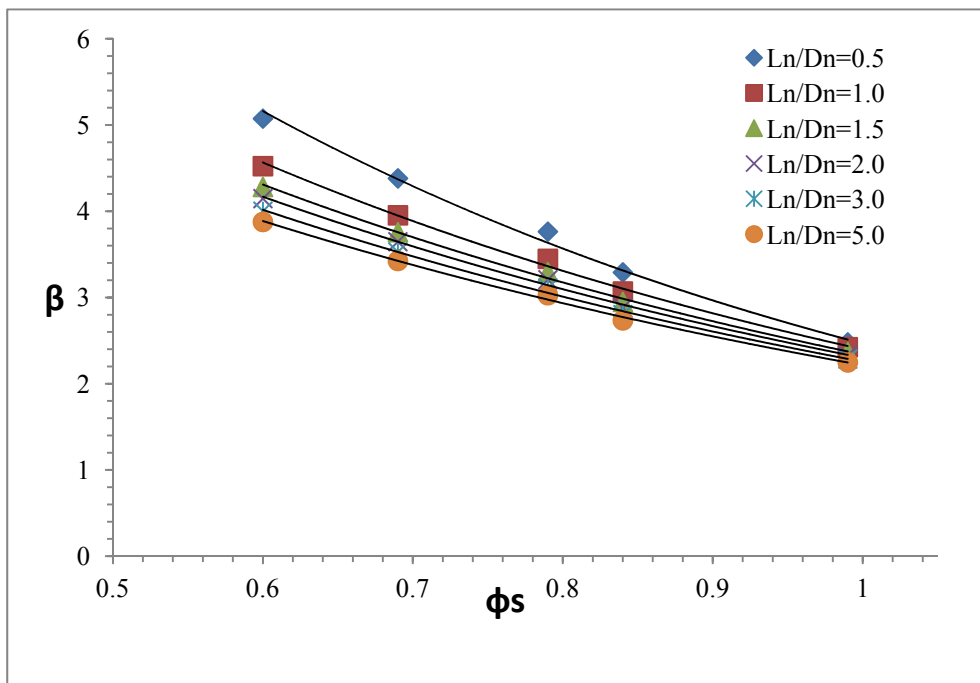


Figure E.28.  $\beta$  vs.  $\phi_s$  curve, Frame 9, BFY-CPY

**E.10. Selected  $\beta - \varphi_s$  plots, sway frames under gravity plus wind loads**

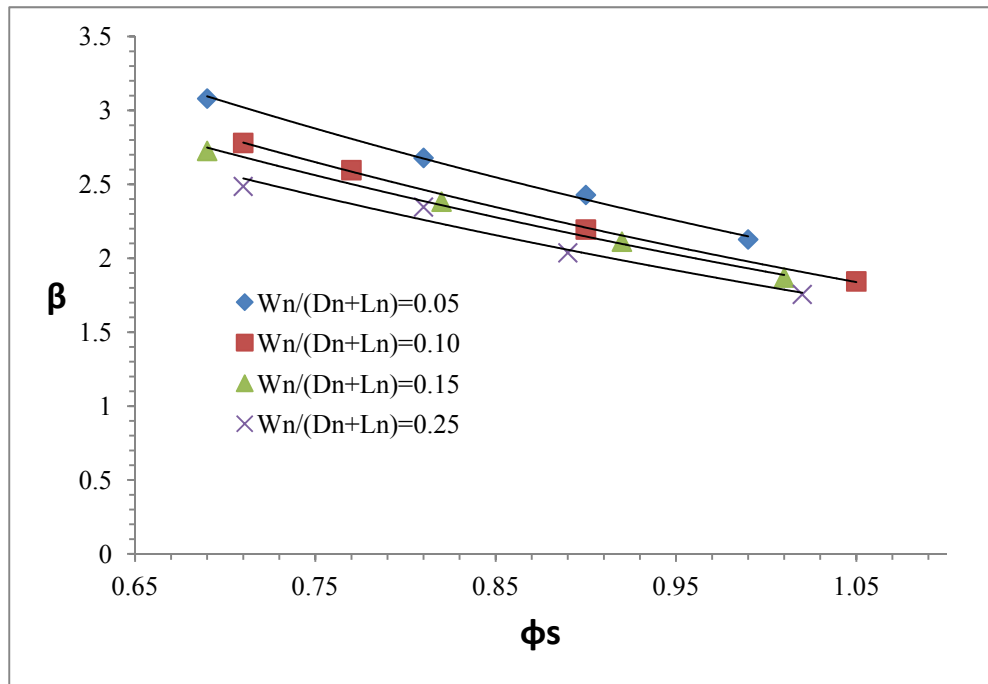


Figure E.29.  $\beta$  vs.  $\varphi_s$  curve, Frame 1, CFY

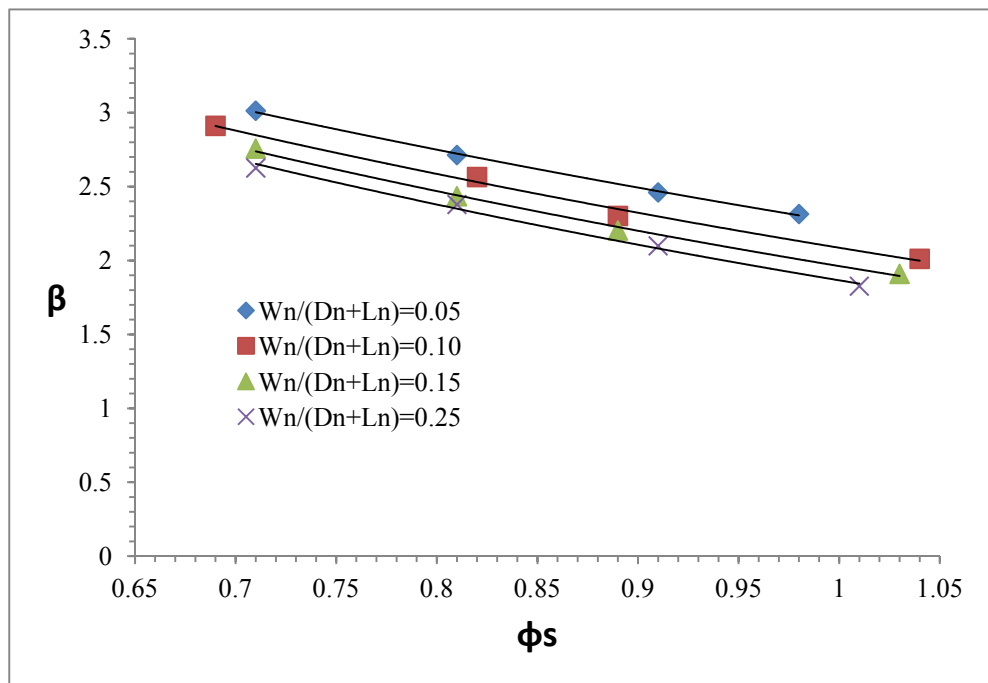


Figure E.30.  $\beta$  vs.  $\varphi_s$  curve, Frame 5, BFY-CFY

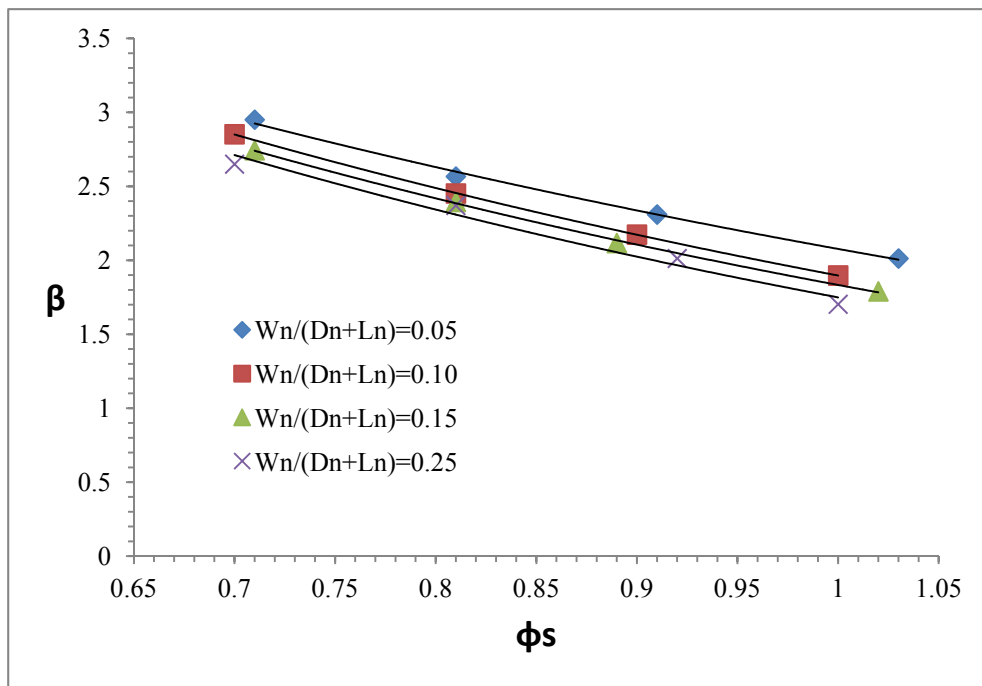


Figure E.31.  $\beta$  vs.  $\phi_s$  curve, Frame 7, BFY-CFY

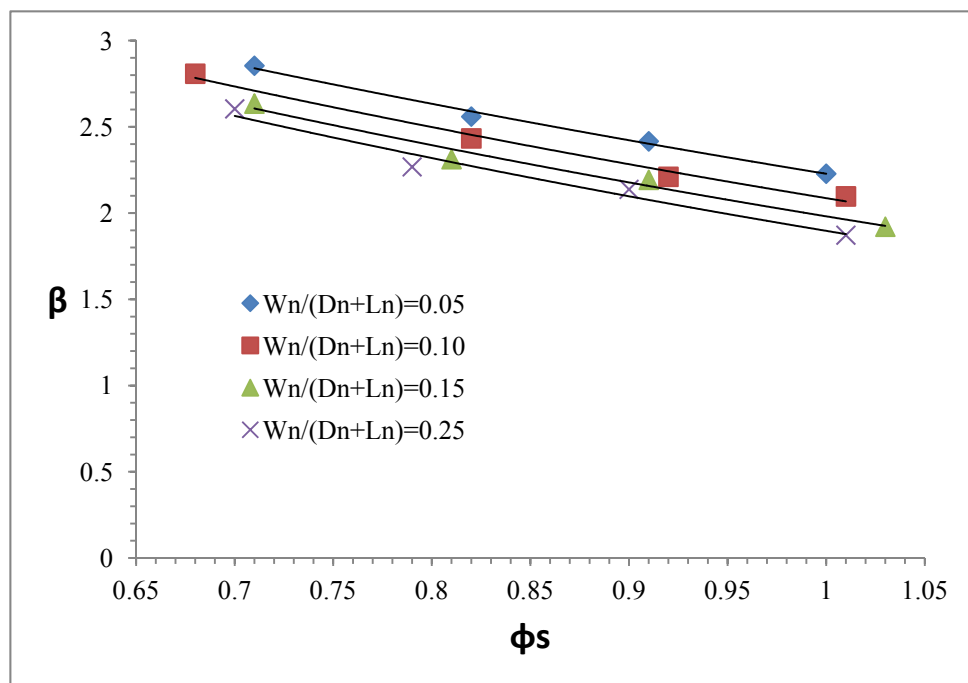


Figure E.32.  $\beta$  vs.  $\phi_s$  curve, Frame 9, BFY-CFY

**E.11. Selected  $\beta - \varphi_s$  plots, hinged joint braced frames under gravity loads**

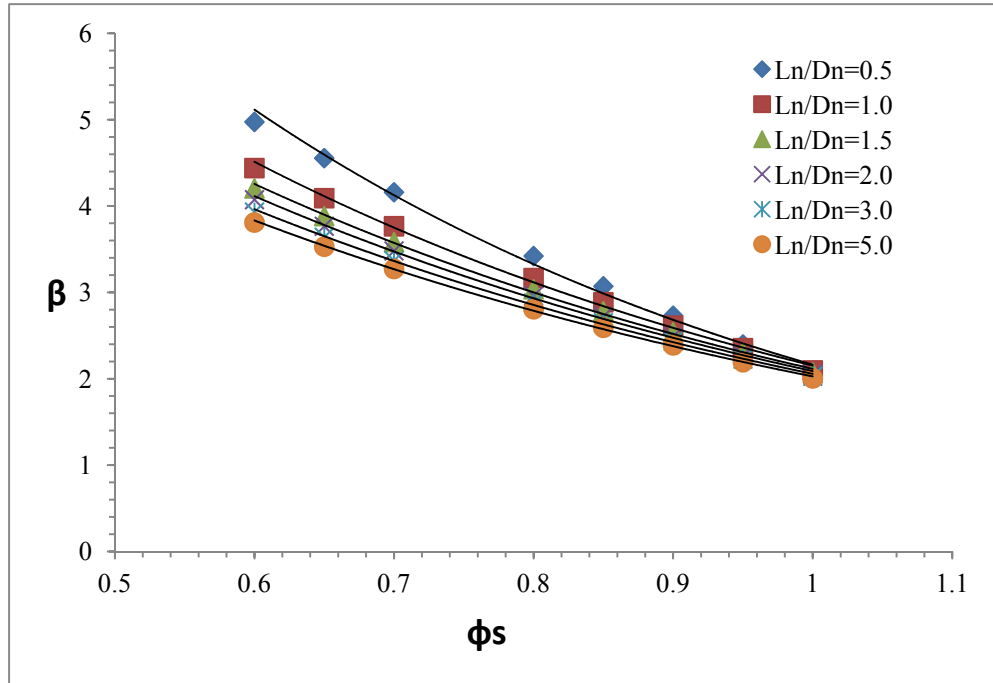


Figure E.33.  $\beta$  vs.  $\varphi_s$  curve, Frame 2, CFY-BPY

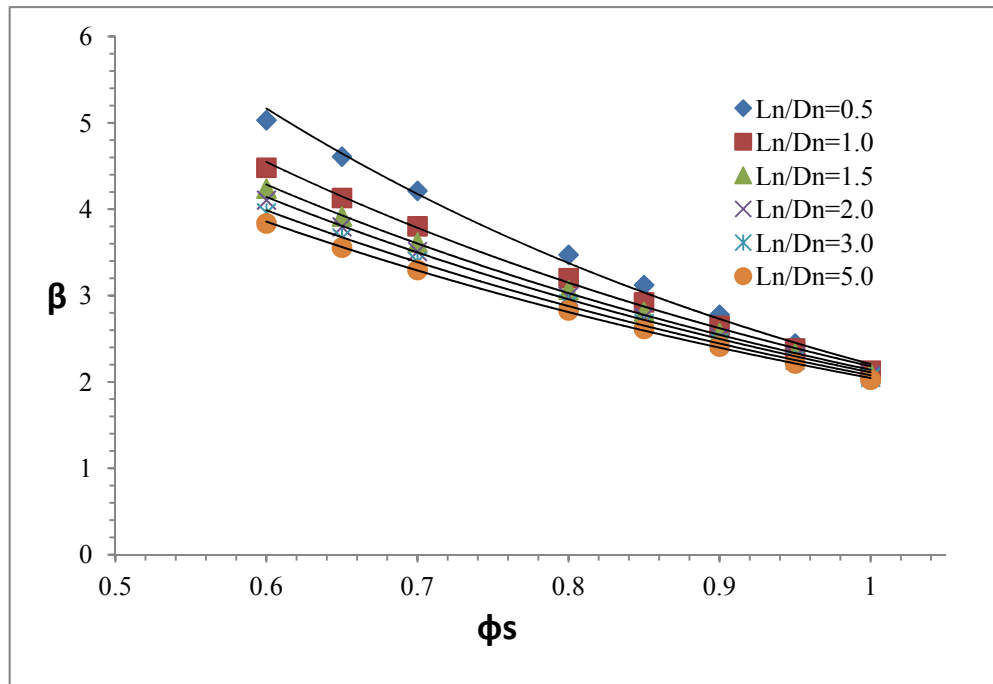
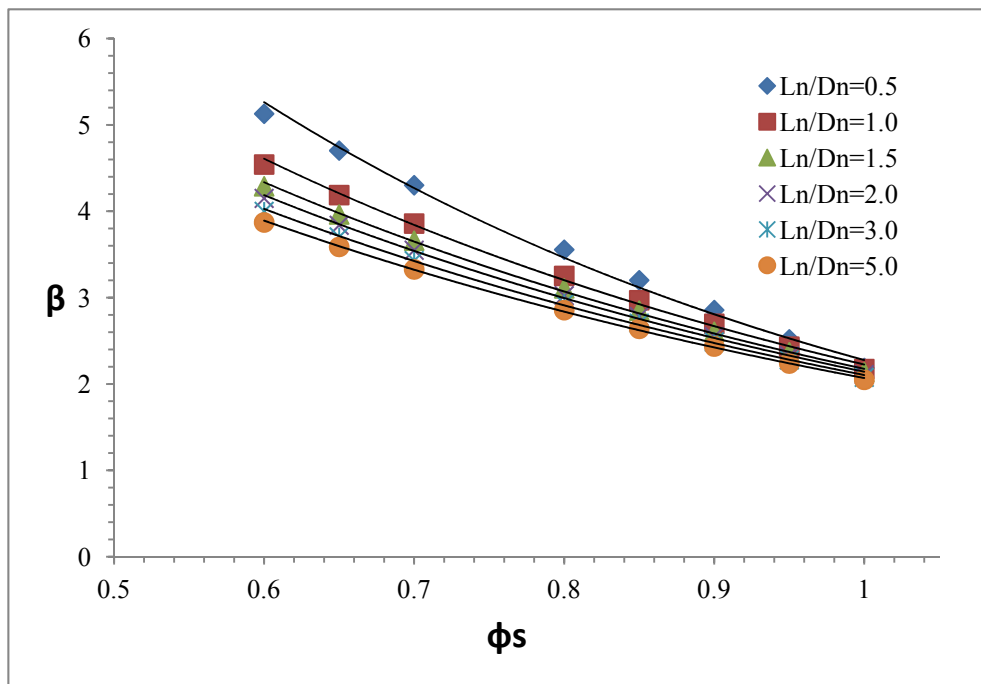
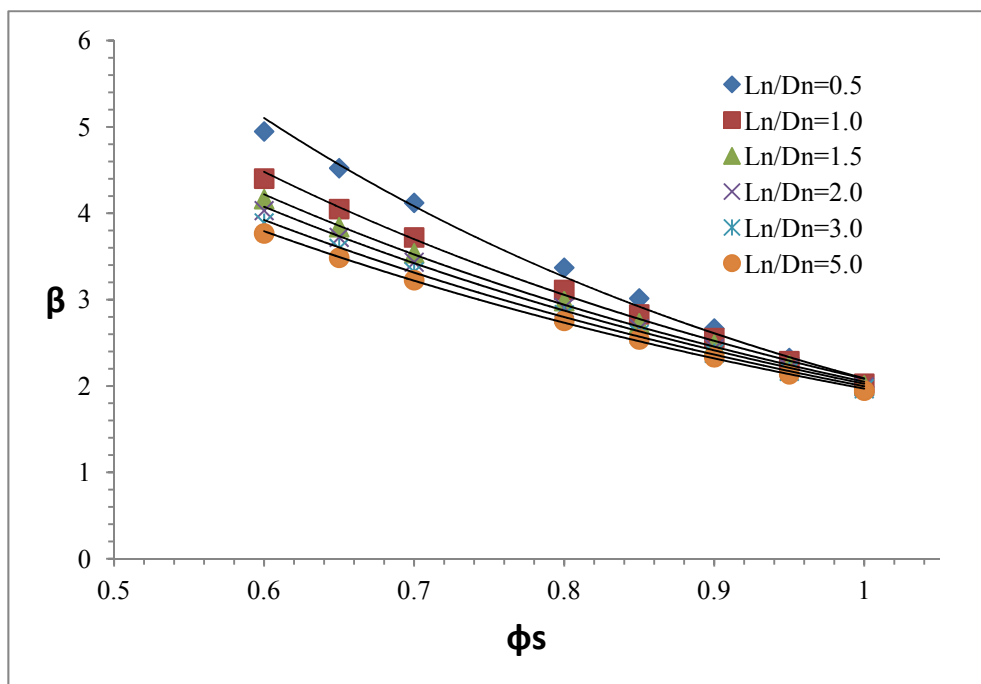


Figure E.34.  $\beta$  vs.  $\varphi_s$  curve, Frame 4, CFY

**E.12. Selected  $\beta - \varphi_s$  plots, rigid joint braced frames under gravity loads**Figure E.35.  $\beta$  vs.  $\varphi_s$  curve, Frame 7, CPY-BFY-CBFigure E.36.  $\beta$  vs.  $\varphi_s$  curve, Frame 9, CFY-BFY

## E.13. Codes

### E.13.1. Matlab script to generate random variables

```

%*****
%This matlab file generates random variables for Frame 7 under gravity
clear;
clc;
%*****
%input data
%*****
%*****
height_column=[6000,6000,6000,4000,4000,4000];
no_col_per_stor=[3,3];
length_beam=[4000,8000,4000,8000];
no_beam_per_bay=[2,2];
total_structure_height=10000;
column_no=6;
beam_no=4;
global_mesh_size=200;
N=350; %number of simulation
%*****
%Nominal values of random variables
%*****
E=[200000];%elastic modulus
E_dist=['L'];
F=[320];%yield stress
F_dist=['L'];
Est=(AS4100);%starin_hardening
Est_dist=['N'];
%section depth
section_name=[15014,20029,25037,31040,31046,41059];
h1=[150,207,256,304,307,406];%200UB18, 200UB29
h1_dist=['N','N','N','N','N','N'];
%section width
b1=[75,134,146,165,166,178];
b1_dist=['N','N','N','N','N','N'];
b2=[75,134,146,165,166,178];
b2_dist=['N','N','N','N','N','N'];
%web thickness
t1=[5,6.3,6.4,6.1,6.7,9.9];
t1_dist=['N','N','N','N','N','N'];
%flange thickness
t21=[7,9.6,10.9,10.2,11.8,12.8];
t21_dist=['N','N','N','N','N','N'];
t22=[7,9.6,10.9,10.2,11.8,12.8];
t22_dist=['N','N','N','N','N','N'];
%*****

%statistical data for random variables

%*****
%mean values
E_m=E;
Fy_m=1.05*F;
Est_m=Est;
h1_m=1.001*h1;
b1_m=1.012*b1;
b2_m=1.015*b2;

```

```

t1_m=1.055*t1;
t21_m=0.988*t21;
t22_m=0.998*t22;
delta_1_m=0.000555556;
delta1_dist=['N'];
delta_2_m=0.000139159;
delta2_dist=['N'];
delta_3_m=7.3429E-05;
delta3_dist=['N'];
Delta_m=0.00002;
Delta_dist=['N'];
Xr_m=1;
Xr_dist=['N'];
%COV
E_cov=0.06;
Fy_cov=0.1;
Est_cov=0.25;
h1_cov=0.00443;
b1_cov=0.01026;
b2_cov=0.00961;
t1_cov=0.04182;
t21_cov=0.04357;
t22_cov=0.04803;
%standard deviation
E_s=E_m*E_cov;
Fy_s=Fy_m*Fy_cov;
Est_s=Est_m*Est_cov;
h1_s=h1_m*h1_cov;
b1_s=b1_m*b1_cov;
b2_s=b2_m*b2_cov;
t1_s=t1_m*t1_cov;
t21_s=t21_m*t21_cov;
t22_s=t22_m*t22_cov;
delta_1_s=0.000426506;
delta_2_s=7.11616E-05;
delta_3_s=7.82244E-05;
Delta_s=0.00173;
Xr_s=0.2;
%number of random variables
l_E=length(E);
l_F=length(F);
l_Est=length(Est);
l_h1=length(h1);
l_b1=length(b1);
l_b2=length(b2);
l_t1=length(t1);
l_t21=length(t21);
l_t22=length(t22);
%*****

%generate all uncorrelated random variables
%Using Latin Hypercube sampling

%*****
***
x_mean=[E_m, Fy_m, Est_m, Delta_m, Xr_m];
x_sdv=[E_s, Fy_s, Est_s, Delta_s, Xr_s];
distribution=[E_dist, F_dist, Est_dist, Delta_dist, Xr_dist];
no_sample=N;
no_var=length(x_mean);

```

## Appendix E

---

```
rd=lhsdesign(no_sample,no_var,'smooth','off');
random_matrix=zeros(no_sample,no_var);
[random_matrix]= generate_random (no_var, rd, distribution, x_mean,
x_sdv);
xlswrite('random_variables_properties.xlsx',random_matrix)
%*****

%generate all correlated random variables (cross-section properties)
%Using Latin Hypercube sampling

%*****

matrix=[];
for i=1:l_h1
x_mean_prop=[h1_m(i), b1_m(i), b2_m(i), t1_m(i), t21_m(i), t22_m(i)];
x_sdv_prop=[h1_s(i), b1_s(i), b2_s(i), t1_s(i), t21_s(i), t22_s(i)];
distribution_prop=[h1_dist(i), b1_dist(i), b2_dist(i), t1_dist(i),
t21_dist(i), t22_dist(i)];
no_sample=N;
no_var=length(x_mean_prop);
%target correlation matrix
correlation=[
1 -0.0068 0.0534 0.0399 -0.0686 -0.0989
-0.0068 1 0.6227 -0.2142 -0.2681 -0.1456
0.0534 0.6227 1 -0.2132 -0.1596 -0.0423
0.0399 -0.2142 -0.2132 1 0.2368 0.2451
0.0686 -0.2681 -0.1596 0.2368 1 0.7634
-0.0989 -0.1456 0.0423 0.2451 0.7634 1];
L = chol(correlation);
z = randn(no_sample,no_var);
y=z*L;
prop=(y.*repmat(x_sdv_prop,no_sample,1))+
repmat(x_mean_prop,no_sample,1);
filename=['UB_', num2str(section_name(i)),'.xlsx'];
xlswrite(filename,prop)
end

%*****

%generate random initial imperfection

%*****

mode_no=3;
storey_no=length(height_column);
bay_no=length(length_beam);
for i=1:storey_no
neleC(i)=nearest(height_column(i)/global_mesh_size);
end
for i=1:bay_no
neleB(i)=nearest(length_beam(i)/global_mesh_size);
end
max_col=max(neleC);
max_beam=max(neleB);
for k=1:storey_no
for j=1:mode_no
for i=1:neleC(k)
col_coeff_matrix(i,j,k)=sin(j*pi*i/neleC(k));
end
end
end
```



```

end
for k=1:storey_no
for i=1:neleC(k)
Delta_coeff(i,k)=i/neleC(k);
end
end
for k=1:bay_no
for j=1:mode_no
for i=1:neleB(k)-1
beam_coeff_matrix(i,j,k)=sin(j*pi*i/neleB(k));
end
end
end
x_mean=[delta_1_m, delta_2_m, delta_3_m ];
x_sdv=[delta_1_s, delta_2_s, delta_3_s ];
distribution=[delta1_dist, delta2_dist, delta3_dist];
no_var=length(x_mean);

%*****
%*****COLUMNS
%*****

matrix=[];
factor=1;
sum=0;
h=height_column(1);
for i=1:no_sample
delta_top(i)=0;
end
for k1=1:column_no
ui=rand(no_sample,no_var);
s=zeros(no_sample,no_var);
[random_matrix]= generate_random (no_var, rd, distribution, x_mean, x_sdv);

%%%%%%%%%%
%generage random sign to assinge to coefficients
%%%%%%%%%%

ui=rand(mode_no,no_sample);
% disp(ui)
for j=1:mode_no
for k=1:no_sample
if ui(j,k)<0.5
sing_base1=col_coeff_matrix(:,j,k11)*-1;
elseif ui(j,k)>=0.5
sing_base1=col_coeff_matrix(:,j,k11);
end
matrix=[matrix,sing_base1];
end
end
for a=1:no_sample*mode_no
if (a>=1 && a<=no_sample)
mat1(:,a)=matrix(:,a);
else if (a>no_sample && a<=2*no_sample)
mat2(:,a-no_sample)=matrix(:,a);
else if (a>2*no_sample && a<=3*no_sample)
mat3(:,a-2*no_sample)=matrix(:,a);
end
end
end
end

```

```

end
for do=1:no_sample
for i=1:neleC(k11)
if random_matrix(do,4)<0
node(do,i,k11)=(-
(mat1(i,do)*s(do,1)+mat2(i,do)*s(do,2)+mat3(i,do)*s(do,3))*height_colum
n(k11)+((1/length(no_col_per_stor))*Delta_coeff(i,k11)*random_matrix(do,
4)+delta_top(do))*total_structure_height;
%
else
node(do,i,k11)=((mat1(i,do)*s(do,1)+mat2(i,do)*s(do,2)+mat3(i,do)*s(do,3
))*height_column(k11)+((1/length(no_col_per_stor))*Delta_coeff(i,k11)*r
andom_matrix(do,4)+delta_top(do))*total_structure_height;
%
end
end
end
if k11==no_col_per_stor(factor)+sum
for i=1:no_sample
delta_top(i)=delta_top(i)+(1/length(no_col_per_stor))*Delta_coeff(neleC(k11),k11)*random_matrix(i,4);
end
sum=sum+no_col_per_stor(factor);
factor=factor+1;
if k11< length(height_column)
h=height_column(k11+1);
end
end
matrix=[];
end
a2=column_no*max_col;
matrix_random_imp_shape=reshape(node,no_sample,a2);
matrix_random_imp_shape=matrix_random_imp_shape(:,any(matrix_random_imp_shape));
xlswrite('random_column_imp.xlsx',matrix_random_imp_shape)
%*****
%*****BEAMS
%*****
factor_b=1;
sum_b=0;
L=length_beam(1);
matrix_beam=[];
for k22=1:beam_no
ui=rand(no_sample,no_var);
s=zeros(no_sample,no_var);
[random_matrix]= generate_random (no_var, rd, distribution, x_mean, x_sdv);

%%%%%%%%%%%%%%
%generage random sign to assinge to coefficents
%%%%%%%%%%%%%%

ui=rand(mode_no,no_sample);
for j=1:mode_no
for k=1:no_sample
if ui(j,k)<0.5
sing_base1=beam_coeff_matrix(:,k22)*-1;
elseif ui(j,k)>=0.5
sing_base1=beam_coeff_matrix(:,k22);
end
matrix_beam=[matrix_beam,sing_base1];
end
end
end

```

```

for a=1:no_sample*mode_no
if (a>=1 && a<=no_sample)
mat1_b(:,a)=matrix_beam(:,a);
else if (a>no_sample && a<=2*no_sample)
mat2_b(:,a-no_sample)=matrix_beam(:,a);
else if (a>2*no_sample && a<=3*no_sample)
mat3_b(:,a-2*no_sample)=matrix_beam(:,a);
end
end
end
end
for do=1:no_sample
for i=1:(neleB(k22)-1)
node_b(do,i,k22)=((mat1_b(i,do)*s(do,1)+mat2_b(i,do)*s(do,2)+mat3_b(i,do)
)*s(do,3))*length_beam(k22);
if k22==3&& do==1 && i==1
end
end
end
if k22==no_beam_per_bay(factor_b)+sum_b
sum=sum+no_beam_per_bay(factor_b);
factor_b=factor_b+1;
if k22< length(length_beam)
L=length_beam(k22+1);
end
end
matrix_beam=[]
;
end
a22=beam_no*(max_beam-1);
matrix_random_imp_shape_beam=reshape(node_b,no_sample,a22);
matrix_random_imp_shape_beam=matrix_random_imp_shape_beam(:,any(matrix_r
andom_imp_shape_beam));
xlswrite('random_beam_imp.xlsx',matrix_random_imp_shape_beam)
disp(matrix_random_imp_shape_beam)
function[random_matrix]= generate_random (no_var, rd, distribution,
x_mean, x_sdv)
for i=1:no_var
p=rd(:,i);
if distribution(i)=='N' || distribution(i)=='L'
a = [ -3.969683028665376e+01 2.209460984245205e+02 -
2.759285104469687e+02 1.383577518672690e+02 -3.066479806614716e+01
2.506628277459239e+00];
b = [ -5.447609879822406e+01 1.615858368580409e+02 -
1.556989798598866e+02 6.680131188771972e+01 -1.328068155288572e+01];
c = [ -7.784894002430293e-03 -3.223964580411365e-01 -
2.400758277161838e+00 -2.549732539343734e+00 4.374664141464968e+00
2.938163982698783e+00];
d = [ 7.784695709041462e-03 3.224671290700398e-01
2.445134137142996e+00 3.754408661907416e+00 ];
plow = 0.02425;
phigh = 1 - plow;
% Initialize output array.
z = zeros(size(p));
% Rational approximation for central region:
k = plow <= p & p <= phigh;
if any(k(:))
q = p(k) - 0.5;
r = q.*q;
z(k) =

```

```

((((a(1)*r+a(2)).*r+a(3)).*r+a(4)).*r+a(5)).*r+a(6)).*q ./ ...
((((b(1)*r+b(2)).*r+b(3)).*r+b(4)).*r+b(5)).*r+1);
end
% Rational approximation for lower region:
k = 0 < p & p < plow;
if any(k(:))
q = sqrt(-2*log(p(k)));
z(k) = (((((c(1)*q+c(2)).*q+c(3)).*q+c(4)).*q+c(5)).*q+c(6))
./ ...
(((d(1)*q+d(2)).*q+d(3)).*q+d(4)).*q+1);
end
% Rational approximation for upper region:
k = phigh < p & p < 1;
if any(k(:))
q = sqrt(-2*log(1-p(k)));
z(k) = -
((((c(1)*q+c(2)).*q+c(3)).*q+c(4)).*q+c(5)).*q+c(6)) ./ ...
(((d(1)*q+d(2)).*q+d(3)).*q+d(4)).*q+1);
end
% Case when P = 0:
z(p == 0) = -Inf;
% Case when P = 1:
z(p == 1) = Inf;
% Cases when output will be NaN:
k = p < 0 | p > 1 | isnan(p);
if any(k(:))
z(k) = NaN;
end
% The relative error of the approximation has absolute value less
% than 1.15e-9. One iteration of Halley's rational method
(third
% order) gives full machine precision.
k = 0 < p & p < 1;
if any(k(:))
e = 0.5*erfc(-z(k)/sqrt(2)) - p(k); % error
u = e * sqrt(2*pi) .* exp(z(k).^2/2); % f(z)/df(z)
z(k) = z(k) - u./( 1 + z(k).*u/2 ); % Halley's
method
end
if distribution(i)=='N'
random_matrix(:,i) = x_mean(i) + z(k)* x_sdv(i);
else if distribution(i)=='L'
v_cov(i)=x_sdv(i)/x_mean(i);
x_sdv_LN(i)=log((v_cov(i))^2+1);
x_mean_LN(i)=log(x_mean(i))-0.5*x_sdv_LN(i);
random_matrix(:,i)=exp(x_mean_LN(i)+z(k)*sqrt(x_sdv_LN(i)));
end
end
else if distribution(i)=='U'
random_matrix(:,i) = x_min(i) + p* (x_max(i)-x_min(i));
end
end
end
end
end

```

## E.13.2. Matlab script to generate ABAQUS input file

```

%This file generates an ABAQUS input file for Frame 7 under gravity
loads
clear;
clc;
tic
%*****
%Required input for frame
%*****
height_column=[6000,6000,6000,4000,4000,4000];
storey_h=[6000,4000];
no_col_per_stor=[3,3];
length_beam=[4000,8000,4000,8000];%write dimentions going horizontally
bay_L=[4000,8000];
no_beam_per_stor=[2,2];
section_col=[15014,31040,25037,15014,25037,25037];
section_beam=[31046,41059,20029,31046];
%joint types
joints=['R','R','R','R','R','R','R','R'];%R for rigid joints and H for
hing joints
beam_loads=[-50,-50,-25,-25];
global_mesh_size=200;
N=350; %number of simulatio
%*****
%*****
v=0.3; %poision rartio
random_var=xlsread('random_variables_properties.xlsx');
imp_col=xlsread('random_column_imp.xlsx');
imp_beam=xlsread('random_beam_imp.xlsx');
%*****
%*****
storey_no=length(height_column);
bay_no=length(length_beam);
for i=1:storey_no
neleC(i)=nearest(height_column(i)/global_mesh_size);
ele_C(i)=height_column(i)/neleC(i);
end
for i=1:bay_no
neleB(i)=nearest(length_beam(i)/global_mesh_size);
ele_B(i)=length_beam(i)/neleB(i);
end
for i=1:storey_no
filename_col=['UB_', num2str(section_col(i)),'.xlsx'];
section_col_file_f=xlsread(filename_col);
matrix_col(:,i)=section_col_file_f;
end
for i=1:bay_no
filename_beam=['UB_', num2str(section_beam(i)),'.xlsx'];
section_beam_file_f=xlsread(filename_beam);
matrix_beam(:,i)=section_beam_file_f;
end
for K=1:N
textfilename = ['Frame_', num2str(K),'.inp'];
File = fopen(textfilename, 'wt');
%*****
%This part writes the frame input file for using by ABAQUS
fprintf(File,'%HEADING\n **This is the input file for a sigle bay frame
for imperfection sensitivity\n');
fprintf(File,'%Preprint, echo=No, model=NO, history=No, contact=No\n');

```

```

fprintf(File,**\n');
fprintf(File,**PARTS\n');
fprintf(File,**\n');
fprintf(File,*Part, name=frame\n');
fprintf(File,*End Part\n');
fprintf(File,**\n');
fprintf(File,**\n');
fprintf(File,**ASSEMBLY\n');
fprintf(File,**\n');
fprintf(File,*Assembly, name=Assembly\n');
fprintf(File,**\n');
fprintf(File,*Instance, name=frame-1, part=frame\n');
%*****
% Generate all nodes for the frame
%*****
fprintf(File,*NODE\n');
y_start=0;
sum=0;
factor=1;
j=1;
k_c_l=1;
z=0;
nodenum=0;%node number
x_start=0;
k_c_l_sum=1;
for i=1:storey_no
y=y_start;
while k_c_l<=neleC(i)
if k_c_l==1 && i<=no_col_per_stor(1)
y=0;
if j==1
if k_c_l==1
x=0;
else
x=imp_col(K,k_c_l_sum);
end
else
if k_c_l==1
x=x_start+bay_L(j-1);
else
x=x_start+bay_L(j-1)+imp_col(K,k_c_l_sum);
end
end
nodenum=nodenum+1;
fprintf(File,%d, %d, %d, %d\n',nodenum,x,y,z);
base(i)=nodenum;
end
if j==1
x=imp_col(K,k_c_l_sum);
else
x=x_start+bay_L(j-1)+imp_col(K,k_c_l_sum);
end
y=y+ele_C(i);
nodenum=nodenum+1;
if k_c_l==neleC(i)
x_shoru_beam(i)=x;
y_top=y;
end
k_c_l=k_c_l+1;
k_c_l_sum=k_c_l_sum+1;

```

```

fprintf(File,'%d, %d, %d, %d\n',nodenum,x,y,z);
end
if j~=1
x_start=x_start+bay_L(j-1);
end
j=j+1;
if i==no_col_per_stor(factor)+sum
sum=sum+no_col_per_stor(factor);
factor=factor+1;
y_start=y_top;
j=1;
x_start=0;
end
k_c_l=1;
fprintf('%d\n',x_shoru_beam(i))
end
y_start=0;
k_b_l=1;
k_b_l_sum=1;
factor=1;
sum=0;
j=1;
for i=1:bay_no
while k_b_l<=neleB(i)+1
x_start=x_shoru_beam(j);
if k_b_l==1
x=x_start;
y=y_start+storey_h(factor);
node_b_start(i)=nodenum+1;
else
x=x+ele_B(i);
if k_b_l==neleB(i)+1
y=y_start+storey_h(factor);
node_b_end(i)=nodenum+1;
else
y=y_start+storey_h(factor)+imp_beam(K,k_b_l_sum);
end
end
nodenum=nodenum+1;
fprintf(File,'%d, %d, %d, %d\n',nodenum,x,y,z) ;
if k_b_l<=neleB(i)+1 && k_b_l~=1
k_b_l_sum=k_b_l_sum+1;
end
if i==1 && k_b_l==1
node_start=nodenum;
end
k_b_l=k_b_l+1;
end
if i~=no_beam_per_stor(factor)+sum
j=j+1;
end
if i==no_beam_per_stor(factor)+sum
y_start=y_start+storey_h(factor);
sum=sum+no_beam_per_stor(factor);
factor=factor+1;
j=j+2;
end
k_b_l=1;
end
%*****

```

```

% Generate all elements for the frame
%*****
elenum=0;
k_c_l=1;
node_1=0;
sum=0;
factor=1;
j=0;
for i=1:storey_no
fprintf(File,'*ELEMENT, TYPE=B31,ELSET=COLUMN_%d\n',i);
while k_c_l<=neleC(i)
if i>no_col_per_stor(1) && k_c_l==1
elenum=elenum+1;
node_1=top_node(j);
node_2=node_2+1;
fprintf(File,'%d, %d, %d\n',elenum,node_1,node_2);
node_1=node_2-1;
elseif i>no_col_per_stor(1) && k_c_l>1
elenum=elenum+1;
node_1=node_1+1;
node_2=node_1+1;
fprintf(File,'%d, %d, %d\n',elenum,node_1,node_2);
else
elenum=elenum+1;
node_1=node_1+1;
node_2=node_1+1;
fprintf(File,'%d, %d, %d\n',elenum,node_1,node_2);
end
k_c_l=k_c_l+1;
end
top_node(i)=node_2;
j=j+1;
if i==no_col_per_stor(factor)+sum
j=sum+1;
sum=sum+no_col_per_stor(factor);
factor=factor+1;
end
k_c_l=1;
node_1=node_1+1;
end
% disp(top_node)
%beam elements
sum=0;
factor=1;
k_b_l=1;
j=1;
for i=1:bay_no
fprintf(File,'*ELEMENT, TYPE=B31,ELSET=BEAM_%d\n',i);
while k_b_l<=(neleB(i))
elenum=elenum+1;
node_1=node_1+1;
node_2=node_1+1;
fprintf(File,'%d, %d, %d\n',elenum,node_1,node_2);
if k_b_l==1
b_start(i)=elenum;
end
if k_b_l==neleB(i)
b_end(i)=elenum;
end
if k_b_l==(neleB(i)/2)

```



```

b_mid(i)=node_2;
end
k_b_l=k_b_l+1;
end
node_1=node_1+1;
k_b_l=1;
end
ele_end=elenum;
elenum=elenum+1;
%*****
%Create and assign Section
%*****
for i=1:storey_no
fprintf(File,'*BEAM SECTION, SECTION=I, ELSET=COLUMN_%d,
MATERIAL=STEEL\n',i);
section_col_file=matrix_col(:,i);
fprintf(File,'%3.2f, %3.2f, %3.2f, %3.2f, %3.2f, %3.2f\n',
(section_col_file(K,1)/2),section_col_file(K,1),section_col_file(K,2),se
ction_col_file(K,3),section_col_file(K,5),section_col_file(K,6),section_
col_file(K,4));
end
for i=1:bay_no
fprintf(File,'*BEAM SECTION, SECTION=I, ELSET=BEAM_%d,
MATERIAL=STEEL\n',i);
section_beam_file=matrix_beam(:,i);
fprintf(File,'%3.2f, %3.2f, %3.2f, %3.2f, %3.2f, %3.2f\n',
(section_beam_file(K,1)/2),section_beam_file(K,1),section_beam_file(K,2)
,section_beam_file(K,3),section_beam_file(K,5),section_beam_file(K,6),se
ction_beam_file(K,4));
end
%*****
fprintf(File,'*END INSTANCE\n');
fprintf(File,'*\n');
%*****
%Joints
%*****
j=0;
sum=0;
factor=1;
sum_b=0;
u=1;
matrix=[];
for i=1:storey_no
if j~=no_beam_per_stor(factor)+sum_b
j=j+1;
end
if i==sum+1
fprintf(File,'*ELEMENT, TYPE=CONN3D2\n');
fprintf(File,'%d,frame-1.%d,frame-
1.%d\n',elenum,top_node(i),node_b_start(j));
matrix=[matrix,elenum];
elenum=elenum+1;
u=u+1;
elseif i==no_col_per_stor(factor)+sum
fprintf(File,'*ELEMENT, TYPE=CONN3D2\n');
fprintf(File,'%d,frame-1.%d,frame-
1.%d\n',elenum,top_node(i),node_b_end(j));
matrix=[matrix,elenum];
elenum=elenum+1;
u=u+1;

```

```

else
fprintf(File,'*ELEMENT, TYPE=CONN3D2\n');
fprintf(File,'%d,frame-1.%d,frame-
1.%d\n',elenum,top_node(i),node_b_end(j-1));
matrix=[matrix,elenum];
elenum=elenum+1;
u=u+1;
fprintf(File,'*ELEMENT, TYPE=CONN3D2\n');
fprintf(File,'%d,frame-1.%d,frame-
1.%d\n',elenum,top_node(i),node_b_start(j));
matrix=[matrix,elenum];
elenum=elenum+1;
u=u+1;
end
if i==no_col_per_stor(factor)+sum
sum=sum+no_col_per_stor(factor);
sum_b=sum_b+no_beam_per_stor(factor);
factor=factor+1;
end
end
%disp(matrix)
shomar=0;
for i=1:length(joints)
if joints(i)=='R'
fprintf(File,'*CONNECTOR SECTION, ELSET=Wire_1_Set_1_%d\n',i);
fprintf(File,'BEAM\n');
elseif joints(i)=='H'
fprintf(File,'*CONNECTOR SECTION, ELSET=Wire_1_Set_1_%d,
BEHAVIOR=HINGE\n',i);
fprintf(File,'CARTESIAN, CARDAN\n');
fprintf(File,'"Datum csys-2"\n');
shomar=1;
end
end
%*****
j=0;
sum=0;
factor=1;
sum_b=0;
u=1;
for i=1:storey_no
if j~=no_beam_per_stor(factor)+sum_b
j=j+1;
end
if i==sum+1
fprintf(File,'*NSET, NSET=Wire_1_Set_1_%d, INSTANCE=frame-
1\n',u);
fprintf(File,'%d, %d\n',top_node(i),node_b_start(j));
%elenum=elenum+1;
u=u+1;
elseif i==no_col_per_stor(factor)+sum
fprintf(File,'*NSET, NSET=Wire_1_Set_1_%d, INSTANCE=frame-
1\n',u);
fprintf(File,'%d, %d\n',top_node(i),node_b_end(j));
%elenum=elenum+1;
u=u+1;
else
fprintf(File,'*NSET, NSET=Wire_1_Set_1_%d, INSTANCE=frame-
1\n',u);
fprintf(File,'%d, %d\n',top_node(i),node_b_end(j-1));

```

```

%elenum=elenum+1;
u=u+1;
fprintf(File,*NSET, NSET=Wire_1_Set_1_%d, INSTANCE=frame-
1\n',u);
fprintf(File,%d, %d,\n', top_node(i),node_b_start(j));
%elenum=elenum+1;
u=u+1;
end
if i==no_col_per_stor(factor)+sum
sum=sum+no_col_per_stor(factor);
sum_b=sum_b+no_beam_per_stor(factor);
factor=factor+1;
end
end
for i=1:length(matrix)
fprintf(File,*ELSET, ELSET=Wire_1_Set_1_%d\n',i);
fprintf(File,%d\n', matrix(1,i))
end
fprintf(File,*ORIENTATION, NAME="Datum csys-2"\n');
fprintf(File,' 1, 0, 0, 0, 1, 0\n');
fprintf(File,'1, 0\n');
%*****
%Printing Node Sets
%*****
fprintf(File,*NSET, NSET=WHOLE_FRAME, GENERATE, INSTANCE=frame-1\n');
fprintf(File,'1, %d\n', node_b_end(bay_no));
fprintf(File,*ELSET, ELSET=WHOLE_FRAME, GENERATE, INSTANCE=frame-1\n');
fprintf(File,'1, %d\n', ele_end);
for i=1:storey_no
fprintf(File,*NSET, NSET=TOP_COL_%d, INSTANCE=frame-1\n',i);
fprintf(File,%d\n',top_node(i));
end
for i=1:bay_no
fprintf(File,*NSET, NSET=START_BEAM_%d, INSTANCE=frame-1\n',i);
fprintf(File,%d\n',node_b_start(i));
end
for i=1:bay_no
fprintf(File,*NSET, NSET=END_BEAM_%d, INSTANCE=frame-1\n',i);
fprintf(File,%d\n',node_b_end(i));
end
for i=1:bay_no
fprintf(File,*NSET, NSET=MID_%d, INSTANCE=frame-1\n',i);
fprintf(File,%d\n',b_mid(i));
end
for i=1:no_col_per_stor(1)
fprintf(File,*NSET, NSET=BASE_%d, INSTANCE=frame-1\n',i);
fprintf(File,%d\n',base(i));
end
for i=1:bay_no
fprintf(File,*ELSET, ELSET=BEAM_%d,GENERATE, INSTANCE=frame-
1\n',i);
fprintf(File,%d, %d, 1\n',b_start(i), b_end(i));
end
fprintf(File,*NSET, NSET=MID_COL_2, INSTANCE=frame-1\n');
fprintf(File,'65\n');
%*****
fprintf(File,*END ASSEMBLY\n');
fprintf(File,**\n');
if shomar==1
fprintf(File,*CONNECTOR BEHAVIOR, NAME=HINGE\n');

```

```
fprintf(File,'*CONNECTOR ELASTICITY, RIGID\n');
fprintf(File,'1, 2, 3, 4\n');
end
%*****
%Generate Material
%*****
fprintf(File,'*MATERIAL, NAME=STEEL\n');
fprintf(File,'*ELASTIC\n%f, %2.1f\n',random_var(K,1),v);
fprintf(File,'*PLASTIC\n');
nominal_stress1=random_var(K,2);
fprintf(File,'%f, 0\n', nominal_stress1);
fprintf(File,'*\n');
%*****
%Residual stress
%*****
fprintf(File,'*INITIAL CONDITIONS, TYPE=STRESS, USER\n');
%*****
%Defining steps, loads and boundary condition
%*****
fprintf(File,'**STEP: apply_load\n');
fprintf(File,'*\n');
fprintf(File,'*STEP, NAME=APPLY_LOAD, NLGEOM=YES, INC=50\n');
fprintf(File,'*STATIC, RIKS\n');
fprintf(File,'0.01, 1, 1e-05,10,10,\n');
fprintf(File,'*\n');
fprintf(File,'**BOUNDARY CONDITIONS\n');
fprintf(File,'*\n');
for i=1:no_col_per_stor(1)
fprintf(File,'*BOUNDARY\n')
fprintf(File,'BASE_%d, 1, 6\n',i)
end
fprintf(File,'*BOUNDARY\n')
fprintf(File,'WHOLE_FRAME, 3, 5\n');
fprintf(File,'*\n');
fprintf(File,'**LOADS\n');
fprintf(File,'*\n');
for i=1:length(beam_loads)
fprintf(File,'*DLOAD\n');
fprintf(File,'BEAM_%d, PY, %f\n',i,beam_loads(i))
end
fprintf(File,'**OUTPUT REQUEST\n');
fprintf(File,'*RESTART, WRITE, FREQUENCY=1\n');
fprintf(File,'*OUTPUT, FIELD, VARIABLE=PRESELECT,FREQUENCY=1\n');
fprintf(File,'*OUTPUT, HISTORY\n');
fprintf(File,'*OUTPUT, HISTORY, VARIABLE=PRESELECT, FREQUENCY=1\n');
fprintf(File,'*END STEP\n');
fclose(File)
end
toc
```

**E.13.3. Matlab script for reliability analysis**

```

%reliability analysis
%Finding beta (FORM)
%R is lognormal
%D is normal
%L is Type I extrem
%*****inputs
clc;
clear;
%factors
textfilename = ['Report.txt'];
File = fopen(textfilename, 'wt');
fprintf(File, 'Based on Probability concept, H.S.Ang, A. and Tang, W.\n');
fprintf(File, '\n');
fai_n=[0.69,0.75,0.82,0.9,0.98];
mean=[2.2012,1.945,1.745,1.58,1.426];
cov=[0.1,0.099,0.099,0.097,0.100];
Rn=[2.093,1.8063,1.6529,1.4855,1.3706];
R_Rn=[];
for i=1:length(mean)
r_ratio=mean(i)/Rn(i);
R_Rn=[R_Rn,r_ratio];
end
load_ratio_n=[0.5,1,1.5,2,3,5];
mat=[];
for j=1:length(load_ratio_n)
beta_mat=[];
sh=[];
load_ratio=load_ratio_n(j);
for i=1:length(fai_n)
fai=fai_n(i);
gama_D=1.2;
gama_L=1.6;
fprintf(File, 'fai=%1.2f\n', fai);
fprintf(File, 'gama_D=%1.2f\n', gama_D);
fprintf(File, 'gama_L=%1.2f\n', gama_L);
fprintf(File, '\n');
%Coefficients of variation
V_R=cov(i);
V_D=0.1;
V_L=0.25;
fprintf(File, 'V_R=%1.2f\n', V_R);
fprintf(File, 'V_D=%1.2f\n', V_D);
fprintf(File, 'V_L=%1.2f\n', V_L);
fprintf(File, '\n');
%Bias Factors
landa_R=R_Rn(i);
landa_D=1.05;
landa_L=1;
fprintf(File, 'landa_R=%1.3f\n', landa_R);
fprintf(File, 'landa_D=%1.2f\n', landa_D);
fprintf(File, 'landa_L=%1.2f\n', landa_L);
fprintf(File, '\n');
% *****calculations
fprintf(File, 'Ln/Dn=%1.2f\n', load_ratio);
fprintf(File, '\n');
fprintf(File, '*****\n');
meanL_meanD=(load_ratio)*(landa_L/landa_D);%3;
mean_D=1;
mean_L=(meanL_meanD)*mean_D;

```

```

%*****Step 2
%optain an initial design points
d_star=mean_D;
l_star=mean_L;
mean_R=((gama_D*mean_D)/landa_D)+((gama_L*mean_L)/landa_L)*(landa_R/fa
i);
r_star=mean_R;%d_star+l_star;%mean_R;
fprintf(File,'r_star_start=%2.6f\n',r_star);
fprintf(File,'l_star_start=%2.6f\n',l_star);
%*****Step 3
%Determaine equivalent mean and standard deviation
%R is lognormal
SD_LnR=sqrt(log(1+(V_R^2)));
sigma_e_R=r_star*SD_LnR;
mean_e_R=r_star*(1-log(r_star/mean_R));
%D is normal
mean_e_D=mean_D;
sigma_e_D=V_D*mean_D;
%L is Type I extrem
alfa=(pi/(V_L*mean_L))*(sqrt(1/6));
u=mean_L-(0.5772/alfa);
F_L_l_star=exp(-exp(-alfa*(l_star-u)));
ff_L_l_star=alfa*exp(-exp(-alfa*(l_star-u)))*exp(-alfa*(l_star-u));
t=sqrt(-log(F_L_l_star^2));
F_L_l_star_star=1-F_L_l_star;
t_star=sqrt(-log(F_L_l_star_star^2));
c_0=2.515517;
c_1=0.802853;
c_2=0.010328;
d_1=1.432788;
d_2=0.189269;
d_3=0.001308;
if F_L_l_star<=0.5
z=-t+(c_0+c_1*t+c_2*t^2)/(1+d_1*t+d_2*t^2+d_3*t^3);
else if F_L_l_star>0.5
z=t_star-
(c_0+c_1*t_star+c_2*t_star^2)/(1+d_1*t_star+d_2*t_star^2+d_3*t_star^3);
end
end
sai=(exp(-0.5*(z^2))/(sqrt(2*pi)));
sigma_e_L=sai/ff_L_l_star;
mean_e_L=l_star-sigma_e_L*(z);
%*****Step 4
%Determine a column vector of {G}
G_1=-sigma_e_R;
G_2=sigma_e_D;
G_3=sigma_e_L;
%*****Step 5
GT_G=(G_1^2)+(G_2^2)+(G_3^2);
alfa_1=G_1/sqrt(GT_G);
alfa_2=G_2/sqrt(GT_G);
alfa_3=G_3/sqrt(GT_G);
%*****Step 6
beta=(mean_e_R-mean_e_Dmean_e_L)/sqrt((sigma_e_R^2)+(sigma_e_D^2)+(sigma_e_L^2));
fprintf(File,'first beta=%2.6f\n',beta);
fprintf(File,'\n');
%Updating the design points
%*****Step 7
%Determine the reduced variates(z*)

```

```

z_1=alfa_1*beta;
z_2=alfa_2*beta;
z_3=alfa_3*beta;
%*****Step 8
%Determine x*i
l_star_new=mean_e_L+z_3*sigma_e_L;
%*****Step 9
%Determine the value of remaining random variable by solving g=0
r_star_new=mean_e_R+z_1*sigma_e_R;
while abs(l_star_new-l_star)>0.00001
%d_star=d_star_new;
l_star=l_star_new;
r_star=r_star_new;
fprintf(File,r_star_new=%2.6f\n',r_star);
fprintf(File,l_star_new=%2.6f\n',l_star);
%*****Step 3
%Determine equivalent mean and standard deviation
%R is lognormal
SD_LnR=sqrt(log(1+(V_R^2)));
sigma_e_R=r_star*SD_LnR;
mean_e_R=r_star*(1-log(r_star/mean_R));
%D is normal
mean_e_D=mean_D;
sigma_e_D=V_D*mean_D;
%L is Type I extrem
alfa=(pi/(V_L*mean_L))*(sqrt(1/6));
u=mean_L-(0.5772/alfa);
F_L_l_star=exp(-exp(-alfa*(l_star-u)));
ff_L_l_star=alfa*exp(-exp(-alfa*(l_star-u)))*exp(-alfa*(l_star-u));
t=sqrt(-log(F_L_l_star^2));
F_L_l_star_star=1-F_L_l_star;
t_star=sqrt(-log(F_L_l_star_star^2));
c_0=2.515517;
c_1=0.802853;
c_2=0.010328;
d_1=1.432788;
d_2=0.189269;
d_3=0.001308;
if F_L_l_star<=0.5
z=-t+(c_0+c_1*t+c_2*t^2)/(1+d_1*t+d_2*t^2+d_3*t^3);
else if F_L_l_star>0.5
z=t_star-
(c_0+c_1*t_star+c_2*t_star^2)/(1+d_1*t_star+d_2*t_star^2+d_3*t_star^3);
end
end
sai=(exp(-0.5*(z^2))/(sqrt(2*pi)));
sigma_e_L=sai/ff_L_l_star;
mean_e_L=l_star-sigma_e_L*(z);
%*****Step 4
%Determine a column vector of {G}
G_1=sigma_e_R;
G_2=sigma_e_D;
G_3=sigma_e_L;
%*****Step 5
GT_G=(G_1^2)+(G_2^2)+(G_3^2);
alfa_1=G_1/sqrt(GT_G);
alfa_2=G_2/sqrt(GT_G);
alfa_3=G_3/sqrt(GT_G);
%*****Step 6
beta=(mean_e_R-mean_e_Dmean_

```

```

e_L)/sqrt((sigma_e_R^2)+(sigma_e_D^2)+(sigma_e_L^2));
%Updating the design points
%*****Step 7
%Determine the reduced variates(z*)
z_1=alfa_1*beta;
z_2=alfa_2*beta;
z_3=alfa_3*beta;
%*****Step 8
%
l_star_new=mean_e_L+z_3*sigma_e_L;
%*****Step 9
%Determine the value of remaining random variable by solving g=0
r_star_new=mean_e_R+z_1*sigma_e_R;
fprintf(File,'beta_new=%2.6f\n',beta);
fprintf(File,'\n');
end
fprintf(File,'*****\n');
fprintf(File,'\n');
fprintf(File,'Final value of beta=%2.6f',beta);
beta_mat=[beta_mat,beta];
gama_total=(gama_D+gama_L*load_ratio)/(1+load_ratio);
safety_factor=gama_total/fai;
end
sh=[sh,beta_mat];
mat=[mat;sh];
end
fai_n=fai_n';
mat=mat';
beta_final=[fai_n,mat];
disp(beta_final)
xlswrite('beta_tang_american.xlsx',beta_final,'Sheet1')
%%%%%%%%%%%%%%%%%%%%%%%%%%%%%%%%%%%%%%%%%%%%%%%%%%%%%%%%
%%%%%%%%%%%%%%%%%%%%%%%%%%%%%%%%%%%%%%%%%%%%%%%%%%%%%%%%
target=[2.5,2.75,3,3.5];
matrix=beta_final;
x=matrix(:,1);
y1=matrix(:,2);
y2=matrix(:,3);
y3=matrix(:,4);
y4=matrix(:,5);
y5=matrix(:,6);
y6=matrix(:,7);
mat_final=[];
mat_final_w=[];
for i=1:length(target)
%*****
p1 = polyfit(x, log(y1), 1);
a1 = exp(p1(2));
b1 = p1(1);
x_new1=log(target(i)/a1)/b1;
%*****
p2 = polyfit(x, log(y2), 1);
a2 = exp(p2(2));
b2 = p2(1);
x_new2=log(target(i)/a2)/b2;
%*****
p3 = polyfit(x, log(y3), 1);
a3 = exp(p3(2));
b3 = p3(1);
x_new3=log(target(i)/a3)/b3;

```



```
%*****
p4 = polyfit(x, log(y4), 1);
a4 = exp(p4(2));
b4 = p4(1);
x_new4=log(target(i)/a4)/b4;
%*****
p5 = polyfit(x, log(y5), 1);
a5 = exp(p5(2));
b5 = p5(1);
x_new5=log(target(i)/a5)/b5;
%*****
p6 = polyfit(x, log(y6), 1);
a6 = exp(p6(2));
b6 = p6(1);
x_new6=log(target(i)/a6)/b6;
%*****
matrix_coff=[x_new1;x_new2;x_new3;x_new4;x_new5;x_new6];
mat_final=[mat_final,matrix_coff];
weight=[10;20;25;35;7;3];
weight_mat=matrix_coff.*weight;
mat_final_w=[mat_final_w,weight_mat];
end
xlswrite('beta_tang_american.xlsx',mat_final,'Sheet2')
fai_1=sum(mat_final_w(:,1))/100;
fai_2=sum(mat_final_w(:,2))/100;
fai_3=sum(mat_final_w(:,3))/100;
fai_4=sum(mat_final_w(:,4))/100;
fai_mat=[fai_1,fai_2,fai_3,fai_4];
xlswrite('beta_tang_american.xlsx',fai_mat,'Sheet3')
disp(mat_final)
disp(mat_final_w)
disp(fai_mat)
```

**E.13.4. Python script to extract load factor and deflection**

```
#!/usr/bin/python
from abaqusConstants import*
from odbAccess import*
import string
import sys, os
import glob
import time
import csv
x11=time.clock()
FOLDER="/home/sshayan/3_bay_irregular/"
os.chdir(FOLDER)
f=open('deflection_u2.txt','a')
l=open('LPF.txt','a')
timemanage=open('time.txt','a')
myodb=openOdb(path='/home/sshayan/3_bay_irregular/Frame_1.odb')
x1=time.clock()
val=myodb.steps['APPLY_LOAD'].historyRegions['Assembly
ASSEMBLY'].historyOutputs['LPF'].data
mynodeset=myodb.rootAssembly.nodeSets['MID_1']
i=0
length=len(val)
while i<length:
    LF1=val[i][1]
    Data=LF1
    Data=str(Data)
    l.write(Data)
    l.write('\n')
    i=i+1
i=0
steplen=len(myodb.steps['APPLY_LOAD'].frames)
while i<steplen:
    myU=myodb.steps['APPLY_LOAD'].frames[i].fieldOutputs['U']
    SubU=myU.getSubset(region=mynodeset)
    sum=0
    for val in SubU.values:
        sum=sum+val
    sum1=str(sum.data[1])
    f.write(sum1)
    f.write('\n')
    i=i+1
x2=time.clock()
timediff=x2-x1
print>>timemanage,timediff
myodb.close()
x22=time.clock()
timetime=x22-x11
print>>timemanage,timetime
timemanage.close()
```

## E.14. Practical application and design examples

The concept and the step-by-step application of the advanced analysis method for steel frame design have been presented in this thesis. The design procedure has been explained and can be grouped into four general steps: (1) load determination, (2) structural modelling, (3) analysis, and (4) limit state check. Five design examples are presented here to provide details of the application of the advanced analysis for practical design. These case studies cover regular and irregular sway frames subjected to both gravity and gravity plus wind combinations as well as braced frames with various joint types under gravity loading. Finally in each example, member sizes determined by advanced analysis are compared with those determined by conventional member-based LRFD design. All column bases are fully fixed. The beam-column connections are modeled as rigid for sway frames while both rigid and hinged joints are considered for braced frames. The influence of connection stiffness on the frame ultimate strength and its failure mode is ignored in this study.

One of the most common floor types is reinforced concrete slabs supported by a steel framing system. This type of construction is used in this study to determine the total dead load (see Figure E.37).

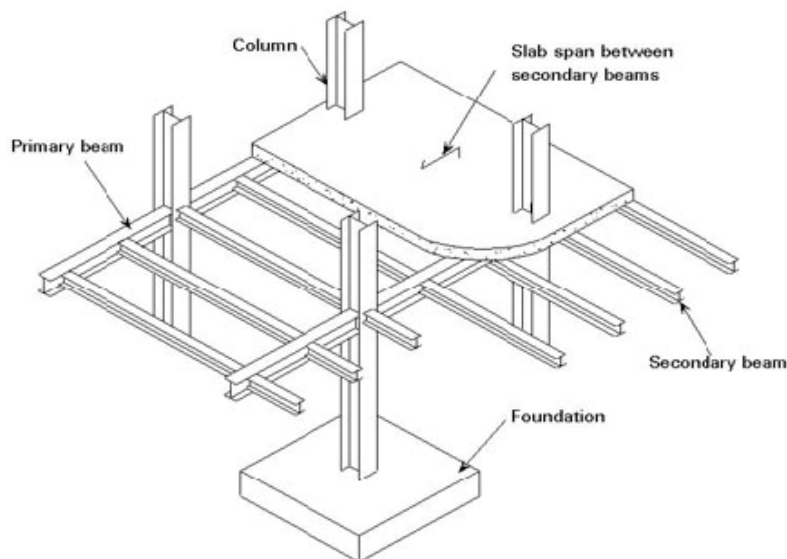


Figure E.37: Floor type

The slab thickness is taken as 200 mm and the distance between frames in the transverse direction is taken as 6m. The typical office live load of 3 kPa is used and the detailed load

calculations are presented in following section. The gravity loads are the same in all examples. For those frames subjected to gravity plus wind, the wind to gravity load ratio of 0.1 ( $W_n/(L_n + D_n) = 0.1$ ) is used, which is the most common case based on the calculation of wind loads for different regions (AISC 360-10).

#### *Load calculation*

Dead load:

Concrete density with reinforcement = 2500 kg/m<sup>3</sup>

Reinforced concrete slab depth = 200 mm

$g=10 \text{ m/s}^2$

Estimated reinforced concrete dead load =  $(2500 \times 10 \times (200/1000))/1000 = 5 \text{ kPa}$

Estimated uniform distributed dead load ( $D_n$ ) =  $5 \times 6 = 30 \text{ kN/m}$

Live load:

Office floor live load=3 kPa

Estimated uniform distributed live load ( $L_n$ ) =  $3 \times 6 = 18 \text{ kN/m}$

The summary of all studied frames including the frame size, support conditions, beam/column connections and load combinations is presented in Table E.77.

Table E.77: Summary of all studied frames

Frame	Type	Size	Support	Beam/column connection	Load combination
3-bay, 5-storey	Sway/regular	Large	Fixed	Rigid	Gravity
2-bay, 2-storey	Braced/regular	Medium	Fixed	Rigid	Gravity
2-bay, 2-storey	Braced/regular	Medium	Fixed	Hinged	Gravity
2-bay, 3-storey	Sway/regular	Medium	Fixed	Rigid	Gravity plus wind
4-bay, 2-storey	Sway/irregular	Medium	Fixed	Rigid	Gravity plus wind

In all examples, the frame is first analysed under applied loads to determine the internal actions using the second-order elastic analysis option of the commercial software of SAP 2000. Following the analysis, the frame is designed to the provisions of the AISC 360-10

Specification using the obtained internal actions. The frame thus initially designed is then modeled using finite element software capable of performing advanced analysis (here ABAQUS) and advanced analysis is conducted to determine the ultimate (collapse) strength of the frame ( $\lambda_n$ ). In addition the failure mode of the frame is obtained. Since all the members have been designed based on a structural Specification, the system ultimate strength is highly likely to satisfy the system design check ( $\lambda_n \geq 1/\phi_s=1.25$ ) but the design may be overly conservative. Subsequently, the frame is designed based on advanced analysis (without check or design of individual members based on a specification) and the system ultimate strength is determined. If the system capacity check is not satisfied (i.e.  $\lambda_n < 1.25$ ), the failed members will be re-proportioned and the frame will be reanalysed. This procedure will be repeated until  $\lambda_n \geq 1/\phi_s$ . The total steel weight is calculated for both cases and compared. Generally, designed-by-advanced-analysis leads to a lighter frame compared to those designed based on specifications. To achieve an optimum design, in both methods, the smallest possible member cross-sections are chosen, although a more practical design in which the member cross-sections in a multi-storey frame would not change in each storey is also considered.

### E.14.1. Example 1: Regular frame under gravity load

The first example is to design a 3-bay, 5-storey unbraced steel frame subjected to gravity. The frame configuration and loading patterns are presented in Figure E.38. The in-plane span length is 8m and the clear floor-to-floor height is 4m. The gravity load per unit of the length ( $w$ ) is 64.8 kN/m ( $1.2 \times 30 + 1.6 \times 18$ ). The roof load is considered as half of the typical floor load. For system based design check the system resistance factor of  $\phi_s=0.8$  is used. The 2D and 3D views of frame model in SAP 2000 is shown in Figure E.39.

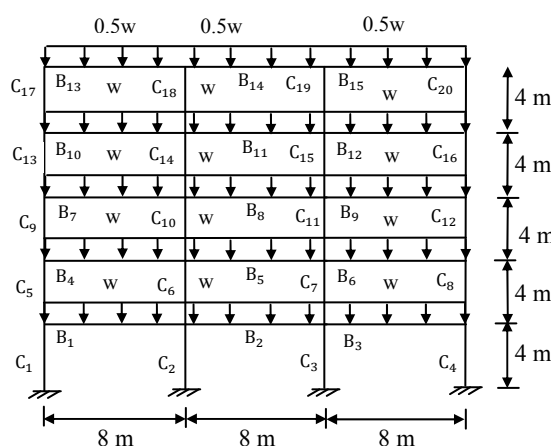


Figure E.38: Example 1, 3-bay, 5-storey frame

The frame second-order elastic analysis results obtained from SAP 2000 are presented in Figures E.40 to E.42. Figure E.40 shows the axial force diagram for the load shown in Figure E.38 and stated in the previous paragraph, followed by the in-plane bending moment and shear force diagram in Figure E.41 and Figure E.42, respectively. All units are in kN and meters.

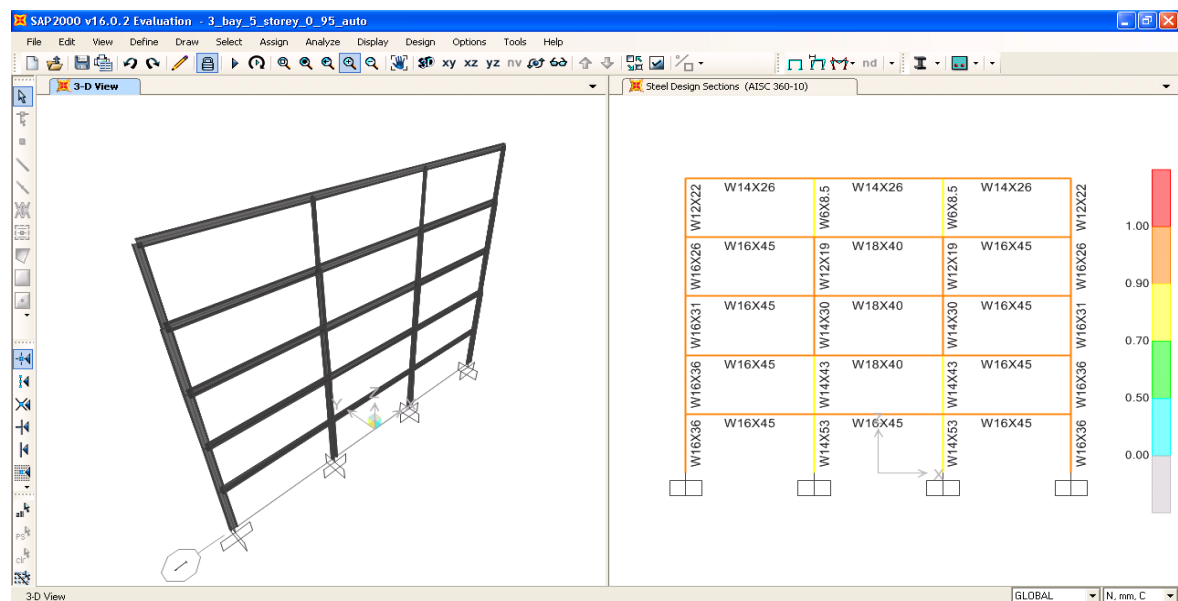


Figure E.39: 3-bay, 5-storey frame, SAP 2000 model

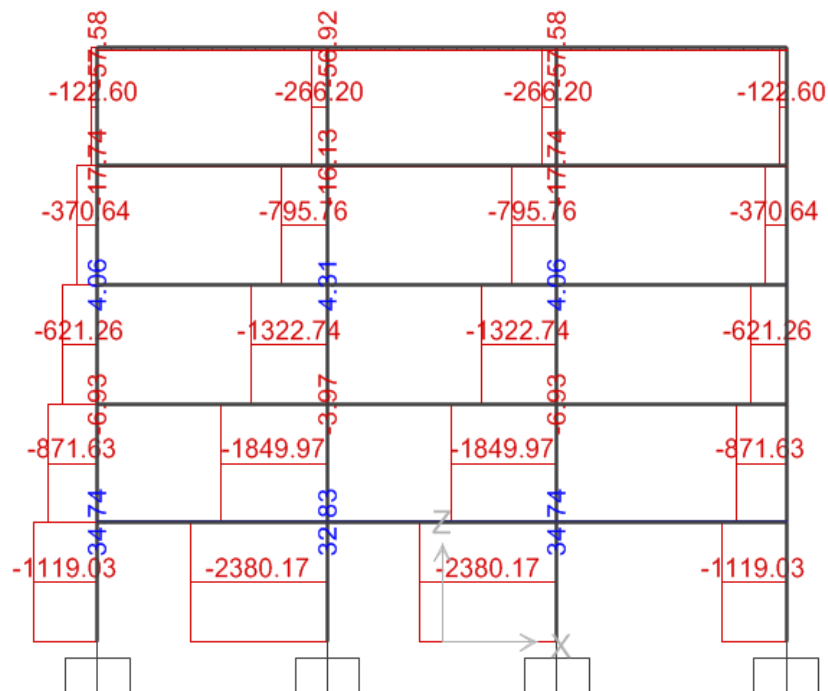


Figure E.40: 3-bay, 5-storey frame, 2<sup>nd</sup> order axial force diagram

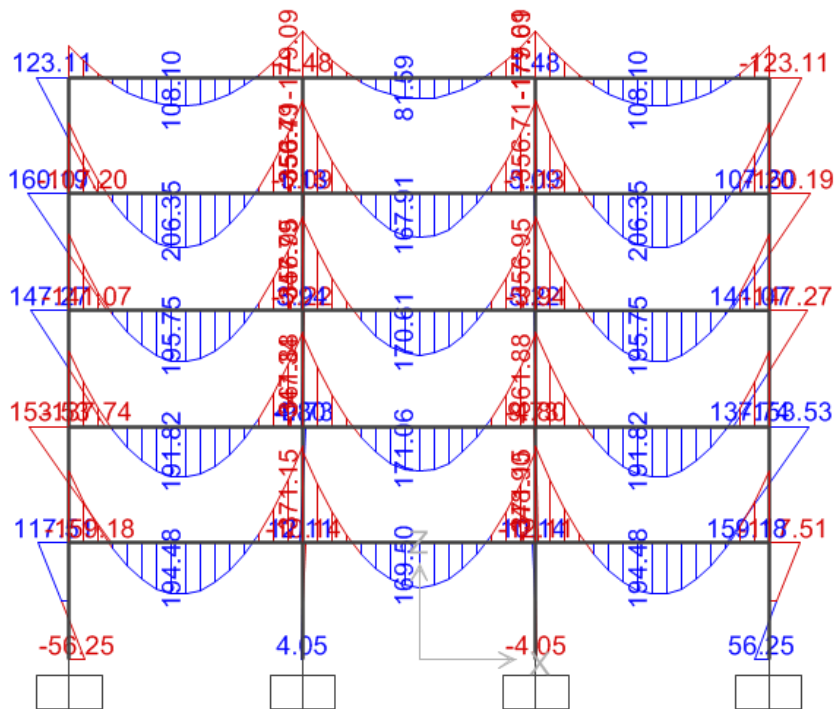


Figure E.41: 3-bay, 5-storey frame, in-plane 2<sup>nd</sup> order bending moment diagram

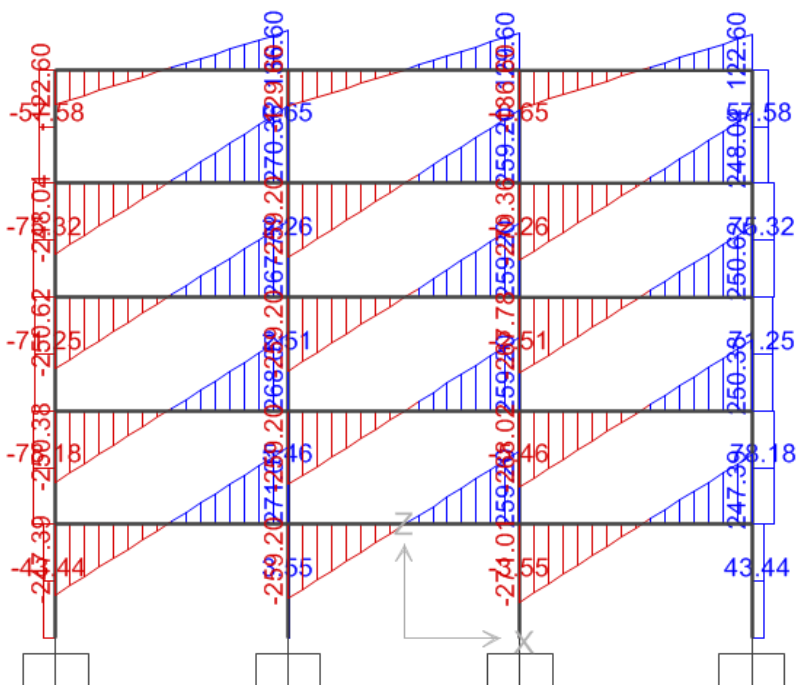


Figure E.42: 3-bay, 5-storey frame, 2<sup>nd</sup> order shear force diagram

In the next step, the members are design based on AISC 360-10 equations to satisfy flexure (in-plane bending), shear, axial force (compression or tension) and combined action capacity checks. The detailed design calculations of some selected members are presented in Section E.14.6. For all members, the combined flexure and axial force limit state was governing and the demand to capacity ratio which should be less than unity to have a safe design are presented in Figure E.43. The member cross-sections are summarized in Table E.79.

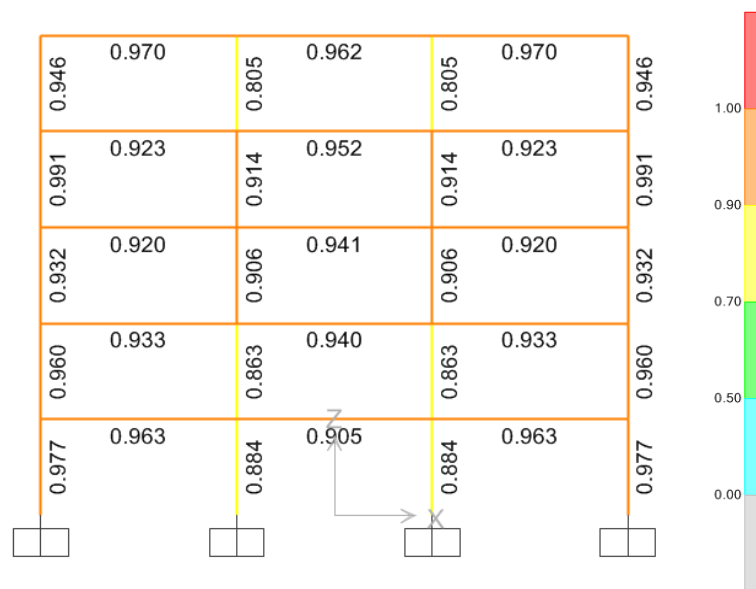


Figure E.43: 3-bay, 5-storey frame, demand to capacity ratios

The frame is then modeled in ABAQUS and an advanced analysis is run which accounts for both geometric and material nonlinearity. To model initial geometric imperfections, the linear superposition of the first 6 buckling modes is used as described in Chapter 5. Using Table 5.6, the scale factor for each mode ( $A_j$ ) can be obtained depending on whether the buckling modes are sway or non-sway. The first buckling modes as well as the scale factors are presented in Table E.78. The residual stress is modelled using the Glambos pattern (see Chapter 6) and applied uniformly to all members. The analysis result reveals that the frame fails by significant yielding of many inner columns and partially yielding of the beams as shown in Figure E.44. The ultimate load factor ( $\lambda_n$ ) obtained from advanced analysis for frame designed based on AISC 360-10 is equal to 1.26 which implies an adequate design.



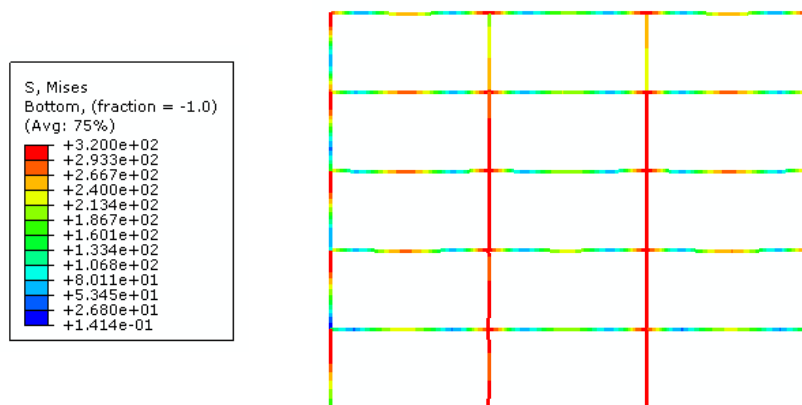
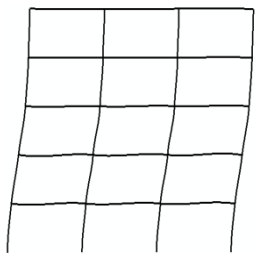
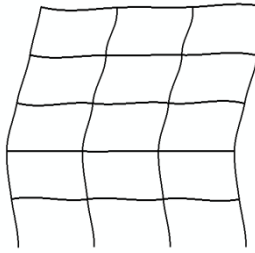
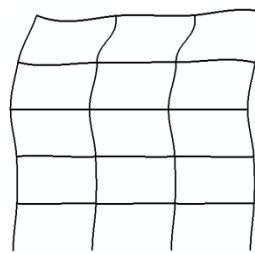
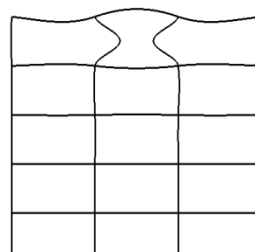
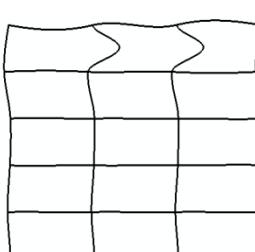
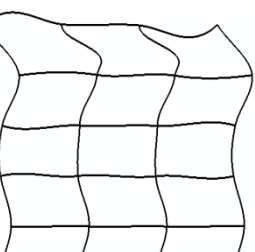


Figure E.44: 3-bay, 5-storey frame, ABAQUS failure mode

Table E.78: 3-bay, 5-storey frame, first six buckling modes

Mode 1	Mode 2	Mode 3
 <p>Sway, <math>L=H=20\text{m}</math>, <math>A_1=21.740</math></p>	 <p>Sway, <math>L=H=20\text{m}</math>, <math>A_2=5.060</math></p>	 <p>Non-sway, <math>L=h=4\text{m}</math>, <math>A_3=1.560</math></p>
Mode 4	Mode 5	Mode 6
 <p>Non-sway, <math>L=h=4\text{m}</math>, <math>A_3=1.556</math></p>	 <p>Non-sway, <math>L=h=4\text{m}</math>, <math>A_3=1.348</math></p>	 <p>Non-sway, <math>L=h=4\text{m}</math>, <math>A_3=1.440</math></p>

In the next step, the frame is designed based on advanced analysis. Before the analysis no separate check of member capacity needs to be carried out. A combination of member cross-sections are chosen based on engineering judgment and the analysis is run including both geometric and material nonlinearity. The ultimate load factor is equal to 1.25 which shows a safe design. The load versus vertical deflection of member B<sub>4</sub> is plotted in Figure E.45

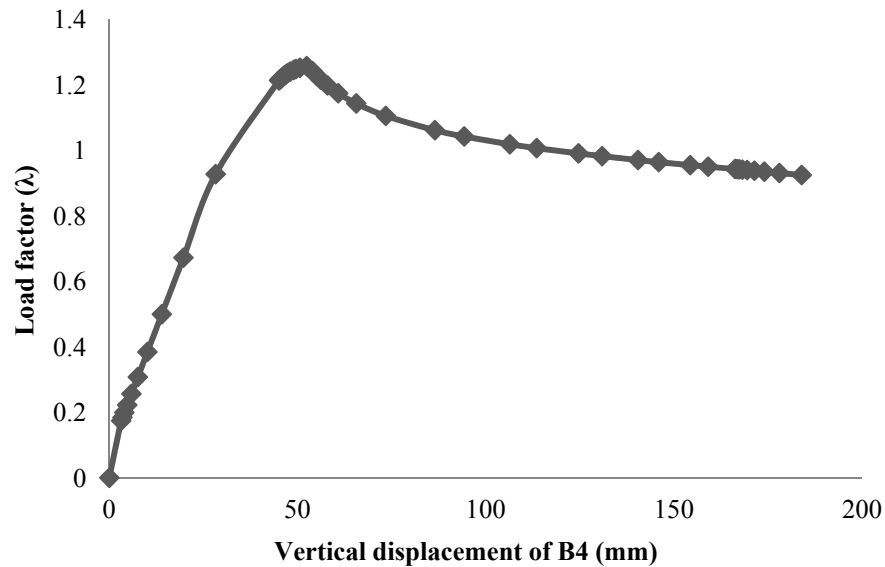


Figure E.45: 3-bay, 5-storey frame, load-deflection response

The member cross-sections obtained from this method of design are summarized in Table E.79 and compared with those determined based on AISC 360-10. The total steel weights in both cases are also presented. As mentioned before the design based on specification leads to a heavier steel structure compared to that obtained using system-based design (advanced analysis method) since all members are designed in their limits. But in reality not all the members are associated in the failure and hence the smaller sections can be chosen for them. Even for those members which participate in the failure, taking into account the effect of moment redistribution leads generally to smaller sections. Comparing the steel weights for both cases shows that the design obtained by the proposed direct method can save about 10.3% of steel in this particular case. Obviously, the more practical case in which the cross-sections are kept the same at least in two or three storeys and in all bays at a same level results in a larger ultimate load factor ( $\lambda_n$ ) and heavier structure since the sections are overestimated for some members.

Table E.79: Comparison of member-based and system-based design of 3-bay, 5-storey frame

Design method	Members	Sections	$\lambda_n$	Failure mode	Steel weight (ton)
Member-based design (AISC 360-10)  (Optimum sections)	$C_1, C_4, C_5, C_8$ $C_2, C_3$ $C_6, C_7$ $C_9, C_{12}$ $C_{10}, C_{11}$ $C_{13}, C_{16}$ $C_{14}, C_{15}$ $C_{17}, C_{20}$ $C_{18}, C_{19}$ $B_{10}, B_4, B_6, B_7, B_9, B_{10}, B_{12}$ $B_5, B_8, B_{11}$ $B_{13}, B_{14}, B_{15}$	W16×36 W14×53 W14×43 W16×31 W14×30 W16×26 W12×19 W12×22 W6×8.5 W16×45 W18×40 W14×26	1.26	Yielding of the columns and partially yielding of the beams	360.73
System-based design (proposed method)  (Optimum sections)	$C_1, C_4, C_5, C_8$ $C_2, C_3$ $C_6, C_7$ $C_9, C_{12}$ $C_{10}, C_{11}$ $C_{13}, C_{16}$ $C_{14}, C_{15}$ $C_{17}, C_{20}$ $C_{18}, C_{19}$ $B_1, B_3$ $B_2, B_4, B_6, B_7, B_9, B_{10}, B_{12}$ $B_5, B_8, B_{11}$ $B_{13}, B_{14}, B_{15}$	W16×31 W14×53 W14×43 W16×26 W14×30 W14×22 W12×19 W12×22 W6×8.5 W16×45 W16×36 W16×36 W14×22	1.25	Yielding of the columns and partially yielding of the beams	322.53
System-based design (proposed method)  (More practical sections)	$C_1, C_4, C_5, C_8, C_9, C_{12}$ $C_2, C_3, C_6, C_7, C_{10}, C_{11}$ $C_{13}, C_{16}, C_{17}, C_{20}$ $C_{14}, C_{15}, C_{18}, C_{19}$ $B_1, B_3$ $B_2, B_4, B_6, B_7, B_9, B_{10}, B_{12}$ $B_5, B_8, B_{11}$ $B_{13}, B_{14}, B_{15}$	W16×31 W14×53 W14×22 W12×19 W16×45 W16×36 W16×36 W14×22	1.25	Yielding of the columns and partially yielding of the beams	397.04

### E.14.2. Example 2: Regular rigid-jointed braced frame under gravity load

The second example is a 2-bay, 2-storey braced steel frame subjected to gravity. The frame configuration and loading patterns are presented in Figure E.46. Although it is common practice to design the connections in braced frames as cost-effective hinged connections, rigid connections may result in smaller beam sizes because the negative moments transferred from beams to columns usually lead to smaller positive moments near the mid-spans of beams. In high-rise braced frames, the space between building floors is costly and hence in some situations, rigid beam-column connections are used in

braced frame construction. Accordingly, for the braced frame shown in Figure E.46, both hinged and rigid beam-column connections are considered. The frame with rigid connections has been studied in this section while the results of hinged-joint frame are presented in the next example. The cross-bracing system is selected for both cases although the brace configuration appears to have no effect on the frame ultimate strength. The braces are connected to other members using hinged joints and their cross-sections are selected from equal-leg L-shape profiles. The frames are designed only for gravity loading since the gravity plus wind combination is not governing for these frames.

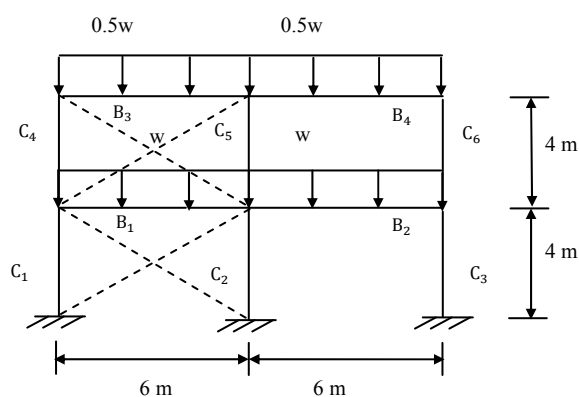


Figure E.46: Example 2, 2-bay, 2-storey braced frame with rigid joints

As in the previous example, the frame is first analysed by second-order elastic analysis and then designed according to AISC 360-10. The internal action diagrams including axial force, in-plane bending moment and shear force are presented in Figures E.47, E.48 and E.49, respectively. The effective length is the same as the actual length for all members since  $K$  is 1.0. Once again, for all members except the braces the combined axial force and bending moment limit state is governing. The demands to capacity ratio of all members are shown in Figure E.50. As it can be seen from the figure the ratios for the brace members are quite low. The reason is that according to Section E2 of AISC 360-10, for members designed on the basis of compression, the slenderness ratio  $KL/r$  preferably should not exceed 200. This limit leads to the larger section than needed based on ultimate strength checks. The details of the design based on AISC 360-10 for member  $B_2$  is presented in Section E.14.6. Subsequently, the frame designed based on the AISC specification is modeled into finite element software (ABAQUS) to determine the ultimate load factor by advanced analysis. The result is then compared with that obtained from the direct advanced analysis design method. The member cross-sections and

ultimate load factors of both methods are summarized in Table E.81. In both methods the sections are chosen optimally (minimum size) but at the same time the results are compared with the more practical case in which the sections do not change in every storey and every bay.

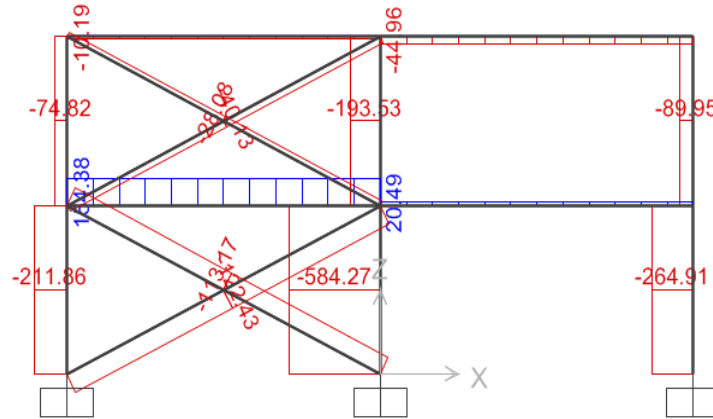


Figure E.47: 2-bay, 2-storey rigid-jointed braced frame, 2th order axial force diagram

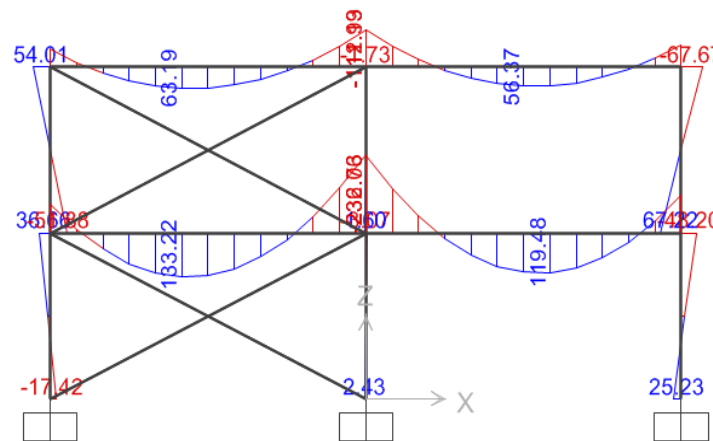


Figure E.48: 2-bay, 2-storey rigid-jointed braced frame, in-plane 2th order bending moment diagram

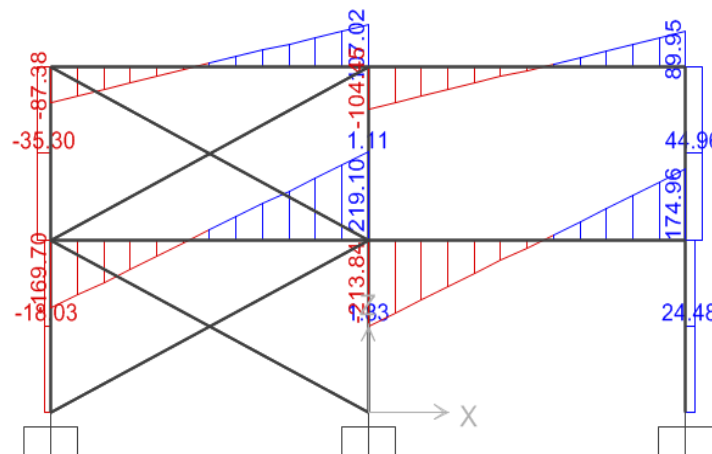


Figure E.49: 2-bay, 2-storey rigid-jointed braced frame, 2<sup>nd</sup> order shear force diagram

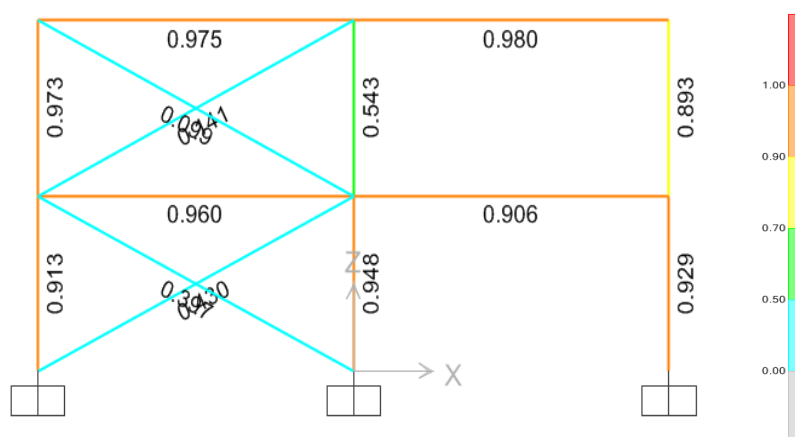


Figure E.50: 2-bay, 2-storey rigid-jointed braced frame, demand to capacity ratio

In the advanced analysis, the braces are considered perfect without any initial geometric imperfections. To avoid those modes in which the braces buckle, in the buckling analyses (but not in the inelastic analyses) the braces are modeled by applying a lateral restraint at each storey level. Table E.80 shows the first six buckling modes of the frame as well as the scale factors incorporated into the advanced analysis.

Table E.80: 2-bay, 2-storey rigid-joint braced frame, first six buckling modes

Mode 1	Mode 2	Mode 3
$L=h=4m, A_1=1.559$	$L=h=4m, A_2=1.467$	$L=h=4m, A_3=1.213$
Mode 4	Mode 5	Mode 6
$L=h=4m, A_4=1.175$	$L=h=4m, A_5=1.348$	$L=h=4m, A_6=1.049$

Table E.81: Comparison of member-based and system-based design of 2-bay, 2-storey rigid-jointed braced frame

Design method	Members	Sections	$\lambda_n$	Failure mode	Steel weight (ton)
Member-based design (AISC 360-10)  (Optimum sections)	$C_1, C_4$ $C_2$ $C_3, C_6$ $C_5$ $B_1, B_2$ $B_3, B_4$ Braces	W10×12 W8×13 W12×14 W6×8.5 W14×34 W12×19 L8×8×1/2	1.57	Yielding of the beams and partially yielding of the columns	32.60
System-based design (proposed method)  (Optimum sections)	$C_1, C_4$ $C_2$ $C_3, C_6$ $C_5$ $B_1, B_2$ $B_3, B_4$ Braces	W10×12 W8×13 W10×12 W6×8.5 W14×26 W12×19 L8×8×1/2	1.30	Yielding of the beams and partially yielding of the columns	30.32
System-based design (proposed method)  (More practical sections)	$C_1, C_4$ $C_2$ $C_3, C_6$ $C_5$ $B_1, B_2$ $B_3, B_4$ Braces	W10×12 W10×12 W10×12 W10×12 W14×26 W12×19 L8×8×1/2	1.30	Yielding of the beams and partially yielding of the columns	30.60

The load versus vertical displacement of member  $B_2$  is plotted in Figure E.51. Comparing the result of member-based and system-based design firstly shows a drop of 17.2% in  $\lambda_n$  taking into account the system effects are considered directly in the design. Lighter members achieved (7% less steel material). The frame failed by the full yielding of several beams and partial yielding of the columns. The ABAQUS failure mode is shown in Figure E.52.

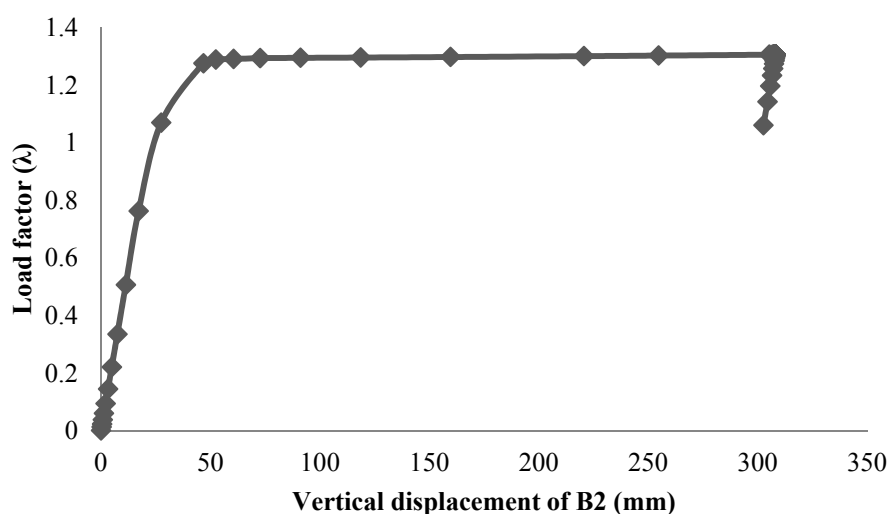


Figure E.51: 2-bay, 2-storey rigid-jointed braced frame, load-deflection

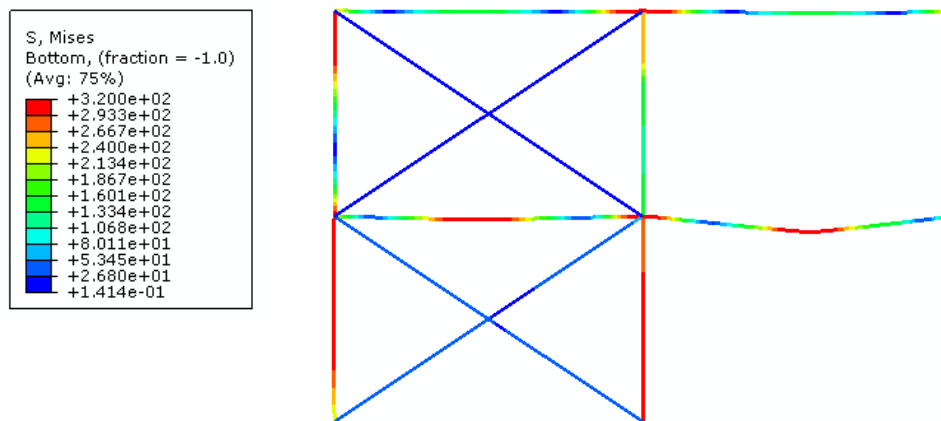


Figure E.52: 2-bay, 2-storey rigid-jointed braced frame, ABAQUS failure mode

### E.14.3. Example 3: Regular hinged-jointed braced frame under gravity load

This example is the same as the previous example, i.e. a 2-bay, 2-storey braced steel frame subjected to gravity loads but with hinged beam-column connections. The internal actions obtained from the elastic second-order analysis are shown in Figures E.53 to E.55. As can be seen from the bending moment diagram, since the beam-column connections are hinged, there is no moment transfer from beams to columns. The demand to capacity ratio for all members is presented in Figure E.56. Member cross-sections and the ultimate load factors from both the member-based and system-based design methods are summarized in Table E.82. The ultimate load factors ( $\lambda_n$ ) using both methods are same and equal to 1.31 which implies safe designs. Since the beams are simply supported, the system effects and moment redistributions do not change the design significantly. Hence, the member-based and system-based design methods lead to the same cross-sections and there is no difference in material use.

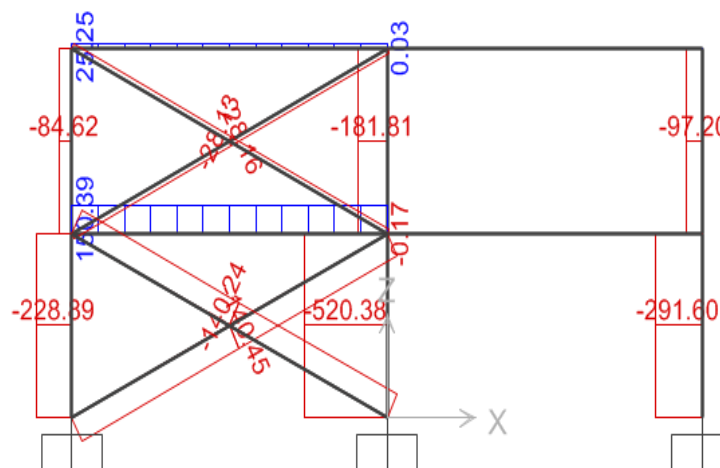


Figure E.53: 2-bay, 2-storey hinged-jointed braced frame, 2th order axial force diagram



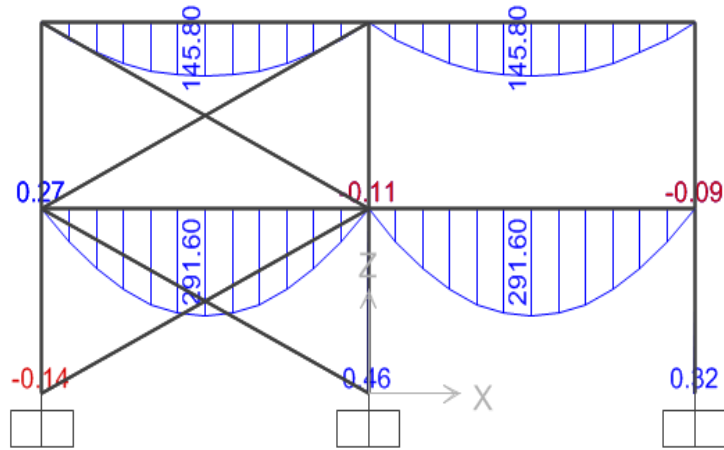


Figure E.54: 2-bay, 2-storey hinged-jointed braced frame, in-plane 2<sup>nd</sup> order bending diagram

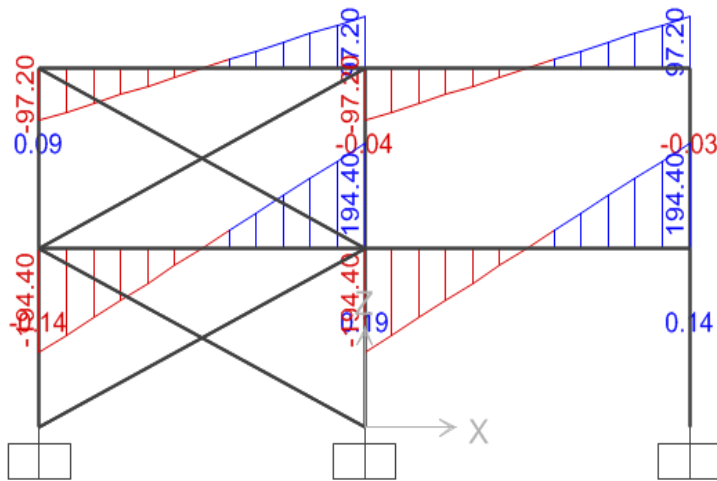


Figure E.55 2-bay, 2-storey hinged-jointed braced frame, 2<sup>nd</sup> order shear force diagram

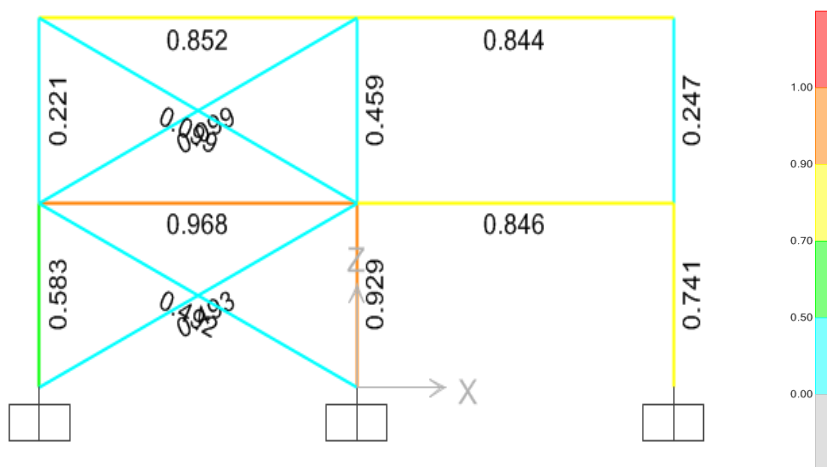


Figure E.56: 2-bay, 2-storey hinged-jointed braced frame, demand to capacity ratio

Table E.82: Comparison of member-based and system-based design of 2-bay, 2-storey hinged-jointed braced frame

Design method	Members	Sections	$\lambda_n$	Failure mode	Steel weight (ton)
Member-based design (AISC 360-10)  (Optimum sections)	$C_1, C_3, C_4, C_5, C_6$ $C_2$ $B_1$ $B_2$ $B_3, B_4$ Braces	W6×8.5 W6×12 W18×35 W16×40 W10×30 L8×8×1/2	1.31	Yielding of the beams and partially yielding of the columns	33.75
System-based design (proposed method)  (Optimum sections)	$C_1, C_3, C_4, C_5, C_6$ $C_2$ $B_1$ $B_2$ $B_3, B_4$ Braces	W6×8.5 W6×12 W18×35 W16×40 W10×30 L8×8×1/2	1.31	Yielding of the beams and partially yielding of the columns	33.75
System-based design (proposed method)  (More practical sections)	$C_1, C_3, C_5, C_6$ $C_2, C_4$ $B_1, B_2$ $B_3, B_4$ Braces	W6×8.5 W6×12 W16×40 W10×30 L8×8×1/2	1.31	Yielding of the beams and partially yielding of the columns	34.72

The first six buckling modes of the frame and the scale factors which need to be applied to each mode to model initial geometric imperfection in advanced analysis are presented in Table E.83. The load versus vertical deflection of member  $B_2$  is plotted in Figure E.57. The failure mode of the frame for all cases is full yielding of the beams and partial yielding of the columns. The ABAQUS frame failure mode is presented in Figure E.58.

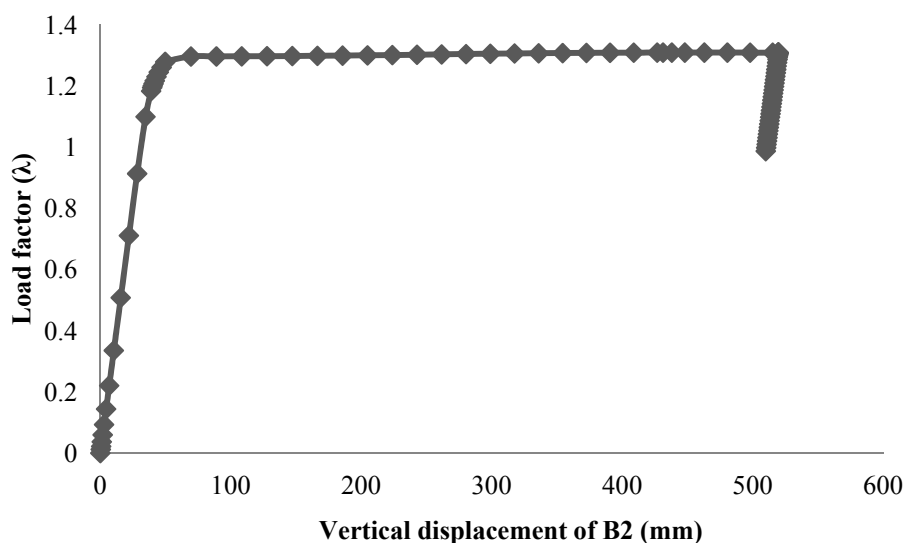
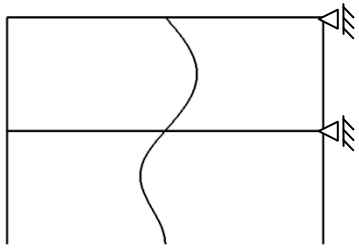
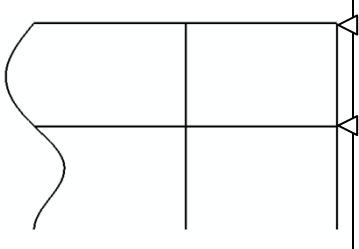
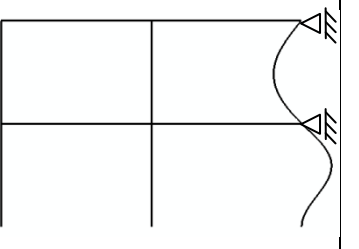
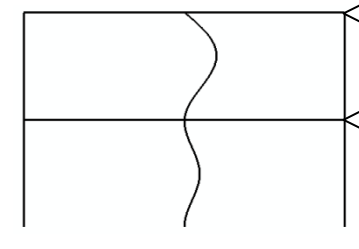
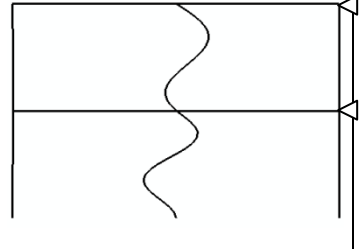
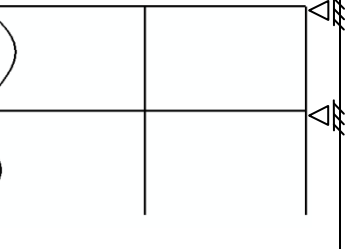


Figure E.57: 2-bay, 2-storey hinged-jointed braced frame, load-deflection response

Table E.83: 2-bay, 2-storey hinged-jointed braced frame, first six buckling modes

Mode 1	Mode 2	Mode 3
		
$L=h=4\text{m}, A_1=1.559$	$L=h=4\text{m}, A_1=1.467$	$L=h=4\text{m}, A_1=1.213$
Mode 4	Mode 5	Mode 6
		
$L=h=4\text{m}, A_1=1.175$	$L=h=4\text{m}, A_1=1.348$	$L=h=4\text{m}, A_1=1.049$

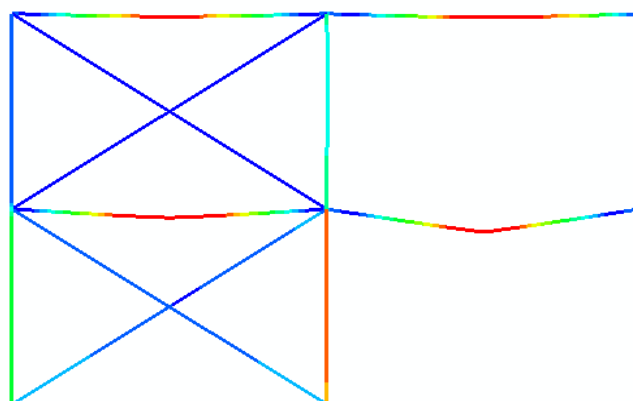
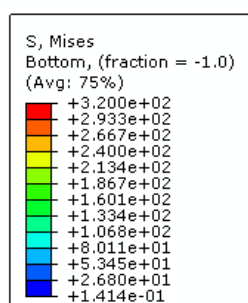


Figure E.58: 2-bay, 2-storey hinged-jointed braced frame, ABAQUS failure mode

#### E.14.4. Example 4: Regular frame under combined gravity and wind

In addition to frames subjected to gravity loading, two medium size steel frames under combined gravity and wind loading are studied in this report. The first frame is a 2-bay, 3-storey regular frame with 6m bays and 4m storey height. The gravity load per unit of

the length ( $w$ ) is 45 kN/m ( $1.2 \times 30 + 0.5 \times 18$ ). The roof load is considered as half of the typical floor load. The wind load is taken as 10% of the total gravity load and has been applied as point loads at each storey level with the roof load being half of the other storey loads. The frame configuration and loadings are presented in Figure E.59. The internal actions obtained from the second-order elastic analysis of SAP 2000 are presented in Figures E.60 to E.62. The demand to capacity ratio for the combined flexure and axial force limit state, which is governing, is presented in Figure E.63.

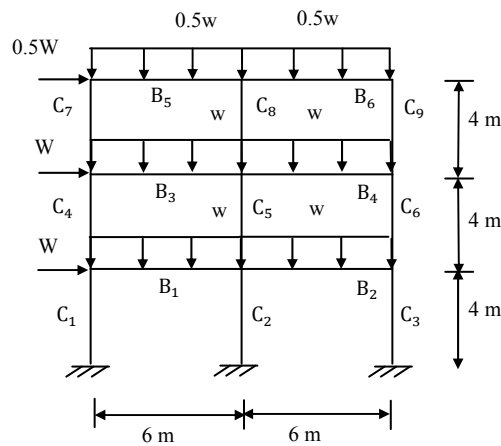


Figure E.59: 2-bay, 3-storey sway frame subjected gravity and wind loads

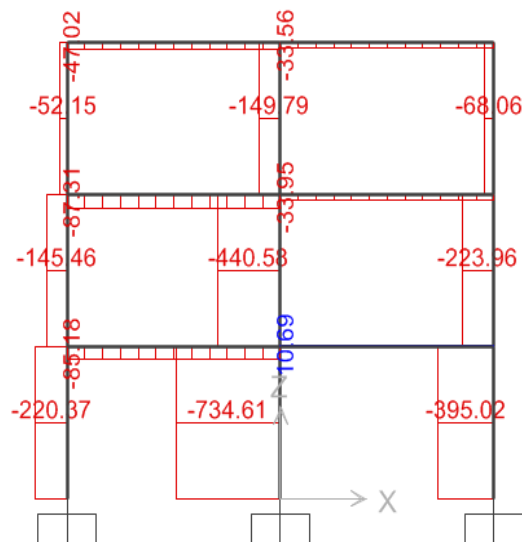


Figure E.60: 2-bay, 3-storey sway frame, 2<sup>nd</sup> order axial force diagram

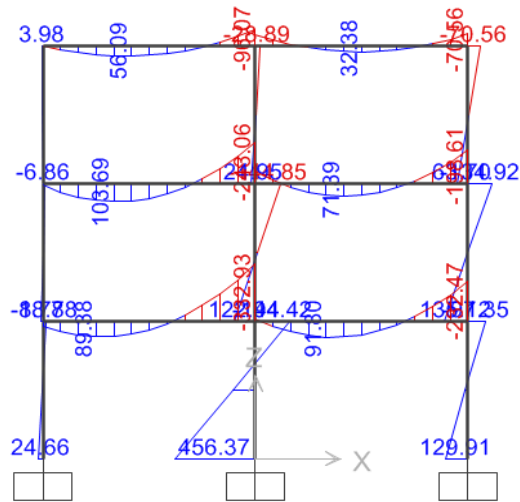


Figure E.61: 2-bay, 3-storey sway frame, 2<sup>nd</sup> order bending moment diagram

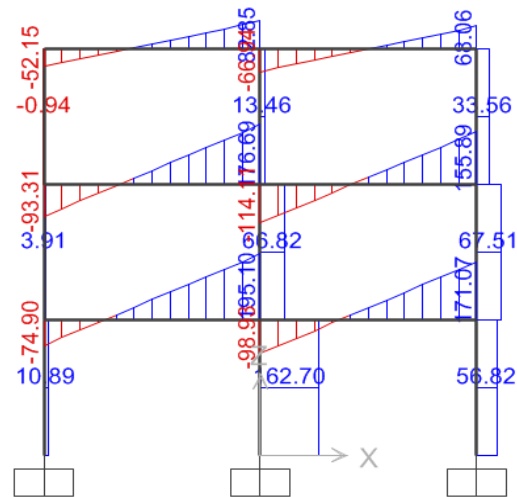


Figure E.62: 2-bay, 3-storey sway frame, 2<sup>nd</sup> order shear force diagram

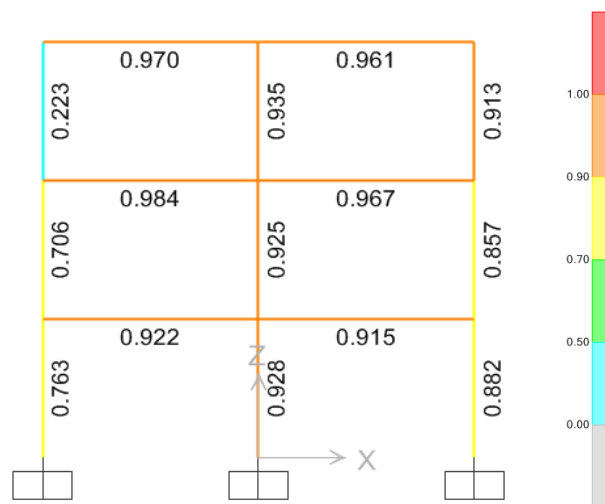


Figure E.63: 2-bay, 3-storey sway frame, demand to capacity ratio

Like the previous examples, the frame is first designed based on AISC 360-10 and subsequently modeled in ABAQUS to check its capacity ( $\lambda_n$ ) by running advanced analysis. The member cross-sections are presented in Table 11. The first six eigen buckling modes and the scale factors to model initial geometric imperfection are presented in Table E.84. To determine the ultimate load factor for frames subject to gravity and wind, the analysis is carried out in two separate steps. In the first step, the gravity loads are applied to the frame and a static pushdown analysis is performed. Once the deformed shape of the frame under gravity loading is obtained, a static lateral pushover analysis is conducted (under constant gravity loads) by increasing the nominal wind load by the factor  $\lambda$  until failure occurs at  $\lambda_n$ . The frame ultimate load is equal to 1.35 and the failure mode is frame sway with yielding of the beams and columns.

In the next step the frame is designed by advanced analysis and with a 6% lighter steel frame the ultimate load factor drops to 1.25. It should be mentioned that applying the gravity load first and then the wind load reflected the actual load sequence, since in reality the gravity loads are permanently present on the structure while wind has a return period. If the lateral and vertical loads are applied simultaneously in a single step, it results in smaller value of ultimate load factor equal to 1.158 (7.26% less). The results for a more practical frame with same cross-sections in several storeys and bays designed by advanced analysis are also presented in Table E.85.

Table E.84: 2-bay, 3-storey sway frame, first six buckling modes

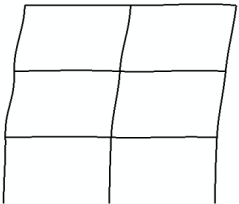
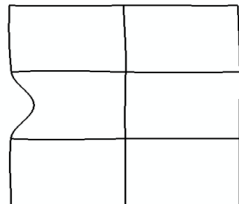
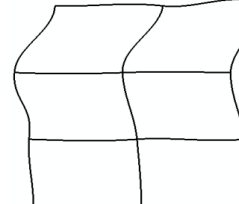
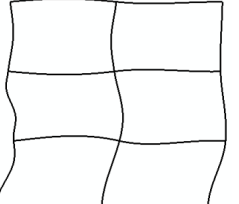
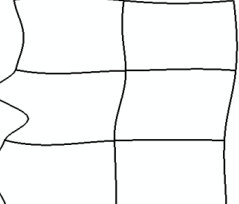
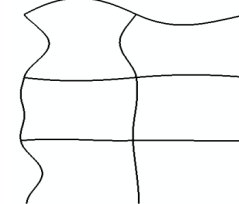
Mode 1	Mode 2	Mode 3
		
$L=h=12\text{m}, A_1=13.044$	$L=h=4\text{m}, A_1=1.012$	$L=h=12\text{m}, A_1=4.680$
Mode 4	Mode 5	Mode 6
		
$L=h=4\text{m}, A_1=1.556$	$L=h=4\text{m}, A_1=1.348$	$L=h=4\text{m}, A_1=1.440$

Table E.85: Comparison of member-based and system-based design of 2-bay, 3-storey sway frame

Design method	Members	Sections	$\lambda_n$	Failure mode	Steel weight (ton)
Member-based design (AISC 360-10)  (Optimum sections)	$C_1$ $C_2$ $C_3, C_6$ $C_4, C_7$ $C_5,$ $C_8$ $C_9$ $B_1$ $B_2, B_3$ $B_4$ $B_5$ $B_6$	W10×12 W24×55 W12×26 W6×8.5 W12×30 W8×10 W12×14 W18×40 W16×31 W16×26 W10×19 W10×15	1.35	Sway (Yielding of the columns and yielding of the beams)	37.5
System-based design (proposed method)  (Optimum sections)	$C_1$ $C_2$ $C_3, C_6$ $C_4, C_7$ $C_5,$ $C_8$ $C_9$ $B_1$ $B_2, B_3$ $B_4$ $B_5$ $B_6$	W8×10 W24×55 W12×26 W6×8.5 W12×30 W8×10 W12×14 W18×35 W16×26 W14×22 W10×19 W10×15	1.25	Sway (Yielding of the columns and yielding of the beams)	35.25
System-based design (proposed method)  (More practical sections)	$C_1$ $C_2$ $C_3, C_6$ $C_4, C_7$ $C_5,$ $C_8$ $C_9$ $B_1$ $B_2$ $B_3, B_4$ $B_5, B_6$	W16×26 W24×55 W16×26 W16×26 W12×30 W12×30 W16×26 W18×35 W18×35 W16×26 W10×19	1.96	Sway (Yielding of the columns and yielding of the beams)	46.18

The load-deflection response and the ABAUS failure mode of the frame designed by advanced analysis are plotted in Figure E.64 and Figure E.65, respectively. As it can be seen from Figure E.65, the failure mode of the frame is sway with yielding of the beams and columns, i.e. same as for the frame designed based on the specification.

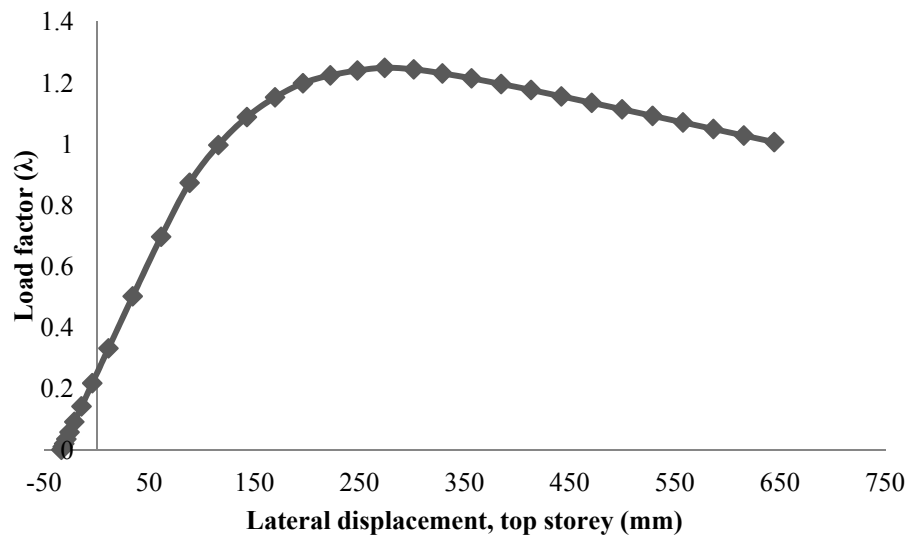


Figure E.64: 2-bay, 3-storey sway frame, load versus top storey lateral deflection

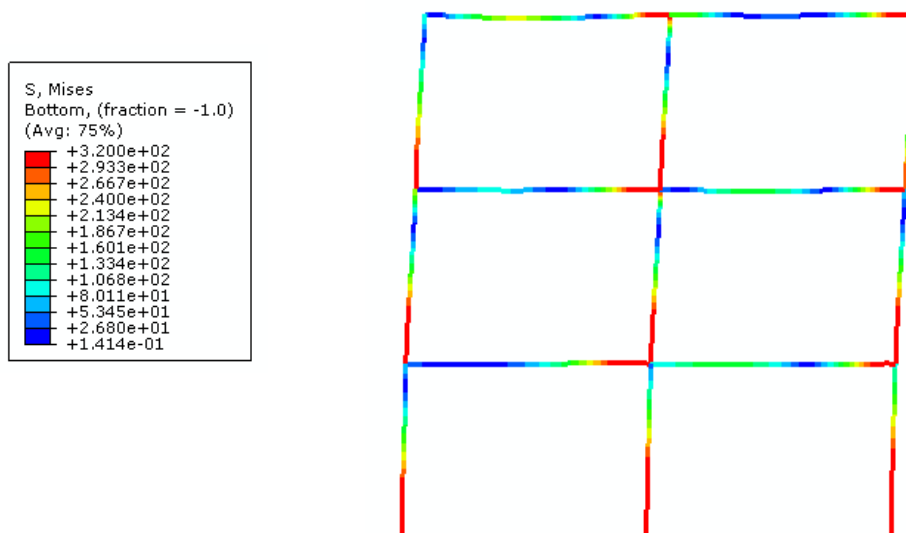


Figure E.65: 2-bay, 3-storey sway frame, ABAQUS failure mode

### E.14.5. Example 5: Irregular frame under combined gravity and wind loading

The last frame is an irregular medium size steel frame subjected to gravity and wind loading. The frame configuration and loading pattern are shown in Figure E.66. The axial force diagram, bending moment diagram and shear force diagram are presented in Figures



E.67, E.68 and E.69 respectively, as obtained from a 2<sup>nd</sup> order elastic analysis. The demand to capacity ratios of all members are shown in Figure E.70.

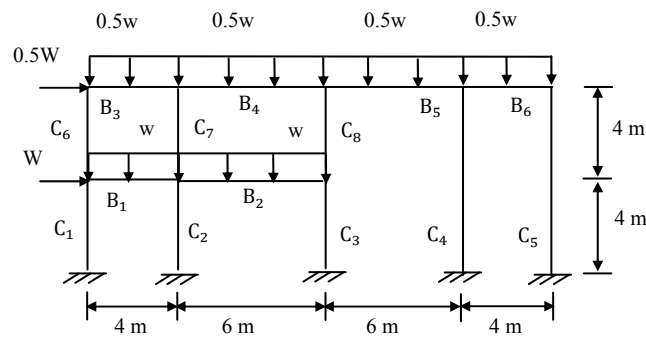


Figure E.66: 4-bay, 2-storey irregular sway frame

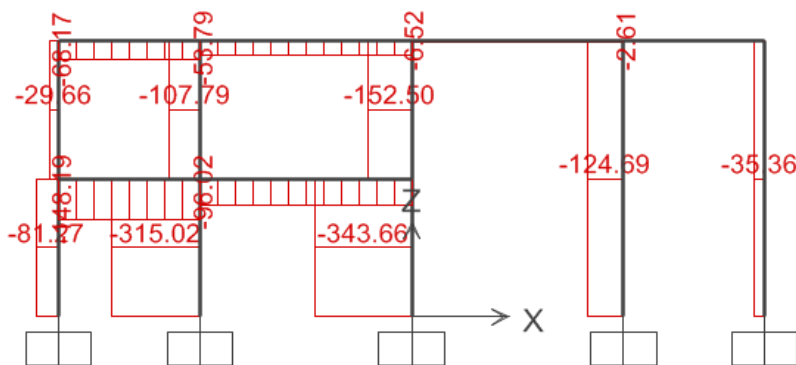


Figure E.67: 4-bay, 2-storey irregular sway frame, 2<sup>nd</sup> order axial force diagram

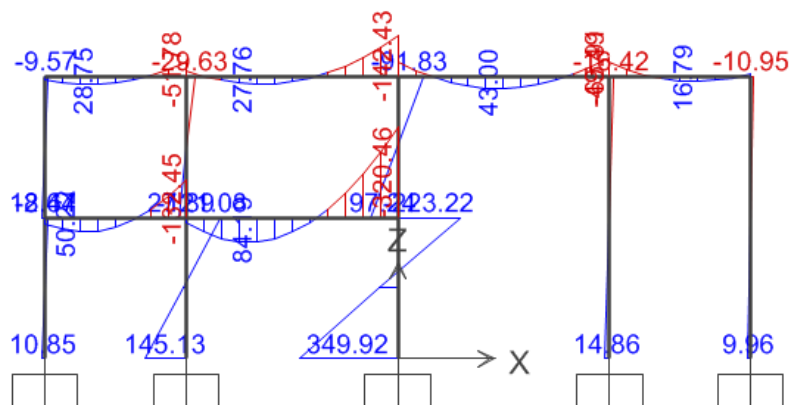


Figure E.68: 4-bay, 2-storey irregular sway frame, 2<sup>nd</sup> order in-plane bending moment diagram

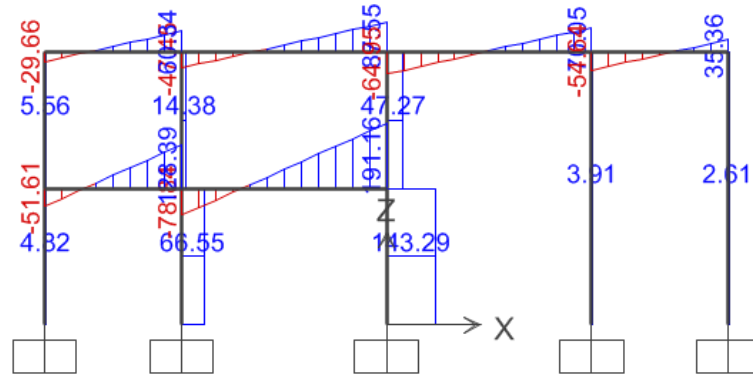


Figure E.69: 4-bay, 2-storey irregular sway frame, 2<sup>nd</sup> order shear force diagram

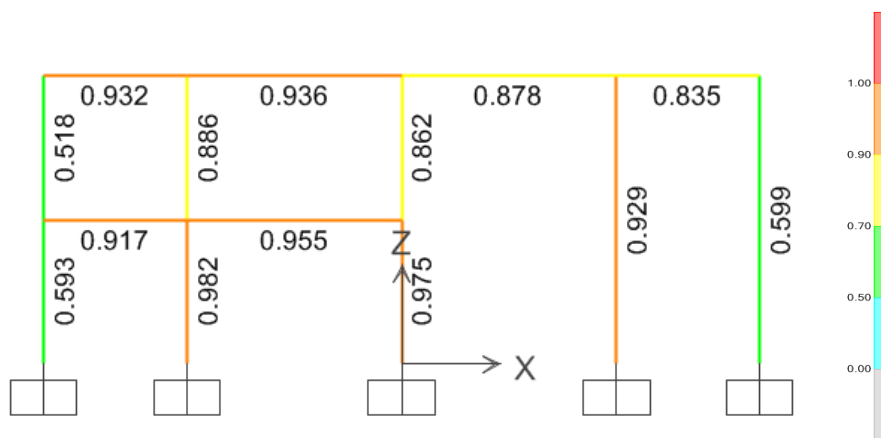


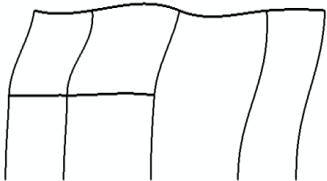
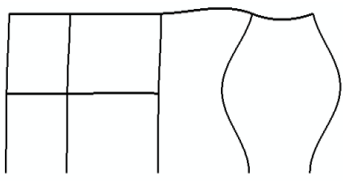
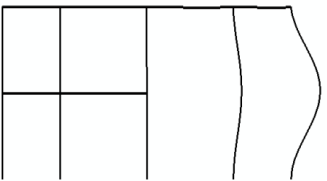
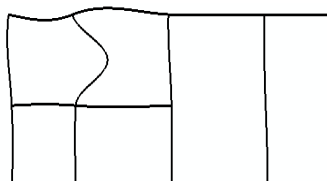
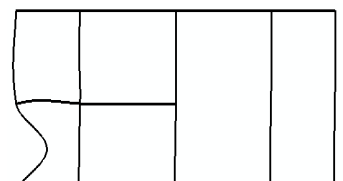
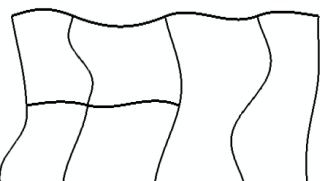
Figure E.70: 4-bay, 2-storey irregular sway frame, demand to capacity ratio

The member-based design is compared with system-based design for both cases of optimum sections and a more practical choice of cross-sections in Table E.86. The advanced analysis of the frame designed based on the code results in the ultimate load factor of 1.40. The ultimate load factor drops to 1.26 when the frame is designed by advanced analysis which leads to an 8.2% lighter frame compared to design based on AISC 360-10. The ultimate load factor for the more practical frame is 1.40. The failure mode is sway with beam and column yielding for all the cases. The first six buckling modes of the frame and the corresponding scale factor of each mode for modeling initial geometric imperfections are presented in Table E.87. The load-deflection response of the frame and the ABAQUS failure mode are shown in Figures E.71 and E.72, respectively.

Table E.86: Comparison of member-based and system-based design of 4-bay, 2-storey irregular sway frame

Design method	Members	Sections	$\lambda_n$	Failure mode	Steel weight (ton)
Member-based design (AISC 360-10)  (Optimum sections)	$C_1, C_5, C_6$ $C_2$ $C_3$ $C_4, C_7$ $C_8$ $B_1, B_4$ $B_2$ $B_3, B_6$ $B_5$	W6×8.5 W12×26 W16×45 W6×12 W10×12 W14×22 W16×40 W10×12 W10×15	1.40	Sway (Yielding of the columns and yielding of the beams)	26.62
System-based design (proposed method)  (Optimum sections)	$C_1, C_5, C_6$ $C_2$ $C_3$ $C_4$ $C_7$ $C_8$ $B_1, B_4$ $B_2$ $B_3, B_5, B_6$	W6×8.5 W12×26 W16×45 W6×12 W6×9 W10×12 W12×19 W16×36 W10×12	1.26	Yielding of the beams and partially yielding of the columns	24.42
System-based design (proposed method)  (More practical sections)	$C_1, C_4, C_5, C_6$ $C_2, C_7$ $C_3, C_8$ $B_1, B_3$ to $B_6$ $B_2$	W6×8.5 W12×19 W16×31 W12×19 W14×30	1.41	Yielding of the beams and partially yielding of the columns	26.98

Table E.87: 2-bay, 2-storey rigid-joint braced frame, first six buckling modes

Mode 1	Mode 2	Mode 3
		
$L=h=12\text{m}, A_1=13.044$	$L=h=4\text{m}, A_2=1.012$	$L=h=12\text{m}, A_3=4.680$
Mode 4	Mode 5	Mode 6
		
$L=h=4\text{m}, A_4=1.556$	$L=h=4\text{m}, A_5=1.348$	$L=h=4\text{m}, A_6=1.440$

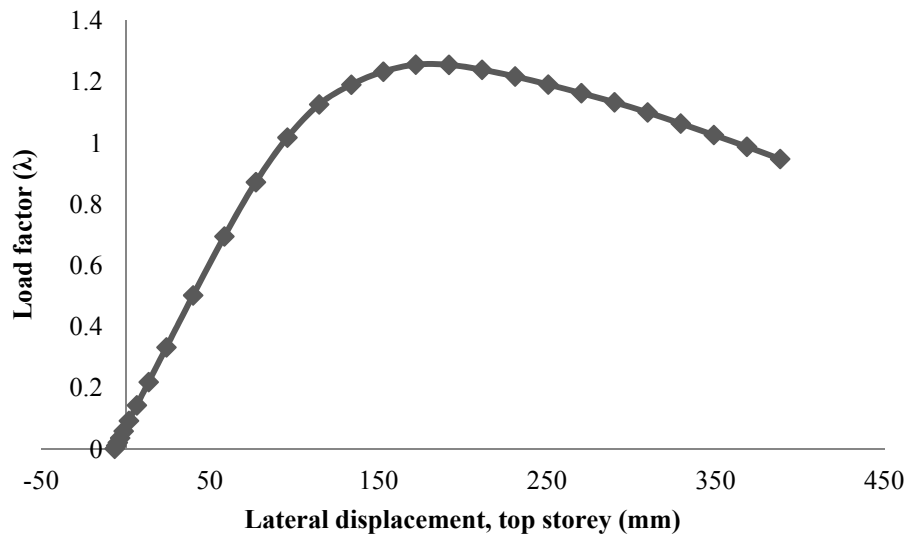


Figure E.71: 4-bay, 2-storey irregular sway frame, load deflection response

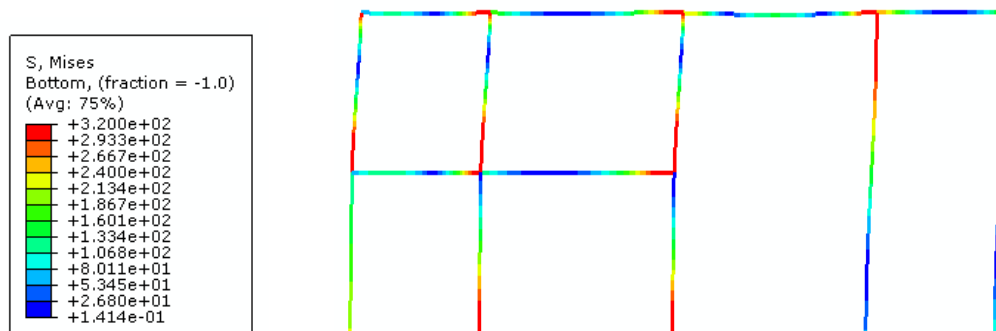


Figure E.72: 4-bay, 2-storey irregular sway frame, ABAQUS failure mode

### E.14.6. Details of selected member design based on AISC360-10

#### 3-bay, 5-storey frame, C3

------(Design Summary)-----

AISC 360-10 Steel Section Check  
 Provision : LRFD  
 Analysis : General Second Order

Type : Column, 2D  
 Member Label : C03  
 Section : W14x53  
 Class : Compact  
 Member length = 4000.0 mm

------(Section Properties)-----

## Appendix E

---

A = 10064.496 mm<sup>2</sup>  
I<sub>x</sub> = 225181201.250 mm<sup>4</sup>  
I<sub>y</sub> = 24016553.257 mm<sup>4</sup>  
r<sub>x</sub> = 149.606 mm  
r<sub>y</sub> = 48.768 mm  
S<sub>x</sub> = 1274913.579 mm<sup>3</sup>  
S<sub>y</sub> = 234335.015 mm<sup>3</sup>  
Z<sub>x</sub> = 1427313.274 mm<sup>3</sup>  
Z<sub>y</sub> = 360515.408 mm<sup>3</sup>  
E = 200000.000 Mpa  
F<sub>y</sub> = 320.000 Mpa  
F<sub>y</sub> = 440.000 Mpa

------(Internal Moment and Forces)-----

P<sub>u</sub> = -2388.027 kN    M<sub>ux</sub> = 8.194 kN.m    M<sub>uy</sub> = 0.000 kN.m    V<sub>ux</sub> = 2.814 kN    V<sub>uy</sub> = 0.000 kN

------(Flexure (Bending))-----

Clause F2, Nominal flextural strength (M<sub>n</sub>) is the lowest value obtained according to the limit states stress of

- (a) yielding
- (b) lateral-torsional buckling
- (c) flange local buckling
- (d) web local buckling

\*\*Frame is 2D, No lateral torsional buckling

\*\*Cross-section is Compact, No local buckling

$$\begin{aligned}\phi \times M_{nx} &= \phi \times F_y \times Z_x < \phi \times 1.5 \times F_y \times S_x \\ &= 0.9 \times 320.000 \times 1427313.274 < 0.9 \times 1.5 \times 320.000 \times 1274913.579 \\ &= 411.066 \text{ kN.m} < 550.763 \text{ kN.m} \quad \text{ok} \\ &= 411.066 \text{ kN.m}\end{aligned}$$

------(Axial (Compression))-----

Clause E3, 2D frame only buckling about x-axis

K = 1.0 according to Section C2

$$\begin{aligned}F_e &> 0.44F_y \\ 2761.263 &> 140.800\end{aligned}$$

$$\begin{aligned}F_{cr} &= 0.658 \wedge (F_y/F_e) \times F_y \\ &= 304.849\end{aligned}$$

$$\begin{aligned}\phi \times P_n &= \phi \times F_{cr} \times A_g \\ &= 2761.334 \text{ kN}\end{aligned}$$

------(Shear)-----

Clause G2

C<sub>v</sub> = 1

$$\begin{aligned}\phi \times V_n &= \phi \times 0.6 \times F_y \times A_w \times C_v \\ &= 637.067 \text{ kN}\end{aligned}$$

------(Combined action (Axial and Bending))-----

## Appendix E

---

Clause H1, Doubly symmetric member subject to flexure and compression

$$P_u/(\phi P_n) > 0.2 \quad (P_u/(\phi P_n)) + (8/9) \times (M_{ux}/(\phi M_{nx})) < 1.0$$

Demand/Capacity Ratio :

$$0.865 + 0.018 = 0.884 < 1.0$$

------(Summary of Demand to Capacity (Design) ratios)-----

Flexure: 0.020

Axial: 0.865

Shear: 0.00442

Combined action: 0.884

\*\* Combined bending and axial force is governing failure mode

### A.2 2-bay, 2-storey rigid-joint braced frame, B2

------(Design Summary)-----

AISC 360-10 Steel Section Check

Provision : LRFD

Analysis : General Second Order

Type : Beam, 2D

Member Label : B02

Section : W14x34

Class : Compact

Member length = 6000.0 mm

------(Section Properties)-----

$$A = 6451.600 \text{ mm}^2$$

$$I_x = 141518684.704 \text{ mm}^4$$

$$I_y = 9698192.216 \text{ mm}^4$$

$$r_x = 148.082 \text{ mm}$$

$$r_y = 38.862 \text{ mm}$$

$$S_x = 796411.310 \text{ mm}^3$$

$$S_y = 113234.612 \text{ mm}^3$$

$$Z_x = 894733.694 \text{ mm}^3$$

$$Z_y = 173702.878 \text{ mm}^3$$

$$E = 200000.000 \text{ Mpa}$$

$$F_y = 320.000 \text{ Mpa}$$

$$F_y = 440.000 \text{ Mpa}$$

------(Internal Moment and Forces)-----

$$P_u = 20.740 \text{ kN} \quad M_{ux} = 232.018 \text{ kN.m} \quad M_{uy} = 0.000 \text{ kN.m} \quad V_{ux} = 213.832 \text{ kN} \quad V_{uy} = 0.000 \text{ kN}$$

------(Flexure (Bending))-----

Clause F2, Nominal flexural strength ( $M_n$ ) is the lowest value obtained according to the limit states stress of

(a) yielding

(b) lateral-torsional buckling

(c) flange local buckling

(d) web local buckling

\*\*Frame is 2D, No lateral torsional buckling

\*\*Cross-section is Compact, No local buckling

$$\begin{aligned}\phi \times M_{nx} &= \phi \times F_y \times Z_x < \phi \times 1.5 \times F_y \times S_x \\ &= 0.9 \times 320.000 \times 894733.694 < 0.9 \times 1.5 \times 320.000 \times 796411.310 \\ &= 257.683 \text{ kN.m} < 344.050 \text{ kN.m} \quad \text{ok} \\ &= 257.683 \text{ kN.m}\end{aligned}$$

------(Axial (Tension))-----

Clause D2, Tensile yielding

$$\begin{aligned}\phi \times P_n &= \phi \times F_y \times A_g \\ &= 1858.061 \text{ kN}\end{aligned}$$

Tensile rupture

$$\begin{aligned}\phi \times P_n &= \phi_t \times F_u \times A_g \\ &= 2129.028 \text{ kN}\end{aligned}$$

$$\begin{aligned}\phi \times P_n &= \min \{1858.061, 2129.028\} \\ &= 1858.061 \text{ kN yielding is governing}\end{aligned}$$

------(Shear)-----

Clause G2

$$C_v = 1$$

$$\begin{aligned}\phi \times V_n &= \phi \times 0.6 \times F_y \times A_w \times C_v \\ &= 494.244 \text{ kN}\end{aligned}$$

------(Combined action (Axial and Bending))-----

Clause H1, Doubly symmetric member subject to flexure and tension

$$P_u / (\phi P_n) < 0.2 (P_u / (2 \times \phi P_n)) + (M_{ux} / (\phi M_{nx})) < 1.0$$

Demand/Capacity Ratio :

$$0.006 + 0.900 = 0.906 < 1.0$$

------(Summary of Demand to Capacity (Design) ratios)-----

Flexure: 0.900

Axial: 0.011

Shear: 0.43264

Combined action: 0.906

\*\* Combined bending and axial force is governing failure mode